

SANDIA REPORT

SAND92-0700/5 • UC-721

Unlimited Release

Printed August 1993

RETAIN HARDCOPY

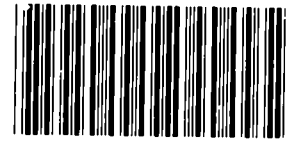
MICROFICHE

Preliminary Performance Assessment for the Waste Isolation Pilot Plant, December 1992

Volume 5: Uncertainty and Sensitivity Analyses of Gas and Brine Migration for Undisturbed Performance

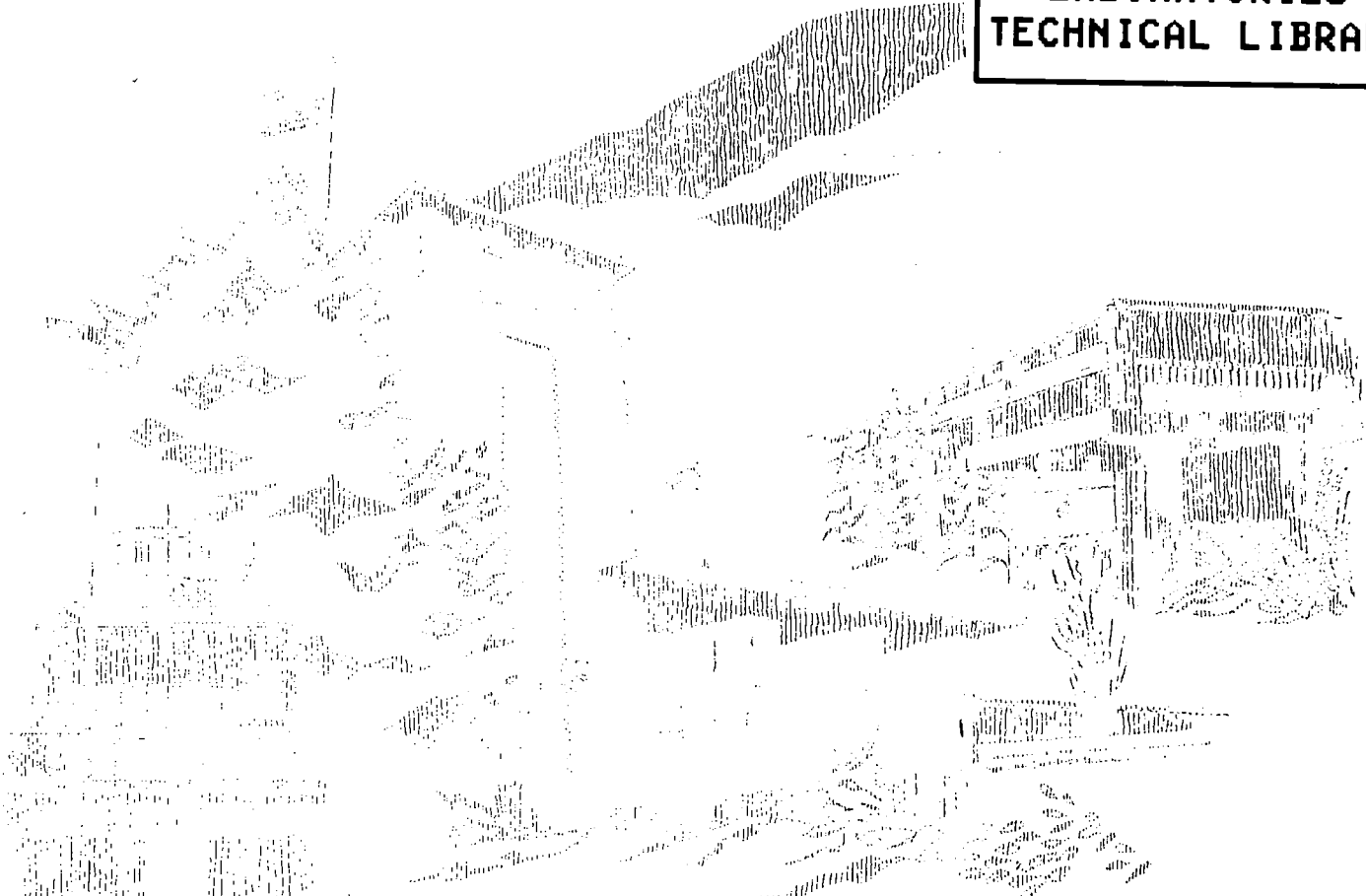
WIPP Performance Assessment Department

Prepared by
Sandia National Laboratories
Albuquerque, New Mexico 87185 and Livermore, California 94550
for the United States Department of Energy
under Contract DE-AC04-76DP00789



8599359

SANDIA NATIONAL
LABORATORIES
TECHNICAL LIBRARY



Issued by Sandia National Laboratories, operated for the United States Department of Energy by Sandia Corporation.

NOTICE: This report was prepared as an account of work sponsored by an agency of the United States Government. Neither the United States Government nor any agency thereof, nor any of their employees, nor any of their contractors, subcontractors, or their employees, makes any warranty, express or implied, or assumes any legal liability or responsibility for the accuracy, completeness, or usefulness of any information, apparatus, product, or process disclosed, or represents that its use would not infringe privately owned rights. Reference herein to any specific commercial product, process, or service by trade name, trademark, manufacturer, or otherwise, does not necessarily constitute or imply its endorsement, recommendation, or favoring by the United States Government, any agency thereof or any of their contractors or subcontractors. The views and opinions expressed herein do not necessarily state or reflect those of the United States Government, any agency thereof or any of their contractors.

Printed in the United States of America. This report has been reproduced directly from the best available copy.

Available to DOE and DOE contractors from
Office of Scientific and Technical Information
PO Box 62
Oak Ridge, TN 37831

Prices available from (615) 576-8401, FTS 626-8401

Available to the public from
National Technical Information Service
US Department of Commerce
5285 Port Royal Rd
Springfield, VA 22161

NTIS price codes
Printed copy: A07
Microfiche copy: A01

Record Copy



TECH REPS, inc. 5000 MARBLE, N.E. • ALBUQUERQUE, NEW MEXICO 87110 • (505) 255-5678/262-2077

Date: November 3, 1993

To: Distribution
From: Faith Puffer, Tech Reps, Inc.
Subject: Addition to Volume 5 of SAND93-0700, *Preliminary Performance Assessment for the Waste Isolation Pilot Plant, December 1992*

To whom it may concern:

The following pages were omitted from your copy of *Volume 5: Uncertainty and Sensitivity Analyses of Gas and Brine Migration for Undisturbed Performance*. Please insert these pages into your copy.

Thank you.

A handwritten signature in black ink, appearing to be 'F. Puffer', written over a printed name.

Faith Puffer

encl: Pages A-5 through A-8

~~NOV 6 11 01 94~~

NOV 10 1993

Preliminary Performance Assessment for the Waste Isolation Pilot Plant, December 1992

Volume 5: Uncertainty and Sensitivity Analyses of Gas and Brine Migration for Undisturbed Performance

WIPP Performance Assessment Department
Sandia National Laboratories
Albuquerque, New Mexico 87185

ABSTRACT

Before disposing of transuranic radioactive waste in the Waste Isolation Pilot Plant (WIPP), the United States Department of Energy (DOE) must evaluate compliance with applicable long-term regulations of the United States Environmental Protection Agency (EPA). Sandia National Laboratories is conducting iterative performance assessments (PAs) of the WIPP for the DOE to provide interim guidance while preparing for a final compliance evaluation. This volume of the 1992 PA contains results of uncertainty and sensitivity analyses with respect to migration of gas and brine from the undisturbed repository. Additional information about the 1992 PA is provided in other volumes. Volume 1 contains an overview of WIPP PA and results of a preliminary comparison with 40 CFR 191, Subpart B. Volume 2 describes the technical basis for the performance assessment, including descriptions of the linked computational models used in the Monte Carlo analyses. Volume 3 contains the reference data base and values for input parameters used in consequence and probability modeling. Volume 4 contains uncertainty and sensitivity analyses with respect to the EPA's *Environmental Standards for the Management and Disposal of Spent Nuclear Fuel, High-Level and Transuranic Radioactive Wastes* (40 CFR 191, Subpart B). Finally, guidance derived from the entire 1992 PA is presented in Volume 6.

Results of the 1992 uncertainty and sensitivity analyses indicate that, conditional on the modeling assumptions and the assigned parameter-value distributions, the most important parameters for which uncertainty has the potential to affect gas and brine migration from the undisturbed repository are: initial liquid saturation in the waste, anhydrite permeability, biodegradation-reaction stoichiometry, gas-generation rates for both corrosion and biodegradation under inundated conditions, and the permeability of the long-term shaft seal. Gas and brine migration are less sensitive to other parameters, although additional information is needed to confirm that the preferred conceptual models and assigned parameter distributions adequately describe reality.

ACKNOWLEDGMENTS

The Waste Isolation Pilot Plant (WIPP) Performance Assessment (PA) Department is comprised of both Sandia National Laboratories (SNL) and contractor employees working as a team to produce preliminary comparisons with Environmental Protection Agency (EPA) regulations, assessments of overall long-term safety of the repository, and interim technical guidance to the program. The on-site team, affiliations, and contributions to the 1992 performance assessment are listed in alphabetical order:

Performance Assessment Department

<u>Name</u>	<u>Affil.*</u>	<u>Primary Author of Major Code</u>	<u>Area of Responsibility</u>
R. Anderson	SNL		Department Manager
B. Baker	TEC		SEC02D, Hydrology, Office Manager
J. Bean	UNM		BRAGFLO, 2-Phase Flow
J. Berglund	UNM	CUTTINGS	Task Ldr., Cuttings/Cavings/ Spallings, Engr. Mech.
S. Bertram- Howery	SNL		PA Liaison with DOE, Criteria Document, Test Phase Plan
W. Beyeler	SAI	PANEL, GARFIELD	Geostatistics, Analytical Models, CAMCON Systems Codes
K. Brinster	SAI		Geohydrology, Conceptual Models
R. Blaine	ECO		SEC02D, SECOTP, & CAMCON Systems Codes
T. Blaine	GC		Drilling Technology, Exposure Pathways Data
K. Byle	UNM		Software and Analysis QA
J. Chapman	TRI		Documentation V.3
D. Duncan	MAC		Data QA
K. Economy	ECO		SECO2D, SECOTP, Hydrology & Transport Task Ldr., Hydrology, Geostatistics, NEA, PSAG
D. Gallegos	SNL		NEA Working Groups, PSAG, PAAG, Human Intrusion
D. Galson	GS		Source Term, Sens. Anal. CAMCON Systems Codes
J. Garner	API	PANEL	Task Ldr., Safety Assessments
A. Gilkey	UNM		EPA Regulations, Documentation V.1, Editor V.1
L. Gomez	SNL		Geology, Scenario Construction
M. Gruebel	TRI		Task Ldr., Uncert./Sens. Anal., Probability Models, Editor V.4
R. Guzowski	SAI		Expert Elicitation, Probability Models
J. Helton	ASU	CCDFPERM	LHS, CAMCON System Codes, Probability Models
S. Hora	UHH		EPA Regulations
H. Iuzzolino	GC	CCDFCALC CCDFPERM	Comp. Fluid Dyn. Hydrology/Geostatistics
R. Klett	SNL		Exposure Pathways
P. Knupp	ECO	SECOTP	Dep. Dept. Manager, Tech. Coord.
M. LaVenue	INT	GRASP-INV	Geostatistics Expert Group Chair
C. Leigh	SNL	GENII-S	CAMCON System Codes
M. Marietta	SNL		Safety Assessments
G. de Marsily	UP		Task Ldr., Inventory
R. McCurley	UNM		Geostatistics
B. Napier	PNL	GENII	
A. Peterson	SNL		
B. RamaRao	INT	GRASP-INV	

Acknowledgments

J. Rath	UNM		CAMCON System Codes
R. Rechar	SNL		Task Ldr., CAMCON, QA
P. Roache	ECO	SECO	Task Ldr., Comp. Fluid Dyn.
D. Rudeen	UNM		STAFF2D, SECOTP, Transport
J. Ruge	ECO		Multigrid Methods/BRAGFLO
T. Russell	ECO		Upscaling
K. Salari	ECO	SECOTP	Transport, Computational Fluid Dynamics
J. Sandha	SAI		INGRES, PA Data Base
J. Schreiber	SAI		BRAGFLO, 2-Phase Flow, Editor V.5
D. Scott	TRI		Documentation V.2
P. Swift	TRI		Task Ldr., Geology, Climate Var., Editor V.1, 2, 4, & 5
M. Tierney	SNL		Task Ldr., CDF Constr., Probability Models, Ref. Data, Editor V.2 & 3
K. Trauth	SNL		Task Ldr., Expert Panels
P. Vaughn	API	BRAGFLO	Task Ldr., 2-Phase Flow & Waste Panel Chemistry, Editor V. 4 & 5
T. Zimmerman	GRA		Geostatistics Test Problem

The foundation of the annual WIPP performance assessment is the underlying data set and understanding of the important processes in the engineered and natural barrier systems. Other SNL Departments are the primary source of these data and understanding. Assistance with the waste inventory comes from Westinghouse Electric Corporation and its contractors. We gratefully acknowledge the support of our departmental and project colleagues. Some individuals have worked closely with the performance assessment team, and we wish to acknowledge their contributions individually:

H. Batchelder	WEC	CH & RH Inventories
R. Beauheim	SNL	Natural Barrier System, Hydrologic Parameters
D. Borns	SNL	Geology, Geophysics
B. Butcher	SNL	Engineered Barrier System, Unmodified Waste-Form Parameters, Disposal Room Systems Parameters
L. Brush	SNL	Engineered Barrier System, Source Term (Solubility) and Gas Generation Parameters
L. Clements	ReS	Computer System Support
T. Corbet	SNL	Natural Barrier System, Geologic & Hydrologic Parameters, Conceptual Models
P. Davies	SNL	Natural Barrier System, Hydrologic & Transport Parameters, & 2-Phase Flow Mechanistic Modeling
P. Drez	DE	CH & RH Inventories
R. Finley	SNL	Repository Isolation Systems Parameters
F. Gelbard	SNL	Natural Barrier System, Retardation
E. Gorham	SNL	Natural Barrier System, Fluid Flow & Transport Parameters
R. Holt	CON	Geology
S. Howarth	SNL	Natural Barrier System, Hydrologic Parameters
R. Kehrman	WEC	CH & RH Waste Characterization
K. Lickliter	BEC	EPA Regulations
R. Lincoln	SNL	Room Modeling
F. Mendenhall	SNL	Engineered Barrier System, Unmodified Waste Form Parameters, Waste Panel Closure (Expansion)
D. Munson	SNL	Reference Stratigraphy, Constitutive Models, Physical & Mechanical Parameters
C. Novak	SNL	Natural Barrier Systems, Chemistry
E. Nowak	SNL	Room Modeling, Source Term
J. Orona	ReS	Computer System Support
A. Stevens	SNL	DOE Liaison

J. Tillerson	SNL	Repository Isolation Systems Parameters
W. Wawersik	SNL	Fracturing
S. Webb	SNL	2-Phase Flow Sensitivity Analysis & Benchmarking

*** Affiliation**

API = Applied Physics Incorporated	ReS = ReSpec
ASU = Arizona State University	SAI = Scientific Applications International Corporation
BEC = Benchmark Environmental Corp.	SNL = Sandia National Laboratories
CON = Consultant	TEC = Technadyne Engineering Consultants
DE = Drez Environmental	TRI = Tech Reqs, Inc.
ECO = Ecodynamics Research Associates	UHH = University of Hawaii at Hilo
GC = Geo-Centers Incorporated	UNM = Univ. of New Mexico/New Mexico Engineering Research Institute
GRA = GRAM, Inc.	UP = University of Paris
GS = Galson Sciences	WEC = Westinghouse Electric Corporation
INT = Intera	
MAC = MACTEC	
PNL = Pacific Northwest Laboratory	

Expert Panels

Futures

M. Baram	Boston University
W. Bell	Yale University
G. Benford	University of California, Irvine
D. Chapman	The World Bank, Cornell University
B. Cohen	University of Pittsburgh
V. Ferkiss	Georgetown University
T. Glickman	Resources for the Future
T. Gordon	Futures Group
C. Kirkwood	Arizona State University
H. Otway	Joint Research Center (Ispra), Los Alamos National Laboratory
M. Pasqualetti	Arizona State University
D. Reicher	Natural Resources Defense Council
N. Rosenberg	Resources for the Future
M. Singer	The Potomac Organization
T. Taylor	Consultant
M. Vinovski	University of Michigan

Markers

D. Ast	Cornell University
V. Baker	University of Arizona
M. Brill	Buffalo Organization for Social and Technological Innovation
F. Drake	University of California at Santa Cruz
B. Finney	University of Hawaii at Manoa
D. Givens	American Anthropological Association
W. Goodenough	University of Pennsylvania
M. Kaplan	Eastern Research Group
J. Lomborg	Consultant
L. Narens	University of California at Irvine
F. Newmeyer	University of Washington
W. Sullivan	University of Washington
W. Williams	Case Western Reserve University

Acknowledgments

Source Term

C. Bruton
I-Ming Chou
D. Hobart
F. Millero

Lawrence Livermore National Laboratory
U.S. Geological Survey
Los Alamos National Laboratory
University of Miami

Retardation

R. Dosch
C. Novak
M. Siegel

Sandia National Laboratories
Sandia National Laboratories
Sandia National Laboratories

Geostatistics Expert Group

G. de Marsily, Chair
R. Bras
J. Carrera
G. Dagan
A. Galli
S. Gorelick
P. Grindrod
A. Gutjahr
D. McLaughlin
S. Neuman
C. Ravenne
Y. Rubin

U. of Paris
Massachusetts Inst. of Tech.
U. Polit cnica de Catalu na
Tel Aviv U.
Ecole des Mines de Paris
Stanford U.
Intera Sciences
New Mexico Tech.
Massachusetts Inst. of Tech.
U. of Arizona
Institut Fran ais du P trole
U. of California, Berkeley

Report Preparation (TRI)

Editors:

Volume 1: M. Minahan (text); D. Marchand (illustrations)
Volume 2: M. Minahan (text); D. Marchand (illustrations)
Volume 3: J. Chapman (text); D. Pulliam (illustrations)
Volume 4: V. Gilliland, M. Minahan (text); S. Laundre-Woerner (illustrations)
Volume 5: S. Strong, F. Puffer (text); D. Marchand (illustrations)

D. Rivard and the Word Processing Department
R. Rohac, R. Andree, and the Illustration and Computer Graphics Departments
S. Tullar and the Production Department

Peer Review

Internal/Sandia

F. Mendenhall
L. Gomez

Management/Sandia

W. Weart

PA Peer Review Panel

R. Heath, Chair

R. Budnitz

T. Cotton

J. Mann

T. Pigford

F. Schwartz

University of Washington

Future Resources Associates, Inc.

JK Research Associates, Inc.

University of Illinois

University of California, Berkeley

Ohio State University

Department of Energy

J. Coffey

Acknowledgments

PREFACE

The *Preliminary Performance Assessment for the Waste Isolation Pilot Plant, December 1992* is currently planned to consist of six volumes. The titles of the volumes are listed below. All analyses reported in the 1992 Preliminary Performance Assessment, including those described in this volume, are based on computer modeling of disposal-system performance that was completed in November 1992.

This report is the fifth in a series of annual reports that document ongoing assessments of the predicted long-term performance of the Waste Isolation Pilot Plant (WIPP); this documentation will continue during the WIPP Test Phase. However, the Test Phase schedule and projected budget may change; if so, the content of the *1992 Preliminary Performance Assessment* report and its production schedule may also change.

- Volume 1: Third Comparison with 40 CFR 191, Subpart B
- Volume 2: Technical Basis
- Volume 3: Model Parameters
- Volume 4: Uncertainty and Sensitivity Analyses for 40 CFR 191, Subpart B
- Volume 5: Uncertainty and Sensitivity Analyses of Gas and Brine Migration for Undisturbed Performance
- Volume 6: Guidance to the WIPP Project from the December 1992 Performance Assessment

CONTENTS

1.	INTRODUCTION	1-1
1.1	Purpose of Volume 5	1-1
1.2	Requirements of 40 CFR 268.6	1-2
1.2.1	Status of WIPP Compliance with 40 CFR 268.6	1-2
1.2.2	The 40 CFR 268 Disposal Unit	1-3
1.2.3	Human Intrusion and 40 CFR 268.6	1-3
1.3	PA Methodology	1-3
1.4	Cases Selected for Analysis	1-5
2.	MODEL DESCRIPTION	2-1
2.1	Conceptual Model for the Repository	2-1
2.2	Computational Model for the Repository/Shaft System	2-1
2.3	Model Geometry	2-2
2.4	Boundary and Initial Conditions	2-7
2.5	Summary of Model Assumptions	2-9
3.	UNCERTAIN VARIABLES USED IN SIMULATIONS OF UNDISTURBED PERFORMANCE	3-1
4.	GAS AND BRINE MIGRATION	4-1
4.1	Four-Shaft Equivalent Geometry	4-1
4.1.1	Repository Behavior	4-2
4.1.2	Brine Flow Behavior	4-14
4.1.3	Gas Flow Behavior	4-29
4.2	Single-Shaft Geometry	4-40
4.2.1	Repository Behavior	4-40
4.2.2	Brine Flow Behavior	4-40
4.2.3	Gas Flow Behavior	4-47
4.3	Four-Shaft Equivalent Geometry without Dynamic Creep Closure	4-47
4.3.1	Repository Behavior	4-50
4.3.2	Brine Flow Behavior	4-50
4.3.3	Gas Flow Behavior	4-54
5.	UNCERTAINTY AND SENSITIVITY ANALYSIS RESULTS	5-1
5.1	Sensitivity Analysis Techniques	5-2
5.2	Gas Generation and Repository Performance	5-7
5.2.1	Gas Generation from Inundated Corrosion	5-7
5.2.2	Gas Generation from Humid Corrosion	5-9
5.2.3	Gas Generation from Inundated and Humid Corrosion	5-10
5.2.4	Gas Generation from Inundated Biodegradation	5-13
5.2.5	Gas Generation from Humid Biodegradation	5-16
5.2.6	Gas Generation from Inundated and Humid Biodegradation	5-18
5.2.7	Gas Generation from Corrosion and Biodegradation	5-20
5.2.8	Iron Remaining in the Waste	5-23
5.2.9	Cellulose Remaining in the Waste	5-24
5.2.10	Repository Pore Volume	5-26
5.2.11	Average Brine Saturation in the Waste	5-29
5.2.12	Pore Pressure in the Waste	5-31

Contents

5.3	Brine Flow	5-33
5.3.1	Cumulative Net Brine Flow from the Repository	5-33
5.3.2	Cumulative Net Brine Flow Out MB139	5-35
5.3.3	Cumulative Net Brine Flow Out Anhydrite a + b	5-37
5.3.4	Cumulative Net Brine Flow Out MB138	5-39
5.3.5	Cumulative Net Brine Flow Upward through Shaft Seal	5-41
5.4	Gas Flow	5-43
5.4.1	Cumulative Net Gas Flow Out MB139	5-43
5.4.2	Cumulative Net Gas Flow Out Anhydrite a + b	5-45
5.4.3	Cumulative Net Gas Flow Out MB138	5-47
5.4.4	Distance Gas Flows Out Anhydrite Layers	5-49
5.4.5	Cumulative Net Gas Flow Upward through Shaft Seal	5-53
5.4.6	Cumulative Net Gas Flow Upward into the Culebra	5-55
6.	SUMMARY AND CONCLUSIONS	6-1
7.	REFERENCES	7-1
	APPENDIX A: MEMORANDUM REGARDING REFERENCE DATA	A-1
	APPENDIX B: BRAGFLO REFERENCE TABLES	B-1

Figures

1-1	Artist's concept of the WIPP disposal system, showing the boundaries of the 40 CFR 268 disposal unit	1-4
1-2	Stratigraphy within the Salado Formation near the repository elevation (after Munson et al., 1989)	1-6
1-3	Proposed WIPP repository, showing transuranic-waste emplacement regions and location of the shafts	1-7
2-1	North-south vertical cross-section showing dimensions of the mesh used in BRAGFLO calculations for this volume	2-3
2-2	Plan view of grid cells 6-8 and 22-24 as initially wrapped around excavated regions	2-5
2-3	Plan view of grid cells after they are unwrapped from around the excavated region	2-6
4-1	Volume Average Pressure in the Waste Repository	4-3
4-2	Volume Average Brine Saturation in the Waste Repository	4-5
4-3	Pore Volume in the Waste Repository	4-6
4-4	Brine Volume in the Waste Repository	4-7
4-5	Iron Remaining in the Waste Repository	4-8
4-6	Cellulose Remaining in the Waste Repository	4-9
4-7	Cumulative Gas Volume Generated (at 30 °C; 0.101 MPa)	4-11
4-8	Cumulative Brine Volume Consumed	4-12
4-9	Cumulative Brine Flow from the Waste Repository	4-13
4-10	Cumulative Brine Flow from the Repository to the Drift Seals	4-15
4-11	Cumulative Upward Brine Flow through Shaft Seal	4-16
4-12	Brine Volume in Lower Shaft	4-17
4-13	Cumulative Brine Flow South out MB138	4-20
4-14	Cumulative Gas Flow South out MB138 (at 30 °C; 0.101 MPa)	4-21
4-15	Cumulative Brine Flow South out Anhydrite Layers a + b	4-23
4-16	Cumulative Gas Flow South out Anhydrite Layers a + b (at 30 °C; 0.101 MPa)	4-24
4-17	Cumulative Brine Flow South out MB139	4-25
4-18	Cumulative Gas Flow South out MB139 (at 30 °C; 0.101 MPa)	4-26
4-19	Cumulative Brine Flow from Drift Seals and Backfill into Shaft	4-27

4-20	Cumulative Brine Flow from Experimental Region into Shaft	4-28
4-21	Cumulative Brine Flow from DRZ into Shaft	4-30
4-22	Cumulative Brine Flow from MB138 into Shaft	4-31
4-23	Cumulative Brine Flow from Transition Zone into Shaft	4-32
4-24	Cumulative Brine Flow from Halite into Shaft	4-33
4-25	Cumulative Brine Flow from Culebra into Shaft	4-34
4-26	Cumulative Gas Flow South in MB139 Past the WIPP Boundary (at 30 °C; 0.101 MPa).....	4-35
4-27	Cumulative Gas Flow South in Anhydrite Layers a + b Past the WIPP Boundary (at 30 °C; 0.101 MPa).....	4-36
4-28	Cumulative Gas Flow South in MB138 Past the WIPP Boundary (at 30 °C; 0.101 MPa).....	4-37
4-29	Cumulative Upward Gas Flow through Shaft Seal (at 30 °C; 0.101 MPa)	4-38
4-30	Cumulative Gas Flow from Drift Seals and Backfill into Shaft (at 30 °C; 0.101 MPa).....	4-39
4-31	Cumulative Gas Flow from DRZ into Shaft (at 30 °C; 0.101 MPa)	4-41
4-32	Volume Average Pressure in the Waste Repository, Single Shaft Model	4-42
4-33	Iron Remaining in the Waste Repository, Single Shaft Model.....	4-43
4-34	Cellulose Remaining in the Waste Repository, Single Shaft Model	4-44
4-35	Cumulative Gas Volume Generated (at 30 °C; 0.101 MPa), Single Shaft Model.....	4-45
4-36	Cumulative Brine Flow from the Waste Repository, Single Shaft Model.....	4-46
4-37	Cumulative Upward Brine Flow through Shaft Seal, Single Shaft Model.....	4-48
4-38	Cumulative Upward Gas Flow through Shaft Seal (at 30 °C; 0.101 MPa), Single Shaft Model	4-49
4-39	Volume Average Pressure in the Waste Repository, Fixed Waste Porosity Model	4-51
4-40	Cumulative Gas Volume Generated (at 30 °C; 0.101 MPa), Fixed Waste Porosity Model	4-52
4-41	Cumulative Brine Flow from the Waste Repository, Fixed Waste Porosity Model.....	4-53
4-42	Cumulative Brine Flow South out MB139, Fixed Waste Porosity Model	4-55
4-43	Cumulative Brine Flow South out Anhydrite Layers a + b, Fixed Waste Porosity Model	4-56
4-44	Cumulative Brine Flow South out MB138, Fixed Waste Porosity Model	4-57
4-45	Cumulative Upward Brine Flow through Shaft Seal, Fixed Waste Porosity Model	4-58
4-46	Cumulative Gas Flow South in Marker Bed 139 Past the WIPP Boundary (at 30 °C; 0.101 MPa), Fixed Waste Porosity Model	4-59
4-47	Cumulative Gas Flow South in Anhydrite Layers a + b Past the WIPP Boundary (at 30 °C; 0.101 MPa), Fixed Waste Porosity Model.....	4-60
4-48	Cumulative Gas Flow South in MB138 Past the WIPP Boundary (at 30 °C; 0.101 MPa), Fixed Waste Porosity Model	4-61
4-49	Cumulative Upward Gas Flow through Shaft Seal (at 30 °C; 0.101 MPa), Fixed Waste Porosity Model	4-62
5-1	Scatterplots and partial rank correlation coefficients for gas generation from inundated corrosion.....	5-8
5-2	Scatterplots and partial rank correlation coefficients for gas generation from humid corrosion.....	5-11
5-3	Scatterplots and partial rank correlation coefficients for gas generation from inundated and humid corrosion.....	5-12
5-4	Scatterplots and partial rank correlation coefficients for gas generation from inundated biodegradation.....	5-15
5-5	Scatterplots and partial rank correlation coefficients for gas generation from humid biodegradation.....	5-17
5-6	Scatterplots and partial rank correlation coefficients for gas generation from inundated and humid biodegradation.....	5-19
5-7	Partial rank correlation coefficients for gas generation from corrosion and biodegradation	5-21
5-8	Scatterplots for coefficients for gas generation from corrosion and biodegradation.....	5-22
5-9	Scatterplots and partial rank correlation coefficients for iron remaining in the waste	5-25
5-10	Scatterplots and partial rank correlation coefficients for cellulose remaining in the waste	5-27
5-11	Scatterplots and partial rank correlation coefficients for repository pore volume	5-28

Contents

5-12	Scatterplots and partial rank correlation coefficients for average brine saturation in the waste	5-30
5-13	Scatterplots and partial rank correlation coefficients for pore pressure in the waste	5-32
5-14	Scatterplots and partial rank correlation coefficients for cumulative net brine flow from the repository	5-34
5-15	Scatterplots and partial rank correlation coefficients for cumulative net brine flow out MB139	5-36
5-16	Scatterplots and partial rank correlation coefficients for cumulative net brine flow out anhydrite a + b	5-38
5-17	Scatterplots and partial rank correlation coefficients for cumulative net brine flow out MB138	5-40
5-18	Scatterplots and partial rank correlation coefficients for cumulative net brine flow upward through shaft seal.....	5-42
5-19	Scatterplots and partial rank correlation coefficients for cumulative net gas flow out MB139	5-44
5-20	Scatterplots and partial rank correlation coefficients for cumulative net gas flow out anhydrite a + b.....	5-46
5-21	Scatterplots and partial rank correlation coefficients for cumulative net gas flow out MB138	5-48
5-22	Scatterplots and partial rank correlation coefficients for the distance gas flows out MB139	5-50
5-23	Scatterplots and partial rank correlation coefficients for cumulative net gas flow upward through the shaft seal	5-54
5-24	Scatterplots and partial rank correlation coefficients for cumulative net gas flow upward through the shaft seal.....	5-56

Tables

2-1	Partial List of Assumptions Used in the BRAGFLO Analyses of Undistributed Performance Reported in Volume 5 of the 1992 WIPP PA.....	2-9
3-1	Variables Sampled in 1992 WIPP Performance Assessment	3-1
4-1	Cumulative Volumes in Anhydrite Layers in BRAGFLO Mesh.....	4-18
4-2	Pore Volumes in Grid Blocks in Anhydrite Layers in BRAGFLO Mesh	4-19
5-1	Latin Hypercube Sample Independent Variables Used in Stepwise Regression and Partial Correlation Analyses	5-4
5-2	Latin Hypercube Sample Dependent Variables Used in Stepwise Regression and Partial Correlation Analyses	5-5
5-3	Stepwise Regression Analysis with Rank-Transformed Data for Total Gas Production Resulting from Inundated Corrosion (QRSCUMGC)	5-9
5-4	Stepwise Regression Analysis with Rank-Transformed Data for Total Gas Production Resulting from Humid Corrosion (QRHCUMGC).....	5-10
5-5	Stepwise Regression Analysis with Rank-Transformed Data for Total Gas Production Resulting from Both Inundated and Humid Corrosion (QRGCORVC)	5-13
5-6	Stepwise Regression Analysis with Rank-Transformed Data for Total Gas Production Resulting from Inundated Biodegradation (QRSCUMGB).....	5-14
5-7	Stepwise Regression Analysis with Rank-Transformed Data for Total Gas Production Resulting from Humid Biodegradation (QRHCUMGB)	5-16
5-8	Stepwise Regression Analysis with Rank-Transformed Data for Total Gas Production Resulting from Both Inundated and Humid Biodegradation (QRGBIOVC).....	5-18
5-9	Stepwise Regression Analysis with Rank-Transformed Data for Total Gas Production Resulting from Corrosion and Biodegradation (GASGENVC).....	5-23
5-10	Stepwise Regression Analysis with Rank-Transformed Data for Iron Remaining in the Repository after 10,000 yr (FECONT).....	5-24
5-11	Stepwise Regression Analysis with Rank-Transformed Data for Cellulosics Remaining in the Repository (BIOCONT)	5-26
5-12	Stepwise Regression Analysis with Rank-Transformed Data for Pore Volume in the Waste (PORVOLW).....	5-29

5-13	Stepwise Regression Analysis with Rank-Transformed Data for Average Brine Saturation in the Waste (SBAVW).....	5-29
5-14	Stepwise Regression Analysis with Rank-Transformed Data for Average Pore Pressure in the Waste (PRESWAST).....	5-31
5-15	Stepwise Regression Analysis with Rank-Transformed Data for Cumulative Net Brine Flow from the Repository (BWSTC).....	5-35
5-16	Stepwise Regression Analysis with Rank-Transformed Data for Cumulative Net Brine Flow South into MB139 (BRNMB9SC).....	5-37
5-17	Stepwise Regression Analysis with Rank-Transformed Data for Cumulative Net Brine Flow South into Anhydrite Layers a + b (BRNANHSC).....	5-39
5-18	Stepwise Regression Analysis with Rank-Transformed Data for Cumulative Net Brine Flow South into MB138 (BRNMB8SC).....	5-41
5-19	Stepwise Regression Analysis with Rank-Transformed Data for Cumulative Net Brine Flow Upward through Shaft Seal (BSHSLUPC).....	5-43
5-20	Stepwise Regression Analysis with Rank-Transformed Data for Cumulative Net Gas Flow South into MB139 (GASMB9SC).....	5-45
5-21	Stepwise Regression Analysis with Rank-Transformed Data for Cumulative Net Gas Flow Out Anhydrite Layers a + b (GASANHSC).....	5-47
5-22	Stepwise Regression Analysis with Rank-Transformed Data for Cumulative Net Gas Flow Out MB138 (GASMB8SC).....	5-49
5-23	Stepwise Regression Analysis with Rank-Transformed Data for Distance Gas Flows Out MB139 (GDSTMB9S).....	5-51
5-24	Stepwise Regression Analysis with Rank-Transformed Data for Gas Migration Distance South Out Anhydrite Layers a + b (GDSTANHS).....	5-52
5-25	Stepwise Regression Analysis with Rank-Transformed Data for Gas Migration Distance South Out MB138 (GDSTMB8S).....	5-52
5-26	Stepwise Regression Analysis with Rank-Transformed Data for Gas Migration Distance South Out the Culebra (GDSTCULS).....	5-53
5-27	Stepwise Regression Analysis with Rank-Transformed Data for Cumulative Net Upward Gas Flow through Shaft Seal (GSHSLUPC).....	5-55
5-28	Stepwise Regression Analysis with Rank-Transformed Data for Cumulative Net Gas Flow into the Culebra (GASCULTC).....	5-55
6-1	Importance of Sampled Parameters with Respect to 40 CFR 268.6.....	6-2

1. INTRODUCTION

The Waste Isolation Pilot Plant (WIPP) is planned as a research and development facility to demonstrate the safe disposal of transuranic (TRU) wastes generated by defense programs of the United States Department of Energy (DOE). Before disposing of waste in the WIPP, the DOE must evaluate compliance with applicable long-term regulations of the United States Environmental Protection Agency (EPA), including 40 CFR 191, Subpart B (*Environmental Standards for the Management and Disposal of Spent Nuclear Fuel, High-Level and Transuranic Radioactive Wastes, Final Rule* [U.S. EPA, 1985]) and 40 CFR 268.6 (Petitions to allow land disposal of a waste prohibited under Subpart C of Part 268 [U.S. EPA, 1986]), which is the portion of the regulations implementing the Resource Conservation and Recovery Act (RCRA) that states the conditions for disposal of specified hazardous wastes. Performance assessments (PAs) will form the basis for evaluating compliance with all applicable long-term regulations of the EPA. The WIPP Performance Assessment (PA) Department of Sandia National Laboratories (SNL) is performing iterative preliminary PAs to provide guidance to the Project while preparing for final compliance evaluation. Previous preliminary PAs for 40 CFR 191, Subpart B, have been documented for 1990 (Bertram-Howery et al., 1990; Rechard et al., 1990; Helton et al., 1991) and 1991 (WIPP PA Division, 1991 a,b,c; Helton et al., 1992).

1.1 Purpose of Volume 5

This volume describes uncertainty and sensitivity analyses of gas and brine migration for undisturbed performance only (i.e., without a breach of the repository by human intrusion). The volume is part of a set documenting the 1992 preliminary PA, and is not intended to provide a stand-alone description of the WIPP or of the compliance-assessment modeling system. Some essential information from other volumes of the 1992 PA is repeated here as necessary, but in general, cross-references are given throughout to more complete discussions elsewhere. Volume 1 of the 1992 PA provides an overview of the 1992 preliminary comparison with 40 CFR 191, Subpart B. Volume 2 describes the technical basis for the compliance assessment modeling system, including conceptual model development, probability modeling, and consequence modeling. Volume 3 compiles model parameters, constructs cumulative distribution functions (CDFs), and discusses their derivation from the pertinent data of disposal-system characterization. Uncertainty and sensitivity analyses specifically related to 40 CFR 191, Subpart B, (including analyses of consequences of human intrusion) are contained in Volume 4. Volume 6 contains guidance to the WIPP Project derived from the entire 1992 PA. Similar analyses of undisturbed performance based on simulations completed earlier in 1992 are documented elsewhere (WIPP PA Department, 1992).

Analyses of undisturbed performance are of interest for both the Individual Protection Requirements (§ 191.15) of 40 CFR 191 and 40 CFR 268.6. As discussed in Volume 4 of this report, brine migration is of interest for 40 CFR 191 because of the potential for radionuclide transport in the liquid phase. Both gas and brine migration are of interest for 40 CFR 268.6 because of the potential for transport of regulated hazardous constituents in both gas and brine phases. However, the preliminary results reported are intended to provide interim guidance to the WIPP Project as it develops a compliance strategy for 40 CFR 268.6, and should not be used as the basis for regulatory decisions. The modeling system and data base remain incomplete, and one potentially important process, the pressure-dependent fracturing of anhydrite interbeds above and below the waste-emplacement region, has not been included in the 1992 PA. Furthermore, transport of radionuclides and heavy metals in brine and volatile organic compounds in gas is not modeled. Performance measures described here apply only to the migration of the fluid

1. Introduction

phases and do not provide information about potential concentrations of contaminants within the fluids. If additional analyses of gas and brine migration continue to show a potential for gas migration beyond regulatory boundaries, a compliance determination for 40 CFR 268.6 will be based on evaluations of hazardous constituent concentrations using expanded data bases and more detailed computational models.

1.2 Requirements of 40 CFR 268.6

The *Land Disposal Restrictions* (40 CFR 268) regulate disposal of specified hazardous wastes. For the WIPP, hazardous constituents mixed with the radioactive transuranic waste can include solids such as lead and other heavy metals, and semivolatile and volatile organic compounds (VOCs) as residual liquids sorbed on waste materials or as gases associated with the waste in waste containers. A detailed inventory of the 40 CFR 268 contaminants anticipated for the WIPP is not available at this time, but a preliminary list of anticipated hazardous constituents were documented in the *Waste Isolation Pilot Plant No-Migration Variance Petition* (DOE, 1990). The Environmental Protection Agency (EPA) subsequently issued the *Conditional No-Migration Determination for the Department of Energy Waste Isolation Pilot Plant (WIPP)*, which mandated waste characterization requirements for the WIPP Test Phase and recommended waste characterization data needs in support of any long-term performance assessment. Methods of sampling and analysis for volatile and semivolatile constituents have been developed for headspace gases (DOE, 1991a) and additional methods for analysis of hazardous constituents in homogeneous solid waste forms are under development as part of the *Waste Characterization Program Plan for WIPP Experimental Waste* (DOE, 1991b).

In general, 40 CFR 268 prohibits the disposal of hazardous wastes unless the owner or operator of the facility petitions for a variance and successfully demonstrates "to a reasonable degree of certainty, that there will be no migration of hazardous constituents from the disposal unit or injection zone for as long as the wastes remain hazardous" or the waste is treated in accordance with applicable standards (40 CFR 268.6 (a), U.S. EPA, 1986). General guidance provided by the EPA on the interpretation of this wording indicates that "no migration" will be defined to be concentrations of hazardous constituents below health-based or environmentally based levels at the disposal-unit boundary (U.S. EPA, 1992). Following guidance from the EPA (U.S. EPA, 1990a, p. 13073) the SNL WIPP PA Department has assumed for the purposes of these analyses that the length of the regulatory period is 10,000 yr.

1.2.1 Status of WIPP Compliance with 40 CFR 268.6

In response to a no-migration variance petition from the DOE (U.S. DOE, 1990a) the EPA issued a conditional no-migration determination (U.S. EPA, 1990b) allowing the emplacement of a limited amount of transuranic mixed waste in the WIPP for experimental purposes during the Test Phase (U.S. DOE, 1993). However, as the EPA states in the supplementary information included with the no-migration determination "[b]efore DOE may move from the test phase to full-scale operations, it must petition EPA again and demonstrate no migration over the long term, that is, it must successfully address current uncertainties about long-term WIPP performance" (U.S. EPA, 1990b, p. 47704). Long-term uncertainties specifically identified by the EPA include "the extent and effects of gas generation, the effects of brine inflow into the repository, and the influence of a 'disturbed rock zone' surrounding the mined repository" (ibid.).

1.2.2 The 40 CFR 268 Disposal Unit

The "disposal unit" for the WIPP as applied to 40 CFR 268.6 (RCRA) is defined to include the entire volume of the Salado Formation from top to bottom within the 41 km² (16 mi²) WIPP land-withdrawal area (U.S. DOE, 1990b) (Figure 1-1). The SNL WIPP PA Department assumes for the purpose of PA modeling that the disposal-unit boundaries will remain unchanged for long-term performance. The RCRA disposal unit contains a smaller volume than that contained within the boundary of the accessible environment used in preliminary comparisons with 40 CFR 191, Subpart B (see Section 3.2 of Volume 1 of this report). As is the case for radionuclides regulated under 40 CFR 191, migration of hazardous constituents is allowed into the Salado Formation within the land-withdrawal area. Unlike the requirements of 40 CFR 191, however, migration of hazardous constituents into the Rustler Formation and other overlying strata within land-withdrawal area constitutes a potential violation.

1.2.3 Human Intrusion and 40 CFR 268.6

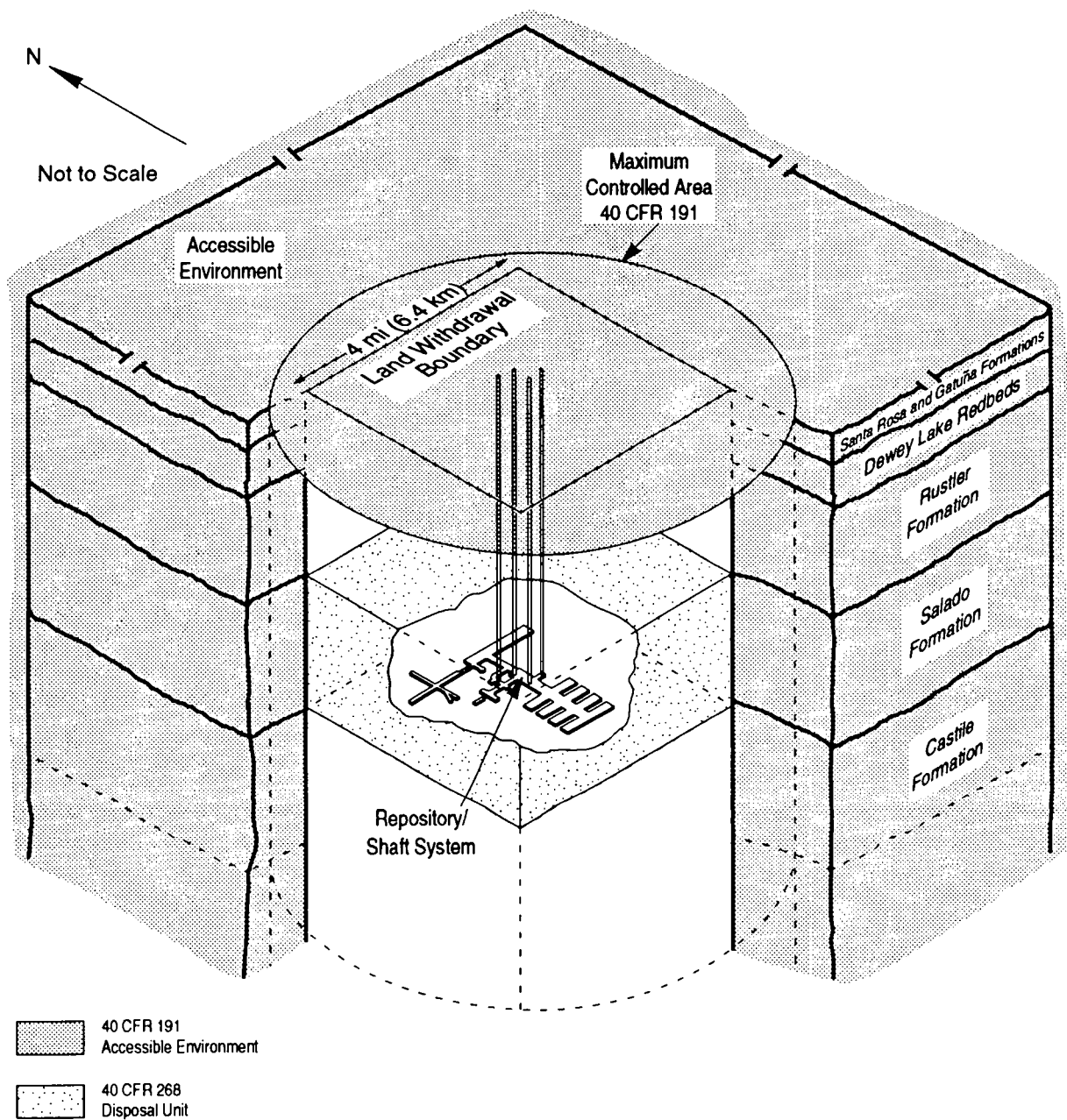
The extent to which estimates of the consequences of human intrusion will be required for long-term compliance evaluations has not been determined. The EPA has determined that human intrusion need not be considered for the Test Phase, and describes it as a long-term issue to "be addressed at the time a petition is considered for permanent disposal" (U.S. EPA, 1990b, p. 47720). Consideration of inadvertent human intrusion is required for compliance with 40 CFR 191, Subpart B, and analyses of the consequences of intrusion during exploratory drilling for hydrocarbons are described in detail in Volumes 1 and 4 of this report.

1.3 PA Methodology

Analyses have been performed using the Monte Carlo methodology and modeling system described in detail in Volume 2 of this report. In keeping with the requirement in 40 CFR 191.13 for probabilistic estimates of performance and a consideration of uncertainty in the results, this methodology relies on multiple realizations using deterministic models of physical processes and a Latin hypercube sampling (LHS) strategy to incorporate uncertainty for input parameters. Values for selected parameters are described by a range and distribution based on available data, and each simulation uses a separate input vector of sampled values drawn from the assigned distributions. The methodology is well suited for conducting uncertainty and sensitivity analyses that provide quantitative and qualitative insights about the potential variability in model results caused by uncertainty in specific input data (Helton et al., 1991, 1992; Helton, 1993). Sensitivity analysis techniques and methods for displaying their results have been summarized by Helton et al. (1991). Scatterplots and stepwise linear regression analyses are used in this volume to evaluate model sensitivity to uncertainty in sampled parameters.

Analyses described in this volume have been performed using the same modeling system and same vectors of sampled input parameters used for the analyses described in other volumes of the 1992 PA. As discussed in Chapter 3, selected parameters have been changed from the previous simulations to examine specific aspects of the disposal-system, such as shaft-seal system performance. Because these analyses are otherwise unchanged from those reported in Volume 4, direct comparisons may be made between specific realizations.

1. Introduction



TRI-6330-7-9

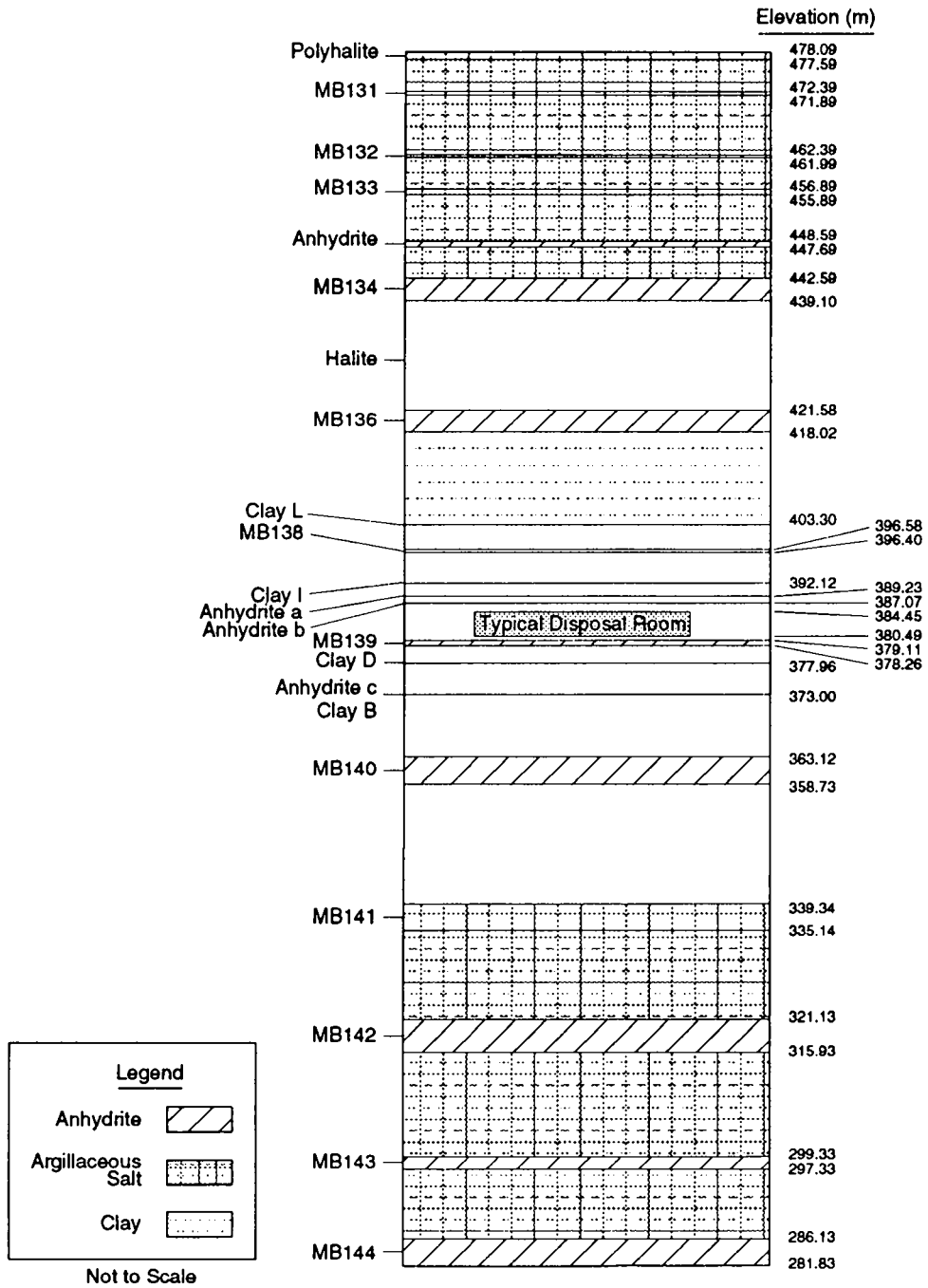
Figure 1-1. Artist's concept of the WIPP disposal system, showing the boundaries of the 40 CFR 268 disposal unit. Boundaries of the accessible environment as defined by 40 CFR 191, Subpart B, are shown for comparison. The scale of the repository/shaft system is exaggerated.

1.4 Cases Selected for Analysis

All analyses reported in this volume use a two-dimensional representation of the repository and surrounding strata as a vertical, north-south cross-section (described in detail in Chapter 2). This geometry is similar to that used in the analyses of undisturbed performance reported in Chapter 4 of Volume 4 of this report, differing only in the representation used for the shaft-seal system. Model stratigraphy is unchanged, and flow of both gas and brine is simulated in lithologies within the Salado Formation including halite, anhydrite Marker Beds 138 and 139, and anhydrite interbeds a and b (combined into a single model unit, anhydrite a + b) (Figure 1-2), as well as in the excavated regions of the repository and the overlying Rustler Formation (represented in the simplified model geometry only by the Culebra Member) (Figure 1-3).

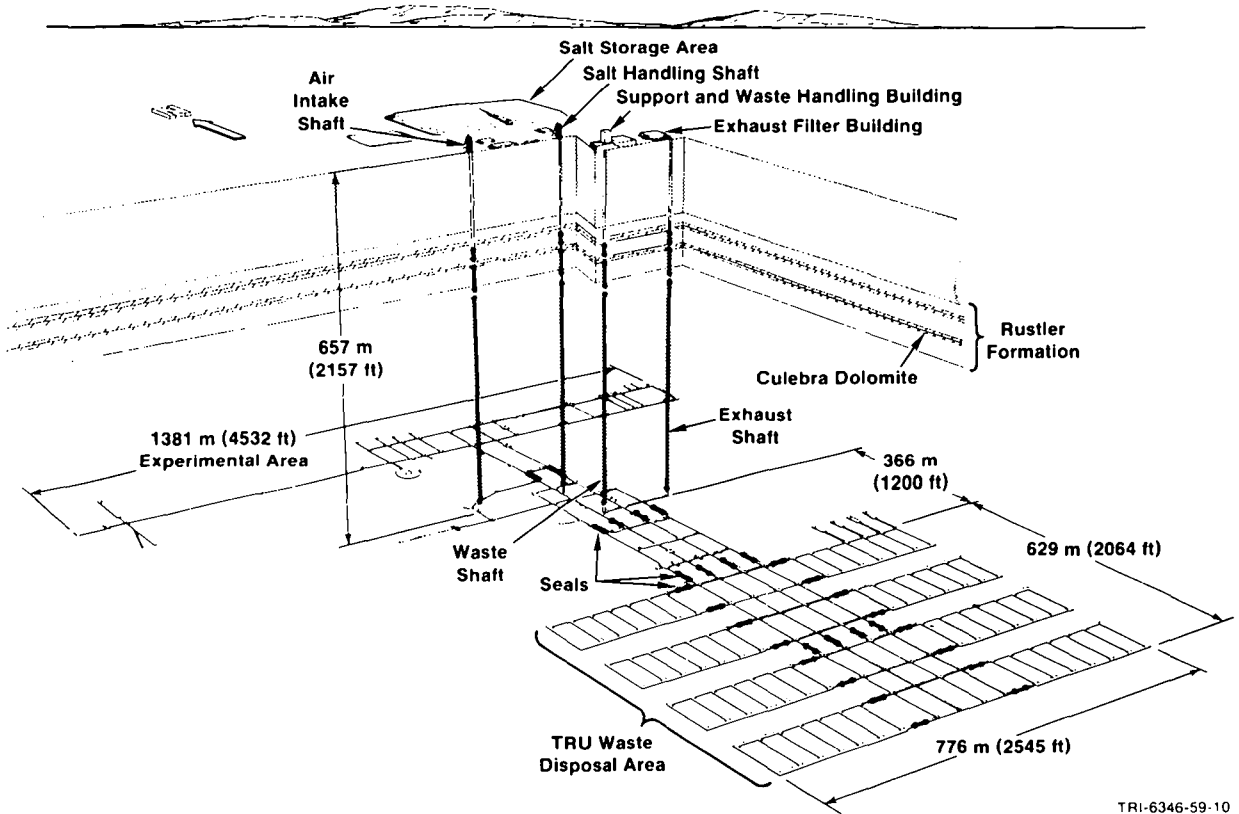
Variations of the modeling system are used to simulate three separate cases: one in which the total volume of all four existing shafts is combined into a single shaft with the total cross-sectional area and the four-shaft-equivalent volume (as was done in Volume 4 of this report); a second case in which the volume and cross-sectional area of only a single shaft was modeled; and a third case using the four-shaft-equivalent-volume geometry in which the dynamic creep closure model was not used, and instead the waste-emplacement regions were assumed to have closed to a final porosity before gas-generation began. The first case represents the PA Department's preferred conceptual model for the behavior of the repository/shaft system. The second case was examined to simulate flow under conditions where only one shaft functioned as a migration pathway. The third case, analogous to cases analyzed in Volume 2 for human intrusion scenarios, was analyzed to provide insight into the effect of including dynamic creep closure on disposal-system performance.

1. Introduction



TRI-6342-1070-0

Figure 1-2. Stratigraphy within the Salado Formation near the repository elevation (after Munson et al., 1989).



TRI-6346-59-10

Figure 1-3. Proposed WIPP repository, showing transuranic-waste emplacement regions and location of the shafts.

2. MODEL DESCRIPTION

This chapter contains descriptions of the geometry, boundary conditions, and initial conditions for the repository model used in these simulations, as well as a brief discussion of the approach used to incorporate dynamic creep closure of the repository into the analysis. In general, the conceptual and computational models used to simulate the disposal system are essentially unchanged from those used in the previous volumes of the 1992 PA, and therefore much of the discussion has not been repeated here. Parameter values used to characterize the various components within the model are described in Chapter 3.

2.1 Conceptual Model for the Repository

The conceptual model used for the repository includes gas generation by corrosion of iron and microbial degradation of cellulosic waste; pressure-dependent two-phase (brine and gas) Darcy flow in the repository and the surrounding strata; development of a disturbed rock zone (DRZ) around the excavated area before the repository is sealed; dynamic pressure-dependent closure of the waste-emplacement region by halite creep after the repository is sealed; isolation of the waste by both panel and shaft seals; and possible fluid migration from the waste through anhydrite interbeds above and below the emplacement region and through the panel- and shaft-seal systems. Brine is assumed initially (i.e., before development of the DRZ) to fill the pore space in all strata surrounding the repository. Pressure-dependent fracturing of anhydrite interbeds as a result of gas generation is not yet included in the conceptual or computational model, but will be included in future PAs. Discussions of the other processes included in the conceptual model can be found in previous volumes of this report, together with extensive references to primary documents: gas generation is described in Sections 1.4.1 and 3.3 of Volume 3; two-phase flow is described in Section 7.2 of Volume 2; properties of the strata around the repository and the DRZ are described in Section 2.3.1 of Volume 2 and Chapter 2 of Volume 3; development of the DRZ and closure by halite creep is described in Chapter 4 of Volume 4; the panel- and shaft-seal systems are described in Section 2.3.2 of Volume 2 and Section 3.2 of Volume 3; and migration pathways are described in Section 4.2.3.1 of Volume 2.

2.2 Computational Model for the Repository/Shaft System

Analyses reported in this volume do not include radionuclide transport or human intrusion, and therefore the computational model for the repository/shaft system uses only two of the computer codes described in previous volumes, BRAGFLO and SANCHO. BRAGFLO (WIPP PA Division, 1991b) simulates gas generation and two-phase flow in the entire model domain, and is described in Appendix A of Volume 2 of this report. SANCHO (Stone et al., 1985) is a finite-element program for the quasistatic, large deformation, inelastic response of two-dimensional solids, and is used to simulate halite creep. The implementation of SANCHO results in BRAGFLO, in terms of emplacement-room porosity as a function of pressure, is described in Chapter 4 of Volume 4.

2.3 Model Geometry

The mesh used in the BRAGFLO simulations attempts to incorporate radial flow phenomena at large distances from the repository and to include the full accessible volume available for multiphase flow. Time and cost constraints currently preclude a full three-dimensional representation of the repository and surrounding strata, so a two-dimensional approximation to the actual geometry was made. In reducing the three dimensions to two, certain measures were preserved. The single most important measure is the volume of various regions. In constructing the mesh (Figure 2-1), the full initial excavated volumes of all excavated regions were preserved. This includes the repository, the drift seals and drift backfill, the shaft, and the experimental region. In addition, the volume of the formations surrounding the repository and other excavated regions could be preserved. In order to include the true volumes of each of these regions, but still reduce the dimensionality to two, other measures had to be compromised. Which of these were preserved and which were compromised in some fashion determined how the mesh was constructed.

The mesh was developed as follows. The repository was modeled as a single large room, with a volume the same as currently planned for the entire waste disposal region, including all rooms and drifts. The initial excavated height, 3.96 m, was preserved. This was desirable because the creep closure treatment is based on porosity changes in a newly excavated and filled room. The height of the room, along with its initial porosity, is one of the few features that can be maintained identically between the original salt creep model done using SANCHO and the model as implemented in BRAGFLO. (This is described briefly in Section 2.1 and in more detail in Section 4.2.2.2 in Volume 4 of this report). It was also considered desirable to preserve the overall length in the north-south direction (847 m). This distance was somewhat arbitrary; it represents a compromise in the maximum distance that contaminated brine must flow from one end of the repository to the access drifts leading to the shaft. In the true repository configuration, some brine could flow a greater distance (e.g., starting from the far southwest corner of the southwest panel). On the other hand, some of this brine is already *at* the drift seals leading to the shaft, so some compromise was necessary. Having fixed the volume, height, and length of the repository, the east-west dimension must be 131.7 m.

The dimensions of the other excavated regions were established in a similar fashion. The distance from the north end of the repository to the nearest shaft (the Waste Shaft) was maintained at 332 m. The height of the access drifts, as well as of the experimental region, was fixed at the same initial excavated height of the waste-disposal region to simplify the mesh. In reality, access drifts and experimental rooms vary in height from about 3.7 to 4.9 m. Having specified the length, height, and volume of the sealed and backfilled access drifts, the width of that region was fixed at 30.35 m, which was approximately the combined widths of the four north-south drifts. Similarly, the distance from the Waste Shaft to the northernmost end of the experimental region was preserved at 561 m, so the east-west width of that region is 49.5 m.

In the base case, the shaft is a composite of the four existing shafts. The volume of the four combined shafts was preserved, and the height was set by the stratigraphy. The horizontal cross-sectional area was therefore the sum of the cross-sectional areas of the four shafts, 94.9 m². It seemed most reasonable to model the shaft as having a square cross section, although the shape is not likely to be important. Thus, the shaft is modeled as a square column 9.74 m on each side. The portion of the shaft below the Rustler Formation but above the shaft seal is referred to as the lower shaft. The upper shaft, above the Culebra, is not modeled here.

TRI-6342-1471-4

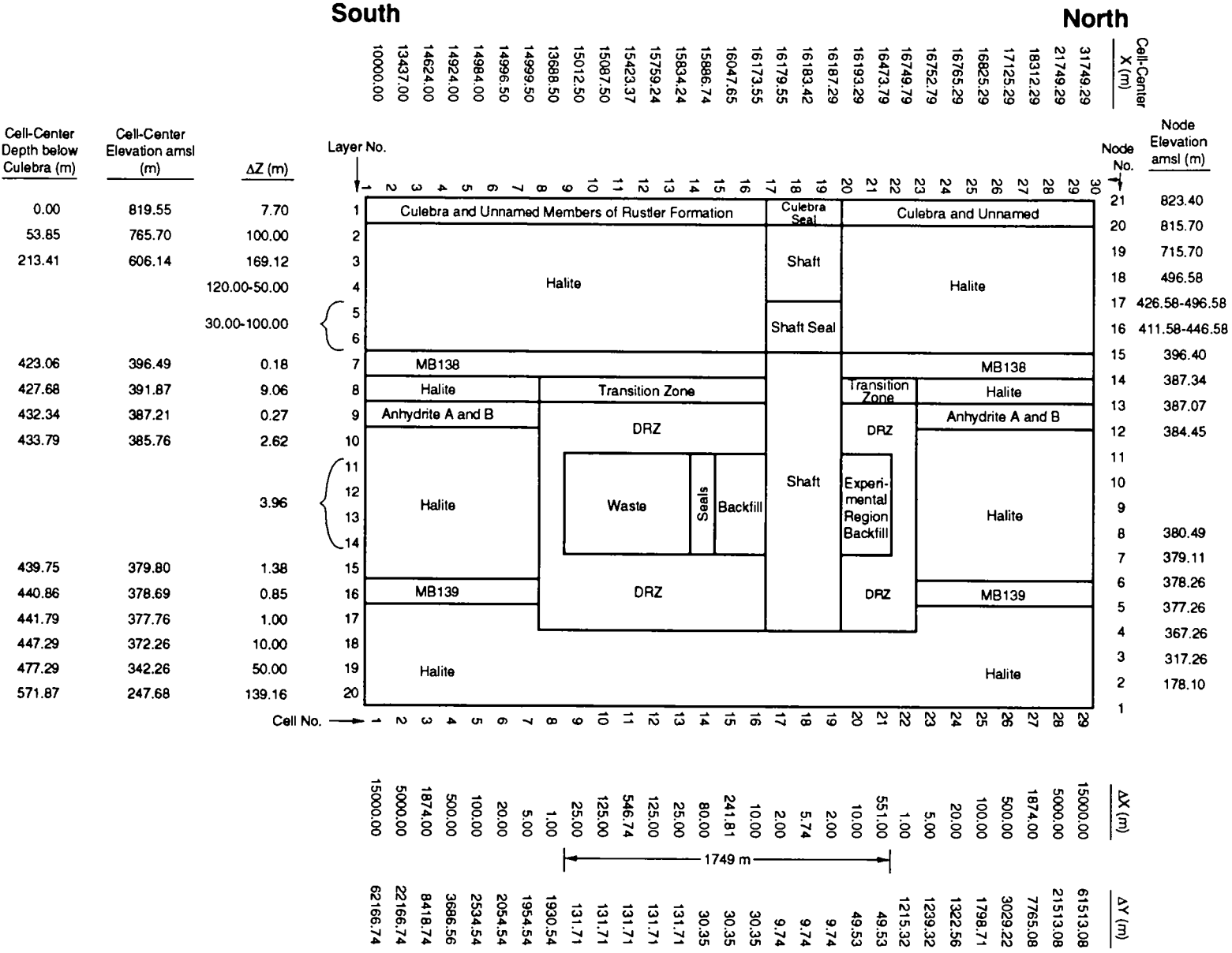


Figure 2-1. North-south vertical cross-section showing dimensions of the mesh used in BRAGFLO calculations for this volume.

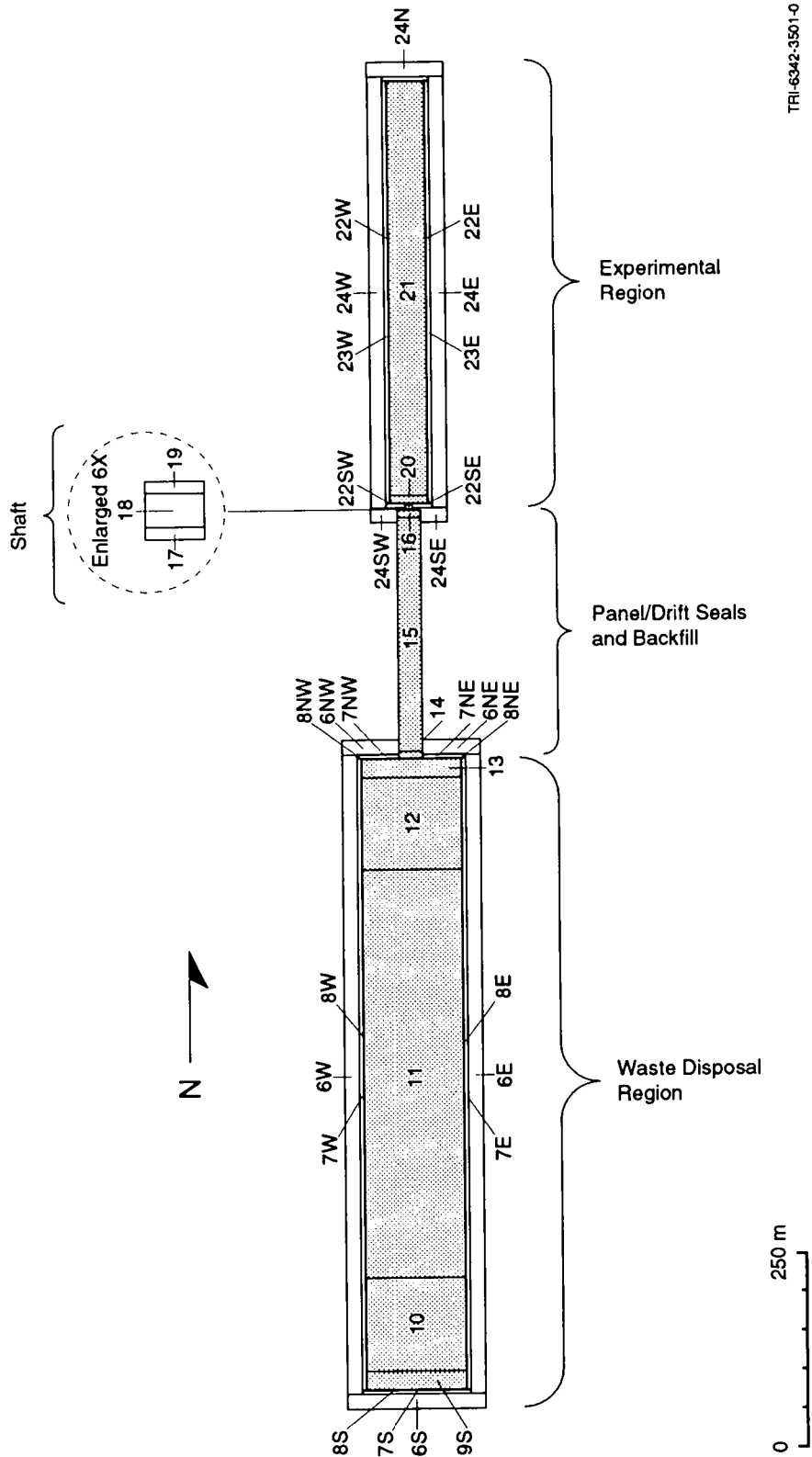
2. Model Description

1 This completely specifies the sizes and shapes of the excavated regions. The next step was to build the mesh
2 surrounding these regions. The objective was to include at any given horizon the entire accessible pore space as far
3 as the mesh extended, that is, to include the pore volume in the east-west direction to the same extent as in the
4 north-south direction. In a plan view at the repository horizon, Figure 2-2, this is done by including volume east
5 and west of the excavated region in the volume of grid cells to the north and south of the excavated regions.

6 If the model were radially symmetrical, this would be easily accomplished by requiring that the east-west
7 dimension, or Δy , be equal to $2\pi r$, where r is the radial distance from the axis of symmetry. Voss (1984) shows that
8 when Δy is varied in this manner using rectilinear geometry, the results are exactly equivalent to solving a true
9 radial problem. This geometry was used in the WIPP PA for human intrusion scenarios, as described in Volumes 2
10 and 4 of this report. Unfortunately, the geometry that has to be used in the undisturbed scenario is not radially
11 symmetrical. It is not clear how the mesh should be "flared" in the Δy -direction at each end of the excavated
12 regions in order to mimic radial symmetry with complete accuracy, if indeed it can be done rigorously. The
13 procedure used in the current calculations essentially divides the excavated regions in two along a vertical east-west
14 plane. Then layers of thickness Δx are "unwrapped" from the outside of the excavated region. The total length of
15 each unwrapped layer becomes the Δy corresponding to that grid cell. Figure 2-3 illustrates this unwrapping. At a
16 given elevation, a layer in the vertical direction of thickness Δz and horizontal north-south width Δx includes the
17 volume of a segment with cross section $\Delta x \Delta z$ both from the east side and the west side of the excavated region.

18 An example will help clarify the procedure. The first grid block south of the repository, Cell 8, is $\Delta x_8 = 1$ m
19 long in the north-south dimension (Figure 2-3). In the east-west direction, the dimension Δy_8 is the sum of the
20 lengths of five segments: 8S, 8E, 8W, 8NE, and 8NW. The first segment (8S in Figure 2-2) is the east-west width
21 of the repository, 131.7 m. The second is the length of a Δx_8 -thick segment, 8E, that extends along the entire east
22 side of the repository, plus $2\Delta x_8$, or 848.7 m. The third segment, 8NE, wraps around the north end of the
23 repository, ending at the seals and backfill regions, for a length of 50.7 m. The fourth and fifth segments, 8W and
24 8NW, are duplicates of the second and third, respectively, except that they wrap around the west side of the
25 repository. Thus, the total width of Cell 8 after it is unwrapped is $\Delta y_8 = 131.7 + 2(848.7 + 50.7) = 1930.5$ m. For
26 Cells 7, 6, and 5, Δy is evaluated in exactly the same manner. Because the same process is carried out at the north
27 end of the mesh, the segments along the east and west sides of the repository will eventually run into the line
28 dividing the north and south ends of the mesh, and will no longer wrap around the north end of the repository. Only
29 Cells 5-8 will wrap around the north end of the repository. Beginning with Cell 4, the segments along the east and
30 west sides of the repository (before being unwrapped) now intersect the north-south midpoint of the mesh, but
31 otherwise each Δy is evaluated the same as for Cells 5-8. Thus, all of the volume of the strata surrounding the
32 excavated regions is included in the mesh. This representation is not strictly equivalent to cylindrical geometry, but
33 is reasonably accurate at large distances from the repository. Very near the repository, this representation requires
34 all flow to go past the end of the repository, rather than through the sides, producing some loss of accuracy.

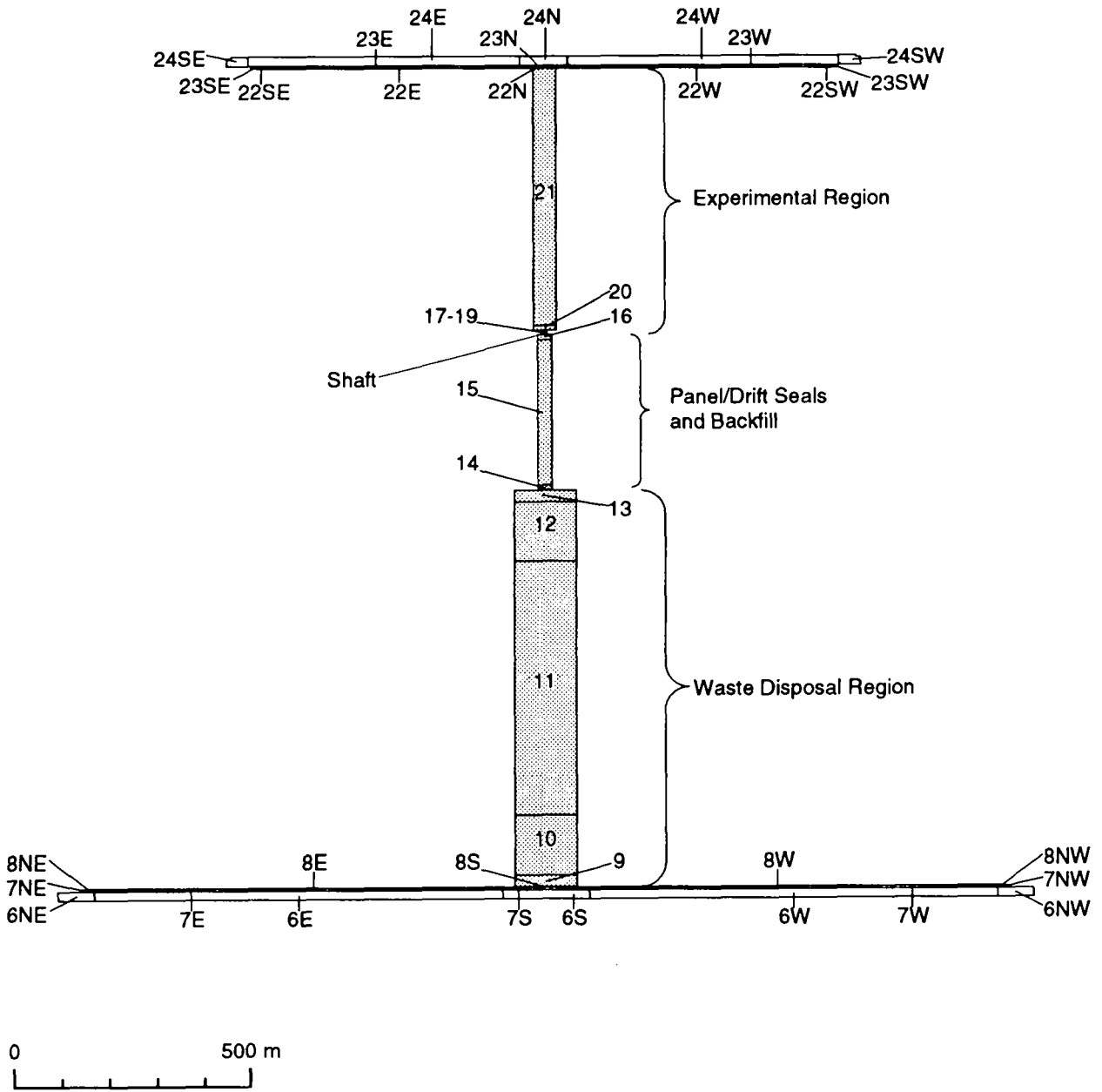
35 This two-dimensional approximation to three-dimensional geometry will be necessary until full three-
36 dimensional simulations become technically and economically feasible. It is doubtful that the full suite of PA
37 simulations can ever be carried out in three dimensions. However, a more limited set will necessarily be done in
38 three dimensions to confirm the approximations used in the two-dimensional calculations. A fast, robust, iterative
39 solver combining a conjugate gradient preconditioner with a multigrid solution algorithm is being adapted to
40 BRAGFLO. Together with newer machines that are more than an order of magnitude faster than those currently
41 used, full three-dimensional simulations should be more practical by next year.



TRI-6342-3501-0

Figure 2-2. Plan view of grid cells 6-8 and 22-24 as initially wrapped around excavated regions.

2. Model Description



TRI-6342-3497-0

Figure 2-3. Plan view of grid cells after they are unwrapped from around the excavated region.

2.4 Boundary and Initial Conditions

Boundary conditions were the same as in all previous BRAGFLO calculations done for PA: there was no flow in the normal directions across all far-field boundaries except the lateral boundaries of the Culebra, where the initial pressure of 1.053 MPa was held constant throughout the simulations. Initial far-field pressure in the Salado Formation was varied hydrostatically from the sampled value for pressure in MB139. This resulted in a pressure discontinuity at the boundary between the Salado and the Culebra that had little effect on fluid flow because of the low permeability of the halite.

Initial conditions were treated the same as for the undisturbed performance calculations discussed in Volume 4 of this report. Rather than simply specifying uniform pressures and saturations in each region at time zero, spatially varying initial conditions were computed over a 50-yr operational or disposal period. This enabled more realistic pressure and saturation distributions to be established in the formations surrounding the repository at the time when the repository is sealed. The procedure used to calculate initial conditions will be summarized here; a more detailed description can be found in Section 4.3 of Volume 4.

During the disposal phase of the WIPP, brine will seep in continually from the surrounding formations, reducing the pressure in the vicinity of the excavated regions. Water in the brine will evaporate into the well-ventilated atmosphere of the excavations or will be pumped out if it accumulates anywhere. Thus, the formations surrounding the excavations will be dewatered and depressurized during the operation. By modeling the time between excavation and decommissioning explicitly, the conditions at decommissioning (time zero) will be much more realistic. In the absence of this calculation, certain unrealistic results are obtained. Foremost among these is the large quantity of brine that immediately drains into excavated regions, in particular the waste, owing to the large pressure gradient between the initially pressurized surrounding formations and the atmospheric excavations. Because brine will be continuously removed during the time each panel is open, it would be incorrect to assume that it is still available to react with waste components to produce gas. When this brine is assumed to react with waste the result is erroneously large estimates of gas generation and inaccuracies in the predicted interaction of gas generation and brine and gas flow throughout the modeled region.

The duration of the disposal phase of the WIPP was assumed to be 50 yr. This may be excessively long for this calculation even if it is an accurate estimate of the duration of the disposal phases because panels will be excavated as needed, not simultaneously, and will be sealed after only a few years. Therefore, only a portion of the excavation is open to the atmosphere at any given time. However, the initial condition calculation does not appear to be highly sensitive to the duration. Most of the depressurization and drainage occurs during the first 20 yr, the duration used in the disturbed performance assessment. A longer duration was used in the undisturbed performance assessment to be consistent with the longer duration of the disposal phase when considering the entire repository instead of a single panel.

The important features of this 50-yr disposal phase or initial condition calculation are as follows. At the beginning of this calculation, pressure in the shaft, drifts, waste, and experimental region are atmospheric (0.101 MPa) and fully gas-saturated. In all other regions, the pressure is hydrostatic relative to the pore pressure in MB139, which is sampled from a range of 12 to 13 MPa. These regions are assumed to be fully brine-saturated. So far, this is how previous PA calculations started at time zero; now they are starting at -50 yr. After 50 yr (i.e., at time zero when the disposal region is sealed), pressure in the waste is reset to atmospheric from the calculated value

2. Model Description

(in most realizations very slightly above atmospheric), and the brine saturation in the waste is set to its sampled value. Any brine in the waste in excess of the sampled saturation is ignored, simulating its disappearance by evaporation or pumping. In all other excavated regions, the brine saturation is set to 1.0, and the pressure is reset to atmospheric. (A hydrostatic gradient would be more accurate, but because of the high permeability of these regions, this is achieved very quickly and much more conveniently in the course of the calculations after time zero.) The permeability of each region is reset at this time. Excavated regions were originally given a very high permeability ($1.0 \times 10^{-10} \text{ m}^2$) and a porosity of 1.0 to simulate cavities. At time zero, these regions take on different characteristics, becoming seals or backfill, each with different permeabilities and porosities, as described in Section 3.

The DRZ receives special treatment. The porosity of the DRZ is assumed to increase at time zero from the porosity of intact halite to the porosity of the highly fractured disturbed zone. One of the more important objectives of this initial condition calculation is to account more accurately for mobile brine content of the DRZ. In previous PA calculations, the DRZ was assumed to be fully saturated at time zero, with a relatively large permeability. This allowed large quantities of brine to drain from the DRZ into the waste, providing much of the brine source for gas generation. The current initial condition calculation recognizes that much of this brine will have been removed during the disposal phase of the WIPP. Therefore, when the porosity of the DRZ increases at time zero, the brine volume is held constant, and the additional pore volume is filled with gas. The pressure in the DRZ, already very close to atmospheric, is set to atmospheric (0.101 MPa) to preclude any gas drive from being artificially created when the DRZ porosity is changed. Such a gas drive could force an immediate and unrealistic surge of remaining DRZ brine into the waste.

The calculations proceed from this calculated initial condition for the 10,000-yr performance period. The most important effect of these more realistic initial conditions is that less brine will flow into the excavated regions (including the waste), because the initial "surge" of brine that occurs upon excavation has been eliminated, and the pressure gradients in the immediate vicinity of excavations have been greatly reduced.

At time zero, waste is assumed to have some initial brine saturation that is available for waste degradation. This is a sampled parameter, ranging from 0.0 to 0.14. When it arrives at the WIPP, waste is expected to contain some small quantity of free liquid. For BRAGFLO simulations, this liquid is assumed to be Salado brine; its actual composition is unknown. The actual liquid content, or saturation, is also unknown. In 1991, the initial brine saturation was varied from 0.0 to 0.276. The maximum (0.276) is the assumed residual brine saturation of the waste (WIPP PA, 1991c). In the absence of real data, residual saturation was selected as the maximum liquid that the waste could contain and still comply with transportation regulations (U.S. DOE, 1991c) that prohibit transporting any waste that contains significant quantities of mobile liquids, i.e., liquids that can flow and, therefore, exceed residual saturation. In 1992, the maximum initial brine saturation was reduced to 0.14. This reduction was necessitated by numerical constraints imposed by the creep closure model that was implemented in 1992. Thus, the range of values over which the initial brine saturation is sampled (0.0 to 0.14) is somewhat arbitrary. However, the range does satisfy two other important criteria: (1) It includes values of initial brine saturation that are physically reasonable and possible. (2) It is sufficiently broad to enable sensitivity analyses to determine how initial brine saturation affects the performance of the WIPP.

2.5 Summary of Model Assumptions

Table 2-1 contains a list of important assumptions made in modeling for the sensitivity analyses reported in this volume. In general, the impact of these assumptions on disposal-system performance is difficult to quantify. Complexities of the coupled processes affecting two-phase flow preclude predictions about how the system will respond to specific changes in modeling assumptions. Assumptions that have a high potential to affect performance, such as the omission of pressure-dependent fracturing of anhydrite interbeds, will be investigated in future analyses as improvements are made in the PA modeling system.

Table 2-1. Partial List of Assumptions Used in the BRAGFLO Analyses of Undisturbed Performance Reported in Volume 5 of the 1992 WIPP PA

General Assumptions

Brine and gas flow obeys generalized Darcy's Law for compressible fluids in all media. Pore space is fully interconnected in all regions.

Dimensions of all regions are fixed and do not change with time.

All gas is assumed to have the physical properties of hydrogen.

All liquid is assumed to be Salado Formation brine.

Gas does not dissolve in brine.

Pressure-dependent fracturing of anhydrite interbeds does not occur.

Stratigraphy is simplified as shown in Section 2.1.

Initial conditions calculated by simulating a 50-yr operational period during which the repository remains open. Time t_0 for the 10,000 yr simulations is at the end of the operational phase, when the repository is sealed. Permeabilities, porosities, and saturations are adjusted at this time as described in Ch. 4 of Volume 4 of this report.

Permeabilities and porosities of selected regions are adjusted at 200 yr to reflect consolidation of the seal system (this volume only).

No hysteresis in capillary pressure curves.

Permeabilities and porosities sampled independently. (Sufficient data are not yet available to correlate permeability with porosity.)

No-flow boundaries everywhere except far-field Culebra, where pressure is specified.

Klinkenberg effect is ignored.

2. Model Description

1 Table 2-1. Partial List of Assumptions Used in the BRAGFLO Analyses of Undisturbed Performance
2 Reported in Volume 5 of the 1992 WIPP PA (Continued).

3 4 **Halite Assumptions**

5 Permeability specified, and constant in time.

6 Initial (pre-excavation) porosity specified; varies with pressure (because of compressibility);
7 unchanged at t_0 .

8 Initial brine saturation specified; unchanged at t_0 .

9 Initial pressures specified, vary with depth; pressures at t_0 are calculated.

10 Threshold capillary pressure a function of permeability; constant in time.

11 **Anhydrite Assumptions**

12 Permeability specified and constant in time.

13 Initial porosity specified as same as intact halite; varies with pressure (because of compressibility).

14 Initial saturation specified.

15 Initial pressure specified.

16 Threshold capillary pressure a function of permeability; constant in time.

17 MB138 not included in the DRZ above the repository.

18 **Disturbed Rock Zone (DRZ) Assumptions**

19 Includes what was originally intact halite between the repository and MB139 and anhydrite a + b;
20 also includes what was originally intact MB139 and anhydrite a + b directly above and below the
21 repository; also includes (for this volume only) one meter of what was originally intact halite below
22 MB139 beneath the repository.

23 Permeability specified and constant during operational phase; changes at t_0 and is constant
24 thereafter; the DRZ does not "heal."

25 Threshold capillary pressure is zero and constant in time.

1 Table 2-1. Partial List of Assumptions Used in the BRAGFLO Analyses of Undisturbed Performance
 2 Reported in Volume 5 of the 1992 WIPP PA (Continued).

3
 4 Initial porosity specified as same as intact halite; varies with pressure (because of compressibility);
 5 changes at t_0 .

6 Initial brine saturation specified, variation calculated during operational phase as brine flows in or
 7 out. At t_0 , brine volume is conserved when porosity changes; brine saturation changes and added
 8 pore volume is filled with gas.

9 Initial pressure same as that of intact halite at the same elevation; calculated during operational
 10 phase. Pressure set to atmospheric at t_0 .

11 Transition Zone Assumptions

12 Located in what was originally intact halite between anhydrite a+b and MB138 above the
 13 repository.

14 Permeability specified as same as that of anhydrite; constant in time.

15 Initial porosity specified as same as intact halite; varies with pressure (because of compressibility).

16 Initial saturation specified.

17 Initial pressure specified.

18 Threshold capillary pressure a function of permeability; constant in time.

19 Culebra Assumptions

20 Initial permeability zero; at t_0 , nonzero permeability specified, uniform, and constant in time.

21
 22 Initial porosity specified, varies with pressure (because of compressibility).

23 Initial saturation specified.

24 Initial pressure specified, not in hydrostatic equilibrium with underlying halite; far-field pressure
 25 constant.

26
 27 Threshold capillary pressure a function of permeability; constant in time.

28
 29

2. Model Description

1 Table 2-1. Partial List of Assumptions Used in the BRAGFLO Analyses of Undisturbed Performance
2 Reported in Volume 5 of the 1992 WIPP PA (Concluded).

3 4 **Waste/Disposal Region Assumptions**

5
6 Initially treated as an empty cavity; very high permeability, porosity equals 1.0 and is constant in
7 time; threshold capillary pressure zero and constant in time; pressure is atmospheric; no gas
8 generation.

9 At t_0 , waste and all panel seals are emplaced simultaneously, and all properties change.

10 Permeability specified, constant in time, independent of porosity.

11 Threshold capillary pressure zero and constant in time.

12 Pressure at t_0 is atmospheric, calculated for later times.

13 Brine content at end of operational phase is discarded (assumed to be removed by ventilation);
14 brine saturation at t_0 is saturation of the newly emplaced waste.

15 Gas-generation rate is dependent on degree of brine saturation, ranging from humid rate to
16 inundated rate; rate is zero if brine saturation is zero. If brine is present, gas continues to be
17 generated until all corrodible and biodegradable material is consumed. No functional dependence
18 of rate on pressure or chemistry. Corrosion consumes water. Biodegradation requires the
19 presence of water. Mineral precipitation is ignored.

20 Dynamic creep closure as a function of pressure in waste results in large porosity changes from
21 the initial specified porosity; porosity changes only as pressure increases, and varies slightly
22 (because of compressibility) if pressure decreases. Dimensions of the modeled waste-disposal
23 region remain constant in time regardless of porosity.

24

25

3. UNCERTAIN VARIABLES USED IN SIMULATIONS OF UNDISTURBED PERFORMANCE

Previous volumes of the 1992 WIPP performance assessment selected 49 imprecisely known variables for consideration (see Table 3-1 of Volume 4 of this report). Nineteen of these parameters are used in simulations of gas and brine migration for undisturbed performance, either directly or to derive the parameters used as BRAGFLO input. Sampled values for these 19 parameters are unchanged in this volume from those used in other analyses in the 1992 PA and are as reported in Appendix C of Volume 4. Six additional parameters related specifically to the performance of the shaft-seal system have been included in sampling for this volume. Values for these parameters are provided in Appendix B of this report, together with values of parameters derived from sampled variables and used directly in BRAGFLO.

Table 3-1 identifies the 25 variables sampled for these analyses, and provides information about ranges, distributions, and sources of additional information for each. The nineteen variables unchanged from earlier volumes are listed first, and are followed by the six additional variables added for these analyses.

Table 3-1. Variables Sampled in 1992 WIPP Performance Assessment^a

Variable	Definition
BCBRSAT	Residual brine saturation for Salado Formation (S_{lr}) (dimensionless). Range: 0.0 to 0.4. Median: 0.2. Distribution: Uniform. Additional information: Section 2.3.1, Volume 3. Variable 13 in Latin hypercube sample (LHS).
BCEXP	Brooks-Corey pore-size distribution parameter for Salado Formation (λ) (dimensionless). Range: 0.2 to 10. Median: 0.7. Distribution: Piecewise uniform. Additional information: Same as BCBRSAT. Variable 11 in LHS.
BCFLG	Pointer variable (flag) for selection of characteristic curve sub-model. Range: 0 or 1. Distribution: 33% 0, 67% 1. Value of 0 selects Van Genuchten/Parker Model; value of 1 selects Brooks-Corey model. Additional information: Section 2.3.1, Volume 3. Variable 12 in LHS.
BCGSSAT	Brooks-Corey residual gas saturation for Salado Formation (S_{gr}) (dimensionless). Range: 0.0 to 0.4. Median: 0.2. Distribution: Uniform. Additional information: Same as BCBRSAT. Variable 14 in LHS.

3. Uncertain Variables

Table 3-1. Variables Sampled in 1992 WIPP Performance Assessment (Continued)

Variable	Definition
BRSAT	Initial liquid (brine) saturation of waste (dimensionless). Range: 0 to 0.14. Median: 0.07. Distribution: Uniform. Additional information: Section 3.4.3, Volume 3. Variable 1 in LHS.
CULPOR	Matrix porosity (Θ_m) in Culebra (dimensionless). Range: 5.8×10^{-2} to 2.53×10^{-1} . Median: 1.39×10^{-1} . Distribution: Piecewise uniform. Additional information: Table 4.4, Kelley and Saulnier, 1990; Table E-8, Lappin et al., 1989; Section 2.6.2, Volume 3. Variable 43 in LHS.
GRCORHF	Scale factor used in definition of gas generation rate for corrosion of steel under humid conditions (dimensionless). Actual gas generation rate is $GRCORH = GRCORHF \cdot GRCORI$. Range: 0 to 0.5. Median: 0.1. Distribution: Piecewise uniform. Additional information: Memo from Brush, July 8, 1991, contained in Appendix A, WIPP PA Division, 1991c; Section 3.3.5, Volume 3. Variable 3 in LHS.
GRCORI	Gas generation rate for corrosion of steel under inundated conditions ($\text{mol}/\text{m}^2 \cdot \text{s}$ surface area steels). Range: 0 to 1.3×10^{-8} . Median: 6.3×10^{-9} . Distribution: Piecewise uniform. Additional information: Same as GRCORHF. Variable 2 in LHS.
GRMICHF	Scale factor used in definition of gas generation rate due to microbial degradation of cellulose under humid conditions ($\text{mol}/\text{kg} \cdot \text{s}$ cellulose). Actual gas generation rate is $GRMICH = GRMICHF \cdot GRMICI$. Range: 0 to 0.2. Median: 0.1. Distribution: Uniform. Additional information: Same as GRCORHF. Variable 6 in LHS.
GRMICI	Gas generation rate due to microbial degradation of cellulose under inundated conditions ($\text{mol}/\text{kg} \cdot \text{s}$ cellulose). Range: 0 to 1.6×10^{-8} . Median: 3.2×10^{-9} . Distribution: Piecewise uniform. Additional information: Same as GRCORHF. Variable 5 in LHS.
MBPERM	Permeability (k) in intact anhydrite marker beds in Salado Formation (m^2). Range: 1×10^{-21} to 1×10^{-16} . Median: 5.0×10^{-20} . Distribution: Piecewise loguniform. Correlation: 0.3 rank correlation with SALPERM. Additional information: Section 2.4.2, Volume 3. Variable 15 in LHS.
MBPOR	Porosity (ϕ) in intact anhydrite marker beds in Salado Formation (dimensionless). Range: 1×10^{-3} to 3×10^{-2} . Median 1×10^{-2} . Distribution: Piecewise uniform. Additional information: Section 2.4.4, Volume 3. Variable 16 in LHS.

Table 3-1. Variables Sampled in 1992 WIPP Performance Assessment (Continued)

Variable	Definition
MBPRES	Far Field Pressure (p) in Salado formation at the MB139 elevation. Range: 1.2×10^7 to 1.3×10^7 . Median: 1.25×10^7 . Distribution: Uniform. Additional information: Section 2.4.3, Volume 3. Variable 18 in LHS.
SALPERM	Permeability (k) in intact halite component of Salado Formation (m^2). Range: 1×10^{-24} to 1×10^{-19} . Median: 2×10^{-21} . Distribution: Piecewise loguniform. Correlation: 0.3 rank correlation with MBPERM. Additional information: Memo from Gorham et al., June 15, 1992, contained in Appendix A, Volume 3; Howarth et al., 1991; Beauheim et al., 1991; Section 2.3.5, Volume 3. Variable 10 in LHS.
STOICCOR	Stoichiometric coefficient for corrosion of steel (dimensionless). Defines proportion of two different chemical reactions taking place during the corrosion process. Range: 0 to 1. Median: 0.5. Distribution: Uniform. Additional information: Brush and Anderson in Lappin et al., 1989, p. A-6; Section 3.3.5, Volume 3. Variable 4 in LHS.
STOICMIC	Stoichiometric coefficient for microbial degradation of cellulosics (mol gas/mol CH_2O). Range: 0 to 1.67. Median: 0.835. Distribution: Uniform. Additional information: Brush and Anderson in Lappin et al., 1989, p. A-10; Section 3.3.5, Volume 3. Variable 7 in LHS.
TZPORF	Scale factor used in definition of transition zone and disturbed rock zone porosity (ϕ_z), with the transition zone and disturbed rock zone porosity defined by $TZPOR = SALPOR + (0.06 - SALPOR) \cdot TZPORF$. Range 0 to 1. Median: 0.5. Distribution: Uniform. Additional information: Section 2.4.4, Volume 3. Variable 17 in LHS.
VMETAL	Fraction of total waste volume that is occupied by IDB (Integrated Data Base) metals and glass waste category (dimensionless). Range: 0.276 to 0.476. Median: 0.376. Distribution: Normal. Additional information: Section 3.4.1, Volume 3. Variable 9 in LHS.
WWOOD	Fraction of total waste volume that is occupied by IDB combustible waste category (dimensionless). Range: 0.285 to 0.484. Median: 0.384. Distribution: Normal. Additional information: Section 3.4.1, Volume 3. Variable 8 in LHS.

3. Uncertain Variables

The following variables were sampled for the undisturbed calculations reported in this volume only, and were not used in the calculations reported in Volume 4. Sampled values for these variables are given in Appendix B of this volume.

Table 3-1. Variables Sampled in 1992 WIPP Performance Assessment (Concluded)

Variable	Definition
BKFLPOR	Porosity of backfill materials in drifts and experimental region and in the shaft below the shaft seal (dimensionless). Range: 0.01 to 0.075. Median: 0.0425. Distribution: Uniform. Additional information: Memorandum by Finley and Vaughn, Appendix A of this volume. Variable 26 in LHS for the Volume 5 calculations
DSEALPRM	Permeability of panel and drift seals (m^2). Range: 1.0×10^{-21} to 1.0×10^{-18} . Also used to define porosity for panel and drift seals (see Appendix B of this volume for definition of relationship). Distribution: lognormal. Additional information: Same as BKFLPOR. Variable 25 in LHS for the Volume 5 calculations.
SEALPRM1	Permeability of the shaft for the time period from 0 to 200 yr (m^2). Range: 1.0×10^{-19} to 5.0×10^{-16} . Median: 7.0×10^{-18} . Distribution: lognormal. Additional information: Same as BKFLPOR. Variable 22 in LHS for the Volume 5 calculations.
SEALPRM2	Permeability of the shaft seal and shaft-fill material within the Salado Formation for the time period from 200 to 10,000 yr (m^2). Range: 1.0×10^{-21} to 1.0×10^{-18} . Median: 3.2×10^{-20} . Distribution: lognormal. Also used to define porosity for the shaft seal and shaft-fill material (see Appendix B of this volume for relationship). Additional information: Same as BKFLPOR. Variable 23 in LHS for the Volume 5 calculations.
SHFTPRM	Permeability of the shaft-fill material within the Salado Formation for the period from 0 to 200 yr (m^2). Range: 1.0×10^{-19} to 1.0×10^{-15} . Median: 1.0×10^{-17} . Distribution: lognormal. Additional information: Same as BKFLPOR. Variable 24 in LHS for the Volume 5 calculations.
SEALTHK	Thickness of the shaft seal within the Salado Formation, as modeled (m). Range: 30 to 100. Median: 65. Distribution: Uniform. Additional information: Same as BKFLPOR. Variable 21 in LHS for the Volume 5 calculations.

^a Adapted from Table 3-1 of Volume 4 and Tables 6.0-1, 6.0-2, and 6.0-3 of Volume 3 of this report.

4. GAS AND BRINE MIGRATION

In this chapter, results are discussed for three cases. In the first, the base case, the shaft is modeled as a composite of the four existing shafts. The second case considers a single shaft instead of combining all four shafts into one, but is otherwise identical to the base case. In the third case, the base case is repeated but without dynamic creep closure; instead, the porosity of the repository is fixed at the median final-state porosity of 19%. This is the best current estimate for the repository-wide average porosity of waste compacted to lithostatic pressure (14.8 MPa) (Butcher, 1990).

In all three cases, the behavior of the repository and the responses of the surrounding strata to changes in the repository is largely determined by the initial brine saturation in the waste. If gas generation is relatively low, primarily as a result of low initial brine content in the waste, the pressure in the repository rises slowly as brine from the far field flows in to equilibrate repository pressure with the far field. Under these conditions, the direction of flow is mostly in toward the repository, and the repository behaves simply as a brine sink. A more common response (in 70% of the realizations) is for gas to be generated sufficiently rapidly so that the pressure in the repository builds quickly, exceeding the far-field pore pressure. In about half of the realizations, the disposal-region pressure exceeds lithostatic pressure. In these cases, brine and gas are driven away from the repository out the most permeable pathways: the three anhydrite layers, and the sealed and backfilled shaft. Despite the high pressures reached in the repository, cumulative brine flow outward through the anhydrite layers is never enough to reach the disposal-unit boundary. Brine flows up the sealed shaft are also small and do not reach the Culebra. Cumulative gas flow out the anhydrite layers is sufficient in 6 of the 70 realizations for gas to flow beyond the disposal-unit boundary. Gas reaches the Culebra in 12 of the 70 realizations.

Results for the single-shaft case differ little from the base case. Cumulative brine flows up the shaft are lower than in the base case in proportion to the cross sectional area of the shaft. Cumulative gas flows into the Culebra are also proportionately lower. Flows of brine and gas out the anhydrite layers are indistinguishable from those of the base case.

Results for the fixed-porosity case differ from the base case primarily in the pressures obtained in the repository. Peak pressures are considerably higher, reaching 39 MPa versus 24 MPa in the base case. However, in the absence of a model for pressure-dependent fracturing of anhydrite interbeds, the higher repository pressures have essentially no effect on the other performance measures examined. Brine and gas flows out the anhydrite layers and up the shaft are unaffected by the use of a fixed repository porosity instead of a time-varying porosity. This conclusion may change in future performance assessments when pressure-dependent fracturing is included in simulations.

4.1 Four-Shaft Equivalent Geometry

Repository behavior is largely dictated by the amount of water initially present in the waste. Pressure in the repository initially increases, either rapidly, as a result of gas generation, or slowly, while gradually equilibrating with far-field pressure if the gas generation rate is low. Peak pressures range from 5.8 to 23.8 MPa. Brine saturation in the waste rises steeply during the first 100-300 yr as creep closure reduces the pore volume of the waste more rapidly than corrosion consumes brine. After peaking at about 300 yr, the brine saturation generally

4. Gas and Brine Migration

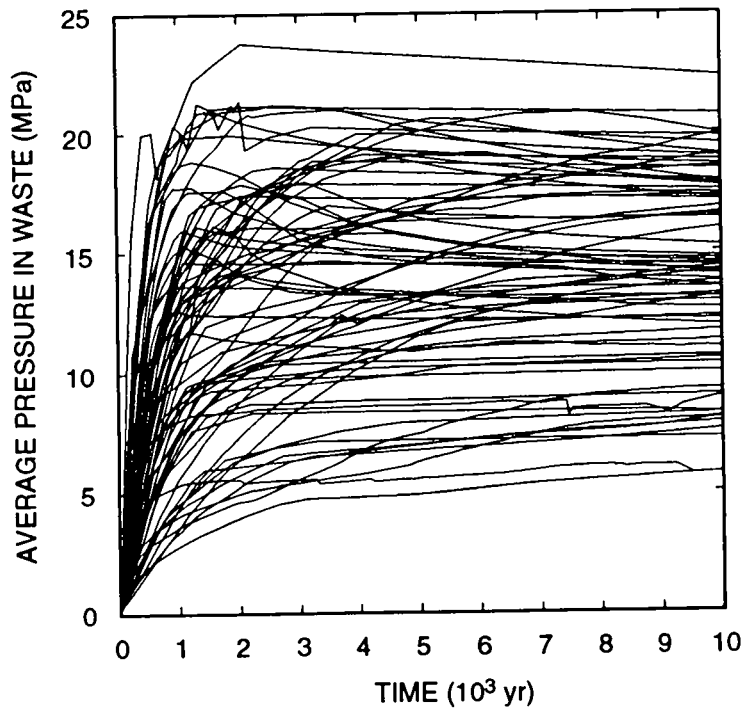
1 decreases continuously during the remainder of the 10,000 yr (unless the initial brine saturation and the corrosion
2 rate are both very low) because corrosion consumes brine faster than it flows into the repository from the far field.
3 Because sufficient brine is not available, the initial iron inventory of the repository is usually not fully consumed
4 within 10,000 yr. The opposite is true for cellulose. As a result of its lower initial inventory and higher reaction
5 rate, cellulose generally is fully consumed fairly early (within the first 3000 yr), when sufficient brine is still
6 available for biodegradation to take place. Although the amount of brine that flows into the repository is usually
7 greater than the amount that flows out, brine inflow has little effect on gas generation because it tends to accumulate
8 in regions of the repository that are depleted of reactants. Thus, the initial brine content of the waste has a far
9 greater impact than brine inflow on how much gas is generated.

10 Cumulative brine flow out the high-permeability pathways — the three anhydrite layers and the shaft —
11 impacts directly on regulatory compliance. In none of the realizations did sufficient brine flow out any of these
12 pathways to reach the disposal-unit boundary. Because transport was not modeled, the analysis is based on
13 quantities of brine flow relative to pathway pore volumes and residual saturations. As expected, the largest volumes
14 of brine flow out MB139. None flows out anhydrite a + b. Although enough brine flowed out MB138 to warrant
15 some concern, it is not clear that the brine there could originate in the waste; it is possible that brine in MB138, as
16 currently modeled, is not contaminated, but instead originates in MB138 or the transition zone above the repository.
17 Small amounts of brine flowed upward through the shaft seal, but not enough to fill the rest of the lower shaft
18 between the seal and the Culebra. Although almost no brine flows *through* the drift seals, it bypasses the drift seals
19 by flowing through the DRZ above and below the seals.

20 Sufficient quantities of gas are produced in 6 of the 70 realizations for gas to flow beyond the disposal-unit
21 boundary. The largest amounts of gas flow out MB139, even though this pathway is also the main conduit for brine
22 flow. Smaller quantities flow out anhydrite a + b and MB138; in the six realizations having flow past the disposal-
23 unit boundary, such flow occurs in all three anhydrite layers. Gas also flows up the shaft into the Culebra in the
24 same six realizations. The panel and drift seals were not completely effective in stopping gas flow: less than 0.01%
25 of the total gas flow from the waste entered the panel and drift seals.

26 4.1.1 Repository Behavior

27 Pressures in the waste (Figure 4-1) increase for at least the first 1000 yr in all realizations. In all cases, the
28 pressures start at atmospheric (0.101 MPa). Some of the increase in pressure results from brine inflow from the far
29 field, and some small component from the reduction of void volume by creep closure. Most of the increase,
30 particularly in those realizations in which pressure rises above the far-field pore pressure (12 to 13 MPa), is caused
31 by gas generation by corrosion and biodegradation of the waste. After 10,000 yr, pressures range from 5.8 to 22.3
32 MPa; peak pressures range from 5.8 to 23.8 MPa. Two general types of behavior can be observed. In about two-
33 thirds of the cases, the pressure profile peaks in less than 10,000 yr, often fairly early — between 1000 and 3000 yr.
34 In these instances, gas is generated faster than pressure can be relieved by fluids flowing out of the anhydrite layers
35 or up the sealed shaft. Eventually, either reactants are fully consumed or brine is no longer available for corrosion,
36 and gas generation stops or slows greatly. From that time on, pressures in the waste gradually equilibrate with the
37 far-field pressures. If the pressure has exceeded the far-field pressure at the elevation of the repository, then the
38 pressure will drop.



TRI-6342-2704-0

Figure 4-1. Volume Average Pressure in the Waste Repository.

4. Gas and Brine Migration

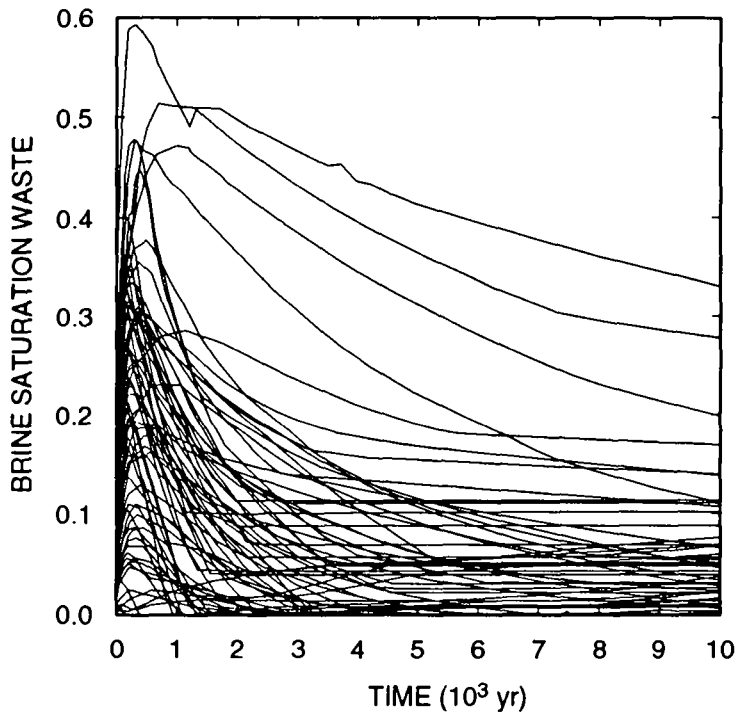
1 Otherwise, the pressure will continue to rise. This is seen in about one-third of the runs, where the pressure has not
2 yet reached the far-field pressure within 10,000 yr, and is increasing so slowly that it may never exceed the far-field
3 pressure. Lithostatic pressure is exceeded in about half of the realizations. Until fracturing of the anhydrite layers is
4 included in the model (planned for 1993), these high repository pressures will always be obtained in some of the
5 realizations.

6 Pressures in the waste can also increase as a result of creep closure reducing the pore volume. In the current
7 implementation of creep closure, it is difficult to determine how much creep closure contributes to pressure
8 increases in the presence of other phenomena. This will be discussed further in Section 4.3. In order for creep
9 closure to have a significant effect, pressures in the waste must first increase independently of creep closure, as a
10 result of either gas generation or influx of fluid from outside the repository.

11 There are a few realizations in which the pressure fluctuates. This generally results when gas generation rates
12 vary rapidly. For example, in the realization producing the highest pressures (see Figure 4-1), the pressure peaks
13 very early at 20 MPa, drops briefly, then rises again to peak at 23.8 MPa. In this case, biodegradation is very rapid,
14 causing pressures to rise rapidly. But when the biodegradable inventory is fully consumed (in about 600 yr), gas
15 generation slows dramatically, resulting in a rapid drop in pressure as gas continues to migrate into the far field.
16 Eventually, gas generation from corrosion brings the pressures back up to the higher peak, when all corrodible
17 materials are finally consumed.

18 Brine saturation in the waste also generally increases initially (Figure 4-2), peaking quite early — within a few
19 hundred years after the repository is sealed. The saturation increase is a direct result of the rapid creep closure
20 during these early times and results in a sharp decrease in pore volume in the waste (Figure 4-3). Although
21 corrosion consumes brine during this time period, which causes the brine volume in the waste to drop (Figure 4-4),
22 the decrease in pore volume is more rapid than the decrease in brine volume. Consequently, brine saturation
23 undergoes a rapid increase initially. Once the repository has crept shut about as far as it can in the current creep
24 closure implementation, brine consumption causes the brine saturation to decrease. Generally, the rate of decrease
25 in brine saturation is quite rapid, dropping to less than 20% of its peak value within 2000 yr. In most cases, once
26 brine saturation begins to decrease, it never rises again during the remainder of the 10,000 yr. Only in a few
27 realizations in which the brine saturation is always quite low (less than 0.05) does the saturation increase after 1000
28 yr. In these cases, the pressure in the repository remains fairly low, typically below hydrostatic (about 7 MPa),
29 because little gas has been generated, and some brine is still able to flow in from outside the repository. However,
30 in most cases, the rate of brine flow in from the far field is quite low as a result of low interbed permeabilities and
31 pressures within the repository that are comparable to the far-field pressures. Any brine that does flow into the
32 repository is usually consumed by corrosion as quickly as it flows in. Thus, there is generally no increase in brine
33 saturation after about 1000 yr.

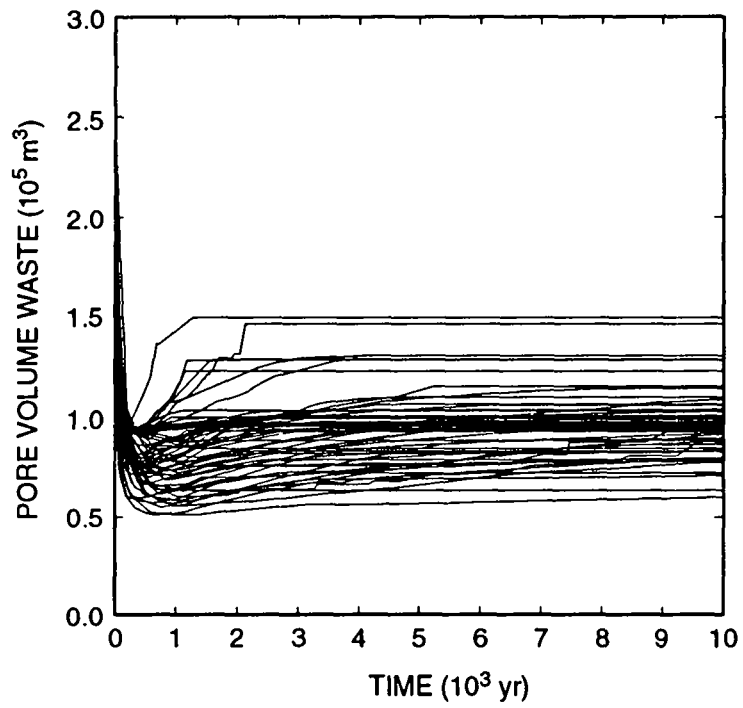
34 The two reactants, iron and cellulose, differ markedly in their time-dependent behavior (Figures 4-5 and 4-6,
35 respectively). In 18 of the 70 realizations, all of the iron is consumed. The initial corrosion rate is generally the
36 highest rate; however, the initial brine content is consumed in most of the realizations, and, given the generally low
37 flow of brine into the waste, much iron is often unreacted after 10,000 yr. In contrast, cellulose is fully consumed in
38 52 of the 70 realizations. This stems from the lower initial content and higher reaction rate for cellulose compared
39 with iron. The median value for the initial mass of cellulose is about 17% that of iron. The median biodegradation



TRI-6342-2705-0

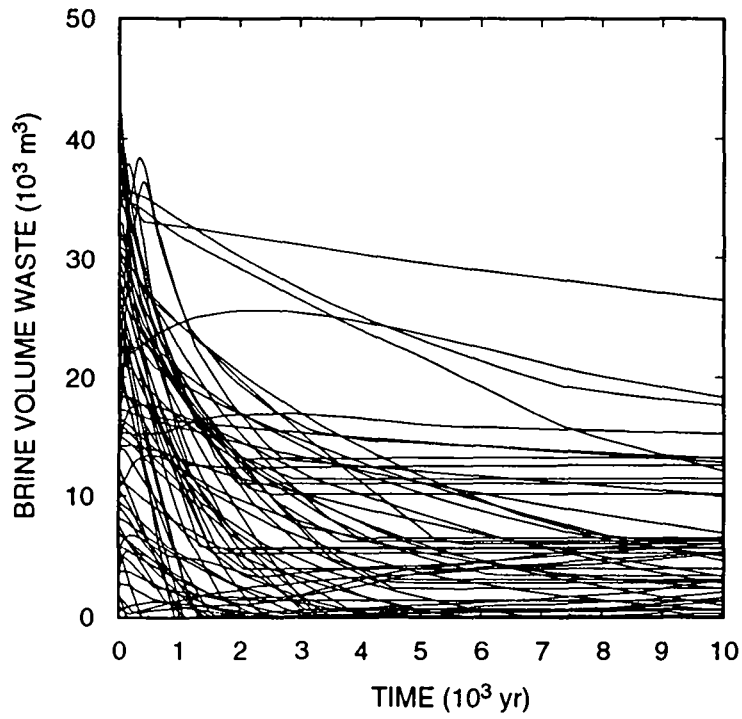
Figure 4-2. Volume Average Brine Saturation in the Waste Repository.

4. Gas and Brine Migration



TRI-6342-2706-0

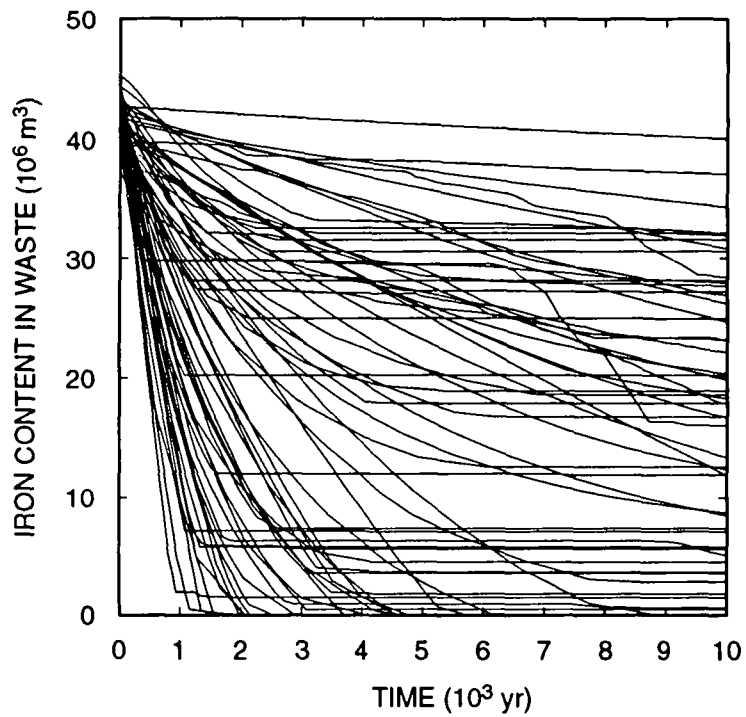
Figure 4-3. Pore Volume in the Waste Repository.



TRI-6342-2707-0

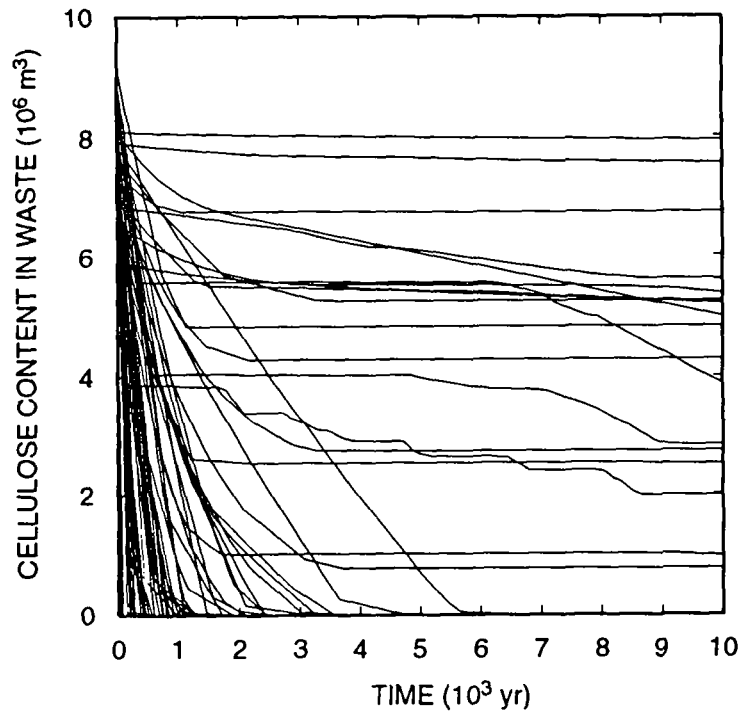
Figure 4-4. Brine Volume in the Waste Repository.

4. Gas and Brine Migration



TRI-6342-2708-0

Figure 4-5. Iron Remaining in the Waste Repository.



TRI-6342-2709-0

Figure 4-6. Cellulose Remaining in the Waste Repository.

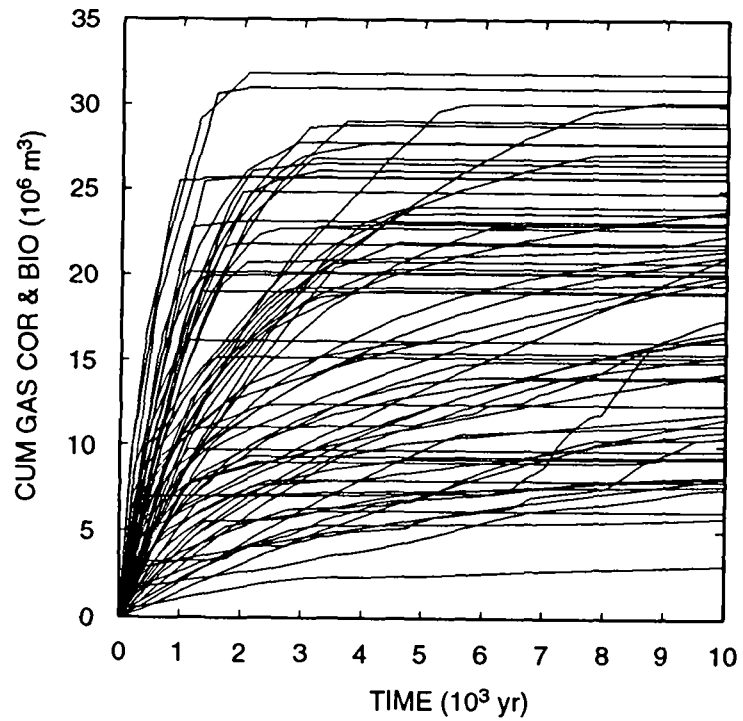
4. Gas and Brine Migration

1 rate among the 70 realizations is about 6 times higher than the median corrosion rate on a mass basis under
2 inundated conditions. Thus, cellulose is expected to be fully consumed in approximately 1/40th of the time required
3 for corrosion, at their full rates. Because of the smaller initial content and higher rate, biodegradation is not
4 inhibited by lack of brine as much as corrosion because it is largely completed while brine is still present in the
5 waste, whereas, brine is depleted in the waste long before corrosion is completed. (Note that although
6 biodegradation is currently assumed not to consume water, there still must be water present in order for
7 biodegradation to occur. Corrosion, as currently modeled, consumes water, so water must also be present for
8 corrosion to take place. These statements are true for both the inundated reactions and the humid reactions. See
9 Sections 1.4.1 and 3.3 of Volume 3 of this report for additional discussions of the gas-generation model.)
10 Averaging over the 70 realizations, 32% of the total initial iron content of the waste remains unreacted after 10,000
11 yr, whereas, only 16% of the total initial biodegradable content remains at that time.

12 The amount of gas generated, Figure 4-7, ranges from 3.0×10^6 to 3.2×10^7 m³ (at reference conditions: 30 °C
13 and 0.101 MPa). This corresponds to 1.3×10^8 to 1.3×10^9 mol H₂ total, or nominally 160 to 1600 mol/drum
14 (based on 6804 drums/room, as modeled). The full potential as currently modeled is 2.0×10^7 to 3.5×10^7 m³ (at
15 reference conditions), or equivalently 8.1×10^8 to 1.4×10^9 mol H₂ total, or 1000 to 1770 mol/drum. Because so
16 much iron remains after 10,000 yr, the average cumulative gas generated (1.8×10^7 m³) is relatively low, only 70
17 percent of the average potential (2.6×10^7 m³).

18 Total brine consumed by corrosion, Figure 4-8, ranges from 1600 to 29,600 m³; compared with the total brine
19 required to complete corrosion, 19,700 to 32,200 m³. In 45 realizations (or 64%), sufficient brine is available in the
20 waste initially to corrode all the iron in the waste without any brine flowing in from outside the waste. However,
21 only in 18 of the realizations (or 26%) was all of the iron fully consumed. In the other 27 realizations, the corrosion
22 rate was too low to consume all of the iron within 10,000 yr, even though enough brine was always available.

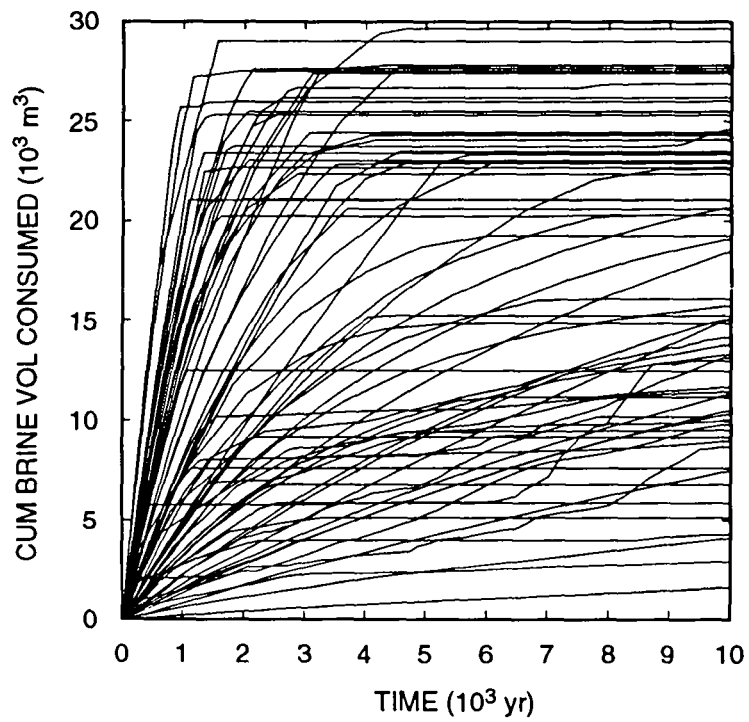
23 As shown in Figure 4-9, there were more realizations (39) in which the net brine flow was *into* the waste, rather
24 than *from* the waste (19), and in 12 of the 70 realizations, there was no brine flow either into or out of the waste.
25 The maximum brine outflow was 11,400 m³. In some realizations, the net cumulative flow of brine was inward
26 because of an early surge of inflowing brine, but there was still a substantial amount of brine outflow. However,
27 even in the most extreme case (the second curve from the bottom in Figure 4-9), only about 7100 m³ of brine
28 flowed back out after having flowed into the waste. It is interesting that in the ten realizations with the highest
29 inflow of brine, none had all the iron fully corroded. This suggests that brine inflow has only a marginal impact, at
30 best, on corrosion, and that corrosion rate is a more important factor influencing corrosion and gas generation,
31 rather than the availability of brine. In contrast, those realizations with the highest brine inflow generally had
32 among the lowest initial brine present in the waste, so, whereas brine inflow may not be important, initial brine
33 content is. Brine inflow has little effect on corrosion because it tends to flow in just at the edges of the repository
34 and then pool in the bottom of the repository. Iron may be largely consumed there, but not enough brine flows in to
35 fill the repository to the top, so iron remains relatively unreacted in the upper portion of the repository.



TRI-6342-2710-0

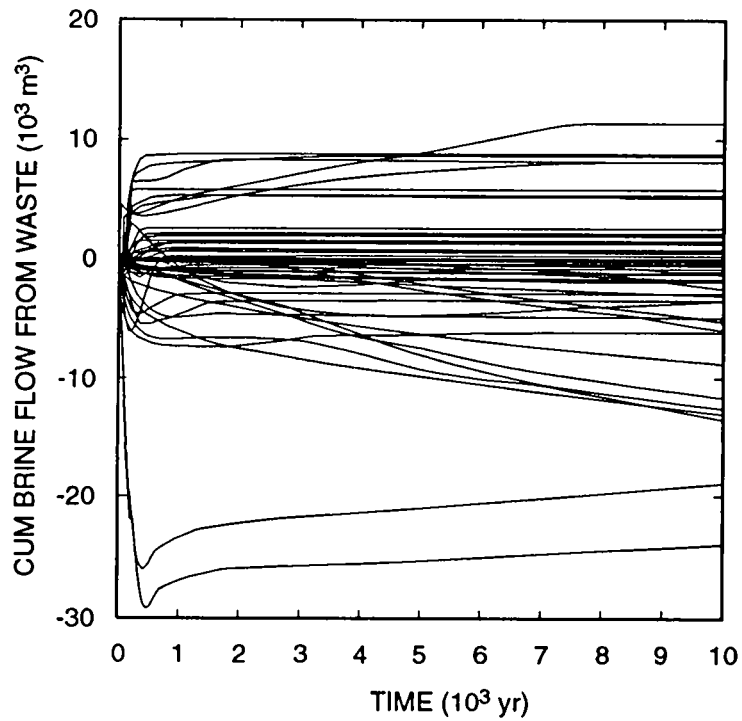
Figure 4-7. Cumulative Gas Volume Generated (at 30 °C; 0.101 MPa).

4. Gas and Brine Migration



TRI-6342-2711-0

Figure 4-8. Cumulative Brine Volume Consumed.



TRI-6342-2712-0

Figure 4-9. Cumulative Brine Flow from the Waste Repository. (Positive values indicate flow OUT from the repository.)

4. Gas and Brine Migration

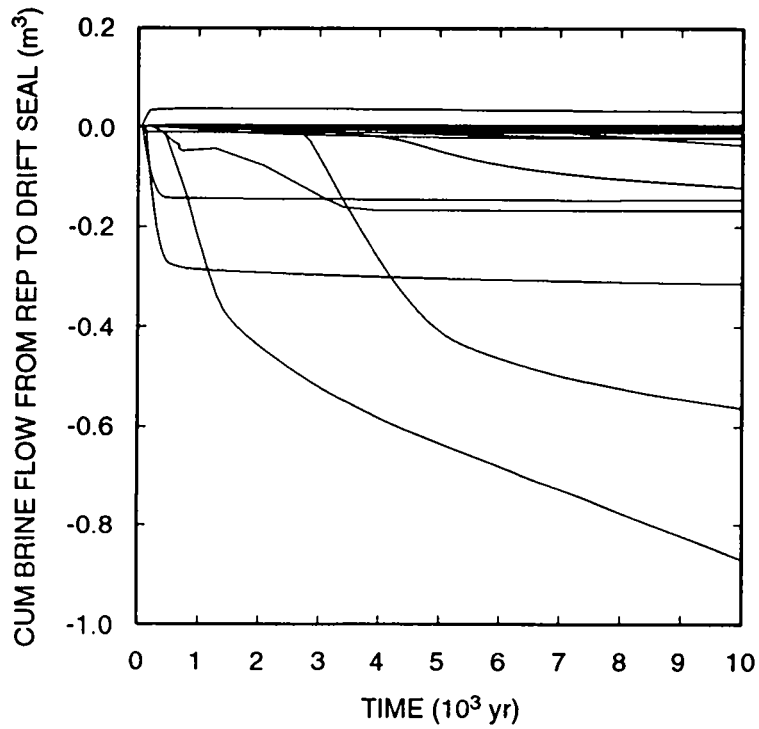
4.1.2 Brine Flow Behavior

A key question for PA to answer is: Where does contaminated brine flow to? Because the presence of brine in the waste results in gas generation, it is also desirable to know where brine comes from, specifically, what are the flow paths taken by brine near the WIPP site over the thousands of years following the sealing of the repository. As discussed above, as much as 11,400 m³ of brine flowed out of the waste. This brine is presumably contaminated with radioactive isotopes and hazardous constituents. Although the model used does not simulate transport, the extent and directions of contaminated brine flow can be estimated, in addition to the sources of brine that flows into the waste. Figure 4-10 shows that almost no brine flowed through the drift seals. The maximum cumulative flow of contaminated brine from the waste into the seals was 0.03 m³. In most realizations, brine flowed from the seals into the waste, but the maximum was still only 0.9 m³. The bulk of flow into or out of the waste was through the DRZ. The drift seals, as currently modeled, are very effective in blocking brine flow from the waste through the seals, but they do not prevent fluids from bypassing the seals by way of the DRZ.

Fluids do not migrate significant distances in the low-permeability halite, and to get to the disposal-unit boundary, contaminated brine must flow through one of the permeable units: the anhydrite layers (Marker Beds 138 or 139 or the combined anhydrite "a" and "b" layer), or up the sealed shaft. As described below, the results of the BRAGFLO simulations show that no contaminated brine would have reached the unit boundaries. This conclusion is based on examinations of the quantities of brine and gas that flowed into various regions, rather than on actual transport calculations because those calculations were not performed.

For these model results, it can safely be stated that no contaminated brine reached the Culebra upward through the shaft seal system. As Figure 4-11 shows, in most realizations, brine flowed downward through the modeled shaft seal, not upward, and did not provide a potential transport medium away from the waste. In seven realizations there was a positive net upward flow of brine, and the maximum flow was only 25 m³. In addition, there were several realizations in which brine flowed downward initially but flowed upward later. To be conservative, it must be assumed that all of this upward-flowing brine is contaminated, although this may not be true. In the worst cases, approximately 40 m³ of brine flows upward (even though in one of those realizations the *net* cumulative flow was 30 m³ downward). However, Figure 4-12 shows that the minimum brine volume in the lower shaft (above the shaft seal but below the Culebra seal) is 370 m³. This figure also shows that the brine volume in the lower shaft is nearly constant in most cases even though that portion of the shaft is never fully saturated with brine after 200 yr, so brine in the lower shaft is never completely displaced by the small amount of brine flowing up through the seal. Therefore, 40 m³ of brine flowing through the shaft seal would flow only about 1/10th of the distance from the seal to the Culebra, never actually reaching the Culebra. In fact, when individual realizations are examined, the quantity of brine that flows through the shaft seal never amounts to more than 1.7% of the brine volume in the lower shaft. (In Figure 4-12, the small drop in brine volume that occurs in every realization at 200 yr results from the change in porosity in the Culebra seal at that time, as described in the memorandum by Finley and Vaughn in Appendix A of this volume.)

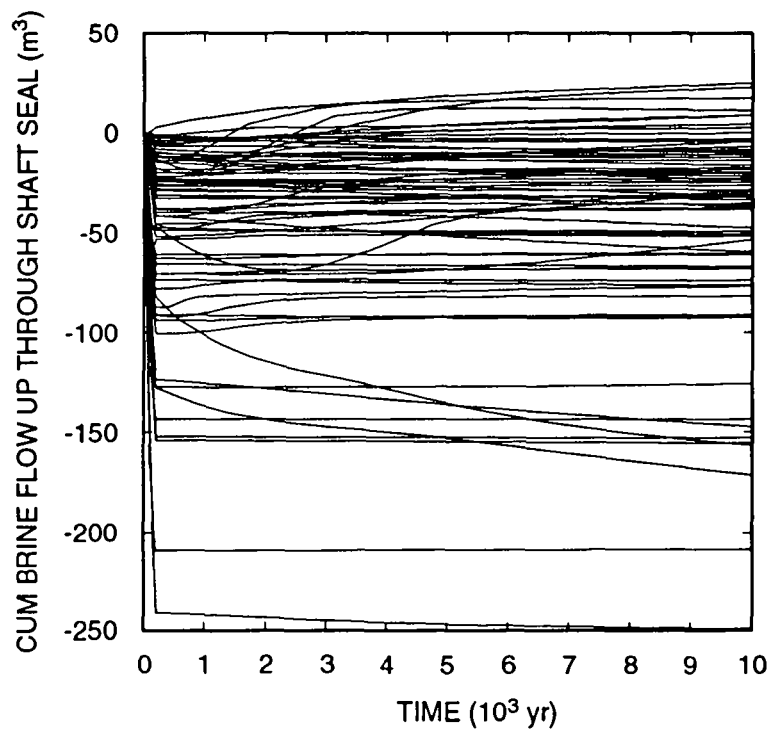
Before considering the other flow paths — the three anhydrite layers — it must be pointed out that the fundamental assumption of plug flow in a porous medium requires that any outward flow of contaminated brine from the waste must displace all the brine-saturated pore volume in a grid block before it can move to the next grid block. Because of the quasi-cylindrical geometry used in the mesh, the volume of grid blocks increases greatly as one moves outward from the repository (see Section 2.3). Table 4-1 lists the cumulative grid block volumes in each anhydrite layer for the mesh used in these calculations, along with the distance from the repository to the outer edge



TRI-6342-2713-0

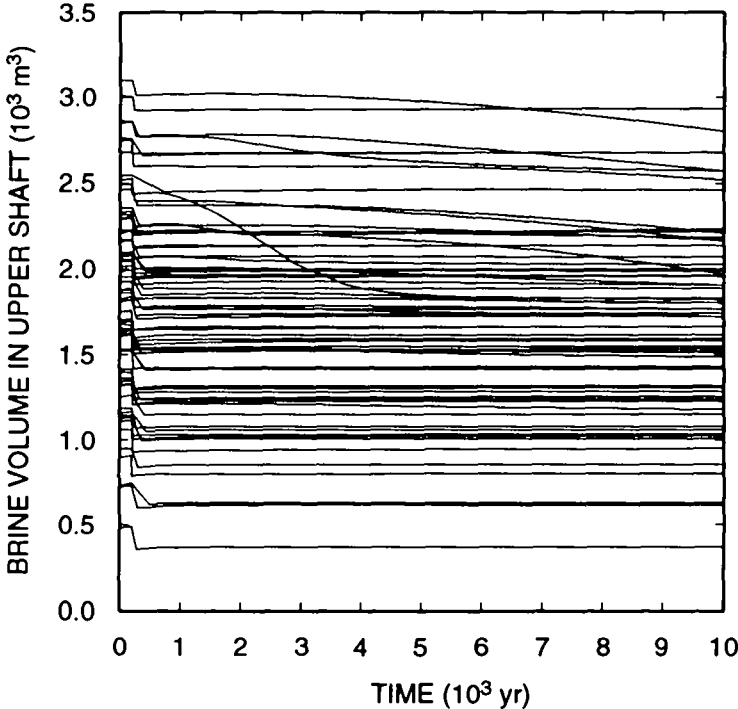
Figure 4-10. Cumulative Brine Flow from the Repository to the Drift Seals. (Positive values indicate flow OUT from the repository, into the drift seals.)

4. Gas and Brine Migration



TRI-6342-2714-0

Figure 4-11. Cumulative Upward Brine Flow through Shaft Seal. (Positive values indicate upward flow.)



TRI-6342-2715-0

Figure 4-12. Brine Volume in Lower Shaft.

4. Gas and Brine Migration

Table 4-1. Cumulative Volumes in Anhydrite Layers in BRAGFLO Mesh (South of Repository) (see Figure 2-1)

Cell No.	Distance (m)	Volume (m ³)		
		Layer 7 MB138	Layer 9 Anhydrite a + b	Layer 16 MB139
8	1	347	521	1,640
7	6	2,110	3,160	9,950
6	26	9,500	14,300	44,900
5	126	55,100	82,700	260,000
4	626	387,000	580,000	1,830,000
3	2,500	3,230,000	4,840,000	15,200,000
2	7,500	23,200,000	34,800,000	109,000,000
1	22,500	191,000,000	287,000,000	902,000,000

of the grid block. Table 4-2 lists initial pore volumes in the same grid blocks. This is the actual volume of brine that must be displaced by contaminated brine and gas flowing out from the repository. This will help to put into perspective the large amount of brine that has to be displaced in order for contaminated brine to reach the disposal-unit boundary. If some of the pore volume is occupied by gas, then the estimates of travel distances must be increased proportionately. The tables give volumes only for the portion of the mesh to the south of the repository. Generally, the cumulative flows of gas and brine are greater south of the repository, so only flows to the south are examined.

Cumulative brine flow southward out through Marker Bed 138 is shown in Figure 4-13. The amount of brine that flows inward toward the repository is generally far greater than the amount that flows outward. In eight realizations was there a net outward flow to the south of the repository, with the maximum being 320 m³. However, in many other cases large quantities of brine flowed in toward the repository initially, but flowed outward later as pressures within the repository built up. This occurred in 40 of the 70 realizations. Although the most brine that flowed south from the repository was 520 m³, which would occupy 54,000 m³ of MB138 volume (at a porosity in this realization of 0.0097), another realization that had 350 m³ brine flow at a lower porosity (0.0046), so that brine occupied 77,000 m³ of the marker bed. Table 4-1 shows that this brine would flow as far south as Cell 4, or 626 m, provided that the marker bed was fully saturated with brine. However, this is generally not true. If some contaminated brine flowed out early on, followed by a large quantity of gas, even small amounts of contaminated brine could be pushed far out. A more accurate way to estimate the distance contaminated brine has flowed is to sum the volumes of brine and gas (at local pressures) that flowed out. The maximum gas flow out through MB138 is 2.8×10⁶ m³ at reference conditions of 0.101 MPa, as shown in Figure 4-14. The repository pressure must exceed the far-field fluid pressure in order for gas to flow out from the repository, so gas pressures in MB138 must be at least 12 MPa, which is the low end of the sampled range of far-field pressures. Thus, the maximum cumulative gas volume that has flowed south out of MB138 is approximately 2.3×10⁴ m³, which, at the minimum sampled marker bed porosity of 0.001159, would occupy 20×10⁶ m³ of the marker bed. Table 4-1 shows that when gas and brine flows are combined, they could flow out into Cell 2, 7500 m south of the repository, or 5 km beyond the disposal-unit boundary, using all the most unfavorable parameter values from the Latin hypercube sampling. Because these extreme combinations of parameter values did not occur in the Latin Hypercube Sample (LHS), the maximum gas

Table 4-2. Pore Volumes in Grid Blocks in Anhydrite Layers in BRAGFLO Mesh (South of Repository)^a
(see Figure 2-1)

Cell No.	Distance (m)	Layer 7 MB138		Layer 9 Anhydrite a + b		Layer 16 MB139	
		Minimum Volume (m ³)	Maximum Volume (m ³)	Minimum Volume (m ³)	Maximum Volume (m ³)	Minimum Volume (m ³)	Maximum Volume (m ³)
8	1	0	10	1	16	2	49
7	6	2	63	4	95	12	298
6	26	11	284	17	426	52	1,340
5	126	64	1,650	96	2,470	302	7,790
4	626	448	11,600	673	17,400	2,120	54,700
3	2,500	3,740	96,500	5,610	145,000	17,700	456,000
2	7,500	26,900	693,000	40,300	1,040,000	127,000	3,270,000
1	22,500	221,000	5,720,000	332,000	8,570,000	1,050,000	27,000,000

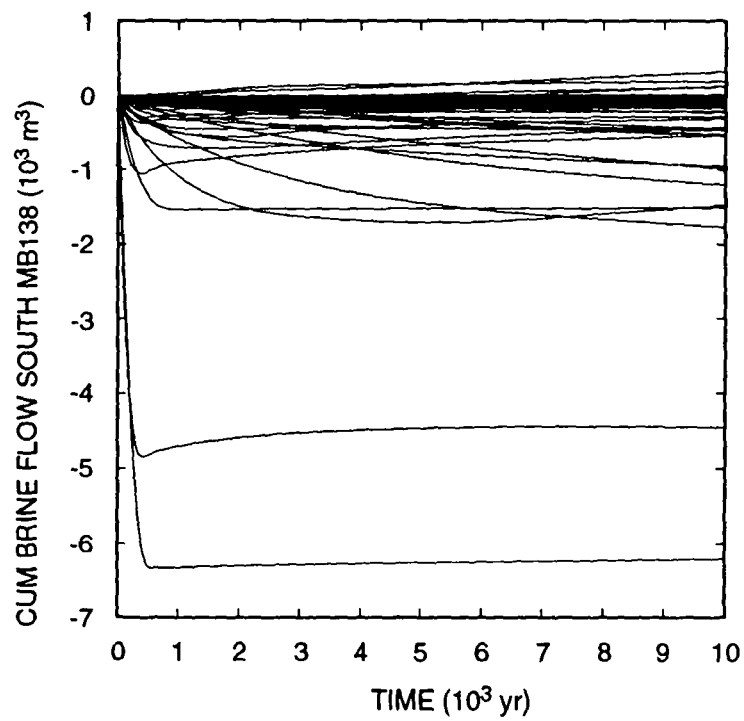
^a Based on actual *sampled* minimum and maximum anhydrite porosity: 0.001159 and 0.02992; *not* on minimum and maximum reported in Volume 3, Table in Volume 3, Table 2.4.4: 0.001 and 0.03.

and brine flow out through MB138 is much less. In only one realization does enough gas flow out through MB138 to occupy all the pore volume in MB138 to a distance beyond the disposal-unit boundary. In this one case, 19,700 m³ of gas at local pressures flows out of MB138, occupying only 4.8×10^6 m³ of marker bed volume, which would only extend into Cell 2 in MB138, the first cell beyond the disposal-unit boundary.

It still cannot be stated with certainty whether contaminated brine actually reached the boundary, however. First, MB138 is not fully saturated with either gas or brine. The residual brine saturation in the realization that potentially crosses the boundary is 0.2001. (This parameter was sampled and is constant in any given realization.) Thus, some brine, contaminated or not, remains as residual saturation rather than being pushed ahead of the gas. This residual brine results in a smaller volume for gas storage in the marker bed, and causes gas to migrate approximately 25% farther than it would if the unit were fully gas-saturated.

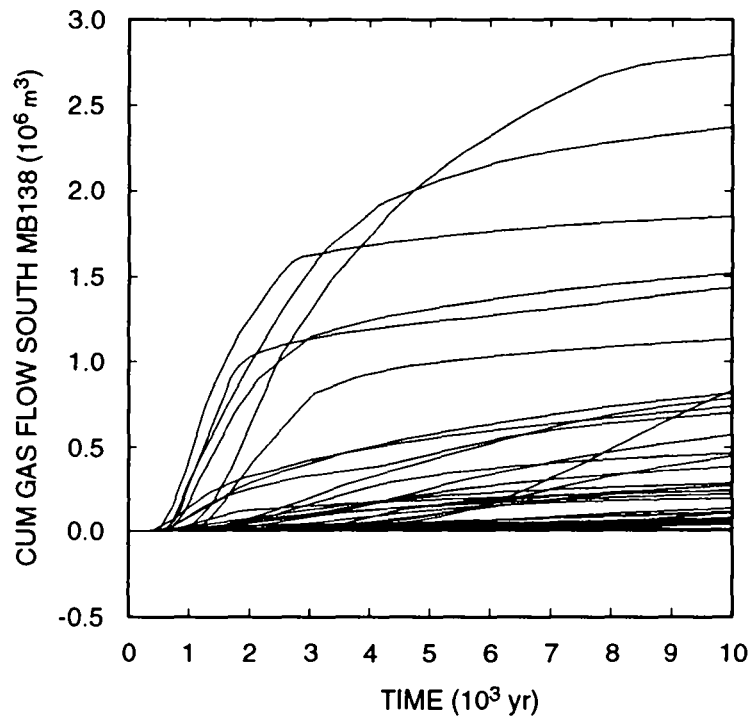
Residual brine volume in MB138 in the realization in which brine potentially reached the unit boundary is 2650 m³, whereas the calculated volume of cumulative brine flow past the disposal-unit boundary is far less at 150 m³. Second, it is necessary to know the history of release of contaminated brine from the waste to know whether the underlying assumption that contaminated brine preceded gas flow out MB138 is true. No brine actually flowed out of the waste in this realization; therefore, no contaminated brine could have reached the disposal-unit boundary. This realization illustrates the hazards involved in making conservative assumptions. With enough bad

4. Gas and Brine Migration



TRI-6342-2716-0

Figure 4-13. Cumulative Brine Flow South out MB138. (Positive values indicate flow southward away from the repository.)



TRI-6342-2717-0

Figure 4-14. Cumulative Gas Flow South out MB138 (at 30 °C; 0.101 MPa). (Positive values indicate flow southward away from the repository.)

4. Gas and Brine Migration

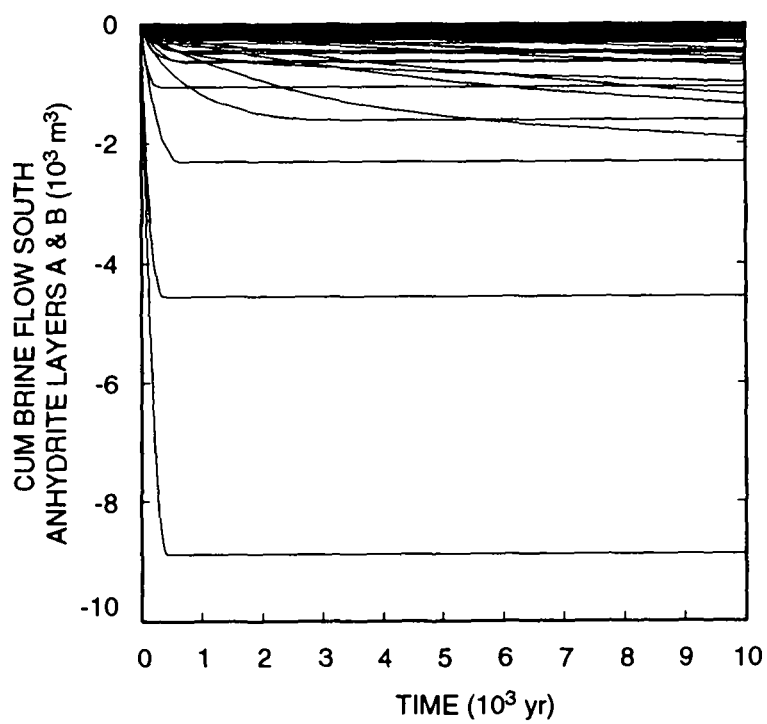
1 assumptions about the results, it would appear that brine crossed the disposal-unit boundary in at least one
2 realization, when in fact, this did not occur.

3 This analysis can be repeated for the anhydrite a + b layer, which is expected to have a larger cumulative gas
4 flow than MB138. The brine flow should be greater simply because this layer is thicker, and, being slightly closer
5 to the repository, the driving pressures are higher. Surprisingly, Figure 4-15 shows that no outward brine flow
6 occurred south of the repository in this layer. Brine flowed only in toward the repository. As pressures quickly
7 built up in the waste, inward brine flow ceased. In more than half of the realizations, this occurred within the first
8 1000 yr. At the same time, gas began to flow outward (Figure 4-16). As expected, the volume of gas flow out
9 through this layer is somewhat higher than in MB138, ranging up to $3.5 \times 10^6 \text{ m}^3$, compared with $2.3 \times 10^4 \text{ m}^3$ in
10 MB138.

11 The analysis for MB139 is similar in complexity to MB138. The net cumulative brine flow out of MB139
12 (Figure 4-17) is positive (i.e., outward) in 13 realizations, with a maximum of 2030 m^3 . From Table 4-2, it can be
13 seen that if MB139 were fully brine saturated, this maximum quantity of brine, which may or may not be
14 contaminated, would flow only as far as Cell 4, or 626 m from the repository, assuming the minimum value for
15 porosity. However, as seen in MB138, more than half of the realizations that had net inward cumulative flows
16 actually had a substantial amount of outward brine flow following a large initial inward surge. The largest of these
17 was 6700 m^3 . In a brine-saturated MB139, assuming minimum porosity, this brine would reach Cell 3, which
18 extends to the disposal-unit boundary. In fact, the realizations having the greatest outward flow of brine do not have
19 the lowest porosity. The realization with the largest brine flow has a porosity of 0.0041, meaning that the brine
20 flows only to Cell 4, or 626 m from the repository, not to the disposal-unit boundary.

21 As shown in the analysis for MB138, gas flow has a major impact on how far contaminated brine might flow.
22 Figure 4-18 shows that as much as $3.6 \times 10^6 \text{ m}^3$ of gas flowed out through MB139. That large quantities of gas
23 flow out through MB139 is surprising; previous work has suggested that brine will tend to pool in the lower portion
24 of the waste and beneath the repository (Bertram-Howery et al., 1990; WIPP PA Division, 1991b; WIPP PA
25 Department, 1992). The main flow path for brine inflow is MB139, but if gas generation in the repository raises the
26 pressure there rapidly enough, little brine ever flows in. Generally, model results indicate that any brine initially
27 present in the repository is converted to gas, which raises the pressure, preventing any further significant influx of
28 brine, and driving large amounts of gas out through MB139. If it is again assumed that contaminated brine precedes
29 any outflowing gas, then it must be concluded that contaminated brine flows past the disposal-unit boundary
30 through MB139. However, at least a residual saturation of brine will remain throughout the anhydrite layers. In the
31 case in which the maximum brine outflow was 6700 m^3 , residual brine volume out to the disposal-unit boundary is
32 12,500 m^3 , nearly double the actual contaminated brine volume that flowed into MB139. So again, no
33 contaminated brine could have reached the disposal-unit boundary through any of the anhydrite layers.

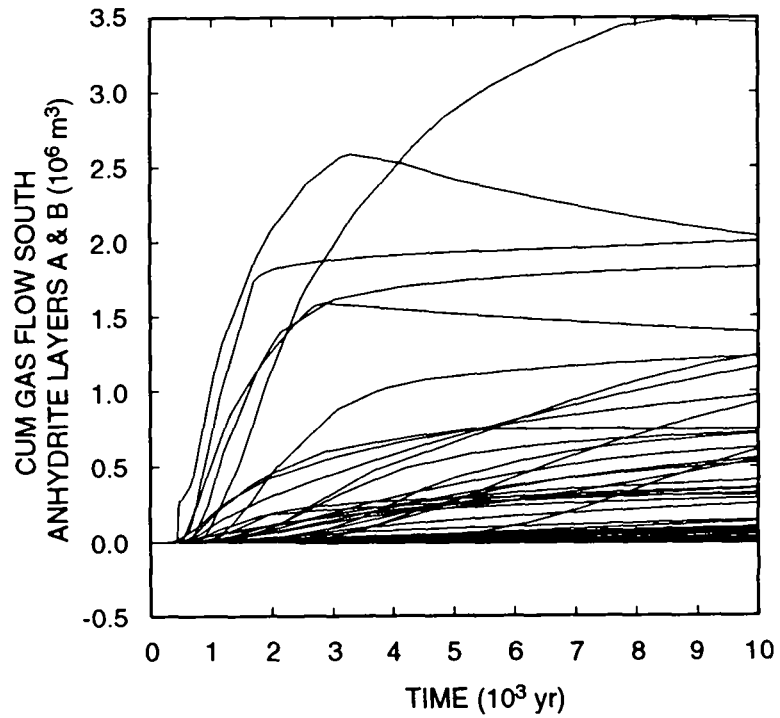
34 The results show that except for flow out the anhydrite layers, there is little movement of brine in the vicinity of
35 the repository. Figure 4-19 shows that almost no brine flowed from the seals and backfill regions into the shaft,
36 while flow in the other direction, cumulative brine flow amounted to less than 800 m^3 . Flow from the experimental
37 region into the shaft, Figure 4-20, is almost a mirror image of flow from the seals and backfill into the shaft,
38 indicating that the shaft does little to impede flow from the experimental region to the seals and backfill.
39 Considering the small volume of the lower shaft, this result is expected. The flow behavior in these regions stems
40 directly from the initial conditions. At time zero, all of the excavated regions except for the repository were
41 assumed to be fully saturated with brine. This assumption was based on the expected brine content of the halite



TRI-6342-2718-0

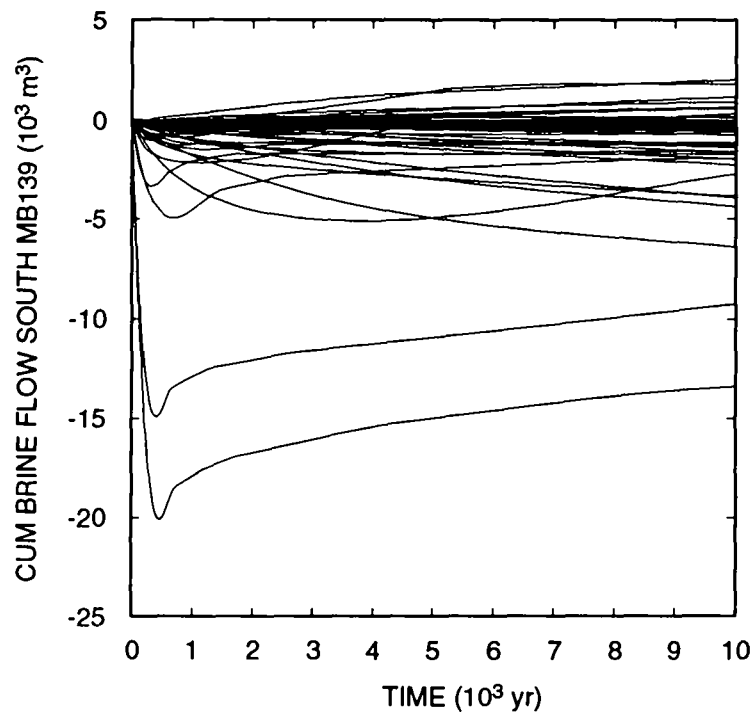
Figure 4-15. Cumulative Brine Flow South out Anhydrite Layers a + b. (Negative values indicate flow northward toward the repository.)

4. Gas and Brine Migration



TRI-6342-2719-0

Figure 4-16. Cumulative Gas Flow South out Anhydrite Layers a + b (at 30 °C; 0.101 MPa). (Positive values indicate flow southward away from the repository.)



TRI-6342-2720-0

Figure 4-17. Cumulative Brine Flow South out MB139. (Positive values indicate flow southward away from the repository.)

4. Gas and Brine Migration

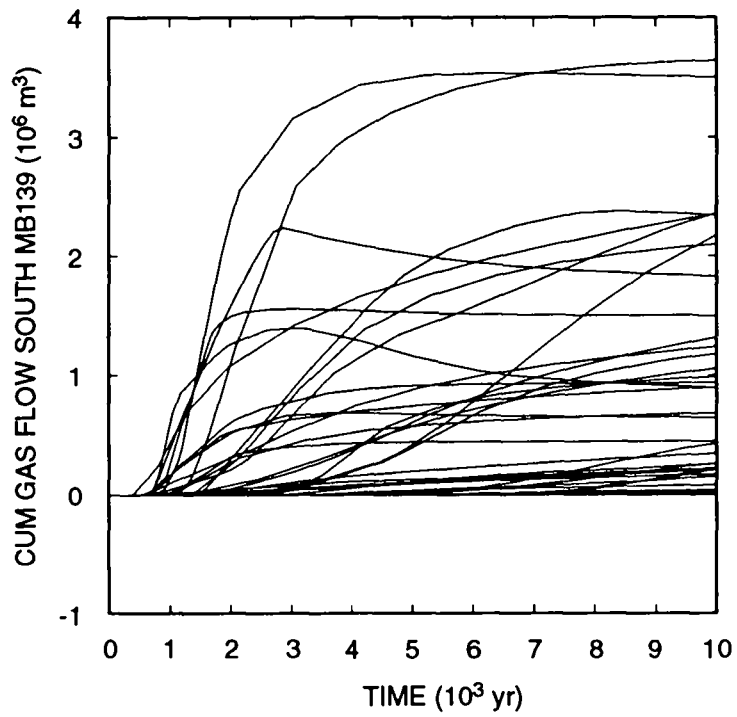
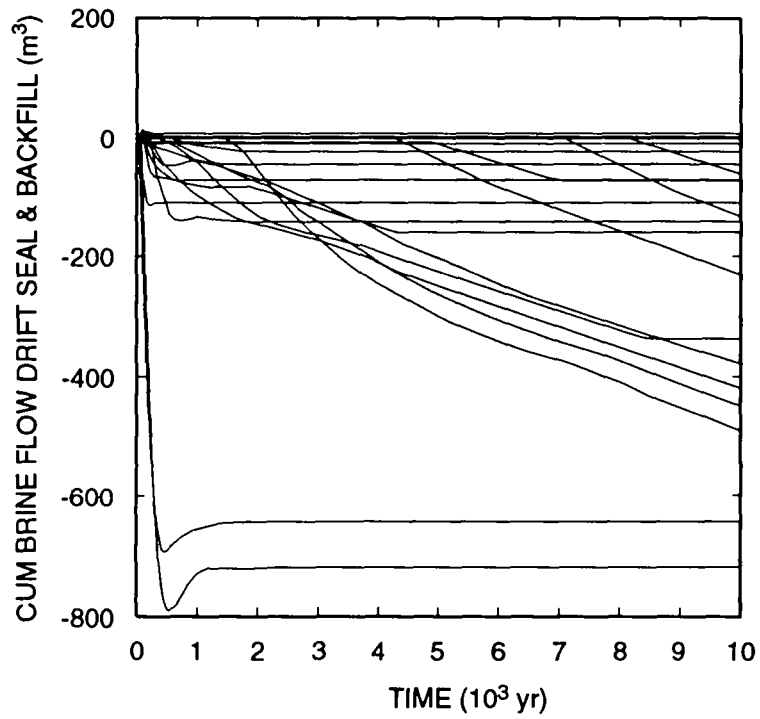


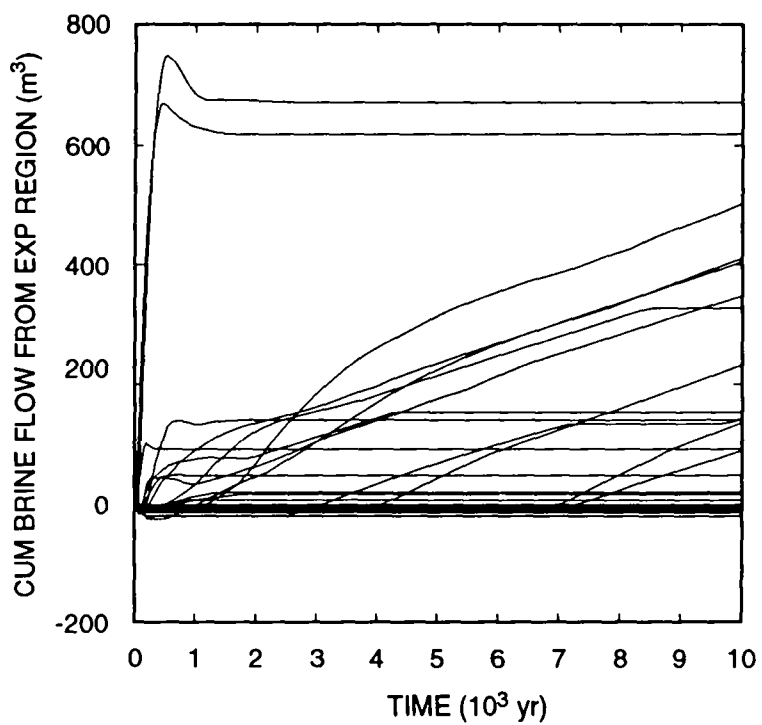
Figure 4-18. Cumulative Gas Flow South out MB139 (at 30 °C; 0.101 MPa). (Positive values indicate flow southward away from the repository.)



TRI-6342-2722-0

Figure 4-19. Cumulative Brine Flow from Drift Seals and Backfill into Shaft. (Positive values indicate flow from seals and backfill into shaft.)

4. Gas and Brine Migration



TRI-6342-2723-0

Figure 4-20. Cumulative Brine Flow from Experimental Region into Shaft.

backfill, estimated to be 5 to 8 weight percent (see memorandum by Finley and Vaughn in Appendix A). Depending on the porosity of the backfill (a sampled parameter), this corresponds to nearly 100% brine saturation. The brine saturation of the DRZ, however, was calculated during the 50-yr operational simulation, then adjusted downward to account for the increased porosity of the DRZ at time zero, when the repository is sealed. The result is that whereas the backfilled excavated regions are fully saturated with brine at time zero, the surrounding DRZ has a relatively low brine saturation, so an immediate flux of brine occurs from the backfilled regions into the DRZ, particularly that portion of the DRZ beneath the seals and backfilled regions. In the majority of realizations, this flow of brine is small, less than 1 m³. But in about 15% of the cases, more than 100 m³ flows into the DRZ.

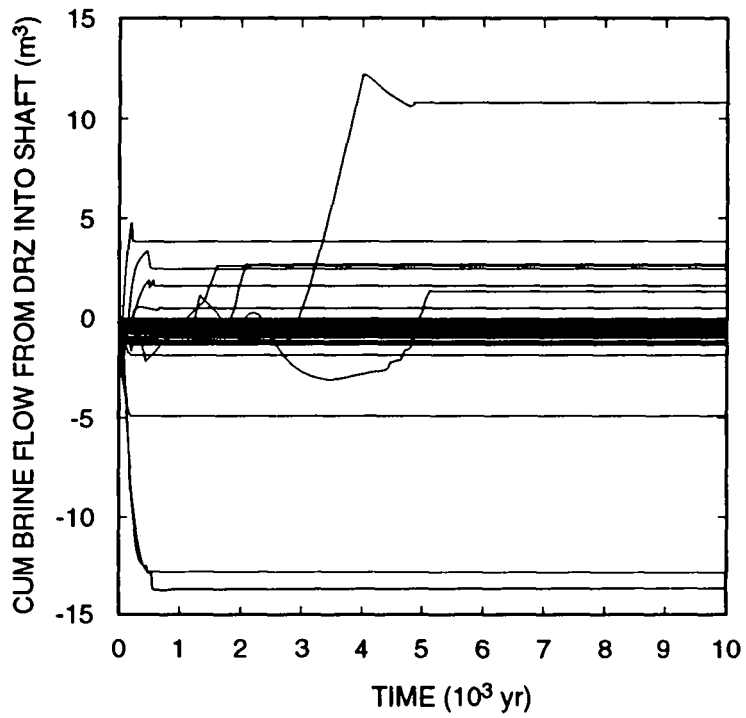
Flow between other regions is generally much smaller. Less than 15 m³ flows between the DRZ and the shaft (Figure 4-21). Except for two realizations, almost no brine flows between MB138 and the shaft (Figure 4-22) or between the transition zone and the shaft (Figure 4-23). Up to 400 m³ of brine flows from the Salado halite into the shaft (Figure 4-24). Although the permeability of the halite is extremely low, the large surface area of the shaft allows a substantial amount of brine to flow in. The one realization in which 700 m³ flows from the shaft into the halite is characterized by the highest halite permeability among the 70 realizations, a highly permeable shaft seal, and large quantities of gas generation that cause the shaft to pressurize much more than in other realizations, thus providing a greater driving force out of the shaft and into the halite. Only seven other realizations have a net flow of brine from the shaft into the halite. Flow through the shaft seal was discussed earlier. In two-thirds of the realizations, brine flows from the shaft into the Culebra (Figure 4-25). This flow is largely driven by gas flowing up the shaft. In the other one-third of the realizations, the shaft is never pressurized enough to prevent brine from draining from the Culebra into the shaft.

4.1.3 Gas Flow Behavior

Gas flow in the anhydrite layers was discussed earlier in connection with its impact on brine flow. It was mentioned then that gas may flow beyond the disposal-unit boundaries in some realizations. This issue will be clarified here. For brevity, the discussion will be restricted to flow in the mesh south of the repository because the cumulative flows are greater there than to the north. Figures 4-26, 4-27, and 4-28 show the cumulative gas flows past the southern disposal-unit boundary in MB139, anhydrite a + b, and in MB138, respectively. Significant volumes of gas (i.e., greater than one m³) flow past the boundary in six realizations. The maximum gas flow past a boundary occurs in MB138, with 1.7×10^6 m³ of gas (at reference conditions). All gas is assumed to have the physical properties of hydrogen. Because the viscosity of hydrogen is lower than that of other gases likely to be present or produced in the waste (CO₂, CH₄, N₂), this assumption should result in greater and more extensive gas flows than if other gases were used.

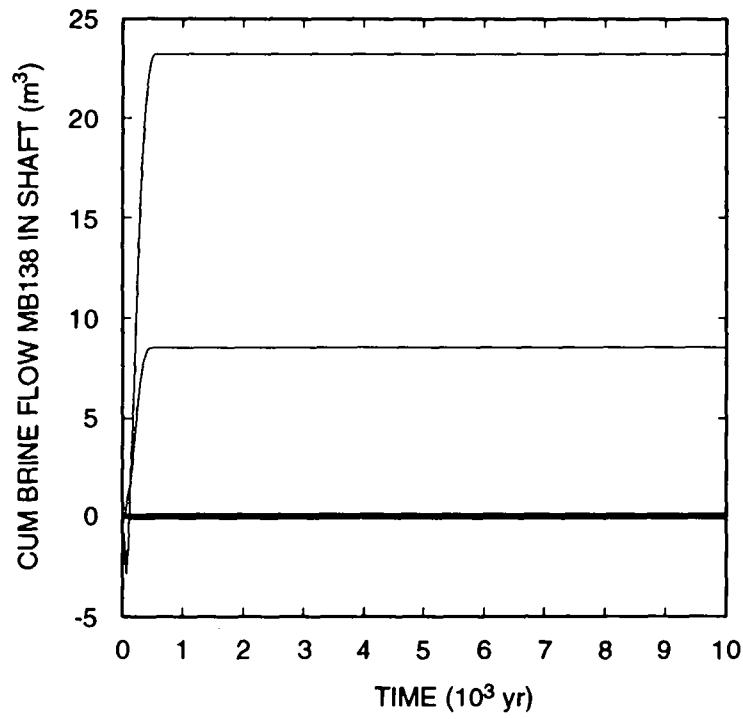
Although no gas flowed past the disposal-unit boundary in the Culebra, it is interesting to see how effective the shaft seal is in preventing gas flow into the Culebra. The cumulative gas flow up through the shaft seal is shown in Figure 4-29. With a maximum of 1.9×10^5 m³, gas flows through the shaft seal are small compared with the flows out the anhydrite layers, where the maxima are more than an order of magnitude higher. Why the upper curve in Figure 4-29 stands out from the others is difficult to explain. The only exceptional parameter in this realization is the halite permeability, which is the highest among the 70 realizations. That the cumulative flow is a factor of five higher than the next highest result suggests that sampling should be more detailed in order to fill in the gap between the one outstanding result and all the rest. The drift seals were relatively ineffective in stopping gas flow toward the shaft for the time scales of this study (Figure 4-30). Nearly as much gas flows through these seals as out each of the

4. Gas and Brine Migration



TRI-6342-2724-0

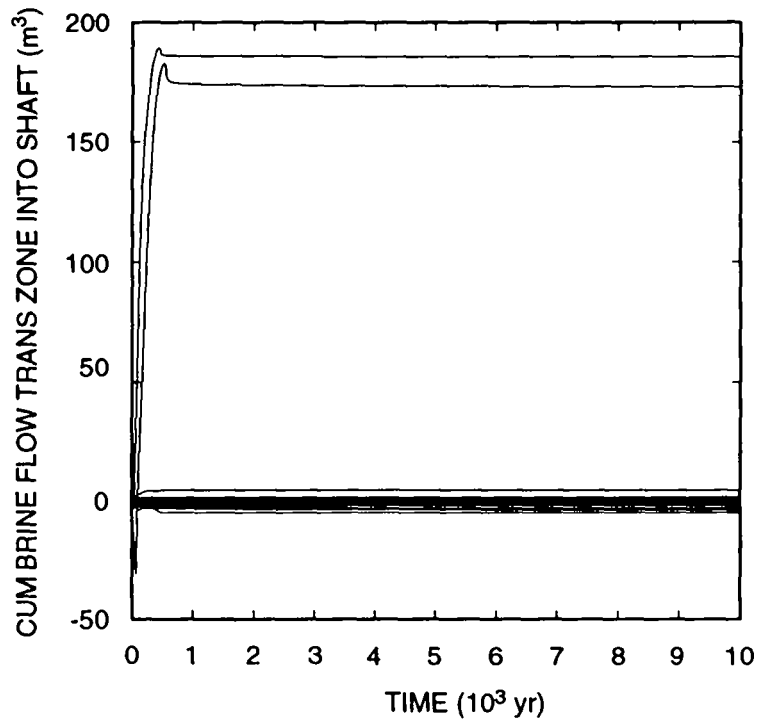
Figure 4-21. Cumulative Brine Flow from DRZ into Shaft.



TRI-6342-2725-0

Figure 4-22. Cumulative Brine Flow from MB138 into Shaft.

4. Gas and Brine Migration



TRI-6342-2726-0

Figure 4-23. Cumulative Brine Flow from Transition Zone into Shaft.

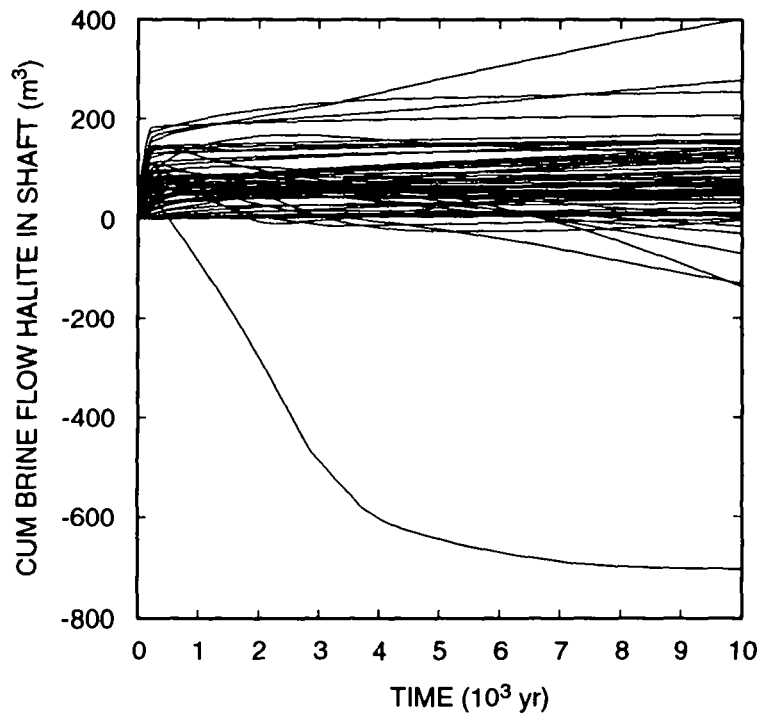
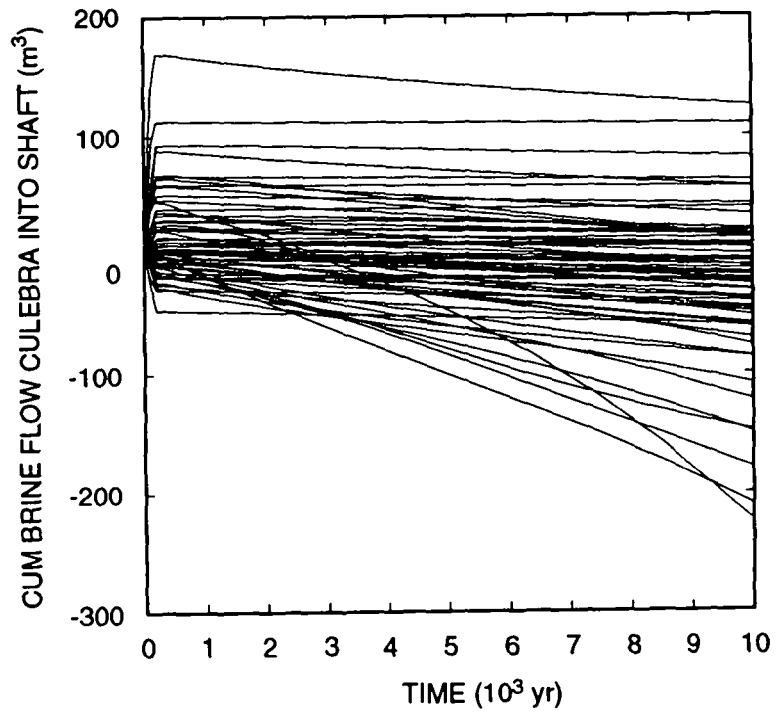


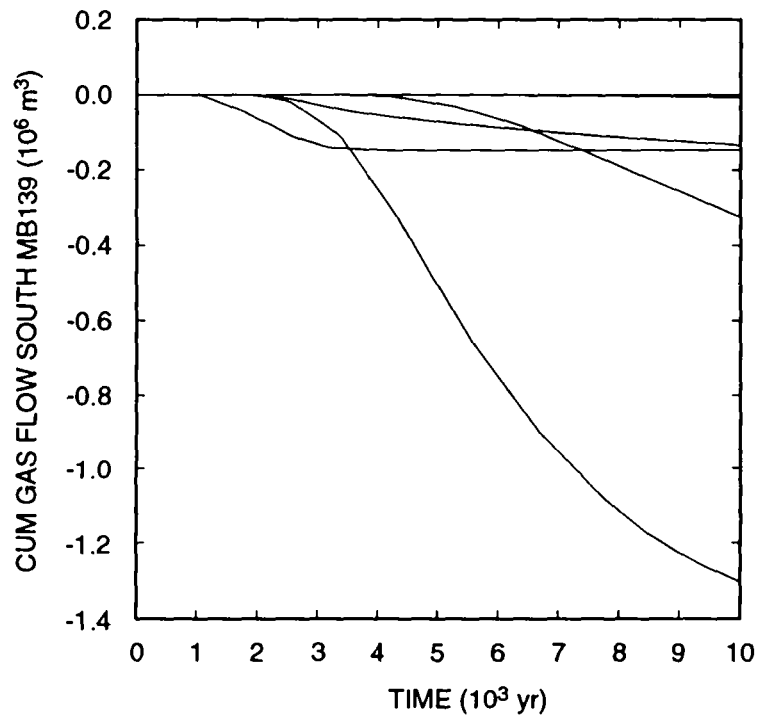
Figure 4-24. Cumulative Brine Flow from Halite into Shaft.

4. Gas and Brine Migration



TRI-6342-2728-0

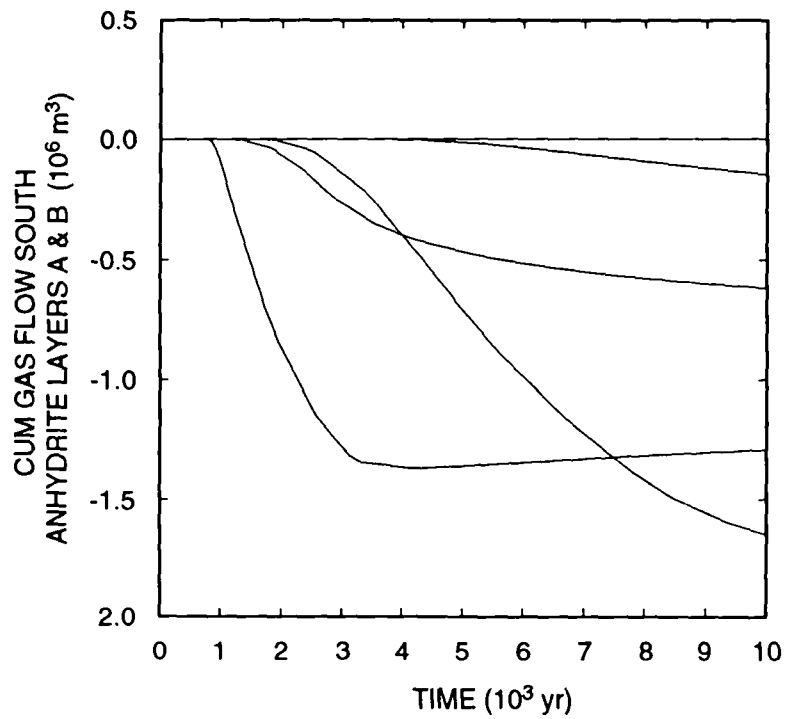
Figure 4-25. Cumulative Brine Flow from Culebra into Shaft.



TRI-6342-2729-0

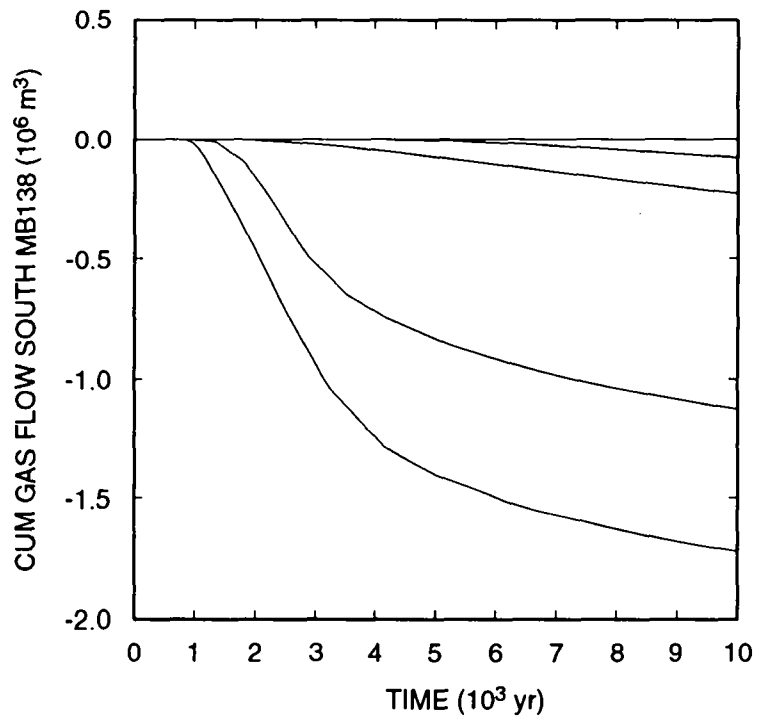
Figure 4-26. Cumulative Gas Flow South in MB139 Past the WIPP Boundary (at 30°C; 0.101 MPa). (Negative values indicate flow southward away from the repository.)

4. Gas and Brine Migration



TRI-6342-2730-0

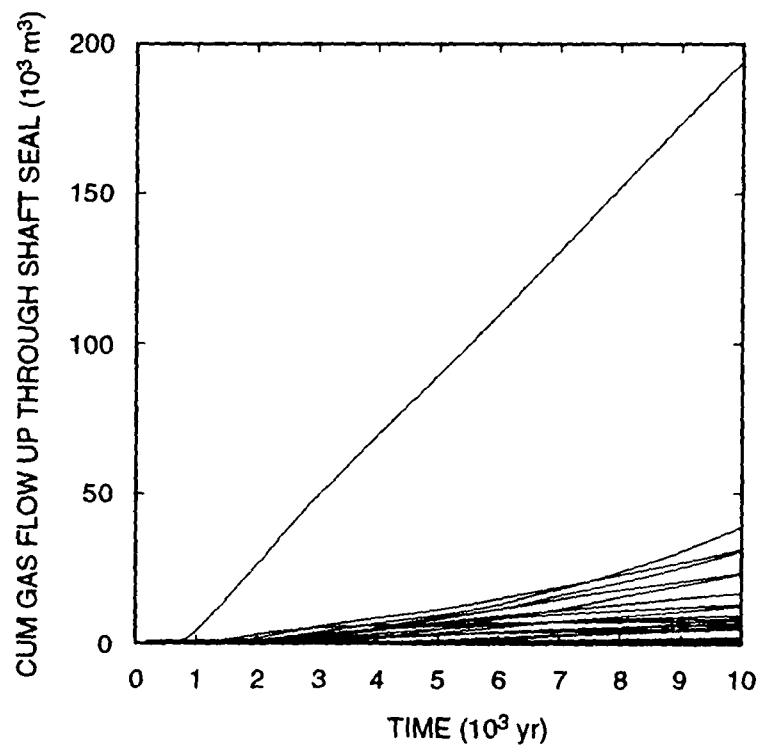
Figure 4-27. Cumulative Gas Flow South in Anhydrite Layers a + b Past the WIPP Boundary (at 30 °C; 0.101 MPa). (Negative values indicate flow southward away from the repository.)



TRI-6342-2731-0

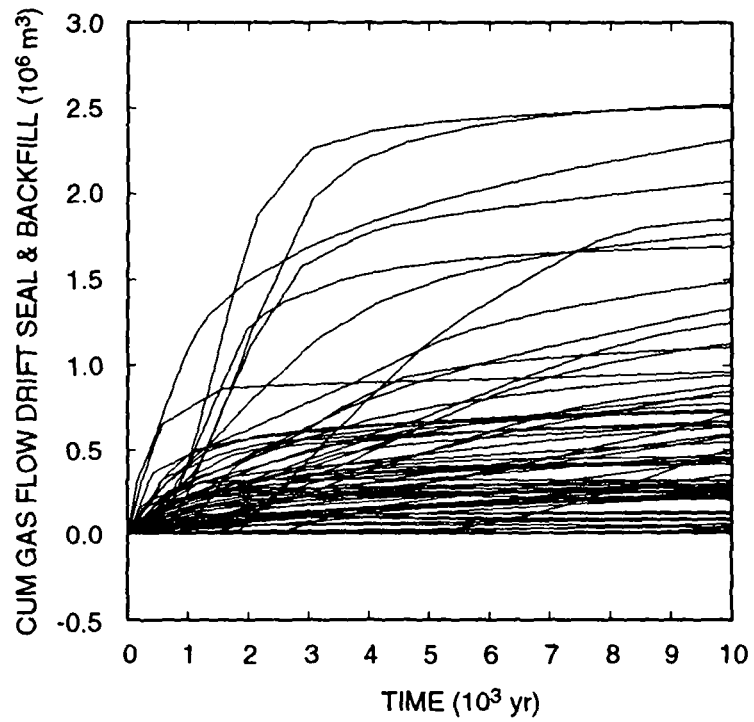
Figure 4-28. Cumulative Gas Flow South in MB138 Past the WIPP Boundary (at 30 °C; 0.101 MPa). (Negative values indicate flow southward away from the repository.)

4. Gas and Brine Migration



TRI-6342-2732-0

Figure 4-29. Cumulative Upward Gas Flow through Shaft Seal (at 30 °C; 0.101 MPa).



TRI-6342-2733-0

Figure 4-30. Cumulative Gas Flow from Drift Seals and Backfill into Shaft (at 30 °C; 0.101 MPa).

4. Gas and Brine Migration

1 three anhydrite layers: a maximum of $2.5 \times 10^6 \text{ m}^3$ versus an average maximum of $3.3 \times 10^6 \text{ m}^3$ to the south in
2 each anhydrite layer. A somewhat greater amount flows through the DRZ into the shaft below the shaft seal (Figure
3 4-31), up to $3.9 \times 10^6 \text{ m}^3$. Gas encounters little resistance between the repository and the shaft, which leaves the
4 shaft seal to prevent gas migration into the Culebra. (It is assumed that there is no DRZ around the shaft above
5 MB138 through which gas could bypass the shaft seal [see Figure 2-1].) Other flow paths between the repository
6 and the shaft are insignificant. Less than $50,000 \text{ m}^3$ of gas flows into the shaft via the transition zone, and less than
7 8000 m^3 by way of MB138; in fact, in some realizations, the flow is in the opposite direction, *from* the shaft, rather
8 than *into* the shaft.

4.2 Single-Shaft Geometry

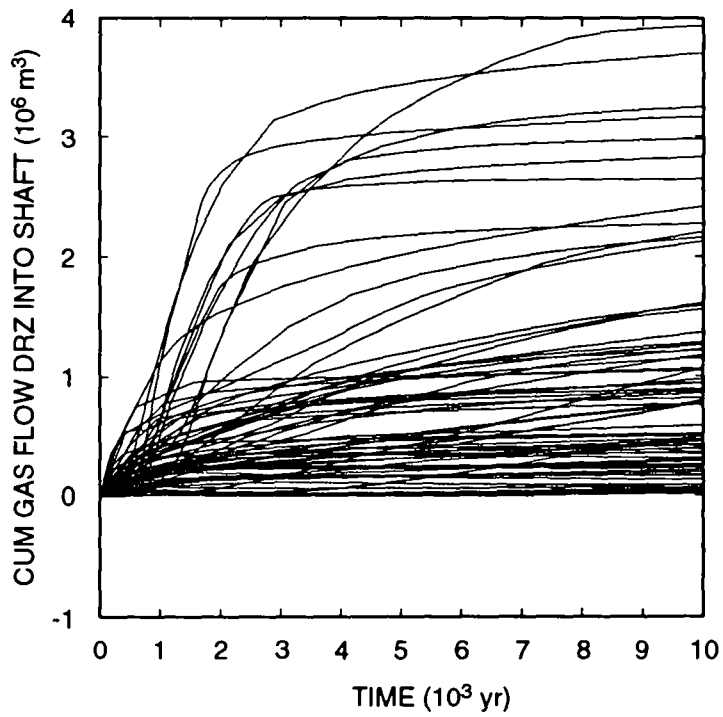
9
10 In these calculations, the shaft was changed from the original configuration (in which all four shafts were
11 combined into one), to a single shaft the size of the Salt Handling Shaft. All other parameters are identical to those
12 used in the four-shaft equivalent geometry calculations. As shown in the following discussion, the affect of
13 reducing the size of the shaft is negligible. Fluid flows up the shaft were reduced in proportion to the shaft cross
14 section reduction. However, shaft flows had only a small effect on the overall performance of the repository in the
15 original calculations. There were no flows of brine and small flows of gas to the top of the Salado Formation in
16 both four-shafts-in-one geometry or the single-shaft geometry. In particular, the shaft seal performance was good
17 enough that the presence of the shaft was of no consequence in either performance assessment, whether there was
18 one shaft or four.

4.2.1 Repository Behavior

19
20 Although minor differences occurred between individual realizations, on the whole, the pressures in the
21 repository differ insignificantly between these single-shaft calculations and the base case (see Figure 4-32). The
22 peak pressure was still 23.8 MPa; after 10,000 yr, pressures ranged from 5.4 to 22.3 MPa, compared with 5.8 to
23 22.3 MPa in the base case. Because the transient pressure behavior in the repository differed little from the base
24 case, other performance measures would also be expected to differ little. Plots of remaining corrodible content,
25 biodegradable content, and total gas generated — Figures 4-33, 4-34, and 4-35, respectively — are nearly
26 indistinguishable from their base case counterparts. Other results describing conditions in the waste are also very
27 similar: pore volumes, cumulative brine consumption, and brine and gas saturations. These results are not
28 surprising. The shaft is a relatively small region located more than 600 m from the waste-disposal region. Its
29 diameter should not and does not have any significant effect on processes that occur in the waste, particularly
30 because the behavior of the repository is largely determined by the amount of brine initially present and by marker
31 bed permeability. Shaft diameter would be expected to have a noticeable effect only on flows up the shaft, although
32 fluid flow in other regions should be considered.

4.2.2 Brine Flow Behavior

33
34 Cumulative brine flow from the repository, Figure 4-36, is virtually identical to the base case, Figure 4-9, which
35 was expected because all other repository responses are unchanged. Plots of cumulative brine flow out each of the



TRI-6342-2734-0

Figure 4-31. Cumulative Gas Flow from DRZ into Shaft (at 30 °C; 0.101 MPa).

4. Gas and Brine Migration

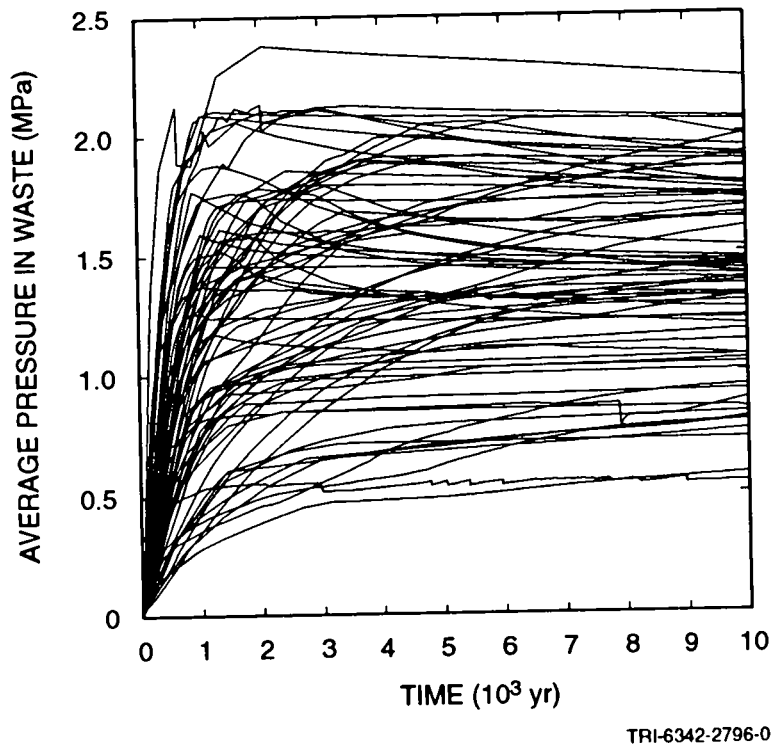
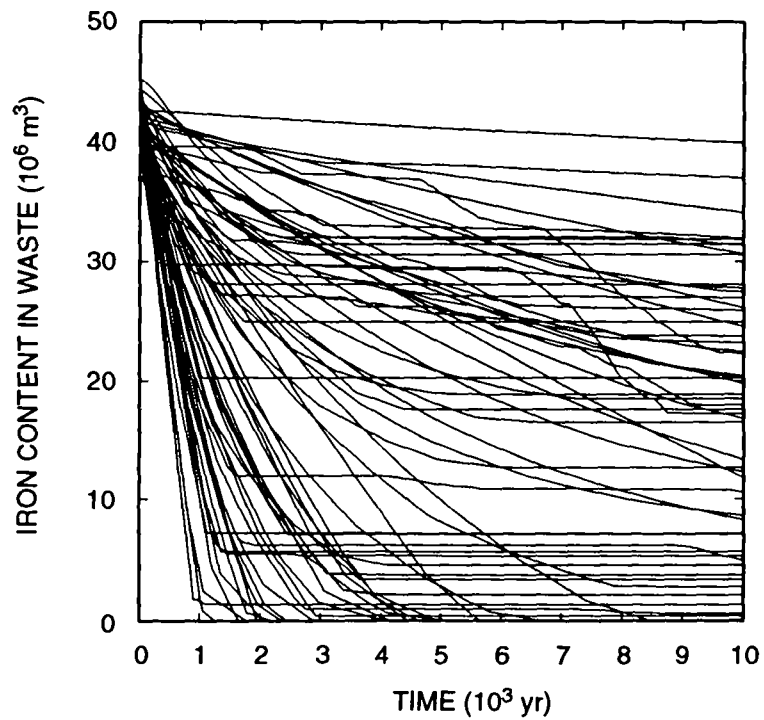


Figure 4-32. Volume Average Pressure in the Waste Repository, Single Shaft Model.



TRI-6342-2797-0

Figure 4-33. Iron Remaining in the Waste Repository, Single Shaft Model.

4. Gas and Brine Migration

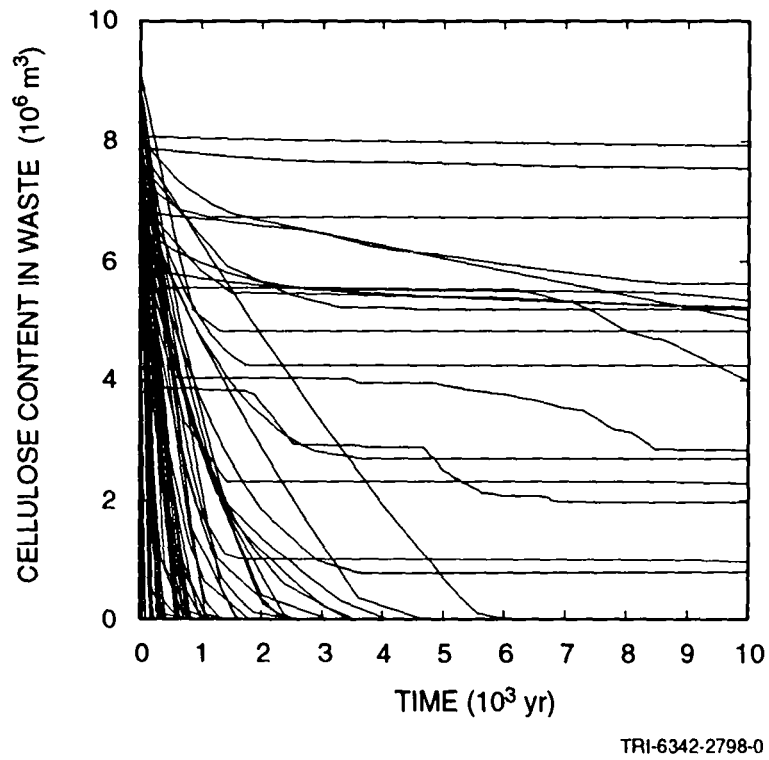
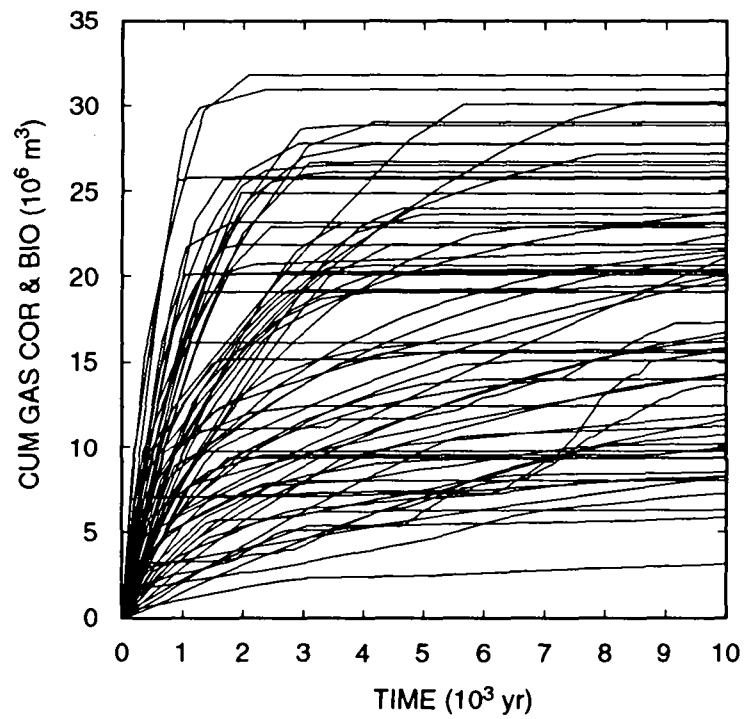


Figure 4-34. Cellulose Remaining in the Waste Repository, Single Shaft Model.



TRI-6342-2799-0

Figure 4-35. Cumulative Gas Volume Generated (at 30 °C; 0.101 MPa), Single Shaft Model.

4. Gas and Brine Migration

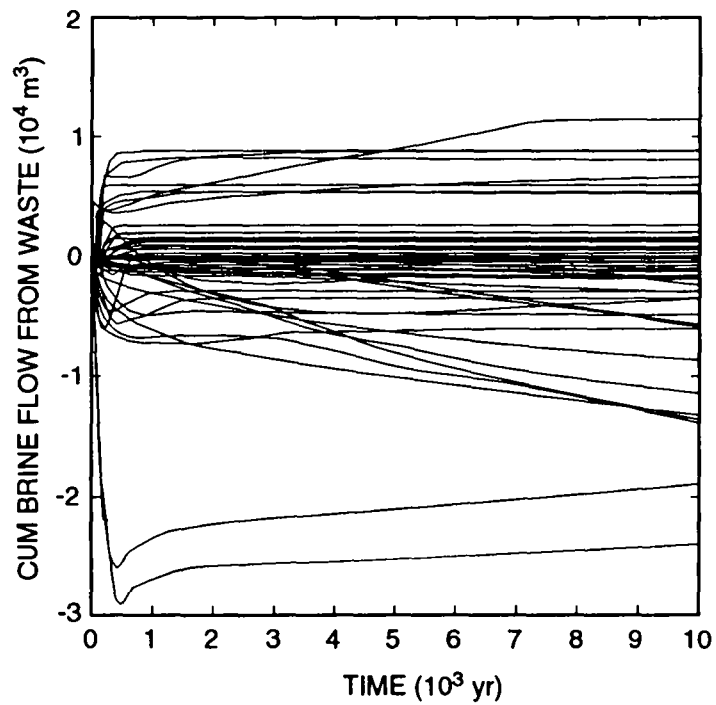


Figure 4-36. Cumulative Brine Flow from the Waste Repository, Single Shaft Model. (Positive values indicate flow away from the repository.)

1 three anhydrite layers overlay plots of the base case exactly and are not repeated here. Where differences are
 2 expected is in flow up the shaft. The most apparent difference between the single-shaft results and the results with
 3 four shafts combined is in flows through the shaft seal, Figure 4-37. Comparing this with the earlier plot, Figure 4-
 4 11, the flow of brine through the shaft seal is reduced by the smaller shaft cross section. The maximum net upward
 5 flow is now 3 m^3 versus 25 m^3 with four combined shafts. However, the minimum pore volume of the lower shaft,
 6 37 m^3 , is still 10 times the volume of brine that flowed up through the shaft seal, just as in the base case. Although
 7 the lower shaft pore volume is smaller with the single shaft, the amount of brine that flowed up the shaft is reduced
 8 proportionately. (Although there were a few realizations in which brine initially flowed downward but later
 9 reversed direction, as in the base case, the total upward flow was still less than 5 m^3 .)

10 The amount of brine that flows out through the anhydrite layers is negligibly different when the shaft is
 11 modeled as a single shaft the size of the Salt Handling Shaft compared to modeling it as all four shafts combined.
 12 Brine flow up the shaft is proportionately smaller when a single shaft is used. Thus, shaft diameter has no effect on
 13 releases of contaminated brine as far as 40 CFR 191B is concerned.

14 4.2.3 Gas Flow Behavior

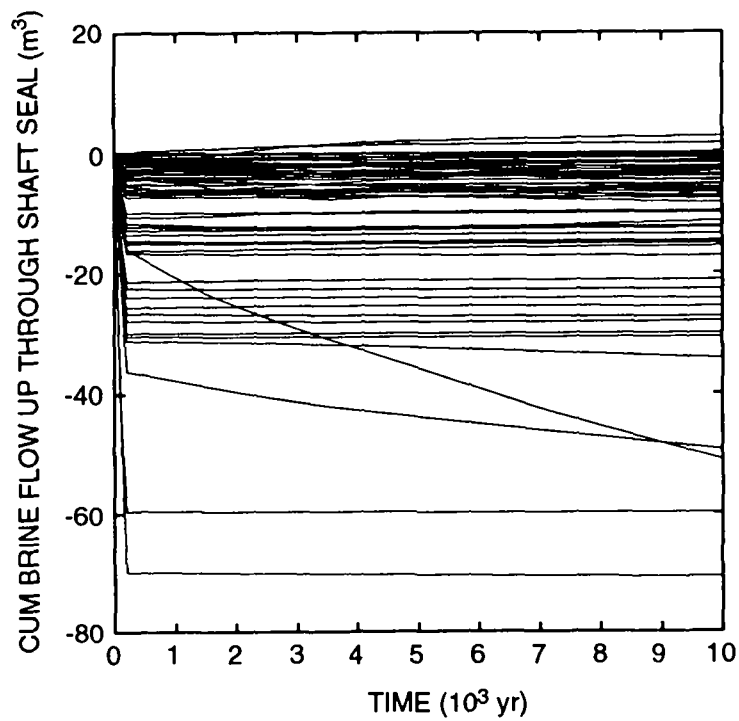
15 As with brine flow, gas flow is largely determined by the behavior of the repository. The shaft has only a
 16 minor impact on repository behavior, since it is more than 600 m away, whereas the anhydrite layers provide flow
 17 paths of much greater capacity. Thus, the same conclusions arrived at with the base case hold true for the single-
 18 shaft case. Cumulative gas flows out each of the anhydrite layers are nearly identical with the base case: Maximum
 19 southward gas flows past the Disposal unit boundary in MB139 are $1.30 \times 10^6 \text{ m}^3$ in both cases; southward flows
 20 out of anhydrite a + b are $1.65 \times 10^6 \text{ m}^3$. Only in MB138 are maximum flows slightly lower: $1.65 \times 10^6 \text{ m}^3$ versus
 21 $1.72 \times 10^6 \text{ m}^3$ in the base case. In the single-shaft calculations, gas flows into the Culebra in twelve realizations,
 22 compared with six realizations in the combined-shafts case. However, the maximum cumulative gas flow are now
 23 $1.9 \times 10^4 \text{ m}^3$, instead of $1.4 \times 10^5 \text{ m}^3$ with combined shafts. With a single shaft, the average cumulative gas flow is
 24 5400 m^3 (for 12 realizations), which is about one-fourth of the four-shaft average, $22,900 \text{ m}^3$ (for 6 realizations).

25 The main difference when using a smaller versus a larger shaft is the flow up through the shaft seal, Figure 4-
 26 38. The obvious difference is the smaller cumulative flows through the seal. The maximum is now $30,000 \text{ m}^3$,
 27 compared with $194,000 \text{ m}^3$ in the base case. In both cases, there were 37 realizations in which the cumulative flow
 28 was greater than 1 m^3 . The average flow among those 37 was 4500 m^3 , compared with $12,400 \text{ m}^3$ in the base case.

29 4.3 Four-Shaft Equivalent Geometry without Dynamic Creep Closure

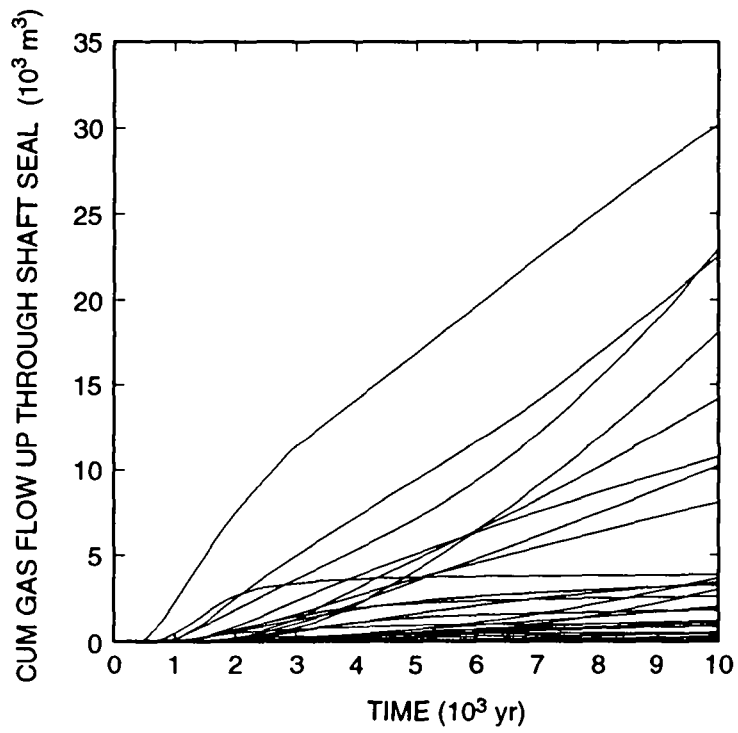
30 This set of calculations is identical to the base case, with all four shafts combined into one, except that the
 31 repository does not undergo creep closure. Instead, the initial porosity is set at 19%, which is the median final
 32 closed porosity of the repository. Small changes in porosity are allowed as a result of compressibility effects.
 33 However, unlike the case of dynamic creep closure, in which the repository porosity varies from an initial value of
 34 66% to as low as 12%, the "fixed porosity" varies by no more than 1.2 percentage points from its initial value (i. e.,
 35 from 19 to 20.2%). This has a major effect on the behavior of the repository, especially on pressures within the
 36 repository. However, the net effect over the 10,000-yr compliance period is negligible, because, ultimately, what

4. Gas and Brine Migration



TRI-6342-2801-0

Figure 4-37. Cumulative Upward Brine Flow through Shaft Seal, Single Shaft Model



TRI-6342-2802-0

Figure 4-38. Cumulative Upward Gas Flow through Shaft Seal (at 30°C; 0.101 MPa), Single Shaft Model.

4. Gas and Brine Migration

drives gas migration is the number of moles of gas generated in the waste, which is primarily dependent on the amount of brine present there initially. Conditional on the conceptual models and parameter distributions used in these analyses, results described have suggested that detailed modeling of the dynamics of creep closure may be unnecessary.

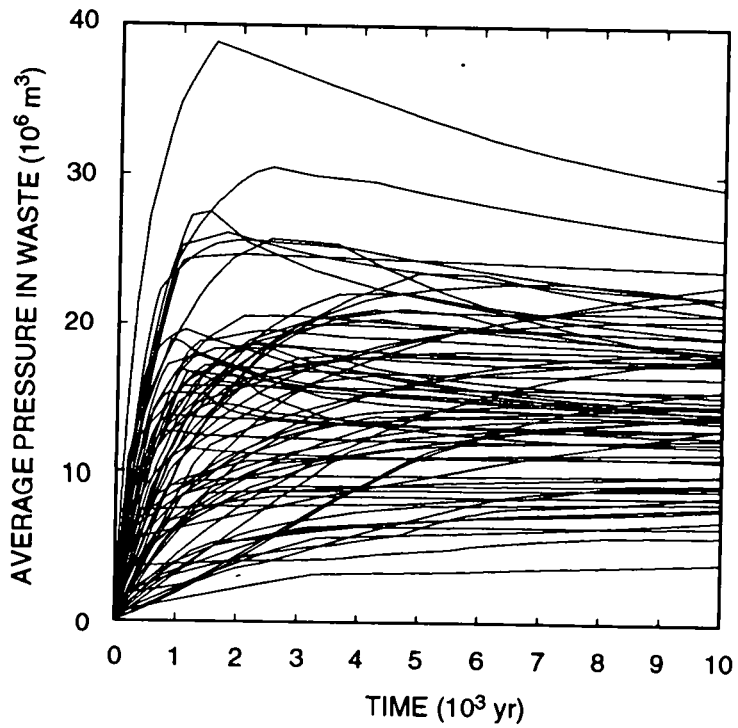
4.3.1 Repository Behavior

Pressures in the waste generally peak at much higher values than in the calculations with dynamic creep closure (Figure 4-39). In order to maintain the gas generation potential in the fixed porosity calculations to be the same as in the dynamic creep closure calculations, the same initial repository brine volume is used. This results in approximately the same amount of gas being generated. (Compare Figures 4-40 and 4-7). With dynamic creep closure, final porosities greater than the median value are often obtained, particularly when large amounts of gas are generated and pressures are relatively high. In fact, in one dynamic closure realization, the repository is forced open to 34% porosity after closing down to 21%. When the porosity in this realization is fixed at 19%, the pressure is proportionately higher. Instead of peaking at 23.8 MPa, it now peaks at 38.8 MPa. At the other extreme, some realizations that result in very low porosities with dynamic closure (as low as 11.6%) because little gas is generated now have lower pressures because the porosity is fixed at 19%. Over time, the differences become less significant. After 10,000 yr, pressures within the repository range from 5.8 to 22.3 MPa using dynamic creep closure, compared with 4.0 to 29.2 MPa with fixed porosities. Even more similar are the averages over the 70 realizations: 14.9 MPa with dynamic closure versus 14.2 MPa with fixed porosity. Thus, it would be expected that a few realizations will display significantly different behavior, but that overall, the results using fixed porosity will not differ much from using dynamic creep closure.

Other performance measures for waste behavior are less affected by the dynamics of porosity changes. Based on the data currently available, gas generation is modeled as a direct function only of brine saturation, not of pressure. As shown earlier, the amount of gas generated, as well as the rate, is strongly influenced by the amount of brine present initially and relatively little by the amount of brine that flows into the repository over time. Porosities and pressures therefore have little effect on the amount of gas generated. Since gas generation is unaffected, the amount of reactants remaining in the waste over time is also unaffected by how the porosity of the waste is modeled.

4.3.2 Brine Flow Behavior

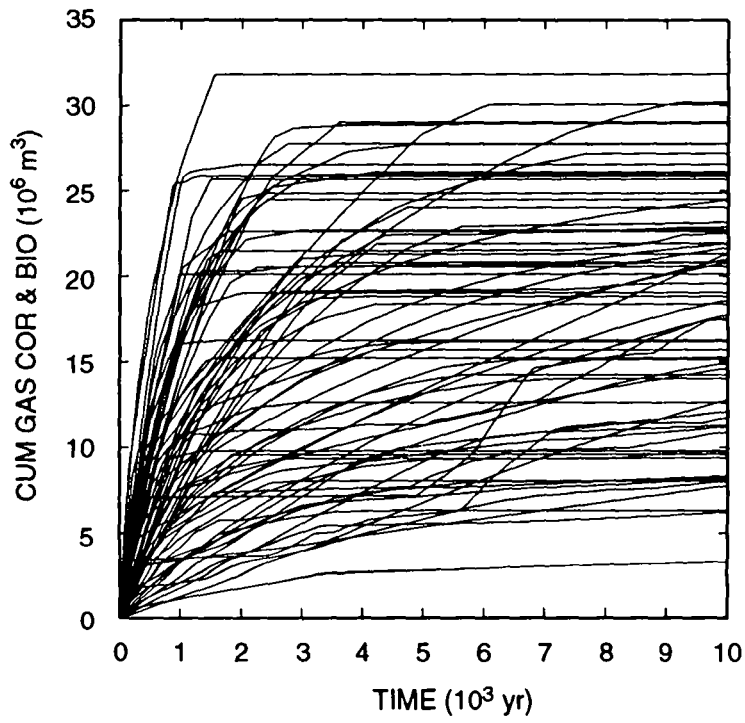
Differences in how the waste porosity is modeled should manifest themselves in fluid flow behavior outside the waste, as a result of differences in peak pressures. Because the initial brine volume is fixed between the two sets of calculations, the initial brine saturation is about 3.5 times higher in the fixed-porosity calculations. Whereas the original brine saturations range from zero to 0.14, where the maximum is half the residual brine saturation, now the initial saturations range as high as 0.48, well above residual saturation. This enables brine to flow from the waste in several of the realizations from the start (Figure 4-41), in contrast to the dynamic closure model, in which brine could flow out of the waste only after the repository has crept shut enough to raise the brine saturation above residual. (Brine could also flow out after first flowing in; this behavior is seen in both models.) With the porosity fixed, the number of realizations in which there is a net positive flow of brine from the repository is larger (25 versus 19), and the maximum outflow is greater (13,300 m³ compared with 11,400 m³ with dynamic closure). While this constitutes a larger source of contaminated brine, the key measure remains the distance this brine flows



TRI-6342-2785-0

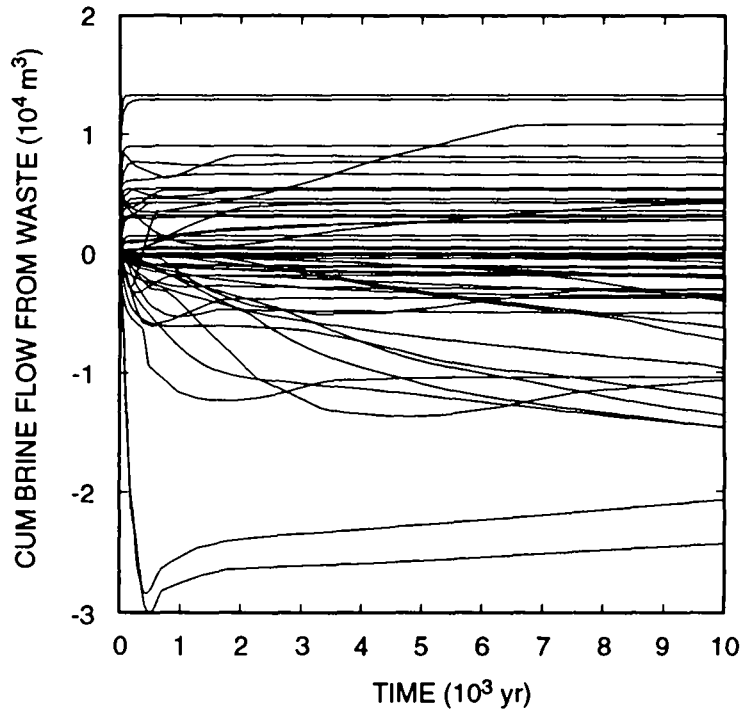
Figure 4-39. Volume Average Pressure in the Waste Repository, Fixed Waste Porosity Model.

4. Gas and Brine Migration



TRI-6342-2786-0

Figure 4-40. Cumulative Gas Volume Generated (at 30 °C; 0.101 MPa), Fixed Waste Porosity Model.



TRI-6342-2787-0

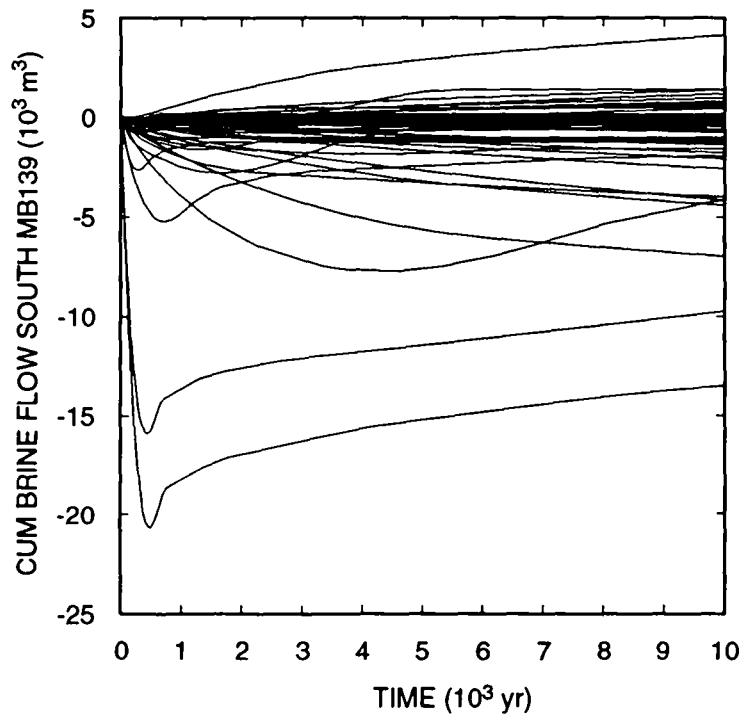
Figure 4-41. Cumulative Brine Flow from the Waste Repository, Fixed Waste Porosity Model. (Positive values indicate flow away from the repository.)

4. Gas and Brine Migration

1 toward the disposal-unit boundaries, and whether it reached the boundaries. In the fixed porosity results, the
2 maximum cumulative brine flows out each of the anhydrite layers in the southern direction are 7200 m³ out MB139
3 (the lowest curve in Figure 4-42, outflow occurs only after approximately 600 yr), zero out anhydrite a + b layer
4 (Figure 4-43), and 540 m³ out MB138 (Figure 4-44). These values differ little from the dynamic closure results
5 reported in Section 4.1.2 (6700 m³ for MB139, zero for anhydrite a + b, and 520 m³ for MB138). In MB139, the
6 realization having the greatest outflow has an anhydrite porosity of 0.0041 and a residual saturation of 0.20, both
7 sampled parameters. Thus, the residual brine in MB139 out to the disposal-unit boundary is 12,500 m³. Even if all
8 of the brine flowing out MB139 is contaminated, it will not even occupy all the volume required for residual brine
9 saturation, and will not reach the disposal-unit boundary. Residual brine occupies 2650 m³ of pore volume in
10 MB138 between the repository and the southern boundary in the realization with the maximum brine outflow, so,
11 again, the amount of potentially contaminated brine flowing south out MB138 will not reach the boundary. The
12 maximum upward brine flow through the shaft seal (Figure 4-45) is 58 m³, somewhat more than the 40 m³ in the
13 dynamic closure calculation, but still not enough to fill the lower shaft to the top of the Salado. Thus, none of the
14 brine flow performance measures shows any significant difference between dynamic creep closure and fixed waste
15 porosity.

16 4.3.3 Gas Flow Behavior

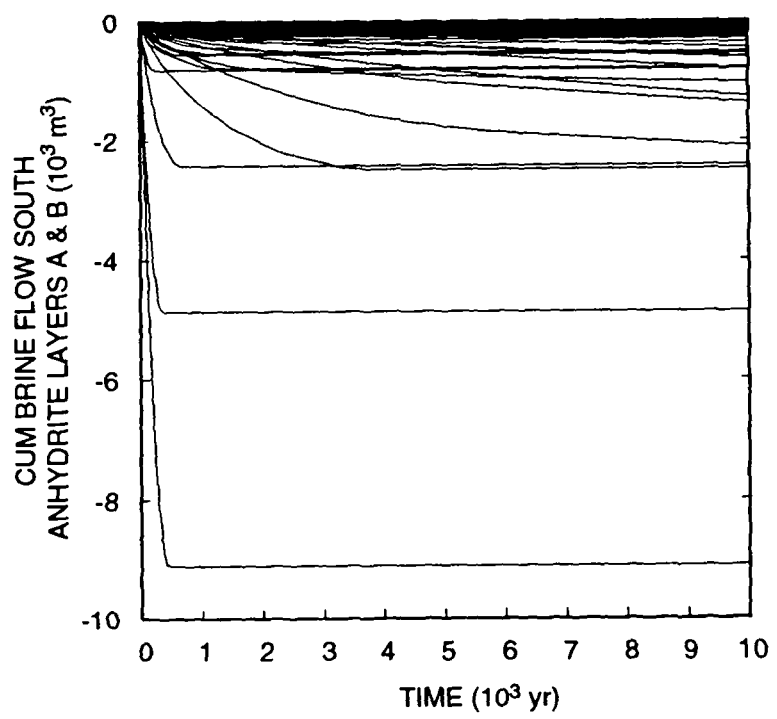
17 Cumulative gas flows out the anhydrite layers and through the shaft seal are similarly unaffected by repository
18 porosity dynamics. The high peak pressures that are obtained when the waste porosity is fixed occur because the
19 low permeability of these pathways prevents significant outflow of gas from the waste. It is only when the
20 permeability of the anhydrite is high that large volumes of gas can flow out these pathways, and in those cases, the
21 driving pressure remains relatively low. As pointed out earlier, it is ultimately the amount of gas generated that
22 causes the driving force for gas migration from the repository. After 10,000 yr, the pore volume of the waste differs
23 little regardless of how the pore volume dynamics are modeled because nearly the same final porosity is attained, so
24 the quantity of gas generated and the permeability of flow paths away from the waste are the controlling factors in
25 determining how far gas migrates. Figures 4-46, 4-47, 4-48, and 4-49 show the amount of gas that flows past the
26 disposal-unit boundary in MB139, anhydrite a + b, MB138, and the shaft seal, respectively. Comparing these with
27 their counterparts in Section 4.1.3 shows that the number of realizations in which gas migrated past the boundary is
28 the same and the total volumes are insignificantly different. Thus, none of the gas flow performance measures
29 shows any significant difference between fixed waste porosity and dynamic creep closure as currently modeled.
30 This conclusion may change when pressure-dependent fracturing of anhydrite interbeds is included in future
31 performance assessments, potentially lowering peak repository pressures and allowing for additional gas migration.



TRI-6342-2788-0

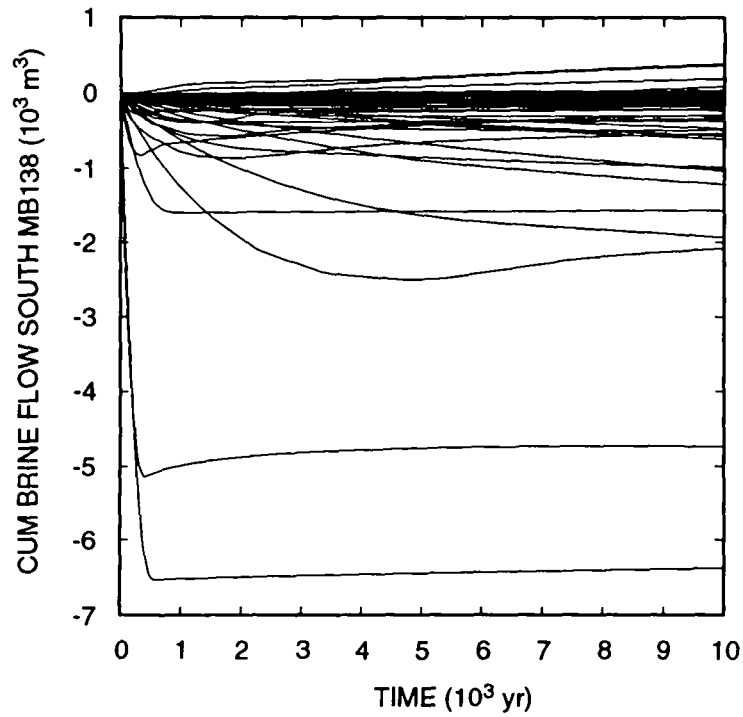
Figure 4-42. Cumulative Brine Flow South out MB139, Fixed Waste Porosity Model. (Positive values indicate flow southward away from the repository.)

4. Gas and Brine Migration



TRI-6342-2789-0

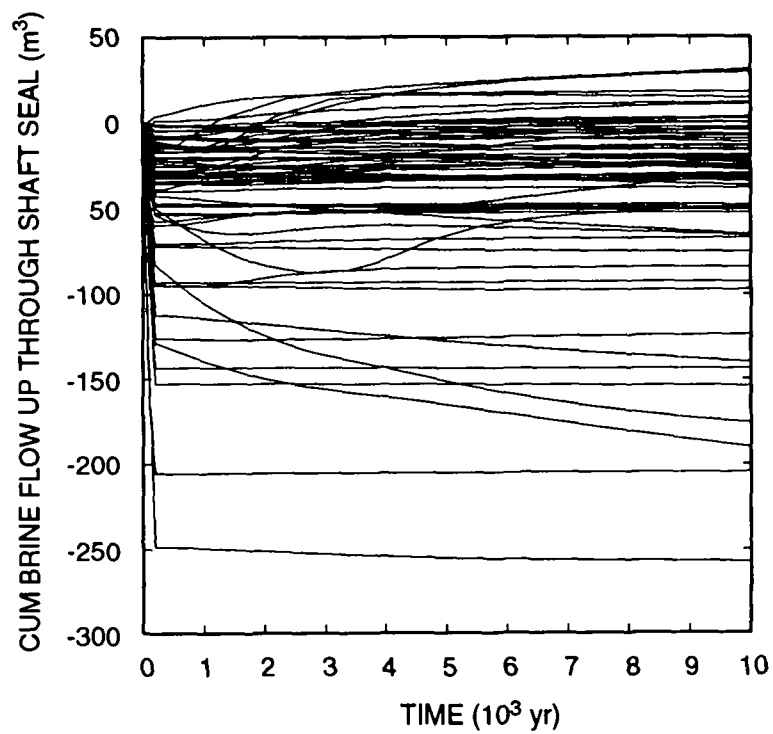
Figure 4-43. Cumulative Brine Flow South out Anhydrite Layers a + b, Fixed Waste Porosity Model. (Negative values indicate flow northward toward repository.)



TRI-6342-2790-0

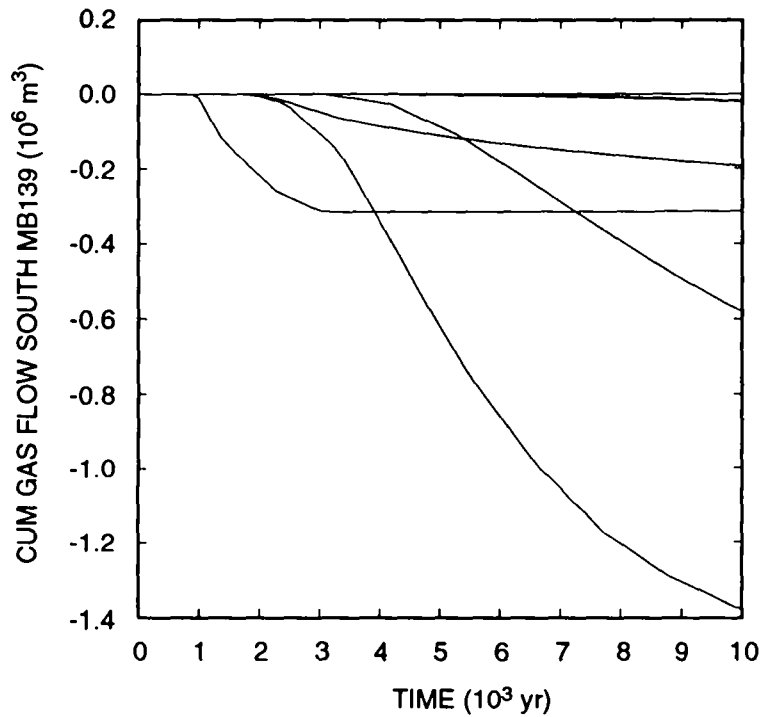
Figure 4-44. Cumulative Brine Flow South out MB138, Fixed Waste Porosity Model. (Negative values indicate flow northward toward repository.)

4. Gas and Brine Migration



TRI-6342-2791-0

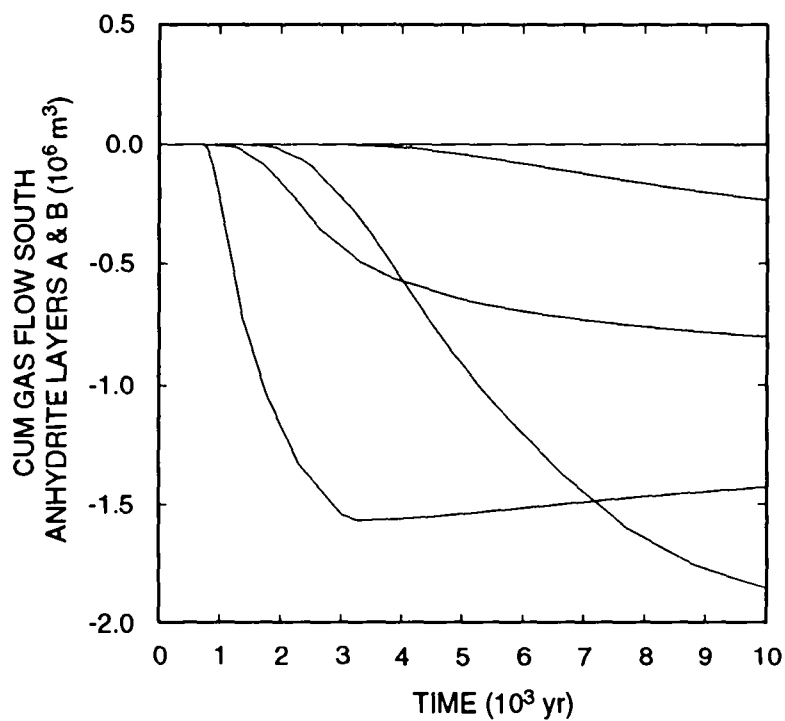
Figure 4-45. Cumulative Upward Brine Flow through Shaft Seal, Fixed Waste Porosity Model. (Positive values indicate flow upward through shaft seal.)



TRI-6342-2792-0

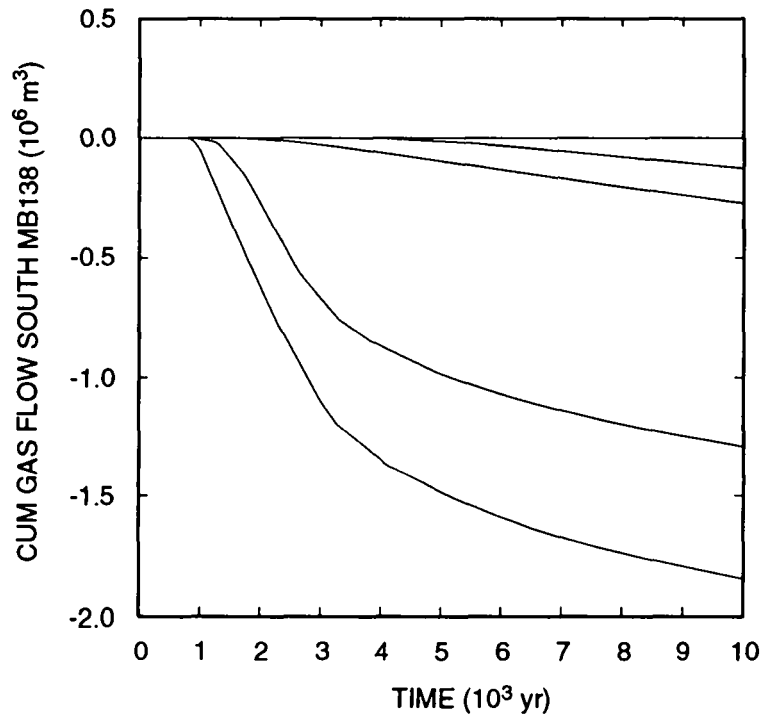
Figure 4-46. Cumulative Gas Flow South in Marker Bed 139 Past the WIPP Boundary (at 30 °C; 0.101 MPa), Fixed Waste Porosity Model. (Negative values indicate flow southward away from repository.)

4. Gas and Brine Migration



TRI-6342-2793-0

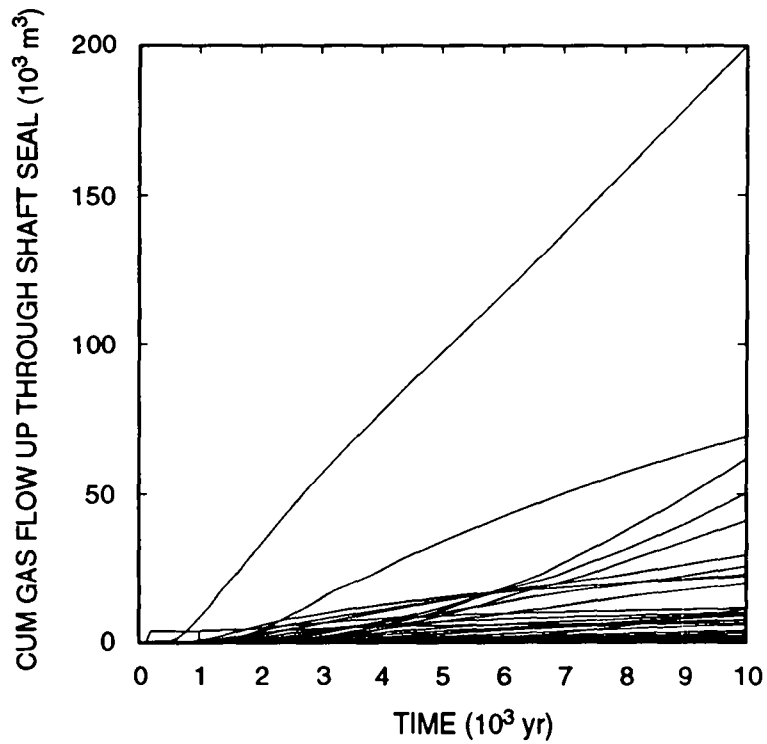
Figure 4-47. Cumulative Gas Flow South in Anhydrite Layers a + b Past the WIPP Boundary (at 30 °C; 0.101 MPa), Fixed Waste Porosity Model. (Negative values indicate flow southward away from repository.)



TRI-6342-2794-0

Figure 4-48. Cumulative Gas Flow South in MBI38 Past the WIPP Boundary (at 30 °C; 0.101 MPa), Fixed Waste Porosity Model. (Negative values indicate flow southward away from the repository.)

4. Gas and Brine Migration



TRI-6342-2795-0

Figure 4-49. Cumulative Upward Gas Flow through Shaft Seal (at 30 °C; 0.101 MPa), Fixed Waste Porosity Model.

5. UNCERTAINTY AND SENSITIVITY ANALYSIS RESULTS

Uncertainty and sensitivity analyses were performed to determine factors that affect gas generation and movement of gas and brine away from the repository. The uncertainty and sensitivity analyses in this presentation use techniques based on Latin hypercube sampling, including examination of scatterplots, partial correlation analysis, and stepwise regression analysis. Specific performance measures examined were cumulative gas and brine flows out through the three anhydrite layers to the south of the repository, cumulative gas and brine flows up through the shaft seal and the distance that gas flowed out through the three anhydrite layers. Only the base case, in which the four shafts were combined into one, was analyzed. Gas and brine flows to the north of the repository were not analyzed because they were generally smaller and, therefore, of less importance from a regulatory standpoint. Also examined were various measures of the behavior of the repository itself, including cumulative gas generation by means of corrosion and biodegradation, pressure in the repository, and repository pore volume. These were analyzed to show how gas generation is affected by variability in the sampled parameters, because gas generation is the driving force behind gas and brine migration away from the repository in the undisturbed scenario.

The results show that the most important parameter affecting gas and brine migration from the repository is the initial brine saturation in the waste. This one parameter has the greatest impact on total gas generation, which effectively controls gas and brine flow into and out of the waste. Other important parameters include the gas-generation rates for corrosion and biodegradation under inundated conditions and the biodegradation stoichiometry. These parameters also affect gas generation, but are secondary to initial brine content in determining the total amount of gas produced. Over the 10,000-yr regulatory period, it is the total volume of gas generated, rather than transient behavior such as pressure in the repository, that most affects how far gas and brine migrate. Thus, *rates* of gas generation are most important only if sufficient brine is available to consume all the reactants in the waste. Biodegradation stoichiometry (i. e., the moles of gas produced per mole of cellulose consumed) is important because its sampled range extends to zero, which can completely nullify the effect of biodegradation. Because the amount of gas produced by biodegradation is directly proportional to the stoichiometric coefficient, gas generation by biodegradation can vary greatly, and, all other things being equal, this parameter can have a major impact. The only other parameter of significance was the shaft-seal permeability, which, for the range sampled, impacts gas flow, but not brine flow, up the shaft. These conclusions are valid only over the ranges of all the parameters used in the calculations and within the limits of the conceptual and numerical models.

Numerous sampled parameters had no noticeable effect on any of the performance measures. These include all four of the relative permeability model parameters (Brooks-Corey exponent, Brooks-Corey weight factor, residual brine saturation, and residual gas saturation for all regions except the waste), the far-field pressure in MB139, the shaft seal thickness, drift seal permeability, shaft porosity, and Culebra porosity. As modeled, drift seals were not effective; higher-permeability DRZ layers above and below the drift seals allowed gas and brine to flow around, rather than through the drift seals, so performance was insensitive to the permeability of the seals. The porosity of the Culebra was also not tested adequately, because little gas and no brine from the waste reached the Culebra; when few realizations result in nonzero flow, the sensitivity to porosity cannot be properly analyzed.

5. Uncertainty and Sensitivity Analysis Results

1 The remaining 10 sampled parameters had, at most, a minor effect on these performance measures. These
2 parameters include: the gas-generation rates for corrosion and biodegradation under humid conditions; corrosion
3 stoichiometry; the initial volume fractions of biodegradables and metals in the waste; the porosity of anhydrite
4 interbeds; the DRZ porosity; the permeabilities of halite and the shaft seal during the first 200 yr; and the
5 permeability of the shaft between the shaft seal and the Culebra during the first 200 yr.

6 These results are strongly dependent on the conceptual models that are currently used. If the conceptual models
7 were modified, the results could differ from those presented here.

8 Each of the performance measures is discussed separately below.

5.1 Sensitivity Analysis Techniques

11 The purpose of sensitivity analysis is to determine the relationships between the uncertainty in the independent
12 variables used in an analysis and the uncertainty in the resultant dependent variables. Uncertainty analysis provides
13 measures of the uncertainty in estimates for dependent variables of interest, including means, variances, and
14 distribution functions. A formal uncertainty analysis is not presented here because such an analysis is not
15 particularly useful in determining relationships among variables. However, uncertainty analysis is incorporated in
16 the sensitivity analysis. This section describes briefly the sensitivity analysis techniques used, including
17 scatterplots, stepwise regression analysis, and partial correlation analysis. A more detailed discussion of these
18 techniques and their application to the WIPP project can be found in Helton et al. (1991).

19 The generation of scatterplots is the simplest sensitivity analysis technique. This approach consists of
20 generating plots of dependent variable value versus independent variable value, with each point on the plot
21 representing one realization. When there is no relationship between the independent and dependent variable, the
22 individual points will be randomly spread over the plot. In contrast, the existence of a well-defined relationship
23 between the independent and dependent variable often will be revealed by the distribution of the individual points.
24 The examination of such plots when Latin hypercube sampling is used can be particularly revealing because of the
25 full stratification over the range of each independent variable. For each dependent variable examined in this
26 chapter, scatterplots are presented only for the two most influential independent variables. As the contribution of
27 additional independent variables to the variability of the dependent variable decreases, the distribution of points in
28 the scatterplots becomes more random and less useful, so additional plots are not presented.

29 In stepwise regression analysis, a sequence of regression models is constructed. The first regression model
30 contains the single independent variable that has the largest impact on the dependent variable. The second
31 regression model contains the two independent variables that have the largest impact on the dependent variable —
32 the independent variable from the first step plus whichever of the remaining variables has the largest impact on the
33 variation not accounted for by the first step. Additional models in the sequence are constructed in the same manner
34 until a point is reached at which further models are unable to increase meaningfully the amount of variation in the
35 dependent variable that can be accounted for. The order in which the variables are selected in the stepwise
36 procedure provides an indication of variable importance, with the most important variables being selected first, the
37 next most important variable being selected second, and so on. The R^2 values (coefficients of determination)
38 indicate how much variation in the dependent variable can be accounted for by all variables selected through that

another step in the regression analysis. When the variables are independent and uncorrelated, as they are assumed to be here, the differences in the R^2 values for each step in the regression models equals the fraction of the total variability in the dependent variable that can be accounted for by the individual independent variable added at each step. When the variation about the regression model is small, the corresponding R^2 value is close to 1, which indicates that the regression model is accounting for most of the variability in the dependent variable. Conversely, an R^2 value close to zero indicates that the regression model is not very successful in accounting for the variability in the dependent variable. In addition to R^2 values, standardized regression coefficients (SRCs) in the individual regression models provide an indication of variable importance, and the sign of the SRC indicates whether the independent and dependent variable tend to increase and decrease together (a positive SRC) or tend to move in opposite directions (a negative SRC).

The statistical program, STEPWISE (Iman et al., 1980; Rechar, 1992), was used to evaluate variable importance using the stepwise regression procedure on rank-transformed data. Regression analyses often perform poorly when the relationships between the independent and dependent variables are nonlinear. Poor linear fits to nonlinear data can often be avoided when the data are replaced with their corresponding ranks and the regression procedures are performed on these ranks (Iman and Conover, 1979). In most cases, the analyses were tried with both raw and ranked data. The rank regressions generally gave better results, meaning that the rank regression models could account for higher percentages of the observed variability in the dependent variables. Only the rank regression analyses are reported, although raw data are shown in the scatterplots.

Stepwise regression analyses were performed on results at the end of the 10,000-yr simulations. Tables 5-1 and 5-2 summarize the variables used in the stepwise regression analysis. It is necessary to have some criterion to stop the regression model construction process. These are discussed in Helton et. al. (1991). In the analyses reported here, an α -value of 0.02 was used to add a variable to the regression model and a value of 0.05 to drop a variable from the model. (The α -value is the probability of obtaining a stronger relationship than the one identified in the analysis as a result of chance variation.) In addition, the Predicted Error Sum of Squares (PRESS) criterion was used to protect against overfit.

Partial correlation analysis provides measures of the linear relationship between a dependent variable and an independent variable when the linear effects of the other independent variables are removed. When a well-defined linear relationship exists between an independent variable and a dependent variable, the partial correlation coefficient will be close to +1 or -1, regardless of the distribution assigned to the independent variable or the magnitude of the impact that the independent variable has on the dependent variable. A positive partial correlation coefficient indicates that two variables tend to increase and decrease together, whereas a negative correlation coefficient indicates that, as one variable increases, the other decreases. Partial correlation coefficients were calculated using time-dependent results, such as those shown in figures in Chapter 4, and show how the impact of different independent variables changes over time. These analyses complement the stepwise regression analyses, which provide more detailed statistics but at a single time. Note that because variables change in importance through time the regression analyses and partial correlation coefficient analyses may identify different variables as being important.

The partial correlation analyses were done using the statistical module PCCSRC (Iman et al., 1985; Rechar, 1992). As with the stepwise regression analyses, these analyses were performed on rank-transformed data. For each dependent variable, a plot of the partial rank correlation coefficients is presented that shows the time dependence of the coefficient for the four most influential independent variables.

5. Uncertainty and Sensitivity Analysis Results

1

2 Table 5-1. Latin Hypercube Sampled Independent Variables Used in Stepwise Regression and Partial
3 Correlation Analyses^a

4

Independent Variables	LHS No.	Description
BCBRSAT	13	Residual brine saturation in all regions except waste
BCEXP	11	Brooks-Corey exponent
BCFLG	12	Brooks-Corey/van Genuchten-Parker weighting factor
BCGSSAT	14	Residual gas saturation in all regions except waste
BKFLPOR	26	Porosity of backfill material in drifts, the experimental region, and in the shaft below the seal
BRSAT	1	Initial brine saturation in waste
CULPOR	27	Culebra porosity
DSEALPRM	25	Permeability of drift seals
GRCORHF	3	Humid corrosion rate factor
GRCORI	2	Inundated corrosion rate
GRMICHF	6	Humid biodegradation rate factor
GRMICI	5	Inundated biodegradation rate
MBPERM	15	Log of anhydrite interbeds permeability
MBPOR	16	Undisturbed anhydrite interbeds porosity
MBPRES	18	Far-field pressure in MB139
SALPERM	10	Intact Salado halite permeability
SEALPRM1	22	Initial shaft seal permeability
SEALPRM2	23	Shaft seal permeability after 200 yr

1 Table 5-1. Latin Hypercube Sampled Independent Variables Used in Stepwise Regression and Partial
 2 Correlation Analyses (Concluded)

Independent Variables	LHS No.	Description
SEALTHK	21	Shaft seal thickness
SHFTPRM	24	Permeability of shaft-fill material above shaft seal
STOICCOR	4	Corrosion stoichiometry factor
STOICMIC	7	Biodegradation stoichiometric coefficient
TZPORF	17	Factor used in calculating DRZ and transition zone porosity
VMETAL	9	Initial volume fraction iron in waste
VWOOD	8	Initial volume fraction cellulose in waste

4
 5 ^a Ranges of values for independent variables are given in Table 3-1. Sampled values are given in
 6 Appendix B

7
 8
 9
 10 Table 5-2. Latin Hypercube Sample Dependent Variables Used in Stepwise Regression and Partial
 11 Correlation Analyses

Dependent Variables	Description
BIOCONT	Cellulose remaining in waste
BRNANHSC	Cumulative brine flow south of repository out anhydrite layers a + b
BRNMB8SC	Cumulative brine flow south of repository out MB138

5. Uncertainty and Sensitivity Analysis Results

1 Table 5-2. Latin Hypercube Sample Dependent Variables Used in Stepwise Regression and Partial
 2 Correlation Analyses (Continued)

3

Dependent Variables	Description
BRNMB9SC	Cumulative brine flow south of repository out MB139
BSHSLUPC	Cumulative brine flow up through shaft seal
BWSTC	Cumulative brine flow from waste
FECONT	Iron remaining in waste
GASANHSC	Cumulative gas flow south of repository out anhydrite layers a + b
GASGENVC	Cumulative gas generated by corrosion and biodegradation
GASMB8SC	Cumulative gas flow south of repository out MB138
GASMB9SC	Cumulative gas flow south of repository out MB139
GASCULTC	Cumulative gas flow into Culebra from shaft
GDSTANHS	Distance from waste that gas flowed south in anhydrite layers a + b
GDSTCULS	Distance from shaft that gas flowed south in Culebra
GDSTMB8S	Distance from waste that gas flowed south in MB138
GDSTMB9S	Distance from waste that gas flowed south in MB139
GSHSLUPC	Cumulative gas flow up through shaft seal
GWSTC	Cumulative gas flow from waste
PORVOLW	Pore volume in waste
PRESWAST	Average pressure in waste
QRGBIOVC	Cumulative gas generated by inundated and humid biodegradation
QRGCORVC	Cumulative gas generated by inundated and humid corrosion
QRHCUMGB	Cumulative gas generated by humid biodegradation

Table 5-2. Latin Hypercube Sample Dependent Variables Used in Stepwise Regression and Partial Correlation Analyses (Concluded)

Dependent Variables	Description
QRHCUMGC	Cumulative gas generated by humid corrosion
QRSCUMGB	Cumulative gas generated by inundated biodegradation
QRSCUMGC	Cumulative gas generated by inundated corrosion
SBAVW	Volume-average brine saturation in waste

5.2 Gas Generation and Repository Performance

In this section, factors that affect gas generation are examined. The focus is on parameters influencing corrosion and microbial degradation. In addition, variables that affect repository performance, including pressure, reactant concentrations, pore volume, and brine saturation, will be determined. Although gas generation and repository behavior are not compliance measures *per se*, it is useful to know how these are affected so that they can, if necessary, be controlled.

5.2.1 Gas Generation from Inundated Corrosion

The regression analysis results in Table 5-3 are for cumulative gas generation resulting from inundated corrosion over 10,000 yr. The first variable selected in the analysis is BRSAT, the initial brine saturation in the waste, which has a positive regression coefficient and can account for 49% of the variability in gas generation by inundated corrosion. The partial rank correlation coefficients shown in Figure 5-1 further support the dominating effect that initial brine saturation has on inundated corrosion. This result is discussed in Section 4.1.1, in which it is apparent even in the behavior of brine saturation in the repository over time that initial brine saturation is the controlling factor.

The next variable selected in the regression analysis is GRCORHF, the humid corrosion rate factor that is multiplied by the inundated rate to give the actual humid corrosion rate. This variable has a negative regression coefficient, indicating that it has an inhibiting effect on gas generation by inundated corrosion. This effect continues increasingly over the 10,000-yr simulation period, as shown in the plot of partial rank correlation coefficients in Figure 5-1. This increasing effect occurs because humid corrosion competes with inundated corrosion. It dominates inundated corrosion, especially later on, because inundated corrosion is limited by the amount of brine present. As long as any amount of brine is present, humid corrosion can proceed at a rate that is proportional to the gas saturation. Except at early times when the brine saturation is relatively large it is more common for the waste to be mostly dry, so humid corrosion will generate gas faster than inundated corrosion. The humid corrosion rate factor contributes another 20% of the variability in gas generation by inundated corrosion.

5. Uncertainty and Sensitivity Analysis Results

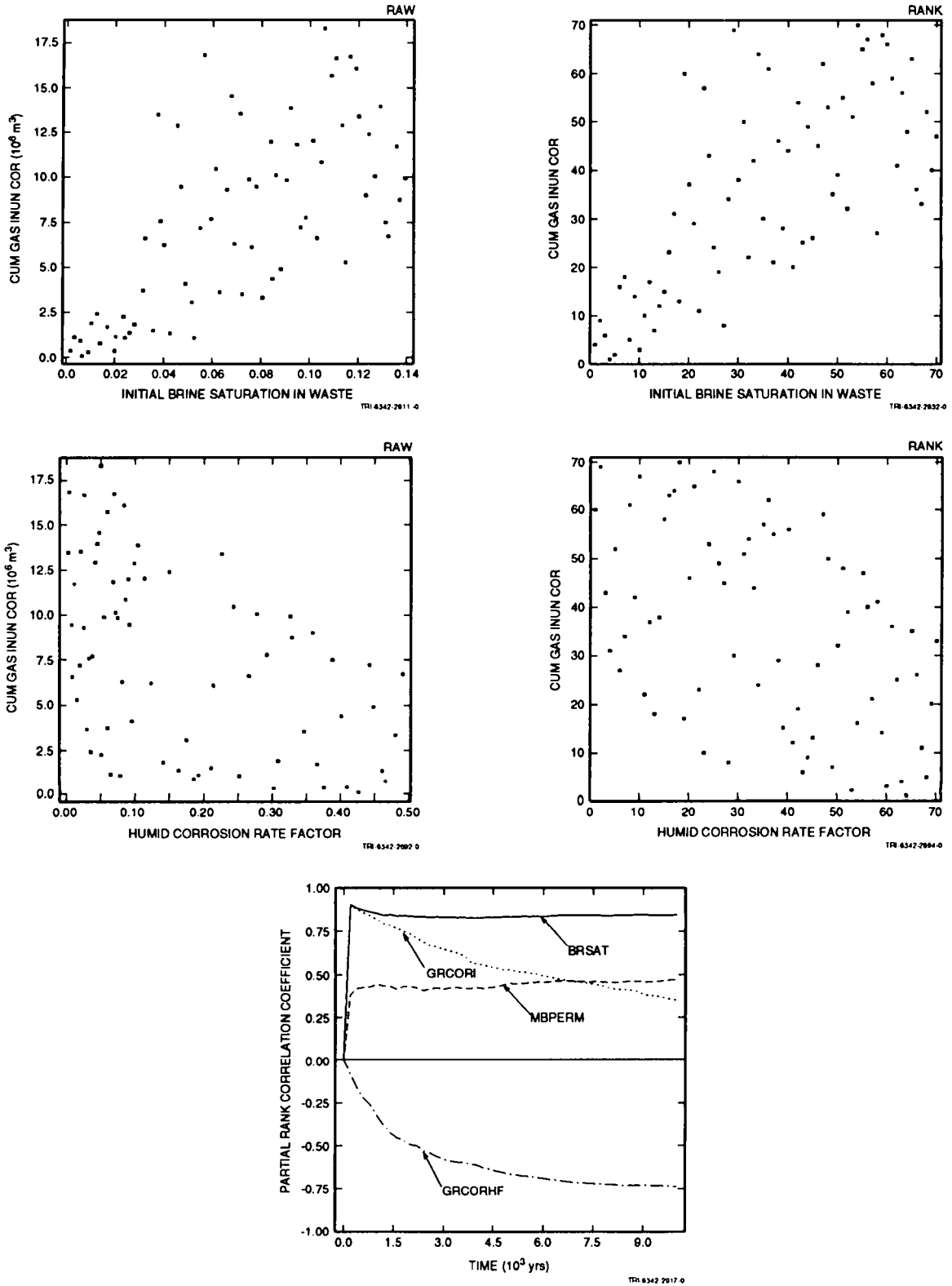


Figure 5-1. Scatterplots and partial rank correlation coefficients for gas generation from inundated corrosion.

The other two variables selected in the analysis, MBPERM (anhydrite permeability) and GRCORI (inundated corrosion rate), play a relatively minor role in affecting inundated corrosion. The small effect of the inundated corrosion rate on inundated corrosion is, in part, a result of the current model used for gas generation and corrosion, in which the inundated rate is proportional to the brine saturation. Because brine saturation tends to decrease over time, the net inundated rate decreases, becoming relatively unimportant after 10,000 yr. These results may not hold true using a different corrosion model, but sufficient data do not yet exist to warrant changing the model.

Scatterplots relating cumulative gas generation to the two dominant variables, BRSAT and GRCORHF, are shown in Figure 5-1. While these two together account for 69% of the variability in gas generation by inundated corrosion, it is apparent from these plots that neither variable is a reliable predictor of gas generation, even though some correlation is evident.

Table 5-3. Stepwise Regression Analysis with Rank-Transformed Data for Total Gas Production Resulting from Inundated Corrosion (QRSCUMGC)

Step	Variable	Description	SRC ^a	R ^{2b}
1	BRSAT	Initial brine saturation in waste	0.68	0.49
2	GRCORHF	Humid corrosion rate factor	-0.47	0.69
3	MBPERM	Log of anhydrite interbeds permeability	0.25	0.75
4	GRCORI	Inundated corrosion rate	0.16	0.78

^a Standard regression coefficients (SRC) for variables in the regression model at each step

^b R² value for the regression model at each step

5.2.2 Gas Generation from Humid Corrosion

Unlike gas generation by inundated corrosion, gas generation by humid corrosion is a fairly strong function of the rate of humid corrosion. (See Volume 3, Section 3.3.5 for a description of the current gas generation model and parameters used in the model.) In Table 5-4, the first variable selected in the regression analysis for gas generation by humid corrosion is GRCORHF, the factor multiplying the inundated rate to obtain the humid corrosion rate. This variable accounts for 64% of the variability in gas generation by humid corrosion. The next variable selected is the inundated corrosion rate, GRCORI. Together, these rate parameters account for 75% of the variability. The regression coefficient for GRCORI is positive now, because humid corrosion does not occur unless inundated corrosion is taking place at the same time. Recall that the corrosion model requires brine to be present for humid corrosion to occur, even though the humid corrosion rate is modeled as proportional to gas saturation.

5. Uncertainty and Sensitivity Analysis Results

The initial brine saturation in the waste, BRSAT, is a less-important variable, accounting for only an additional 8% of the variability in gas generation by humid corrosion. The plot of partial rank correlation coefficients in Figure 5-2 shows that BRSAT had a negative effect at first, becoming significantly positive only after about 3000 yr. This results from the changing relative importance of inundated corrosion compared with humid corrosion. Initially, when the brine saturation is usually highest, the total reaction rate is dominated by the inundated reaction. Later, as the brine saturation in the waste decreases, having been consumed predominantly by inundated corrosion, humid corrosion becomes more important.

Scatterplots of the first two variables selected in the regression analysis, Figure 5-2, show some clear trends for the first variable, GRCORHF. The correlation is much weaker for the second variable, GRCORI.

Table 5-4. Stepwise Regression Analysis with Rank-Transformed Data for Total Gas Production Resulting from Humid Corrosion (QRHCUMGC)

Step	Variable	Description	SRC	R ²
1	GRCORHF	Humid corrosion rate factor	0.79	0.64
2	GRCORI	Inundated corrosion rate	0.32	0.75
3	BRSAT	Initial brine saturation in waste	0.29	0.83

5.2.3 Gas Generation from Inundated and Humid Corrosion

When both inundated and humid corrosion are considered together, the regression analysis selects BRSAT first, accounting for 56% of the variability in gas generation by corrosion. This suggests that corrosion under inundated conditions contributes more to the amount of gas produced by corrosion than humid conditions, since BRSAT has a strong positive impact on inundated corrosion, but only a weak effect on humid corrosion. The scatterplot relating cumulative gas generation by corrosion to initial brine saturation in the waste, Figure 5-3, shows a clear trend, even more so than for inundated corrosion alone, with the amount of gas generated increasing as the initial brine saturation increases. The plot of partial rank correlation coefficients in Figure 5-3 shows that BRSAT has a strong effect throughout the 10,000 yr, although other variables were slightly more important at first, when inundated corrosion was not yet inhibited by a lack of brine.

The inundated corrosion rate, GRCORI, was selected next, accounting for an additional 11% of the variability in gas generation by corrosion. The scatterplot relating cumulative gas generation by corrosion after 10,000 yr to inundated corrosion rate in Figure 5-3, however, shows only the slightest of trends to increasing gas generation as the rate increases. As shown in the plot of partial rank correlation coefficients, Figure 5-3, GRCORI has the greatest impact during the first 3000 yr, when adequate sources of brine remain from the initial brine saturation. Its influence gradually decreases from the start, as brine is consumed.

5.2 Gas Generation and Repository Performance

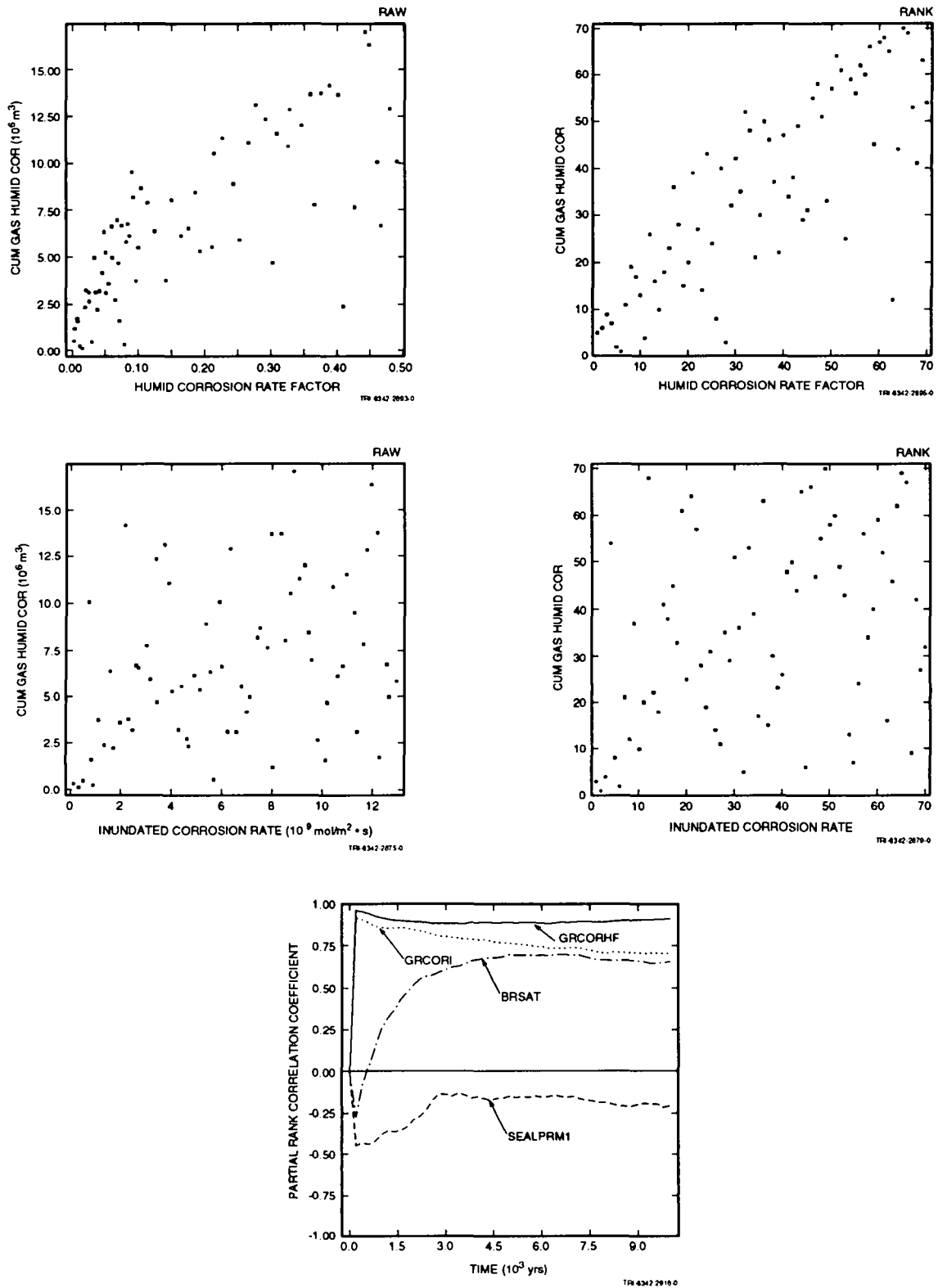


Figure 5-2. Scatterplots and partial rank correlation coefficients for gas generation from humid corrosion.

5. Uncertainty and Sensitivity Analysis Results

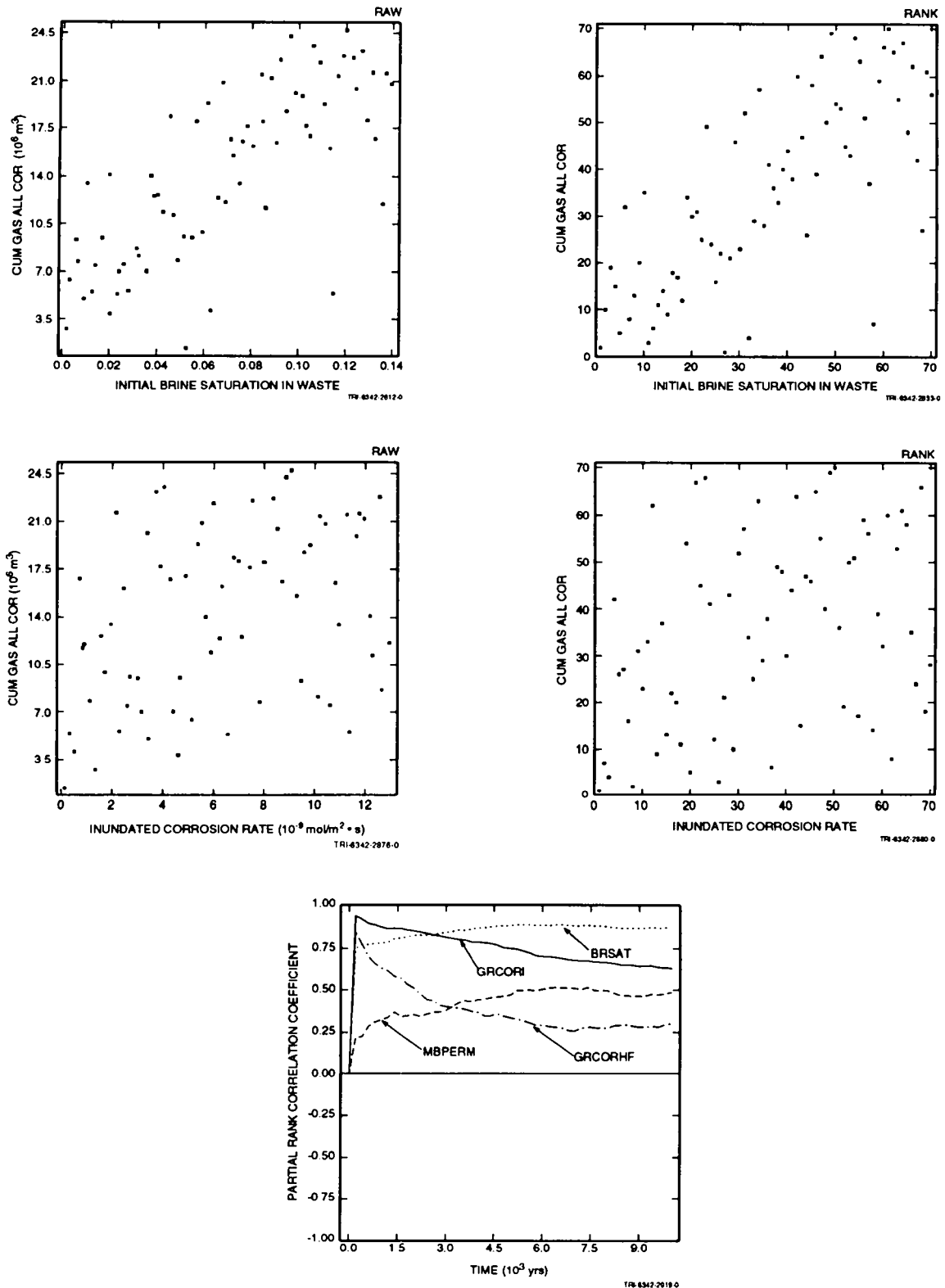


Figure 5-3. Scatterplots and partial rank correlation coefficients for gas generation from inundated and humid corrosion.

The regression analysis (Table 5-5) selected three more variables as having some measurable effect on total gas generation by corrosion: MBPERM, the permeability of anhydrite interbeds; STOICCOR, a factor that determines the relative importance of two corrosion reactions and thus the stoichiometry for corrosion; and GRCORHF, the humid corrosion rate factor. Together, these three account for an additional 12% of the variability in gas generation by corrosion. The linear correlation with five variables accounts for 79% of the variability. STOICCOR has a negative correlation coefficient, indicating that as this variable increases, gas generation decreases. This occurs because the corrosion stoichiometric coefficient, or the moles of gas generated per mole of iron consumed, decreases as STOICCOR increases: the stoichiometric coefficient has a value of 1.333 when STOICCOR is 1.0, and a value of 1.0 when STOICCOR is 0. The minor effect of STOICCOR stems from the relatively narrow range of values taken by the stoichiometric coefficient. Anhydrite permeability has a small effect on gas generation by affecting the amount of brine that can flow into the repository and contribute to additional corrosion. As discussed in Section 4.1.1, little brine flows into the waste in general, so the effect is not great.

Table 5-5. Stepwise Regression Analysis with Rank-Transformed Data for Total Gas Production Resulting from Both Inundated and Humid Corrosion (QRGCRVC)

Step	Variable	Description	SRC	R ²
1	BRSAT	Initial brine saturation in waste	0.74	0.56
2	GRCORI	Inundated corrosion rate	0.33	0.67
3	MBPERM	Log of anhydrite interbeds permeability	0.24	0.73
4	STOICCOR	Corrosion stoichiometry factor	-0.17	0.76
5	GRCORHF	Humid corrosion rate factor	0.16	0.79

5.2.4 Gas Generation from Inundated Biodegradation

The sensitivity analysis done for gas generation by corrosion is repeated for gas generation by biodegradation. For inundated biodegradation, the regression analysis in Table 5-6 selected STOICMIC, the biodegradation stoichiometric coefficient, as the most important variable. This variable accounts for 36% of the variability in gas generation by inundated biodegradation. The scatterplot relating cumulative gas generation to this variable, Figure 5-4, shows a definite trend, with the amount of gas generated increasing as STOICMIC increases. This result is exactly as expected, since this is the definition of the stoichiometric coefficient (moles of gas produced per mole of cellulose consumed).

5. Uncertainty and Sensitivity Analysis Results

1 This analysis found eight variables having a measurable effect, although the additional influence of each of the
 2 last five is very slight. As with inundated corrosion, biodegradation under inundated conditions requires brine to be
 3 present, although biodegradation is currently assumed not to consume water. Thus, the next most important
 4 variable selected is BRSAT, which shows a trend similar to that for STOICMIC, but less pronounced. As expected,
 5 the inundated biodegradation rate, GRMICI, is one of the more important variables, but it is surprising that it
 6 accounts for only 8% of the variability in gas production by inundated biodegradation. As the partial rank
 7 correlation coefficient plot in Figure 5-4 shows, GRMICI was the dominant variable early, but its influence
 8 decreased steadily over the first 1000 yr as brine in the waste was consumed. In addition, as seen earlier in Figure
 9 4-6, much of the cellulose in the waste was fully consumed within that same time period, which explains why the
 10 curves in the plot of partial rank correlation coefficients are flat after about 1500 yr. GRCORHF has a negative
 11 regression coefficient, indicating that humid corrosion competes with inundated biodegradation by consuming brine
 12 needed for inundated biodegradation. As the partial rank correlation coefficient plot shows, GRCORHF becomes
 13 significant only after the microbial rate becomes less significant. At later times, humid corrosion tends to consume
 14 the remaining brine required for any further inundated biodegradation.

15 Table 5-6. Stepwise Regression Analysis with Rank-Transformed Data for Total Gas Production
 16 Resulting from Inundated Biodegradation (QRSCUMGB)

Step	Variable	Description	SRC	R ²
1	STOICMIC	Biodegradation stoichiometric coefficient	0.61	0.36
2	BRSAT	Initial brine saturation in waste	0.42	0.53
3	GRMICI	Inundated biodegradation rate	0.28	0.61
4	GRCORHF	Humid corrosion rate factor	-0.22	0.65
5	BCEXP	Brooks-Corey exponent	0.18	0.69
6	GRMICHF	Humid biodegradation rate factor	0.20	0.72
7	VWOOD	Initial volume fraction cellulose in waste	-0.18	0.75
8	SEALPRM2	Shaft seal permeability after 200 yr	0.17	0.78

5.2 Gas Generation and Repository Performance

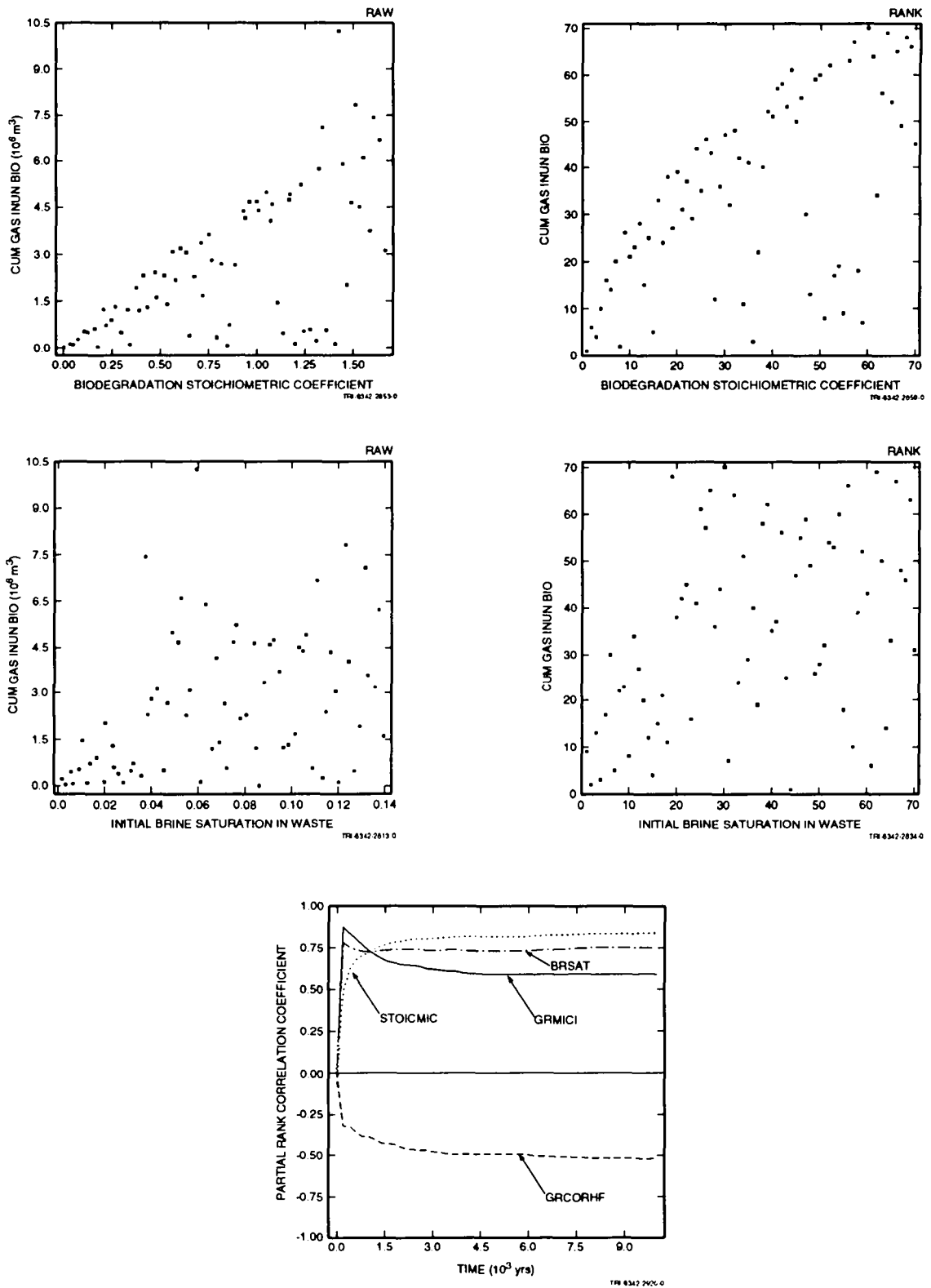


Figure 5-4. Scatterplots and partial rank correlation coefficients for gas generation from inundated biodegradation.

5.2.5 Gas Generation from Humid Biodegradation

The regression analysis in Table 5-7 is for cumulative gas generation by humid biodegradation. As with humid corrosion, humid biodegradation, as currently modeled, requires brine to be present. However, as with inundated biodegradation, it is assumed to consume no brine, in contrast to corrosion, in which both inundated and humid reactions consume brine. The first variable selected in the regression analysis is STOICMIC, the biodegradation stoichiometric coefficient. It accounts for only 29% of the variability in gas generation by humid biodegradation, making it somewhat less important here than in inundated biodegradation, although the scatterplot in Figure 5-5 still shows a clear trend. As it was under inundated conditions, STOICMIC is important because it strongly affects the amount of gas produced for a given amount of reactants. The second variable selected, GRMICHF (humid biodegradation rate factor), contributes nearly as much as STOICMIC to the variability in cumulative gas generation by humid biodegradation. The scatterplot for this variable also shows an apparent trend, but with more scatter than shown by STOICMIC. The partial rank correlation coefficients in Figure 5-5 show STOICMIC becoming more important apparently at the expense of the inundated biodegradation rate, GRMICI, which dominated at first. The inundated corrosion rate, GRCORI, has a very small positive effect on gas generation by humid biodegradation by consuming brine, thereby increasing the gas saturation, which results in more gas production under humid, rather than inundated conditions.

Table 5-7. Stepwise Regression Analysis with Rank-Transformed Data for Total Gas Production Resulting from Humid Biodegradation (QRHCUMGB)

Step	Variable	Description	SRC	R ²
1	STOICMIC	Biodegradation stoichiometric coefficient	0.55	0.29
2	GRMICHF	Humid biodegradation rate factor	0.50	0.53
3	GRMICI	Inundated biodegradation rate	0.34	0.64
4	GRCORI	Inundated corrosion rate	0.20	0.68

5.2 Gas Generation and Repository Performance

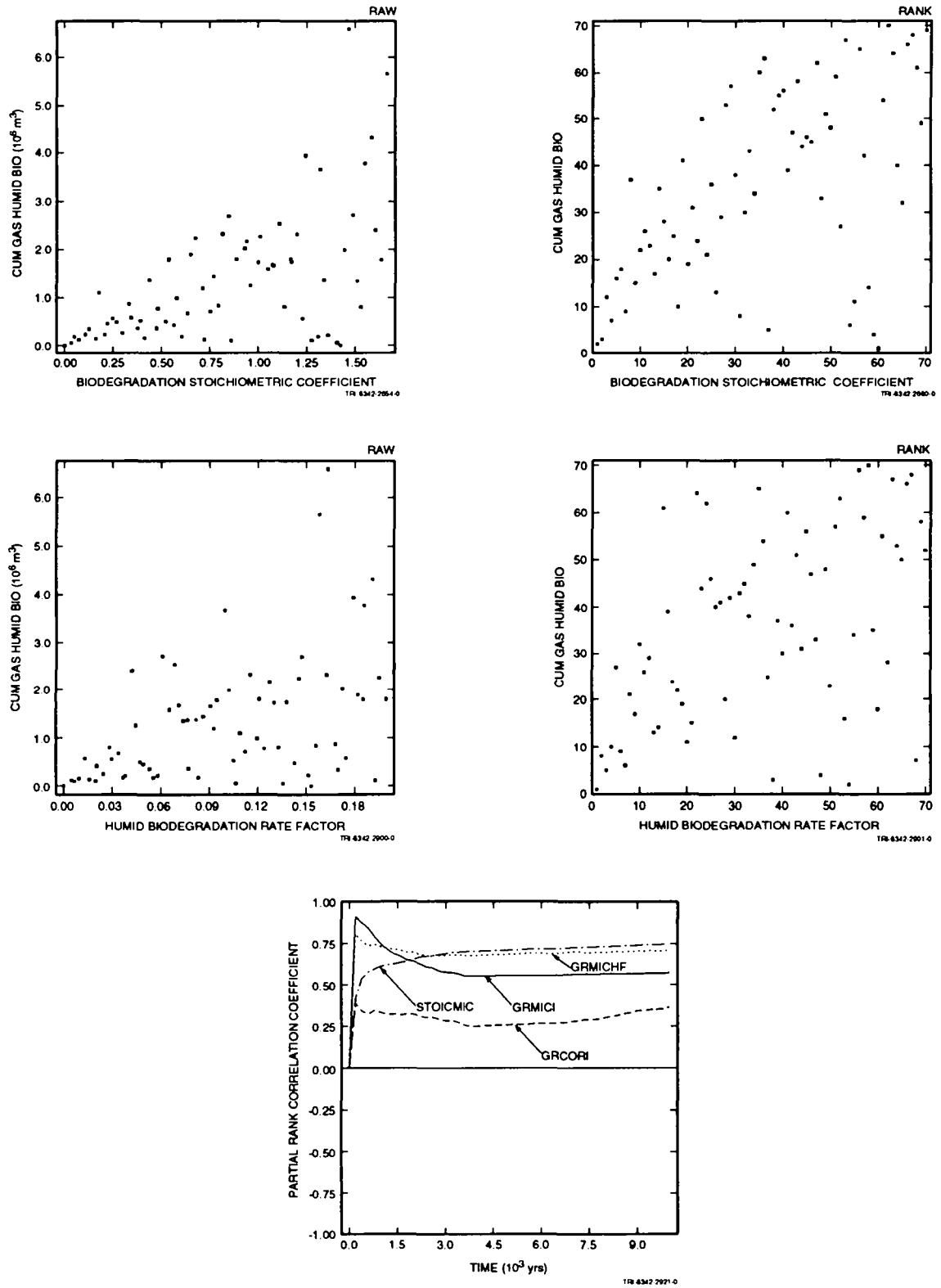


Figure 5-5. Scatterplots and partial rank correlation coefficients for gas generation from humid biodegradation.

5.2.6 Gas Generation from Inundated and Humid Biodegradation

The regression analysis for cumulative gas generation by both inundated and humid biodegradation, shown in Table 5-8, selected STOICMIC as the dominant variable in determining the variability of gas generation. It accounts for 50% of the variability. The scatterplot relating gas generation to biodegradation stoichiometry, in Figure 5-6, confirms the strong influence that stoichiometry has on the amount of gas generated. Because STOICMIC was most influential under both inundated and humid conditions, this result is not surprising.

The next variable selected, GRMICI, contributes another 14% to the variability in gas generation. GRMICI plays a measurably significant, if minor, role because a large portion of the gas produced by biodegradation takes place under inundated conditions. This can be deduced from Figures 4-2 and 4-6, which show the time-dependent behavior of brine saturation in the waste and cellulose content remaining in the waste, respectively. However, its scatterplot indicates that the effect is not very strong.

The influence of initial brine saturation, BRSAT, is understandable, because, in the absence of a large influx of brine from outside the waste, initial brine saturation essentially provides the driving force for biodegradation. However, it actually contributes very little to the variability of total gas generation from biodegradation, only 4%. The partial rank correlation coefficients in Figure 5-6 show the same trends as for inundated and humid biodegradation separately, with the inundated rate, GRMICI, dominating at first, to be superseded later by STOICMIC. This ordering of influence consistently occurs because, as brine and reactants (cellulose) are depleted, the amount of gas produced per unit quantity of reactant has an increasingly greater impact on total gas generated, whereas the *rate* becomes irrelevant. Gas generation per unit of reactant, as measured by the stoichiometric coefficient, also has a far greater impact than potential. The original basis for potential, VWOOD (the volume fraction of cellulose in the initial inventory), has no discernible effect because the stoichiometry, which ranges from 0.0 to 1.67, completely determines how much of this initial cellulose inventory will be converted to gas. This will be true as long as any cellulose is present initially. If the initial cellulose content of the waste were also varied over a range that extended to zero, it could possibly become as important as STOICMIC in determining the variability in

Table 5-8. Stepwise Regression Analysis with Rank-Transformed Data for Total Gas Production Resulting from Both Inundated and Humid Biodegradation (QRGBIOVC)

Step	Variable	Description	SRC	R ²
1	STOICMIC	Biodegradation stoichiometric coefficient	0.70	0.50
2	GRMICI	Inundated biodegradation rate	0.38	0.64
3	BRSAT	Initial brine saturation in waste	0.23	0.69
4	GRCORHF	Humid corrosion rate factor	-0.18	0.72

5.2 Gas Generation and Repository Performance

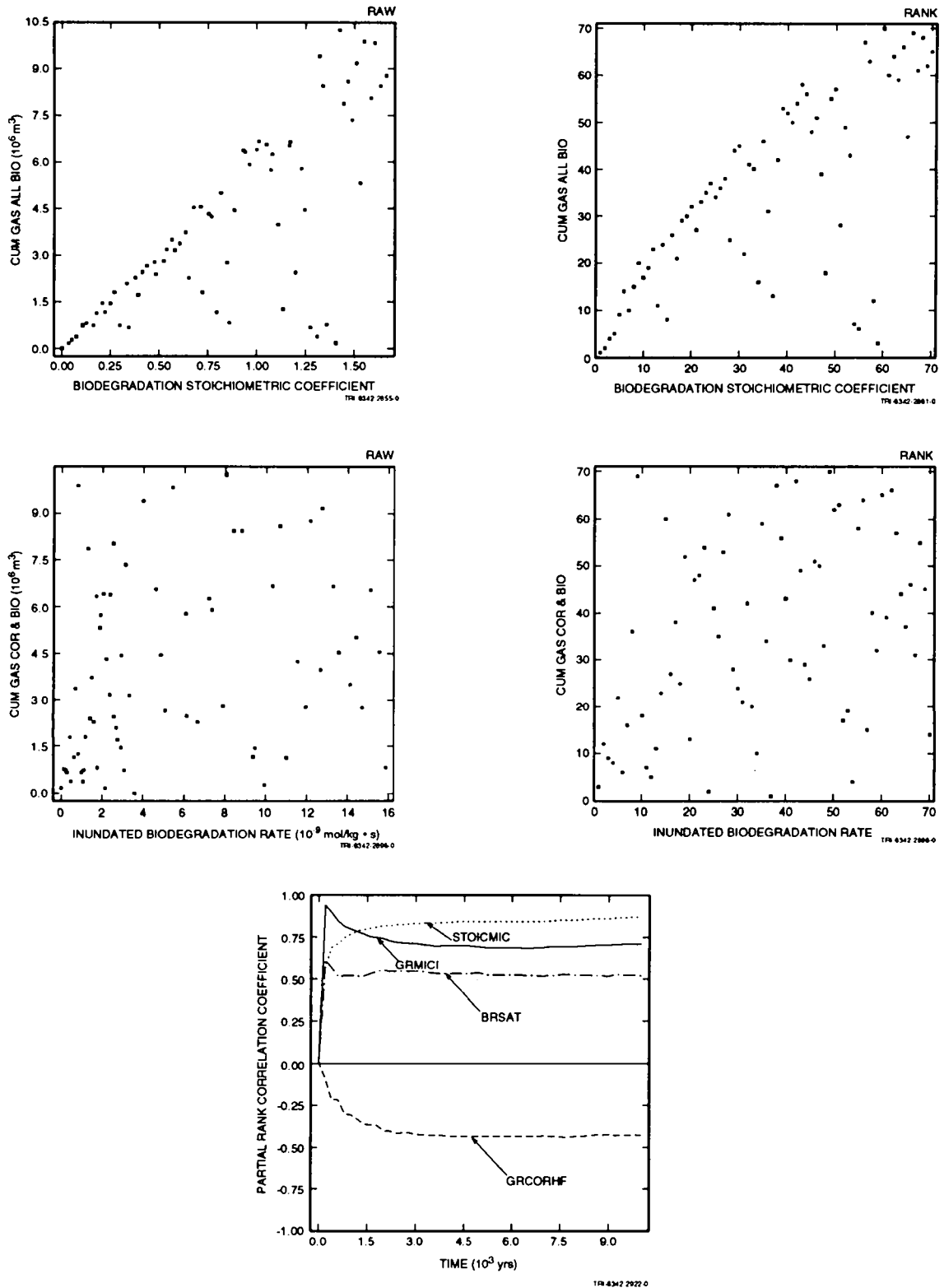


Figure 5-6. Scatterplots and partial rank correlation coefficients for gas generation from inundated and humid biodegradation.

5. Uncertainty and Sensitivity Analysis Results

1 gas generation. However, cellulose will be present in some of the waste (as wood and paper products), and the
2 fraction of cellulose in the initial waste inventory, VWOOD, is assumed to range from 0.284 to 0.484. Therefore,
3 the sampled value for initial cellulose content will always be nonzero, and its range will be relatively narrow
4 compared to the currently assumed range of stoichiometric coefficients.

5 The other two variables selected in the regression analysis contribute very little to the variability in gas
6 generation. BRSAT continues to have some influence, but is dominated by the stoichiometry and inundated
7 biodegradation rate. The correlation coefficient for GRCORHF is negative, indicating that it continues to show a
8 competing effect on gas generation by consuming brine that must be present for biodegradation to take place.

9 5.2.7 Gas Generation from Corrosion and Biodegradation

10 When gas generation by both corrosion and biodegradation are considered, the regression analysis, Table 5-9,
11 shows that the initial brine saturation of the waste is the dominant variable, accounting for 55% of the variability in
12 the amount of gas generated. The plot of partial rank correlation coefficients in Figure 5-7 indicates that this is true
13 almost from the beginning. The scatterplot relating the amount of gas generated to initial brine saturation (Figure 5-
14 7) shows a clear trend. The biodegradation stoichiometry, which is dominant in determining gas generation by
15 biodegradation, also has a significant impact on the total gas generation, although the scatterplot is less convincing.
16 The inundated biodegradation rate, GRMICI, is a major influence at first, but, as cellulose is rapidly consumed, its
17 effect decreases greatly, as seen in the plot of partial rank correlation coefficients. The inundated corrosion rate is
18 also a dominant variable at first, but its influence gradually decreases over time, as the amount of gas generated
19 under more prevalent humid conditions increases.

20 Anhydrite permeability continues to show up in the regression analysis. Accounting for 5% of the variability in
21 gas generation, it is clearly not a dominant variable, but still cannot be ignored, because it controls the flow of brine
22 into the waste as well as the flow of gas out of the repository. Gas flow does not affect gas generation directly, but
23 when the pressure in the repository approaches that of the far field, it can strongly inhibit the influx of brine from
24 outside the waste. Higher anhydrite permeability over the range of sampled values can allow the pressure in the
25 repository to be relieved, in turn allowing more brine to flow inward. However, because the permeability is so low,
26 little brine can flow under any circumstances, and these mechanisms are relatively unimportant. Thus, the overall
27 impact of anhydrite permeability on gas generation is minor. Knowing that absolute permeability has only a small
28 effect over the range of sampled values, it is understandable that *relative* permeability has no discernible effect.
29 Neither of the relative permeability parameters, BCEXP and BCFLG, was selected in the stepwise regression
30 analysis. Scatterplots relating cumulative gas generation to these two variables, Figure 5-8, show completely
31 random scatter and suggest no trends. These results reinforce the conclusions that brine flow has little effect on gas
32 generation and that the initial state of the waste, along with parameters directly affecting gas generation, largely
33 control how much gas is generated.

5.2 Gas Generation and Repository Performance

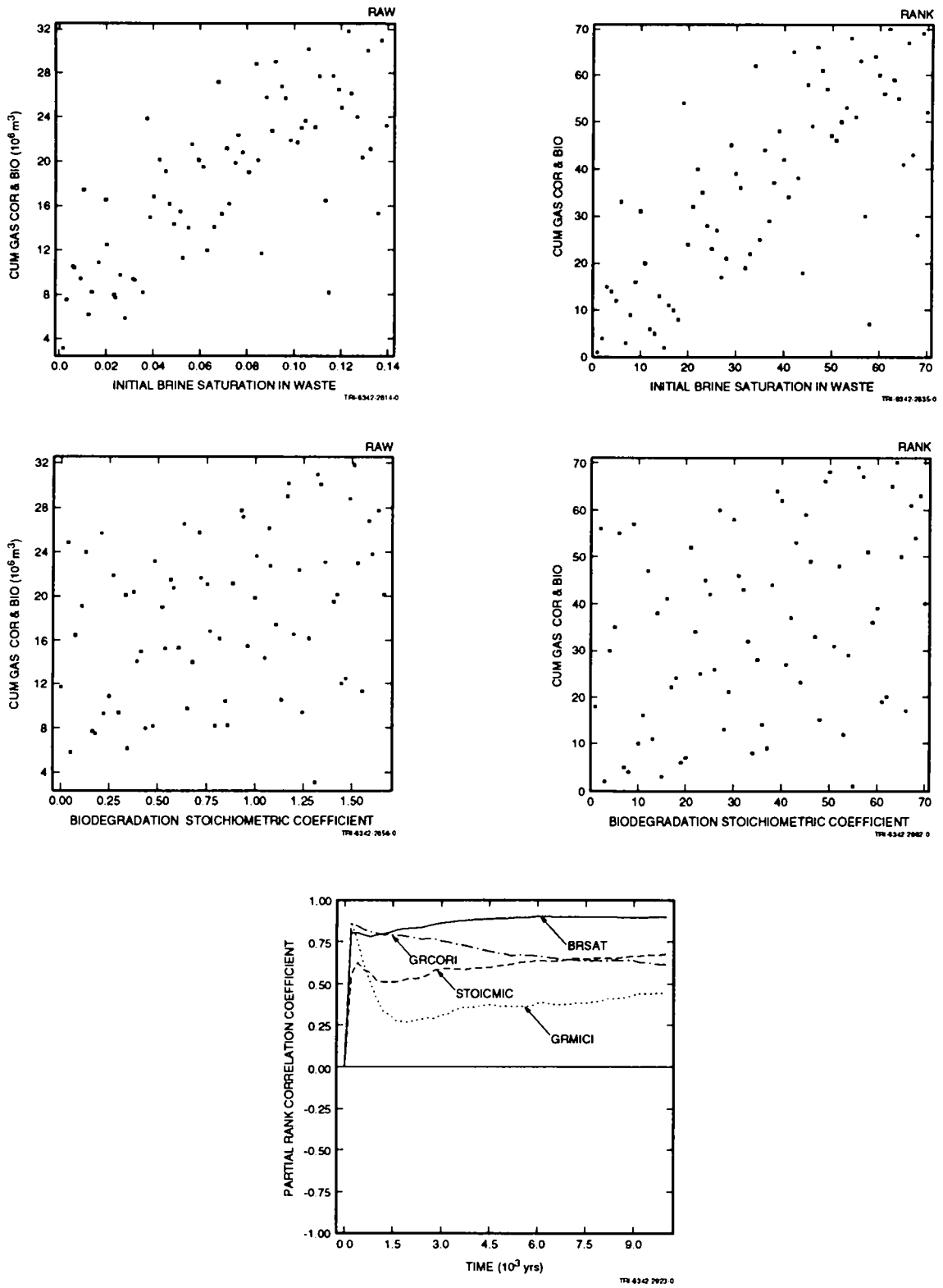


Figure 5-7. Partial rank correlation coefficients for gas generation from corrosion and biodegradation.

5. Uncertainty and Sensitivity Analysis Results

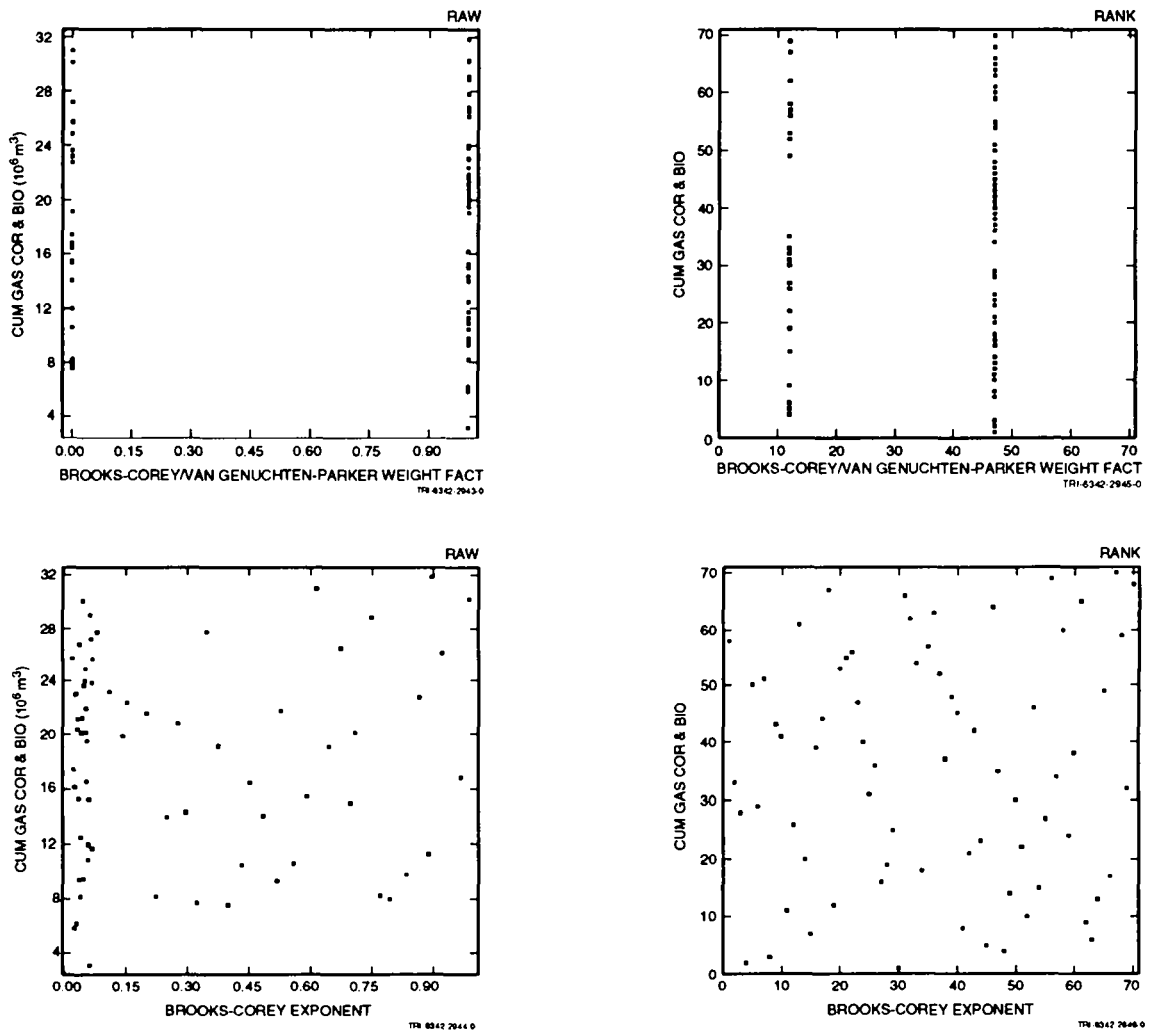


Figure 5-8. Scatterplots for coefficients for gas generation from corrosion and biodegradation.

Table 5-9. Stepwise Regression Analysis with Rank-Transformed Data for Total Gas Production Resulting from Corrosion and Biodegradation (GASGENVC)

Step	Variable	Description	SRC	R ²
1	BRSAT	Initial brine saturation in waste	0.73	0.55
2	STOICMIC	Biodegradation stoichiometric coefficient	0.32	0.66
3	GRCORI	Inundated corrosion rate	0.28	0.73
4	MBPERM	Log of anhydrite interbeds permeability	0.20	0.78
5	GRMICI	Inundated biodegradation rate	0.16	0.80
6	STOICCOR	Corrosion stoichiometry factor	-0.15	0.83

5.2.8 Iron Remaining in the Waste

Analysis of other performance measures will help to understand the behavior of the repository. Table 5-10 shows the regression analysis for iron content remaining in the waste, FECONT. Initial brine saturation in the waste, BRSAT, is the first variable selected, accounting for 61% of the variability in FECONT. The correlation coefficient is negative, indicating, as expected, that the more brine present initially in the waste, the less iron will remain after 10,000 yr. The corrosion rate under inundated conditions, GRCORI, also has some influence, but the rate is sufficiently high that if the waste were fully inundated at all times, all of the iron would be consumed in most realizations within 10,000 yr. As seen earlier with gas generation, potentials become more important over the long term than rates. In the case of corrosion, initial brine content in the waste is one of these potentials, because so little brine flows in from outside the waste. Another potential measure, VMETAL, the initial volume fraction of corrodible metal in the waste, also shows up in the regression analysis, but accounts for only 3% of the variability in FECONT because the limiting potential is the amount of brine available.

Anhydrite permeability, MBPERM, has a small effect, accounting for 4% of the variability in FECONT. The correlation coefficient is negative, so higher permeabilities result in more iron being consumed, indicating that brine influx does contribute to gas generation. However, because anhydrite permeability has so little influence on remaining iron content, it is clear that brine influx has at most a minor impact on gas generation.

5. Uncertainty and Sensitivity Analysis Results

The plot of partial rank correlation coefficients in Figure 5-9 illustrates the dominating effect that initial brine saturation has on the amount of iron remaining in the repository.

The scatterplot relating iron content to initial brine saturation, Figure 5-9, shows the strong negative effect that brine saturation has on the amount of iron that remains after 10,000 yr. The relationship between remaining iron content and the next most influential variable, inundated corrosion rate, also in Figure 5-9, shows the large amount of random scatter typical of an independent variable that accounts for only 11% of the variability of a dependent variable.

Table 5-10. Stepwise Regression Analysis with Rank-Transformed Data for Iron Remaining in the Repository after 10,000 yr (FECONT)

Step	Variable	Description	SRC	R ²
1	BRSAT	Initial brine saturation in waste	-0.77	0.61
2	GRCORI	Inundated corrosion rate	-0.33	0.72
3	VMETAL	Initial volume fraction iron in waste	0.20	0.75
4	MBPERM	Log of anhydrite interbeds permeability	-0.18	0.79
5	GRCORHF	Humid corrosion rate factor	-0.17	0.82

5.2.9 Cellulose Remaining in the Waste

The amount of cellulose remaining after 10,000 yr, BIOCONT, is not strongly dependent on any single variable. The most influential, GRMICI, accounts for only 29% of the variability in BIOCONT, as shown in the regression analysis in Table 5-11. BRSAT appears once again, with nearly as much influence as the biodegradation rate. The scatterplots for each of these two variables, Figure 5-10, show some correlation for GRMICI and less for BRSAT. The partial rank correlation coefficients in Figure 5-10 show that these variables, as well as STOICMIC, dominate at very early times, but their influence degrades over time.

5.2 Gas Generation and Repository Performance

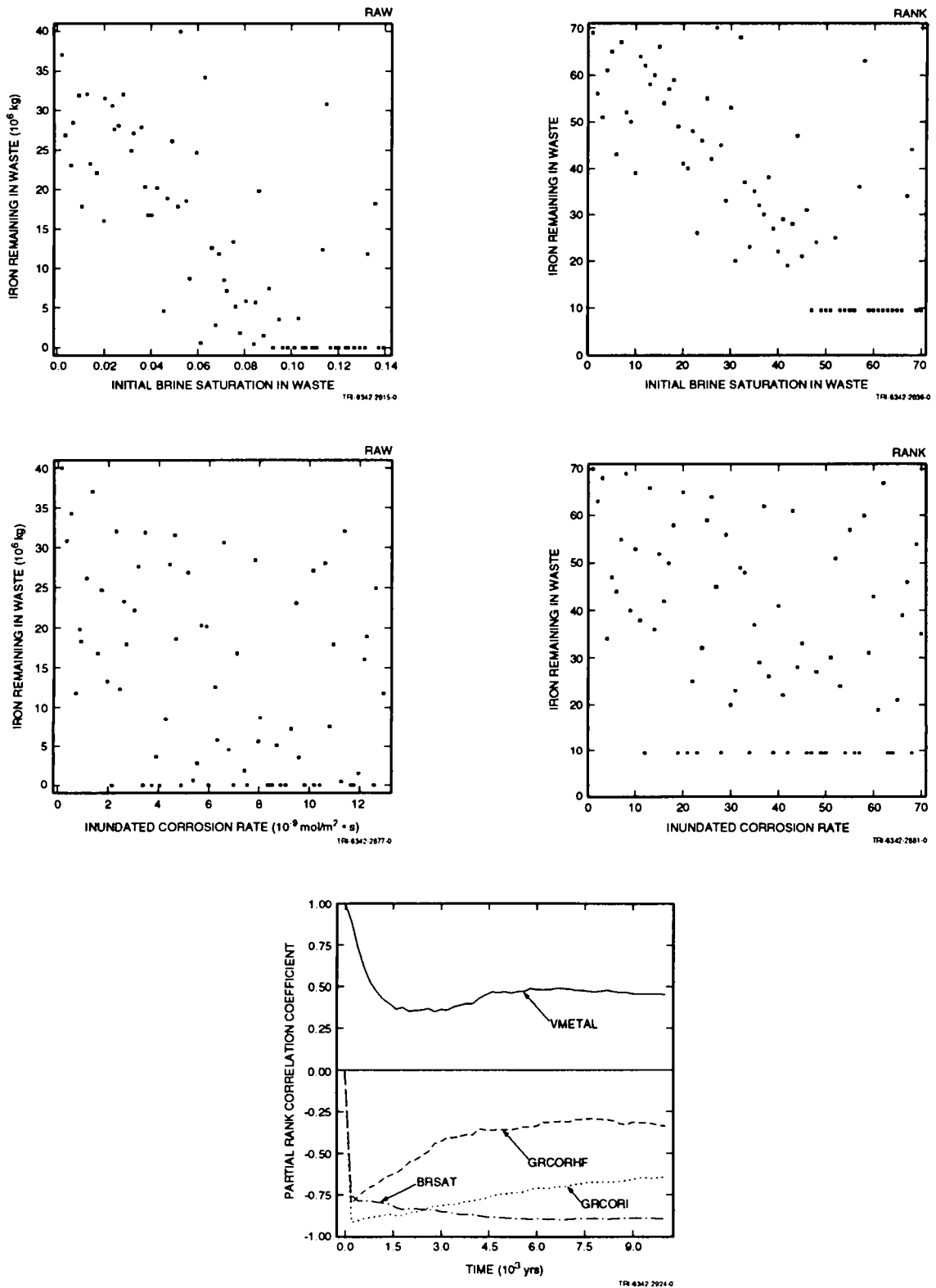


Figure 5-9. Scatterplots and partial rank correlation coefficients for iron remaining in the waste. (Rows of points in the rank plots with identical ranks result from the convention used to assign ranks to realizations with identical raw results [i.e., zero]).

5. Uncertainty and Sensitivity Analysis Results

Table 5-11. Stepwise Regression Analysis with Rank-Transformed Data for Cellulosics Remaining in the Repository (BIOCONT)

Step	Variable	Description	SRC	R ²
1	GRMICI	Inundated biodegradation rate	-0.47	0.21
2	BRSAT	Initial brine saturation in waste	-0.42	0.38
3	GRCORHF	Humid corrosion rate factor	0.25	0.45
4	STOICMIC	Biodegradation stoichiometric coefficient	0.25	0.51
5	GRCORI	Inundated corrosion rate	0.22	0.56

5.2.10 Repository Pore Volume

Pore volume in the repository is of interest primarily as a measure of the impact of creep closure on repository performance. The stepwise regression analysis (Table 5-12) selected initial brine saturation in the waste as the first variable, accounting for 57% of the variability in PORVOLW. The strength of this correlation is confirmed by the scatterplot shown in Figure 5-11, in which there is a clear trend to increasing the pore volume as the brine saturation increases. The effect is actually an indirect one. Higher initial brine saturation results in more gas being generated, which in turn raises the pressure in the repository. This initially coincides with a decrease in pore volume. Thus, the partial rank correlation coefficient, Figure 5-11, shows that brine saturation initially has a negative correlation with pore volume. However, as seen in Figure 4-3, the porosity in the waste quickly reaches a minimum and then starts to increase again as the pressure continues to rise. The reduction in pore volume, in itself, contributes to this pressure rise. Three other variables influence the pressure measurably at early times: STOICMIC, GRCORI, and GRMICI. The impact of these variables decreases over time, leaving BRSAT to dominate over the 10,000-yr period, as the plot of partial rank correlations shows. According to the creep closure model as currently implemented, once the pressure begins to decline, the porosity is fixed (except for small compressibility effects). Thus, the pore volume at 10,000 yr is strongly affected by the peak pressure attained, usually fairly early, which is heavily influenced by initial brine saturation.

5.2 Gas Generation and Repository Performance

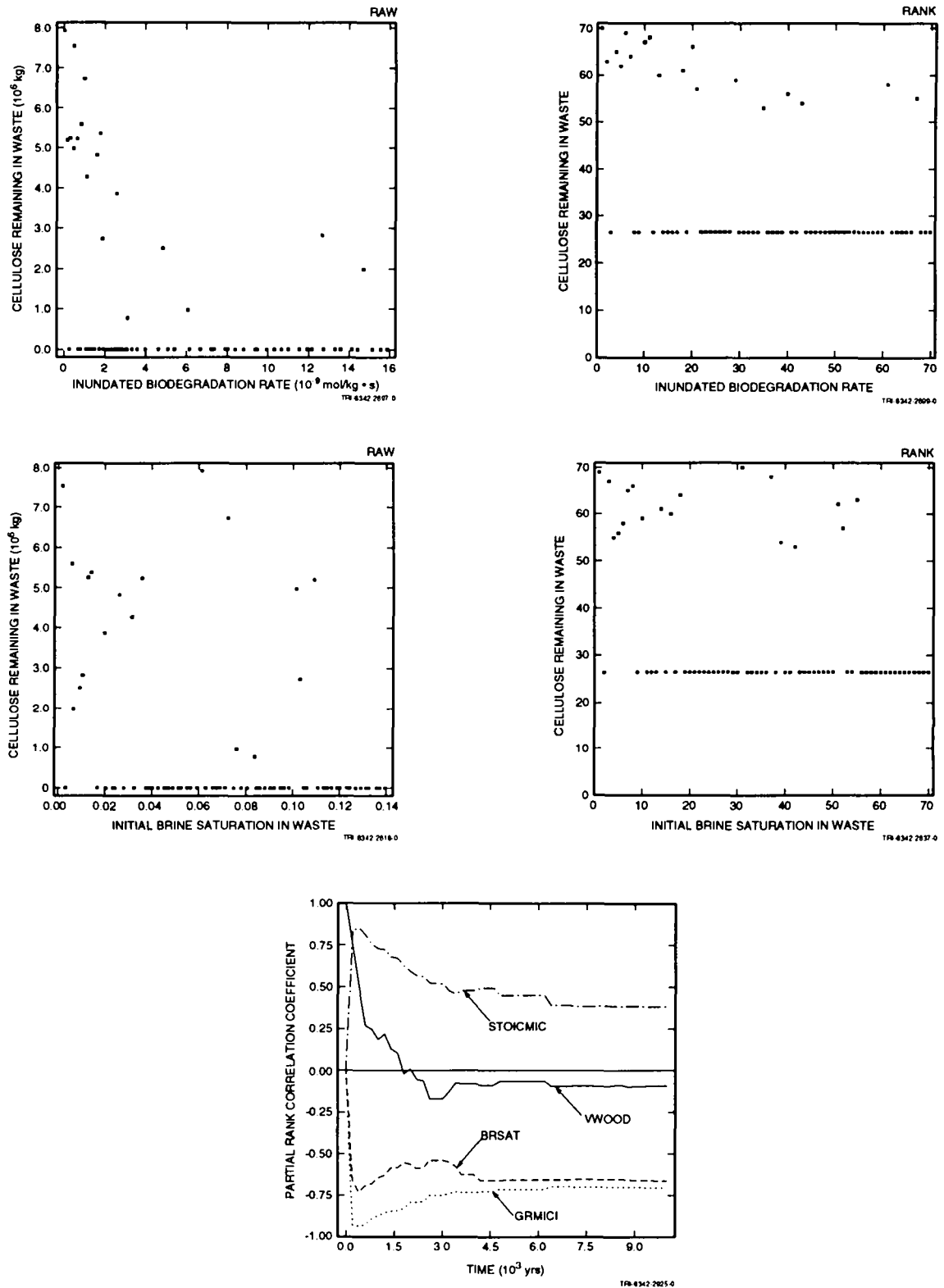


Figure 5-10. Scatterplots and partial rank correlation coefficients for cellulose remaining in the waste. (Rows of points in the rank plots with identical ranks result from the convention used to assign ranks to realizations with identical raw results [i.e., zero]).

5. Uncertainty and Sensitivity Analysis Results

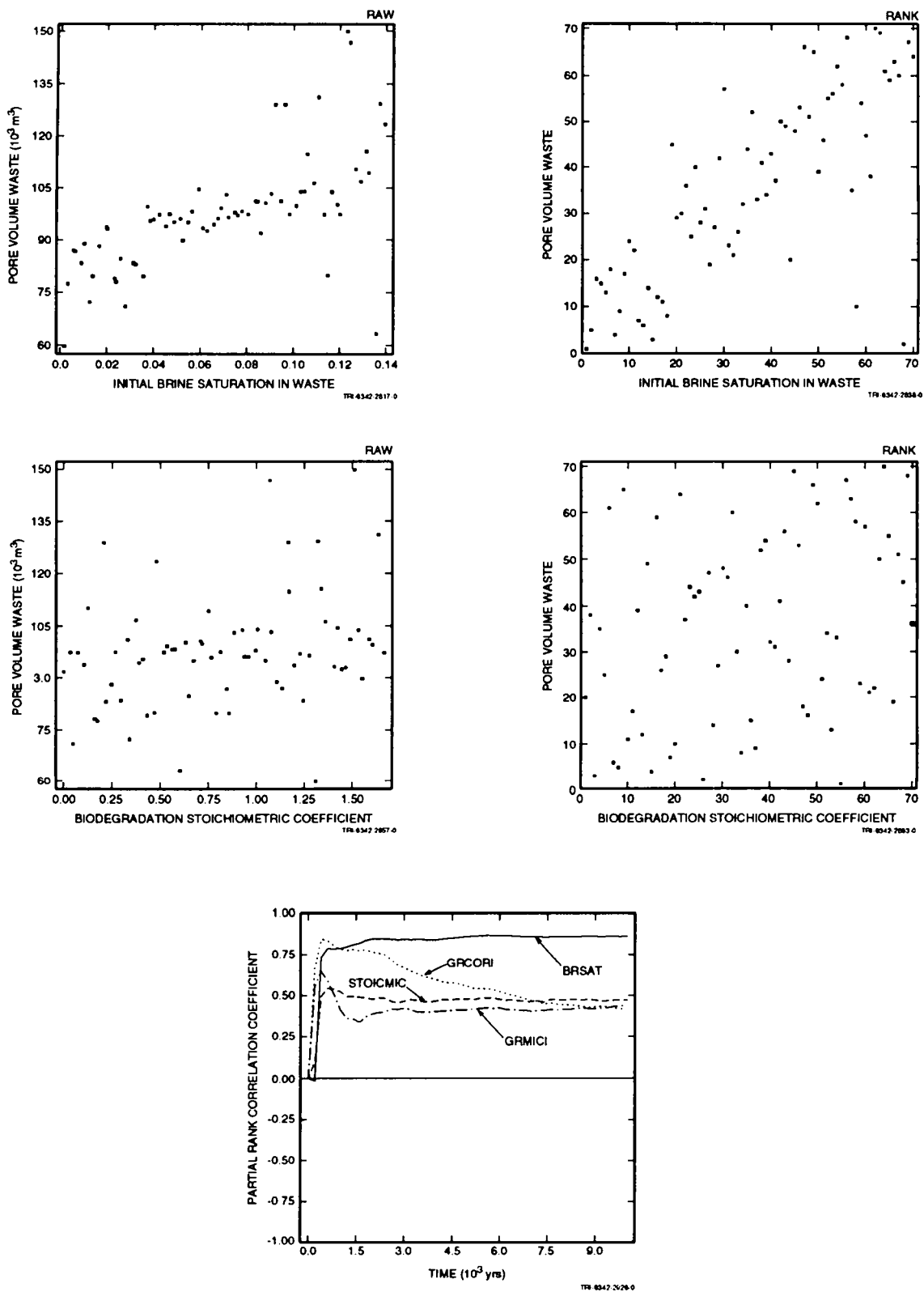


Figure 5-11. Scatterplots and partial rank correlation coefficients for repository pore volume.

1 Table 5-12. Stepwise Regression Analysis with Rank-Transformed Data for Pore Volume in the Waste
 2 (PORVOLW)

Step	Variable	Description	SRC	R ²
1	BRSAT	Initial brine saturation in waste	0.75	0.57
2	STOICMIC	Biodegradation stoichiometric coefficient	0.28	0.65
3	GRCORI	Inundated corrosion rate	0.23	0.70
4	GRMICI	Inundated biodegradation rate	0.22	0.75

4 5.2.11 Average Brine Saturation in the Waste

5 The stepwise regression analysis (Table 5-13) found seven variables that have some impact on the average
 6 brine saturation in the waste, SBAVW. However, none of them alone contributes greatly to the variability.
 7 Scatterplots of the two variables that affect SBAVW most strongly, Figure 5-12, confirm that the relationships are
 8 weak. The plot of partial rank correlation coefficients shows that, at first, initial brine saturation in the waste
 9 dominates; by definition, there should be a perfect correlation initially. Later, as corrosion consumed brine, the
 10 inundated corrosion rate has a strong influence. However, by 10,000 yr, no variable dominates, even though many
 11 have some small effect.

12 Table 5-13. Stepwise Regression Analysis with Rank-Transformed Data for Average Brine Saturation in
 13 the Waste (SBAVW)

Step	Variable	Description	SRC	R ²
1	BRSAT	Initial brine saturation in waste	0.39	0.14
2	GRCORI	Inundated corrosion rate	-0.36	0.26
3	TZPORF	Factor used in calculating DRZ and transition zone porosity	-0.29	0.35

5. Uncertainty and Sensitivity Analysis Results

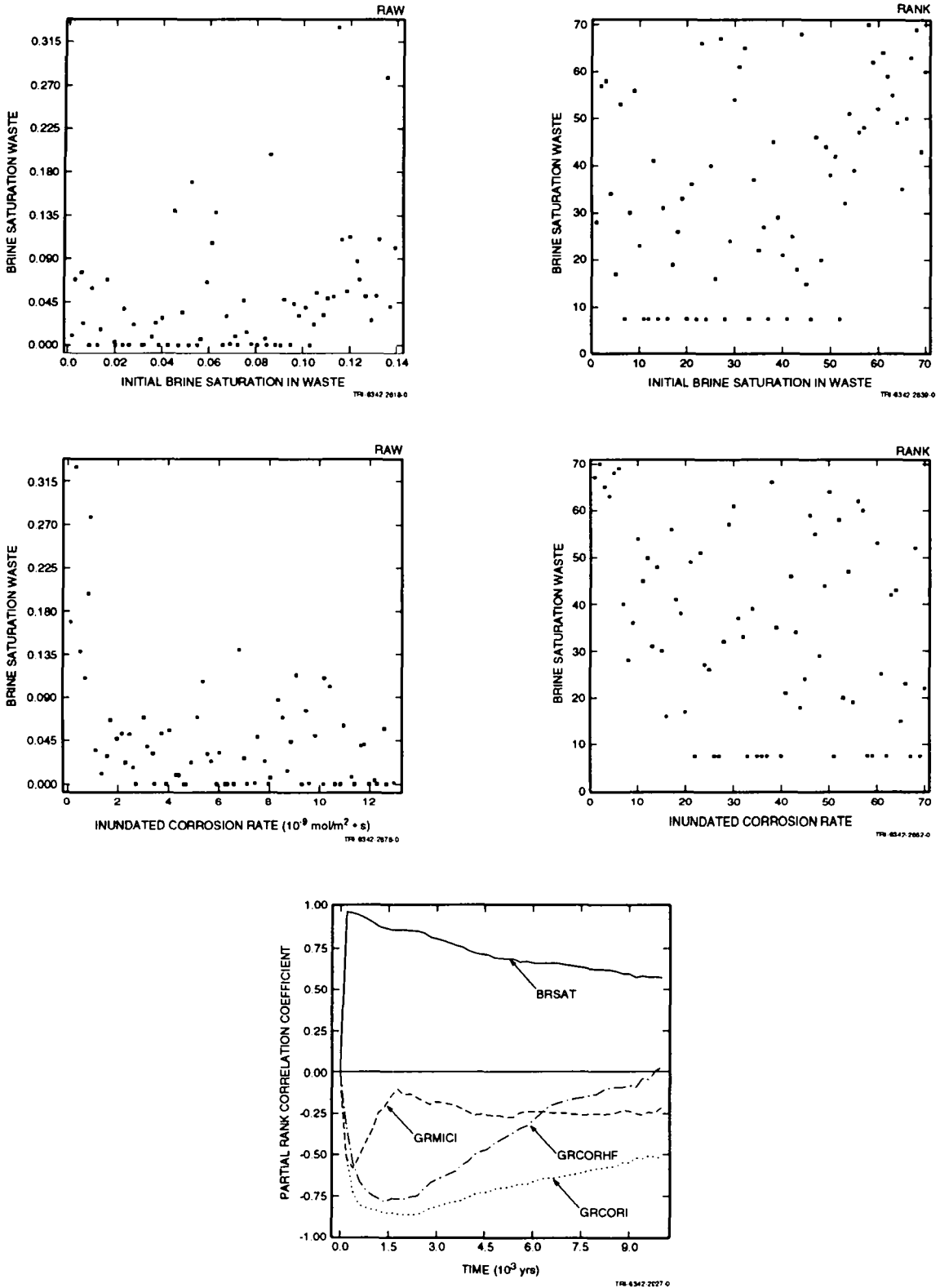


Figure 5-12. Scatterplots and partial rank correlation coefficients for average brine saturation in the waste. (Rows of points in the rank plots with identical ranks result from the convention used to assign ranks to realizations with identical raw results [i.e., zero]).

1 Table 5-13. Stepwise Regression Analysis with Rank-Transformed Data for Average Brine Saturation in
 2 the Waste (SBAVW) (Concluded)

Step	Variable	Description	SRC	R ²
4	SALPERM	Intact Salado halite permeability	0.29	0.41
5	STOICCOR	Corrosion stoichiometry factor	-0.28	0.49
6	SHFTPRM	Permeability of shaft-fill material above shaft seal	0.23	0.54
7	BCFLG	Brooks-Corey/van Genuchten-Parker weighting factor	-0.23	0.59

4 5.2.12 Pore Pressure in the Waste

5 Because the pressure in the waste results from gas generation, the variables that affect gas generation, reactant
 6 content, and pore volume should also affect pressure. The regression analysis, Table 5-14, confirms this. Once
 7 again, the dominant variable is the initial brine saturation in the waste, accounting for 62% of the variability in
 8 repository pressure. The scatterplot relating pressure to initial brine saturation shows the strong correlation between
 9 them. Two other variables have only minor impacts, although their influence was considerably greater at early
 10 times, as shown by the partial rank correlation coefficients in Figure 5-13

11 Table 5-14. Stepwise Regression Analysis with Rank-Transformed Data for Average Pore Pressure in the
 12 Waste (PRESWAST)

Step	Variable	Description	SRC	R ²
1	BRSAT	Initial brine saturation in waste	0.79	0.62
2	STOICMIC	Biodegradation stoichiometric coefficient	0.24	0.68
3	GRMICI	Inundated biodegradation rate	0.21	0.72

5. Uncertainty and Sensitivity Analysis Results

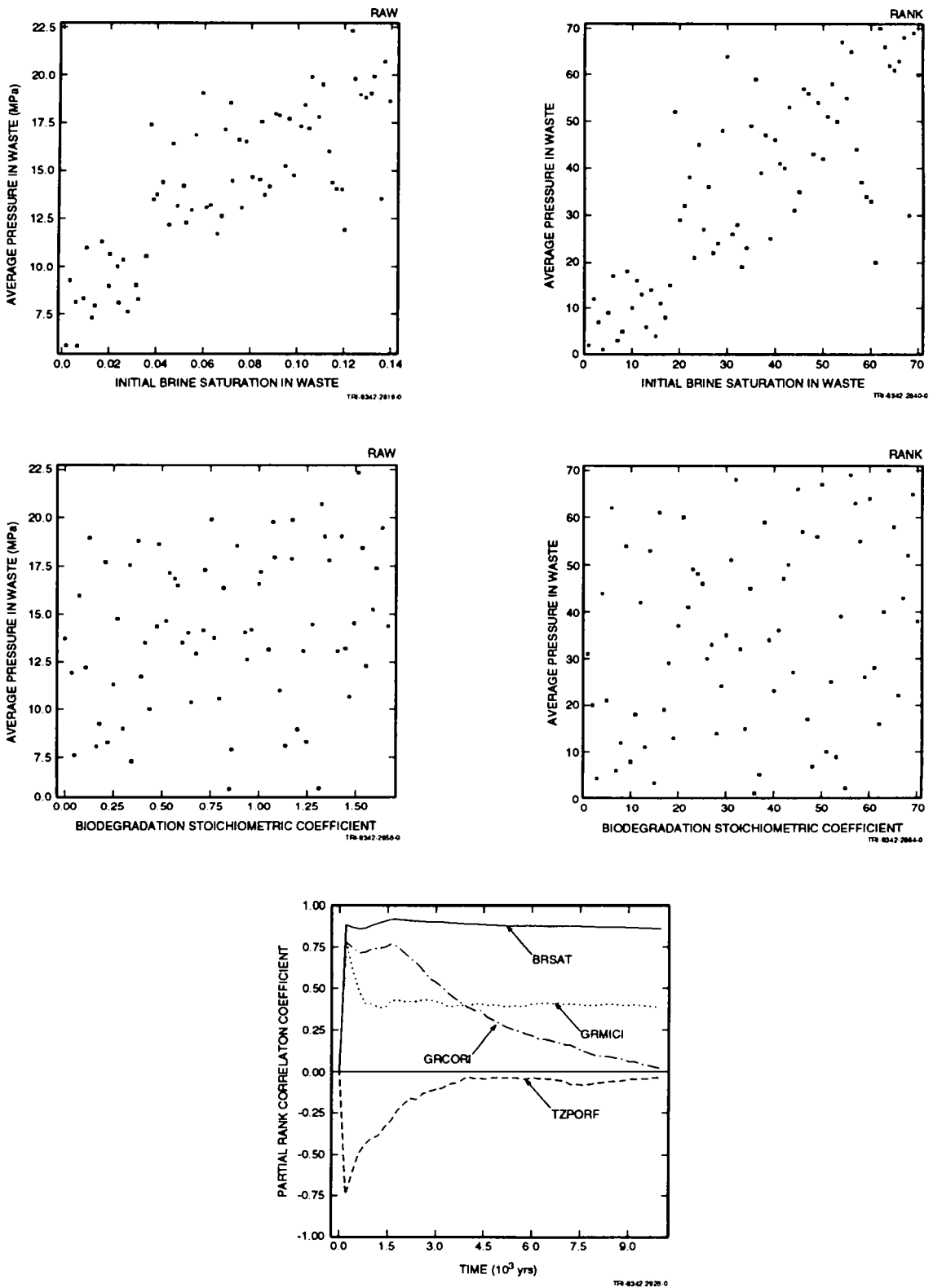


Figure 5-13. Scatterplots and partial rank correlation coefficients for pore pressure in the waste.

5.3 Brine Flow

A key performance measure for the WIPP under undisturbed conditions is the amount of contaminants (either radionuclides or hazardous chemical constituents) in brine that flows beyond the disposal unit boundaries. In the absence of actual modeling of contaminant transport, surrogate key measures are simply the amounts of brine that flow out the various flow paths from the repository, including the three anhydrite layers and the sealed shafts. In this section, these performance measures are examined to determine which sampled parameters affect them. This analysis provides insight into which parameters require more attention (and perhaps more measured data), and which conceptual features of the model may require more sophisticated treatment. It also identifies parameters or conceptual models that are *not* important and can therefore be further simplified.

5.3.1 Cumulative Net Brine Flow from the Repository

In Table 5-15, the regression analysis for cumulative net brine flow from the repository selected the initial brine saturation of the waste as the first variable. The scatterplot relating brine flow to brine saturation, Figure 5-14, shows brine flow tending to increase as initial brine saturation increases. Net brine flows out of the repository range from -24,000 m³ to +11,400 m³, implying that some minimum initial brine saturation is necessary for brine to flow out of the waste. Because the initial brine saturation is at most half of the residual brine saturation of the waste, the initial saturation itself is not sufficient to cause flow from the waste. Rather, when more brine is present initially, less inflow is required to exceed residual before allowing brine to flow out. Also affecting this correlation is the creep closure model. Brine saturation is increased more rapidly and residual saturation is reached more quickly, allowing some of the initial brine content of the waste to flow out in some realizations. Under these circumstances, it is not necessary for any brine to flow in first, although, as seen in Figure 4-9, this does occur in some realizations. The partial rank correlation coefficients in Figure 5-14 confirm that BRSAT is the dominant variable affecting net flow from the waste.

Anhydrite porosity accounts for an additional 8% of the variability in brine flow from the waste. It has a negative correlation coefficient, indicating that brine outflow decreases as the anhydrite porosity increases. Higher porosities allow more brine to flow in toward the repository because the storage capacity of the anhydrite is greater, so the distance over which the brine must travel is less. Similarly, brine flowing out of the repository must displace brine in the anhydrite over a greater distance when the porosity is lower.

Anhydrite permeability also has a small influence on brine flow from the waste. It has a negative correlation coefficient, as anhydrite porosity does, for the same reasons. High permeabilities contribute to brine flow in from the far field. This brine inflow eventually fills the DRZ enough to allow brine to flow into the waste, where it may be consumed by corrosion. Although some brine does flow out of the repository in some realizations, it most often occurs because creep closure has increased the brine saturation in the waste independently of brine inflow from the far field. Thus, anhydrite permeability enhances brine flow into the waste, and inhibits outflow by filling the DRZ that surrounds the repository with brine.

5. Uncertainty and Sensitivity Analysis Results

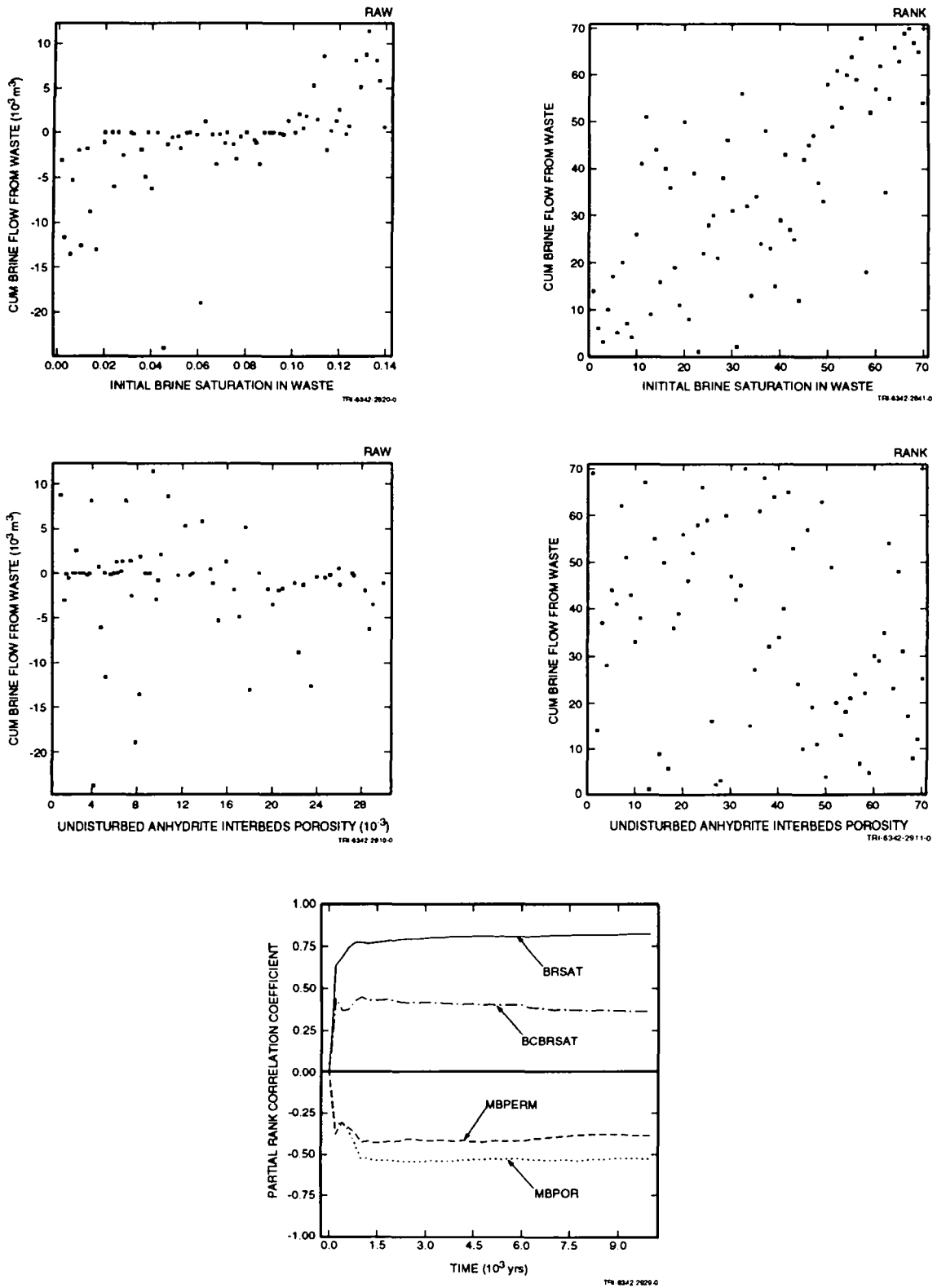


Figure 5-14. Scatterplots and partial rank correlation coefficients for cumulative net brine flow from the repository.

1 Table 5-15. Stepwise Regression Analysis with Rank-Transformed Data for Cumulative Net Brine Flow
 2 from the Repository (BWSTC)

3

Step	Variable	Description	SRC	R ²
1	BRSAT	Initial brine saturation in waste	0.72	0.53
2	MBPOR	Undisturbed anhydrite interbeds porosity	-0.30	0.61
3	MBPERM	Log of anhydrite interbeds permeability	-0.24	0.67
4	BCBRSAT	Residual brine saturation in all regions except waste	0.18	0.70

4 5.3.2 Cumulative Net Brine Flow Out MB139

5 The stepwise regression analysis (Table 5-16) for cumulative net brine flow out MB139 to the south of the
 6 repository (from Cell 8 to Cell 7 in Figure 2-2) selected BRSAT as the first variable. It accounts for 45% of the
 7 variability in brine flow. The scatterplot relating MB139 brine flow to initial waste brine saturation, in Figure 5-15,
 8 shows that brine flow out is negative in most realizations, that is, brine flows toward the repository. Generally, the
 9 inward brine flow is greatest when the initial brine saturation is lowest because less gas is generated in the waste,
 10 leaving the pressure in the waste lower, and thereby offering less resistance to brine flow from the far field.

11 Anhydrite permeability is also an influential parameter affecting brine flow in MB139, accounting for an
 12 additional 16% of the variability in brine flow. The scatterplot in Figure 5-15 shows that when the permeability is
 13 high, net brine outflow is more likely to be negative, or toward the repository, especially at early times when the
 14 pressure gradient from the far field to the repository is greatest. This is the same effect that was seen on the
 15 cumulative brine flow from the waste. Intermediate values of permeability (10^{-18} to 10^{-20} m²) can allow some
 16 outward flow, which is a concern from a regulatory standpoint. In these cases, creep closure and gas generation
 17 may reverse the pressure gradient while elevating the waste brine saturation to the point where brine can flow from
 18 the waste. If the rate at which these processes take place is faster than the rate of brine inflow through MB139 when
 19 the anhydrite permeability is intermediate in value, brine flow out MB139 will result. When the permeability is less
 20 than 10^{-20} m², brine movement in the anhydrite layers tends to become insignificant. The partial rank correlation
 21 coefficients show that permeability is more important at early times, but its influence gradually decreases over the
 22 first 2000 yr. This occurs because, when there is a large quantity of brine flow, it generally takes place early, when
 23 the waste pressure is still very low and the pressure gradient from the far field to the waste is largest. As the
 24 pressure in the waste builds, the relative importance of permeability decreases compared with the initial brine
 25 saturation, which strongly influences pressure buildup.

5. Uncertainty and Sensitivity Analysis Results

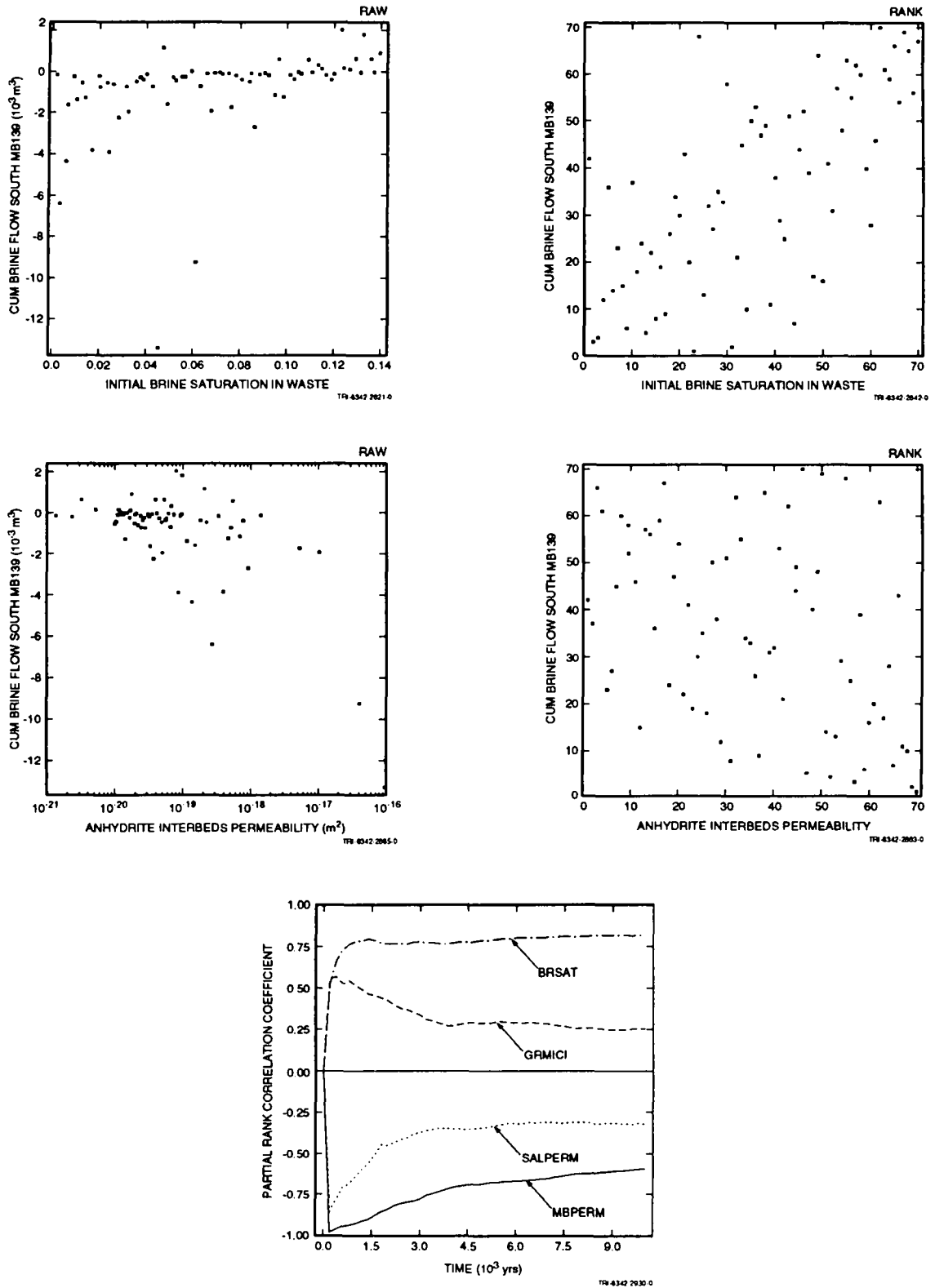


Figure 5-15. Scatterplots and partial rank correlation coefficients for cumulative net brine flow out MB139.

The third variable selected in the regression analysis, TZPORF, is a measure of the DRZ porosity. It has a small negative effect on brine flow out MB139 for the same reason that BCBRSAT affects brine flow from the repository, BWSTC. A high DRZ porosity constitutes a larger storage capacity in the DRZ, effectively damping out the interchange of fluids between the repository and the anhydrite layers. For brine flow out MB139 to occur, the DRZ must first fill at least to residual saturation with brine. Whether that brine comes from initial inflow from MB139 or, as it must eventually, from the waste, the more pore volume in the DRZ, the longer brine flow out MB139 will be delayed.

Anhydrite porosity and halite permeability each account for 3% of the variability in brine flow out MB139. Higher porosity tends to result in greater brine flows by providing more source and sink capacity close to the repository. Higher halite permeability allows brine to flow vertically out of the anhydrite layer and into halite instead of through the anhydrite, thus reducing flow out MB139.

Table 5-16. Stepwise Regression Analysis with Rank-Transformed Data for Cumulative Net Brine Flow South into MB139 (BRNMB9SC)

Step	Variable	Description	SRC	R ²
1	BRSAT	Initial brine saturation in waste	0.65	0.45
2	MBPERM	Log of anhydrite interbeds permeability	-0.35	0.61
3	TZPORF	Factor used in calculating DRZ and transition zone porosity	-0.26	0.68
4	MBPOR	Undisturbed anhydrite interbeds porosity	0.17	0.71
5	SALPERM	Intact Salado halite permeability	-0.18	0.74

5.3.3 Cumulative Net Brine Flow Out Anhydrite a + b

Brine flow out through the anhydrite a + b layer differs in one major respect from flow in MB139: there is no net outward brine flow in any of the 70 realizations. Brine flows in early when the pressure gradient from the far field to the waste is high. But this brine either flows into the repository or ends up further down in the DRZ or MB139. When the pressure in the waste exceeds the far-field pressure, there is no "pool" of brine at the repository end of anhydrite a + b to flow back out. Anhydrite permeability, as might be expected, is the dominant variable affecting brine flow. The scatterplot (Figure 5-16) shows that, as with MB139, cumulative flows into the waste can be large when the anhydrite permeability is greater than 10^{-18} m², and are nearly zero when the permeability is less than 10^{-20} m².

5. Uncertainty and Sensitivity Analysis Results

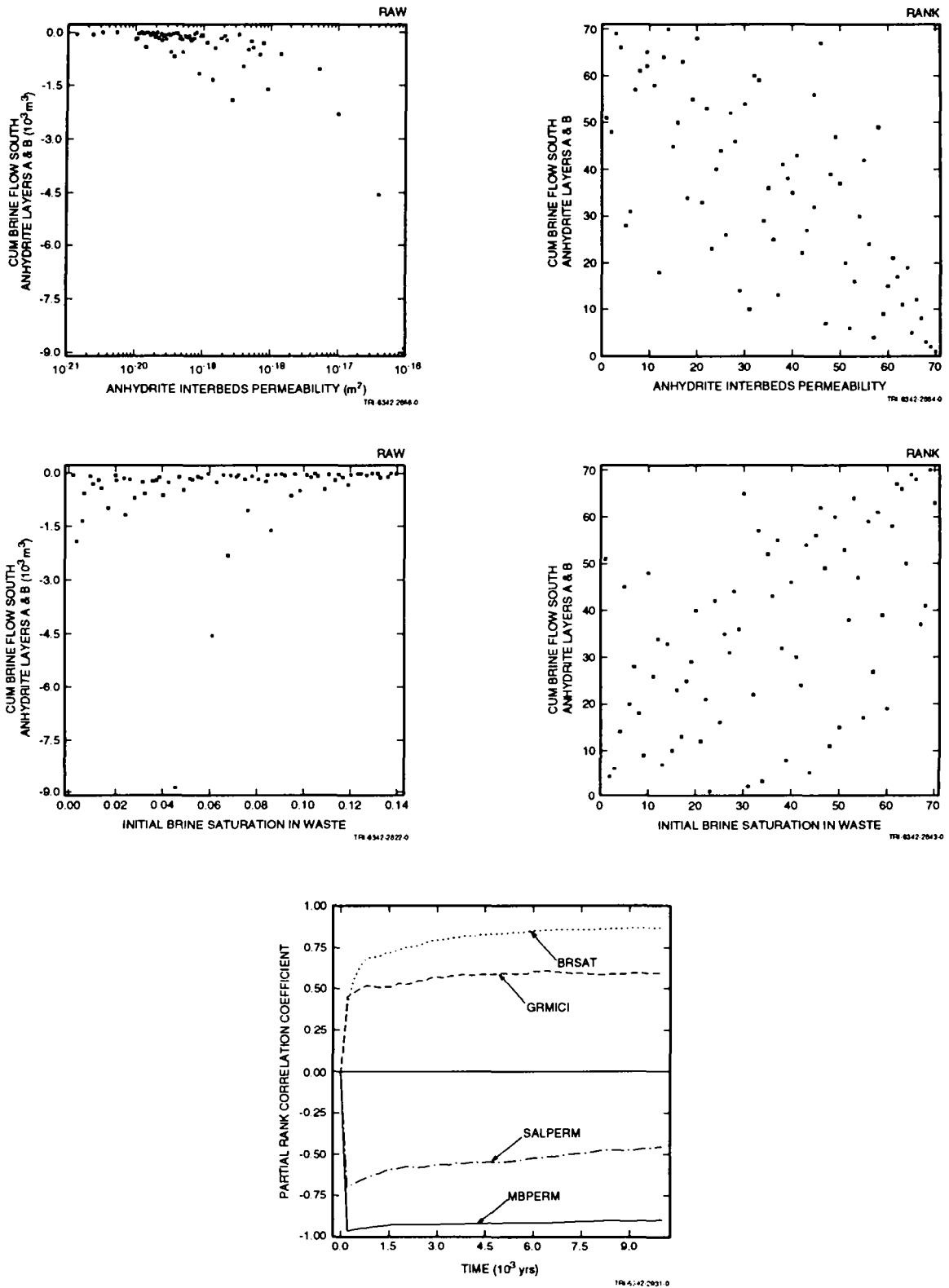


Figure 5-16. Scatterplots and partial rank correlation coefficients for cumulative net brine flow out anhydrite a + b.

1 Although the regression analysis (Tables 5-17) indicates that the initial brine saturation also has a moderate
 2 influence on brine flow in anhydrite a + b, the scatterplot in Figure 5-16 suggests that the effect is not really very
 3 predictable. Intermediate values of brine saturation can result in large flows toward the repository, but low values
 4 of initial brine saturation have a more consistent effect. When there is little brine in the waste, the back pressure
 5 created in the waste remains low, allowing more brine to flow inward through anhydrite a + b. The plot of partial
 6 rank correlation coefficients in Figure 5-16 indicates that the effect of initial waste brine saturation grows slightly
 7 over 10,000 yr, while the influence of permeability starts high and remains steady.

8 Other gas-generation-related variables also have a small effect, essentially contributing to the increase in back
 9 pressure that eventually stops the flow of brine through anhydrite a + b. As in MB139, higher halite permeability
 10 tends to reduce flow through the anhydrite layer by allowing some brine to enter the halite instead of continuing to
 11 flow through the anhydrite.

12 Table 5-17. Stepwise Regression Analysis with Rank-Transformed Data for Cumulative Net Brine Flow
 13 South into Anhydrite Layers a + b (BRNANHSC)

Step	Variable	Description	SRC	R ²
1	MBPERM	Log of anhydrite interbeds permeability	-0.64	0.46
2	BRSAT	Initial brine saturation in waste	0.52	0.74
3	GRMICI	Inundated biodegradation rate	0.23	0.79
4	SALPERM	Intact Salado halite permeability	-0.17	0.82
5	STOICMIC	Biodegradation stoichiometric coefficient	0.12	0.84
6	GRCORI	Inundated corrosion rate	0.12	0.85

15 5.3.4 Cumulative Net Brine Flow Out MB138

16 The regression analysis for net brine flow out MB138, Table 5-18, shows that the initial brine saturation in the
 17 waste and anhydrite permeability are about equally influential variables, although neither one provides a very strong
 18 correlation. Scatterplots for these variables in Figure 5-17 look very similar to those for the same variables in
 19 anhydrite a + b. The partial rank correlation coefficients, Figure 5-17, show similar trends, although the effect of
 20 permeability decreases slightly more over time than for anhydrite a + b.

5. Uncertainty and Sensitivity Analysis Results

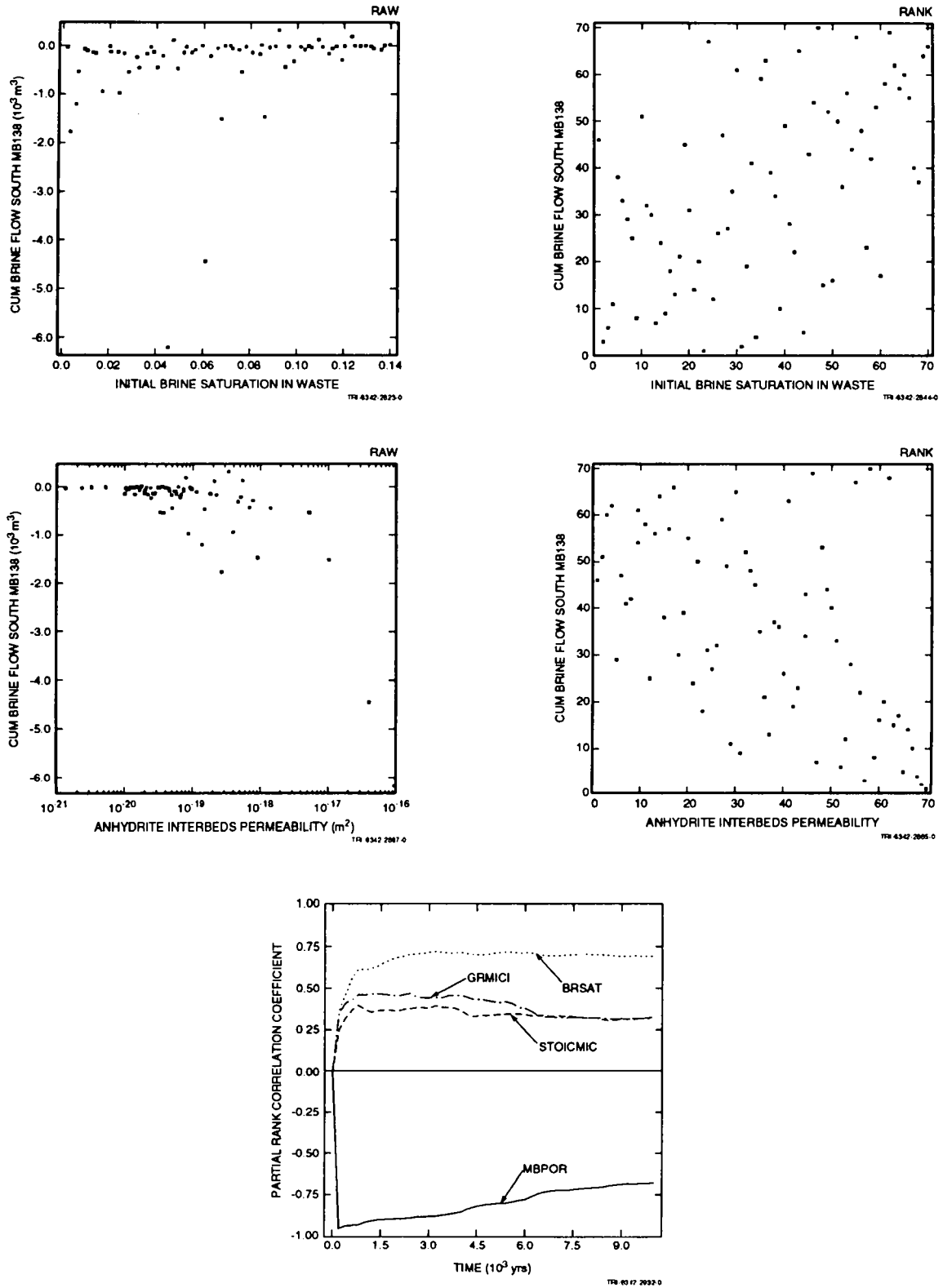


Figure 5-17. Scatterplots and partial rank correlation coefficients for cumulative net brine flow out MB138.

Table 5-18. Stepwise Regression Analysis with Rank-Transformed Data for Cumulative Net Brine Flow South into MB138 (BRNMB8SC)

Step	Variable	Description	SRC	R ²
1	BRSAT	Initial brine saturation in waste	0.51	0.27
2	MBPERM	Log of anhydrite interbeds permeability	-0.51	0.52
3	STOICMIC	Biodegradation stoichiometric coefficient	0.22	0.57

5.3.5 Cumulative Net Brine Flow Upward through Shaft Seal

The stepwise regression analysis (Table 5-19) performed for cumulative net upward flow of brine through the shaft seal, BSHSLUPC, shows that the dominant variable is the permeability during the first 200 yr of the shaft above the shaft seal but below the Culebra (SHFTPRM), not the long-term shaft seal permeability, as one might expect. However, this accounts for only 33% of the variability in brine flow through the shaft seal. Shaft seal permeability during the first 200 yr (SEALPRM1) is nearly as important, contributing another 26% to the variability in brine flow. Scatterplots in Figure 5-18 confirm that neither variable alone is very strongly correlated to brine flow. Shaft permeability during the first 200 yr (SHFTPRM) was sampled from a range that is nearly identical to the range of seal permeability for that same time period. Because that portion of the shaft is 319 to 389 m long compared to 30 to 100 m for the shaft seal (a sampled parameter, SEALTHK), it is reasonable to believe that permeability of the lower shaft is slightly more significant than seal permeability in determining brine flow through the seal. However, the impact of these variables is somewhat distorted because most of the cumulative flow through the shaft seal was downward drainage by gravity during the first 200 yr. In more than half of the realizations, the flow direction eventually reverses. Upward flow that takes place over the last 9000 yr or so is small compared to the initial downward surge, but is potentially much more important to regulatory compliance. (See Section 4.1.2 for additional discussion of brine flow.)

Halite permeability has an additional effect, but it is of secondary importance. Because of the large surface area of the shaft-halite interface, some brine drains into the shaft from the surrounding halite, even though the highest surge of brine occurred during the 50-yr disposal phase. That brine was removed from the simulation at time zero (reflecting evaporation before the repository is sealed), leaving a depressurized zone around the shaft at time zero. Despite this, when the permeability of halite is sufficiently high, some seepage from the Salado into the shaft often continues, as seen in Figure 4-24. This contributes to the downward flow of brine through the shaft seal, but should not greatly impact upward flow.

5. Uncertainty and Sensitivity Analysis Results

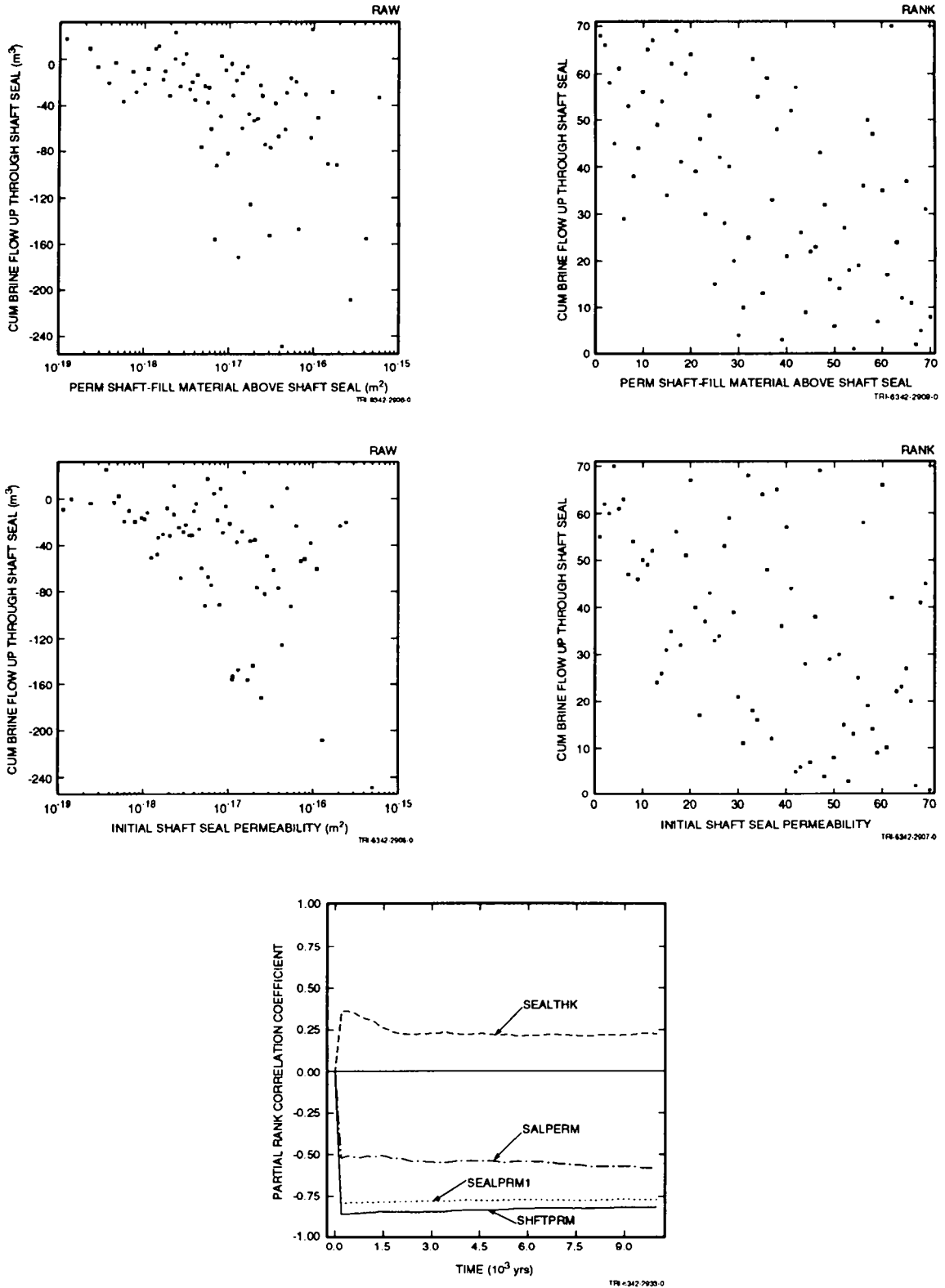


Figure 5-18. Scatterplots and partial rank correlation coefficients for cumulative net brine flow upward through shaft seal.

All three variables have negative correlation coefficients, indicating that larger values result in larger downward flows. The process being observed here is gravity drainage, which would be aided by higher seal and shaft permeabilities. If only the upward component of brine flow during 10,000 yr was analyzed, positive correlation coefficients would be expected.

Table 5-19. Stepwise Regression Analysis with Rank-Transformed Data for Cumulative Net Brine Flow Upward through Shaft Seal (BSHSLUPC)

Step	Variable	Description	SRC	R ²
1	SHFTPRM	Permeability of shaft-fill material above shaft seal	-0.58	0.33
2	SEALPRM1	Initial shaft seal permeability	-0.51	0.59
3	SALPERM	Intact Salado halite permeability	-0.34	0.71

5.4 Gas Flow

A key performance measure for the WIPP under undisturbed conditions is the amount of volatile organic compounds (VOCs) dissolved in gas that flows beyond the disposal unit boundaries. Because transport of VOCs has not yet been modeled using the two-phase flow model, measures discussed here are the amount and distance that gas flows out the various flow paths from the repository, including the three anhydrite layers and the sealed shaft leading to the Culebra. These measures provide insight into which parameters control migration of VOCs, which parameters require more attention (and perhaps more measured data), and which conceptual features of the model may require more sophisticated treatment. Two-phase flow modeling also provides insight into parameters or conceptual models that are *not* important and can therefore be further simplified or omitted in future performance assessments.

5.4.1 Cumulative Net Gas Flow Out MB139

The first three performance measures to be examined are the cumulative flows southward out each of the anhydrite layers. The stepwise regression analysis for flow out MB139, shown in Table 5-20, selected BRSAT, the initial brine saturation in the waste, as the first variable. The correlation is not strong, but it is reasonable that the key parameter affecting gas generation plays an important role in determining how much gas flows out MB139. The second variable selected, the permeability of the anhydrite layers, is also an obvious choice to affect gas flow. Another gas-generation parameter, the biodegradation stoichiometric coefficient, STOICMIC, also has a small effect. Altogether, the three variables selected account for only half of the variability in cumulative gas flow. The scatterplots for the first two variables, BRSAT and MBPERM, in Figure 5-19, illustrate the relatively poor

5. Uncertainty and Sensitivity Analysis Results

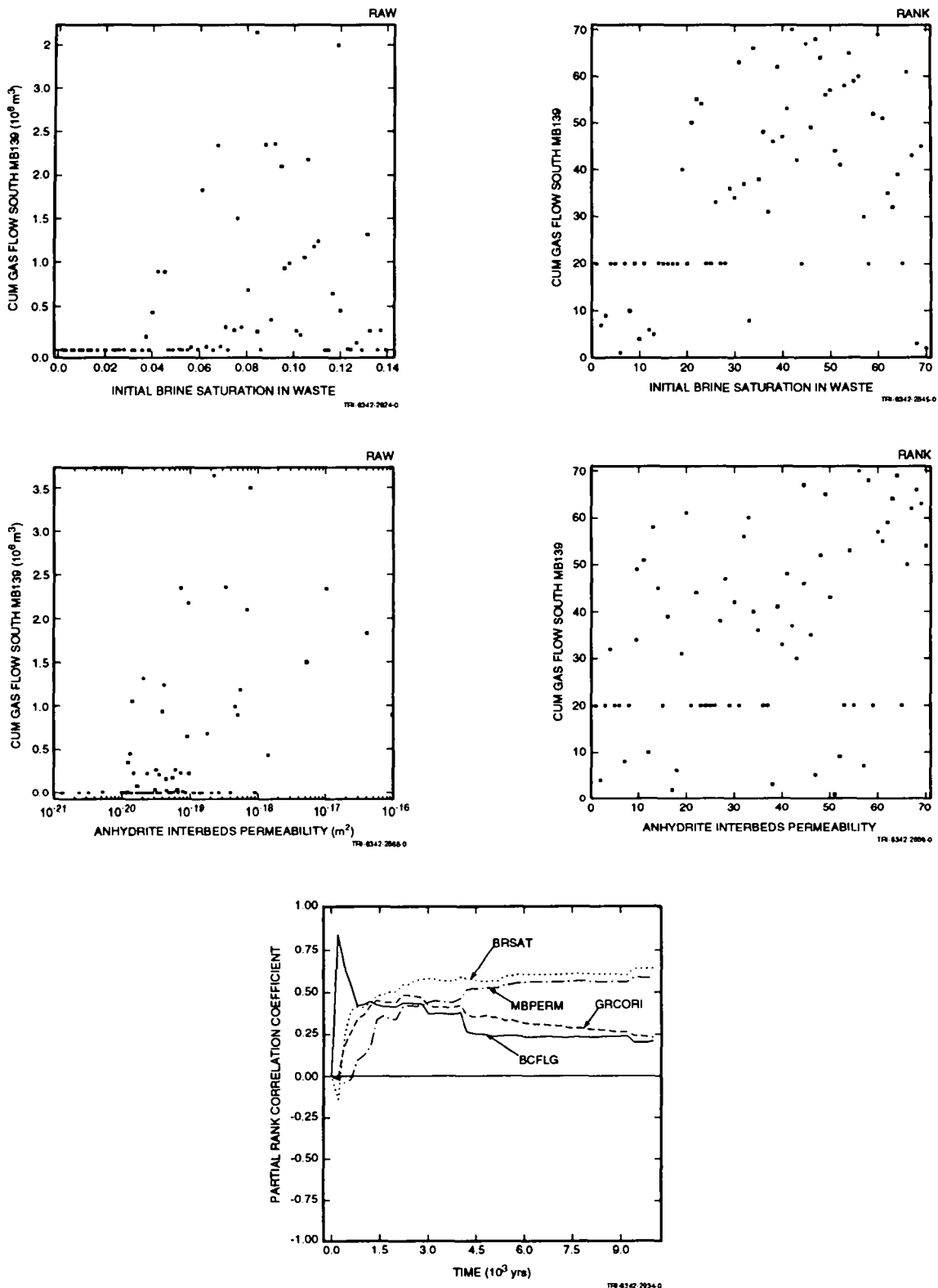


Figure 5-19. Scatterplots and partial rank correlation coefficients for cumulative net gas flow out MB139. (Rows of points in the rank plots with identical ranks result from the convention used to assign ranks to realizations with identical raw results [i.e., zero]).

1 correlation between cumulative gas flows and each variable. The partial rank correlation coefficients in Figure 5-19
 2 show that BRSAT was most important over the last 9000 yr, but that it really does not dominate the other variables.
 3 Very early on, all three variables actually had small negative correlation coefficients, with higher values resulting in
 4 smaller gas flows out MB139. However, the effects may have been too small to be significant at that time because
 5 almost no gas had flowed out in any realization. One interesting feature that shows up in the scatterplots is that
 6 there appear to be cutoff values in both BRSAT and MBPERM below which there is no gas flow out MB139. For
 7 BRSAT, this value is about 4% initial brine saturation in the waste. When the initial brine saturation is too low,
 8 insufficient gas is generated to raise the pressure in the repository and push gas out the anhydrite layers. For
 9 anhydrite permeability, the cutoff is about 10^{-20} m², the same value below which brine flow becomes insignificant.

10 Table 5-20. Stepwise Regression Analysis with Rank-Transformed Data for Cumulative Net Gas Flow
 11 South into MB139 (GASMB9SC)

Step	Variable	Description	SRC	R ²
1	BRSAT	Initial brine saturation in waste	0.49	0.25
2	MBPERM	Log of anhydrite interbeds permeability	0.41	0.43
3	STOICMIC	Biodegradation stoichiometric coefficient	0.27	0.50

13 5.4.2 Cumulative Net Gas Flow Out Anhydrite a + b

14 The regression analysis for cumulative gas flow south out through anhydrite layers a + b, in Table 5-21, also
 15 selected BRSAT as the first variable. The correlation is somewhat stronger than it was in MB139. Because gas
 16 flow is not competing with brine outflow, gas generation, which is largely controlled by the initial brine saturation,
 17 has a more direct impact on gas flow. Anhydrite permeability and biodegradation stoichiometry were again
 18 selected. Together, these three account for 66% of the variability in gas flow out anhydrite a + b. Gas generation,
 19 again, has a strong influence on the amount of gas that flows out the anhydrite layer. The plot of partial rank
 20 correlation coefficients, Figure 5-20, shows that BRSAT and MBPERM dominate in determining the cumulative gas
 21 flows over the last 8000 yr. Scatterplots of BRSAT and MBPERM, in Figure 5-20, show lower limits below which
 22 gas does not flow out anhydrite a+ b, the values again being 4% for brine saturation and 10^{-20} m² for permeability.

5. Uncertainty and Sensitivity Analysis Results

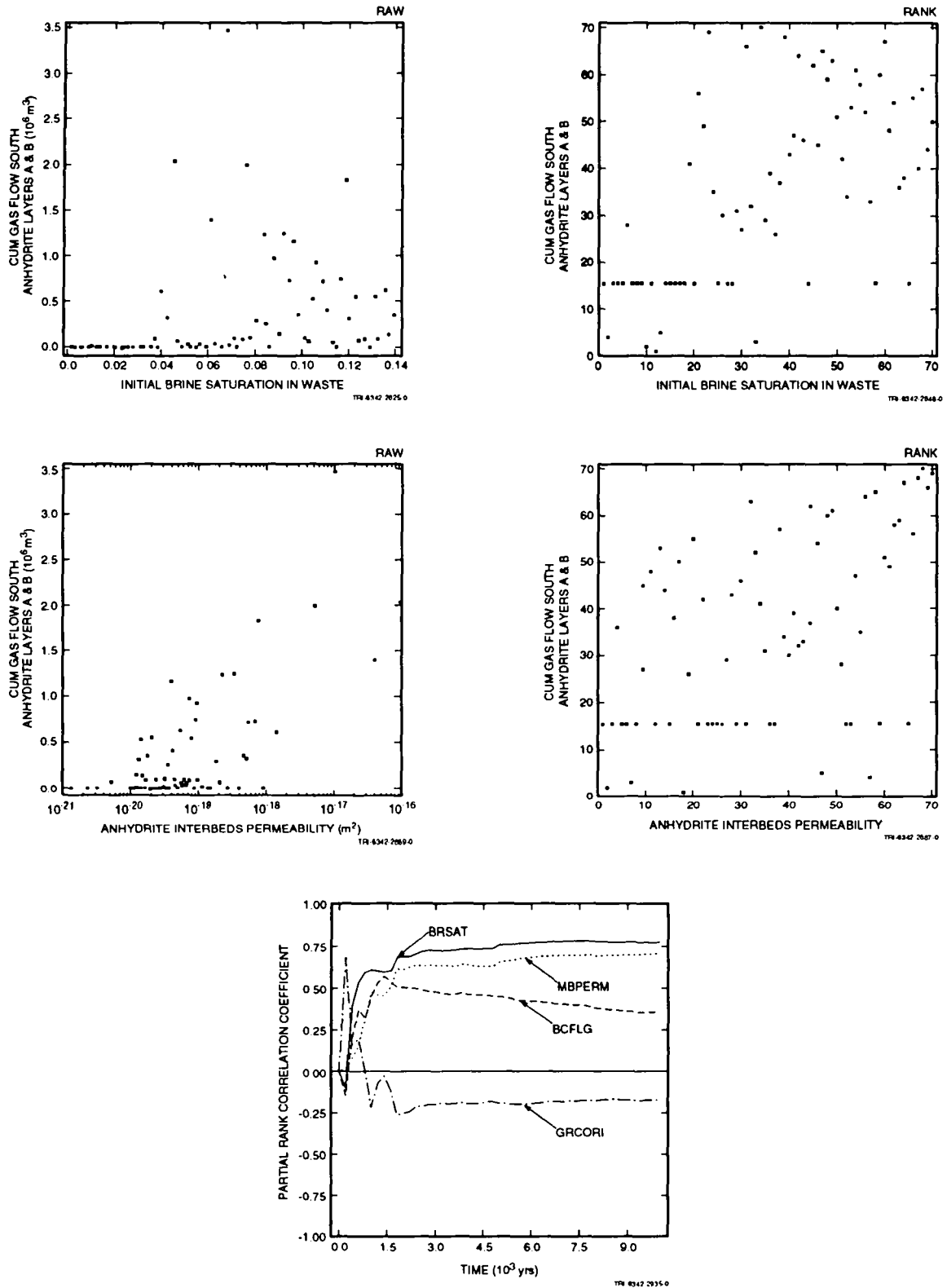


Figure 5-20. Scatterplots and partial rank correlation coefficients for cumulative net gas flow out anhydrite a + b. (Rows of points in the rank plots with identical ranks result from the convention used to assign ranks to realizations with identical raw results [i.e., zero]).

Table 5-21. Stepwise Regression Analysis with Rank-Transformed Data for Cumulative Net Gas Flow Out Anhydrite Layers a + b (GASANHSC)

Step	Variable	Description	SRC	R ²
1	BRSAT	Initial brine saturation in waste	0.59	0.37
2	MBPERM	Log of anhydrite interbeds permeability	0.50	0.61
3	STOICMIC	Biodegradation stoichiometric coefficient	0.22	0.66
4	GRCORI	Inundated corrosion rate	0.20	0.69

5.4.3 Cumulative Net Gas Flow Out MB138

The regression analysis for cumulative gas flow south out through MB138, Table 5-22, as for the other two anhydrite layers, selected BRSAT and MBPERM as the two most important variables affecting gas flow (Figure 5-21). Two other gas generation parameters, STOICMIC and GRCORI (inundated corrosion rate), also made small contributions to the variability of gas flow out MB138. Comments made above regarding the other two anhydrite layers apply also to MB138.

One other parameter, BCFLG, which is the weighting factor that determines which relative permeability model to use, showed a small influence in all three anhydrite layers (but only in the plots of partial rank correlation coefficients for MB139 and anhydrite a + b). When BCFLG = 0, the van Genuchten-Parker model is used; when BCFLG = 1, the Brooks-Corey model is used. In MB139, BCFLG had a positive correlation coefficient, whereas in anhydrite a + b and in MB138, it had a negative correlation. It is positive during the first 500 yr or so in all three layers, but there is almost no gas flow during this period in any realization. Therefore, the high value that seems to dominate all other variables over that time period is apparently spurious. Once gas flows have started in most realizations, the influence of BCFLG quickly becomes insignificant.

5. Uncertainty and Sensitivity Analysis Results

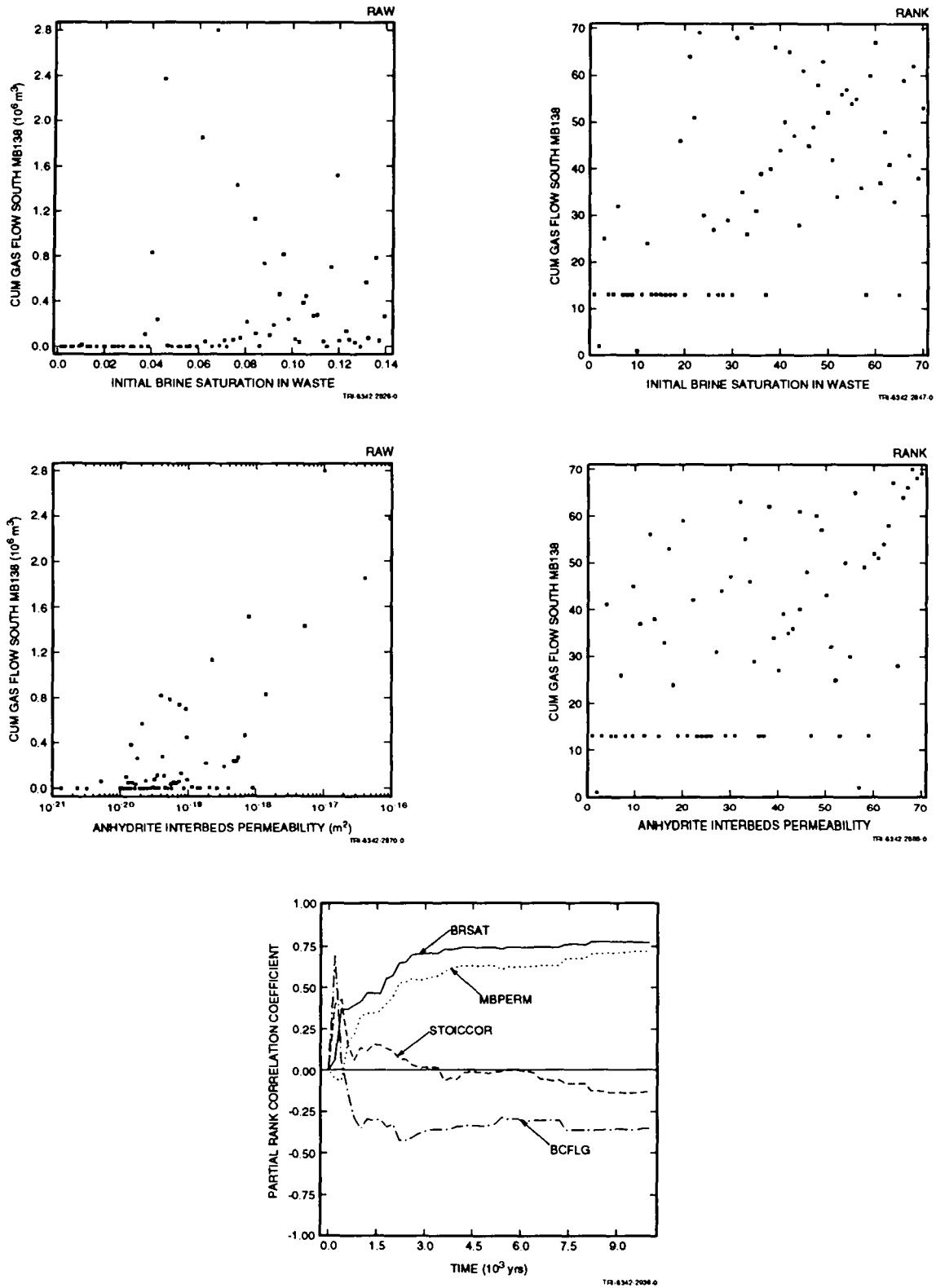


Figure 5-21. Scatterplots and partial rank correlation coefficients for cumulative net gas flow out of MB138. (Rows of points in the rank plots with identical ranks result from the convention used to assign ranks to realizations with identical raw results [i.e., zero]).

Table 5-22. Stepwise Regression Analysis with Rank-Transformed Data for Cumulative Net Gas Flow Out MB138 (GASMB8SC)

Step	Variable	Description	SRC	R ²
1	BRSAT	Initial brine saturation in waste	0.58	0.34
2	MBPERM	Log of anhydrite interbeds permeability	0.53	0.61
3	BCFLG	Brooks-Corey/van Genuchten-Parker weighting factor	-0.22	0.64
4	STOICMIC	Biodegradation stoichiometric coefficient	0.20	0.68
5	GRCORI	Inundated corrosion rate	0.17	0.71

5.4.4 Distance Gas Flows Out Anhydrite Layers

Three additional performance measures test the possible impact of the storage capacity of various regions. These measures are the distances that gas flows out each of the three anhydrite layers. Factors that affect storage or retention of fluids would be expected to influence how far gas can flow.

The results of the stepwise regression analyses and partial rank correlation analyses continue to show that the initial brine saturation in the waste is the most important variable affecting how far gas flows away from the repository. No storage factors, such as anhydrite porosity and DRZ porosity, and no retention parameters, such as residual saturations, have any measurable effect on the distance that gas migrates from the repository.

The stepwise regression analysis for distance that gas flows out MB139, shown in Table 5-23, selected BRSAT as the first variable. Although it has greater influence than any other variable, its impact is fairly weak, accounting for only 27% of the variability in gas flow distance. Nearly as influential is anhydrite permeability. As seen in preceding analyses, initial brine saturation in the waste results in the main driving force for gas migration away from the repository, whereas anhydrite permeability determines the ease with which gas flows out as it is generated. Scatterplots relating gas flow distance to these two variables, Figure 5-22, confirm the slight trends in the raw data. Gas migration distances appear at a small number of fixed values. These are the distances from the repository to the outer edge of the grid cells in the mesh, as shown in Table 4-1. Gas is assumed to have reached that distance when the saturation in a grid cell exceeds 1.0×10^{-12} . Volumes of gas in grid cells at this minimum saturation are extremely small (i.e., less than one m³).

5. Uncertainty and Sensitivity Analysis Results

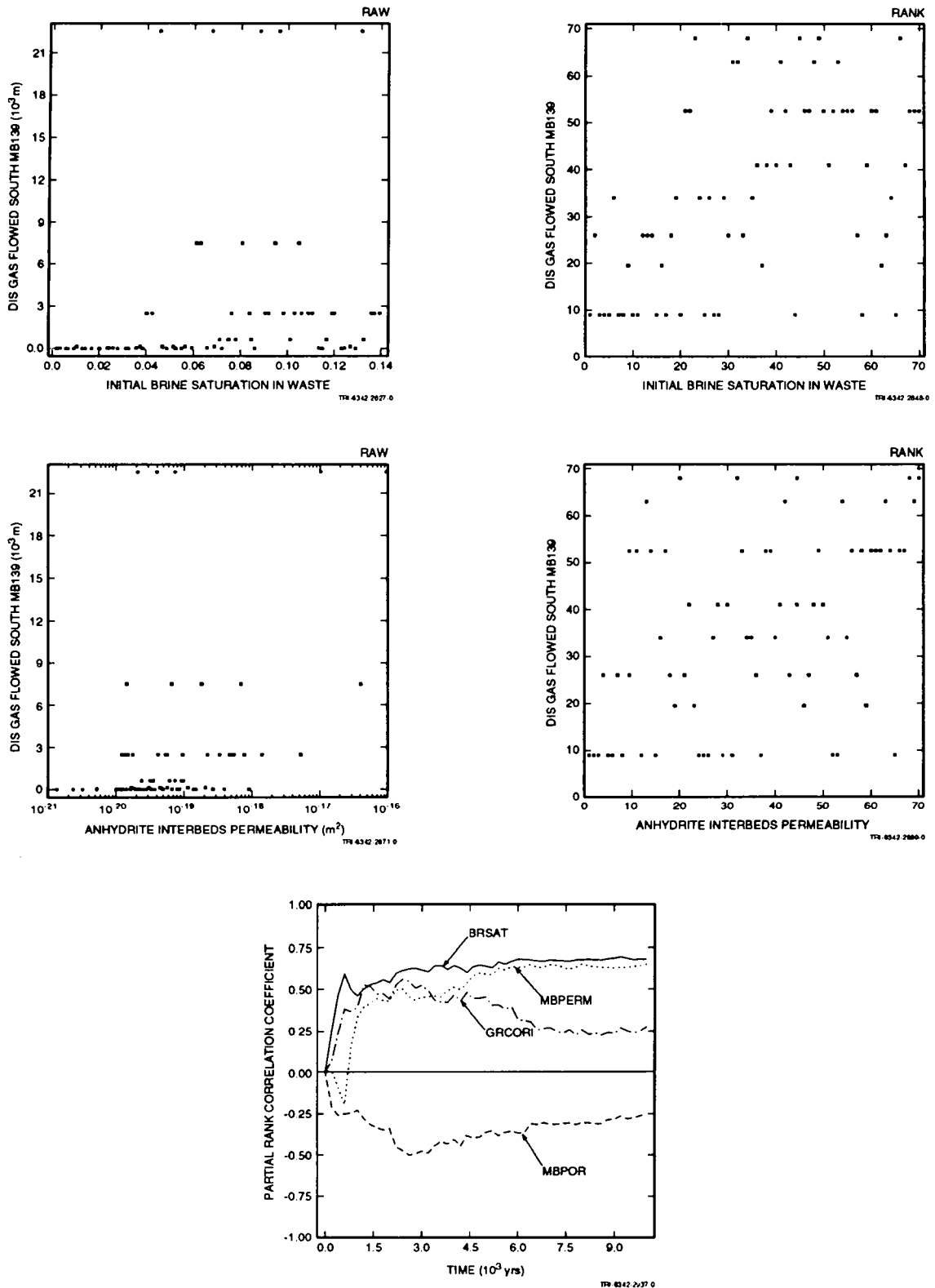


Figure 5-22. Scatterplots and partial rank correlation coefficients for distance gas flows out MB139. (Rows of points in the rank plots with identical ranks result from the convention used to assign ranks to realizations with identical raw results [i.e., zero]).

The next variable selected in the regression analysis is the relative permeability model weight factor, BCFLG. This variable has a negative regression coefficient, indicating that gas migration distance tends to be less when BCFLG = 1 (i. e., when the Brooks-Corey model is used), and migration distances tend to be greater when the van Genuchten-Parker model is used. The effect is minor, but seems to stem from the differences in capillary pressure between the two models. Unlike the Brooks-Corey model, the van Genuchten-Parker model uses a threshold capillary pressure of zero, so there is no minimum gas pressure required for flow to occur. The slightly greater ease with which gas flow is initiated using the van Genuchten-Parker model results in greater migration distances.

The last variable selected in the regression analysis is STOICMIC, the biodegradation stoichiometric coefficient. Although its influence is slight, it contributes to the driving force behind gas migration in the same way that BRSAT does.

The plots of partial rank correlation coefficients shown in Figure 5-22 indicate that the influence of the first three variables increases slowly over at least the last 8000 yr. The inundated corrosion rate shows some impact during the first 3000 yr, but its influence wanes after that.

Table 5-23. Stepwise Regression Analysis with Rank-Transformed Data for Distance Gas Flows Out MB139 (GDSTMB9S)

Step	Variable	Description	SRC	R ²
1	BRSAT	Initial brine saturation in waste	0.52	0.27
2	MBPERM	Log of anhydrite interbeds permeability	0.45	0.46
3	BCFLG	Brooks-Corey/van Genuchten-Parker weighting factor	-0.36	0.56
4	STOICMIC	Biodegradation stoichiometric coefficient	0.21	0.60

The regression analysis (Table 5-24) for gas migration distance out through anhydrite a + b is essentially identical to that of MB139, but with slightly better correlations.

The regression analysis (Table 5-25) for gas migration distance out through MB138 is also nearly identical to that of MB139 and anhydrite a + b, but with still slightly better correlations. An additional gas generation parameter has been added, although its effect is barely measurable.

5. Uncertainty and Sensitivity Analysis Results

1 Table 5-24. Stepwise Regression Analysis with Rank-Transformed Data for Gas Migration Distance South
 2 Out Anhydrite Layers a + b (GDSTANHS)

Step	Variable	Description	SRC	R ²
1	BRSAT	Initial brine saturation in waste	0.59	0.34
2	MBPERM	Log of anhydrite interbeds permeability	0.45	0.53
3	BCFLG	Brooks-Corey/van Genuchten-Parker weighting factor	-0.35	0.62
4	STOICMIC	Biodegradation stoichiometric coefficient	0.24	0.68

4
 5 Table 5-25. Stepwise Regression Analysis with Rank-Transformed Data for Gas Migration Distance South
 6 Out MB138 (GDSTMB8S)

Step	Variable	Description	SRC	R ²
1	BRSAT	Initial brine saturation in waste	0.58	0.34
2	MBPERM	Log of anhydrite interbeds permeability	0.51	0.57
3	BCFLG	Brooks-Corey/van Genuchten-Parker weighting factor	-0.41	0.71
4	STOICMIC	Biodegradation stoichiometric coefficient	0.19	0.75

8

The regression analysis for gas migration distance out through the Culebra, shown in Table 5-26, selected BCFLG as the most influential variable, although its effect is minor. The low values of R^2 are obtained because only eight realizations resulted in gas migration distances from the shaft into the Culebra that were greater than zero. With so few non-zero responses, little significance can be assigned to this analysis.

Table 5-26. Stepwise Regression Analysis with Rank-Transformed Data for Gas Migration Distance South Out the Culebra (GDSTCULS)

Step	Variable	Description	SRC	R^2
1	BCFLG	Brooks-Corey/van Genuchten-Parker weighting factor	-0.49	0.18
2	BCEXP	Brooks-Corey exponent	-0.35	0.29
3	SALPERM	Intact Salado halite permeability	0.27	0.36

5.4.5 Cumulative Net Gas Flow Upward through Shaft Seal

Two more crucial performance measures are flow through the shaft seal and flow into the Culebra layer of the BRAGFLO model. Since the lower shaft is assumed to have zero residual gas saturation, any amount of gas that gets through the shaft seal can, in principle, reach the Culebra layer, which is outside the disposal unit boundary. (The top of the Salado Formation is the boundary for purposes of evaluating gas migration.) Cumulative flow into the Culebra, GASCULTC (which is actually measured from the Culebra shaft seal into the Culebra), is greater than zero in 6 of the 70 realizations. Flows range from 109 to 136,000 m^3 .

The regression analysis for cumulative gas flow through the shaft seal, Table 5-27, once again selected the initial brine saturation in the waste as the first variable. As in the anhydrite analyses, the correlation between gas flow and brine saturation is not particularly strong, but the scatterplot, Figure 5-23, shows an apparent minimum value of brine saturation (6%) below which no gas flows through the shaft seal. This again stems from a minimum gas and pressure generation required for gas to migrate beyond the repository. The plot of partial rank correlation coefficients, Figure 5-23, shows that BRSAT is the dominant variable over the full 10,000 yr. Together with STOICMIC, gas generation parameters account for at least 47% of the variability in gas flow through the shaft seal.

5. Uncertainty and Sensitivity Analysis Results

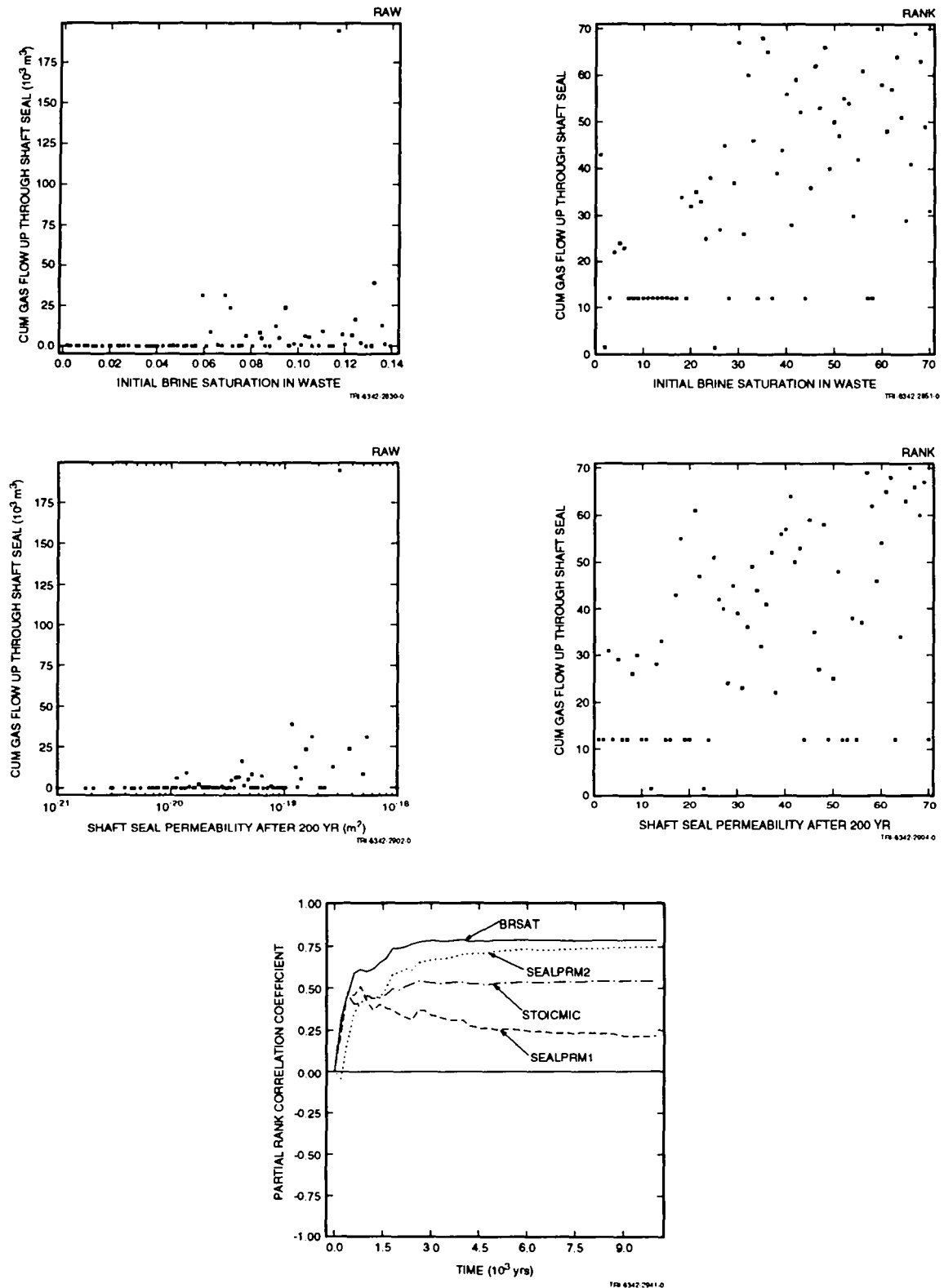


Figure 5-23. Scatterplots and partial rank correlation coefficients for cumulative net gas flow upward through the shaft seal. (Rows of points in the rank plots with identical ranks result from the convention used to assign ranks to realizations with identical raw results [i.e., zero]).

Table 5-27. Stepwise Regression Analysis with Rank-Transformed Data for Cumulative Net Upward Gas Flow through Shaft Seal (GSHSLUPC)

Step	Variable	Description	SRC	R ²
1	BRSAT	Initial brine saturation in waste	0.60	0.37
2	SEALPRM2	Shaft seal permeability after 200 yr	0.50	0.60
3	STOICMIC	Biodegradation stoichiometric coefficient	0.31	0.70

5.4.6 Cumulative Net Gas Flow Upward into the Culebra

The regression analysis for cumulative net gas flow into the Culebra from the Culebra shaft seal, in Table 5-28, selected the permeability of the shaft seal after 200 yr as the first variable. As expected, the higher the permeability, the more gas flowed into the Culebra. The correlation is not strong, accounting for only 30% of the variability in GASCULTC, but this is largely a result of the few occurrences of flow into the Culebra; there were only six realizations in which there was any significant flow. (Two more realizations had minute quantities of gas flow into the Culebra — enough to result in measurable gas migration distances.) Whereas five of these ranged from 110 m³ to 1070 m³, there was one realization that resulted in 136,000 m³. The scatterplots shown in Figure 5-24 illustrate how this correlation is unduly weighted by a single outlying data point, although the regression analysis supports intuitively finding that seal permeability and parameters that control gas generation have the most influence on the amount of gas that flows into the Culebra. The partial rank correlation coefficients, Figure 5-24, indicate that the influence of these two parameters is growing with time. The step-like behavior of the curves is indicative of the few realizations in which flow into the Culebra actually resulted.

Table 5-28. Stepwise Regression Analysis with Rank-Transformed Data for Cumulative Net Gas Flow into the Culebra (GASCULTC)

Step	Variable	Description	SRC	R ²
1	SEALPRM2	Shaft seal permeability after 200 yr	0.55	0.30
2	BRSAT	Initial brine saturation in waste	0.38	0.45

5. Uncertainty and Sensitivity Analysis Results

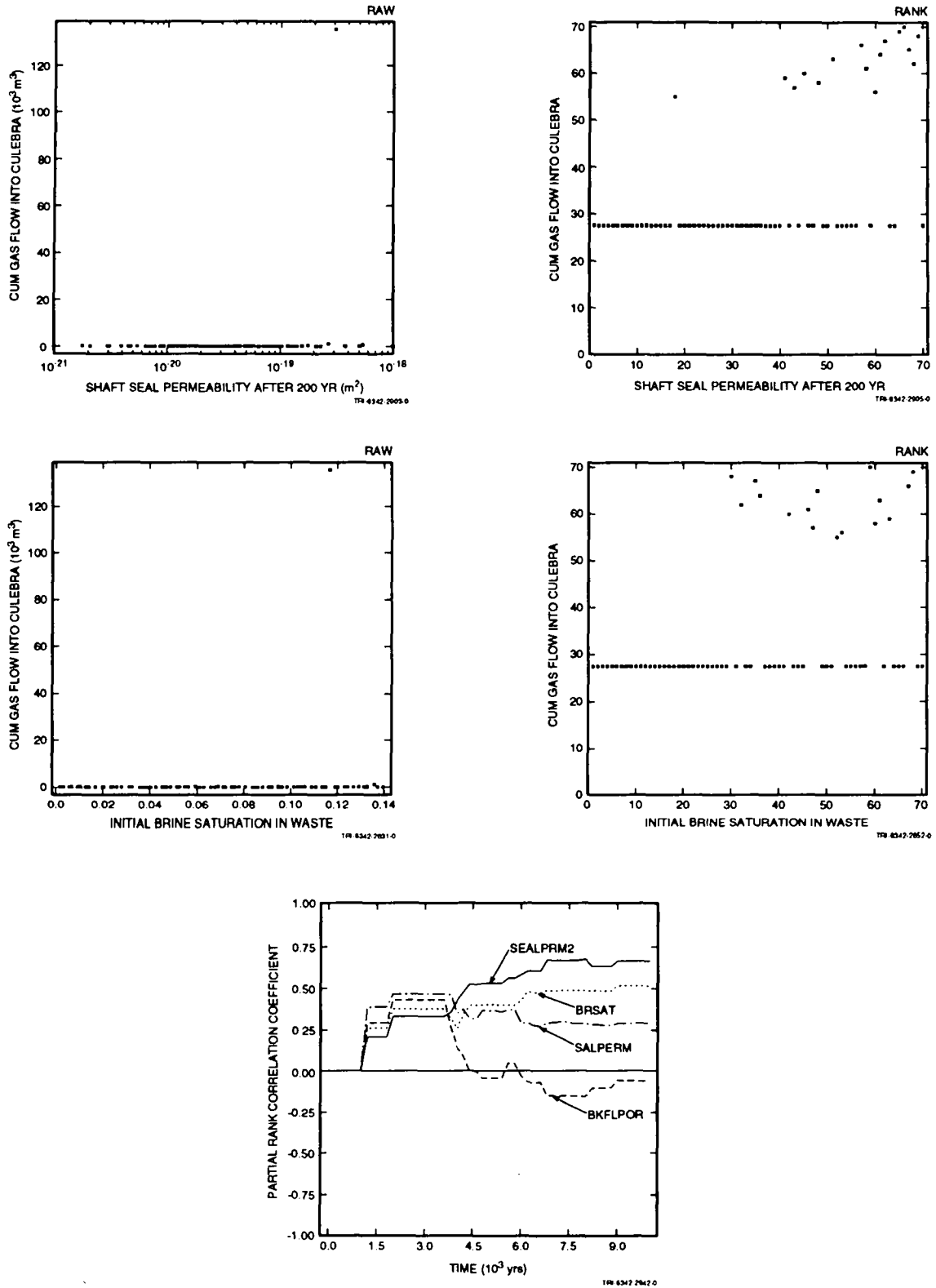


Figure 5-24. Scatterplots and partial rank correlation coefficients for cumulative net gas flow upward through the shaft seal. (Rows of points in the rank plots with identical ranks result from the convention used to assign ranks to realizations with identical raw results [i.e., zero]).

6. SUMMARY AND CONCLUSIONS

Conclusions based on these analyses are conditional on the modeling assumptions and parameter-value distributions used in the 1992 preliminary PA. These analyses do not represent a final performance assessment, and results should not be used for comparisons to regulatory standards. The 1992 PA modeling system does not yet include all potentially important physical processes that may affect disposal-system performance (e.g., pressure-dependent fracturing of anhydrites and effects of possible channeling of fluid flow are not included in 1992, and will be included in future PAs), nor are all portions of the data base complete. Results are presented here to provide interim guidance to the WIPP Project as it plans for a final compliance evaluation.

Of the 25 parameters that were selected for sampling in the analyses of undisturbed performance, 6 have significant effects on the performance measures considered. These 6 parameters are listed in Table 6-1 as "very important," reflecting their potential impact on gas and brine migration from the repository. The single most important parameter, as shown in the sensitivity analyses described in Chapter 5 of this volume, is the initial brine saturation in the waste. Few data are available for this parameter (see Section 2.4 of this volume), but for the range of values sampled here, the initial water content of the waste effectively controls the amount of gas that is generated. The total amount of gas generated, in turn, controls how much gas flows out through the various release pathways. Unless the overall gas-generation rate is very small, the full gas-generation potential allowed by the amount of water initially present will be realized over 10,000 yr. Unless the permeability of the anhydrite layers is near the lower limit of the sampled range, this time period is sufficient for gas to flow to the disposal-unit boundaries as long as enough water is initially present to generate the amount of gas required to flow that far. The other five parameters listed as "very important" also play a major role in influencing gas and brine migration from the repository, but their effect is secondary to that of the initial brine saturation. The range of initial brine saturation currently used does not have a sound basis in measured data, and is expected to change. Because this one parameter so dominates the undisturbed performance, a different range of values may produce different results, and even the conclusions with the strongest statistical support in this report should be regarded as preliminary.

Most of the other sampled parameters had a smaller impact on gas and brine migration, and are listed as "important" in Table 6-1. These parameters each appear in only a few of the regression analyses reported in Chapter 5. Their importance, however, is conditional on the conceptual models used to describe the repository and its surroundings, and may change in future analyses as conceptual models are refined.

The final category of parameters listed in Table 6-1, "less important," includes those that were not identified in any of the regression analyses reported in Chapter 5. Conditional on all assumptions of the 1992 PA, the distributions used for these parameters had no effect on the undisturbed performance measures considered. Essentially any value could have been selected from the distributions and used as a fixed value throughout without affecting performance, implying that, unless conceptual models change significantly, these parameters could be omitted from future samplings if the present ranges are shown to be defensible. However, these conclusions apply only to undisturbed performance; some parameters that are insignificant here (e.g., Culebra matrix porosity) may be more important in assessing performance following human intrusion.

6. Summary and Conclusions

1 Table 6-1. Importance of Sampled Parameters with Respect to 40 CFR 268.6. Results apply only to
 2 undisturbed performance of the repository (no human intrusion), and are conditional on
 3 modeling assumptions, the choice of parameters sampled, and the assumed parameter-value
 4 distributions. Comparable results for 40 CFR 191B (disturbed performance) can be found in
 5 Volume 4 of this report.
 6

Parameter Name	Parameter Description
Very Important Parameters (listed in order of importance)	
BRSAT	Initial brine saturation in waste*
MBPERM	Salado anhydrite permeability
STOICMIC	Biodegradation stoichiometric coefficient
GRCORI	Corrosion gas-generation rate, inundated conditions
GRMICI	Biodegradation gas-generation rate, inundated conditions
SEALPERM2	Shaft seal permeability after 200 yr
Important Parameters (listed in alphabetical order)	
BCFLG	Brooks-Corey/van Genuchten-Parker pointer
GRCORHF	Corrosion gas-generation rate factor, humid conditions
GRMICHF	Biodegradation gas-generation rate factor, humid conditions
MBPOR	Salado anhydrite porosity
SALPERM	Salado halite permeability
SEALPERM1	Shaft seal permeability, 0-200 yr
SHFTPRM	Lower shaft permeability, 0-200 yr
STOICCOR	Corrosion stoichiometric coefficient
TZPORF	Transition zone and DRZ porosity factor
VMETAL	Initial volume fraction of metals and glass in waste
VWOOD	Initial volume fraction of combustibles in waste
Less Important Parameters (listed in alphabetical order)	
BCBRSAT	Residual brine saturation in Salado Fm.
BCEXP	Brooks-Corey relative permeability model exponent
BCGSSAT	Residual gas saturation in Salado Fm.
BKFLPOR	Porosity of backfill in drifts, experimental region, and shaft below seal
CULPOR	Matrix porosity of Culebra
DSEALPRM	Drift and panel seal permeability
MBPRES	Far-field pressure in Salado Fm.
SEALTHK	Shaft seal vertical thickness

* Importance of initial brine saturation in the waste may be highly sensitive to the assumed parameter-value distribution. See text for additional information.

7. REFERENCES

- Beauheim, R.L., G.J. Saulnier, Jr., and J.D. Avis. 1991 *Interpretation of Brine-Permeability Tests of the Salado Formation at the Waste Isolation Pilot Plant Site: First Interim Report*. SAND90-0083. Albuquerque, NM: Sandia National Laboratories.
- Bertram-Howery, S.G., M.G. Marietta, R.P. Rechar, P.N. Swift, D.R. Anderson, B.L. Baker, J.E. Bean, Jr., W. Beyeler, K.F. Brinster, R.V. Guzowski, J.C. Helton, R.D. McCurley, D.K. Rudeen, J.D. Schreiber, and P. Vaughn. 1990. *Preliminary Comparison with 40 CFR Part 191, Subpart B for the Waste Isolation Pilot Plant, December 1990*. SAND90-2347. Albuquerque, NM: Sandia National Laboratories.
- Butcher, B.M. 1990. Appendix A: "Memo 5: Disposal Room Porosity and Permeability Values for Disposal Room Performance Assessment," *Data Used in Preliminary Performance Assessment of the Waste Isolation Pilot Plant (1990)*. R.P. Rechar, H. Iuzzolino, and J.S. Sandha. SAND89-2408. Albuquerque, NM: Sandia National Laboratories. A-93 through A-102.
- Helton, J.C. 1993. "Risk, Uncertainty in Risk, and the EPA Release Limits for Radioactive Waste Disposal," *Nuclear Technology*. SAND91-1255J. Vol. 101, no. 1, 18-39.
- Helton, J.C., J.W. Garner, R.D. McCurley, and D.K. Rudeen. 1991. *Sensitivity Analysis Techniques and Results for Performance Assessment at the Waste Isolation Pilot Plant*. SAND90-7103. Albuquerque, NM: Sandia National Laboratories.
- Helton, J.C., J.W. Garner, R.P. Rechar, D.K. Rudeen, and P.N. Swift. 1992. *Preliminary Comparison with 40 CFR Part 191, Subpart B for the Waste Isolation Pilot Plant, December 1991—Volume 4: Uncertainty and Sensitivity Analysis Results*. SAND91-0893/4. Albuquerque, NM: Sandia National Laboratories.
- Howarth, S.M., E.W. Peterson, P.L. Lagus, K. Lie, S.J. Finley, and E.J. Nowak. 1991. "Interpretation of In-Situ Pressure and Flow Measurements of the Salado Formation at the Waste Isolation Pilot Plant," *1991 Joint Rocky Mountain Regional Meeting and Low Permeability Reservoirs Symposium, Society of Petroleum Engineers, Denver, CO, April 15-17, 1991*. SPE-21840. Richardson, TX: Society of Petroleum Engineers. 355-369.
- Iman, R.L., and W.J. Conover. 1979. "The Use of the Rank Transform in Regression," *Technometrics*. Vol. 21, No. 4, 499-509.
- Iman, R.L., J.M. Davenport, E.L. Frost, and M.J. Shortencarier. 1980. *Stepwise Regression with PRESS and Rank Regression (Program and User's Guide)*. SAND79-1472. Albuquerque, NM: Sandia National Laboratories.
- Iman, R.L., M.J. Shortencarier, and J.D. Johnson. 1985. *A FORTRAN 77 Program and User's Guide for the Calculation of Partial Correlation and Standardized Regression Coefficients*. NUREG/CR-4122, SAND85-0044. Albuquerque, NM: Sandia National Laboratories.
- Kelley, V.A., and G.J. Saulnier, Jr. 1990 *Core Analyses for Selected Samples from the Culebra Dolomite at the Waste Isolation Pilot Plant Site*. SAND90-7011. Albuquerque, NM: Sandia National Laboratories.

References

- Lappin, A.R., R.L. Hunter, D.P. Garber, P.B. Davies, R.L. Beauheim, D.J. Borns, L.H. Brush, B.M. Butcher, T. Cauffman, M.S.Y. Chu, L.S. Gomez, R.V. Guzowski, H.J. Iuzzolino, V. Kelley, S.J. Lambert, M.G. Marietta, J.W. Mercer, E.J. Nowak, J. Pickens, R.P. Rechard, M. Reeves, K.L. Robinson, and M.D. Siegel. 1989. *Systems Analysis, Long-Term Radionuclide Transport, and Dose Assessments, Waste Isolation Pilot Plant (WIPP), Southeastern New Mexico; March 1989*. SAND89-0462. Albuquerque, NM: Sandia National Laboratories.
- Munson, D.E., A.F. Fossum, and P.E. Senseny. 1989. *Advances in Resolution of Discrepancies Between Predicted and Measured In Situ WIPP Room Closures*. SAND88-2948. Albuquerque, NM: Sandia National Laboratories.
- Rechard, R.P., ed. 1992. *User's Reference Manual for CAMCON: Compliance Assessment Methodology Controller Version 3.0*. SAND90-1983. Albuquerque, NM: Sandia National Laboratories.
- Rechard, R.P., W. Beyeler, R.D. McCurley, D.K. Rudeen, J.E. Bean, and J.D. Schreiber. 1990. *Parameter Sensitivity Studies of Selected Components of the Waste Isolation Pilot Plant Repository/Shaft System*. SAND89-2030. Albuquerque, NM: Sandia National Laboratories.
- Stone, C.M., R.D. Krieg, and Z.E. Beisinger. 1985. *SANCHO: A Finite Element Computer Program for the Quasistatic, Large Deformation, Inelastic Response of Two-Dimensional Solids*. SAND84-2618. Albuquerque, NM: Sandia National Laboratories.
- U.S. DOE (Department of Energy). 1990a. *Waste Isolation Pilot Plant No-Migration Variance Petition*. DOE/WIPP 89-003, Revision 1. Carlsbad, NM: Westinghouse Electric Corporation, Waste Isolation Division.
- U.S. DOE (Department of Energy). 1990b. *Draft Plan for the Waste Isolation Pilot Plant Test Phase: Performance Assessment and Operations Demonstration*. DOE/WIPP 89-011. Carlsbad, NM: U.S. Department of Energy, Waste Isolation Pilot Plant. (Copy on file at the Waste Management and Transportation Library, Sandia National Laboratories, Albuquerque, NM.)
- U.S. DOE (Department of Energy). 1991a. *Quality Assurance Program Plan for the Waste Isolation Pilot Plant Experimental Waste-Characterization Program*. DOE/EM/48063-1, Rev. 1, Washington, D.C.
- U.S. DOE (Department of Energy). 1991b. *Waste Characterization Program Plan for WIPP Experimental Waste*. DOE/WIPP 89-025, Rev. 1, Carlsbad, NM: Westinghouse Electric Corporation.
- U.S. DOE (Department of Energy). 1991c. *Waste Acceptance Criteria for the Waste Isolation Pilot Plant, December 1991*. DOE/WIPP-069, Rev. 4. Carlsbad, NM: Westinghouse Electric Corporation.
- U.S. DOE (Department of Energy). 1993. *Test Phase Plan for the Waste Isolation Pilot Plant*. DOE/WIPP 89-011, Rev. 1. Albuquerque, NM: U.S. Department of Energy, WIPP Project Integration Office.
- U.S. EPA (Environmental Protection Agency). 1985. "40 CFR 191: Environmental Standards for the Management and Disposal of Spent Nuclear Fuel, High-Level and Transuranic Radioactive Wastes, Final Rule," *Federal Register*. Vol. 50, no. 182, 38066-38089.

- U.S. EPA (Environmental Protection Agency). 1986. "Land Disposal Restrictions," *Code of Federal Regulations 40, Part 268*. Washington, DC: Office of the Federal Register, National Archives and Records Administration.
- U.S. EPA (Environmental Protection Agency). 1990a. "Hazardous and Solid Waste; Conditional Variance to Department of Energy Waste Isolation Pilot Plant; Notice of Proposed Decision," *Federal Register*, V. 55, No. 67, 13068-13094.
- U.S. EPA (Environmental Protection Agency). 1990b. "Conditional No-Migration Determination for the Department of Energy Waste Isolation Pilot Plant (WIPP)," *Federal Register*. Vol. 55. no. 220, 47700-47721.
- U.S. EPA (Environmental Protection Agency). 1992. *"No Migration" Variances to the Hazardous Waste Land Disposal Prohibitions: A Guidance Manual for Petitioners, Draft, July 1992*. EPA 530/R/92/03. Washington, DC: U.S. Environmental Protection Agency, Office of Solid Waste. (Copy on file at the Waste Management and Transportation Library, Sandia National Laboratories, Albuquerque, NM.)
- Voss, C. I. 1984. *SUTRA (Saturated-Unsaturated TRANsport): A Finite-Element Simulation Model for Saturated-Unsaturated, Fluid-Density-Dependent Ground-Water Flow with Energy Transport or Chemically-Reactive Single-Species Solute Transport*. Water-Resources Investigations Report 84-4369. Reston, VA: U. S. Geological Survey National Center.
- WIPP PA (Performance Assessment) Department. 1992. *Long-Term Gas and Brine Migration at the Waste Isolation Pilot Plant: Preliminary Sensitivity Analyses for Post-Closure 40 CFR 268 (RCRA), May 1992*. SAND92-1933. Albuquerque, NM: Sandia National Laboratories.
- WIPP PA (Performance Assessment) Division. 1991a. *Preliminary Comparison with 40 CFR Part 191, Subpart B for the Waste Isolation Pilot Plant, December 1991. Volume 1: Methodology and Results*. SAND91-0893/1. Albuquerque, NM: Sandia National Laboratories.
- WIPP PA (Performance Assessment) Division. 1991b. *Preliminary Comparison with 40 CFR Part 191, Subpart B for the Waste Isolation Pilot Plant, December 1991. Volume 2: Probability and Consequence Modeling*. SAND91-0893/2. Albuquerque, NM: Sandia National Laboratories.
- WIPP PA (Performance Assessment) Division. 1991c. *Preliminary Comparison with 40 CFR Part 191, Subpart B for the Waste Isolation Pilot Plant, December 1991. Volume 3: Reference Data*. SAND91-0893/3. Albuquerque, NM: Sandia National Laboratories.

APPENDIX A: MEMORANDUM REGARDING REFERENCE DATA

APPENDIX A: MEMORANDUM REGARDING REFERENCE DATA

Referenced Memorandum

Finley and Vaughn, February 17, 1993 A-5

2/17/93

WIPP Performance Assessment Dept. 6342

Ray E. Finley, 6121, and Palmer Vaughn, 6342

Seal and Backfill Information

A series of meetings was held between the Repository Isolation Systems Dept. (6121) and the WIPP Performance Assessment Dept. (6342) personnel to develop seal and backfill parameters for the 1993 gas migration calculations to be performed by Dept. 6342. Estimates for seal and backfill parameters were developed from available literature for two time periods: 0-200 years, and 200-10,000 years. The modeling to be done by 6342 requires upper and lower bound estimates, and in some cases "best guess" estimates for each parameter of interest for each time period. Table 1 (attached) lists the various seal and backfill locations and parameters required for the Gas Migration calculations.

The estimates listed in Table 1 assume that the water-bearing-zone seals are effective at limiting water inflow into the facility. Also, these estimates do not take into consideration the DRZ in the surrounding halite or in the interbeds (primarily MB139).

It should be stressed that the values in Table 1 are estimates and could change as our understanding of the nature and behavior of the seal materials changes. Also, the estimates are limited by the assumptions used in the reference materials.

Implicit in Table 1 are various assumptions of correlations between certain parameters; e.g., porosities are correlated to permeabilities, although the correlation is not stated. The threshold capillary pressure is assumed to be correlated to permeability.

Although the values shown in Table 1 represent the current best estimates, modeling constraints and the need to be more consistent in making assumptions resulted in some changes in values. The values actually used in the calculations are shown in Table 2. Correlations implicit in Table 1 were clarified and are shown more explicitly in Table 2. In particular, note that porosities are correlated to the log of permeabilities.

Initial brine saturations were originally assumed to correspond to 5-8 wt% of the salt and backfill. However, given the ranges of porosities in Table 2 and using values of bulk density and brine density measured for WIPP halite and Salado brine (2140 kg/m³ and 1230 kg/m³, respectively), it was found that 5-8 wt% brine corresponds to more than 90% brine saturation. The lowest brine saturation corresponds to 5 wt% brine added to halite having a compacted porosity of 9%. If 5 wt% brine is added to crush halite having a porosity of 9% after compaction, the pore space will be 90% saturated with brine. Rather than sample a narrow

range of initial brine saturations in the backfill/seal/shaft components (90-100%) a fixed value of 100% is assumed (1.0, Table 2).

In Table 1, the porosity of the Shaft Seal is shown changing after 200 years, and the Shaft Fill porosity differs from that of the Shaft Seal. Furthermore, it is anticipated that the Shaft Fill porosity will become identical to that of the Shaft Seal after 200 years. However, these changes create problems in modeling because they constitute instantaneous changes in brine mass that introduce mass balance errors into the calculations. It is difficult to rationalize these errors, which are artifacts of the model. To avoid this difficulty, the porosities of these two materials will be assumed to be equal and constant in time, rather than changing at 200 years. This is expected to result in more accurate results even though the porosity change that is actually believed to occur is ignored.

The parameter values listed in Table 1 were developed from information contained in the following references:

Arguello, J.G., 1988, "WIPP Panel Entryway Seal - Numerical Simulation of Seal Composite Interaction for Preliminary Design Evaluation," SAND87-2804, Sandia National Laboratories, Albuquerque, NM.

Butcher, B.M., 1991, "The Advantages of a Salt/Bentonite Backfill for Waste Isolation Pilot Plant Disposal Rooms," SAND90-3074, Sandia National Laboratories, Albuquerque, NM.

Ehgartner, B., 1990, "Geomechanical Analyses in Support of the Waste Isolation Pilot Plant (WIPP)," SAND90-0285, Sandia National Laboratories, Albuquerque, NM.

Ehgartner, B., 1991, "A Coupled Mechanical/Hydrological Model for WIPP Shaft Seals," SAND90-2826, Sandia National Laboratories, Albuquerque, NM.

Finley, R.E., and J.R. Tillerson, 1992, "WIPP Small Scale Seal Performance Tests - Status and Impacts" SAND91-2247, Sandia National Laboratories, Albuquerque, NM.

Morgan, H.S., 1987, "TRU Storage Room Calculation with Stratigraphy," Memo to D.E. Munson, December 9, 1987, Sandia National Laboratories, Albuquerque, NM.

Nowak, E.J., J.R. Tillerson, and T.M. Torres, 1990, "Initial Reference Seal System Design: Waste Isolation Pilot Plant," SAND90-0355, Sandia National Laboratories, Albuquerque, NM.

Stormont, J.C., and C.L. Howard, 1987, "Development, Implementation, and Early Results: Test Series C of the Small-Scale Seal Performance Tests," SAND87-2203, Sandia National Laboratories, Albuquerque, NM.

Weatherby, J.R., W.T. Brown, and B.M. Butcher, 1991, "The Closure of WIPP Disposal Rooms Filled with Various Waste and Backfill Combination," Proceedings of the 33rd U.S. Rock Mechanics Symposium, A.A. Balkema, Pub.

Table 1. Parameter Values Initially Determined for Use in Gas Migration Calculations Using BRAGFLO.

Material	Time Period 1 0-200 yrs	Time Period 2 200-10,000 yrs
Shaft Seal		
Permeability (m ²)	5.0x10 ⁻¹⁶ > 1.0x10 ⁻¹⁸ > 1.0x10 ⁻¹⁹	1.0x10 ⁻¹⁸ - 1.0x10 ⁻²¹
Porosity	12% > 9% > 7%	9% - 1%
Brine saturation	5% - 8% (wt.)	---
Capillary pressure Length (m)	Correlation 30 - 90	Correlation Remainder of Shaft
Shaft Fill		
Permeability (m ²)	1.0x10 ⁻¹⁵ - 1.0x10 ⁻¹⁹	Same
Porosity	16% - 7%	as
Brine saturation	5% - 8% (wt.)	Shaft
Capillary pressure	Correlation	Seal
Backfill/Experimental/Lower Shaft		
Permeability (m ²)	1.0x10 ⁻¹⁵ - 1.0x10 ⁻¹⁷	1.0x10 ⁻¹⁵ - 1.0x10 ⁻¹⁷
Porosity	2% < 10% < 12%	1% - 7.5%
Brine saturation	5% - 8% (wt.)	---
Capillary pressure	Correlation	Correlation
Culebra Seal		
Permeability (m ²)	1.0x10 ⁻¹⁸	Same
Porosity	Values for concrete	as
Brine saturation	100%	Shaft
Capillary pressure	Correlation	Fill
Panel Seals		
Permeability (m ²)	1.0x10 ⁻¹⁸ - 1.0x10 ⁻²¹	Same
Porosity	5% - 9%	as
Brine saturation	5% - 8%	Time
Capillary pressure	---	Period 1

Note: All values based on water-bearing zone seals being effective at minimizing inflow and no significant contribution to saturation from halite.

Table 2. Modified Parameter Values to be Used in Gas Migration Calculations Using BRAGFLO.

Material/Property	Time Period 1 0-200 yrs	Time Period 2 200-10,000 yrs
Shaft Seal		
Permeability (m ²)	1.0x10 ⁻¹⁹ - 5.0x10 ⁻¹⁶	1.0x10 ⁻²¹ - 1.0x10 ⁻¹⁸
Porosity	Same as period 2	0.01 - 0.09
Brine saturation	1.00	---
Length (m)	30 - 100	Rest of Upper Shaft
Shaft Fill		
Permeability (m ²)	1.0x10 ⁻¹⁹ - 1.0x10 ⁻¹⁵	Same as Shaft Seal
Porosity	same as Shaft Seal	Shaft Seal
Brine saturation	1.00	---
Backfill/Experimental/Lower Shaft		
Permeability (m ²)	1.0x10 ⁻¹⁵	Same as
Porosity	0.01 - 0.075	Period 1
Brine saturation	1.00	---
Culebra Seal		
Permeability (m ²)	1.0x10 ⁻¹⁸	Same as
Porosity	0.20 ^a	Shaft Seal
Brine saturation	1.00	---
Length (m)	7.7	7.7
Panel Seals		
Permeability (m ²)	1.0x10 ⁻²¹ - 1.0x10 ⁻¹⁸	Same as
Porosity	0.05 - 0.09	Period 1
Brine saturation	1.00	---

- Note: 1) "Brine saturation" is Initial Brine Saturation.
 2) Porosity of Shaft Seal (Period 2) correlated linearly to log of Shaft Seal permeability (Period 2).
 3) Porosity of Panel Seal correlated linearly to log of Panel Seal permeability.
 a) Value for concrete from Neville, A.M., 'Properties of Concrete', John Wiley & Sons, NY, 1973

APPENDIX B: BRAGFLO REFERENCE TABLES

APPENDIX B: BRAGFLO REFERENCE TABLES

Table B-1. Variable Parameters for Volume 5 BRAGFLO Calculations

Halite

(1) Permeability k	$= 10^k$ = Sampled variable (LHS variable #10) LHS distribution type: Cumulative Range: -24.0 to -19.0	[m ²]
(2) Porosity	= Sampled anhydrite porosity (LHS variable #16) LHS distribution type: Cumulative Range: 1.0×10^{-3} to 3.0×10^{-2}	[dimensionless]
(3) Compressibility	$= \left(\frac{S_s}{\rho_f g \phi} - \beta_f \right)$	[Pa ⁻¹]
S_s	= Specific storage = 1.4×10^{-6}	[m ⁻¹]
ρ_f	= Salado brine fluid density = 1.23×10^3	[kg/m ³]
g	= Acceleration due to gravity = 9.79	[m/s ²]
ϕ	= Porosity	[dimensionless]
β_f	= Salado brine fluid compressibility = 2.5×10^{-10}	[Pa ⁻¹]
(4) BCEXP	= Sampled Brooks-Corey exponent (LHS variable #11) LHS distribution type: Cumulative Range: 2.0×10^{-2} to 1.0	[dimensionless]
(5) BCBRSAT	= Sampled residual brine saturation (LHS variable #13) LHS distribution type: Uniform Range: 0.0 to 0.4	[dimensionless]
(6) BCGSSAT	= Sampled residual gas saturation (LHS variable #14) LHS distribution type: Uniform Range: 0.0 to 0.4	[dimensionless]
(7) BCFLG	= Sampled Brooks-Corey weighting factor (LHS variable #12) LHS distribution type: Delta Range: 0.0 to 1.0	[dimensionless]
(8) BC_PCT	= Brooks-Corey Threshold Capillary Pressure = $0.56 \cdot (\text{Permeability})^{-0.346}$	[Pa]

Table B-1. Variable Parameters for Volume 5 BRAGFLO Calculations (Continued)**Initial Disturbed Rock Zone (DRZ)**

(Initial DRZ used during time period of -50 years to 0 years)

(1) Permeability	= 1.0×10^{-17}	
(2) Porosity	= Sampled anhydrite porosity (LHS variable #16) LHS distribution type: Cumulative Range: 1.0×10^{-3} to 3.0×10^{-2}	[dimensionless]
(3) Compressibility	= $\left(\frac{S_s}{\rho_f g \phi} - \beta_f \right)$	[Pa ⁻¹]
S_s	= Specific storage = 1.4×10^{-6}	[m ⁻¹]
ρ_f	= Salado brine fluid density = 1.23×10^3	[kg/m ³]
g	= Acceleration due to gravity = 9.79	[m/s ²]
ϕ	= Porosity	[dimensionless]
β_f	= Salado brine fluid compressibility = 2.5×10^{-10}	[Pa ⁻¹]
(4) BCEXP	= Sampled halite Brooks-Corey exponent (LHS variable #11) LHS distribution type: Cumulative Range: 2.0×10^{-2} to 1.0	[dimensionless]
(5) BCBRSAT	= Sampled halite residual brine saturation (LHS variable #13) LHS distribution type: Uniform Range: 0.0 to 0.4	[dimensionless]
(6) BCGSSAT	= Sampled halite residual gas saturation (LHS variable #14) LHS distribution type: Uniform Range: 0.0 to 0.4	[dimensionless]
(7) BCFLG	= Brooks-Corey weighting factor = 1.0	[dimensionless]
(8) BC_PCT	= Brooks-Corey Threshold Capillary Pressure = $0.56 \cdot (\text{Permeability})^{-0.346}$	[Pa]

Table B-1. Variable Parameters for Volume 5 BRAGFLO Calculations (Continued)**Transition Zone**

(1) Permeability k	= 10^k = Sampled variable (LHS variable #15) LHS distribution type: Cumulative Range: -21.0 to -16.0	[m ²]
(2) Porosity	= Sampled anhydrite porosity (LHS variable #16) LHS distribution type: Cumulative Range: 1.0×10^{-3} to 3.0×10^{-2}	[dimensionless]
(3) Compressibility	= $\left(\frac{S_s}{\rho_f g \phi} - \beta_f \right)$	[Pa ⁻¹]
S_s	= Specific storage = 1.4×10^{-6}	[m ⁻¹]
ρ_f	= Salado brine fluid density = 1.23×10^3	[kg/m ³]
g	= Acceleration due to gravity = 9.79	[m/s ²]
ϕ	= Porosity	[dimensionless]
β_f	= Salado brine fluid compressibility = 2.5×10^{-10}	[Pa ⁻¹]
(4) BCEXP	= Sampled halite Brooks-Corey exponent (LHS variable #11) LHS distribution type: Cumulative Range: 2.0×10^{-2} to 1.0	[dimensionless]
(5) BCBRSAT	= Sampled halite residual brine saturation (LHS variable #13) LHS distribution type: Uniform Range: 0.0 to 0.4	[dimensionless]
(6) BCGSSAT	= Sampled halite residual gas saturation (LHS variable #14) LHS distribution type: Uniform Range: 0.0 to 0.4	[dimensionless]
(7) BCFLG	= Brooks-Corey weighting factor = 1.0	[dimensionless]
(8) BC_PCT	= Brooks-Corey Threshold Capillary Pressure = $0.56 \cdot (\text{Permeability})^{-0.346}$	[Pa]

Table B-1. Variable Parameters for Volume 5 BRAGFLO Calculations (Continued)**Anhydrite**

(1) Permeability k	= 10^k = Sampled variable (LHS variable #15) LHS distribution type: Cumulative Range: -21.0 to -16.0	[m ²]
(2) Porosity	= Sampled variable (LHS variable #16) LHS distribution type: Cumulative Range: 1.0×10^{-3} to 3.0×10^{-2}	[dimensionless]
(3) Compressibility	$= \left(\frac{S_s}{\rho_f g \phi} - \beta_f \right)$	[Pa ⁻¹]
S_s	= Specific storage = 1.0×10^{-6}	[m ⁻¹]
ρ_f	= Salado brine fluid density = 1.23×10^3	[kg/m ³]
g	= Acceleration due to gravity = 9.79	[m/s ²]
ϕ	= Porosity	[dimensionless]
β_f	= Salado brine fluid compressibility = 2.5×10^{-10}	[dimensionless]
(4) BCEXP	= Sampled halite Brooks-Corey exponent (LHS variable #11) LHS distribution type: Cumulative Range: 2.0×10^{-2} to 1.0	[dimensionless]
(5) BCBRSAT	= Sampled halite residual brine saturation (LHS variable #13) LHS distribution type: Uniform Range: 0.0 to 0.4	[dimensionless]
(6) BCGSSAT	= Sampled halite residual gas saturation (LHS variable #14) LHS distribution type: Uniform Range: 0.0 to 0.4	[dimensionless]
(7) BCFLG	= Sampled SALADO Brooks-Corey weighting factor (LHS variable #12) LHS distribution type: Delta Range: 0.0 to 1.0	[dimensionless]

Table B-1. Variable Parameters for Volume 5 BRAGFLO Calculations (Continued)**Anhydrite (Concluded)**

(8) BC_PCT = Brooks-Corey Threshold Capillary Pressure [Pa]
 = $0.56 \cdot (\text{Permeability})^{-0.346}$

Table B-1. Variable Parameters for Volume 5 BRAGFLO Calculations (Continued)**Cavity 1**

(Cavity 1 used to describe waste-emplacement region during time period of -50 years to 0 years)

(1) Permeability	= 1.0×10^{-10}	[m ²]
(2) Porosity	= 1.0	[dimensionless]
(3) Compressibility	= 0.0	[Pa ⁻¹]
(4) BCEXP	= Sampled halite Brooks-Corey exponent (LHS variable #11) LHS distribution type: Cumulative Range: 2.0×10^{-2} to 1.0	[dimensionless]
(5) BCBSAT	= Residual brine saturation = 0.0	[dimensionless]
(6) BCGSSAT	= Residual gas saturation = 0.0	[dimensionless]
(7) BCFLG	= Brooks-Corey weighting factor = 1.0	[dimensionless]
(8) BC_PCT	= Brooks-Corey Threshold Capillary Pressure = 0.0	[Pa]

Table B-1. Variable Parameters for Volume 5 BRAGFLO Calculations (Continued)**Culebra 1**

(Culebra 1 used during time period of -50 years to 0 years)

(1) Permeability	= 0.0	[m ²]
(2) Porosity	= Sampled Culebra porosity (LHS variable #43) LHS distribution type: Data Range: 5.80565 x 10 ⁻² to 2.5250 x 10 ⁻¹	[dimensionless]
(3) Compressibility	= 0.0	[Pa ⁻¹]
(4) BCEXP	= Brooks-Corey exponent = 0.7	[dimensionless]
(5) BCBRSAT	= Residual brine saturation = 0.2	[dimensionless]
(6) BCGSSAT	= Residual gas saturation = 0.2	[dimensionless]
(7) BCFLG	= Brooks-Corey weighting factor = 1.0	[dimensionless]
(8) BC_PCT	= Brooks-Corey Threshold Capillary Pressure = 0.0	[Pa]

Table B-1. Variable Parameters for Volume 5 BRAGFLO Calculations (Continued)**Cavity 2**

(Cavity 2 used to describe excavated volume other than waste-emplacement region during time period of -50 years to 0 years)

(1) Permeability	= 1.0×10^{-10}	[m ²]
(2) Porosity	= 1.0	[dimensionless]
(3) Compressibility	= 0.0	[Pa ⁻¹]
(4) BCEXP	= Sampled halite Brooks-Corey exponent (LHS variable #11) LHS distribution type: Cumulative Range: 2.0×10^{-2} to 1.0	[dimensionless]
(5) BCBRSAT	= Residual brine saturation = 0.0	[dimensionless]
(6) BCGSSAT	= Residual gas saturation = 0.0	[dimensionless]
(7) BCFLG	= Brooks-Corey weighting factor = 1.0	[dimensionless]
(8) BC_PCT	= Brooks-Corey Threshold Capillary Pressure = 0.0	[Pa]

Table B-1. Variable Parameters for Volume 5 BRAGFLO Calculations (Continued)**Waste**

(Waste replaces Cavity 1 at time=0 years)

(1) Permeability	= 1.0×10^{-13}	[m ²]
(2) Porosity	= 6.601785×10^{-1}	[dimensionless]
(3) Compressibility	= 1.6×10^{-9}	[Pa ⁻¹]
(4) BCEXP	= Brooks-Corey exponent = 2.89	[dimensionless]
(5) BCBRSAT	= Residual brine saturation = 2.76×10^{-1}	[dimensionless]
(6) BCGSSAT	= Residual gas saturation = 0.7	[dimensionless]
(7) BCFLG	= Brooks-Corey weighting factor = 1.0	[dimensionless]
(8) BC_PCT	= Brooks-Corey Threshold Capillary Pressure = 0.0	[Pa]

(9) Initial Iron (Fe) Concentration: [kg/m³]

$$= \frac{WTDRMET \cdot (WTFRFE/VDRUM) \cdot \omega \cdot VWASTE + WTFECONT}{VREPOS}$$

<i>WTDRMET</i>	= Mass of contents of one drum of metal+glass = 64.5	[kg]
<i>WTFRFE</i>	= Mass fraction of corrodable metal in metal+glass = 0.7210021	[dimensionless]
ω	= Volume fraction of metal (i.e. Fe) = Sampled variable (LHS variable #9) LHS distribution type: Normal Range: 2.76×10^{-1} to 4.76×10^{-1}	[dimensionless]
<i>VDRUM</i>	= Volume (internal capacity) of one drum = 0.21	[m ³]
<i>VWASTE</i>	= Design volume of waste in repository = 1.75564×10^5	[m ³]
<i>WTFECONT</i>	= Mass of Fe in containers = 2.6132656×10^7	[kg]
<i>VREPOS</i>	= Total excavated storage volume of repository = $4.36023214418 \times 10^5$	[m ³]

Table B-1. Variable Parameters for Volume 5 BRAGFLO Calculations (Continued)**Waste (Continued)**

(Waste replaces Cavity 1 at time=0 years)

(10) Initial Cellulose Concentration:		[kg/m ³]
=	<i>CONCBIOI</i>	
=	$\frac{WTDRCOMB \cdot WTFRBIO \cdot \omega \cdot (VWASTE/VDRUM) + WTBIOCONT}{VREPOS}$	
<i>WTDRCOMB</i>	= Mass of contents of one drum of combustibles = 40.0	[kg]
<i>WTFRBIO</i>	= Mass fraction of biodegradables in combustibles = 0.5546459	[dimensionless]
ω	= Volume fraction of combustibles = Sampled variable (LHS variable #8) LHS distribution type: Normal Range: 2.84×10^{-1} to 4.84×10^{-1}	[dimensionless]
<i>VWASTE</i>	= Design volume of waste in repository = 1.75564×10^5	[m ³]
<i>VDRUM</i>	= Volume (internal capacity) of one drum = 0.21	[m ³]
<i>WTBIOCONT</i>	= Mass of biodegradables in containers = 0.0	[kg]
<i>VREPOS</i>	= Total excavated storage volume of repository = $4.36023214418 \times 10^5$	[m ³]
(11) Gas Production Rate, Corrosion, Inundated		[mol Fe/(m ³ ·s)]
	$= \lambda \cdot \frac{(ASDRUM \cdot DRPANEL)}{((4.0 - \omega)/3.0) \cdot VPANELX}$	
λ	= Sampled variable (LHS variable #2) LHS distribution type: Cumulative Range: 0.0 to 1.3×10^{-8}	[mol Fe/(m ² ·s)]
<i>ASDRUM</i>	= Surface area of corrodable metal per drum = 6.0	[m ²]
<i>DRPANEL</i>	= Number of Drums in one Panel = 8.606362×10^4	[dimensionless]
<i>VPANELX</i>	= Excavated volume of one panel = 46097.6458546	[m ³]
$\frac{4.0 - \omega}{3.0}$	= Anoxic Iron Corrosion Stoichiometry	[dimensionless]
ω	= Sampled variable (LHS variable #4) LHS distribution type: Uniform Range: 0.0 to 1.0	[dimensionless]

Table B-1. Variable Parameters for Volume 5 BRAGFLO Calculations (Continued)**Waste (Continued)**

(Waste replaces Cavity 1 at time=0 years)

(12) Gas Production Rate, Microbial, Inundated:		[mol cellulose/(m ³ ·s)]
	$= \lambda \cdot \text{CONCBIOI} / \text{STOIMIC}$	
λ	= Sampled variable (LHS variable #5) LHS distribution type: Cumulative Range: 0.0 to 1.6 x 10 ⁻⁸	[mol cellulose/(kg·s)]
<i>CONCBIOI</i>	= Initial Cellulose Concentration (same as equation (10))	[kg/m ³]
	$= \frac{\text{WTDRCOMB} \cdot \text{WTFRBIO} \cdot \omega \cdot (\text{VWASTE} / \text{VDRUM}) + \text{WTBIOCONT}}{\text{VREPOS}}$	
<i>WTDRCOMB</i>	= Mass of contents of one drum of combustibles = 40.0	[kg]
<i>WTFRBIO</i>	= Mass fraction of biodegradables in combustibles = 0.5546459	[dimensionless]
ω	= Volume fraction of combustibles = Sampled variable (LHS variable #8) LHS distribution type: Normal Range: 2.84 x 10 ⁻¹ to 4.84 x 10 ⁻¹	[dimensionless]
<i>VWASTE</i>	= Design volume of waste in repository = 1.75564 x 10 ⁵	[m ³]
<i>VDRUM</i>	= Volume (internal capacity) of one drum = 0.21	[m ³]
<i>WTBIOCONT</i>	= Mass of biodegradables in containers = 0.0	[kg]
<i>VREPOS</i>	= Total excavated storage volume of repository = 4.36023214418 x 10 ⁵	[m ³]
<i>STOIMIC</i>	= Microbial Stoichiometry = Sampled variable (LHS variable #7) LHS distribution type: Uniform Range: 0.0 to 1.67	[dimensionless]
(13) Humidity Factor, Corrosion =	Sampled variable (LHS variable #3) LHS distribution type: Cumulative Range: 0.0 to 0.5	[dimensionless]
(14) Humidity Factor, Microbial =	Sampled variable (LHS variable #6) LHS distribution type: Uniform Range: 0.0 to 0.2	[dimensionless]

Table B-1. Variable Parameters for Volume 5 BRAGFLO Calculations (Continued)**Waste (Concluded)**

(Waste replaces Cavity 1 at time=0 years)

(15) Anoxic Iron Corrosion Stoichiometry = $\frac{4.0 - \omega}{3.0}$ [dimensionless]

ω = Sampled variable (LHS variable #4)
 LHS distribution type: Uniform
 Range: 0.0 to 1.0

(16) Microbial Stoichiometry = Sampled variable [dimensionless]
 (LHS variable #7)
 LHS distribution type: Uniform
 Range: 0.0 to 1.67

Table B-1. Variable Parameters for Volume 5 BRAGFLO Calculations (Continued)**Final Disturbed Rock Zone (DRZ)**

(Final DRZ replaces Initial DRZ at time=0 years)

(1) Permeability k	= 10^k = Sampled variable (LHS variable #10) LHS distribution type: Cumulative Range: -24.0 to -19.0	[m ²]
(2) Porosity ϕ_A	= $\phi_A + \omega(0.06 - \phi_A)$ = Sampled anhydrite (LHS variable #16)	[dimensionless]
ω	= Sampled variable (LHS variable #17) LHS distribution type: Uniform Range: 0.0 to 1.0	[dimensionless]
(3) Compressibility	= $\left(\frac{S_s}{\rho_f g \phi} - \beta_f \right)$	[Pa ⁻¹]
S_s	= Specific storage = 1.4×10^{-6}	[m ⁻¹]
ρ_f	= Salado brine fluid density = 1.23×10^3	[kg/m ³]
g	= Acceleration due to gravity = 9.79	[m/s ²]
ϕ	= Porosity	[dimensionless]
β_f	= Salado brine fluid compressibility = 2.5×10^{-10}	[Pa ⁻¹]
(4) BCEXP	= Sampled halite Brooks-Corey exponent (LHS variable #11) LHS distribution type: Cumulative Range: 2.0×10^{-2} to 1.0	[dimensionless]
(5) BCBRSAT	= Sampled halite residual brine saturation (LHS variable #13) LHS distribution type: Uniform Range: 0.0 to 0.4	[dimensionless]
(6) BCGSSAT	= Sampled halite residual gas saturation (LHS variable #14) LHS distribution type: Uniform Range: 0.0 to 0.4	[dimensionless]
(7) BCFLG	= Brooks-Corey weighting factor = 1.0	[dimensionless]

Table B-1. Variable Parameters for Volume 5 BRAGFLO Calculations (Continued)

Final Disturbed Rock Zone (DRZ) (Concluded)

(Final DRZ replaces Initial DRZ at time=0 years)

(8) BC_PCT = Brooks-Corey Threshold Capillary Pressure [Pa]
 = $0.56 \cdot (\text{Permeability})^{-0.346}$

Table B-1. Variable Parameters for Volume 5 BRAGFLO Calculations (Continued)**Culebra**

(Culebra replaces Culebra 1 at time=0 years)

(1) Permeability	$= \frac{\kappa\mu}{\rho_f g}$	[m ²]
κ	= Hydraulic Conductivity = 2.24×10^{-7}	[m/s]
μ	= Culebra brine viscosity = 1.0×10^{-3}	[kg/(m·s)]
ρ_f	= Culebra brine fluid density = 1.09×10^3	[kg/m ³]
g	= Acceleration due to gravity = 9.79	[m/s ²]
(2) Porosity	= Sampled variable (LHS variable #43) LHS distribution type: Data Range: 5.80565×10^{-2} to 2.52500×10^{-1}	[dimensionless]
(3) Compressibility	$= \frac{S}{t\rho_f\phi g} - \beta_f$	[Pa ⁻¹]
S	= Storage coefficient (= Specific storage x thickness) = 2.0×10^{-5}	[dimensionless]
t	= Culebra layer thickness = 7.7	[m]
ρ_f	= Culebra brine fluid density = 1.09×10^3	[kg/m ³]
ϕ	= Porosity	[dimensionless]
g	= Acceleration due to gravity = 9.79	[m/s ²]
β_f	= Culebra brine fluid compressibility = 2.5×10^{-10}	[Pa ⁻¹]
(4) BCEXP	= Brooks-Corey exponent = 0.7	[dimensionless]
(5) BCBRSAT	= Residual brine saturation = 0.2	[dimensionless]
(6) BCGSSAT	= Residual gas saturation = 0.2	[dimensionless]
(7) BCFLG	= Brooks-Corey weighting factor = 1.0	[dimensionless]

Table B-1. Variable Parameters for Volume 5 BRAGFLO Calculations (Continued)

Culebra (Concluded)

(Culebra replaces Culebra 1 at time=0 years)

(8) BC_PCT = Brooks-Corey Threshold Capillary Pressure [Pa]
 = $0.56 \cdot (\text{Permeability})^{-0.346}$

Table B-1. Variable Parameters for Volume 5 BRAGFLO Calculations (Continued)**Shaft Seal**

(Shaft Seal, Upper Shaft, Lower Shaft, Backfill, Culebra Seal, and Experimental Region replaces Cavity 2 at time=0 years)

(1) Permeability	= Sampled variable (LHS variable #22) LHS distribution type: Lognormal Range: 1.0×10^{-19} to 5.0×10^{-16}	[m ²]
(2) Porosity	$= \left(\frac{\text{LOG}_{10} \omega - \text{LOG}_{10}(1.0 \times 10^{-21})}{\text{LOG}_{10}(1.0 \times 10^{-18}) - \text{LOG}_{10}(1.0 \times 10^{-21})} \right) (0.09 - 0.01) + 0.01$	[dimensionless]
ω	= Sampled variable (LHS variable #23) LHS distribution type: Lognormal Range: 1.0×10^{-21} to 1.0×10^{-18}	[m ²]
(3) Compressibility	$= \left(\frac{S_s}{\rho_f g \phi} - \beta_f \right)$	[Pa ⁻¹]
S_s	= Specific storage = 1.4×10^{-6}	[m ⁻¹]
ρ_f	= Salado brine fluid density = 1.23×10^3	[kg/m ³]
ϕ	= Porosity	[dimensionless]
g	= Acceleration due to gravity = 9.79	[m/s ²]
β_f	= Salado brine fluid compressibility = 2.5×10^{-10}	[Pa ⁻¹]
(4) BCEXP	= Brooks-Corey exponent = 0.7	[dimensionless]
(5) BCBRSAT	= Residual brine saturation = 0.2	[dimensionless]
(6) BCGSSAT	= Residual gas saturation = 0.0	[dimensionless]
(7) BCFLG	= Brooks-Corey weighting factor = 1.0	[dimensionless]
(8) BC_PCT	= Brooks-Corey Threshold Capillary Pressure = $0.56 \cdot (\text{Permeability})^{-0.346}$	[Pa]

Table B-1. Variable Parameters for Volume 5 BRAGFLO Calculations (Continued)**Upper Shaft**

(Shaft Seal, Upper Shaft, Lower Shaft, Backfill, Culebra Seal, and Experimental Region replaces Cavity 2 at time=0 years)

(1) Permeability	= Sampled variable (LHS variable #24) LHS distribution type: Lognormal Range: 1.0×10^{-19} to 5.0×10^{-15}	[m ²]
(2) Porosity	$= \left(\frac{\text{LOG}_{10}\omega - \text{LOG}_{10}(1.0 \times 10^{-21})}{\text{LOG}_{10}(1.0 \times 10^{-18}) - \text{LOG}_{10}(1.0 \times 10^{-21})} \right) (0.09 - 0.01) + 0.01$	[dimensionless]
ω	= Sampled variable (LHS variable #23) LHS distribution type: Lognormal Range: 1.0×10^{-21} to 1.0×10^{-18}	[m ²]
(3) Compressibility	$= \left(\frac{S_s}{\rho_f g \phi} - \beta_f \right)$	[Pa ⁻¹]
S_s	= Specific storage = 1.4×10^{-6}	[m ⁻¹]
ρ_f	= Salado brine fluid density = 1.23×10^3	[kg/m ³]
ϕ	= Porosity	[dimensionless]
g	= Acceleration due to gravity = 9.79	[m/s ²]
β_f	= Salado brine fluid compressibility = 2.5×10^{-10}	[Pa ⁻¹]
(4) BCEXP	= Brooks-Corey exponent = 0.7	[dimensionless]
(5) BCBRSAT	= Residual brine saturation = 0.2	[dimensionless]
(6) BCGSSAT	= Residual gas saturation = 0.0	[dimensionless]
(7) BCFLG	= Brooks-Corey weighting factor = 1.0	[dimensionless]
(8) BC_PCT	= Brooks-Corey Threshold Capillary Pressure = $0.56 \cdot (\text{Permeability})^{-0.346}$	[Pa]

Table B-1. Variable Parameters for Volume 5 BRAGFLO Calculations (Continued)**Lower Shaft**

(Shaft Seal, Upper Shaft, Lower Shaft, Backfill, Culebra Seal, and Experimental Region replaces Cavity 2 at time=0 years)

(1) Permeability	= 1.0×10^{-15}	[m ²]
(2) Porosity	= Sampled variable (LHS variable #26) LHS distribution type: Uniform Range: 1.0×10^{-2} to 7.5×10^{-2}	[dimensionless]
(3) Compressibility	= $\left(\frac{S_s}{\rho_f g \phi} - \beta_f \right)$	[Pa ⁻¹]
S_s	= Specific storage = 1.4×10^{-6}	[m ⁻¹]
ρ_f	= Salado brine fluid density = 1.23×10^3	[kg/m ³]
ϕ	= Porosity	[dimensionless]
g	= Acceleration due to gravity = 9.79	[m/s ²]
β_f	= Salado brine fluid compressibility = 2.5×10^{-10}	[Pa ⁻¹]
(4) BCEXP	= Brooks-Corey exponent = 0.7	[dimensionless]
(5) BCBRSAT	= Residual brine saturation = 0.2	[dimensionless]
(6) BCGSSAT	= Residual gas saturation = 0.0	[dimensionless]
(7) BCFLG	= Brooks-Corey weighting factor = 1.0	[dimensionless]
(8) BC_PCT	= Brooks-Corey Threshold Capillary Pressure = $0.56 \cdot (\text{Permeability})^{-0.346}$	[Pa]

Table B-1. Variable Parameters for Volume 5 BRAGFLO Calculations (Continued)**Backfill**

(Shaft Seal, Upper Shaft, Lower Shaft, Backfill, Culebra Seal, and Experimental Region replaces Cavity 2 at time=0 years)

(1) Permeability	= 1.0×10^{-15}	[m ²]
(2) Porosity	= Sampled LOWER SHAFT porosity (LHS variable #26) LHS distribution type: Uniform Range: 1.0×10^{-2} to 7.5×10^{-2}	[dimensionless]
(3) Compressibility	= $\left(\frac{S_s}{\rho_f g \phi} - \beta_f \right)$	[Pa ⁻¹]
S_s	= Specific storage = 1.4×10^{-6}	[m ⁻¹]
ρ_f	= Salado brine fluid density = 1.23×10^3	[kg/m ³]
ϕ	= Porosity	[dimensionless]
g	= Acceleration due to gravity = 9.79	[m/s ²]
β_f	= Salado brine fluid compressibility = 2.5×10^{-10}	[Pa ⁻¹]
(4) BCEXP	= Brooks-Corey exponent = 0.7	[dimensionless]
(5) BCBRSAT	= Residual brine saturation = 0.2	[dimensionless]
(6) BCGSSAT	= Residual gas saturation = 0.0	[dimensionless]
(7) BCFLG	= Brooks-Corey weighting factor = 1.0	[dimensionless]
(8) BC_PCT	= Brooks-Corey Threshold Capillary Pressure = $0.56 \cdot (\text{Permeability})^{-0.346}$	[Pa]

Table B-1. Variable Parameters for Volume 5 BRAGFLO Calculations (Continued)**Experimental Region**

(Shaft Seal, Upper Shaft, Lower Shaft, Backfill, Culebra Seal, and Experimental Region replaces Cavity 2 at time=0 years)

(1) Permeability	= 1.0×10^{-15}	[m ²]
(2) Porosity	= Sampled Lower Shaft porosity (LHS variable #26) LHS distribution type: Uniform Range: 1.0×10^{-2} to 7.5×10^{-2}	[dimensionless]
(3) Compressibility	= $\left(\frac{S_s}{\rho_f g \phi} - \beta_f \right)$	[Pa ⁻¹]
S_s	= Specific storage = 1.4×10^{-6}	[m ⁻¹]
ρ_f	= Salado brine fluid density = 1.23×10^3	[kg/m ³]
ϕ	= Porosity	[dimensionless]
g	= Acceleration due to gravity = 9.79	[m/s ²]
β_f	= Salado brine fluid compressibility = 2.5×10^{-10}	[Pa ⁻¹]
(4) BCEXP	= Brooks-Corey exponent = 0.7	[dimensionless]
(5) BCBRSAT	= Residual brine saturation = 0.2	[dimensionless]
(6) BCGSSAT	= Residual gas saturation = 0.0	[dimensionless]
(7) BCFLG	= Brooks-Corey weighting factor = 1.0	[dimensionless]
(8) BC_PCT	= Brooks-Corey Threshold Capillary Pressure = $0.56 \cdot (\text{Permeability})^{-0.346}$	[Pa]

Table B-1. Variable Parameters for Volume 5 BRAGFLO Calculations (Continued)**Shaft Seal 2**

(Shaft Seal 2 replaces Culebra Seal, Upper Shaft, and Shaft Seal at time=200 years)

(1) Permeability	= Sampled Shaft Seal permeability (LHS variable #22) LHS distribution type: Lognormal Range: 1.0×10^{-19} to 5.0×10^{-16}	[m ²]
(2) Porosity	$= \left(\frac{\text{LOG}_{10}\omega - \text{LOG}_{10}(1.0 \times 10^{-21})}{\text{LOG}_{10}(1.0 \times 10^{-18}) - \text{LOG}_{10}(1.0 \times 10^{-21})} \right) (0.09 - 0.01) + 0.01$	[dimensionless]
ω	= Sampled variable (LHS variable #23) LHS distribution type: Lognormal Range: 1.0×10^{-21} to 1.0×10^{-18}	[dimensionless]
(3) Compressibility	$= \left(\frac{S_s}{\rho_f g \phi} - \beta_f \right)$	[Pa ⁻¹]
S_s	= Specific storage = 1.4×10^{-6}	[m ⁻¹]
ρ_f	= Salado brine fluid density = 1.23×10^3	[kg/m ³]
ϕ	= Porosity	[dimensionless]
g	= Acceleration due to gravity = 9.79	[m/s ²]
β_f	= Salado brine fluid compressibility = 2.5×10^{-10}	[Pa ⁻¹]
(4) BCEXP	= Brooks-Corey exponent = 0.7	[dimensionless]
(5) BCBRSAT	= Residual brine saturation = 0.2	[dimensionless]
(6) BCGSSAT	= Residual gas saturation = 0.0	[dimensionless]
(7) BCFLG	= Brooks-Corey weighting factor = 1.0	[dimensionless]
(8) BC_PCT	= Brooks-Corey Threshold Capillary Pressure = $0.56 \cdot (\text{Permeability})^{-0.346}$	[Pa]

Table B-1. Variable Parameters for Volume 5 BRAGFLO Calculations (Continued)**Panel Seal**

(1) Permeability	= Sampled variable (LHS variable #25) LHS distribution type: Lognormal Range: 1.0×10^{-21} to 1.0×10^{-18}	[m ²]
(2) Porosity	$= \left(\frac{\text{LOG}_{10}(\text{Permeability}) - \text{LOG}_{10}(1.0 \times 10^{-21})}{\text{LOG}_{10}(1.0 \times 10^{-18}) - \text{LOG}_{10}(1.0 \times 10^{-21})} \right) (0.09 - 0.05) + 0.05$	[dimensionless]
(3) Compressibility	$= \left(\frac{S_s}{\rho_f g \phi} - \beta_f \right)$	[Pa ⁻¹]
S_s	= Specific storage = 1.4×10^{-6}	[m ⁻¹]
ρ_f	= Salado brine fluid density = 1.23×10^3	[kg/m ³]
ϕ	= Porosity	[dimensionless]
g	= Acceleration due to gravity = 9.79	[m/s ²]
β_f	= Salado brine fluid compressibility = 2.5×10^{-10}	[Pa ⁻¹]
(4) BCEXP	= Brooks-Corey exponent = 0.7	[dimensionless]
(5) BCBRSAT	= Residual brine saturation = 0.2	[dimensionless]
(6) BCGSSAT	= Residual gas saturation = 0.0	[dimensionless]
(7) BCFLG	= Brooks-Corey weighting factor = 1.0	[dimensionless]
(8) BC_PCT	= Brooks-Corey Threshold Capillary Pressure = $0.56 \cdot (\text{Permeability})^{-0.346}$	[Pa]

Table B-1. Variable Parameters for Volume 5 BRAGFLO Calculations (Concluded)**Culebra Seal**

(1) Permeability	= 1.0×10^{-18}	[m ²]
(2) Porosity	= 0.2	[dimensionless]
(3) Compressibility	= $\left(\frac{S_s}{\rho_f g \phi} - \beta_f \right)$	[Pa ⁻¹]
S_s	= Specific storage = 1.4×10^{-6}	[m ⁻¹]
ρ_f	= Salado brine fluid density = 1.23×10^3	[kg/m ³]
ϕ	= Porosity	[dimensionless]
g	= Acceleration due to gravity = 9.79	[m/s ²]
β_f	= Salado brine fluid compressibility = 2.5×10^{-10}	[Pa ⁻¹]
(4) BCEXP	= Brooks-Corey exponent = 0.7	[dimensionless]
(5) BCBRSAT	= Residual brine saturation = 0.2	[dimensionless]
(6) BCGSSAT	= Residual gas saturation = 0.0	[dimensionless]
(7) BCFLG	= Brooks-Corey weighting factor = 1.0	[dimensionless]
(8) BC_PCT	= Brooks-Corey Threshold Capillary Pressure = $0.56 \cdot (\text{Permeability})^{-0.346}$	[Pa]

Table B-2. 1992 BRAGFLO Computed Variable Values for ANHYDRITE

Run No.	Porosity	Permeability	Compressibility	BCEXP	BCBRSAT	BCGSSAT	BCFLG	BC PCT
1	2.8660x10 ⁻²	1.4125x10 ⁻¹⁸	2.6476x10 ⁻⁹	9.6790	8.7890x10 ⁻²	2.3300x10 ⁻¹	0.0000	8.4002x10 ⁵
2	6.9900x10 ⁻³	1.6982x10 ⁻²⁰	1.1631x10 ⁻⁸	4.9660x10 ⁻¹	1.4570x10 ⁻¹	1.2590x10 ⁻¹	1.0000	3.8780x10 ⁶
3	2.8970x10 ⁻²	9.1201x10 ⁻¹⁹	2.6166x10 ⁻⁹	6.7900x10 ⁻¹	1.8490x10 ⁻¹	2.1660x10 ⁻¹	1.0000	9.7730x10 ⁵
4	5.6130x10 ⁻³	5.0119x10 ⁻²⁰	1.4545x10 ⁻⁸	5.1820	1.7260x10 ⁻¹	1.8900x10 ⁻¹	1.0000	2.6668x10 ⁶
5	2.0560x10 ⁻²	1.1482x10 ⁻²⁰	3.7891x10 ⁻⁹	4.0710x10 ⁻¹	1.9880x10 ⁻¹	1.4590x10 ⁻¹	1.0000	4.4405x10 ⁶
6	1.3750x10 ⁻²	1.5136x10 ⁻²⁰	5.7896x10 ⁻⁹	6.1420	3.3170x10 ⁻¹	4.7930x10 ⁻²	0.0000	4.0356x10 ⁶
7	2.5930x10 ⁻²	1.7783x10 ⁻²⁰	2.9526x10 ⁻⁹	1.0990	3.5430x10 ⁻²	1.6220x10 ⁻¹	0.0000	3.8167x10 ⁶
8	3.1850x10 ⁻³	1.8197x10 ⁻¹⁹	2.5824x10 ⁻⁸	6.4480	3.8660x10 ⁻¹	2.8520x10 ⁻²	1.0000	1.7070x10 ⁶
9	2.7270x10 ⁻²	1.2303x10 ⁻²⁰	2.7953x10 ⁻⁹	4.2610x10 ⁻¹	3.4080x10 ⁻¹	1.8690x10 ⁻¹	1.0000	4.3356x10 ⁶
10	9.6770x10 ⁻³	5.2481x10 ⁻¹⁸	8.3317x10 ⁻⁹	1.5170	7.9000x10 ⁻²	3.4810x10 ⁻¹	1.0000	5.3342x10 ⁵
11	2.5730x10 ⁻³	1.3183x10 ⁻²⁰	3.2026x10 ⁻⁸	5.1250x10 ⁻¹	2.7170x10 ⁻¹	2.0030x10 ⁻¹	0.0000	4.2332x10 ⁶
12	9.8270x10 ⁻³	2.2387x10 ⁻¹⁹	8.2007x10 ⁻⁹	7.4960	1.4100x10 ⁻¹	2.8620x10 ⁻¹	1.0000	1.5889x10 ⁶
13	1.6610x10 ⁻²	4.8978x10 ⁻²⁰	4.7497x10 ⁻⁹	2.2490	3.6500x10 ⁻¹	2.9370x10 ⁻¹	1.0000	2.6881x10 ⁶
14	1.9600x10 ⁻²	1.0000x10 ⁻²⁰	3.9870x10 ⁻⁹	3.0620x10 ⁻¹	8.3660x10 ⁻³	1.7360x10 ⁻¹	1.0000	4.6579x10 ⁶
15	1.1590x10 ⁻³	2.0893x10 ⁻²⁰	7.1402x10 ⁻⁸	4.4620x10 ⁻¹	2.3100x10 ⁻¹	3.8350x10 ⁻¹	0.0000	3.6097x10 ⁶
16	5.8700x10 ⁻³	5.1286x10 ⁻¹⁹	1.3897x10 ⁻⁸	5.3590x10 ⁻¹	3.7890x10 ⁻¹	2.1720x10 ⁻¹	1.0000	1.1927x10 ⁶
17	2.3950x10 ⁻²	5.7544x10 ⁻²⁰	3.2174x10 ⁻⁹	5.9190	1.1130x10 ⁻¹	3.8060x10 ⁻¹	0.0000	2.5423x10 ⁶
18	6.1370x10 ⁻³	6.6069x10 ⁻²⁰	1.3282x10 ⁻⁸	5.8730x10 ⁻¹	2.9470x10 ⁻¹	8.6120x10 ⁻³	0.0000	2.4236x10 ⁶
19	6.2550x10 ⁻³	4.5709x10 ⁻²⁰	1.3026x10 ⁻⁸	2.0050	1.1640x10 ⁻¹	1.6670x10 ⁻¹	1.0000	2.7531x10 ⁶
20	1.7070x10 ⁻²	4.4668x10 ⁻²⁰	4.6150x10 ⁻⁹	6.7090x10 ⁻¹	1.2940x10 ⁻¹	3.2110x10 ⁻¹	1.0000	2.7752x10 ⁶
21	2.3500x10 ⁻²	1.1481x10 ⁻¹⁹	3.2838x10 ⁻⁹	2.2590x10 ⁻¹	1.9770x10 ⁻²	2.2330x10 ⁻¹	0.0000	2.0018x10 ⁶
22	2.6030x10 ⁻²	7.4131x10 ⁻²⁰	2.9403x10 ⁻⁹	1.4340	2.1830x10 ⁻¹	1.8710x10 ⁻²	1.0000	2.3290x10 ⁶
23	2.9920x10 ⁻²	3.5481x10 ⁻²⁰	2.5256x10 ⁻⁹	7.0990	2.3880x10 ⁻¹	4.5230x10 ⁻²	1.0000	3.0053x10 ⁶
24	1.4710x10 ⁻²	6.1660x10 ⁻²⁰	5.3955x10 ⁻⁹	4.3270x10 ⁻¹	6.1270x10 ⁻²	2.6430x10 ⁻¹	1.0000	2.4823x10 ⁶
25	2.4720x10 ⁻²	3.2359x10 ⁻²⁰	3.1094x10 ⁻⁹	2.7610	3.0510x10 ⁻¹	9.9900x10 ⁻²	1.0000	3.1026x10 ⁶
26	1.8820x10 ⁻²	2.3988x10 ⁻²⁰	4.1626x10 ⁻⁹	5.2660	2.4700x10 ⁻¹	6.8060x10 ⁻²	1.0000	3.4412x10 ⁶
27	2.2740x10 ⁻³	2.1878x10 ⁻²⁰	3.6269x10 ⁻⁸	8.3330	2.1280x10 ⁻¹	7.5730x10 ⁻²	1.0000	3.5526x10 ⁶
28	2.8830x10 ⁻³	1.9499x10 ⁻²⁰	2.8555x10 ⁻⁸	7.9460	3.4740x10 ⁻¹	1.5270x10 ⁻¹	0.0000	3.6970x10 ⁶
29	1.2680x10 ⁻²	3.0903x10 ⁻²⁰	6.2993x10 ⁻⁹	6.0410x10 ⁻¹	3.3040x10 ⁻¹	3.5780x10 ⁻¹	1.0000	3.1525x10 ⁶
30	8.7910x10 ⁻³	7.4131x10 ⁻²⁰	9.1966x10 ⁻⁹	2.0040x10 ⁻¹	1.4050x10 ⁻²	1.5530x10 ⁻¹	0.0000	2.3290x10 ⁶
31	1.7650x10 ⁻²	3.2359x10 ⁻²¹	4.4551x10 ⁻⁹	3.3160x10 ⁻¹	2.1130x10 ⁻¹	2.4050x10 ⁻¹	1.0000	6.8822x10 ⁶
32	2.0930x10 ⁻²	1.0471x10 ⁻²⁰	3.7177x10 ⁻⁹	8.8800	3.1430x10 ⁻¹	3.7550x10 ⁻¹	1.0000	4.5842x10 ⁶
33	6.6640x10 ⁻³	4.6774x10 ⁻¹⁹	1.2212x10 ⁻⁸	5.2200x10 ⁻¹	1.0530x10 ⁻¹	3.4190x10 ⁻¹	1.0000	1.2313x10 ⁶
34	9.1030x10 ⁻³	1.2303x10 ⁻²⁰	8.8728x10 ⁻⁹	8.6520	2.5150x10 ⁻¹	3.6280x10 ⁻¹	0.0000	4.3356x10 ⁶
35	2.4230x10 ⁻³	2.8184x10 ⁻²⁰	3.4024x10 ⁻⁸	3.9470x10 ⁻¹	2.9070x10 ⁻¹	1.3390x10 ⁻¹	1.0000	3.2545x10 ⁶
36	2.7120x10 ⁻²	1.9953x10 ⁻²⁰	2.8121x10 ⁻⁹	2.7500x10 ⁻¹	3.7090x10 ⁻¹	3.6960x10 ⁻¹	1.0000	3.6677x10 ⁶
37	5.0960x10 ⁻³	2.5704x10 ⁻²⁰	1.6046x10 ⁻⁸	6.9780	2.2650x10 ⁻¹	3.0790x10 ⁻²	1.0000	3.3599x10 ⁶
38	1.8940x10 ⁻³	1.5136x10 ⁻¹⁹	4.3596x10 ⁻⁸	2.9640	1.7810x10 ⁻¹	3.9620x10 ⁻¹	1.0000	1.8193x10 ⁶
39	1.0090x10 ⁻²	5.6234x10 ⁻²⁰	7.9804x10 ⁻⁹	2.6060x10 ⁻¹	1.6330x10 ⁻¹	3.7240x10 ⁻²	1.0000	2.5626x10 ⁶
40	2.2760x10 ⁻²	2.0893x10 ⁻¹⁹	3.3987x10 ⁻⁹	2.4160x10 ⁻¹	2.4340x10 ⁻¹	1.1100x10 ⁻¹	1.0000	1.6273x10 ⁶
41	1.8020x10 ⁻²	3.9811x10 ⁻¹⁹	4.3585x10 ⁻⁹	5.7490x10 ⁻¹	1.3340x10 ⁻¹	1.0650x10 ⁻¹	1.0000	1.3019x10 ⁶
42	2.1990x10 ⁻²	2.3442x10 ⁻²¹	3.5265x10 ⁻⁹	5.4840x10 ⁻¹	3.9640x10 ⁻¹	3.3500x10 ⁻¹	0.0000	7.6943x10 ⁶
43	5.1790x10 ⁻³	2.6915x10 ⁻¹⁹	1.5785x10 ⁻⁸	4.0000	3.9070x10 ⁻¹	1.2040x10 ⁻¹	0.0000	1.4908x10 ⁶
44	3.9010x10 ⁻³	5.3703x10 ⁻²⁰	2.1038x10 ⁻⁸	3.6050x10 ⁻¹	2.5980x10 ⁻¹	5.7350x10 ⁻²	0.0000	2.6038x10 ⁶
45	9.3870x10 ⁻³	9.7724x10 ⁻²⁰	8.5968x10 ⁻⁹	3.2390x10 ⁻¹	1.5830x10 ⁻¹	9.4190x10 ⁻²	1.0000	2.1166x10 ⁶
46	2.8280x10 ⁻²	1.6596x10 ⁻²⁰	2.6865x10 ⁻⁹	4.6060x10 ⁻¹	6.5170x10 ⁻²	2.3880x10 ⁻¹	1.0000	3.9090x10 ⁶
47	6.5700x10 ⁻³	9.1201x10 ⁻²⁰	1.2390x10 ⁻⁸	3.4760	3.1780x10 ⁻¹	2.6060x10 ⁻¹	1.0000	2.1678x10 ⁶
48	2.2390x10 ⁻²	1.4125x10 ⁻²⁰	3.4590x10 ⁻⁹	7.7080	4.5510x10 ⁻²	2.0750x10 ⁻¹	0.0000	4.1332x10 ⁶
49	1.6820x10 ⁻³	6.9183x10 ⁻¹⁹	4.9123x10 ⁻⁸	3.7530x10 ⁻¹	5.0110x10 ⁻²	6.9900x10 ⁻²	1.0000	1.0753x10 ⁶
50	1.2890x10 ⁻²	2.4547x10 ⁻²⁰	6.1926x10 ⁻⁹	3.5390x10 ⁻¹	1.8990x10 ⁻¹	1.9850x10 ⁻¹	1.0000	3.4139x10 ⁶
51	7.8440x10 ⁻³	4.0738x10 ⁻¹⁷	1.0337x10 ⁻⁸	5.6000x10 ⁻¹	2.3180x10 ⁻²	1.1810x10 ⁻²	1.0000	2.6250x10 ⁵
52	4.7130x10 ⁻³	8.7097x10 ⁻²⁰	1.7370x10 ⁻⁸	3.2370	1.5040x10 ⁻¹	3.8860x10 ⁻¹	0.0000	2.2027x10 ⁶

Appendix B: BRAGFLO Reference Tables

Table B-2. 1992 BRA GFLO Computed Variable Values for ANHYDRITE (Concluded)

Run No.	Porosity	Permeability	Compressibility	BCEXP	BCBRSAT	BCGSSAT	BCFLG	BC PCT
53	1.5900x10 ⁻²	7.7625x10 ⁻¹⁹	4.9729x10 ⁻⁹	6.7410	2.8470x10 ⁻¹	1.8060x10 ⁻¹	1.0000	1.0334x10 ⁶
54	1.4500x10 ⁻²	1.4454x10 ⁻²⁰	5.4772x10 ⁻⁹	4.7200x10 ⁻¹	1.6590x10 ⁻¹	2.7290x10 ⁻¹	0.0000	4.1004x10 ⁶
55	2.0030x10 ⁻²	1.0233x10 ⁻¹⁷	3.8960x10 ⁻⁹	6.5030x10 ⁻¹	3.2450x10 ⁻¹	3.0330x10 ⁻¹	0.0000	4.2338x10 ⁵
56	1.1650x10 ⁻²	1.0965x10 ⁻²⁰	6.8783x10 ⁻⁹	4.8480	9.2770x10 ⁻²	5.2210x10 ⁻²	0.0000	4.5118x10 ⁶
57	4.5630x10 ⁻³	5.2481x10 ⁻²¹	1.7950x10 ⁻⁸	9.2110	5.1160x10 ⁻³	2.7770x10 ⁻¹	1.0000	5.8219x10 ⁶
58	8.7110x10 ⁻³	3.3884x10 ⁻¹⁹	9.2833x10 ⁻⁹	6.4060x10 ⁻¹	3.4880x10 ⁻¹	3.2980x10 ⁻¹	1.0000	1.3766x10 ⁶
59	2.5160x10 ⁻²	7.9433x10 ⁻²⁰	3.0507x10 ⁻⁹	8.9580	8.5120x10 ⁻²	3.1270x10 ⁻¹	1.0000	2.2740x10 ⁶
60	8.2600x10 ⁻³	9.5499x10 ⁻²⁰	9.8038x10 ⁻⁹	9.8620	7.0380x10 ⁻²	8.1940x10 ⁻²	1.0000	2.1336x10 ⁶
61	7.3840x10 ⁻³	4.1687x10 ⁻²⁰	1.0997x10 ⁻⁸	8.0490x10 ⁻¹	2.7910x10 ⁻¹	1.3890x10 ⁻¹	1.0000	2.8423x10 ⁶
62	1.2250x10 ⁻²	5.4954x10 ⁻¹⁹	6.5292x10 ⁻⁹	2.8630x10 ⁻¹	3.5990x10 ⁻¹	2.5120x10 ⁻¹	1.0000	1.1645x10 ⁶
63	4.1090x10 ⁻³	9.5499x10 ⁻¹⁷	1.9961x10 ⁻⁸	3.7540	2.0010x10 ⁻¹	2.8360x10 ⁻¹	0.0000	1.9548x10 ⁵
64	3.7390x10 ⁻³	2.6915x10 ⁻²⁰	2.1960x10 ⁻⁸	2.4950	2.9320x10 ⁻²	8.7020x10 ⁻²	1.0000	3.3068x10 ⁶
65	7.4700x10 ⁻³	3.7153x10 ⁻²⁰	1.0867x10 ⁻⁸	2.5410x10 ⁻¹	2.6410x10 ⁻¹	3.5100x10 ⁻¹	1.0000	2.9578x10 ⁶
66	3.5330x10 ⁻³	3.9811x10 ⁻²⁰	2.3255x10 ⁻⁸	6.9150x10 ⁻¹	1.2380x10 ⁻¹	3.1630x10 ⁻¹	0.0000	2.8879x10 ⁶
67	8.1910x10 ⁻³	1.3804x10 ⁻¹⁹	9.8885x10 ⁻⁹	5.5890	5.6350x10 ⁻²	2.5370x10 ⁻¹	0.0000	1.8782x10 ⁶
68	1.0760x10 ⁻²	6.7608x10 ⁻²⁰	7.4679x10 ⁻⁹	4.5200	3.0240x10 ⁻¹	2.9970x10 ⁻¹	0.0000	2.4044x10 ⁶
69	1.5190x10 ⁻²	3.3113x10 ⁻²⁰	5.2171x10 ⁻⁹	4.3270	3.7150x10 ⁻¹	4.8390x10 ⁻³	1.0000	3.0780x10 ⁶
70	1.4890x10 ⁻³	1.3490x10 ⁻²¹	5.5522x10 ⁻⁸	6.2770x10 ⁻¹	1.0130x10 ⁻¹	1.1920x10 ⁻¹	1.0000	9.3155x10 ⁶

Table B-2 1992 BRAGFLO Ranks of Computed Variable Values for ANHYDRITE

Run No.	Porosity	Permeability	Compressibility	BCEXP	BCBRSAT	BCGSSAT	BCFLG	BC PCT
1	68.	66.	3.	69.	16.	41.	1.	5.
2	24.	16.	47.	21.	26.	23.	24.	55.
3	69.	65.	2.	34.	33.	38.	24.	6.
4	18.	37.	53.	52.	31.	34.	24.	34.
5	54.	8.	17.	15.	35.	26.	24.	63.
6	42.	14.	29.	56.	59.	9.	1.	57.
7	63.	17.	8.	37.	7.	29.	1.	54.
8	9.	54.	62.	57.	68.	5.	24.	17.
9	66.	9.	5.	16.	60.	33.	24.	61.
10	34.	67.	37.	39.	14.	61.	24.	4.
11	7.	11.	64.	22.	48.	36.	1.	60.
12	35.	56.	36.	61.	25.	51.	24.	15.
13	47.	36.	24.	41.	64.	52.	24.	35.
14	52.	5.	19.	8.	2.	31.	24.	66.
15	1.	20.	70.	18.	41.	68.	1.	51.
16	19.	61.	52.	24.	67.	39.	24.	10.
17	60.	40.	11.	55.	20.	67.	1.	31.
18	20.	42.	51.	28.	52.	2.	1.	29.
19	21.	35.	50.	40.	21.	30.	24.	36.
20	48.	34.	23.	33.	23.	57.	24.	37.
21	59.	51.	12.	2.	4.	40.	1.	20.
22	64.	44.	7.	38.	39.	4.	24.	26.
23	70.	30.	1.	60.	42.	8.	24.	41.
24	44.	41.	27.	17.	11.	47.	24.	30.
25	61.	28.	10.	43.	54.	18.	24.	43.
26	51.	22.	20.	53.	44.	12.	24.	49.
27	5.	21.	66.	64.	38.	14.	24.	50.
28	8.	18.	63.	63.	61.	27.	1.	53.
29	40.	27.	31.	29.	58.	63.	24.	44.
30	31.	44.	40.	1.	3.	28.	1.	26.
31	49.	3.	22.	10.	37.	43.	24.	68.
32	55.	6.	16.	66.	55.	66.	24.	65.
33	23.	60.	48.	23.	19.	60.	24.	11.
34	32.	9.	39.	65.	45.	64.	1.	61.
35	6.	26.	65.	14.	51.	24.	24.	45.
36	65.	19.	6.	6.	65.	65.	24.	52.
37	16.	24.	55.	59.	40.	6.	24.	47.
38	4.	53.	67.	44.	32.	70.	24.	18.
39	36.	39.	35.	5.	29.	7.	24.	32.
40	58.	55.	13.	3.	43.	20.	24.	16.
41	50.	59.	21.	27.	24.	19.	24.	12.
42	56.	2.	15.	25.	70.	59.	1.	69.
43	17.	57.	54.	48.	69.	22.	1.	14.
44	12.	38.	59.	12.	46.	11.	1.	33.
45	33.	50.	38.	9.	28.	17.	24.	21.
46	67.	15.	4.	19.	12.	42.	24.	56.
47	22.	48.	49.	46.	56.	46.	24.	23.
48	57.	12.	14.	62.	8.	37.	1.	59.
49	3.	63.	68.	13.	9.	13.	24.	8.
50	41.	23.	30.	11.	34.	35.	24.	48.
51	27.	69.	44.	26.	5.	3.	24.	2.
52	15.	47.	56.	45.	27.	69.	1.	24.

Appendix B: BRAGFLO Reference Tables

Table B-2 1992 BRAGFLO Ranks of Computed Variable Values for ANHYDRITE (Concluded)

Run No.	Porosity	Permeability	Compressibility	BCEXP	BCBRSAT	BCGSSAT	BCFLG	BC PCT
53	46.	64.	25.	58.	50.	32.	24.	7.
54	43.	13.	28.	20.	30.	48.	1.	58.
55	53.	68.	18.	32.	57.	54.	1.	3.
56	38.	7.	33.	51.	17.	10.	1.	64.
57	14.	4.	57.	68.	1.	49.	24.	67.
58	30.	58.	41.	31.	62.	58.	24.	13.
59	62.	46.	9.	67.	15.	55.	24.	25.
60	29.	49.	42.	70.	13.	15.	24.	22.
61	25.	33.	46.	36.	49.	25.	24.	38.
62	39.	62.	32.	7.	63.	44.	24.	9.
63	13.	70.	58.	47.	36.	50.	1.	1.
64	11.	25.	60.	42.	6.	16.	24.	46.
65	26.	31.	45.	4.	47.	62.	24.	40.
66	10.	32.	61.	35.	22.	56.	1.	39.
67	28.	52.	43.	54.	10.	45.	1.	19.
68	37.	43.	34.	50.	53.	53.	1.	28.
69	45.	29.	26.	49.	66.	1.	24.	42.
70	2.	1.	69.	30.	18.	21.	24.	70.

Table B-2 1992 BRAGFLO Computed Variable Values for BACKFILL

Run No.	Porosity	Permeability	Compressibility	BCEXP	BCBRSAT	BCGSSAT	BCFLG	BC PCT
1	2.4490x10 ⁻²	1.0000x10 ⁻¹⁵	4.4974x10 ⁻⁹	7.0000x10 ⁻¹	2.0000x10 ⁻¹	0.0000	1.0000	8.6734x10 ⁴
2	1.1240x10 ⁻²	1.0000x10 ⁻¹⁵	1.0094x10 ⁻⁸	7.0000x10 ⁻¹	2.0000x10 ⁻¹	0.0000	1.0000	8.6734x10 ⁴
3	5.1030x10 ⁻²	1.0000x10 ⁻¹⁵	2.0283x10 ⁻⁹	7.0000x10 ⁻¹	2.0000x10 ⁻¹	0.0000	1.0000	8.6734x10 ⁴
4	1.6070x10 ⁻²	1.0000x10 ⁻¹⁵	6.9848x10 ⁻⁹	7.0000x10 ⁻¹	2.0000x10 ⁻¹	0.0000	1.0000	8.6734x10 ⁴
5	4.3250x10 ⁻²	1.0000x10 ⁻¹⁵	2.4381x10 ⁻⁹	7.0000x10 ⁻¹	2.0000x10 ⁻¹	0.0000	1.0000	8.6734x10 ⁴
6	5.8630x10 ⁻²	1.0000x10 ⁻¹⁵	1.7330x10 ⁻⁹	7.0000x10 ⁻¹	2.0000x10 ⁻¹	0.0000	1.0000	8.6734x10 ⁴
7	6.6520x10 ⁻²	1.0000x10 ⁻¹⁵	1.4978x10 ⁻⁹	7.0000x10 ⁻¹	2.0000x10 ⁻¹	0.0000	1.0000	8.6734x10 ⁴
8	3.6140x10 ⁻²	1.0000x10 ⁻¹⁵	2.9670x10 ⁻⁹	7.0000x10 ⁻¹	2.0000x10 ⁻¹	0.0000	1.0000	8.6734x10 ⁴
9	1.9210x10 ⁻²	1.0000x10 ⁻¹⁵	5.8022x10 ⁻⁹	7.0000x10 ⁻¹	2.0000x10 ⁻¹	0.0000	1.0000	8.6734x10 ⁴
10	4.7300x10 ⁻²	1.0000x10 ⁻¹⁵	2.2080x10 ⁻⁹	7.0000x10 ⁻¹	2.0000x10 ⁻¹	0.0000	1.0000	8.6734x10 ⁴
11	6.7690x10 ⁻²	1.0000x10 ⁻¹⁵	1.4676x10 ⁻⁹	7.0000x10 ⁻¹	2.0000x10 ⁻¹	0.0000	1.0000	8.6734x10 ⁴
12	2.5040x10 ⁻²	1.0000x10 ⁻¹⁵	4.3931x10 ⁻⁹	7.0000x10 ⁻¹	2.0000x10 ⁻¹	0.0000	1.0000	8.6734x10 ⁴
13	7.0630x10 ⁻²	1.0000x10 ⁻¹⁵	1.3961x10 ⁻⁹	7.0000x10 ⁻¹	2.0000x10 ⁻¹	0.0000	1.0000	8.6734x10 ⁴
14	4.0420x10 ⁻²	1.0000x10 ⁻¹⁵	2.6264x10 ⁻⁹	7.0000x10 ⁻¹	2.0000x10 ⁻¹	0.0000	1.0000	8.6734x10 ⁴
15	2.1150x10 ⁻²	1.0000x10 ⁻¹⁵	5.2470x10 ⁻⁹	7.0000x10 ⁻¹	2.0000x10 ⁻¹	0.0000	1.0000	8.6734x10 ⁴
16	7.2500x10 ⁻²	1.0000x10 ⁻¹⁵	1.3536x10 ⁻⁹	7.0000x10 ⁻¹	2.0000x10 ⁻¹	0.0000	1.0000	8.6734x10 ⁴
17	4.9250x10 ⁻²	1.0000x10 ⁻¹⁵	2.1107x10 ⁻⁹	7.0000x10 ⁻¹	2.0000x10 ⁻¹	0.0000	1.0000	8.6734x10 ⁴
18	1.3450x10 ⁻²	1.0000x10 ⁻¹⁵	8.3941x10 ⁻⁹	7.0000x10 ⁻¹	2.0000x10 ⁻¹	0.0000	1.0000	8.6734x10 ⁴
19	7.4520x10 ⁻²	1.0000x10 ⁻¹⁵	1.3101x10 ⁻⁹	7.0000x10 ⁻¹	2.0000x10 ⁻¹	0.0000	1.0000	8.6734x10 ⁴
20	3.7170x10 ⁻²	1.0000x10 ⁻¹⁵	2.8779x10 ⁻⁹	7.0000x10 ⁻¹	2.0000x10 ⁻¹	0.0000	1.0000	8.6734x10 ⁴
21	5.5630x10 ⁻²	1.0000x10 ⁻¹⁵	1.8399x10 ⁻⁹	7.0000x10 ⁻¹	2.0000x10 ⁻¹	0.0000	1.0000	8.6734x10 ⁴
22	4.4090x10 ⁻²	1.0000x10 ⁻¹⁵	2.3869x10 ⁻⁹	7.0000x10 ⁻¹	2.0000x10 ⁻¹	0.0000	1.0000	8.6734x10 ⁴
23	6.0100x10 ⁻²	1.0000x10 ⁻¹⁵	1.6845x10 ⁻⁹	7.0000x10 ⁻¹	2.0000x10 ⁻¹	0.0000	1.0000	8.6734x10 ⁴
24	6.9800x10 ⁻²	1.0000x10 ⁻¹⁵	1.4157x10 ⁻⁹	7.0000x10 ⁻¹	2.0000x10 ⁻¹	0.0000	1.0000	8.6734x10 ⁴
25	6.1100x10 ⁻²	1.0000x10 ⁻¹⁵	1.6528x10 ⁻⁹	7.0000x10 ⁻¹	2.0000x10 ⁻¹	0.0000	1.0000	8.6734x10 ⁴
26	5.6930x10 ⁻²	1.0000x10 ⁻¹⁵	1.7922x10 ⁻⁹	7.0000x10 ⁻¹	2.0000x10 ⁻¹	0.0000	1.0000	8.6734x10 ⁴
27	2.8620x10 ⁻²	1.0000x10 ⁻¹⁵	3.8123x10 ⁻⁹	7.0000x10 ⁻¹	2.0000x10 ⁻¹	0.0000	1.0000	8.6734x10 ⁴
28	4.1490x10 ⁻²	1.0000x10 ⁻¹⁵	2.5522x10 ⁻⁹	7.0000x10 ⁻¹	2.0000x10 ⁻¹	0.0000	1.0000	8.6734x10 ⁴
29	1.4260x10 ⁻²	1.0000x10 ⁻¹⁵	7.9031x10 ⁻⁹	7.0000x10 ⁻¹	2.0000x10 ⁻¹	0.0000	1.0000	8.6734x10 ⁴
30	3.2140x10 ⁻²	1.0000x10 ⁻¹⁵	3.3674x10 ⁻⁹	7.0000x10 ⁻¹	2.0000x10 ⁻¹	0.0000	1.0000	8.6734x10 ⁴
31	2.6760x10 ⁻²	1.0000x10 ⁻¹⁵	4.0946x10 ⁻⁹	7.0000x10 ⁻¹	2.0000x10 ⁻¹	0.0000	1.0000	8.6734x10 ⁴
32	3.9190x10 ⁻²	1.0000x10 ⁻¹⁵	2.7166x10 ⁻⁹	7.0000x10 ⁻¹	2.0000x10 ⁻¹	0.0000	1.0000	8.6734x10 ⁴
33	4.5660x10 ⁻²	1.0000x10 ⁻¹⁵	2.2963x10 ⁻⁹	7.0000x10 ⁻¹	2.0000x10 ⁻¹	0.0000	1.0000	8.6734x10 ⁴
34	3.4580x10 ⁻²	1.0000x10 ⁻¹⁵	3.1121x10 ⁻⁹	7.0000x10 ⁻¹	2.0000x10 ⁻¹	0.0000	1.0000	8.6734x10 ⁴
35	3.8780x10 ⁻²	1.0000x10 ⁻¹⁵	2.7480x10 ⁻⁹	7.0000x10 ⁻¹	2.0000x10 ⁻¹	0.0000	1.0000	8.6734x10 ⁴
36	4.6630x10 ⁻²	1.0000x10 ⁻¹⁵	2.2433x10 ⁻⁹	7.0000x10 ⁻¹	2.0000x10 ⁻¹	0.0000	1.0000	8.6734x10 ⁴
37	1.6500x10 ⁻²	1.0000x10 ⁻¹⁵	6.7962x10 ⁻⁹	7.0000x10 ⁻¹	2.0000x10 ⁻¹	0.0000	1.0000	8.6734x10 ⁴
38	6.7530x10 ⁻²	1.0000x10 ⁻¹⁵	1.4716x10 ⁻⁹	7.0000x10 ⁻¹	2.0000x10 ⁻¹	0.0000	1.0000	8.6734x10 ⁴
39	6.2320x10 ⁻²	1.0000x10 ⁻¹⁵	1.6156x10 ⁻⁹	7.0000x10 ⁻¹	2.0000x10 ⁻¹	0.0000	1.0000	8.6734x10 ⁴
40	5.4740x10 ⁻²	1.0000x10 ⁻¹⁵	1.8739x10 ⁻⁹	7.0000x10 ⁻¹	2.0000x10 ⁻¹	0.0000	1.0000	8.6734x10 ⁴
41	6.3580x10 ⁻²	1.0000x10 ⁻¹⁵	1.5786x10 ⁻⁹	7.0000x10 ⁻¹	2.0000x10 ⁻¹	0.0000	1.0000	8.6734x10 ⁴
42	7.1460x10 ⁻²	1.0000x10 ⁻¹⁵	1.3770x10 ⁻⁹	7.0000x10 ⁻¹	2.0000x10 ⁻¹	0.0000	1.0000	8.6734x10 ⁴
43	4.4580x10 ⁻²	1.0000x10 ⁻¹⁵	2.3580x10 ⁻⁹	7.0000x10 ⁻¹	2.0000x10 ⁻¹	0.0000	1.0000	8.6734x10 ⁴
44	7.3870x10 ⁻²	1.0000x10 ⁻¹⁵	1.3239x10 ⁻⁹	7.0000x10 ⁻¹	2.0000x10 ⁻¹	0.0000	1.0000	8.6734x10 ⁴
45	2.9730x10 ⁻²	1.0000x10 ⁻¹⁵	3.6606x10 ⁻⁹	7.0000x10 ⁻¹	2.0000x10 ⁻¹	0.0000	1.0000	8.6734x10 ⁴
46	1.2610x10 ⁻²	1.0000x10 ⁻¹⁵	8.9699x10 ⁻⁹	7.0000x10 ⁻¹	2.0000x10 ⁻¹	0.0000	1.0000	8.6734x10 ⁴
47	6.0510x10 ⁻²	1.0000x10 ⁻¹⁵	1.6714x10 ⁻⁹	7.0000x10 ⁻¹	2.0000x10 ⁻¹	0.0000	1.0000	8.6734x10 ⁴
48	3.3090x10 ⁻²	1.0000x10 ⁻¹⁵	3.2635x10 ⁻⁹	7.0000x10 ⁻¹	2.0000x10 ⁻¹	0.0000	1.0000	8.6734x10 ⁴
49	4.1760x10 ⁻²	1.0000x10 ⁻¹⁵	2.5341x10 ⁻⁹	7.0000x10 ⁻¹	2.0000x10 ⁻¹	0.0000	1.0000	8.6734x10 ⁴
50	3.0510x10 ⁻²	1.0000x10 ⁻¹⁵	3.5606x10 ⁻⁹	7.0000x10 ⁻¹	2.0000x10 ⁻¹	0.0000	1.0000	8.6734x10 ⁴
51	1.8180x10 ⁻²	1.0000x10 ⁻¹⁵	6.1451x10 ⁻⁹	7.0000x10 ⁻¹	2.0000x10 ⁻¹	0.0000	1.0000	8.6734x10 ⁴
52	6.5110x10 ⁻²	1.0000x10 ⁻¹⁵	1.5356x10 ⁻⁹	7.0000x10 ⁻¹	2.0000x10 ⁻¹	0.0000	1.0000	8.6734x10 ⁴

Appendix B: BRAGFLO Reference Tables

Table B-2 1992 BRAGFLO Computed Variable Values for BACKFILL (Concluded)

Run No.	Porosity	Permeability	Compressibility	BCEXP	BCBRSAT	BCGSSAT	BCFLG	BC PCT
53	2.0520x10 ⁻²	1.0000x10 ⁻¹⁵	5.4158x10 ⁻⁹	7.0000x10 ⁻¹	2.0000x10 ⁻¹	0.0000	1.0000	8.6734x10 ⁴
54	6.4400x10 ⁻²	1.0000x10 ⁻¹⁵	1.5553x10 ⁻⁹	7.0000x10 ⁻¹	2.0000x10 ⁻¹	0.0000	1.0000	8.6734x10 ⁴
55	2.6330x10 ⁻²	1.0000x10 ⁻¹⁵	4.1656x10 ⁻⁹	7.0000x10 ⁻¹	2.0000x10 ⁻¹	0.0000	1.0000	8.6734x10 ⁴
56	3.5470x10 ⁻²	1.0000x10 ⁻¹⁵	3.0278x10 ⁻⁹	7.0000x10 ⁻¹	2.0000x10 ⁻¹	0.0000	1.0000	8.6734x10 ⁴
57	1.9820x10 ⁻²	1.0000x10 ⁻¹⁵	5.6159x10 ⁻⁹	7.0000x10 ⁻¹	2.0000x10 ⁻¹	0.0000	1.0000	8.6734x10 ⁴
58	2.3880x10 ⁻²	1.0000x10 ⁻¹⁵	4.6186x10 ⁻⁹	7.0000x10 ⁻¹	2.0000x10 ⁻¹	0.0000	1.0000	8.6734x10 ⁴
59	5.7990x10 ⁻²	1.0000x10 ⁻¹⁵	1.7549x10 ⁻⁹	7.0000x10 ⁻¹	2.0000x10 ⁻¹	0.0000	1.0000	8.6734x10 ⁴
60	6.9150x10 ⁻²	1.0000x10 ⁻¹⁵	1.4313x10 ⁻⁹	7.0000x10 ⁻¹	2.0000x10 ⁻¹	0.0000	1.0000	8.6734x10 ⁴
61	1.5400x10 ⁻²	1.0000x10 ⁻¹⁵	7.2995x10 ⁻⁹	7.0000x10 ⁻¹	2.0000x10 ⁻¹	0.0000	1.0000	8.6734x10 ⁴
62	2.7890x10 ⁻²	1.0000x10 ⁻¹⁵	3.9186x10 ⁻⁹	7.0000x10 ⁻¹	2.0000x10 ⁻¹	0.0000	1.0000	8.6734x10 ⁴
63	5.2340x10 ⁻²	1.0000x10 ⁻¹⁵	1.9713x10 ⁻⁹	7.0000x10 ⁻¹	2.0000x10 ⁻¹	0.0000	1.0000	8.6734x10 ⁴
64	5.3500x10 ⁻²	1.0000x10 ⁻¹⁵	1.9231x10 ⁻⁹	7.0000x10 ⁻¹	2.0000x10 ⁻¹	0.0000	1.0000	8.6734x10 ⁴
65	1.0820x10 ⁻²	1.0000x10 ⁻¹⁵	1.0495x10 ⁻⁸	7.0000x10 ⁻¹	2.0000x10 ⁻¹	0.0000	1.0000	8.6734x10 ⁴
66	5.0410x10 ⁻²	1.0000x10 ⁻¹⁵	2.0563x10 ⁻⁹	7.0000x10 ⁻¹	2.0000x10 ⁻¹	0.0000	1.0000	8.6734x10 ⁴
67	3.3230x10 ⁻²	1.0000x10 ⁻¹⁵	3.2487x10 ⁻⁹	7.0000x10 ⁻¹	2.0000x10 ⁻¹	0.0000	1.0000	8.6734x10 ⁴
68	2.2660x10 ⁻²	1.0000x10 ⁻¹⁵	4.8807x10 ⁻⁹	7.0000x10 ⁻¹	2.0000x10 ⁻¹	0.0000	1.0000	8.6734x10 ⁴
69	4.8950x10 ⁻²	1.0000x10 ⁻¹⁵	2.1251x10 ⁻⁹	7.0000x10 ⁻¹	2.0000x10 ⁻¹	0.0000	1.0000	8.6734x10 ⁴
70	5.3660x10 ⁻²	1.0000x10 ⁻¹⁵	1.9166x10 ⁻⁹	7.0000x10 ⁻¹	2.0000x10 ⁻¹	0.0000	1.0000	8.6734x10 ⁴

Table B-2 1992 BRAGFLO Ranks of Computed Variable Values for BACKFILL

Run No.	Porosity	Permeability	Compressibility	BCEXP	BCBRSAT	BCGSSAT	BCFLG	BC.PCT
1	16.	1.	55.	1.	1.	1.	1.	1.
2	2.	1.	69.	1.	1.	1.	1.	1.
3	45.	1.	26.	1.	1.	1.	1.	1.
4	7.	1.	64.	1.	1.	1.	1.	1.
5	36.	1.	35.	1.	1.	1.	1.	1.
6	53.	1.	18.	1.	1.	1.	1.	1.
7	61.	1.	10.	1.	1.	1.	1.	1.
8	29.	1.	42.	1.	1.	1.	1.	1.
9	10.	1.	61.	1.	1.	1.	1.	1.
10	41.	1.	30.	1.	1.	1.	1.	1.
11	63.	1.	8.	1.	1.	1.	1.	1.
12	17.	1.	54.	1.	1.	1.	1.	1.
13	66.	1.	5.	1.	1.	1.	1.	1.
14	33.	1.	38.	1.	1.	1.	1.	1.
15	13.	1.	58.	1.	1.	1.	1.	1.
16	68.	1.	3.	1.	1.	1.	1.	1.
17	43.	1.	28.	1.	1.	1.	1.	1.
18	4.	1.	67.	1.	1.	1.	1.	1.
19	70.	1.	1.	1.	1.	1.	1.	1.
20	30.	1.	41.	1.	1.	1.	1.	1.
21	50.	1.	21.	1.	1.	1.	1.	1.
22	37.	1.	34.	1.	1.	1.	1.	1.
23	54.	1.	17.	1.	1.	1.	1.	1.
24	65.	1.	6.	1.	1.	1.	1.	1.
25	56.	1.	15.	1.	1.	1.	1.	1.
26	51.	1.	20.	1.	1.	1.	1.	1.
27	21.	1.	50.	1.	1.	1.	1.	1.
28	34.	1.	37.	1.	1.	1.	1.	1.
29	5.	1.	66.	1.	1.	1.	1.	1.
30	24.	1.	47.	1.	1.	1.	1.	1.
31	19.	1.	52.	1.	1.	1.	1.	1.
32	32.	1.	39.	1.	1.	1.	1.	1.
33	39.	1.	32.	1.	1.	1.	1.	1.
34	27.	1.	44.	1.	1.	1.	1.	1.
35	31.	1.	40.	1.	1.	1.	1.	1.
36	40.	1.	31.	1.	1.	1.	1.	1.
37	8.	1.	63.	1.	1.	1.	1.	1.
38	62.	1.	9.	1.	1.	1.	1.	1.
39	57.	1.	14.	1.	1.	1.	1.	1.
40	49.	1.	22.	1.	1.	1.	1.	1.
41	58.	1.	13.	1.	1.	1.	1.	1.
42	67.	1.	4.	1.	1.	1.	1.	1.
43	38.	1.	33.	1.	1.	1.	1.	1.
44	69.	1.	2.	1.	1.	1.	1.	1.
45	22.	1.	49.	1.	1.	1.	1.	1.
46	3.	1.	68.	1.	1.	1.	1.	1.
47	55.	1.	16.	1.	1.	1.	1.	1.
48	25.	1.	46.	1.	1.	1.	1.	1.
49	35.	1.	36.	1.	1.	1.	1.	1.
50	23.	1.	48.	1.	1.	1.	1.	1.
51	9.	1.	62.	1.	1.	1.	1.	1.
52	60.	1.	11.	1.	1.	1.	1.	1.

Appendix B: BRAGFLO Reference Tables

Table B-2 1992 BRAGFLO Ranks of Computed Variable Values for BACKFILL (Concluded)

Run No.	Porosity	Permeability	Compressibility	BCEXP	BCBRSAT	BCGSSAT	BCFLG	BC PCT
53	12.	1.	59.	1.	1.	1.	1.	1.
54	59.	1.	12.	1.	1.	1.	1.	1.
55	18.	1.	53.	1.	1.	1.	1.	1.
56	28.	1.	43.	1.	1.	1.	1.	1.
57	11.	1.	60.	1.	1.	1.	1.	1.
58	15.	1.	56.	1.	1.	1.	1.	1.
59	52.	1.	19.	1.	1.	1.	1.	1.
60	64.	1.	7.	1.	1.	1.	1.	1.
61	6.	1.	65.	1.	1.	1.	1.	1.
62	20.	1.	51.	1.	1.	1.	1.	1.
63	46.	1.	25.	1.	1.	1.	1.	1.
64	47.	1.	24.	1.	1.	1.	1.	1.
65	1.	1.	70.	1.	1.	1.	1.	1.
66	44.	1.	27.	1.	1.	1.	1.	1.
67	26.	1.	45.	1.	1.	1.	1.	1.
68	14.	1.	57.	1.	1.	1.	1.	1.
69	42.	1.	29.	1.	1.	1.	1.	1.
70	48.	1.	23.	1.	1.	1.	1.	1.

Table B-2 1992 BRAGFLO Computed Variable Values for CAVITY_1

Run No.	Porosity	Permeability	Compressibility	BCEXP	BCBRSAT	BCGSSAT	BCFLG	BC PCT
1	1.0000	1.0000x10 ⁻¹⁰	0.0000	9.6790	0.0000	0.0000	1.0000	0.0000
2	1.0000	1.0000x10 ⁻¹⁰	0.0000	4.9660x10 ⁻¹	0.0000	0.0000	1.0000	0.0000
3	1.0000	1.0000x10 ⁻¹⁰	0.0000	6.7900x10 ⁻¹	0.0000	0.0000	1.0000	0.0000
4	1.0000	1.0000x10 ⁻¹⁰	0.0000	5.1820	0.0000	0.0000	1.0000	0.0000
5	1.0000	1.0000x10 ⁻¹⁰	0.0000	4.0710x10 ⁻¹	0.0000	0.0000	1.0000	0.0000
6	1.0000	1.0000x10 ⁻¹⁰	0.0000	6.1420	0.0000	0.0000	1.0000	0.0000
7	1.0000	1.0000x10 ⁻¹⁰	0.0000	1.0990	0.0000	0.0000	1.0000	0.0000
8	1.0000	1.0000x10 ⁻¹⁰	0.0000	6.4480	0.0000	0.0000	1.0000	0.0000
9	1.0000	1.0000x10 ⁻¹⁰	0.0000	4.2610x10 ⁻¹	0.0000	0.0000	1.0000	0.0000
10	1.0000	1.0000x10 ⁻¹⁰	0.0000	1.5170	0.0000	0.0000	1.0000	0.0000
11	1.0000	1.0000x10 ⁻¹⁰	0.0000	5.1250x10 ⁻¹	0.0000	0.0000	1.0000	0.0000
12	1.0000	1.0000x10 ⁻¹⁰	0.0000	7.4960	0.0000	0.0000	1.0000	0.0000
13	1.0000	1.0000x10 ⁻¹⁰	0.0000	2.2490	0.0000	0.0000	1.0000	0.0000
14	1.0000	1.0000x10 ⁻¹⁰	0.0000	3.0620x10 ⁻¹	0.0000	0.0000	1.0000	0.0000
15	1.0000	1.0000x10 ⁻¹⁰	0.0000	4.4620x10 ⁻¹	0.0000	0.0000	1.0000	0.0000
16	1.0000	1.0000x10 ⁻¹⁰	0.0000	5.3590x10 ⁻¹	0.0000	0.0000	1.0000	0.0000
17	1.0000	1.0000x10 ⁻¹⁰	0.0000	5.9190	0.0000	0.0000	1.0000	0.0000
18	1.0000	1.0000x10 ⁻¹⁰	0.0000	5.8730x10 ⁻¹	0.0000	0.0000	1.0000	0.0000
19	1.0000	1.0000x10 ⁻¹⁰	0.0000	2.0050	0.0000	0.0000	1.0000	0.0000
20	1.0000	1.0000x10 ⁻¹⁰	0.0000	6.7090x10 ⁻¹	0.0000	0.0000	1.0000	0.0000
21	1.0000	1.0000x10 ⁻¹⁰	0.0000	2.2590x10 ⁻¹	0.0000	0.0000	1.0000	0.0000
22	1.0000	1.0000x10 ⁻¹⁰	0.0000	1.4340	0.0000	0.0000	1.0000	0.0000
23	1.0000	1.0000x10 ⁻¹⁰	0.0000	7.0990	0.0000	0.0000	1.0000	0.0000
24	1.0000	1.0000x10 ⁻¹⁰	0.0000	4.3270x10 ⁻¹	0.0000	0.0000	1.0000	0.0000
25	1.0000	1.0000x10 ⁻¹⁰	0.0000	2.7610	0.0000	0.0000	1.0000	0.0000
26	1.0000	1.0000x10 ⁻¹⁰	0.0000	5.2660	0.0000	0.0000	1.0000	0.0000
27	1.0000	1.0000x10 ⁻¹⁰	0.0000	8.3330	0.0000	0.0000	1.0000	0.0000
28	1.0000	1.0000x10 ⁻¹⁰	0.0000	7.9460	0.0000	0.0000	1.0000	0.0000
29	1.0000	1.0000x10 ⁻¹⁰	0.0000	6.0410x10 ⁻¹	0.0000	0.0000	1.0000	0.0000
30	1.0000	1.0000x10 ⁻¹⁰	0.0000	2.0040x10 ⁻¹	0.0000	0.0000	1.0000	0.0000
31	1.0000	1.0000x10 ⁻¹⁰	0.0000	3.3160x10 ⁻¹	0.0000	0.0000	1.0000	0.0000
32	1.0000	1.0000x10 ⁻¹⁰	0.0000	8.8800	0.0000	0.0000	1.0000	0.0000
33	1.0000	1.0000x10 ⁻¹⁰	0.0000	5.2200x10 ⁻¹	0.0000	0.0000	1.0000	0.0000
34	1.0000	1.0000x10 ⁻¹⁰	0.0000	8.6520	0.0000	0.0000	1.0000	0.0000
35	1.0000	1.0000x10 ⁻¹⁰	0.0000	3.9470x10 ⁻¹	0.0000	0.0000	1.0000	0.0000
36	1.0000	1.0000x10 ⁻¹⁰	0.0000	2.7500x10 ⁻¹	0.0000	0.0000	1.0000	0.0000
37	1.0000	1.0000x10 ⁻¹⁰	0.0000	6.9780	0.0000	0.0000	1.0000	0.0000
38	1.0000	1.0000x10 ⁻¹⁰	0.0000	2.9640	0.0000	0.0000	1.0000	0.0000
39	1.0000	1.0000x10 ⁻¹⁰	0.0000	2.6060x10 ⁻¹	0.0000	0.0000	1.0000	0.0000
40	1.0000	1.0000x10 ⁻¹⁰	0.0000	2.4160x10 ⁻¹	0.0000	0.0000	1.0000	0.0000
41	1.0000	1.0000x10 ⁻¹⁰	0.0000	5.7490x10 ⁻¹	0.0000	0.0000	1.0000	0.0000
42	1.0000	1.0000x10 ⁻¹⁰	0.0000	5.4840x10 ⁻¹	0.0000	0.0000	1.0000	0.0000
43	1.0000	1.0000x10 ⁻¹⁰	0.0000	4.0000	0.0000	0.0000	1.0000	0.0000
44	1.0000	1.0000x10 ⁻¹⁰	0.0000	3.6050x10 ⁻¹	0.0000	0.0000	1.0000	0.0000
45	1.0000	1.0000x10 ⁻¹⁰	0.0000	3.2390x10 ⁻¹	0.0000	0.0000	1.0000	0.0000
46	1.0000	1.0000x10 ⁻¹⁰	0.0000	4.6060x10 ⁻¹	0.0000	0.0000	1.0000	0.0000
47	1.0000	1.0000x10 ⁻¹⁰	0.0000	3.4760	0.0000	0.0000	1.0000	0.0000
48	1.0000	1.0000x10 ⁻¹⁰	0.0000	7.7080	0.0000	0.0000	1.0000	0.0000
49	1.0000	1.0000x10 ⁻¹⁰	0.0000	3.7530x10 ⁻¹	0.0000	0.0000	1.0000	0.0000
50	1.0000	1.0000x10 ⁻¹⁰	0.0000	3.5390x10 ⁻¹	0.0000	0.0000	1.0000	0.0000
51	1.0000	1.0000x10 ⁻¹⁰	0.0000	5.6000x10 ⁻¹	0.0000	0.0000	1.0000	0.0000
52	1.0000	1.0000x10 ⁻¹⁰	0.0000	3.2370	0.0000	0.0000	1.0000	0.0000

Appendix B: BRAGFLO Reference Tables

Table B-2 1992 BRAGFLO Computed Variable Values for CAVITY_1 (Concluded)

Run No.	Porosity	Permeability	Compressibility	BCEXP	BCBRSAT	BCGSSAT	BCFLG	BCPCT
53	1.0000	1.0000x10 ⁻¹⁰	0.0000	6.7410	0.0000	0.0000	1.0000	0.0000
54	1.0000	1.0000x10 ⁻¹⁰	0.0000	4.7200x10 ⁻¹	0.0000	0.0000	1.0000	0.0000
55	1.0000	1.0000x10 ⁻¹⁰	0.0000	6.5030x10 ⁻¹	0.0000	0.0000	1.0000	0.0000
56	1.0000	1.0000x10 ⁻¹⁰	0.0000	4.8480	0.0000	0.0000	1.0000	0.0000
57	1.0000	1.0000x10 ⁻¹⁰	0.0000	9.2110	0.0000	0.0000	1.0000	0.0000
58	1.0000	1.0000x10 ⁻¹⁰	0.0000	6.4060x10 ⁻¹	0.0000	0.0000	1.0000	0.0000
59	1.0000	1.0000x10 ⁻¹⁰	0.0000	8.9580	0.0000	0.0000	1.0000	0.0000
60	1.0000	1.0000x10 ⁻¹⁰	0.0000	9.8620	0.0000	0.0000	1.0000	0.0000
61	1.0000	1.0000x10 ⁻¹⁰	0.0000	8.0490x10 ⁻¹	0.0000	0.0000	1.0000	0.0000
62	1.0000	1.0000x10 ⁻¹⁰	0.0000	2.8630x10 ⁻¹	0.0000	0.0000	1.0000	0.0000
63	1.0000	1.0000x10 ⁻¹⁰	0.0000	3.7540	0.0000	0.0000	1.0000	0.0000
64	1.0000	1.0000x10 ⁻¹⁰	0.0000	2.4950	0.0000	0.0000	1.0000	0.0000
65	1.0000	1.0000x10 ⁻¹⁰	0.0000	2.5410x10 ⁻¹	0.0000	0.0000	1.0000	0.0000
66	1.0000	1.0000x10 ⁻¹⁰	0.0000	6.9150x10 ⁻¹	0.0000	0.0000	1.0000	0.0000
67	1.0000	1.0000x10 ⁻¹⁰	0.0000	5.5890	0.0000	0.0000	1.0000	0.0000
68	1.0000	1.0000x10 ⁻¹⁰	0.0000	4.5200	0.0000	0.0000	1.0000	0.0000
69	1.0000	1.0000x10 ⁻¹⁰	0.0000	4.3270	0.0000	0.0000	1.0000	0.0000
70	1.0000	1.0000x10 ⁻¹⁰	0.0000	6.2770x10 ⁻¹	0.0000	0.0000	1.0000	0.0000

Table B-2 1992 BRAGFLO Ranks of Computed Variable Values for CAVITY_1

Run No.	Porosity	Permeability	Compressibility	BCEXP	BCBRSAT	BCGSSAT	BCFLG	BC PCT
1	1.	1.	1.	69.	1.	1.	1.	1.
2	1.	1.	1.	21.	1.	1.	1.	1.
3	1.	1.	1.	34.	1.	1.	1.	1.
4	1.	1.	1.	52.	1.	1.	1.	1.
5	1.	1.	1.	15.	1.	1.	1.	1.
6	1.	1.	1.	56.	1.	1.	1.	1.
7	1.	1.	1.	37.	1.	1.	1.	1.
8	1.	1.	1.	57.	1.	1.	1.	1.
9	1.	1.	1.	16.	1.	1.	1.	1.
10	1.	1.	1.	39.	1.	1.	1.	1.
11	1.	1.	1.	22.	1.	1.	1.	1.
12	1.	1.	1.	61.	1.	1.	1.	1.
13	1.	1.	1.	41.	1.	1.	1.	1.
14	1.	1.	1.	8.	1.	1.	1.	1.
15	1.	1.	1.	18.	1.	1.	1.	1.
16	1.	1.	1.	24.	1.	1.	1.	1.
17	1.	1.	1.	55.	1.	1.	1.	1.
18	1.	1.	1.	28.	1.	1.	1.	1.
19	1.	1.	1.	40.	1.	1.	1.	1.
20	1.	1.	1.	33.	1.	1.	1.	1.
21	1.	1.	1.	2.	1.	1.	1.	1.
22	1.	1.	1.	38.	1.	1.	1.	1.
23	1.	1.	1.	60.	1.	1.	1.	1.
24	1.	1.	1.	17.	1.	1.	1.	1.
25	1.	1.	1.	43.	1.	1.	1.	1.
26	1.	1.	1.	53.	1.	1.	1.	1.
27	1.	1.	1.	64.	1.	1.	1.	1.
28	1.	1.	1.	63.	1.	1.	1.	1.
29	1.	1.	1.	29.	1.	1.	1.	1.
30	1.	1.	1.	1.	1.	1.	1.	1.
31	1.	1.	1.	10.	1.	1.	1.	1.
32	1.	1.	1.	66.	1.	1.	1.	1.
33	1.	1.	1.	23.	1.	1.	1.	1.
34	1.	1.	1.	65.	1.	1.	1.	1.
35	1.	1.	1.	14.	1.	1.	1.	1.
36	1.	1.	1.	6.	1.	1.	1.	1.
37	1.	1.	1.	59.	1.	1.	1.	1.
38	1.	1.	1.	44.	1.	1.	1.	1.
39	1.	1.	1.	5.	1.	1.	1.	1.
40	1.	1.	1.	3.	1.	1.	1.	1.
41	1.	1.	1.	27.	1.	1.	1.	1.
42	1.	1.	1.	25.	1.	1.	1.	1.
43	1.	1.	1.	48.	1.	1.	1.	1.
44	1.	1.	1.	12.	1.	1.	1.	1.
45	1.	1.	1.	9.	1.	1.	1.	1.
46	1.	1.	1.	19.	1.	1.	1.	1.
47	1.	1.	1.	46.	1.	1.	1.	1.
48	1.	1.	1.	62.	1.	1.	1.	1.
49	1.	1.	1.	13.	1.	1.	1.	1.
50	1.	1.	1.	11.	1.	1.	1.	1.
51	1.	1.	1.	26.	1.	1.	1.	1.
52	1.	1.	1.	45.	1.	1.	1.	1.

Appendix B: BRAGFLO Reference Tables

Table B-2 1992 BRAGFLO Ranks of Computed Variable Values for CAVITY_1 (Concluded)

<u>Run No.</u>	<u>Porosity</u>	<u>Permeability</u>	<u>Compressibility</u>	<u>BCEXP</u>	<u>BCBRSAT</u>	<u>BCGSSAT</u>	<u>BCFLG</u>	<u>BC PCT</u>
53	1.	1.	1.	58.	1.	1.	1.	1.
54	1.	1.	1.	20.	1.	1.	1.	1.
55	1.	1.	1.	32.	1.	1.	1.	1.
56	1.	1.	1.	51.	1.	1.	1.	1.
57	1.	1.	1.	68.	1.	1.	1.	1.
58	1.	1.	1.	31.	1.	1.	1.	1.
59	1.	1.	1.	67.	1.	1.	1.	1.
60	1.	1.	1.	70.	1.	1.	1.	1.
61	1.	1.	1.	36.	1.	1.	1.	1.
62	1.	1.	1.	7.	1.	1.	1.	1.
63	1.	1.	1.	47.	1.	1.	1.	1.
64	1.	1.	1.	42.	1.	1.	1.	1.
65	1.	1.	1.	4.	1.	1.	1.	1.
66	1.	1.	1.	35.	1.	1.	1.	1.
67	1.	1.	1.	54.	1.	1.	1.	1.
68	1.	1.	1.	50.	1.	1.	1.	1.
69	1.	1.	1.	49.	1.	1.	1.	1.
70	1.	1.	1.	30.	1.	1.	1.	1.

Table B-2 1992 BRAGFLO Computed Variable Values for CAVITY_2

Run No.	Porosity	Permeability	Compressibility	BCEXP	BCBRSAT	BCGSSAT	BCFLG	BC PCT
1	1.0000	1.0000x10 ⁻¹⁰	0.0000	9.6790	0.0000	0.0000	1.0000	0.0000
2	1.0000	1.0000x10 ⁻¹⁰	0.0000	4.9660x10 ⁻¹	0.0000	0.0000	1.0000	0.0000
3	1.0000	1.0000x10 ⁻¹⁰	0.0000	6.7900x10 ⁻¹	0.0000	0.0000	1.0000	0.0000
4	1.0000	1.0000x10 ⁻¹⁰	0.0000	5.1820	0.0000	0.0000	1.0000	0.0000
5	1.0000	1.0000x10 ⁻¹⁰	0.0000	4.0710x10 ⁻¹	0.0000	0.0000	1.0000	0.0000
6	1.0000	1.0000x10 ⁻¹⁰	0.0000	6.1420	0.0000	0.0000	1.0000	0.0000
7	1.0000	1.0000x10 ⁻¹⁰	0.0000	1.0990	0.0000	0.0000	1.0000	0.0000
8	1.0000	1.0000x10 ⁻¹⁰	0.0000	6.4480	0.0000	0.0000	1.0000	0.0000
9	1.0000	1.0000x10 ⁻¹⁰	0.0000	4.2610x10 ⁻¹	0.0000	0.0000	1.0000	0.0000
10	1.0000	1.0000x10 ⁻¹⁰	0.0000	1.5170	0.0000	0.0000	1.0000	0.0000
11	1.0000	1.0000x10 ⁻¹⁰	0.0000	5.1250x10 ⁻¹	0.0000	0.0000	1.0000	0.0000
12	1.0000	1.0000x10 ⁻¹⁰	0.0000	7.4960	0.0000	0.0000	1.0000	0.0000
13	1.0000	1.0000x10 ⁻¹⁰	0.0000	2.2490	0.0000	0.0000	1.0000	0.0000
14	1.0000	1.0000x10 ⁻¹⁰	0.0000	3.0620x10 ⁻¹	0.0000	0.0000	1.0000	0.0000
15	1.0000	1.0000x10 ⁻¹⁰	0.0000	4.4620x10 ⁻¹	0.0000	0.0000	1.0000	0.0000
16	1.0000	1.0000x10 ⁻¹⁰	0.0000	5.3590x10 ⁻¹	0.0000	0.0000	1.0000	0.0000
17	1.0000	1.0000x10 ⁻¹⁰	0.0000	5.9190	0.0000	0.0000	1.0000	0.0000
18	1.0000	1.0000x10 ⁻¹⁰	0.0000	5.8730x10 ⁻¹	0.0000	0.0000	1.0000	0.0000
19	1.0000	1.0000x10 ⁻¹⁰	0.0000	2.0050	0.0000	0.0000	1.0000	0.0000
20	1.0000	1.0000x10 ⁻¹⁰	0.0000	6.7090x10 ⁻¹	0.0000	0.0000	1.0000	0.0000
21	1.0000	1.0000x10 ⁻¹⁰	0.0000	2.2590x10 ⁻¹	0.0000	0.0000	1.0000	0.0000
22	1.0000	1.0000x10 ⁻¹⁰	0.0000	1.4340	0.0000	0.0000	1.0000	0.0000
23	1.0000	1.0000x10 ⁻¹⁰	0.0000	7.0990	0.0000	0.0000	1.0000	0.0000
24	1.0000	1.0000x10 ⁻¹⁰	0.0000	4.3270x10 ⁻¹	0.0000	0.0000	1.0000	0.0000
25	1.0000	1.0000x10 ⁻¹⁰	0.0000	2.7610	0.0000	0.0000	1.0000	0.0000
26	1.0000	1.0000x10 ⁻¹⁰	0.0000	5.2660	0.0000	0.0000	1.0000	0.0000
27	1.0000	1.0000x10 ⁻¹⁰	0.0000	8.3330	0.0000	0.0000	1.0000	0.0000
28	1.0000	1.0000x10 ⁻¹⁰	0.0000	7.9460	0.0000	0.0000	1.0000	0.0000
29	1.0000	1.0000x10 ⁻¹⁰	0.0000	6.0410x10 ⁻¹	0.0000	0.0000	1.0000	0.0000
30	1.0000	1.0000x10 ⁻¹⁰	0.0000	2.0040x10 ⁻¹	0.0000	0.0000	1.0000	0.0000
31	1.0000	1.0000x10 ⁻¹⁰	0.0000	3.3160x10 ⁻¹	0.0000	0.0000	1.0000	0.0000
32	1.0000	1.0000x10 ⁻¹⁰	0.0000	8.8800	0.0000	0.0000	1.0000	0.0000
33	1.0000	1.0000x10 ⁻¹⁰	0.0000	5.2200x10 ⁻¹	0.0000	0.0000	1.0000	0.0000
34	1.0000	1.0000x10 ⁻¹⁰	0.0000	8.6520	0.0000	0.0000	1.0000	0.0000
35	1.0000	1.0000x10 ⁻¹⁰	0.0000	3.9470x10 ⁻¹	0.0000	0.0000	1.0000	0.0000
36	1.0000	1.0000x10 ⁻¹⁰	0.0000	2.7500x10 ⁻¹	0.0000	0.0000	1.0000	0.0000
37	1.0000	1.0000x10 ⁻¹⁰	0.0000	6.9780	0.0000	0.0000	1.0000	0.0000
38	1.0000	1.0000x10 ⁻¹⁰	0.0000	2.9640	0.0000	0.0000	1.0000	0.0000
39	1.0000	1.0000x10 ⁻¹⁰	0.0000	2.6060x10 ⁻¹	0.0000	0.0000	1.0000	0.0000
40	1.0000	1.0000x10 ⁻¹⁰	0.0000	2.4160x10 ⁻¹	0.0000	0.0000	1.0000	0.0000
41	1.0000	1.0000x10 ⁻¹⁰	0.0000	5.7490x10 ⁻¹	0.0000	0.0000	1.0000	0.0000
42	1.0000	1.0000x10 ⁻¹⁰	0.0000	5.4840x10 ⁻¹	0.0000	0.0000	1.0000	0.0000
43	1.0000	1.0000x10 ⁻¹⁰	0.0000	4.0000	0.0000	0.0000	1.0000	0.0000
44	1.0000	1.0000x10 ⁻¹⁰	0.0000	3.6050x10 ⁻¹	0.0000	0.0000	1.0000	0.0000
45	1.0000	1.0000x10 ⁻¹⁰	0.0000	3.2390x10 ⁻¹	0.0000	0.0000	1.0000	0.0000
46	1.0000	1.0000x10 ⁻¹⁰	0.0000	4.6060x10 ⁻¹	0.0000	0.0000	1.0000	0.0000
47	1.0000	1.0000x10 ⁻¹⁰	0.0000	3.4760	0.0000	0.0000	1.0000	0.0000
48	1.0000	1.0000x10 ⁻¹⁰	0.0000	7.7080	0.0000	0.0000	1.0000	0.0000
49	1.0000	1.0000x10 ⁻¹⁰	0.0000	3.7530x10 ⁻¹	0.0000	0.0000	1.0000	0.0000
50	1.0000	1.0000x10 ⁻¹⁰	0.0000	3.5390x10 ⁻¹	0.0000	0.0000	1.0000	0.0000
51	1.0000	1.0000x10 ⁻¹⁰	0.0000	5.6000x10 ⁻¹	0.0000	0.0000	1.0000	0.0000
52	1.0000	1.0000x10 ⁻¹⁰	0.0000	3.2370	0.0000	0.0000	1.0000	0.0000

Appendix B: BRAGFLO Reference Tables

Table B-2 1992 BRAGFLO Computed Variable Values for CAVITY_2 (Concluded)

<u>Run No.</u>	<u>Porosity</u>	<u>Permeability</u>	<u>Compressibility</u>	<u>BCEXP</u>	<u>BCBRSAT</u>	<u>BCGSSAT</u>	<u>BCFLG</u>	<u>BC PCT</u>
53	1.0000	1.0000x10 ⁻¹⁰	0.0000	6.7410	0.0000	0.0000	1.0000	0.0000
54	1.0000	1.0000x10 ⁻¹⁰	0.0000	4.7200x10 ⁻¹	0.0000	0.0000	1.0000	0.0000
55	1.0000	1.0000x10 ⁻¹⁰	0.0000	6.5030x10 ⁻¹	0.0000	0.0000	1.0000	0.0000
56	1.0000	1.0000x10 ⁻¹⁰	0.0000	4.8480	0.0000	0.0000	1.0000	0.0000
57	1.0000	1.0000x10 ⁻¹⁰	0.0000	9.2110	0.0000	0.0000	1.0000	0.0000
58	1.0000	1.0000x10 ⁻¹⁰	0.0000	6.4060x10 ⁻¹	0.0000	0.0000	1.0000	0.0000
59	1.0000	1.0000x10 ⁻¹⁰	0.0000	8.9580	0.0000	0.0000	1.0000	0.0000
60	1.0000	1.0000x10 ⁻¹⁰	0.0000	9.8620	0.0000	0.0000	1.0000	0.0000
61	1.0000	1.0000x10 ⁻¹⁰	0.0000	8.0490x10 ⁻¹	0.0000	0.0000	1.0000	0.0000
62	1.0000	1.0000x10 ⁻¹⁰	0.0000	2.8630x10 ⁻¹	0.0000	0.0000	1.0000	0.0000
63	1.0000	1.0000x10 ⁻¹⁰	0.0000	3.7540	0.0000	0.0000	1.0000	0.0000
64	1.0000	1.0000x10 ⁻¹⁰	0.0000	2.4950	0.0000	0.0000	1.0000	0.0000
65	1.0000	1.0000x10 ⁻¹⁰	0.0000	2.5410x10 ⁻¹	0.0000	0.0000	1.0000	0.0000
66	1.0000	1.0000x10 ⁻¹⁰	0.0000	6.9150x10 ⁻¹	0.0000	0.0000	1.0000	0.0000
67	1.0000	1.0000x10 ⁻¹⁰	0.0000	5.5890	0.0000	0.0000	1.0000	0.0000
68	1.0000	1.0000x10 ⁻¹⁰	0.0000	4.5200	0.0000	0.0000	1.0000	0.0000
69	1.0000	1.0000x10 ⁻¹⁰	0.0000	4.3270	0.0000	0.0000	1.0000	0.0000
70	1.0000	1.0000x10 ⁻¹⁰	0.0000	6.2770x10 ⁻¹	0.0000	0.0000	1.0000	0.0000

Table B-2 1992 BRAGFLO Ranks of Computed Variable Values for CAVITY_2

Run No.	Porosity	Permeability	Compressibility	BCEXP	BCBRSAT	BCGSSAT	BCFLG	BCPCT
1	1.	1.	1.	69.	1.	1.	1.	1.
2	1.	1.	1.	21.	1.	1.	1.	1.
3	1.	1.	1.	34.	1.	1.	1.	1.
4	1.	1.	1.	52.	1.	1.	1.	1.
5	1.	1.	1.	15.	1.	1.	1.	1.
6	1.	1.	1.	56.	1.	1.	1.	1.
7	1.	1.	1.	37.	1.	1.	1.	1.
8	1.	1.	1.	57.	1.	1.	1.	1.
9	1.	1.	1.	16.	1.	1.	1.	1.
10	1.	1.	1.	39.	1.	1.	1.	1.
11	1.	1.	1.	22.	1.	1.	1.	1.
12	1.	1.	1.	61.	1.	1.	1.	1.
13	1.	1.	1.	41.	1.	1.	1.	1.
14	1.	1.	1.	8.	1.	1.	1.	1.
15	1.	1.	1.	18.	1.	1.	1.	1.
16	1.	1.	1.	24.	1.	1.	1.	1.
17	1.	1.	1.	55.	1.	1.	1.	1.
18	1.	1.	1.	28.	1.	1.	1.	1.
19	1.	1.	1.	40.	1.	1.	1.	1.
20	1.	1.	1.	33.	1.	1.	1.	1.
21	1.	1.	1.	2.	1.	1.	1.	1.
22	1.	1.	1.	38.	1.	1.	1.	1.
23	1.	1.	1.	60.	1.	1.	1.	1.
24	1.	1.	1.	17.	1.	1.	1.	1.
25	1.	1.	1.	43.	1.	1.	1.	1.
26	1.	1.	1.	53.	1.	1.	1.	1.
27	1.	1.	1.	64.	1.	1.	1.	1.
28	1.	1.	1.	63.	1.	1.	1.	1.
29	1.	1.	1.	29.	1.	1.	1.	1.
30	1.	1.	1.	1.	1.	1.	1.	1.
31	1.	1.	1.	10.	1.	1.	1.	1.
32	1.	1.	1.	66.	1.	1.	1.	1.
33	1.	1.	1.	23.	1.	1.	1.	1.
34	1.	1.	1.	65.	1.	1.	1.	1.
35	1.	1.	1.	14.	1.	1.	1.	1.
36	1.	1.	1.	6.	1.	1.	1.	1.
37	1.	1.	1.	59.	1.	1.	1.	1.
38	1.	1.	1.	44.	1.	1.	1.	1.
39	1.	1.	1.	5.	1.	1.	1.	1.
40	1.	1.	1.	3.	1.	1.	1.	1.
41	1.	1.	1.	27.	1.	1.	1.	1.
42	1.	1.	1.	25.	1.	1.	1.	1.
43	1.	1.	1.	48.	1.	1.	1.	1.
44	1.	1.	1.	12.	1.	1.	1.	1.
45	1.	1.	1.	9.	1.	1.	1.	1.
46	1.	1.	1.	19.	1.	1.	1.	1.
47	1.	1.	1.	46.	1.	1.	1.	1.
48	1.	1.	1.	62.	1.	1.	1.	1.
49	1.	1.	1.	13.	1.	1.	1.	1.
50	1.	1.	1.	11.	1.	1.	1.	1.
51	1.	1.	1.	26.	1.	1.	1.	1.
52	1.	1.	1.	45.	1.	1.	1.	1.

Appendix B: BRAGFLO Reference Tables

Table B-2 1992 BRAGFLO Ranks of Computed Variable Values for CAVITY_2 (Concluded)

<u>Run No.</u>	<u>Porosity</u>	<u>Permeability</u>	<u>Compressibility</u>	<u>BCEXP</u>	<u>BCBRSAT</u>	<u>BCGSSAT</u>	<u>BCFLG</u>	<u>BC PCT</u>
53	1.	1.	1.	58.	1.	1.	1.	1.
54	1.	1.	1.	20.	1.	1.	1.	1.
55	1.	1.	1.	32.	1.	1.	1.	1.
56	1.	1.	1.	51.	1.	1.	1.	1.
57	1.	1.	1.	68.	1.	1.	1.	1.
58	1.	1.	1.	31.	1.	1.	1.	1.
59	1.	1.	1.	67.	1.	1.	1.	1.
60	1.	1.	1.	70.	1.	1.	1.	1.
61	1.	1.	1.	36.	1.	1.	1.	1.
62	1.	1.	1.	7.	1.	1.	1.	1.
63	1.	1.	1.	47.	1.	1.	1.	1.
64	1.	1.	1.	42.	1.	1.	1.	1.
65	1.	1.	1.	4.	1.	1.	1.	1.
66	1.	1.	1.	35.	1.	1.	1.	1.
67	1.	1.	1.	54.	1.	1.	1.	1.
68	1.	1.	1.	50.	1.	1.	1.	1.
69	1.	1.	1.	49.	1.	1.	1.	1.
70	1.	1.	1.	30.	1.	1.	1.	1.

Table B-2 1992 BRAGFLO Computed Variable Values for CULEBRA

Run No.	Porosity	Permeability	Compressibility	BCEXP	BCRSAT	BCGSSAT	BCFLG	BC PCT
1	1.1430x10 ⁻¹	2.0991x10 ⁻¹⁴	1.8795x10 ⁻⁹	7.0000x10 ⁻¹	2.0000x10 ⁻¹	2.0000x10 ⁻¹	1.0000	3.0253x10 ⁴
2	1.8220x10 ⁻¹	2.0991x10 ⁻¹⁴	1.0859x10 ⁻⁹	7.0000x10 ⁻¹	2.0000x10 ⁻¹	2.0000x10 ⁻¹	1.0000	3.0253x10 ⁴
3	1.7260x10 ⁻¹	2.0991x10 ⁻¹⁴	1.1602x10 ⁻⁹	7.0000x10 ⁻¹	2.0000x10 ⁻¹	2.0000x10 ⁻¹	1.0000	3.0253x10 ⁴
4	1.2840x10 ⁻¹	2.0991x10 ⁻¹⁴	1.6457x10 ⁻⁹	7.0000x10 ⁻¹	2.0000x10 ⁻¹	2.0000x10 ⁻¹	1.0000	3.0253x10 ⁴
5	1.2200x10 ⁻¹	2.0991x10 ⁻¹⁴	1.7451x10 ⁻⁹	7.0000x10 ⁻¹	2.0000x10 ⁻¹	2.0000x10 ⁻¹	1.0000	3.0253x10 ⁴
6	1.7830x10 ⁻¹	2.0991x10 ⁻¹⁴	1.1151x10 ⁻⁹	7.0000x10 ⁻¹	2.0000x10 ⁻¹	2.0000x10 ⁻¹	1.0000	3.0253x10 ⁴
7	1.2060x10 ⁻¹	2.0991x10 ⁻¹⁴	1.7683x10 ⁻⁹	7.0000x10 ⁻¹	2.0000x10 ⁻¹	2.0000x10 ⁻¹	1.0000	3.0253x10 ⁴
8	1.0450x10 ⁻¹	2.0991x10 ⁻¹⁴	2.0792x10 ⁻⁹	7.0000x10 ⁻¹	2.0000x10 ⁻¹	2.0000x10 ⁻¹	1.0000	3.0253x10 ⁴
9	1.2100x10 ⁻¹	2.0991x10 ⁻¹⁴	1.7616x10 ⁻⁹	7.0000x10 ⁻¹	2.0000x10 ⁻¹	2.0000x10 ⁻¹	1.0000	3.0253x10 ⁴
10	1.6340x10 ⁻¹	2.0991x10 ⁻¹⁴	1.2396x10 ⁻⁹	7.0000x10 ⁻¹	2.0000x10 ⁻¹	2.0000x10 ⁻¹	1.0000	3.0253x10 ⁴
11	1.7880x10 ⁻¹	2.0991x10 ⁻¹⁴	1.1113x10 ⁻⁹	7.0000x10 ⁻¹	2.0000x10 ⁻¹	2.0000x10 ⁻¹	1.0000	3.0253x10 ⁴
12	1.3740x10 ⁻¹	2.0991x10 ⁻¹⁴	1.5215x10 ⁻⁹	7.0000x10 ⁻¹	2.0000x10 ⁻¹	2.0000x10 ⁻¹	1.0000	3.0253x10 ⁴
13	1.1150x10 ⁻¹	2.0991x10 ⁻¹⁴	1.9330x10 ⁻⁹	7.0000x10 ⁻¹	2.0000x10 ⁻¹	2.0000x10 ⁻¹	1.0000	3.0253x10 ⁴
14	1.2590x10 ⁻¹	2.0991x10 ⁻¹⁴	1.6833x10 ⁻⁹	7.0000x10 ⁻¹	2.0000x10 ⁻¹	2.0000x10 ⁻¹	1.0000	3.0253x10 ⁴
15	1.0750x10 ⁻¹	2.0991x10 ⁻¹⁴	2.0142x10 ⁻⁹	7.0000x10 ⁻¹	2.0000x10 ⁻¹	2.0000x10 ⁻¹	1.0000	3.0253x10 ⁴
16	1.2290x10 ⁻¹	2.0991x10 ⁻¹⁴	1.7305x10 ⁻⁹	7.0000x10 ⁻¹	2.0000x10 ⁻¹	2.0000x10 ⁻¹	1.0000	3.0253x10 ⁴
17	1.4460x10 ⁻¹	2.0991x10 ⁻¹⁴	1.4333x10 ⁻⁹	7.0000x10 ⁻¹	2.0000x10 ⁻¹	2.0000x10 ⁻¹	1.0000	3.0253x10 ⁴
18	1.7820x10 ⁻¹	2.0991x10 ⁻¹⁴	1.1159x10 ⁻⁹	7.0000x10 ⁻¹	2.0000x10 ⁻¹	2.0000x10 ⁻¹	1.0000	3.0253x10 ⁴
19	7.6020x10 ⁻²	2.0991x10 ⁻¹⁴	2.9519x10 ⁻⁹	7.0000x10 ⁻¹	2.0000x10 ⁻¹	2.0000x10 ⁻¹	1.0000	3.0253x10 ⁴
20	2.0520x10 ⁻¹	2.0991x10 ⁻¹⁴	9.3619x10 ⁻¹⁰	7.0000x10 ⁻¹	2.0000x10 ⁻¹	2.0000x10 ⁻¹	1.0000	3.0253x10 ⁴
21	1.0500x10 ⁻¹	2.0991x10 ⁻¹⁴	2.0682x10 ⁻⁹	7.0000x10 ⁻¹	2.0000x10 ⁻¹	2.0000x10 ⁻¹	1.0000	3.0253x10 ⁴
22	1.3110x10 ⁻¹	2.0991x10 ⁻¹⁴	1.6066x10 ⁻⁹	7.0000x10 ⁻¹	2.0000x10 ⁻¹	2.0000x10 ⁻¹	1.0000	3.0253x10 ⁴
23	1.4220x10 ⁻¹	2.0991x10 ⁻¹⁴	1.4617x10 ⁻⁹	7.0000x10 ⁻¹	2.0000x10 ⁻¹	2.0000x10 ⁻¹	1.0000	3.0253x10 ⁴
24	1.4510x10 ⁻¹	2.0991x10 ⁻¹⁴	1.4275x10 ⁻⁹	7.0000x10 ⁻¹	2.0000x10 ⁻¹	2.0000x10 ⁻¹	1.0000	3.0253x10 ⁴
25	2.0340x10 ⁻¹	2.0991x10 ⁻¹⁴	9.4668x10 ⁻¹⁰	7.0000x10 ⁻¹	2.0000x10 ⁻¹	2.0000x10 ⁻¹	1.0000	3.0253x10 ⁴
26	2.0780x10 ⁻¹	2.0991x10 ⁻¹⁴	9.2134x10 ⁻¹⁰	7.0000x10 ⁻¹	2.0000x10 ⁻¹	2.0000x10 ⁻¹	1.0000	3.0253x10 ⁴
27	1.6470x10 ⁻¹	2.0991x10 ⁻¹⁴	1.2279x10 ⁻⁹	7.0000x10 ⁻¹	2.0000x10 ⁻¹	2.0000x10 ⁻¹	1.0000	3.0253x10 ⁴
28	1.8890x10 ⁻¹	2.0991x10 ⁻¹⁴	1.0385x10 ⁻⁹	7.0000x10 ⁻¹	2.0000x10 ⁻¹	2.0000x10 ⁻¹	1.0000	3.0253x10 ⁴
29	1.5540x10 ⁻¹	2.0991x10 ⁻¹⁴	1.3163x10 ⁻⁹	7.0000x10 ⁻¹	2.0000x10 ⁻¹	2.0000x10 ⁻¹	1.0000	3.0253x10 ⁴
30	1.6620x10 ⁻¹	2.0991x10 ⁻¹⁴	1.2145x10 ⁻⁹	7.0000x10 ⁻¹	2.0000x10 ⁻¹	2.0000x10 ⁻¹	1.0000	3.0253x10 ⁴
31	1.0200x10 ⁻¹	2.0991x10 ⁻¹⁴	2.1363x10 ⁻⁹	7.0000x10 ⁻¹	2.0000x10 ⁻¹	2.0000x10 ⁻¹	1.0000	3.0253x10 ⁴
32	1.2240x10 ⁻¹	2.0991x10 ⁻¹⁴	1.7386x10 ⁻⁹	7.0000x10 ⁻¹	2.0000x10 ⁻¹	2.0000x10 ⁻¹	1.0000	3.0253x10 ⁴
33	1.2550x10 ⁻¹	2.0991x10 ⁻¹⁴	1.6895x10 ⁻⁹	7.0000x10 ⁻¹	2.0000x10 ⁻¹	2.0000x10 ⁻¹	1.0000	3.0253x10 ⁴
34	1.4580x10 ⁻¹	2.0991x10 ⁻¹⁴	1.4195x10 ⁻⁹	7.0000x10 ⁻¹	2.0000x10 ⁻¹	2.0000x10 ⁻¹	1.0000	3.0253x10 ⁴
35	2.0210x10 ⁻¹	2.0991x10 ⁻¹⁴	9.5438x10 ⁻¹⁰	7.0000x10 ⁻¹	2.0000x10 ⁻¹	2.0000x10 ⁻¹	1.0000	3.0253x10 ⁴
36	1.7180x10 ⁻¹	2.0991x10 ⁻¹⁴	1.1668x10 ⁻⁹	7.0000x10 ⁻¹	2.0000x10 ⁻¹	2.0000x10 ⁻¹	1.0000	3.0253x10 ⁴
37	1.0990x10 ⁻¹	2.0991x10 ⁻¹⁴	1.9648x10 ⁻⁹	7.0000x10 ⁻¹	2.0000x10 ⁻¹	2.0000x10 ⁻¹	1.0000	3.0253x10 ⁴
38	1.1960x10 ⁻¹	2.0991x10 ⁻¹⁴	1.7852x10 ⁻⁹	7.0000x10 ⁻¹	2.0000x10 ⁻¹	2.0000x10 ⁻¹	1.0000	3.0253x10 ⁴
39	1.3280x10 ⁻¹	2.0991x10 ⁻¹⁴	1.5829x10 ⁻⁹	7.0000x10 ⁻¹	2.0000x10 ⁻¹	2.0000x10 ⁻¹	1.0000	3.0253x10 ⁴
40	1.9160x10 ⁻¹	2.0991x10 ⁻¹⁴	1.0204x10 ⁻⁹	7.0000x10 ⁻¹	2.0000x10 ⁻¹	2.0000x10 ⁻¹	1.0000	3.0253x10 ⁴
41	1.4310x10 ⁻¹	2.0991x10 ⁻¹⁴	1.4510x10 ⁻⁹	7.0000x10 ⁻¹	2.0000x10 ⁻¹	2.0000x10 ⁻¹	1.0000	3.0253x10 ⁴
42	9.5620x10 ⁻²	2.0991x10 ⁻¹⁴	2.2955x10 ⁻⁹	7.0000x10 ⁻¹	2.0000x10 ⁻¹	2.0000x10 ⁻¹	1.0000	3.0253x10 ⁴
43	1.2150x10 ⁻¹	2.0991x10 ⁻¹⁴	1.7533x10 ⁻⁹	7.0000x10 ⁻¹	2.0000x10 ⁻¹	2.0000x10 ⁻¹	1.0000	3.0253x10 ⁴
44	1.5930x10 ⁻¹	2.0991x10 ⁻¹⁴	1.2780x10 ⁻⁹	7.0000x10 ⁻¹	2.0000x10 ⁻¹	2.0000x10 ⁻¹	1.0000	3.0253x10 ⁴
45	1.6170x10 ⁻¹	2.0991x10 ⁻¹⁴	1.2553x10 ⁻⁹	7.0000x10 ⁻¹	2.0000x10 ⁻¹	2.0000x10 ⁻¹	1.0000	3.0253x10 ⁴
46	1.3680x10 ⁻¹	2.0991x10 ⁻¹⁴	1.5293x10 ⁻⁹	7.0000x10 ⁻¹	2.0000x10 ⁻¹	2.0000x10 ⁻¹	1.0000	3.0253x10 ⁴
47	7.9990x10 ⁻²	2.0991x10 ⁻¹⁴	2.7930x10 ⁻⁹	7.0000x10 ⁻¹	2.0000x10 ⁻¹	2.0000x10 ⁻¹	1.0000	3.0253x10 ⁴
48	1.4620x10 ⁻¹	2.0991x10 ⁻¹⁴	1.4149x10 ⁻⁹	7.0000x10 ⁻¹	2.0000x10 ⁻¹	2.0000x10 ⁻¹	1.0000	3.0253x10 ⁴
49	1.2310x10 ⁻¹	2.0991x10 ⁻¹⁴	1.7273x10 ⁻⁹	7.0000x10 ⁻¹	2.0000x10 ⁻¹	2.0000x10 ⁻¹	1.0000	3.0253x10 ⁴
50	6.4050x10 ⁻²	2.0991x10 ⁻¹⁴	3.5502x10 ⁻⁹	7.0000x10 ⁻¹	2.0000x10 ⁻¹	2.0000x10 ⁻¹	1.0000	3.0253x10 ⁴
51	1.0650x10 ⁻¹	2.0991x10 ⁻¹⁴	2.0355x10 ⁻⁹	7.0000x10 ⁻¹	2.0000x10 ⁻¹	2.0000x10 ⁻¹	1.0000	3.0253x10 ⁴
52	2.4520x10 ⁻¹	2.0991x10 ⁻¹⁴	7.4268x10 ⁻¹⁰	7.0000x10 ⁻¹	2.0000x10 ⁻¹	2.0000x10 ⁻¹	1.0000	3.0253x10 ⁴

Appendix B: BRAGFLO Reference Tables

Table B-2 1992 BRAGFLO Computed Variable Values for CULEBRA (Concluded)

Run No.	Porosity	Permeability	Compressibility	BCEXP	BCBR SAT	BCGSSAT	BCFLG	BC PCT
53	1.6180x10 ⁻¹	2.0991x10 ⁻¹⁴	1.2544x10 ⁻⁹	7.0000x10 ⁻¹	2.0000x10 ⁻¹	2.0000x10 ⁻¹	1.0000	3.0253x10 ⁴
54	2.1840x10 ⁻¹	2.0991x10 ⁻¹⁴	8.6449x10 ⁻¹⁰	7.0000x10 ⁻¹	2.0000x10 ⁻¹	2.0000x10 ⁻¹	1.0000	3.0253x10 ⁴
55	1.7930x10 ⁻¹	2.0991x10 ⁻¹⁴	1.1075x10 ⁻⁹	7.0000x10 ⁻¹	2.0000x10 ⁻¹	2.0000x10 ⁻¹	1.0000	3.0253x10 ⁴
56	1.6170x10 ⁻¹	2.0991x10 ⁻¹⁴	1.2553x10 ⁻⁹	7.0000x10 ⁻¹	2.0000x10 ⁻¹	2.0000x10 ⁻¹	1.0000	3.0253x10 ⁴
57	1.4880x10 ⁻¹	2.0991x10 ⁻¹⁴	1.3858x10 ⁻⁹	7.0000x10 ⁻¹	2.0000x10 ⁻¹	2.0000x10 ⁻¹	1.0000	3.0253x10 ⁴
58	1.7840x10 ⁻¹	2.0991x10 ⁻¹⁴	1.1144x10 ⁻⁹	7.0000x10 ⁻¹	2.0000x10 ⁻¹	2.0000x10 ⁻¹	1.0000	3.0253x10 ⁴
59	1.4090x10 ⁻¹	2.0991x10 ⁻¹⁴	1.4775x10 ⁻⁹	7.0000x10 ⁻¹	2.0000x10 ⁻¹	2.0000x10 ⁻¹	1.0000	3.0253x10 ⁴
60	9.7870x10 ⁻²	2.0991x10 ⁻¹⁴	2.2370x10 ⁻⁹	7.0000x10 ⁻¹	2.0000x10 ⁻¹	2.0000x10 ⁻¹	1.0000	3.0253x10 ⁴
61	1.1710x10 ⁻¹	2.0991x10 ⁻¹⁴	1.8286x10 ⁻⁹	7.0000x10 ⁻¹	2.0000x10 ⁻¹	2.0000x10 ⁻¹	1.0000	3.0253x10 ⁴
62	1.7810x10 ⁻¹	2.0991x10 ⁻¹⁴	1.1167x10 ⁻⁹	7.0000x10 ⁻¹	2.0000x10 ⁻¹	2.0000x10 ⁻¹	1.0000	3.0253x10 ⁴
63	1.1510x10 ⁻¹	2.0991x10 ⁻¹⁴	1.8647x10 ⁻⁹	7.0000x10 ⁻¹	2.0000x10 ⁻¹	2.0000x10 ⁻¹	1.0000	3.0253x10 ⁴
64	1.6240x10 ⁻¹	2.0991x10 ⁻¹⁴	1.2488x10 ⁻⁹	7.0000x10 ⁻¹	2.0000x10 ⁻¹	2.0000x10 ⁻¹	1.0000	3.0253x10 ⁴
65	1.0040x10 ⁻¹	2.0991x10 ⁻¹⁴	2.1744x10 ⁻⁹	7.0000x10 ⁻¹	2.0000x10 ⁻¹	2.0000x10 ⁻¹	1.0000	3.0253x10 ⁴
66	2.0620x10 ⁻¹	2.0991x10 ⁻¹⁴	9.3043x10 ⁻¹⁰	7.0000x10 ⁻¹	2.0000x10 ⁻¹	2.0000x10 ⁻¹	1.0000	3.0253x10 ⁴
67	2.3870x10 ⁻¹	2.0991x10 ⁻¹⁴	7.6971x10 ⁻¹⁰	7.0000x10 ⁻¹	2.0000x10 ⁻¹	2.0000x10 ⁻¹	1.0000	3.0253x10 ⁴
68	1.2380x10 ⁻¹	2.0991x10 ⁻¹⁴	1.7161x10 ⁻⁹	7.0000x10 ⁻¹	2.0000x10 ⁻¹	2.0000x10 ⁻¹	1.0000	3.0253x10 ⁴
69	1.7800x10 ⁻¹	2.0991x10 ⁻¹⁴	1.1175x10 ⁻⁹	7.0000x10 ⁻¹	2.0000x10 ⁻¹	2.0000x10 ⁻¹	1.0000	3.0253x10 ⁴
70	1.6170x10 ⁻¹	2.0991x10 ⁻¹⁴	1.2553x10 ⁻⁹	7.0000x10 ⁻¹	2.0000x10 ⁻¹	2.0000x10 ⁻¹	1.0000	3.0253x10 ⁴

Table B-2 1992 BRAGFLO Ranks of Computed Variable Values for CULEBRA

Run No.	Porosity	Permeability	Compressibility	BCEXP	BCBRSAT	BCGSSAT	BCFLG	BCPCT
1	14.	1.	57.	1.	1.	1.	1.	1.
2	60.	1.	11.	1.	1.	1.	1.	1.
3	52.	1.	19.	1.	1.	1.	1.	1.
4	28.	1.	43.	1.	1.	1.	1.	1.
5	21.	1.	50.	1.	1.	1.	1.	1.
6	56.	1.	15.	1.	1.	1.	1.	1.
7	18.	1.	53.	1.	1.	1.	1.	1.
8	8.	1.	63.	1.	1.	1.	1.	1.
9	19.	1.	52.	1.	1.	1.	1.	1.
10	48.	1.	23.	1.	1.	1.	1.	1.
11	58.	1.	13.	1.	1.	1.	1.	1.
12	32.	1.	39.	1.	1.	1.	1.	1.
13	13.	1.	58.	1.	1.	1.	1.	1.
14	27.	1.	44.	1.	1.	1.	1.	1.
15	11.	1.	60.	1.	1.	1.	1.	1.
16	23.	1.	48.	1.	1.	1.	1.	1.
17	36.	1.	35.	1.	1.	1.	1.	1.
18	55.	1.	16.	1.	1.	1.	1.	1.
19	2.	1.	69.	1.	1.	1.	1.	1.
20	65.	1.	6.	1.	1.	1.	1.	1.
21	9.	1.	62.	1.	1.	1.	1.	1.
22	29.	1.	42.	1.	1.	1.	1.	1.
23	34.	1.	37.	1.	1.	1.	1.	1.
24	37.	1.	34.	1.	1.	1.	1.	1.
25	64.	1.	7.	1.	1.	1.	1.	1.
26	67.	1.	4.	1.	1.	1.	1.	1.
27	49.	1.	22.	1.	1.	1.	1.	1.
28	61.	1.	10.	1.	1.	1.	1.	1.
29	41.	1.	30.	1.	1.	1.	1.	1.
30	50.	1.	21.	1.	1.	1.	1.	1.
31	7.	1.	64.	1.	1.	1.	1.	1.
32	22.	1.	49.	1.	1.	1.	1.	1.
33	26.	1.	45.	1.	1.	1.	1.	1.
34	38.	1.	33.	1.	1.	1.	1.	1.
35	63.	1.	8.	1.	1.	1.	1.	1.
36	51.	1.	20.	1.	1.	1.	1.	1.
37	12.	1.	59.	1.	1.	1.	1.	1.
38	17.	1.	54.	1.	1.	1.	1.	1.
39	30.	1.	41.	1.	1.	1.	1.	1.
40	62.	1.	9.	1.	1.	1.	1.	1.
41	35.	1.	36.	1.	1.	1.	1.	1.
42	4.	1.	67.	1.	1.	1.	1.	1.
43	20.	1.	51.	1.	1.	1.	1.	1.
44	42.	1.	29.	1.	1.	1.	1.	1.
45	43.	1.	26.	1.	1.	1.	1.	1.
46	31.	1.	40.	1.	1.	1.	1.	1.
47	3.	1.	68.	1.	1.	1.	1.	1.
48	39.	1.	32.	1.	1.	1.	1.	1.
49	24.	1.	47.	1.	1.	1.	1.	1.
50	1.	1.	70.	1.	1.	1.	1.	1.
51	10.	1.	61.	1.	1.	1.	1.	1.
52	70.	1.	1.	1.	1.	1.	1.	1.

Appendix B: BRAGFLO Reference Tables

Table B-2 1992 BRAGFLO Ranks of Computed Variable Values for CULEBRA (Concluded)

Run No.	Porosity	Permeability	Compressibility	BCEXP	BCBRSAT	BGSSAT	BCFLG	BC PCT
53	46.	1.	25.	1.	1.	1.	1.	1.
54	68.	1.	3.	1.	1.	1.	1.	1.
55	59.	1.	12.	1.	1.	1.	1.	1.
56	43.	1.	26.	1.	1.	1.	1.	1.
57	40.	1.	31.	1.	1.	1.	1.	1.
58	57.	1.	14.	1.	1.	1.	1.	1.
59	33.	1.	38.	1.	1.	1.	1.	1.
60	5.	1.	66.	1.	1.	1.	1.	1.
61	16.	1.	55.	1.	1.	1.	1.	1.
62	54.	1.	17.	1.	1.	1.	1.	1.
63	15.	1.	56.	1.	1.	1.	1.	1.
64	47.	1.	24.	1.	1.	1.	1.	1.
65	6.	1.	65.	1.	1.	1.	1.	1.
66	66.	1.	5.	1.	1.	1.	1.	1.
67	69.	1.	2.	1.	1.	1.	1.	1.
68	25.	1.	46.	1.	1.	1.	1.	1.
69	53.	1.	18.	1.	1.	1.	1.	1.
70	43.	1.	26.	1.	1.	1.	1.	1.

Table B-2 1992 BRAGFLO Computed Variable Values for CULEBRA 1

Run No.	Porosity	Permeability	Compressibility	BCEXP	BCBR SAT	BCGSSAT	BCFLG	BC PCT
1	1.1430x10 ⁻¹	0.0000	0.0000	7.0000x10 ⁻¹	2.0000x10 ⁻¹	2.0000x10 ⁻¹	1.0000	0.0000
2	1.8220x10 ⁻¹	0.0000	0.0000	7.0000x10 ⁻¹	2.0000x10 ⁻¹	2.0000x10 ⁻¹	1.0000	0.0000
3	1.7260x10 ⁻¹	0.0000	0.0000	7.0000x10 ⁻¹	2.0000x10 ⁻¹	2.0000x10 ⁻¹	1.0000	0.0000
4	1.2840x10 ⁻¹	0.0000	0.0000	7.0000x10 ⁻¹	2.0000x10 ⁻¹	2.0000x10 ⁻¹	1.0000	0.0000
5	1.2200x10 ⁻¹	0.0000	0.0000	7.0000x10 ⁻¹	2.0000x10 ⁻¹	2.0000x10 ⁻¹	1.0000	0.0000
6	1.7830x10 ⁻¹	0.0000	0.0000	7.0000x10 ⁻¹	2.0000x10 ⁻¹	2.0000x10 ⁻¹	1.0000	0.0000
7	1.2060x10 ⁻¹	0.0000	0.0000	7.0000x10 ⁻¹	2.0000x10 ⁻¹	2.0000x10 ⁻¹	1.0000	0.0000
8	1.0450x10 ⁻¹	0.0000	0.0000	7.0000x10 ⁻¹	2.0000x10 ⁻¹	2.0000x10 ⁻¹	1.0000	0.0000
9	1.2100x10 ⁻¹	0.0000	0.0000	7.0000x10 ⁻¹	2.0000x10 ⁻¹	2.0000x10 ⁻¹	1.0000	0.0000
10	1.6340x10 ⁻¹	0.0000	0.0000	7.0000x10 ⁻¹	2.0000x10 ⁻¹	2.0000x10 ⁻¹	1.0000	0.0000
11	1.7880x10 ⁻¹	0.0000	0.0000	7.0000x10 ⁻¹	2.0000x10 ⁻¹	2.0000x10 ⁻¹	1.0000	0.0000
12	1.3740x10 ⁻¹	0.0000	0.0000	7.0000x10 ⁻¹	2.0000x10 ⁻¹	2.0000x10 ⁻¹	1.0000	0.0000
13	1.1150x10 ⁻¹	0.0000	0.0000	7.0000x10 ⁻¹	2.0000x10 ⁻¹	2.0000x10 ⁻¹	1.0000	0.0000
14	1.2590x10 ⁻¹	0.0000	0.0000	7.0000x10 ⁻¹	2.0000x10 ⁻¹	2.0000x10 ⁻¹	1.0000	0.0000
15	1.0750x10 ⁻¹	0.0000	0.0000	7.0000x10 ⁻¹	2.0000x10 ⁻¹	2.0000x10 ⁻¹	1.0000	0.0000
16	1.2290x10 ⁻¹	0.0000	0.0000	7.0000x10 ⁻¹	2.0000x10 ⁻¹	2.0000x10 ⁻¹	1.0000	0.0000
17	1.4460x10 ⁻¹	0.0000	0.0000	7.0000x10 ⁻¹	2.0000x10 ⁻¹	2.0000x10 ⁻¹	1.0000	0.0000
18	1.7820x10 ⁻¹	0.0000	0.0000	7.0000x10 ⁻¹	2.0000x10 ⁻¹	2.0000x10 ⁻¹	1.0000	0.0000
19	7.6020x10 ⁻²	0.0000	0.0000	7.0000x10 ⁻¹	2.0000x10 ⁻¹	2.0000x10 ⁻¹	1.0000	0.0000
20	2.0520x10 ⁻¹	0.0000	0.0000	7.0000x10 ⁻¹	2.0000x10 ⁻¹	2.0000x10 ⁻¹	1.0000	0.0000
21	1.0500x10 ⁻¹	0.0000	0.0000	7.0000x10 ⁻¹	2.0000x10 ⁻¹	2.0000x10 ⁻¹	1.0000	0.0000
22	1.3110x10 ⁻¹	0.0000	0.0000	7.0000x10 ⁻¹	2.0000x10 ⁻¹	2.0000x10 ⁻¹	1.0000	0.0000
23	1.4220x10 ⁻¹	0.0000	0.0000	7.0000x10 ⁻¹	2.0000x10 ⁻¹	2.0000x10 ⁻¹	1.0000	0.0000
24	1.4510x10 ⁻¹	0.0000	0.0000	7.0000x10 ⁻¹	2.0000x10 ⁻¹	2.0000x10 ⁻¹	1.0000	0.0000
25	2.0340x10 ⁻¹	0.0000	0.0000	7.0000x10 ⁻¹	2.0000x10 ⁻¹	2.0000x10 ⁻¹	1.0000	0.0000
26	2.0780x10 ⁻¹	0.0000	0.0000	7.0000x10 ⁻¹	2.0000x10 ⁻¹	2.0000x10 ⁻¹	1.0000	0.0000
27	1.6470x10 ⁻¹	0.0000	0.0000	7.0000x10 ⁻¹	2.0000x10 ⁻¹	2.0000x10 ⁻¹	1.0000	0.0000
28	1.8890x10 ⁻¹	0.0000	0.0000	7.0000x10 ⁻¹	2.0000x10 ⁻¹	2.0000x10 ⁻¹	1.0000	0.0000
29	1.5540x10 ⁻¹	0.0000	0.0000	7.0000x10 ⁻¹	2.0000x10 ⁻¹	2.0000x10 ⁻¹	1.0000	0.0000
30	1.6620x10 ⁻¹	0.0000	0.0000	7.0000x10 ⁻¹	2.0000x10 ⁻¹	2.0000x10 ⁻¹	1.0000	0.0000
31	1.0200x10 ⁻¹	0.0000	0.0000	7.0000x10 ⁻¹	2.0000x10 ⁻¹	2.0000x10 ⁻¹	1.0000	0.0000
32	1.2240x10 ⁻¹	0.0000	0.0000	7.0000x10 ⁻¹	2.0000x10 ⁻¹	2.0000x10 ⁻¹	1.0000	0.0000
33	1.2550x10 ⁻¹	0.0000	0.0000	7.0000x10 ⁻¹	2.0000x10 ⁻¹	2.0000x10 ⁻¹	1.0000	0.0000
34	1.4580x10 ⁻¹	0.0000	0.0000	7.0000x10 ⁻¹	2.0000x10 ⁻¹	2.0000x10 ⁻¹	1.0000	0.0000
35	2.0210x10 ⁻¹	0.0000	0.0000	7.0000x10 ⁻¹	2.0000x10 ⁻¹	2.0000x10 ⁻¹	1.0000	0.0000
36	1.7180x10 ⁻¹	0.0000	0.0000	7.0000x10 ⁻¹	2.0000x10 ⁻¹	2.0000x10 ⁻¹	1.0000	0.0000
37	1.0990x10 ⁻¹	0.0000	0.0000	7.0000x10 ⁻¹	2.0000x10 ⁻¹	2.0000x10 ⁻¹	1.0000	0.0000
38	1.1960x10 ⁻¹	0.0000	0.0000	7.0000x10 ⁻¹	2.0000x10 ⁻¹	2.0000x10 ⁻¹	1.0000	0.0000
39	1.3280x10 ⁻¹	0.0000	0.0000	7.0000x10 ⁻¹	2.0000x10 ⁻¹	2.0000x10 ⁻¹	1.0000	0.0000
40	1.9160x10 ⁻¹	0.0000	0.0000	7.0000x10 ⁻¹	2.0000x10 ⁻¹	2.0000x10 ⁻¹	1.0000	0.0000
41	1.4310x10 ⁻¹	0.0000	0.0000	7.0000x10 ⁻¹	2.0000x10 ⁻¹	2.0000x10 ⁻¹	1.0000	0.0000
42	9.5620x10 ⁻²	0.0000	0.0000	7.0000x10 ⁻¹	2.0000x10 ⁻¹	2.0000x10 ⁻¹	1.0000	0.0000
43	1.2150x10 ⁻¹	0.0000	0.0000	7.0000x10 ⁻¹	2.0000x10 ⁻¹	2.0000x10 ⁻¹	1.0000	0.0000
44	1.5930x10 ⁻¹	0.0000	0.0000	7.0000x10 ⁻¹	2.0000x10 ⁻¹	2.0000x10 ⁻¹	1.0000	0.0000
45	1.6170x10 ⁻¹	0.0000	0.0000	7.0000x10 ⁻¹	2.0000x10 ⁻¹	2.0000x10 ⁻¹	1.0000	0.0000
46	1.3680x10 ⁻¹	0.0000	0.0000	7.0000x10 ⁻¹	2.0000x10 ⁻¹	2.0000x10 ⁻¹	1.0000	0.0000
47	7.9990x10 ⁻²	0.0000	0.0000	7.0000x10 ⁻¹	2.0000x10 ⁻¹	2.0000x10 ⁻¹	1.0000	0.0000
48	1.4620x10 ⁻¹	0.0000	0.0000	7.0000x10 ⁻¹	2.0000x10 ⁻¹	2.0000x10 ⁻¹	1.0000	0.0000
49	1.2310x10 ⁻¹	0.0000	0.0000	7.0000x10 ⁻¹	2.0000x10 ⁻¹	2.0000x10 ⁻¹	1.0000	0.0000
50	6.4050x10 ⁻²	0.0000	0.0000	7.0000x10 ⁻¹	2.0000x10 ⁻¹	2.0000x10 ⁻¹	1.0000	0.0000
51	1.0650x10 ⁻¹	0.0000	0.0000	7.0000x10 ⁻¹	2.0000x10 ⁻¹	2.0000x10 ⁻¹	1.0000	0.0000
52	2.4520x10 ⁻¹	0.0000	0.0000	7.0000x10 ⁻¹	2.0000x10 ⁻¹	2.0000x10 ⁻¹	1.0000	0.0000

Appendix B: BRAGFLO Reference Tables

Table B-2 1992 BRAGFLO Computed Variable Values for CULEBRA1 (Concluded)

Run No.	Porosity	Permeability	Compressibility	BCEXP	BCBRSAT	BCGSSAT	BCFLG	BC PCT
53	1.6180x10 ⁻¹	0.0000	0.0000	7.0000x10 ⁻¹	2.0000x10 ⁻¹	2.0000x10 ⁻¹	1.0000	0.0000
54	2.1840x10 ⁻¹	0.0000	0.0000	7.0000x10 ⁻¹	2.0000x10 ⁻¹	2.0000x10 ⁻¹	1.0000	0.0000
55	1.7930x10 ⁻¹	0.0000	0.0000	7.0000x10 ⁻¹	2.0000x10 ⁻¹	2.0000x10 ⁻¹	1.0000	0.0000
56	1.6170x10 ⁻¹	0.0000	0.0000	7.0000x10 ⁻¹	2.0000x10 ⁻¹	2.0000x10 ⁻¹	1.0000	0.0000
57	1.4880x10 ⁻¹	0.0000	0.0000	7.0000x10 ⁻¹	2.0000x10 ⁻¹	2.0000x10 ⁻¹	1.0000	0.0000
58	1.7840x10 ⁻¹	0.0000	0.0000	7.0000x10 ⁻¹	2.0000x10 ⁻¹	2.0000x10 ⁻¹	1.0000	0.0000
59	1.4090x10 ⁻¹	0.0000	0.0000	7.0000x10 ⁻¹	2.0000x10 ⁻¹	2.0000x10 ⁻¹	1.0000	0.0000
60	9.7870x10 ⁻²	0.0000	0.0000	7.0000x10 ⁻¹	2.0000x10 ⁻¹	2.0000x10 ⁻¹	1.0000	0.0000
61	1.1710x10 ⁻¹	0.0000	0.0000	7.0000x10 ⁻¹	2.0000x10 ⁻¹	2.0000x10 ⁻¹	1.0000	0.0000
62	1.7810x10 ⁻¹	0.0000	0.0000	7.0000x10 ⁻¹	2.0000x10 ⁻¹	2.0000x10 ⁻¹	1.0000	0.0000
63	1.1510x10 ⁻¹	0.0000	0.0000	7.0000x10 ⁻¹	2.0000x10 ⁻¹	2.0000x10 ⁻¹	1.0000	0.0000
64	1.6240x10 ⁻¹	0.0000	0.0000	7.0000x10 ⁻¹	2.0000x10 ⁻¹	2.0000x10 ⁻¹	1.0000	0.0000
65	1.0040x10 ⁻¹	0.0000	0.0000	7.0000x10 ⁻¹	2.0000x10 ⁻¹	2.0000x10 ⁻¹	1.0000	0.0000
66	2.0620x10 ⁻¹	0.0000	0.0000	7.0000x10 ⁻¹	2.0000x10 ⁻¹	2.0000x10 ⁻¹	1.0000	0.0000
67	2.3870x10 ⁻¹	0.0000	0.0000	7.0000x10 ⁻¹	2.0000x10 ⁻¹	2.0000x10 ⁻¹	1.0000	0.0000
68	1.2380x10 ⁻¹	0.0000	0.0000	7.0000x10 ⁻¹	2.0000x10 ⁻¹	2.0000x10 ⁻¹	1.0000	0.0000
69	1.7800x10 ⁻¹	0.0000	0.0000	7.0000x10 ⁻¹	2.0000x10 ⁻¹	2.0000x10 ⁻¹	1.0000	0.0000
70	1.6170x10 ⁻¹	0.0000	0.0000	7.0000x10 ⁻¹	2.0000x10 ⁻¹	2.0000x10 ⁻¹	1.0000	0.0000

Table B-2 1992 BRAGFLO Ranks of Computed Variable Values for CULEBRA1

Run No.	Porosity	Permeability	Compressibility	BCEXP	BCBRSAT	BCGSSAT	BCFLG	BC PCT
1	14.	1.	1.	1.	1.	1.	1.	1.
2	60.	1.	1.	1.	1.	1.	1.	1.
3	52.	1.	1.	1.	1.	1.	1.	1.
4	28.	1.	1.	1.	1.	1.	1.	1.
5	21.	1.	1.	1.	1.	1.	1.	1.
6	56.	1.	1.	1.	1.	1.	1.	1.
7	18.	1.	1.	1.	1.	1.	1.	1.
8	8.	1.	1.	1.	1.	1.	1.	1.
9	19.	1.	1.	1.	1.	1.	1.	1.
10	48.	1.	1.	1.	1.	1.	1.	1.
11	58.	1.	1.	1.	1.	1.	1.	1.
12	32.	1.	1.	1.	1.	1.	1.	1.
13	13.	1.	1.	1.	1.	1.	1.	1.
14	27.	1.	1.	1.	1.	1.	1.	1.
15	11.	1.	1.	1.	1.	1.	1.	1.
16	23.	1.	1.	1.	1.	1.	1.	1.
17	36.	1.	1.	1.	1.	1.	1.	1.
18	55.	1.	1.	1.	1.	1.	1.	1.
19	2.	1.	1.	1.	1.	1.	1.	1.
20	65.	1.	1.	1.	1.	1.	1.	1.
21	9.	1.	1.	1.	1.	1.	1.	1.
22	29.	1.	1.	1.	1.	1.	1.	1.
23	34.	1.	1.	1.	1.	1.	1.	1.
24	37.	1.	1.	1.	1.	1.	1.	1.
25	64.	1.	1.	1.	1.	1.	1.	1.
26	67.	1.	1.	1.	1.	1.	1.	1.
27	49.	1.	1.	1.	1.	1.	1.	1.
28	61.	1.	1.	1.	1.	1.	1.	1.
29	41.	1.	1.	1.	1.	1.	1.	1.
30	50.	1.	1.	1.	1.	1.	1.	1.
31	7.	1.	1.	1.	1.	1.	1.	1.
32	22.	1.	1.	1.	1.	1.	1.	1.
33	26.	1.	1.	1.	1.	1.	1.	1.
34	38.	1.	1.	1.	1.	1.	1.	1.
35	63.	1.	1.	1.	1.	1.	1.	1.
36	51.	1.	1.	1.	1.	1.	1.	1.
37	12.	1.	1.	1.	1.	1.	1.	1.
38	17.	1.	1.	1.	1.	1.	1.	1.
39	30.	1.	1.	1.	1.	1.	1.	1.
40	62.	1.	1.	1.	1.	1.	1.	1.
41	35.	1.	1.	1.	1.	1.	1.	1.
42	4.	1.	1.	1.	1.	1.	1.	1.
43	20.	1.	1.	1.	1.	1.	1.	1.
44	42.	1.	1.	1.	1.	1.	1.	1.
45	43.	1.	1.	1.	1.	1.	1.	1.
46	31.	1.	1.	1.	1.	1.	1.	1.
47	3.	1.	1.	1.	1.	1.	1.	1.
48	39.	1.	1.	1.	1.	1.	1.	1.
49	24.	1.	1.	1.	1.	1.	1.	1.
50	1.	1.	1.	1.	1.	1.	1.	1.
51	10.	1.	1.	1.	1.	1.	1.	1.
52	70.	1.	1.	1.	1.	1.	1.	1.

Appendix B: BRAGFLO Reference Tables

Table B-2 1992 BRAGFLO Ranks of Computed Variable Values for CULEBRA1 (Concluded)

Run No.	Porosity	Permeability	Compressibility	BCEXP	BCBRSAT	BCGSSAT	BCFLG	BC PCT
53	46.	1.	1.	1.	1.	1.	1.	1.
54	68.	1.	1.	1.	1.	1.	1.	1.
55	59.	1.	1.	1.	1.	1.	1.	1.
56	43.	1.	1.	1.	1.	1.	1.	1.
57	40.	1.	1.	1.	1.	1.	1.	1.
58	57.	1.	1.	1.	1.	1.	1.	1.
59	33.	1.	1.	1.	1.	1.	1.	1.
60	5.	1.	1.	1.	1.	1.	1.	1.
61	16.	1.	1.	1.	1.	1.	1.	1.
62	54.	1.	1.	1.	1.	1.	1.	1.
63	15.	1.	1.	1.	1.	1.	1.	1.
64	47.	1.	1.	1.	1.	1.	1.	1.
65	6.	1.	1.	1.	1.	1.	1.	1.
66	66.	1.	1.	1.	1.	1.	1.	1.
67	69.	1.	1.	1.	1.	1.	1.	1.
68	25.	1.	1.	1.	1.	1.	1.	1.
69	53.	1.	1.	1.	1.	1.	1.	1.
70	43.	1.	1.	1.	1.	1.	1.	1.

Appendix B: BRAGFLO Reference Tables

Table B-2 1992 BRAGFLO Computed Variable Values for CULEBRA_SEAL (Concluded)

Run No.	Porosity	Permeability	Compressibility	BCEXP	BCBRSAT	BCGSSAT	BCFLG	BC PCT
53	2.0000x10 ⁻¹	1.0000x10 ⁻¹⁸	3.3131x10 ⁻¹⁰	7.0000x10 ⁻¹	2.0000x10 ⁻¹	0.0000	1.0000	9.4665x10 ⁵
54	2.0000x10 ⁻¹	1.0000x10 ⁻¹⁸	3.3131x10 ⁻¹⁰	7.0000x10 ⁻¹	2.0000x10 ⁻¹	0.0000	1.0000	9.4665x10 ⁵
55	2.0000x10 ⁻¹	1.0000x10 ⁻¹⁸	3.3131x10 ⁻¹⁰	7.0000x10 ⁻¹	2.0000x10 ⁻¹	0.0000	1.0000	9.4665x10 ⁵
56	2.0000x10 ⁻¹	1.0000x10 ⁻¹⁸	3.3131x10 ⁻¹⁰	7.0000x10 ⁻¹	2.0000x10 ⁻¹	0.0000	1.0000	9.4665x10 ⁵
57	2.0000x10 ⁻¹	1.0000x10 ⁻¹⁸	3.3131x10 ⁻¹⁰	7.0000x10 ⁻¹	2.0000x10 ⁻¹	0.0000	1.0000	9.4665x10 ⁵
58	2.0000x10 ⁻¹	1.0000x10 ⁻¹⁸	3.3131x10 ⁻¹⁰	7.0000x10 ⁻¹	2.0000x10 ⁻¹	0.0000	1.0000	9.4665x10 ⁵
59	2.0000x10 ⁻¹	1.0000x10 ⁻¹⁸	3.3131x10 ⁻¹⁰	7.0000x10 ⁻¹	2.0000x10 ⁻¹	0.0000	1.0000	9.4665x10 ⁵
60	2.0000x10 ⁻¹	1.0000x10 ⁻¹⁸	3.3131x10 ⁻¹⁰	7.0000x10 ⁻¹	2.0000x10 ⁻¹	0.0000	1.0000	9.4665x10 ⁵
61	2.0000x10 ⁻¹	1.0000x10 ⁻¹⁸	3.3131x10 ⁻¹⁰	7.0000x10 ⁻¹	2.0000x10 ⁻¹	0.0000	1.0000	9.4665x10 ⁵
62	2.0000x10 ⁻¹	1.0000x10 ⁻¹⁸	3.3131x10 ⁻¹⁰	7.0000x10 ⁻¹	2.0000x10 ⁻¹	0.0000	1.0000	9.4665x10 ⁵
63	2.0000x10 ⁻¹	1.0000x10 ⁻¹⁸	3.3131x10 ⁻¹⁰	7.0000x10 ⁻¹	2.0000x10 ⁻¹	0.0000	1.0000	9.4665x10 ⁵
64	2.0000x10 ⁻¹	1.0000x10 ⁻¹⁸	3.3131x10 ⁻¹⁰	7.0000x10 ⁻¹	2.0000x10 ⁻¹	0.0000	1.0000	9.4665x10 ⁵
65	2.0000x10 ⁻¹	1.0000x10 ⁻¹⁸	3.3131x10 ⁻¹⁰	7.0000x10 ⁻¹	2.0000x10 ⁻¹	0.0000	1.0000	9.4665x10 ⁵
66	2.0000x10 ⁻¹	1.0000x10 ⁻¹⁸	3.3131x10 ⁻¹⁰	7.0000x10 ⁻¹	2.0000x10 ⁻¹	0.0000	1.0000	9.4665x10 ⁵
67	2.0000x10 ⁻¹	1.0000x10 ⁻¹⁸	3.3131x10 ⁻¹⁰	7.0000x10 ⁻¹	2.0000x10 ⁻¹	0.0000	1.0000	9.4665x10 ⁵
68	2.0000x10 ⁻¹	1.0000x10 ⁻¹⁸	3.3131x10 ⁻¹⁰	7.0000x10 ⁻¹	2.0000x10 ⁻¹	0.0000	1.0000	9.4665x10 ⁵
69	2.0000x10 ⁻¹	1.0000x10 ⁻¹⁸	3.3131x10 ⁻¹⁰	7.0000x10 ⁻¹	2.0000x10 ⁻¹	0.0000	1.0000	9.4665x10 ⁵
70	2.0000x10 ⁻¹	1.0000x10 ⁻¹⁸	3.3131x10 ⁻¹⁰	7.0000x10 ⁻¹	2.0000x10 ⁻¹	0.0000	1.0000	9.4665x10 ⁵

Table B-2 1992 BRAGFLO Ranks of Computed Variable Values for CULEBRA_SEAL

<u>Run No.</u>	<u>Porosity</u>	<u>Permeability</u>	<u>Compressibility</u>	<u>BCEXP</u>	<u>BCBRSAT</u>	<u>BCGSSAT</u>	<u>BCFLG</u>	<u>BC PCT</u>
1	1.	1.	1.	1.	1.	1.	1.	1.
2	1.	1.	1.	1.	1.	1.	1.	1.
3	1.	1.	1.	1.	1.	1.	1.	1.
4	1.	1.	1.	1.	1.	1.	1.	1.
5	1.	1.	1.	1.	1.	1.	1.	1.
6	1.	1.	1.	1.	1.	1.	1.	1.
7	1.	1.	1.	1.	1.	1.	1.	1.
8	1.	1.	1.	1.	1.	1.	1.	1.
9	1.	1.	1.	1.	1.	1.	1.	1.
10	1.	1.	1.	1.	1.	1.	1.	1.
11	1.	1.	1.	1.	1.	1.	1.	1.
12	1.	1.	1.	1.	1.	1.	1.	1.
13	1.	1.	1.	1.	1.	1.	1.	1.
14	1.	1.	1.	1.	1.	1.	1.	1.
15	1.	1.	1.	1.	1.	1.	1.	1.
16	1.	1.	1.	1.	1.	1.	1.	1.
17	1.	1.	1.	1.	1.	1.	1.	1.
18	1.	1.	1.	1.	1.	1.	1.	1.
19	1.	1.	1.	1.	1.	1.	1.	1.
20	1.	1.	1.	1.	1.	1.	1.	1.
21	1.	1.	1.	1.	1.	1.	1.	1.
22	1.	1.	1.	1.	1.	1.	1.	1.
23	1.	1.	1.	1.	1.	1.	1.	1.
24	1.	1.	1.	1.	1.	1.	1.	1.
25	1.	1.	1.	1.	1.	1.	1.	1.
26	1.	1.	1.	1.	1.	1.	1.	1.
27	1.	1.	1.	1.	1.	1.	1.	1.
28	1.	1.	1.	1.	1.	1.	1.	1.
29	1.	1.	1.	1.	1.	1.	1.	1.
30	1.	1.	1.	1.	1.	1.	1.	1.
31	1.	1.	1.	1.	1.	1.	1.	1.
32	1.	1.	1.	1.	1.	1.	1.	1.
33	1.	1.	1.	1.	1.	1.	1.	1.
34	1.	1.	1.	1.	1.	1.	1.	1.
35	1.	1.	1.	1.	1.	1.	1.	1.
36	1.	1.	1.	1.	1.	1.	1.	1.
37	1.	1.	1.	1.	1.	1.	1.	1.
38	1.	1.	1.	1.	1.	1.	1.	1.
39	1.	1.	1.	1.	1.	1.	1.	1.
40	1.	1.	1.	1.	1.	1.	1.	1.
41	1.	1.	1.	1.	1.	1.	1.	1.
42	1.	1.	1.	1.	1.	1.	1.	1.
43	1.	1.	1.	1.	1.	1.	1.	1.
44	1.	1.	1.	1.	1.	1.	1.	1.
45	1.	1.	1.	1.	1.	1.	1.	1.
46	1.	1.	1.	1.	1.	1.	1.	1.
47	1.	1.	1.	1.	1.	1.	1.	1.
48	1.	1.	1.	1.	1.	1.	1.	1.
49	1.	1.	1.	1.	1.	1.	1.	1.
50	1.	1.	1.	1.	1.	1.	1.	1.
51	1.	1.	1.	1.	1.	1.	1.	1.
52	1.	1.	1.	1.	1.	1.	1.	1.

Appendix B: BRAGFLO Reference Tables

Table B-2 1992 BRAGFLO Ranks of Computed Variable Values for CULEBRA_SEAL (Concluded)

<u>Run No.</u>	<u>Porosity</u>	<u>Permeability</u>	<u>Compressibility</u>	<u>BCEXP</u>	<u>BCBRSAT</u>	<u>BCGSSAT</u>	<u>BCFLG</u>	<u>BCPCT</u>
53	1.	1.	1.	1.	1.	1.	1.	1.
54	1.	1.	1.	1.	1.	1.	1.	1.
55	1.	1.	1.	1.	1.	1.	1.	1.
56	1.	1.	1.	1.	1.	1.	1.	1.
57	1.	1.	1.	1.	1.	1.	1.	1.
58	1.	1.	1.	1.	1.	1.	1.	1.
59	1.	1.	1.	1.	1.	1.	1.	1.
60	1.	1.	1.	1.	1.	1.	1.	1.
61	1.	1.	1.	1.	1.	1.	1.	1.
62	1.	1.	1.	1.	1.	1.	1.	1.
63	1.	1.	1.	1.	1.	1.	1.	1.
64	1.	1.	1.	1.	1.	1.	1.	1.
65	1.	1.	1.	1.	1.	1.	1.	1.
66	1.	1.	1.	1.	1.	1.	1.	1.
67	1.	1.	1.	1.	1.	1.	1.	1.
68	1.	1.	1.	1.	1.	1.	1.	1.
69	1.	1.	1.	1.	1.	1.	1.	1.
70	1.	1.	1.	1.	1.	1.	1.	1.

Table B-2 1992 BRAGFLO Computed Variable Values for EXPERIMENTAL_REGION

Run No.	Porosity	Permeability	Compressibility	BCEXP	BCRSAT	BCGSSAT	BCFLG	BCPCT
1	2.4490x10 ⁻²	1.0000x10 ⁻¹⁵	4.4974x10 ⁻⁹	7.0000x10 ⁻¹	2.0000x10 ⁻¹	0.0000	1.0000	8.6734x10 ⁴
2	1.1240x10 ⁻²	1.0000x10 ⁻¹⁵	1.0094x10 ⁻⁸	7.0000x10 ⁻¹	2.0000x10 ⁻¹	0.0000	1.0000	8.6734x10 ⁴
3	5.1030x10 ⁻²	1.0000x10 ⁻¹⁵	2.0283x10 ⁻⁹	7.0000x10 ⁻¹	2.0000x10 ⁻¹	0.0000	1.0000	8.6734x10 ⁴
4	1.6070x10 ⁻²	1.0000x10 ⁻¹⁵	6.9848x10 ⁻⁹	7.0000x10 ⁻¹	2.0000x10 ⁻¹	0.0000	1.0000	8.6734x10 ⁴
5	4.3250x10 ⁻²	1.0000x10 ⁻¹⁵	2.4381x10 ⁻⁹	7.0000x10 ⁻¹	2.0000x10 ⁻¹	0.0000	1.0000	8.6734x10 ⁴
6	5.8630x10 ⁻²	1.0000x10 ⁻¹⁵	1.7330x10 ⁻⁹	7.0000x10 ⁻¹	2.0000x10 ⁻¹	0.0000	1.0000	8.6734x10 ⁴
7	6.6520x10 ⁻²	1.0000x10 ⁻¹⁵	1.4978x10 ⁻⁹	7.0000x10 ⁻¹	2.0000x10 ⁻¹	0.0000	1.0000	8.6734x10 ⁴
8	3.6140x10 ⁻²	1.0000x10 ⁻¹⁵	2.9670x10 ⁻⁹	7.0000x10 ⁻¹	2.0000x10 ⁻¹	0.0000	1.0000	8.6734x10 ⁴
9	1.9210x10 ⁻²	1.0000x10 ⁻¹⁵	5.8022x10 ⁻⁹	7.0000x10 ⁻¹	2.0000x10 ⁻¹	0.0000	1.0000	8.6734x10 ⁴
10	4.7300x10 ⁻²	1.0000x10 ⁻¹⁵	2.2080x10 ⁻⁹	7.0000x10 ⁻¹	2.0000x10 ⁻¹	0.0000	1.0000	8.6734x10 ⁴
11	6.7690x10 ⁻²	1.0000x10 ⁻¹⁵	1.4676x10 ⁻⁹	7.0000x10 ⁻¹	2.0000x10 ⁻¹	0.0000	1.0000	8.6734x10 ⁴
12	2.5040x10 ⁻²	1.0000x10 ⁻¹⁵	4.3931x10 ⁻⁹	7.0000x10 ⁻¹	2.0000x10 ⁻¹	0.0000	1.0000	8.6734x10 ⁴
13	7.0630x10 ⁻²	1.0000x10 ⁻¹⁵	1.3961x10 ⁻⁹	7.0000x10 ⁻¹	2.0000x10 ⁻¹	0.0000	1.0000	8.6734x10 ⁴
14	4.0420x10 ⁻²	1.0000x10 ⁻¹⁵	2.6264x10 ⁻⁹	7.0000x10 ⁻¹	2.0000x10 ⁻¹	0.0000	1.0000	8.6734x10 ⁴
15	2.1150x10 ⁻²	1.0000x10 ⁻¹⁵	5.2470x10 ⁻⁹	7.0000x10 ⁻¹	2.0000x10 ⁻¹	0.0000	1.0000	8.6734x10 ⁴
16	7.2500x10 ⁻²	1.0000x10 ⁻¹⁵	1.3536x10 ⁻⁹	7.0000x10 ⁻¹	2.0000x10 ⁻¹	0.0000	1.0000	8.6734x10 ⁴
17	4.9250x10 ⁻²	1.0000x10 ⁻¹⁵	2.1107x10 ⁻⁹	7.0000x10 ⁻¹	2.0000x10 ⁻¹	0.0000	1.0000	8.6734x10 ⁴
18	1.3450x10 ⁻²	1.0000x10 ⁻¹⁵	8.3941x10 ⁻⁹	7.0000x10 ⁻¹	2.0000x10 ⁻¹	0.0000	1.0000	8.6734x10 ⁴
19	7.4520x10 ⁻²	1.0000x10 ⁻¹⁵	1.3101x10 ⁻⁹	7.0000x10 ⁻¹	2.0000x10 ⁻¹	0.0000	1.0000	8.6734x10 ⁴
20	3.7170x10 ⁻²	1.0000x10 ⁻¹⁵	2.8779x10 ⁻⁹	7.0000x10 ⁻¹	2.0000x10 ⁻¹	0.0000	1.0000	8.6734x10 ⁴
21	5.5630x10 ⁻²	1.0000x10 ⁻¹⁵	1.8399x10 ⁻⁹	7.0000x10 ⁻¹	2.0000x10 ⁻¹	0.0000	1.0000	8.6734x10 ⁴
22	4.4090x10 ⁻²	1.0000x10 ⁻¹⁵	2.3869x10 ⁻⁹	7.0000x10 ⁻¹	2.0000x10 ⁻¹	0.0000	1.0000	8.6734x10 ⁴
23	6.0100x10 ⁻²	1.0000x10 ⁻¹⁵	1.6845x10 ⁻⁹	7.0000x10 ⁻¹	2.0000x10 ⁻¹	0.0000	1.0000	8.6734x10 ⁴
24	6.9800x10 ⁻²	1.0000x10 ⁻¹⁵	1.4157x10 ⁻⁹	7.0000x10 ⁻¹	2.0000x10 ⁻¹	0.0000	1.0000	8.6734x10 ⁴
25	6.1100x10 ⁻²	1.0000x10 ⁻¹⁵	1.6528x10 ⁻⁹	7.0000x10 ⁻¹	2.0000x10 ⁻¹	0.0000	1.0000	8.6734x10 ⁴
26	5.6930x10 ⁻²	1.0000x10 ⁻¹⁵	1.7922x10 ⁻⁹	7.0000x10 ⁻¹	2.0000x10 ⁻¹	0.0000	1.0000	8.6734x10 ⁴
27	2.8620x10 ⁻²	1.0000x10 ⁻¹⁵	3.8123x10 ⁻⁹	7.0000x10 ⁻¹	2.0000x10 ⁻¹	0.0000	1.0000	8.6734x10 ⁴
28	4.1490x10 ⁻²	1.0000x10 ⁻¹⁵	2.5522x10 ⁻⁹	7.0000x10 ⁻¹	2.0000x10 ⁻¹	0.0000	1.0000	8.6734x10 ⁴
29	1.4260x10 ⁻²	1.0000x10 ⁻¹⁵	7.9031x10 ⁻⁹	7.0000x10 ⁻¹	2.0000x10 ⁻¹	0.0000	1.0000	8.6734x10 ⁴
30	3.2140x10 ⁻²	1.0000x10 ⁻¹⁵	3.3674x10 ⁻⁹	7.0000x10 ⁻¹	2.0000x10 ⁻¹	0.0000	1.0000	8.6734x10 ⁴
31	2.6760x10 ⁻²	1.0000x10 ⁻¹⁵	4.0946x10 ⁻⁹	7.0000x10 ⁻¹	2.0000x10 ⁻¹	0.0000	1.0000	8.6734x10 ⁴
32	3.9190x10 ⁻²	1.0000x10 ⁻¹⁵	2.7166x10 ⁻⁹	7.0000x10 ⁻¹	2.0000x10 ⁻¹	0.0000	1.0000	8.6734x10 ⁴
33	4.5660x10 ⁻²	1.0000x10 ⁻¹⁵	2.2963x10 ⁻⁹	7.0000x10 ⁻¹	2.0000x10 ⁻¹	0.0000	1.0000	8.6734x10 ⁴
34	3.4580x10 ⁻²	1.0000x10 ⁻¹⁵	3.1121x10 ⁻⁹	7.0000x10 ⁻¹	2.0000x10 ⁻¹	0.0000	1.0000	8.6734x10 ⁴
35	3.8780x10 ⁻²	1.0000x10 ⁻¹⁵	2.7480x10 ⁻⁹	7.0000x10 ⁻¹	2.0000x10 ⁻¹	0.0000	1.0000	8.6734x10 ⁴
36	4.6630x10 ⁻²	1.0000x10 ⁻¹⁵	2.2433x10 ⁻⁹	7.0000x10 ⁻¹	2.0000x10 ⁻¹	0.0000	1.0000	8.6734x10 ⁴
37	1.6500x10 ⁻²	1.0000x10 ⁻¹⁵	6.7962x10 ⁻⁹	7.0000x10 ⁻¹	2.0000x10 ⁻¹	0.0000	1.0000	8.6734x10 ⁴
38	6.7530x10 ⁻²	1.0000x10 ⁻¹⁵	1.4716x10 ⁻⁹	7.0000x10 ⁻¹	2.0000x10 ⁻¹	0.0000	1.0000	8.6734x10 ⁴
39	6.2320x10 ⁻²	1.0000x10 ⁻¹⁵	1.6156x10 ⁻⁹	7.0000x10 ⁻¹	2.0000x10 ⁻¹	0.0000	1.0000	8.6734x10 ⁴
40	5.4740x10 ⁻²	1.0000x10 ⁻¹⁵	1.8739x10 ⁻⁹	7.0000x10 ⁻¹	2.0000x10 ⁻¹	0.0000	1.0000	8.6734x10 ⁴
41	6.3580x10 ⁻²	1.0000x10 ⁻¹⁵	1.5786x10 ⁻⁹	7.0000x10 ⁻¹	2.0000x10 ⁻¹	0.0000	1.0000	8.6734x10 ⁴
42	7.1460x10 ⁻²	1.0000x10 ⁻¹⁵	1.3770x10 ⁻⁹	7.0000x10 ⁻¹	2.0000x10 ⁻¹	0.0000	1.0000	8.6734x10 ⁴
43	4.4580x10 ⁻²	1.0000x10 ⁻¹⁵	2.3580x10 ⁻⁹	7.0000x10 ⁻¹	2.0000x10 ⁻¹	0.0000	1.0000	8.6734x10 ⁴
44	7.3870x10 ⁻²	1.0000x10 ⁻¹⁵	1.3239x10 ⁻⁹	7.0000x10 ⁻¹	2.0000x10 ⁻¹	0.0000	1.0000	8.6734x10 ⁴
45	2.9730x10 ⁻²	1.0000x10 ⁻¹⁵	3.6606x10 ⁻⁹	7.0000x10 ⁻¹	2.0000x10 ⁻¹	0.0000	1.0000	8.6734x10 ⁴
46	1.2610x10 ⁻²	1.0000x10 ⁻¹⁵	8.9699x10 ⁻⁹	7.0000x10 ⁻¹	2.0000x10 ⁻¹	0.0000	1.0000	8.6734x10 ⁴
47	6.0510x10 ⁻²	1.0000x10 ⁻¹⁵	1.6714x10 ⁻⁹	7.0000x10 ⁻¹	2.0000x10 ⁻¹	0.0000	1.0000	8.6734x10 ⁴
48	3.3090x10 ⁻²	1.0000x10 ⁻¹⁵	3.2635x10 ⁻⁹	7.0000x10 ⁻¹	2.0000x10 ⁻¹	0.0000	1.0000	8.6734x10 ⁴
49	4.1760x10 ⁻²	1.0000x10 ⁻¹⁵	2.5341x10 ⁻⁹	7.0000x10 ⁻¹	2.0000x10 ⁻¹	0.0000	1.0000	8.6734x10 ⁴
50	3.0510x10 ⁻²	1.0000x10 ⁻¹⁵	3.5606x10 ⁻⁹	7.0000x10 ⁻¹	2.0000x10 ⁻¹	0.0000	1.0000	8.6734x10 ⁴
51	1.8180x10 ⁻²	1.0000x10 ⁻¹⁵	6.1451x10 ⁻⁹	7.0000x10 ⁻¹	2.0000x10 ⁻¹	0.0000	1.0000	8.6734x10 ⁴
52	6.5110x10 ⁻²	1.0000x10 ⁻¹⁵	1.5356x10 ⁻⁹	7.0000x10 ⁻¹	2.0000x10 ⁻¹	0.0000	1.0000	8.6734x10 ⁴

Appendix B: BRAGFLO Reference Tables

Table B-2 1992 BRAGFLO Computed Variable Values for EXPERIMENTAL_REGION (Concluded)

Run No.	Porosity	Permeability	Compressibility	BCEXP	BCBRSAT	BCGSSAT	BCFLG	BCPCT
53	2.0520x10 ⁻²	1.0000x10 ⁻¹⁵	5.4158x10 ⁻⁹	7.0000x10 ⁻¹	2.0000x10 ⁻¹	0.0000	1.0000	8.6734x10 ⁴
54	6.4400x10 ⁻²	1.0000x10 ⁻¹⁵	1.5553x10 ⁻⁹	7.0000x10 ⁻¹	2.0000x10 ⁻¹	0.0000	1.0000	8.6734x10 ⁴
55	2.6330x10 ⁻²	1.0000x10 ⁻¹⁵	4.1656x10 ⁻⁹	7.0000x10 ⁻¹	2.0000x10 ⁻¹	0.0000	1.0000	8.6734x10 ⁴
56	3.5470x10 ⁻²	1.0000x10 ⁻¹⁵	3.0278x10 ⁻⁹	7.0000x10 ⁻¹	2.0000x10 ⁻¹	0.0000	1.0000	8.6734x10 ⁴
57	1.9820x10 ⁻²	1.0000x10 ⁻¹⁵	5.6159x10 ⁻⁹	7.0000x10 ⁻¹	2.0000x10 ⁻¹	0.0000	1.0000	8.6734x10 ⁴
58	2.3880x10 ⁻²	1.0000x10 ⁻¹⁵	4.6186x10 ⁻⁹	7.0000x10 ⁻¹	2.0000x10 ⁻¹	0.0000	1.0000	8.6734x10 ⁴
59	5.7990x10 ⁻²	1.0000x10 ⁻¹⁵	1.7549x10 ⁻⁹	7.0000x10 ⁻¹	2.0000x10 ⁻¹	0.0000	1.0000	8.6734x10 ⁴
60	6.9150x10 ⁻²	1.0000x10 ⁻¹⁵	1.4313x10 ⁻⁹	7.0000x10 ⁻¹	2.0000x10 ⁻¹	0.0000	1.0000	8.6734x10 ⁴
61	1.5400x10 ⁻²	1.0000x10 ⁻¹⁵	7.2995x10 ⁻⁹	7.0000x10 ⁻¹	2.0000x10 ⁻¹	0.0000	1.0000	8.6734x10 ⁴
62	2.7890x10 ⁻²	1.0000x10 ⁻¹⁵	3.9186x10 ⁻⁹	7.0000x10 ⁻¹	2.0000x10 ⁻¹	0.0000	1.0000	8.6734x10 ⁴
63	5.2340x10 ⁻²	1.0000x10 ⁻¹⁵	1.9713x10 ⁻⁹	7.0000x10 ⁻¹	2.0000x10 ⁻¹	0.0000	1.0000	8.6734x10 ⁴
64	5.3500x10 ⁻²	1.0000x10 ⁻¹⁵	1.9231x10 ⁻⁹	7.0000x10 ⁻¹	2.0000x10 ⁻¹	0.0000	1.0000	8.6734x10 ⁴
65	1.0820x10 ⁻²	1.0000x10 ⁻¹⁵	1.0495x10 ⁻⁸	7.0000x10 ⁻¹	2.0000x10 ⁻¹	0.0000	1.0000	8.6734x10 ⁴
66	5.0410x10 ⁻²	1.0000x10 ⁻¹⁵	2.0563x10 ⁻⁹	7.0000x10 ⁻¹	2.0000x10 ⁻¹	0.0000	1.0000	8.6734x10 ⁴
67	3.3230x10 ⁻²	1.0000x10 ⁻¹⁵	3.2487x10 ⁻⁹	7.0000x10 ⁻¹	2.0000x10 ⁻¹	0.0000	1.0000	8.6734x10 ⁴
68	2.2660x10 ⁻²	1.0000x10 ⁻¹⁵	4.8807x10 ⁻⁹	7.0000x10 ⁻¹	2.0000x10 ⁻¹	0.0000	1.0000	8.6734x10 ⁴
69	4.8950x10 ⁻²	1.0000x10 ⁻¹⁵	2.1251x10 ⁻⁹	7.0000x10 ⁻¹	2.0000x10 ⁻¹	0.0000	1.0000	8.6734x10 ⁴
70	5.3660x10 ⁻²	1.0000x10 ⁻¹⁵	1.9166x10 ⁻⁹	7.0000x10 ⁻¹	2.0000x10 ⁻¹	0.0000	1.0000	8.6734x10 ⁴

Table B-2 1992 BRAGFLO Ranks of Computed Variable Values for EXPERIMENTAL_REGION

Run No.	Porosity	Permeability	Compressibility	BCEXP	BCBRSAT	BCGSSAT	BCFLG	BCPCT
1	16.	1.	55.	1.	1.	1.	1.	1.
2	2.	1.	69.	1.	1.	1.	1.	1.
3	45.	1.	26.	1.	1.	1.	1.	1.
4	7.	1.	64.	1.	1.	1.	1.	1.
5	36.	1.	35.	1.	1.	1.	1.	1.
6	53.	1.	18.	1.	1.	1.	1.	1.
7	61.	1.	10.	1.	1.	1.	1.	1.
8	29.	1.	42.	1.	1.	1.	1.	1.
9	10.	1.	61.	1.	1.	1.	1.	1.
10	41.	1.	30.	1.	1.	1.	1.	1.
11	63.	1.	8.	1.	1.	1.	1.	1.
12	17.	1.	54.	1.	1.	1.	1.	1.
13	66.	1.	5.	1.	1.	1.	1.	1.
14	33.	1.	38.	1.	1.	1.	1.	1.
15	13.	1.	58.	1.	1.	1.	1.	1.
16	68.	1.	3.	1.	1.	1.	1.	1.
17	43.	1.	28.	1.	1.	1.	1.	1.
18	4.	1.	67.	1.	1.	1.	1.	1.
19	70.	1.	1.	1.	1.	1.	1.	1.
20	30.	1.	41.	1.	1.	1.	1.	1.
21	50.	1.	21.	1.	1.	1.	1.	1.
22	37.	1.	34.	1.	1.	1.	1.	1.
23	54.	1.	17.	1.	1.	1.	1.	1.
24	65.	1.	6.	1.	1.	1.	1.	1.
25	56.	1.	15.	1.	1.	1.	1.	1.
26	51.	1.	20.	1.	1.	1.	1.	1.
27	21.	1.	50.	1.	1.	1.	1.	1.
28	34.	1.	37.	1.	1.	1.	1.	1.
29	5.	1.	66.	1.	1.	1.	1.	1.
30	24.	1.	47.	1.	1.	1.	1.	1.
31	19.	1.	52.	1.	1.	1.	1.	1.
32	32.	1.	39.	1.	1.	1.	1.	1.
33	39.	1.	32.	1.	1.	1.	1.	1.
34	27.	1.	44.	1.	1.	1.	1.	1.
35	31.	1.	40.	1.	1.	1.	1.	1.
36	40.	1.	31.	1.	1.	1.	1.	1.
37	8.	1.	63.	1.	1.	1.	1.	1.
38	62.	1.	9.	1.	1.	1.	1.	1.
39	57.	1.	14.	1.	1.	1.	1.	1.
40	49.	1.	22.	1.	1.	1.	1.	1.
41	58.	1.	13.	1.	1.	1.	1.	1.
42	67.	1.	4.	1.	1.	1.	1.	1.
43	38.	1.	33.	1.	1.	1.	1.	1.
44	69.	1.	2.	1.	1.	1.	1.	1.
45	22.	1.	49.	1.	1.	1.	1.	1.
46	3.	1.	68.	1.	1.	1.	1.	1.
47	55.	1.	16.	1.	1.	1.	1.	1.
48	25.	1.	46.	1.	1.	1.	1.	1.
49	35.	1.	36.	1.	1.	1.	1.	1.
50	23.	1.	48.	1.	1.	1.	1.	1.
51	9.	1.	62.	1.	1.	1.	1.	1.
52	60.	1.	11.	1.	1.	1.	1.	1.

Appendix B: BRAGFLO Reference Tables

Table B-2 1992 BRAGFLO Ranks of Computed Variable Values for EXPERIMENTAL_REGION (Concluded)

Run No.	Porosity	Permeability	Compressibility	BCEXP	BCBRSAT	BCGSSAT	BCFLG	BCPCT
53	12.	1.	59.	1.	1.	1.	1.	1.
54	59.	1.	12.	1.	1.	1.	1.	1.
55	18.	1.	53.	1.	1.	1.	1.	1.
56	28.	1.	43.	1.	1.	1.	1.	1.
57	11.	1.	60.	1.	1.	1.	1.	1.
58	15.	1.	56.	1.	1.	1.	1.	1.
59	52.	1.	19.	1.	1.	1.	1.	1.
60	64.	1.	7.	1.	1.	1.	1.	1.
61	6.	1.	65.	1.	1.	1.	1.	1.
62	20.	1.	51.	1.	1.	1.	1.	1.
63	46.	1.	25.	1.	1.	1.	1.	1.
64	47.	1.	24.	1.	1.	1.	1.	1.
65	1.	1.	70.	1.	1.	1.	1.	1.
66	44.	1.	27.	1.	1.	1.	1.	1.
67	26.	1.	45.	1.	1.	1.	1.	1.
68	14.	1.	57.	1.	1.	1.	1.	1.
69	42.	1.	29.	1.	1.	1.	1.	1.
70	48.	1.	23.	1.	1.	1.	1.	1.

Table B-2 1992 BRAGFLO Computed Variable Values for FINAL_SALADO_DRZ

Run No.	Porosity	Permeability	Compressibility	BCEXP	BCBRSAT	BCGSSAT	BCFLG	BCPCT
1	2.9338x10 ⁻²	1.0000x10 ⁻¹⁵	3.7128x10 ⁻⁹	9.6790	8.7890x10 ⁻²	2.3300x10 ⁻¹	1.0000	8.6734x10 ⁴
2	3.2244x10 ⁻²	1.0000x10 ⁻¹⁵	3.3557x10 ⁻⁹	4.9660x10 ⁻¹	1.4570x10 ⁻¹	1.2590x10 ⁻¹	1.0000	8.6734x10 ⁴
3	5.1073x10 ⁻²	1.0000x10 ⁻¹⁵	2.0264x10 ⁻⁹	6.7900x10 ⁻¹	1.8490x10 ⁻¹	2.1660x10 ⁻¹	1.0000	8.6734x10 ⁴
4	5.9880x10 ⁻²	1.0000x10 ⁻¹⁵	1.6916x10 ⁻⁹	5.1820	1.7260x10 ⁻¹	1.8900x10 ⁻¹	1.0000	8.6734x10 ⁴
5	2.3095x10 ⁻²	1.0000x10 ⁻¹⁵	4.7841x10 ⁻⁹	4.0710x10 ⁻¹	1.9880x10 ⁻¹	1.4590x10 ⁻¹	1.0000	8.6734x10 ⁴
6	5.8159x10 ⁻²	1.0000x10 ⁻¹⁵	1.7490x10 ⁻⁹	6.1420	3.3170x10 ⁻¹	4.7930x10 ⁻²	1.0000	8.6734x10 ⁴
7	3.5160x10 ⁻²	1.0000x10 ⁻¹⁵	3.0567x10 ⁻⁹	1.0990	3.5430x10 ⁻²	1.6220x10 ⁻¹	1.0000	8.6734x10 ⁴
8	3.5393x10 ⁻²	1.0000x10 ⁻¹⁵	3.0349x10 ⁻⁹	6.4480	3.8660x10 ⁻¹	2.8520x10 ⁻²	1.0000	8.6734x10 ⁴
9	4.1674x10 ⁻²	1.0000x10 ⁻¹⁵	2.5398x10 ⁻⁹	4.2610x10 ⁻¹	3.4080x10 ⁻¹	1.8690x10 ⁻¹	1.0000	8.6734x10 ⁴
10	2.4250x10 ⁻²	1.0000x10 ⁻¹⁵	4.5442x10 ⁻⁹	1.5170	7.9000x10 ⁻²	3.4810x10 ⁻¹	1.0000	8.6734x10 ⁴
11	3.8769x10 ⁻²	1.0000x10 ⁻¹⁵	2.7488x10 ⁻⁹	5.1250x10 ⁻¹	2.7170x10 ⁻¹	2.0030x10 ⁻¹	1.0000	8.6734x10 ⁴
12	3.7282x10 ⁻²	1.0000x10 ⁻¹⁵	2.8685x10 ⁻⁹	7.4960	1.4100x10 ⁻¹	2.8620x10 ⁻¹	1.0000	8.6734x10 ⁴
13	1.9799x10 ⁻²	1.0000x10 ⁻¹⁵	5.6222x10 ⁻⁹	2.2490	3.6500x10 ⁻¹	2.9370x10 ⁻¹	1.0000	8.6734x10 ⁴
14	3.7667x10 ⁻²	1.0000x10 ⁻¹⁵	2.8366x10 ⁻⁹	3.0620x10 ⁻¹	8.3660x10 ⁻³	1.7360x10 ⁻¹	1.0000	8.6734x10 ⁴
15	5.1892x10 ⁻²	1.0000x10 ⁻¹⁵	1.9905x10 ⁻⁹	4.4620x10 ⁻¹	2.3100x10 ⁻¹	3.8350x10 ⁻¹	1.0000	8.6734x10 ⁴
16	4.6976x10 ⁻²	1.0000x10 ⁻¹⁵	2.2249x10 ⁻⁹	5.3590x10 ⁻¹	3.7890x10 ⁻¹	2.1720x10 ⁻¹	1.0000	8.6734x10 ⁴
17	5.4383x10 ⁻²	1.0000x10 ⁻¹⁵	1.8878x10 ⁻⁹	5.9190	1.1130x10 ⁻¹	3.8060x10 ⁻¹	1.0000	8.6734x10 ⁴
18	2.6960x10 ⁻²	1.0000x10 ⁻¹⁵	4.0623x10 ⁻⁹	5.8730x10 ⁻¹	2.9470x10 ⁻¹	8.6120x10 ⁻³	1.0000	8.6734x10 ⁴
19	4.8939x10 ⁻²	1.0000x10 ⁻¹⁵	2.1257x10 ⁻⁹	2.0050	1.1640x10 ⁻¹	1.6670x10 ⁻¹	1.0000	8.6734x10 ⁴
20	4.8916x10 ⁻²	1.0000x10 ⁻¹⁵	2.1268x10 ⁻⁹	6.7090x10 ⁻¹	1.2940x10 ⁻¹	3.2110x10 ⁻¹	1.0000	8.6734x10 ⁴
21	3.1377x10 ⁻²	1.0000x10 ⁻¹⁵	3.4554x10 ⁻⁹	2.2590x10 ⁻¹	1.9770x10 ⁻²	2.2330x10 ⁻¹	1.0000	8.6734x10 ⁴
22	5.0492x10 ⁻²	1.0000x10 ⁻¹⁵	2.0526x10 ⁻⁹	1.4340	2.1830x10 ⁻¹	1.8710x10 ⁻²	1.0000	8.6734x10 ⁴
23	5.4561x10 ⁻²	1.0000x10 ⁻¹⁵	1.8808x10 ⁻⁹	7.0990	2.3880x10 ⁻¹	4.5230x10 ⁻²	1.0000	8.6734x10 ⁴
24	2.3356x10 ⁻²	1.0000x10 ⁻¹⁵	4.7279x10 ⁻⁹	4.3270x10 ⁻¹	6.1270x10 ⁻²	2.6430x10 ⁻¹	1.0000	8.6734x10 ⁴
25	5.5692x10 ⁻²	1.0000x10 ⁻¹⁵	1.8376x10 ⁻⁹	2.7610	3.0510x10 ⁻¹	9.9900x10 ⁻²	1.0000	8.6734x10 ⁴
26	5.1986x10 ⁻²	1.0000x10 ⁻¹⁵	1.9864x10 ⁻⁹	5.2660	2.4700x10 ⁻¹	6.8060x10 ⁻²	1.0000	8.6734x10 ⁴
27	3.1097x10 ⁻²	1.0000x10 ⁻¹⁵	3.4888x10 ⁻⁹	8.3330	2.1280x10 ⁻¹	7.5730x10 ⁻²	1.0000	8.6734x10 ⁴
28	1.4826x10 ⁻²	1.0000x10 ⁻¹⁵	7.5917x10 ⁻⁹	7.9460	3.4740x10 ⁻¹	1.5270x10 ⁻¹	1.0000	8.6734x10 ⁴
29	1.8131x10 ⁻²	1.0000x10 ⁻¹⁵	6.1623x10 ⁻⁹	6.0410x10 ⁻¹	3.3040x10 ⁻¹	3.5780x10 ⁻¹	1.0000	8.6734x10 ⁴
30	5.5555x10 ⁻²	1.0000x10 ⁻¹⁵	1.8427x10 ⁻⁹	2.0040x10 ⁻¹	1.4050x10 ⁻²	1.5530x10 ⁻¹	1.0000	8.6734x10 ⁴
31	3.3857x10 ⁻²	1.0000x10 ⁻¹⁵	3.1839x10 ⁻⁹	3.3160x10 ⁻¹	2.1130x10 ⁻¹	2.4050x10 ⁻¹	1.0000	8.6734x10 ⁴
32	5.7726x10 ⁻²	1.0000x10 ⁻¹⁵	1.7640x10 ⁻⁹	8.8800	3.1430x10 ⁻¹	3.7550x10 ⁻¹	1.0000	8.6734x10 ⁴
33	5.9040x10 ⁻²	1.0000x10 ⁻¹⁵	1.7192x10 ⁻⁹	5.2200x10 ⁻¹	1.0530x10 ⁻¹	3.4190x10 ⁻¹	1.0000	8.6734x10 ⁴
34	3.8766x10 ⁻²	1.0000x10 ⁻¹⁵	2.7491x10 ⁻⁹	8.6520	2.5150x10 ⁻¹	3.6280x10 ⁻¹	1.0000	8.6734x10 ⁴
35	4.7477x10 ⁻²	1.0000x10 ⁻¹⁵	2.1988x10 ⁻⁹	3.9470x10 ⁻¹	2.9070x10 ⁻¹	1.3390x10 ⁻¹	1.0000	8.6734x10 ⁴
36	4.7765x10 ⁻²	1.0000x10 ⁻¹⁵	2.1840x10 ⁻⁹	2.7500x10 ⁻¹	3.7090x10 ⁻¹	3.6960x10 ⁻¹	1.0000	8.6734x10 ⁴
37	3.4118x10 ⁻²	1.0000x10 ⁻¹⁵	3.1576x10 ⁻⁹	6.9780	2.2650x10 ⁻¹	3.0790x10 ⁻²	1.0000	8.6734x10 ⁴
38	3.9355x10 ⁻²	1.0000x10 ⁻¹⁵	2.7042x10 ⁻⁹	2.9640	1.7810x10 ⁻¹	3.9620x10 ⁻¹	1.0000	8.6734x10 ⁴
39	4.3649x10 ⁻²	1.0000x10 ⁻¹⁵	2.4136x10 ⁻⁹	2.6060x10 ⁻¹	1.6330x10 ⁻¹	3.7240x10 ⁻²	1.0000	8.6734x10 ⁴
40	2.6845x10 ⁻²	1.0000x10 ⁻¹⁵	4.0808x10 ⁻⁹	2.4160x10 ⁻¹	2.4340x10 ⁻¹	1.1100x10 ⁻¹	1.0000	8.6734x10 ⁴
41	2.4393x10 ⁻²	1.0000x10 ⁻¹⁵	4.5163x10 ⁻⁹	5.7490x10 ⁻¹	1.3340x10 ⁻¹	1.0650x10 ⁻¹	1.0000	8.6734x10 ⁴
42	3.7631x10 ⁻²	1.0000x10 ⁻¹⁵	2.8395x10 ⁻⁹	5.4840x10 ⁻¹	3.9640x10 ⁻¹	3.3500x10 ⁻¹	1.0000	8.6734x10 ⁴
43	2.8231x10 ⁻²	1.0000x10 ⁻¹⁵	3.8682x10 ⁻⁹	4.0000	3.9070x10 ⁻¹	1.2040x10 ⁻¹	1.0000	8.6734x10 ⁴
44	1.7825x10 ⁻²	1.0000x10 ⁻¹⁵	6.2725x10 ⁻⁹	3.6050x10 ⁻¹	2.5980x10 ⁻¹	5.7350x10 ⁻²	1.0000	8.6734x10 ⁴
45	2.3493x10 ⁻²	1.0000x10 ⁻¹⁵	4.6989x10 ⁻⁹	3.2390x10 ⁻¹	1.5830x10 ⁻¹	9.4190x10 ⁻²	1.0000	8.6734x10 ⁴
46	5.6711x10 ⁻²	1.0000x10 ⁻¹⁵	1.8001x10 ⁻⁹	4.6060x10 ⁻¹	6.5170x10 ⁻²	2.3880x10 ⁻¹	1.0000	8.6734x10 ⁴
47	1.4114x10 ⁻²	1.0000x10 ⁻¹⁵	7.9872x10 ⁻⁹	3.4760	3.1780x10 ⁻¹	2.6060x10 ⁻¹	1.0000	8.6734x10 ⁴
48	5.7247x10 ⁻²	1.0000x10 ⁻¹⁵	1.7809x10 ⁻⁹	7.7080	4.5510x10 ⁻²	2.0750x10 ⁻¹	1.0000	8.6734x10 ⁴
49	5.6909x10 ⁻²	1.0000x10 ⁻¹⁵	1.7930x10 ⁻⁹	3.7530x10 ⁻¹	5.0110x10 ⁻²	6.9900x10 ⁻²	1.0000	8.6734x10 ⁴
50	4.5726x10 ⁻²	1.0000x10 ⁻¹⁵	2.2926x10 ⁻⁹	3.5390x10 ⁻¹	1.8990x10 ⁻¹	1.9850x10 ⁻¹	1.0000	8.6734x10 ⁴
51	2.3898x10 ⁻²	1.0000x10 ⁻¹⁵	4.6150x10 ⁻⁹	5.6000x10 ⁻¹	2.3180x10 ⁻²	1.1810x10 ⁻²	1.0000	8.6734x10 ⁴
52	4.5974x10 ⁻²	1.0000x10 ⁻¹⁵	2.2789x10 ⁻⁹	3.2370	1.5040x10 ⁻¹	3.8860x10 ⁻¹	1.0000	8.6734x10 ⁴

Appendix B: BRAGFLO Reference Tables

Table B-2 1992 BRAGFLO Computed Variable Values for FINAL_SALADO_DRZ (Concluded)

Run No.	Porosity	Permeability	Compressibility	BCEXP	BCBRSAT	BCGSSAT	BCFLG	BCPCT
53	3.0815x10 ⁻²	1.0000x10 ⁻¹⁵	3.5230x10 ⁻⁹	6.7410	2.8470x10 ⁻¹	1.8060x10 ⁻¹	1.0000	8.6734x10 ⁴
54	3.0693x10 ⁻²	1.0000x10 ⁻¹⁵	3.5379x10 ⁻⁹	4.7200x10 ⁻¹	1.6590x10 ⁻¹	2.7290x10 ⁻¹	1.0000	8.6734x10 ⁴
55	4.0163x10 ⁻²	1.0000x10 ⁻¹⁵	2.6448x10 ⁻⁹	6.5030x10 ⁻¹	3.2450x10 ⁻¹	3.0330x10 ⁻¹	1.0000	8.6734x10 ⁴
56	5.2274x10 ⁻²	1.0000x10 ⁻¹⁵	1.9741x10 ⁻⁹	4.8480	9.2770x10 ⁻²	5.2210x10 ⁻²	1.0000	8.6734x10 ⁴
57	7.0516x10 ⁻³	1.0000x10 ⁻¹⁵	1.6238x10 ⁻⁸	9.2110	5.1160x10 ⁻³	2.7770x10 ⁻¹	1.0000	8.6734x10 ⁴
58	2.5041x10 ⁻²	1.0000x10 ⁻¹⁵	4.3928x10 ⁻⁹	6.4060x10 ⁻¹	3.4880x10 ⁻¹	3.2980x10 ⁻¹	1.0000	8.6734x10 ⁴
59	2.8428x10 ⁻²	1.0000x10 ⁻¹⁵	3.8398x10 ⁻⁹	8.9580	8.5120x10 ⁻²	3.1270x10 ⁻¹	1.0000	8.6734x10 ⁴
60	3.9407x10 ⁻²	1.0000x10 ⁻¹⁵	2.7003x10 ⁻⁹	9.8620	7.0380x10 ⁻²	8.1940x10 ⁻²	1.0000	8.6734x10 ⁴
61	1.6302x10 ⁻²	1.0000x10 ⁻¹⁵	6.8816x10 ⁻⁹	8.0490x10 ⁻¹	2.7910x10 ⁻¹	1.3890x10 ⁻¹	1.0000	8.6734x10 ⁴
62	2.9951x10 ⁻²	1.0000x10 ⁻¹⁵	3.6318x10 ⁻⁹	2.8630x10 ⁻¹	3.5990x10 ⁻¹	2.5120x10 ⁻¹	1.0000	8.6734x10 ⁴
63	4.1109x10 ⁻²	1.0000x10 ⁻¹⁵	2.5782x10 ⁻⁹	3.7540	2.0010x10 ⁻¹	2.8360x10 ⁻¹	1.0000	8.6734x10 ⁴
64	3.0137x10 ⁻²	1.0000x10 ⁻¹⁵	3.6079x10 ⁻⁹	2.4950	2.9320x10 ⁻²	8.7020x10 ⁻²	1.0000	8.6734x10 ⁴
65	3.8978x10 ⁻²	1.0000x10 ⁻¹⁵	2.7328x10 ⁻⁹	2.5410x10 ⁻¹	2.6410x10 ⁻¹	3.5100x10 ⁻¹	1.0000	8.6734x10 ⁴
66	3.7103x10 ⁻³	1.0000x10 ⁻¹⁵	3.1085x10 ⁻⁸	6.9150x10 ⁻¹	1.2380x10 ⁻¹	3.1630x10 ⁻¹	1.0000	8.6734x10 ⁴
67	2.0750x10 ⁻²	1.0000x10 ⁻¹⁵	5.3531x10 ⁻⁹	5.5890	5.6350x10 ⁻²	2.5370x10 ⁻¹	1.0000	8.6734x10 ⁴
68	3.6434x10 ⁻²	1.0000x10 ⁻¹⁵	2.9411x10 ⁻⁹	4.5200	3.0240x10 ⁻¹	2.9970x10 ⁻¹	1.0000	8.6734x10 ⁴
69	2.3166x10 ⁻²	1.0000x10 ⁻¹⁵	4.7686x10 ⁻⁹	4.3270	3.7150x10 ⁻¹	4.8390x10 ⁻³	1.0000	8.6734x10 ⁴
70	3.6159x10 ⁻³	1.0000x10 ⁻¹⁵	3.1903x10 ⁻⁸	6.2770x10 ⁻¹	1.0130x10 ⁻¹	1.1920x10 ⁻¹	1.0000	8.6734x10 ⁴

Table B-2 1992 BRAGFLO Ranks of Computed Variable Values for FINAL_SALADO_DRZ

Run No.	Porosity	Permeability	Compressibility	BCEXP	BCBRSAT	BCGSSAT	BCFLG	BCPCT
1	23.	1.	48.	69.	16.	41.	1.	1.
2	30.	1.	41.	21.	26.	23.	1.	1.
3	56.	1.	15.	34.	33.	38.	1.	1.
4	70.	1.	1.	52.	31.	34.	1.	1.
5	11.	1.	60.	15.	35.	26.	1.	1.
6	68.	1.	3.	56.	59.	9.	1.	1.
7	33.	1.	38.	37.	7.	29.	1.	1.
8	34.	1.	37.	57.	68.	5.	1.	1.
9	46.	1.	25.	16.	60.	33.	1.	1.
10	16.	1.	55.	39.	14.	61.	1.	1.
11	40.	1.	31.	22.	48.	36.	1.	1.
12	36.	1.	35.	61.	25.	51.	1.	1.
13	9.	1.	62.	41.	64.	52.	1.	1.
14	38.	1.	33.	8.	2.	31.	1.	1.
15	57.	1.	14.	18.	41.	68.	1.	1.
16	50.	1.	21.	24.	67.	39.	1.	1.
17	60.	1.	11.	55.	20.	67.	1.	1.
18	20.	1.	51.	28.	52.	2.	1.	1.
19	54.	1.	17.	40.	21.	30.	1.	1.
20	53.	1.	18.	33.	23.	57.	1.	1.
21	29.	1.	42.	2.	4.	40.	1.	1.
22	55.	1.	16.	38.	39.	4.	1.	1.
23	61.	1.	10.	60.	42.	8.	1.	1.
24	13.	1.	58.	17.	11.	47.	1.	1.
25	63.	1.	8.	43.	54.	18.	1.	1.
26	58.	1.	13.	53.	44.	12.	1.	1.
27	28.	1.	43.	64.	38.	14.	1.	1.
28	5.	1.	66.	63.	61.	27.	1.	1.
29	8.	1.	63.	29.	58.	63.	1.	1.
30	62.	1.	9.	1.	3.	28.	1.	1.
31	31.	1.	40.	10.	37.	43.	1.	1.
32	67.	1.	4.	66.	55.	66.	1.	1.
33	69.	1.	2.	23.	19.	60.	1.	1.
34	39.	1.	32.	65.	45.	64.	1.	1.
35	51.	1.	20.	14.	51.	24.	1.	1.
36	52.	1.	19.	6.	65.	65.	1.	1.
37	32.	1.	39.	59.	40.	6.	1.	1.
38	42.	1.	29.	44.	32.	70.	1.	1.
39	47.	1.	24.	5.	29.	7.	1.	1.
40	19.	1.	52.	3.	43.	20.	1.	1.
41	17.	1.	54.	27.	24.	19.	1.	1.
42	37.	1.	34.	25.	70.	59.	1.	1.
43	21.	1.	50.	48.	69.	22.	1.	1.
44	7.	1.	64.	12.	46.	11.	1.	1.
45	14.	1.	57.	9.	28.	17.	1.	1.
46	64.	1.	7.	19.	12.	42.	1.	1.
47	4.	1.	67.	46.	56.	46.	1.	1.
48	66.	1.	5.	62.	8.	37.	1.	1.
49	65.	1.	6.	13.	9.	13.	1.	1.
50	48.	1.	23.	11.	34.	35.	1.	1.
51	15.	1.	56.	26.	5.	3.	1.	1.
52	49.	1.	22.	45.	27.	69.	1.	1.

Appendix B: BRAGFLO Reference Tables

Table B-2 1992 BRAGFLO Ranks of Computed Variable Values for FINAL_SALADO_DRZ (Concluded)

Run No.	Porosity	Permeability	Compressibility	BCEXP	BCBRSAT	BCGSSAT	BCFLG	BCPCT
53	27.	1.	44.	58.	50.	32.	1.	1.
54	26.	1.	45.	20.	30.	48.	1.	1.
55	44.	1.	27.	32.	57.	54.	1.	1.
56	59.	1.	12.	51.	17.	10.	1.	1.
57	3.	1.	68.	68.	1.	49.	1.	1.
58	18.	1.	53.	31.	62.	58.	1.	1.
59	22.	1.	49.	67.	15.	55.	1.	1.
60	43.	1.	28.	70.	13.	15.	1.	1.
61	6.	1.	65.	36.	49.	25.	1.	1.
62	24.	1.	47.	7.	63.	44.	1.	1.
63	45.	1.	26.	47.	36.	50.	1.	1.
64	25.	1.	46.	42.	6.	16.	1.	1.
65	41.	1.	30.	4.	47.	62.	1.	1.
66	2.	1.	69.	35.	22.	56.	1.	1.
67	10.	1.	61.	54.	10.	45.	1.	1.
68	35.	1.	36.	50.	53.	53.	1.	1.
69	12.	1.	59.	49.	66.	1.	1.	1.
70	1.	1.	70.	30.	18.	21.	1.	1.

Table B-2 1992 BRAGFLO Computed Variable Values for INITIAL_SALADO_DRZ

Run No.	Porosity	Permeability	Compressibility	BCEXP	BCBRSAT	BCGSSAT	BCFLG	BCPCT
1	2.8660x10 ⁻²	1.0000x10 ⁻¹⁷	3.8066x10 ⁻⁹	9.6790	8.7890x10 ⁻²	2.3300x10 ⁻¹	1.0000	4.2676x10 ⁵
2	6.9900x10 ⁻³	1.0000x10 ⁻¹⁷	1.6383x10 ⁻⁸	4.9660x10 ⁻¹	1.4570x10 ⁻¹	1.2590x10 ⁻¹	1.0000	4.2676x10 ⁵
3	2.8970x10 ⁻²	1.0000x10 ⁻¹⁷	3.7632x10 ⁻⁹	6.7900x10 ⁻¹	1.8490x10 ⁻¹	2.1660x10 ⁻¹	1.0000	4.2676x10 ⁵
4	5.6130x10 ⁻³	1.0000x10 ⁻¹⁷	2.0463x10 ⁻⁸	5.1820	1.7260x10 ⁻¹	1.8900x10 ⁻¹	1.0000	4.2676x10 ⁵
5	2.0560x10 ⁻²	1.0000x10 ⁻¹⁷	5.4048x10 ⁻⁹	4.0710x10 ⁻¹	1.9880x10 ⁻¹	1.4590x10 ⁻¹	1.0000	4.2676x10 ⁵
6	1.3750x10 ⁻²	1.0000x10 ⁻¹⁷	8.2055x10 ⁻⁹	6.1420	3.3170x10 ⁻¹	4.7930x10 ⁻²	1.0000	4.2676x10 ⁵
7	2.5930x10 ⁻²	1.0000x10 ⁻¹⁷	4.2337x10 ⁻⁹	1.0990	3.5430x10 ⁻²	1.6220x10 ⁻¹	1.0000	4.2676x10 ⁵
8	3.1850x10 ⁻³	1.0000x10 ⁻¹⁷	3.6253x10 ⁻⁸	6.4480	3.8660x10 ⁻¹	2.8520x10 ⁻²	1.0000	4.2676x10 ⁵
9	2.7270x10 ⁻²	1.0000x10 ⁻¹⁷	4.0134x10 ⁻⁹	4.2610x10 ⁻¹	3.4080x10 ⁻¹	1.8690x10 ⁻¹	1.0000	4.2676x10 ⁵
10	9.6770x10 ⁻³	1.0000x10 ⁻¹⁷	1.1764x10 ⁻⁸	1.5170	7.9000x10 ⁻²	3.4810x10 ⁻¹	1.0000	4.2676x10 ⁵
11	2.5730x10 ⁻³	1.0000x10 ⁻¹⁷	4.4936x10 ⁻⁸	5.1250x10 ⁻¹	2.7170x10 ⁻¹	2.0030x10 ⁻¹	1.0000	4.2676x10 ⁵
12	9.8270x10 ⁻³	1.0000x10 ⁻¹⁷	1.1581x10 ⁻⁸	7.4960	1.4100x10 ⁻¹	2.8620x10 ⁻¹	1.0000	4.2676x10 ⁵
13	1.6610x10 ⁻²	1.0000x10 ⁻¹⁷	6.7496x10 ⁻⁹	2.2490	3.6500x10 ⁻¹	2.9370x10 ⁻¹	1.0000	4.2676x10 ⁵
14	1.9600x10 ⁻²	1.0000x10 ⁻¹⁷	5.6818x10 ⁻⁹	3.0620x10 ⁻¹	8.3660x10 ⁻³	1.7360x10 ⁻¹	1.0000	4.2676x10 ⁵
15	1.1590x10 ⁻³	1.0000x10 ⁻¹⁷	1.0006x10 ⁻⁷	4.4620x10 ⁻¹	2.3100x10 ⁻¹	3.8350x10 ⁻¹	1.0000	4.2676x10 ⁵
16	5.8700x10 ⁻³	1.0000x10 ⁻¹⁷	1.9556x10 ⁻⁸	5.3590x10 ⁻¹	3.7890x10 ⁻¹	2.1720x10 ⁻¹	1.0000	4.2676x10 ⁵
17	2.3950x10 ⁻²	1.0000x10 ⁻¹⁷	4.6044x10 ⁻⁹	5.9190	1.1130x10 ⁻¹	3.8060x10 ⁻¹	1.0000	4.2676x10 ⁵
18	6.1370x10 ⁻³	1.0000x10 ⁻¹⁷	1.8695x10 ⁻⁸	5.8730x10 ⁻¹	2.9470x10 ⁻¹	8.6120x10 ⁻³	1.0000	4.2676x10 ⁵
19	6.2550x10 ⁻³	1.0000x10 ⁻¹⁷	1.8337x10 ⁻⁸	2.0050	1.1640x10 ⁻¹	1.6670x10 ⁻¹	1.0000	4.2676x10 ⁵
20	1.7070x10 ⁻²	1.0000x10 ⁻¹⁷	6.5609x10 ⁻⁹	6.7090x10 ⁻¹	1.2940x10 ⁻¹	3.2110x10 ⁻¹	1.0000	4.2676x10 ⁵
21	2.3500x10 ⁻²	1.0000x10 ⁻¹⁷	4.6974x10 ⁻⁹	2.2590x10 ⁻¹	1.9770x10 ⁻²	2.2330x10 ⁻¹	1.0000	4.2676x10 ⁵
22	2.6030x10 ⁻²	1.0000x10 ⁻¹⁷	4.2165x10 ⁻⁹	1.4340	2.1830x10 ⁻¹	1.8710x10 ⁻²	1.0000	4.2676x10 ⁵
23	2.9920x10 ⁻²	1.0000x10 ⁻¹⁷	3.6358x10 ⁻⁹	7.0990	2.3880x10 ⁻¹	4.5230x10 ⁻²	1.0000	4.2676x10 ⁵
24	1.4710x10 ⁻²	1.0000x10 ⁻¹⁷	7.6537x10 ⁻⁹	4.3270x10 ⁻¹	6.1270x10 ⁻²	2.6430x10 ⁻¹	1.0000	4.2676x10 ⁵
25	2.4720x10 ⁻²	1.0000x10 ⁻¹⁷	4.4532x10 ⁻⁹	2.7610	3.0510x10 ⁻¹	9.9900x10 ⁻²	1.0000	4.2676x10 ⁵
26	1.8820x10 ⁻²	1.0000x10 ⁻¹⁷	5.9276x10 ⁻⁹	5.2660	2.4700x10 ⁻¹	6.8060x10 ⁻²	1.0000	4.2676x10 ⁵
27	2.2740x10 ⁻³	1.0000x10 ⁻¹⁷	5.0877x10 ⁻⁸	8.3330	2.1280x10 ⁻¹	7.5730x10 ⁻²	1.0000	4.2676x10 ⁵
28	2.8830x10 ⁻³	1.0000x10 ⁻¹⁷	4.0077x10 ⁻⁸	7.9460	3.4740x10 ⁻¹	1.5270x10 ⁻¹	1.0000	4.2676x10 ⁵
29	1.2680x10 ⁻²	1.0000x10 ⁻¹⁷	8.9190x10 ⁻⁹	6.0410x10 ⁻¹	3.3040x10 ⁻¹	3.5780x10 ⁻¹	1.0000	4.2676x10 ⁵
30	8.7910x10 ⁻³	1.0000x10 ⁻¹⁷	1.2975x10 ⁻⁸	2.0040x10 ⁻¹	1.4050x10 ⁻²	1.5530x10 ⁻¹	1.0000	4.2676x10 ⁵
31	1.7650x10 ⁻²	1.0000x10 ⁻¹⁷	6.3371x10 ⁻⁹	3.3160x10 ⁻¹	2.1130x10 ⁻¹	2.4050x10 ⁻¹	1.0000	4.2676x10 ⁵
32	2.0930x10 ⁻²	1.0000x10 ⁻¹⁷	5.3048x10 ⁻⁹	8.8800	3.1430x10 ⁻¹	3.7550x10 ⁻¹	1.0000	4.2676x10 ⁵
33	6.6640x10 ⁻³	1.0000x10 ⁻¹⁷	1.7196x10 ⁻⁸	5.2200x10 ⁻¹	1.0530x10 ⁻¹	3.4190x10 ⁻¹	1.0000	4.2676x10 ⁵
34	9.1030x10 ⁻³	1.0000x10 ⁻¹⁷	1.2522x10 ⁻⁸	8.6520	2.5150x10 ⁻¹	3.6280x10 ⁻¹	1.0000	4.2676x10 ⁵
35	2.4230x10 ⁻³	1.0000x10 ⁻¹⁷	4.7733x10 ⁻⁸	3.9470x10 ⁻¹	2.9070x10 ⁻¹	1.3390x10 ⁻¹	1.0000	4.2676x10 ⁵
36	2.7120x10 ⁻²	1.0000x10 ⁻¹⁷	4.0370x10 ⁻⁹	2.7500x10 ⁻¹	3.7090x10 ⁻¹	3.6960x10 ⁻¹	1.0000	4.2676x10 ⁵
37	5.0960x10 ⁻³	1.0000x10 ⁻¹⁷	2.2564x10 ⁻⁸	6.9780	2.2650x10 ⁻¹	3.0790x10 ⁻²	1.0000	4.2676x10 ⁵
38	1.8940x10 ⁻³	1.0000x10 ⁻¹⁷	6.1135x10 ⁻⁸	2.9640	1.7810x10 ⁻¹	3.9620x10 ⁻¹	1.0000	4.2676x10 ⁵
39	1.0090x10 ⁻²	1.0000x10 ⁻¹⁷	1.1273x10 ⁻⁸	2.6060x10 ⁻¹	1.6330x10 ⁻¹	3.7240x10 ⁻²	1.0000	4.2676x10 ⁵
40	2.2760x10 ⁻²	1.0000x10 ⁻¹⁷	4.8582x10 ⁻⁹	2.4160x10 ⁻¹	2.4340x10 ⁻¹	1.1100x10 ⁻¹	1.0000	4.2676x10 ⁵
41	1.8020x10 ⁻²	1.0000x10 ⁻¹⁷	6.2019x10 ⁻⁹	5.7490x10 ⁻¹	1.3340x10 ⁻¹	1.0650x10 ⁻¹	1.0000	4.2676x10 ⁵
42	2.1990x10 ⁻²	1.0000x10 ⁻¹⁷	5.0371x10 ⁻⁹	5.4840x10 ⁻¹	3.9640x10 ⁻¹	3.3500x10 ⁻¹	1.0000	4.2676x10 ⁵
43	5.1790x10 ⁻³	1.0000x10 ⁻¹⁷	2.2199x10 ⁻⁸	4.0000	3.9070x10 ⁻¹	1.2040x10 ⁻¹	1.0000	4.2676x10 ⁵
44	3.9010x10 ⁻³	1.0000x10 ⁻¹⁷	2.9553x10 ⁻⁸	3.6050x10 ⁻¹	2.5980x10 ⁻¹	5.7350x10 ⁻²	1.0000	4.2676x10 ⁵
45	9.3870x10 ⁻³	1.0000x10 ⁻¹⁷	1.2135x10 ⁻⁸	3.2390x10 ⁻¹	1.5830x10 ⁻¹	9.4190x10 ⁻²	1.0000	4.2676x10 ⁵
46	2.8280x10 ⁻²	1.0000x10 ⁻¹⁷	3.8611x10 ⁻⁹	4.6060x10 ⁻¹	6.5170x10 ⁻²	2.3880x10 ⁻¹	1.0000	4.2676x10 ⁵
47	6.5700x10 ⁻³	1.0000x10 ⁻¹⁷	1.7446x10 ⁻⁸	3.4760	3.1780x10 ⁻¹	2.6060x10 ⁻¹	1.0000	4.2676x10 ⁵
48	2.2390x10 ⁻²	1.0000x10 ⁻¹⁷	4.9426x10 ⁻⁹	7.7080	4.5510x10 ⁻²	2.0750x10 ⁻¹	1.0000	4.2676x10 ⁵
49	1.6820x10 ⁻³	1.0000x10 ⁻¹⁷	6.8872x10 ⁻⁸	3.7530x10 ⁻¹	5.0110x10 ⁻²	6.9900x10 ⁻²	1.0000	4.2676x10 ⁵
50	1.2890x10 ⁻²	1.0000x10 ⁻¹⁷	8.7696x10 ⁻⁹	3.5390x10 ⁻¹	1.8990x10 ⁻¹	1.9850x10 ⁻¹	1.0000	4.2676x10 ⁵
51	7.8440x10 ⁻³	1.0000x10 ⁻¹⁷	1.4572x10 ⁻⁸	5.6000x10 ⁻¹	2.3180x10 ⁻²	1.1810x10 ⁻²	1.0000	4.2676x10 ⁵
52	4.7130x10 ⁻³	1.0000x10 ⁻¹⁷	2.4418x10 ⁻⁸	3.2370	1.5040x10 ⁻¹	3.8860x10 ⁻¹	1.0000	4.2676x10 ⁵

Appendix B: BRAGFLO Reference Tables

Table B-2 1992 BRAGFLO Computed Variable Values for INITIAL_SALADO_DRZ (Concluded)

Run No.	Porosity	Permeability	Compressibility	BCEXP	BCBRSAT	BCGSSAT	BCFLG	BCPCT
53	1.5900x10 ⁻²	1.0000x10 ⁻¹⁷	7.0621x10 ⁻⁹	6.7410	2.8470x10 ⁻¹	1.8060x10 ⁻¹	1.0000	4.2676x10 ⁵
54	1.4500x10 ⁻²	1.0000x10 ⁻¹⁷	7.7681x10 ⁻⁹	4.7200x10 ⁻¹	1.6590x10 ⁻¹	2.7290x10 ⁻¹	1.0000	4.2676x10 ⁵
55	2.0030x10 ⁻²	1.0000x10 ⁻¹⁷	5.5544x10 ⁻⁹	6.5030x10 ⁻¹	3.2450x10 ⁻¹	3.0330x10 ⁻¹	1.0000	4.2676x10 ⁵
56	1.1650x10 ⁻²	1.0000x10 ⁻¹⁷	9.7296x10 ⁻⁹	4.8480	9.2770x10 ⁻²	5.2210x10 ⁻²	1.0000	4.2676x10 ⁵
57	4.5630x10 ⁻³	1.0000x10 ⁻¹⁷	2.5229x10 ⁻⁸	9.2110	5.1160x10 ⁻³	2.7770x10 ⁻¹	1.0000	4.2676x10 ⁵
58	8.7110x10 ⁻³	1.0000x10 ⁻¹⁷	1.3097x10 ⁻⁸	6.4060x10 ⁻¹	3.4880x10 ⁻¹	3.2980x10 ⁻¹	1.0000	4.2676x10 ⁵
59	2.5160x10 ⁻²	1.0000x10 ⁻¹⁷	4.3709x10 ⁻⁹	8.9580	8.5120x10 ⁻²	3.1270x10 ⁻¹	1.0000	4.2676x10 ⁵
60	8.2600x10 ⁻³	1.0000x10 ⁻¹⁷	1.3825x10 ⁻⁸	9.8620	7.0380x10 ⁻²	8.1940x10 ⁻²	1.0000	4.2676x10 ⁵
61	7.3840x10 ⁻³	1.0000x10 ⁻¹⁷	1.5495x10 ⁻⁸	8.0490x10 ⁻¹	2.7910x10 ⁻¹	1.3890x10 ⁻¹	1.0000	4.2676x10 ⁵
62	1.2250x10 ⁻²	1.0000x10 ⁻¹⁷	9.2408x10 ⁻⁹	2.8630x10 ⁻¹	3.5990x10 ⁻¹	2.5120x10 ⁻¹	1.0000	4.2676x10 ⁵
63	4.1090x10 ⁻³	1.0000x10 ⁻¹⁷	2.8045x10 ⁻⁸	3.7540	2.0010x10 ⁻¹	2.8360x10 ⁻¹	1.0000	4.2676x10 ⁵
64	3.7390x10 ⁻³	1.0000x10 ⁻¹⁷	3.0845x10 ⁻⁸	2.4950	2.9320x10 ⁻²	8.7020x10 ⁻²	1.0000	4.2676x10 ⁵
65	7.4700x10 ⁻³	1.0000x10 ⁻¹⁷	1.5314x10 ⁻⁸	2.5410x10 ⁻¹	2.6410x10 ⁻¹	3.5100x10 ⁻¹	1.0000	4.2676x10 ⁵
66	3.5330x10 ⁻³	1.0000x10 ⁻¹⁷	3.2658x10 ⁻⁸	6.9150x10 ⁻¹	1.2380x10 ⁻¹	3.1630x10 ⁻¹	1.0000	4.2676x10 ⁵
67	8.1910x10 ⁻³	1.0000x10 ⁻¹⁷	1.3944x10 ⁻⁸	5.5890	5.6350x10 ⁻²	2.5370x10 ⁻¹	1.0000	4.2676x10 ⁵
68	1.0760x10 ⁻²	1.0000x10 ⁻¹⁷	1.0555x10 ⁻⁸	4.5200	3.0240x10 ⁻¹	2.9970x10 ⁻¹	1.0000	4.2676x10 ⁵
69	1.5190x10 ⁻²	1.0000x10 ⁻¹⁷	7.4039x10 ⁻⁹	4.3270	3.7150x10 ⁻¹	4.8390x10 ⁻³	1.0000	4.2676x10 ⁵
70	1.4890x10 ⁻³	1.0000x10 ⁻¹⁷	7.7831x10 ⁻⁸	6.2770x10 ⁻¹	1.0130x10 ⁻¹	1.1920x10 ⁻¹	1.0000	4.2676x10 ⁵

Table B-2 1992 BRAGFLO Ranks of Computed Variable Values for INITIAL_SALADO_DRZ

Run No.	Porosity	Permeability	Compressibility	BCEXP	BCBRSAT	BCGSSAT	BCFLG	BCPCT
1	68.	1.	3.	69.	16.	41.	1.	1.
2	24.	1.	47.	21.	26.	23.	1.	1.
3	69.	1.	2.	34.	33.	38.	1.	1.
4	18.	1.	53.	52.	31.	34.	1.	1.
5	54.	1.	17.	15.	35.	26.	1.	1.
6	42.	1.	29.	56.	59.	9.	1.	1.
7	63.	1.	8.	37.	7.	29.	1.	1.
8	9.	1.	62.	57.	68.	5.	1.	1.
9	66.	1.	5.	16.	60.	33.	1.	1.
10	34.	1.	37.	39.	14.	61.	1.	1.
11	7.	1.	64.	22.	48.	36.	1.	1.
12	35.	1.	36.	61.	25.	51.	1.	1.
13	47.	1.	24.	41.	64.	52.	1.	1.
14	52.	1.	19.	8.	2.	31.	1.	1.
15	1.	1.	70.	18.	41.	68.	1.	1.
16	19.	1.	52.	24.	67.	39.	1.	1.
17	60.	1.	11.	55.	20.	67.	1.	1.
18	20.	1.	51.	28.	52.	2.	1.	1.
19	21.	1.	50.	40.	21.	30.	1.	1.
20	48.	1.	23.	33.	23.	57.	1.	1.
21	59.	1.	12.	2.	4.	40.	1.	1.
22	64.	1.	7.	38.	39.	4.	1.	1.
23	70.	1.	1.	60.	42.	8.	1.	1.
24	44.	1.	27.	17.	11.	47.	1.	1.
25	61.	1.	10.	43.	54.	18.	1.	1.
26	51.	1.	20.	53.	44.	12.	1.	1.
27	5.	1.	66.	64.	38.	14.	1.	1.
28	8.	1.	63.	63.	61.	27.	1.	1.
29	40.	1.	31.	29.	58.	63.	1.	1.
30	31.	1.	40.	1.	3.	28.	1.	1.
31	49.	1.	22.	10.	37.	43.	1.	1.
32	55.	1.	16.	66.	55.	66.	1.	1.
33	23.	1.	48.	23.	19.	60.	1.	1.
34	32.	1.	39.	65.	45.	64.	1.	1.
35	6.	1.	65.	14.	51.	24.	1.	1.
36	65.	1.	6.	6.	65.	65.	1.	1.
37	16.	1.	55.	59.	40.	6.	1.	1.
38	4.	1.	67.	44.	32.	70.	1.	1.
39	36.	1.	35.	5.	29.	7.	1.	1.
40	58.	1.	13.	3.	43.	20.	1.	1.
41	50.	1.	21.	27.	24.	19.	1.	1.
42	56.	1.	15.	25.	70.	59.	1.	1.
43	17.	1.	54.	48.	69.	22.	1.	1.
44	12.	1.	59.	12.	46.	11.	1.	1.
45	33.	1.	38.	9.	28.	17.	1.	1.
46	67.	1.	4.	19.	12.	42.	1.	1.
47	22.	1.	49.	46.	56.	46.	1.	1.
48	57.	1.	14.	62.	8.	37.	1.	1.
49	3.	1.	68.	13.	9.	13.	1.	1.
50	41.	1.	30.	11.	34.	35.	1.	1.
51	27.	1.	44.	26.	5.	3.	1.	1.
52	15.	1.	56.	45.	27.	69.	1.	1.

Appendix B: BRAGFLO Reference Tables

Table B-2 1992 BRAGFLO Ranks of Computed Variable Values for INITIAL_SALADO_DRZ (Concluded)

Run No.	Porosity	Permeability	Compressibility	BCEXP	BCBRSAT	BCGSSAT	BCFLG	BCPCT
53	46.	1.	25.	58.	50.	32.	1.	1.
54	43.	1.	28.	20.	30.	48.	1.	1.
55	53.	1.	18.	32.	57.	54.	1.	1.
56	38.	1.	33.	51.	17.	10.	1.	1.
57	14.	1.	57.	68.	1.	49.	1.	1.
58	30.	1.	41.	31.	62.	58.	1.	1.
59	62.	1.	9.	67.	15.	55.	1.	1.
60	29.	1.	42.	70.	13.	15.	1.	1.
61	25.	1.	46.	36.	49.	25.	1.	1.
62	39.	1.	32.	7.	63.	44.	1.	1.
63	13.	1.	58.	47.	36.	50.	1.	1.
64	11.	1.	60.	42.	6.	16.	1.	1.
65	26.	1.	45.	4.	47.	62.	1.	1.
66	10.	1.	61.	35.	22.	56.	1.	1.
67	28.	1.	43.	54.	10.	45.	1.	1.
68	37.	1.	34.	50.	53.	53.	1.	1.
69	45.	1.	26.	49.	66.	1.	1.	1.
70	2.	1.	69.	30.	18.	21.	1.	1.

Table B-2 1992 BRAGFLO Computed Variable Values for LOWER_SHAFT

Run No.	Porosity	Permeability	Compressibility	BCEXP	BCRSAT	BCGSSAT	BCFLG	BCPCT
1	2.4490x10 ⁻²	1.0000x10 ⁻¹⁵	4.4974x10 ⁻⁹	7.0000x10 ⁻¹	2.0000x10 ⁻¹	0.0000	1.0000	8.6734x10 ⁴
2	1.1240x10 ⁻²	1.0000x10 ⁻¹⁵	1.0094x10 ⁻⁸	7.0000x10 ⁻¹	2.0000x10 ⁻¹	0.0000	1.0000	8.6734x10 ⁴
3	5.1030x10 ⁻²	1.0000x10 ⁻¹⁵	2.0283x10 ⁻⁹	7.0000x10 ⁻¹	2.0000x10 ⁻¹	0.0000	1.0000	8.6734x10 ⁴
4	1.6070x10 ⁻²	1.0000x10 ⁻¹⁵	6.9848x10 ⁻⁹	7.0000x10 ⁻¹	2.0000x10 ⁻¹	0.0000	1.0000	8.6734x10 ⁴
5	4.3250x10 ⁻²	1.0000x10 ⁻¹⁵	2.4381x10 ⁻⁹	7.0000x10 ⁻¹	2.0000x10 ⁻¹	0.0000	1.0000	8.6734x10 ⁴
6	5.8630x10 ⁻²	1.0000x10 ⁻¹⁵	1.7330x10 ⁻⁹	7.0000x10 ⁻¹	2.0000x10 ⁻¹	0.0000	1.0000	8.6734x10 ⁴
7	6.6520x10 ⁻²	1.0000x10 ⁻¹⁵	1.4978x10 ⁻⁹	7.0000x10 ⁻¹	2.0000x10 ⁻¹	0.0000	1.0000	8.6734x10 ⁴
8	3.6140x10 ⁻²	1.0000x10 ⁻¹⁵	2.9670x10 ⁻⁹	7.0000x10 ⁻¹	2.0000x10 ⁻¹	0.0000	1.0000	8.6734x10 ⁴
9	1.9210x10 ⁻²	1.0000x10 ⁻¹⁵	5.8022x10 ⁻⁹	7.0000x10 ⁻¹	2.0000x10 ⁻¹	0.0000	1.0000	8.6734x10 ⁴
10	4.7300x10 ⁻²	1.0000x10 ⁻¹⁵	2.2080x10 ⁻⁹	7.0000x10 ⁻¹	2.0000x10 ⁻¹	0.0000	1.0000	8.6734x10 ⁴
11	6.7690x10 ⁻²	1.0000x10 ⁻¹⁵	1.4676x10 ⁻⁹	7.0000x10 ⁻¹	2.0000x10 ⁻¹	0.0000	1.0000	8.6734x10 ⁴
12	2.5040x10 ⁻²	1.0000x10 ⁻¹⁵	4.3931x10 ⁻⁹	7.0000x10 ⁻¹	2.0000x10 ⁻¹	0.0000	1.0000	8.6734x10 ⁴
13	7.0630x10 ⁻²	1.0000x10 ⁻¹⁵	1.3961x10 ⁻⁹	7.0000x10 ⁻¹	2.0000x10 ⁻¹	0.0000	1.0000	8.6734x10 ⁴
14	4.0420x10 ⁻²	1.0000x10 ⁻¹⁵	2.6264x10 ⁻⁹	7.0000x10 ⁻¹	2.0000x10 ⁻¹	0.0000	1.0000	8.6734x10 ⁴
15	2.1150x10 ⁻²	1.0000x10 ⁻¹⁵	5.2470x10 ⁻⁹	7.0000x10 ⁻¹	2.0000x10 ⁻¹	0.0000	1.0000	8.6734x10 ⁴
16	7.2500x10 ⁻²	1.0000x10 ⁻¹⁵	1.3536x10 ⁻⁹	7.0000x10 ⁻¹	2.0000x10 ⁻¹	0.0000	1.0000	8.6734x10 ⁴
17	4.9250x10 ⁻²	1.0000x10 ⁻¹⁵	2.1107x10 ⁻⁹	7.0000x10 ⁻¹	2.0000x10 ⁻¹	0.0000	1.0000	8.6734x10 ⁴
18	1.3450x10 ⁻²	1.0000x10 ⁻¹⁵	8.3941x10 ⁻⁹	7.0000x10 ⁻¹	2.0000x10 ⁻¹	0.0000	1.0000	8.6734x10 ⁴
19	7.4520x10 ⁻²	1.0000x10 ⁻¹⁵	1.3101x10 ⁻⁹	7.0000x10 ⁻¹	2.0000x10 ⁻¹	0.0000	1.0000	8.6734x10 ⁴
20	3.7170x10 ⁻²	1.0000x10 ⁻¹⁵	2.8779x10 ⁻⁹	7.0000x10 ⁻¹	2.0000x10 ⁻¹	0.0000	1.0000	8.6734x10 ⁴
21	5.5630x10 ⁻²	1.0000x10 ⁻¹⁵	1.8399x10 ⁻⁹	7.0000x10 ⁻¹	2.0000x10 ⁻¹	0.0000	1.0000	8.6734x10 ⁴
22	4.4090x10 ⁻²	1.0000x10 ⁻¹⁵	2.3869x10 ⁻⁹	7.0000x10 ⁻¹	2.0000x10 ⁻¹	0.0000	1.0000	8.6734x10 ⁴
23	6.0100x10 ⁻²	1.0000x10 ⁻¹⁵	1.6845x10 ⁻⁹	7.0000x10 ⁻¹	2.0000x10 ⁻¹	0.0000	1.0000	8.6734x10 ⁴
24	6.9800x10 ⁻²	1.0000x10 ⁻¹⁵	1.4157x10 ⁻⁹	7.0000x10 ⁻¹	2.0000x10 ⁻¹	0.0000	1.0000	8.6734x10 ⁴
25	6.1100x10 ⁻²	1.0000x10 ⁻¹⁵	1.6528x10 ⁻⁹	7.0000x10 ⁻¹	2.0000x10 ⁻¹	0.0000	1.0000	8.6734x10 ⁴
26	5.6930x10 ⁻²	1.0000x10 ⁻¹⁵	1.7922x10 ⁻⁹	7.0000x10 ⁻¹	2.0000x10 ⁻¹	0.0000	1.0000	8.6734x10 ⁴
27	2.8620x10 ⁻²	1.0000x10 ⁻¹⁵	3.8123x10 ⁻⁹	7.0000x10 ⁻¹	2.0000x10 ⁻¹	0.0000	1.0000	8.6734x10 ⁴
28	4.1490x10 ⁻²	1.0000x10 ⁻¹⁵	2.5522x10 ⁻⁹	7.0000x10 ⁻¹	2.0000x10 ⁻¹	0.0000	1.0000	8.6734x10 ⁴
29	1.4260x10 ⁻²	1.0000x10 ⁻¹⁵	7.9031x10 ⁻⁹	7.0000x10 ⁻¹	2.0000x10 ⁻¹	0.0000	1.0000	8.6734x10 ⁴
30	3.2140x10 ⁻²	1.0000x10 ⁻¹⁵	3.3674x10 ⁻⁹	7.0000x10 ⁻¹	2.0000x10 ⁻¹	0.0000	1.0000	8.6734x10 ⁴
31	2.6760x10 ⁻²	1.0000x10 ⁻¹⁵	4.0946x10 ⁻⁹	7.0000x10 ⁻¹	2.0000x10 ⁻¹	0.0000	1.0000	8.6734x10 ⁴
32	3.9190x10 ⁻²	1.0000x10 ⁻¹⁵	2.7166x10 ⁻⁹	7.0000x10 ⁻¹	2.0000x10 ⁻¹	0.0000	1.0000	8.6734x10 ⁴
33	4.5660x10 ⁻²	1.0000x10 ⁻¹⁵	2.2963x10 ⁻⁹	7.0000x10 ⁻¹	2.0000x10 ⁻¹	0.0000	1.0000	8.6734x10 ⁴
34	3.4580x10 ⁻²	1.0000x10 ⁻¹⁵	3.1121x10 ⁻⁹	7.0000x10 ⁻¹	2.0000x10 ⁻¹	0.0000	1.0000	8.6734x10 ⁴
35	3.8780x10 ⁻²	1.0000x10 ⁻¹⁵	2.7480x10 ⁻⁹	7.0000x10 ⁻¹	2.0000x10 ⁻¹	0.0000	1.0000	8.6734x10 ⁴
36	4.6630x10 ⁻²	1.0000x10 ⁻¹⁵	2.2433x10 ⁻⁹	7.0000x10 ⁻¹	2.0000x10 ⁻¹	0.0000	1.0000	8.6734x10 ⁴
37	1.6500x10 ⁻²	1.0000x10 ⁻¹⁵	6.7962x10 ⁻⁹	7.0000x10 ⁻¹	2.0000x10 ⁻¹	0.0000	1.0000	8.6734x10 ⁴
38	6.7530x10 ⁻²	1.0000x10 ⁻¹⁵	1.4716x10 ⁻⁹	7.0000x10 ⁻¹	2.0000x10 ⁻¹	0.0000	1.0000	8.6734x10 ⁴
39	6.2320x10 ⁻²	1.0000x10 ⁻¹⁵	1.6156x10 ⁻⁹	7.0000x10 ⁻¹	2.0000x10 ⁻¹	0.0000	1.0000	8.6734x10 ⁴
40	5.4740x10 ⁻²	1.0000x10 ⁻¹⁵	1.8739x10 ⁻⁹	7.0000x10 ⁻¹	2.0000x10 ⁻¹	0.0000	1.0000	8.6734x10 ⁴
41	6.3580x10 ⁻²	1.0000x10 ⁻¹⁵	1.5786x10 ⁻⁹	7.0000x10 ⁻¹	2.0000x10 ⁻¹	0.0000	1.0000	8.6734x10 ⁴
42	7.1460x10 ⁻²	1.0000x10 ⁻¹⁵	1.3770x10 ⁻⁹	7.0000x10 ⁻¹	2.0000x10 ⁻¹	0.0000	1.0000	8.6734x10 ⁴
43	4.4580x10 ⁻²	1.0000x10 ⁻¹⁵	2.3580x10 ⁻⁹	7.0000x10 ⁻¹	2.0000x10 ⁻¹	0.0000	1.0000	8.6734x10 ⁴
44	7.3870x10 ⁻²	1.0000x10 ⁻¹⁵	1.3239x10 ⁻⁹	7.0000x10 ⁻¹	2.0000x10 ⁻¹	0.0000	1.0000	8.6734x10 ⁴
45	2.9730x10 ⁻²	1.0000x10 ⁻¹⁵	3.6606x10 ⁻⁹	7.0000x10 ⁻¹	2.0000x10 ⁻¹	0.0000	1.0000	8.6734x10 ⁴
46	1.2610x10 ⁻²	1.0000x10 ⁻¹⁵	8.9699x10 ⁻⁹	7.0000x10 ⁻¹	2.0000x10 ⁻¹	0.0000	1.0000	8.6734x10 ⁴
47	6.0510x10 ⁻²	1.0000x10 ⁻¹⁵	1.6714x10 ⁻⁹	7.0000x10 ⁻¹	2.0000x10 ⁻¹	0.0000	1.0000	8.6734x10 ⁴
48	3.3090x10 ⁻²	1.0000x10 ⁻¹⁵	3.2635x10 ⁻⁹	7.0000x10 ⁻¹	2.0000x10 ⁻¹	0.0000	1.0000	8.6734x10 ⁴
49	4.1760x10 ⁻²	1.0000x10 ⁻¹⁵	2.5341x10 ⁻⁹	7.0000x10 ⁻¹	2.0000x10 ⁻¹	0.0000	1.0000	8.6734x10 ⁴
50	3.0510x10 ⁻²	1.0000x10 ⁻¹⁵	3.5606x10 ⁻⁹	7.0000x10 ⁻¹	2.0000x10 ⁻¹	0.0000	1.0000	8.6734x10 ⁴
51	1.8180x10 ⁻²	1.0000x10 ⁻¹⁵	6.1451x10 ⁻⁹	7.0000x10 ⁻¹	2.0000x10 ⁻¹	0.0000	1.0000	8.6734x10 ⁴
52	6.5110x10 ⁻²	1.0000x10 ⁻¹⁵	1.5356x10 ⁻⁹	7.0000x10 ⁻¹	2.0000x10 ⁻¹	0.0000	1.0000	8.6734x10 ⁴

Appendix B: BRAGFLO Reference Tables

Table B-2 1992 BRAGFLO Computed Variable Values for LOWER_SHAFT (Concluded)

Run No.	Porosity	Permeability	Compressibility	BCEXP	BCBRSAT	BCGSSAT	BCFLG	BCPCT
53	2.0520x10 ⁻²	1.0000x10 ⁻¹⁵	5.4158x10 ⁻⁹	7.0000x10 ⁻¹	2.0000x10 ⁻¹	0.0000	1.0000	8.6734x10 ⁴
54	6.4400x10 ⁻²	1.0000x10 ⁻¹⁵	1.5553x10 ⁻⁹	7.0000x10 ⁻¹	2.0000x10 ⁻¹	0.0000	1.0000	8.6734x10 ⁴
55	2.6330x10 ⁻²	1.0000x10 ⁻¹⁵	4.1656x10 ⁻⁹	7.0000x10 ⁻¹	2.0000x10 ⁻¹	0.0000	1.0000	8.6734x10 ⁴
56	3.5470x10 ⁻²	1.0000x10 ⁻¹⁵	3.0278x10 ⁻⁹	7.0000x10 ⁻¹	2.0000x10 ⁻¹	0.0000	1.0000	8.6734x10 ⁴
57	1.9820x10 ⁻²	1.0000x10 ⁻¹⁵	5.6159x10 ⁻⁹	7.0000x10 ⁻¹	2.0000x10 ⁻¹	0.0000	1.0000	8.6734x10 ⁴
58	2.3880x10 ⁻²	1.0000x10 ⁻¹⁵	4.6186x10 ⁻⁹	7.0000x10 ⁻¹	2.0000x10 ⁻¹	0.0000	1.0000	8.6734x10 ⁴
59	5.7990x10 ⁻²	1.0000x10 ⁻¹⁵	1.7549x10 ⁻⁹	7.0000x10 ⁻¹	2.0000x10 ⁻¹	0.0000	1.0000	8.6734x10 ⁴
60	6.9150x10 ⁻²	1.0000x10 ⁻¹⁵	1.4313x10 ⁻⁹	7.0000x10 ⁻¹	2.0000x10 ⁻¹	0.0000	1.0000	8.6734x10 ⁴
61	1.5400x10 ⁻²	1.0000x10 ⁻¹⁵	7.2995x10 ⁻⁹	7.0000x10 ⁻¹	2.0000x10 ⁻¹	0.0000	1.0000	8.6734x10 ⁴
62	2.7890x10 ⁻²	1.0000x10 ⁻¹⁵	3.9186x10 ⁻⁹	7.0000x10 ⁻¹	2.0000x10 ⁻¹	0.0000	1.0000	8.6734x10 ⁴
63	5.2340x10 ⁻²	1.0000x10 ⁻¹⁵	1.9713x10 ⁻⁹	7.0000x10 ⁻¹	2.0000x10 ⁻¹	0.0000	1.0000	8.6734x10 ⁴
64	5.3500x10 ⁻²	1.0000x10 ⁻¹⁵	1.9231x10 ⁻⁹	7.0000x10 ⁻¹	2.0000x10 ⁻¹	0.0000	1.0000	8.6734x10 ⁴
65	1.0820x10 ⁻²	1.0000x10 ⁻¹⁵	1.0495x10 ⁻⁸	7.0000x10 ⁻¹	2.0000x10 ⁻¹	0.0000	1.0000	8.6734x10 ⁴
66	5.0410x10 ⁻²	1.0000x10 ⁻¹⁵	2.0563x10 ⁻⁹	7.0000x10 ⁻¹	2.0000x10 ⁻¹	0.0000	1.0000	8.6734x10 ⁴
67	3.3230x10 ⁻²	1.0000x10 ⁻¹⁵	3.2487x10 ⁻⁹	7.0000x10 ⁻¹	2.0000x10 ⁻¹	0.0000	1.0000	8.6734x10 ⁴
68	2.2660x10 ⁻²	1.0000x10 ⁻¹⁵	4.8807x10 ⁻⁹	7.0000x10 ⁻¹	2.0000x10 ⁻¹	0.0000	1.0000	8.6734x10 ⁴
69	4.8950x10 ⁻²	1.0000x10 ⁻¹⁵	2.1251x10 ⁻⁹	7.0000x10 ⁻¹	2.0000x10 ⁻¹	0.0000	1.0000	8.6734x10 ⁴
70	5.3660x10 ⁻²	1.0000x10 ⁻¹⁵	1.9166x10 ⁻⁹	7.0000x10 ⁻¹	2.0000x10 ⁻¹	0.0000	1.0000	8.6734x10 ⁴

Table B-2 1992 BRAGFLO Ranks of Computed Variable Values for LOWER_SHAFT

Run No.	Porosity	Permeability	Compressibility	BCEXP	BCBRSAT	BCGSSAT	BCFLG	BCPCT
1	16.	1.	55.	1.	1.	1.	1.	1.
2	2.	1.	69.	1.	1.	1.	1.	1.
3	45.	1.	26.	1.	1.	1.	1.	1.
4	7.	1.	64.	1.	1.	1.	1.	1.
5	36.	1.	35.	1.	1.	1.	1.	1.
6	53.	1.	18.	1.	1.	1.	1.	1.
7	61.	1.	10.	1.	1.	1.	1.	1.
8	29.	1.	42.	1.	1.	1.	1.	1.
9	10.	1.	61.	1.	1.	1.	1.	1.
10	41.	1.	30.	1.	1.	1.	1.	1.
11	63.	1.	8.	1.	1.	1.	1.	1.
12	17.	1.	54.	1.	1.	1.	1.	1.
13	66.	1.	5.	1.	1.	1.	1.	1.
14	33.	1.	38.	1.	1.	1.	1.	1.
15	13.	1.	58.	1.	1.	1.	1.	1.
16	68.	1.	3.	1.	1.	1.	1.	1.
17	43.	1.	28.	1.	1.	1.	1.	1.
18	4.	1.	67.	1.	1.	1.	1.	1.
19	70.	1.	1.	1.	1.	1.	1.	1.
20	30.	1.	41.	1.	1.	1.	1.	1.
21	50.	1.	21.	1.	1.	1.	1.	1.
22	37.	1.	34.	1.	1.	1.	1.	1.
23	54.	1.	17.	1.	1.	1.	1.	1.
24	65.	1.	6.	1.	1.	1.	1.	1.
25	56.	1.	15.	1.	1.	1.	1.	1.
26	51.	1.	20.	1.	1.	1.	1.	1.
27	21.	1.	50.	1.	1.	1.	1.	1.
28	34.	1.	37.	1.	1.	1.	1.	1.
29	5.	1.	66.	1.	1.	1.	1.	1.
30	24.	1.	47.	1.	1.	1.	1.	1.
31	19.	1.	52.	1.	1.	1.	1.	1.
32	32.	1.	39.	1.	1.	1.	1.	1.
33	39.	1.	32.	1.	1.	1.	1.	1.
34	27.	1.	44.	1.	1.	1.	1.	1.
35	31.	1.	40.	1.	1.	1.	1.	1.
36	40.	1.	31.	1.	1.	1.	1.	1.
37	8.	1.	63.	1.	1.	1.	1.	1.
38	62.	1.	9.	1.	1.	1.	1.	1.
39	57.	1.	14.	1.	1.	1.	1.	1.
40	49.	1.	22.	1.	1.	1.	1.	1.
41	58.	1.	13.	1.	1.	1.	1.	1.
42	67.	1.	4.	1.	1.	1.	1.	1.
43	38.	1.	33.	1.	1.	1.	1.	1.
44	69.	1.	2.	1.	1.	1.	1.	1.
45	22.	1.	49.	1.	1.	1.	1.	1.
46	3.	1.	68.	1.	1.	1.	1.	1.
47	55.	1.	16.	1.	1.	1.	1.	1.
48	25.	1.	46.	1.	1.	1.	1.	1.
49	35.	1.	36.	1.	1.	1.	1.	1.
50	23.	1.	48.	1.	1.	1.	1.	1.
51	9.	1.	62.	1.	1.	1.	1.	1.
52	60.	1.	11.	1.	1.	1.	1.	1.

Appendix B: BRAGFLO Reference Tables

Table B-2 1992 BRAGFLO Ranks of Computed Variable Values for LOWER_SHAFT (Concluded)

Run No.	Porosity	Permeability	Compressibility	BCEXP	BCBRSAT	BCGSSAT	BCFLG	BCPCT
53	12.	1.	59.	1.	1.	1.	1.	1.
54	59.	1.	12.	1.	1.	1.	1.	1.
55	18.	1.	53.	1.	1.	1.	1.	1.
56	28.	1.	43.	1.	1.	1.	1.	1.
57	11.	1.	60.	1.	1.	1.	1.	1.
58	15.	1.	56.	1.	1.	1.	1.	1.
59	52.	1.	19.	1.	1.	1.	1.	1.
60	64.	1.	7.	1.	1.	1.	1.	1.
61	6.	1.	65.	1.	1.	1.	1.	1.
62	20.	1.	51.	1.	1.	1.	1.	1.
63	46.	1.	25.	1.	1.	1.	1.	1.
64	47.	1.	24.	1.	1.	1.	1.	1.
65	1.	1.	70.	1.	1.	1.	1.	1.
66	44.	1.	27.	1.	1.	1.	1.	1.
67	26.	1.	45.	1.	1.	1.	1.	1.
68	14.	1.	57.	1.	1.	1.	1.	1.
69	42.	1.	29.	1.	1.	1.	1.	1.
70	48.	1.	23.	1.	1.	1.	1.	1.

Table B-2 1992 BRAGFLO Computed Variable Values for PANEL_SEAL

Run No.	Porosity	Permeability	Compressibility	BCEXP	BCBRSAT	BCGSSAT	BCFLG	BCPCT
1	6.4546x10 ⁻²	1.2330x10 ⁻²⁰	1.5512x10 ⁻⁹	7.0000x10 ⁻¹	2.0000x10 ⁻¹	0.0000	1.0000	4.3323x10 ⁶
2	6.9050x10 ⁻²	2.6840x10 ⁻²⁰	1.4337x10 ⁻⁹	7.0000x10 ⁻¹	2.0000x10 ⁻¹	0.0000	1.0000	3.3100x10 ⁶
3	6.4267x10 ⁻²	1.1750x10 ⁻²⁰	1.5591x10 ⁻⁹	7.0000x10 ⁻¹	2.0000x10 ⁻¹	0.0000	1.0000	4.4051x10 ⁶
4	7.4080x10 ⁻²	6.3970x10 ⁻²⁰	1.3194x10 ⁻⁹	7.0000x10 ⁻¹	2.0000x10 ⁻¹	0.0000	1.0000	2.4509x10 ⁶
5	7.0423x10 ⁻²	3.4020x10 ⁻²⁰	1.4009x10 ⁻⁹	7.0000x10 ⁻¹	2.0000x10 ⁻¹	0.0000	1.0000	3.0494x10 ⁶
6	6.7501x10 ⁻²	2.0540x10 ⁻²⁰	1.4724x10 ⁻⁹	7.0000x10 ⁻¹	2.0000x10 ⁻¹	0.0000	1.0000	3.6310x10 ⁶
7	6.7660x10 ⁻²	2.1110x10 ⁻²⁰	1.4683x10 ⁻⁹	7.0000x10 ⁻¹	2.0000x10 ⁻¹	0.0000	1.0000	3.5968x10 ⁶
8	7.4185x10 ⁻²	6.5140x10 ⁻²⁰	1.3172x10 ⁻⁹	7.0000x10 ⁻¹	2.0000x10 ⁻¹	0.0000	1.0000	2.4356x10 ⁶
9	6.7849x10 ⁻²	2.1810x10 ⁻²⁰	1.4636x10 ⁻⁹	7.0000x10 ⁻¹	2.0000x10 ⁻¹	0.0000	1.0000	3.5564x10 ⁶
10	6.5015x10 ⁻²	1.3370x10 ⁻²⁰	1.5382x10 ⁻⁹	7.0000x10 ⁻¹	2.0000x10 ⁻¹	0.0000	1.0000	4.2126x10 ⁶
11	8.3154x10 ⁻²	3.0660x10 ⁻¹⁹	1.1482x10 ⁻⁹	7.0000x10 ⁻¹	2.0000x10 ⁻¹	0.0000	1.0000	1.4251x10 ⁶
12	6.0920x10 ⁻²	6.5920x10 ⁻²¹	1.6584x10 ⁻⁹	7.0000x10 ⁻¹	2.0000x10 ⁻¹	0.0000	1.0000	5.3803x10 ⁶
13	6.2562x10 ⁻²	8.7530x10 ⁻²¹	1.6084x10 ⁻⁹	7.0000x10 ⁻¹	2.0000x10 ⁻¹	0.0000	1.0000	4.8776x10 ⁶
14	7.7689x10 ⁻²	1.1930x10 ⁻¹⁹	1.2465x10 ⁻⁹	7.0000x10 ⁻¹	2.0000x10 ⁻¹	0.0000	1.0000	1.9755x10 ⁶
15	7.4789x10 ⁻²	7.2300x10 ⁻²⁰	1.3046x10 ⁻⁹	7.0000x10 ⁻¹	2.0000x10 ⁻¹	0.0000	1.0000	2.3492x10 ⁶
16	8.6557x10 ⁻²	5.5180x10 ⁻¹⁹	1.0932x10 ⁻⁹	7.0000x10 ⁻¹	2.0000x10 ⁻¹	0.0000	1.0000	1.1629x10 ⁶
17	6.0226x10 ⁻²	5.8470x10 ⁻²¹	1.6805x10 ⁻⁹	7.0000x10 ⁻¹	2.0000x10 ⁻¹	0.0000	1.0000	5.6083x10 ⁶
18	7.2424x10 ⁻²	4.8060x10 ⁻²⁰	1.3553x10 ⁻⁹	7.0000x10 ⁻¹	2.0000x10 ⁻¹	0.0000	1.0000	2.7058x10 ⁶
19	7.8301x10 ⁻²	1.3260x10 ⁻¹⁹	1.2348x10 ⁻⁹	7.0000x10 ⁻¹	2.0000x10 ⁻¹	0.0000	1.0000	1.9045x10 ⁶
20	6.2783x10 ⁻²	9.0940x10 ⁻²¹	1.6018x10 ⁻⁹	7.0000x10 ⁻¹	2.0000x10 ⁻¹	0.0000	1.0000	4.8135x10 ⁶
21	5.9353x10 ⁻²	5.0290x10 ⁻²¹	1.7088x10 ⁻⁹	7.0000x10 ⁻¹	2.0000x10 ⁻¹	0.0000	1.0000	5.9085x10 ⁶
22	7.7349x10 ⁻²	1.1250x10 ⁻¹⁹	1.2531x10 ⁻⁹	7.0000x10 ⁻¹	2.0000x10 ⁻¹	0.0000	1.0000	2.0160x10 ⁶
23	6.3790x10 ⁻²	1.0820x10 ⁻²⁰	1.5726x10 ⁻⁹	7.0000x10 ⁻¹	2.0000x10 ⁻¹	0.0000	1.0000	4.5326x10 ⁶
24	7.6220x10 ⁻²	9.2570x10 ⁻²⁰	1.2754x10 ⁻⁹	7.0000x10 ⁻¹	2.0000x10 ⁻¹	0.0000	1.0000	2.1567x10 ⁶
25	5.7045x10 ⁻²	3.3760x10 ⁻²¹	1.7881x10 ⁻⁹	7.0000x10 ⁻¹	2.0000x10 ⁻¹	0.0000	1.0000	6.7820x10 ⁶
26	7.1304x10 ⁻²	3.9610x10 ⁻²⁰	1.3805x10 ⁻⁹	7.0000x10 ⁻¹	2.0000x10 ⁻¹	0.0000	1.0000	2.8930x10 ⁶
27	6.6134x10 ⁻²	1.6220x10 ⁻²⁰	1.5080x10 ⁻⁹	7.0000x10 ⁻¹	2.0000x10 ⁻¹	0.0000	1.0000	3.9401x10 ⁶
28	8.3995x10 ⁻²	3.5450x10 ⁻¹⁹	1.1342x10 ⁻⁹	7.0000x10 ⁻¹	2.0000x10 ⁻¹	0.0000	1.0000	1.3553x10 ⁶
29	7.0821x10 ⁻²	3.6440x10 ⁻²⁰	1.3916x10 ⁻⁹	7.0000x10 ⁻¹	2.0000x10 ⁻¹	0.0000	1.0000	2.9777x10 ⁶
30	8.0747x10 ⁻²	2.0230x10 ⁻¹⁹	1.1898x10 ⁻⁹	7.0000x10 ⁻¹	2.0000x10 ⁻¹	0.0000	1.0000	1.6456x10 ⁶
31	6.6460x10 ⁻²	1.7160x10 ⁻²⁰	1.4994x10 ⁻⁹	7.0000x10 ⁻¹	2.0000x10 ⁻¹	0.0000	1.0000	3.8641x10 ⁶
32	7.9457x10 ⁻²	1.6190x10 ⁻¹⁹	1.2132x10 ⁻⁹	7.0000x10 ⁻¹	2.0000x10 ⁻¹	0.0000	1.0000	1.7774x10 ⁶
33	6.1584x10 ⁻²	7.3930x10 ⁻²¹	1.6379x10 ⁻⁹	7.0000x10 ⁻¹	2.0000x10 ⁻¹	0.0000	1.0000	5.1710x10 ⁶
34	6.8752x10 ⁻²	2.5490x10 ⁻²⁰	1.4410x10 ⁻⁹	7.0000x10 ⁻¹	2.0000x10 ⁻¹	0.0000	1.0000	3.3696x10 ⁶
35	5.7582x10 ⁻²	3.7040x10 ⁻²¹	1.7691x10 ⁻⁹	7.0000x10 ⁻¹	2.0000x10 ⁻¹	0.0000	1.0000	6.5679x10 ⁶
36	6.6807x10 ⁻²	1.8220x10 ⁻²⁰	1.4903x10 ⁻⁹	7.0000x10 ⁻¹	2.0000x10 ⁻¹	0.0000	1.0000	3.7848x10 ⁶
37	6.3385x10 ⁻²	1.0090x10 ⁻²⁰	1.5842x10 ⁻⁹	7.0000x10 ⁻¹	2.0000x10 ⁻¹	0.0000	1.0000	4.6435x10 ⁶
38	6.0375x10 ⁻²	6.0000x10 ⁻²¹	1.6757x10 ⁻⁹	7.0000x10 ⁻¹	2.0000x10 ⁻¹	0.0000	1.0000	5.5584x10 ⁶
39	6.9617x10 ⁻²	2.9600x10 ⁻²⁰	1.4200x10 ⁻⁹	7.0000x10 ⁻¹	2.0000x10 ⁻¹	0.0000	1.0000	3.1998x10 ⁶
40	7.1929x10 ⁻²	4.4120x10 ⁻²⁰	1.3664x10 ⁻⁹	7.0000x10 ⁻¹	2.0000x10 ⁻¹	0.0000	1.0000	2.7870x10 ⁶
41	8.5712x10 ⁻²	4.7690x10 ⁻¹⁹	1.1064x10 ⁻⁹	7.0000x10 ⁻¹	2.0000x10 ⁻¹	0.0000	1.0000	1.2231x10 ⁶
42	6.1966x10 ⁻²	7.8970x10 ⁻²¹	1.6262x10 ⁻⁹	7.0000x10 ⁻¹	2.0000x10 ⁻¹	0.0000	1.0000	5.0544x10 ⁶
43	8.0322x10 ⁻²	1.8800x10 ⁻¹⁹	1.1975x10 ⁻⁹	7.0000x10 ⁻¹	2.0000x10 ⁻¹	0.0000	1.0000	1.6878x10 ⁶
44	6.8201x10 ⁻²	2.3180x10 ⁻²⁰	1.4547x10 ⁻⁹	7.0000x10 ⁻¹	2.0000x10 ⁻¹	0.0000	1.0000	3.4822x10 ⁶
45	6.9955x10 ⁻²	3.1380x10 ⁻²⁰	1.4120x10 ⁻⁹	7.0000x10 ⁻¹	2.0000x10 ⁻¹	0.0000	1.0000	3.1358x10 ⁶
46	7.6523x10 ⁻²	9.7550x10 ⁻²⁰	1.2693x10 ⁻⁹	7.0000x10 ⁻¹	2.0000x10 ⁻¹	0.0000	1.0000	2.1180x10 ⁶
47	6.7080x10 ⁻²	1.9100x10 ⁻²⁰	1.4832x10 ⁻⁹	7.0000x10 ⁻¹	2.0000x10 ⁻¹	0.0000	1.0000	3.7235x10 ⁶
48	7.5590x10 ⁻²	8.3030x10 ⁻²⁰	1.2881x10 ⁻⁹	7.0000x10 ⁻¹	2.0000x10 ⁻¹	0.0000	1.0000	2.2394x10 ⁶
49	5.5156x10 ⁻²	2.4360x10 ⁻²¹	1.8579x10 ⁻⁹	7.0000x10 ⁻¹	2.0000x10 ⁻¹	0.0000	1.0000	7.5927x10 ⁶
50	7.3176x10 ⁻²	5.4730x10 ⁻²⁰	1.3388x10 ⁻⁹	7.0000x10 ⁻¹	2.0000x10 ⁻¹	0.0000	1.0000	2.5868x10 ⁶
51	7.0199x10 ⁻²	3.2730x10 ⁻²⁰	1.4062x10 ⁻⁹	7.0000x10 ⁻¹	2.0000x10 ⁻¹	0.0000	1.0000	3.0904x10 ⁶
52	7.1211x10 ⁻²	3.8980x10 ⁻²⁰	1.3826x10 ⁻⁹	7.0000x10 ⁻¹	2.0000x10 ⁻¹	0.0000	1.0000	2.9091x10 ⁶

Appendix B: BRAGFLO Reference Tables

Table B-2 1992 BRAGFLO Computed Variable Values for PANEL_SEAL (Concluded)

Run No.	Porosity	Permeability	Compressibility	BCEXP	BCBRSAT	BCGSSAT	BCFLG	BCPCT
53	8.1495x10 ⁻²	2.3020x10 ⁻¹⁹	1.1766x10 ⁻⁹	7.0000x10 ⁻¹	2.0000x10 ⁻¹	0.0000	1.0000	1.5736x10 ⁶
54	7.8822x10 ⁻²	1.4510x10 ⁻¹⁹	1.2250x10 ⁻⁹	7.0000x10 ⁻¹	2.0000x10 ⁻¹	0.0000	1.0000	1.8461x10 ⁶
55	8.2516x10 ⁻²	2.7460x10 ⁻¹⁹	1.1590x10 ⁻⁹	7.0000x10 ⁻¹	2.0000x10 ⁻¹	0.0000	1.0000	1.4805x10 ⁶
56	6.5560x10 ⁻²	1.4690x10 ⁻²⁰	1.5234x10 ⁻⁹	7.0000x10 ⁻¹	2.0000x10 ⁻¹	0.0000	1.0000	4.0775x10 ⁶
57	7.4885x10 ⁻²	7.3510x10 ⁻²⁰	1.3026x10 ⁻⁹	7.0000x10 ⁻¹	2.0000x10 ⁻¹	0.0000	1.0000	2.3358x10 ⁶
58	5.1492x10 ⁻²	1.2940x10 ⁻²¹	2.0079x10 ⁻⁹	7.0000x10 ⁻¹	2.0000x10 ⁻¹	0.0000	1.0000	9.4506x10 ⁶
59	9.0000x10 ⁻²	1.0000x10 ⁻¹⁸	1.0418x10 ⁻⁹	7.0000x10 ⁻¹	2.0000x10 ⁻¹	0.0000	1.0000	9.4665x10 ⁵
60	5.5835x10 ⁻²	2.7390x10 ⁻²¹	1.8323x10 ⁻⁹	7.0000x10 ⁻¹	2.0000x10 ⁻¹	0.0000	1.0000	7.2909x10 ⁶
61	7.6860x10 ⁻²	1.0340x10 ⁻¹⁹	1.2626x10 ⁻⁹	7.0000x10 ⁻¹	2.0000x10 ⁻¹	0.0000	1.0000	2.0757x10 ⁶
62	7.1746x10 ⁻²	4.2750x10 ⁻²⁰	1.3705x10 ⁻⁹	7.0000x10 ⁻¹	2.0000x10 ⁻¹	0.0000	1.0000	2.8176x10 ⁶
63	7.3762x10 ⁻²	6.0550x10 ⁻²⁰	1.3262x10 ⁻⁹	7.0000x10 ⁻¹	2.0000x10 ⁻¹	0.0000	1.0000	2.4979x10 ⁶
64	7.5663x10 ⁻²	8.4080x10 ⁻²⁰	1.2866x10 ⁻⁹	7.0000x10 ⁻¹	2.0000x10 ⁻¹	0.0000	1.0000	2.2297x10 ⁶
65	7.3045x10 ⁻²	5.3500x10 ⁻²⁰	1.3417x10 ⁻⁹	7.0000x10 ⁻¹	2.0000x10 ⁻¹	0.0000	1.0000	2.6072x10 ⁶
66	5.1070x10 ⁻²	1.2030x10 ⁻²¹	2.0265x10 ⁻⁹	7.0000x10 ⁻¹	2.0000x10 ⁻¹	0.0000	1.0000	9.6921x10 ⁶
67	7.2562x10 ⁻²	4.9220x10 ⁻²⁰	1.3523x10 ⁻⁹	7.0000x10 ⁻¹	2.0000x10 ⁻¹	0.0000	1.0000	2.6835x10 ⁶
68	6.9149x10 ⁻²	2.7300x10 ⁻²⁰	1.4313x10 ⁻⁹	7.0000x10 ⁻¹	2.0000x10 ⁻¹	0.0000	1.0000	3.2906x10 ⁶
69	5.8844x10 ⁻²	4.6060x10 ⁻²¹	1.7258x10 ⁻⁹	7.0000x10 ⁻¹	2.0000x10 ⁻¹	0.0000	1.0000	6.0909x10 ⁶
70	6.5148x10 ⁻²	1.3680x10 ⁻²⁰	1.5346x10 ⁻⁹	7.0000x10 ⁻¹	2.0000x10 ⁻¹	0.0000	1.0000	4.1793x10 ⁶

Table B-2 1992 BRAGFLO Ranks of Computed Variable Values for PANEL_SEAL

Run No.	Porosity	Permeability	Compressibility	BCEXP	BCBRSAT	BCGSSAT	BCFLG	BCPCT
1	19.	19.	52.	1.	1.	1.	1.	52.
2	32.	32.	39.	1.	1.	1.	1.	39.
3	18.	18.	53.	1.	1.	1.	1.	53.
4	48.	48.	23.	1.	1.	1.	1.	23.
5	37.	37.	34.	1.	1.	1.	1.	34.
6	27.	27.	44.	1.	1.	1.	1.	44.
7	28.	28.	43.	1.	1.	1.	1.	43.
8	49.	49.	22.	1.	1.	1.	1.	22.
9	29.	29.	42.	1.	1.	1.	1.	42.
10	20.	20.	51.	1.	1.	1.	1.	51.
11	66.	66.	5.	1.	1.	1.	1.	5.
12	11.	11.	60.	1.	1.	1.	1.	60.
13	14.	14.	57.	1.	1.	1.	1.	57.
14	58.	58.	13.	1.	1.	1.	1.	13.
15	50.	50.	21.	1.	1.	1.	1.	21.
16	69.	69.	2.	1.	1.	1.	1.	2.
17	9.	9.	62.	1.	1.	1.	1.	62.
18	43.	43.	28.	1.	1.	1.	1.	28.
19	59.	59.	12.	1.	1.	1.	1.	12.
20	15.	15.	56.	1.	1.	1.	1.	56.
21	8.	8.	63.	1.	1.	1.	1.	63.
22	57.	57.	14.	1.	1.	1.	1.	14.
23	17.	17.	54.	1.	1.	1.	1.	54.
24	54.	54.	17.	1.	1.	1.	1.	17.
25	5.	5.	66.	1.	1.	1.	1.	66.
26	40.	40.	31.	1.	1.	1.	1.	31.
27	23.	23.	48.	1.	1.	1.	1.	48.
28	67.	67.	4.	1.	1.	1.	1.	4.
29	38.	38.	33.	1.	1.	1.	1.	33.
30	63.	63.	8.	1.	1.	1.	1.	8.
31	24.	24.	47.	1.	1.	1.	1.	47.
32	61.	61.	10.	1.	1.	1.	1.	10.
33	12.	12.	59.	1.	1.	1.	1.	59.
34	31.	31.	40.	1.	1.	1.	1.	40.
35	6.	6.	65.	1.	1.	1.	1.	65.
36	25.	25.	46.	1.	1.	1.	1.	46.
37	16.	16.	55.	1.	1.	1.	1.	55.
38	10.	10.	61.	1.	1.	1.	1.	61.
39	34.	34.	37.	1.	1.	1.	1.	37.
40	42.	42.	29.	1.	1.	1.	1.	29.
41	68.	68.	3.	1.	1.	1.	1.	3.
42	13.	13.	58.	1.	1.	1.	1.	58.
43	62.	62.	9.	1.	1.	1.	1.	9.
44	30.	30.	41.	1.	1.	1.	1.	41.
45	35.	35.	36.	1.	1.	1.	1.	36.
46	55.	55.	16.	1.	1.	1.	1.	16.
47	26.	26.	45.	1.	1.	1.	1.	45.
48	52.	52.	19.	1.	1.	1.	1.	19.
49	3.	3.	68.	1.	1.	1.	1.	68.
50	46.	46.	25.	1.	1.	1.	1.	25.
51	36.	36.	35.	1.	1.	1.	1.	35.
52	39.	39.	32.	1.	1.	1.	1.	32.

Appendix B: BRAGFLO Reference Tables

Table B-2 1992 BRAGFLO Ranks of Computed Variable Values for PANEL_SEAL (Concluded)

Run No.	Porosity	Permeability	Compressibility	BCEXP	BCBRSAT	BCGSSAT	BCFLG	BCPCT
53	64.	64.	7.	1.	1.	1.	1.	7.
54	60.	60.	11.	1.	1.	1.	1.	11.
55	65.	65.	6.	1.	1.	1.	1.	6.
56	22.	22.	49.	1.	1.	1.	1.	49.
57	51.	51.	20.	1.	1.	1.	1.	20.
58	2.	2.	69.	1.	1.	1.	1.	69.
59	70.	70.	1.	1.	1.	1.	1.	1.
60	4.	4.	67.	1.	1.	1.	1.	67.
61	56.	56.	15.	1.	1.	1.	1.	15.
62	41.	41.	30.	1.	1.	1.	1.	30.
63	47.	47.	24.	1.	1.	1.	1.	24.
64	53.	53.	18.	1.	1.	1.	1.	18.
65	45.	45.	26.	1.	1.	1.	1.	26.
66	1.	1.	70.	1.	1.	1.	1.	70.
67	44.	44.	27.	1.	1.	1.	1.	27.
68	33.	33.	38.	1.	1.	1.	1.	38.
69	7.	7.	64.	1.	1.	1.	1.	64.
70	21.	21.	50.	1.	1.	1.	1.	50.

Table B-2 1992 BRAGFLO Computed Variable Values for SALADO

Run No.	Porosity	Permeability	Compressibility	BCEXP	BCBRSAT	BCGSSAT	BCFLG	BCPCT
1	2.8660x10 ⁻²	3.6308x10 ⁻²¹	3.8066x10 ⁻⁹	9.6790	8.7890x10 ⁻²	2.3300x10 ⁻¹	0.0000	6.6135x10 ⁶
2	6.9900x10 ⁻³	9.7724x10 ⁻²¹	1.6383x10 ⁻⁸	4.9660x10 ⁻¹	1.4570x10 ⁻¹	1.2590x10 ⁻¹	1.0000	4.6951x10 ⁶
3	2.8970x10 ⁻²	1.3183x10 ⁻²¹	3.7632x10 ⁻⁹	6.7900x10 ⁻¹	1.8490x10 ⁻¹	2.1660x10 ⁻¹	1.0000	9.3900x10 ⁶
4	5.6130x10 ⁻³	1.5136x10 ⁻²¹	2.0463x10 ⁻⁸	5.1820	1.7260x10 ⁻¹	1.8900x10 ⁻¹	1.0000	8.9517x10 ⁶
5	2.0560x10 ⁻²	2.8840x10 ⁻²²	5.4048x10 ⁻⁹	4.0710x10 ⁻¹	1.9880x10 ⁻¹	1.4590x10 ⁻¹	1.0000	1.5887x10 ⁷
6	1.3750x10 ⁻²	7.2444x10 ⁻²⁴	8.2055x10 ⁻⁹	6.1420	3.3170x10 ⁻¹	4.7930x10 ⁻²	0.0000	5.6837x10 ⁷
7	2.5930x10 ⁻²	1.1481x10 ⁻²²	4.2337x10 ⁻⁹	1.0990	3.5430x10 ⁻²	1.6220x10 ⁻¹	0.0000	2.1849x10 ⁷
8	3.1850x10 ⁻³	4.8978x10 ⁻²²	3.6253x10 ⁻⁸	6.4480	3.8660x10 ⁻¹	2.8520x10 ⁻²	1.0000	1.3227x10 ⁷
9	2.7270x10 ⁻²	4.7863x10 ⁻²⁴	4.0134x10 ⁻⁹	4.2610x10 ⁻¹	3.4080x10 ⁻¹	1.8690x10 ⁻¹	1.0000	6.5601x10 ⁷
10	9.6770x10 ⁻³	3.9811x10 ⁻²¹	1.1764x10 ⁻⁸	1.5170	7.9000x10 ⁻²	3.4810x10 ⁻¹	1.0000	6.4060x10 ⁶
11	2.5730x10 ⁻³	7.7625x10 ⁻²¹	4.4936x10 ⁻⁸	5.1250x10 ⁻¹	2.7170x10 ⁻¹	2.0030x10 ⁻¹	0.0000	5.0845x10 ⁶
12	9.8270x10 ⁻³	9.1201x10 ⁻²¹	1.1581x10 ⁻⁸	7.4960	1.4100x10 ⁻¹	2.8620x10 ⁻¹	1.0000	4.8087x10 ⁶
13	1.6610x10 ⁻²	8.7096x10 ⁻²⁴	6.7496x10 ⁻⁹	2.2490	3.6500x10 ⁻¹	2.9370x10 ⁻¹	1.0000	5.3327x10 ⁷
14	1.9600x10 ⁻²	7.0795x10 ⁻²³	5.6818x10 ⁻⁹	3.0620x10 ⁻¹	8.3660x10 ⁻³	1.7360x10 ⁻¹	1.0000	2.5828x10 ⁷
15	1.1590x10 ⁻³	3.0200x10 ⁻²⁴	1.0006x10 ⁻⁷	4.4620x10 ⁻¹	2.3100x10 ⁻¹	3.8350x10 ⁻¹	0.0000	7.6932x10 ⁷
16	5.8700x10 ⁻³	1.9953x10 ⁻²¹	1.9556x10 ⁻⁸	5.3590x10 ⁻¹	3.7890x10 ⁻¹	2.1720x10 ⁻¹	1.0000	8.1356x10 ⁶
17	2.3950x10 ⁻²	1.2882x10 ⁻²²	4.6044x10 ⁻⁹	5.9190	1.1130x10 ⁻¹	3.8060x10 ⁻¹	0.0000	2.0996x10 ⁷
18	6.1370x10 ⁻³	6.7608x10 ⁻²²	1.8695x10 ⁻⁸	5.8730x10 ⁻¹	2.9470x10 ⁻¹	8.6120x10 ⁻³	0.0000	1.1831x10 ⁷
19	6.2550x10 ⁻³	3.9811x10 ⁻²³	1.8337x10 ⁻⁸	2.0050	1.1640x10 ⁻¹	1.6670x10 ⁻¹	1.0000	3.1520x10 ⁷
20	1.7070x10 ⁻²	1.8197x10 ⁻²⁰	6.5609x10 ⁻⁹	6.7090x10 ⁻¹	1.2940x10 ⁻¹	3.2110x10 ⁻¹	1.0000	3.7864x10 ⁶
21	2.3500x10 ⁻²	2.8840x10 ⁻²⁰	4.6974x10 ⁻⁹	2.2590x10 ⁻¹	1.9770x10 ⁻²	2.2330x10 ⁻¹	0.0000	3.2287x10 ⁶
22	2.6030x10 ⁻²	5.4954x10 ⁻²¹	4.2165x10 ⁻⁹	1.4340	2.1830x10 ⁻¹	1.8710x10 ⁻²	1.0000	5.7299x10 ⁶
23	2.9920x10 ⁻²	5.4954x10 ⁻²²	3.6358x10 ⁻⁹	7.0990	2.3880x10 ⁻¹	4.5230x10 ⁻²	1.0000	1.2710x10 ⁷
24	1.4710x10 ⁻²	1.2023x10 ⁻²¹	7.6537x10 ⁻⁹	4.3270x10 ⁻¹	6.1270x10 ⁻²	2.6430x10 ⁻¹	1.0000	9.6941x10 ⁶
25	2.4720x10 ⁻²	7.0795x10 ⁻²¹	4.4532x10 ⁻⁹	2.7610	3.0510x10 ⁻¹	9.9900x10 ⁻²	1.0000	5.2491x10 ⁶
26	1.8820x10 ⁻²	1.7378x10 ⁻²¹	5.9276x10 ⁻⁹	5.2660	2.4700x10 ⁻¹	6.8060x10 ⁻²	1.0000	8.5339x10 ⁶
27	2.2740x10 ⁻³	5.1286x10 ⁻²²	5.0877x10 ⁻⁸	8.3330	2.1280x10 ⁻¹	7.5730x10 ⁻²	1.0000	1.3018x10 ⁷
28	2.8830x10 ⁻³	4.5709x10 ⁻²²	4.0077x10 ⁻⁸	7.9460	3.4740x10 ⁻¹	1.5270x10 ⁻¹	0.0000	1.3547x10 ⁷
29	1.2680x10 ⁻²	2.3442x10 ⁻²¹	8.9190x10 ⁻⁹	6.0410x10 ⁻¹	3.3040x10 ⁻¹	3.5780x10 ⁻¹	1.0000	7.6943x10 ⁶
30	8.7910x10 ⁻³	7.9433x10 ⁻²²	1.2975x10 ⁻⁸	2.0040x10 ⁻¹	1.4050x10 ⁻²	1.5530x10 ⁻¹	0.0000	1.1189x10 ⁷
31	1.7650x10 ⁻²	3.3884x10 ⁻²²	6.3371x10 ⁻⁹	3.3160x10 ⁻¹	2.1130x10 ⁻¹	2.4050x10 ⁻¹	1.0000	1.5025x10 ⁷
32	2.0930x10 ⁻²	6.1660x10 ⁻²¹	5.3048x10 ⁻⁹	8.8800	3.1430x10 ⁻¹	3.7550x10 ⁻¹	1.0000	5.5061x10 ⁶
33	6.6640x10 ⁻³	1.0000x10 ⁻²¹	1.7196x10 ⁻⁸	5.2200x10 ⁻¹	1.0530x10 ⁻¹	3.4190x10 ⁻¹	1.0000	1.0332x10 ⁷
34	9.1030x10 ⁻³	2.3988x10 ⁻²²	1.2522x10 ⁻⁸	8.6520	2.5150x10 ⁻¹	3.6280x10 ⁻¹	0.0000	1.6932x10 ⁷
35	2.4230x10 ⁻³	3.0903x10 ⁻²¹	4.7733x10 ⁻⁸	3.9470x10 ⁻¹	2.9070x10 ⁻¹	1.3390x10 ⁻¹	1.0000	6.9928x10 ⁶
36	2.7120x10 ⁻²	1.5849x10 ⁻²²	4.0370x10 ⁻⁹	2.7500x10 ⁻¹	3.7090x10 ⁻¹	3.6960x10 ⁻¹	1.0000	1.9543x10 ⁷
37	5.0960x10 ⁻³	8.5114x10 ⁻²²	2.2564x10 ⁻⁸	6.9780	2.2650x10 ⁻¹	3.0790x10 ⁻²	1.0000	1.0925x10 ⁷
38	1.8940x10 ⁻³	5.1286x10 ⁻²¹	6.1135x10 ⁻⁸	2.9640	1.7810x10 ⁻¹	3.9620x10 ⁻¹	1.0000	5.8685x10 ⁶
39	1.0090x10 ⁻²	7.5858x10 ⁻²²	1.1273x10 ⁻⁸	2.6060x10 ⁻¹	1.6330x10 ⁻¹	3.7240x10 ⁻²	1.0000	1.1369x10 ⁷
40	2.2760x10 ⁻²	2.5704x10 ⁻²³	4.8582x10 ⁻⁹	2.4160x10 ⁻¹	2.4340x10 ⁻¹	1.1100x10 ⁻¹	1.0000	3.6671x10 ⁷
41	1.8020x10 ⁻²	5.8884x10 ⁻²¹	6.2019x10 ⁻⁹	5.7490x10 ⁻¹	1.3340x10 ⁻¹	1.0650x10 ⁻¹	1.0000	5.5946x10 ⁶
42	2.1990x10 ⁻²	6.3096x10 ⁻²²	5.0371x10 ⁻⁹	5.4840x10 ⁻¹	3.9640x10 ⁻¹	3.3500x10 ⁻¹	0.0000	1.2117x10 ⁷
43	5.1790x10 ⁻³	2.4547x10 ⁻²¹	2.2199x10 ⁻⁸	4.0000	3.9070x10 ⁻¹	1.2040x10 ⁻¹	0.0000	7.5727x10 ⁶
44	3.9010x10 ⁻³	3.9811x10 ⁻²¹	2.9553x10 ⁻⁸	3.6050x10 ⁻¹	2.5980x10 ⁻¹	5.7350x10 ⁻²	0.0000	6.4060x10 ⁶
45	9.3870x10 ⁻³	2.8840x10 ⁻²¹	1.2135x10 ⁻⁸	3.2390x10 ⁻¹	1.5830x10 ⁻¹	9.4190x10 ⁻²	1.0000	7.1619x10 ⁶
46	2.8280x10 ⁻²	1.0471x10 ⁻²⁴	3.8611x10 ⁻⁹	4.6060x10 ⁻¹	6.5170x10 ⁻²	2.3880x10 ⁻¹	1.0000	1.1099x10 ⁸
47	6.5700x10 ⁻³	5.7544x10 ⁻²⁰	1.7446x10 ⁻⁸	3.4760	3.1780x10 ⁻¹	2.6060x10 ⁻¹	1.0000	2.5423x10 ⁶
48	2.2390x10 ⁻²	2.8184x10 ⁻²¹	4.9426x10 ⁻⁹	7.7080	4.5510x10 ⁻²	2.0750x10 ⁻¹	0.0000	7.2192x10 ⁶
49	1.6820x10 ⁻³	1.9953x10 ⁻²²	6.8872x10 ⁻⁸	3.7530x10 ⁻¹	5.0110x10 ⁻²	6.9900x10 ⁻²	1.0000	1.8046x10 ⁷
50	1.2890x10 ⁻²	1.8621x10 ⁻²²	8.7696x10 ⁻⁹	3.5390x10 ⁻¹	1.8990x10 ⁻¹	1.9850x10 ⁻¹	1.0000	1.8483x10 ⁷
51	7.8440x10 ⁻³	8.7096x10 ⁻²¹	1.4572x10 ⁻⁸	5.6000x10 ⁻¹	2.3180x10 ⁻²	1.1810x10 ⁻²	1.0000	4.8859x10 ⁶
52	4.7130x10 ⁻³	1.9953x10 ⁻²¹	2.4418x10 ⁻⁸	3.2370	1.5040x10 ⁻¹	3.8860x10 ⁻¹	0.0000	8.1356x10 ⁶

Appendix B: BRAGFLO Reference Tables

Table B-2 1992 BRAGFLO Computed Variable Values for SALADO (Concluded)

Run No.	Porosity	Permeability	Compressibility	BCEXP	BCBRSAT	BCGSSAT	BCFLG	BCPCT
53	1.5900x10 ⁻²	4.6774x10 ⁻²¹	7.0621x10 ⁻⁹	6.7410	2.8470x10 ⁻¹	1.8060x10 ⁻¹	1.0000	6.0585x10 ⁶
54	1.4500x10 ⁻²	3.7154x10 ⁻²²	7.7681x10 ⁻⁹	4.7200x10 ⁻¹	1.6590x10 ⁻¹	2.7290x10 ⁻¹	0.0000	1.4554x10 ⁷
55	2.0030x10 ⁻²	1.4125x10 ⁻²²	5.5544x10 ⁻⁹	6.5030x10 ⁻¹	3.2450x10 ⁻¹	3.0330x10 ⁻¹	0.0000	2.0337x10 ⁷
56	1.1650x10 ⁻²	1.6596x10 ⁻²⁴	9.7296x10 ⁻⁹	4.8480	9.2770x10 ⁻²	5.2210x10 ⁻²	0.0000	9.4639x10 ⁷
57	4.5630x10 ⁻³	3.8904x10 ⁻²²	2.5229x10 ⁻⁸	9.2110	5.1160x10 ⁻³	2.7770x10 ⁻¹	1.0000	1.4324x10 ⁷
58	8.7110x10 ⁻³	2.1878x10 ⁻²³	1.3097x10 ⁻⁸	6.4060x10 ⁻¹	3.4880x10 ⁻¹	3.2980x10 ⁻¹	1.0000	3.8775x10 ⁷
59	2.5160x10 ⁻²	1.4791x10 ⁻²³	4.3709x10 ⁻⁹	8.9580	8.5120x10 ⁻²	3.1270x10 ⁻¹	1.0000	4.4398x10 ⁷
60	8.2600x10 ⁻³	9.1201x10 ⁻²³	1.3825x10 ⁻⁸	9.8620	7.0380x10 ⁻²	8.1940x10 ⁻²	1.0000	2.3661x10 ⁷
61	7.3840x10 ⁻³	1.0715x10 ⁻²¹	1.5495x10 ⁻⁸	8.0490x10 ⁻¹	2.7910x10 ⁻¹	1.3890x10 ⁻¹	1.0000	1.0088x10 ⁷
62	1.2250x10 ⁻²	1.2303x10 ⁻²²	9.2408x10 ⁻⁹	2.8630x10 ⁻¹	3.5990x10 ⁻¹	2.5120x10 ⁻¹	1.0000	2.1333x10 ⁷
63	4.1090x10 ⁻³	3.0903x10 ⁻²²	2.8045x10 ⁻⁸	3.7540	2.0010x10 ⁻¹	2.8360x10 ⁻¹	0.0000	1.5511x10 ⁷
64	3.7390x10 ⁻³	1.6982x10 ⁻²²	3.0845x10 ⁻⁸	2.4950	2.9320x10 ⁻²	8.7020x10 ⁻²	1.0000	1.9081x10 ⁷
65	7.4700x10 ⁻³	1.5488x10 ⁻²¹	1.5314x10 ⁻⁸	2.5410x10 ⁻¹	2.6410x10 ⁻¹	3.5100x10 ⁻¹	1.0000	8.8807x10 ⁶
66	3.5330x10 ⁻³	4.8978x10 ⁻²³	3.2658x10 ⁻⁸	6.9150x10 ⁻¹	1.2380x10 ⁻¹	3.1630x10 ⁻¹	0.0000	2.9339x10 ⁷
67	8.1910x10 ⁻³	1.1482x10 ⁻²¹	1.3944x10 ⁻⁸	5.5890	5.6350x10 ⁻²	2.5370x10 ⁻¹	0.0000	9.8498x10 ⁶
68	1.0760x10 ⁻²	2.2387x10 ⁻²²	1.0555x10 ⁻⁸	4.5200	3.0240x10 ⁻¹	2.9970x10 ⁻¹	0.0000	1.7342x10 ⁷
69	1.5190x10 ⁻²	2.5704x10 ⁻²²	7.4039x10 ⁻⁹	4.3270	3.7150x10 ⁻¹	4.8390x10 ⁻³	1.0000	1.6532x10 ⁷
70	1.4890x10 ⁻³	2.5704x10 ⁻²⁴	7.7831x10 ⁻⁸	6.2770x10 ⁻¹	1.0130x10 ⁻¹	1.1920x10 ⁻¹	1.0000	8.1344x10 ⁷

Table B-2 1992 BRAGFLO Ranks of Computed Variable Values for SALADO

Run No.	Porosity	Permeability	Compressibility	BCEXP	BCBRSAT	BCGSSAT	BCFLG	BCPCT
1	68.	55.	3.	69.	16.	41.	1.	16.
2	24.	67.	47.	21.	26.	23.	24.	4.
3	69.	44.	2.	34.	33.	38.	24.	27.
4	18.	45.	53.	52.	31.	34.	24.	26.
5	54.	26.	17.	15.	35.	26.	24.	45.
6	42.	6.	29.	56.	59.	9.	1.	65.
7	63.	15.	8.	37.	7.	29.	1.	56.
8	9.	32.	62.	57.	68.	5.	24.	39.
9	66.	5.	5.	16.	60.	33.	24.	66.
10	34.	56.	37.	39.	14.	61.	24.	14.
11	7.	64.	64.	22.	48.	36.	1.	7.
12	35.	66.	36.	61.	25.	51.	24.	5.
13	47.	7.	24.	41.	64.	52.	24.	64.
14	52.	13.	19.	8.	2.	31.	24.	58.
15	1.	4.	70.	18.	41.	68.	1.	67.
16	19.	48.	52.	24.	67.	39.	24.	22.
17	60.	17.	11.	55.	20.	67.	1.	54.
18	20.	36.	51.	28.	52.	2.	1.	35.
19	21.	11.	50.	40.	21.	30.	24.	60.
20	48.	68.	23.	33.	23.	57.	24.	3.
21	59.	69.	12.	2.	4.	40.	1.	2.
22	64.	60.	7.	38.	39.	4.	24.	11.
23	70.	34.	1.	60.	42.	8.	24.	37.
24	44.	43.	27.	17.	11.	47.	24.	28.
25	61.	63.	10.	43.	54.	18.	24.	8.
26	51.	47.	20.	53.	44.	12.	24.	24.
27	5.	33.	66.	64.	38.	14.	24.	38.
28	8.	31.	63.	63.	61.	27.	1.	40.
29	40.	50.	31.	29.	58.	63.	24.	21.
30	31.	38.	40.	1.	3.	28.	1.	33.
31	49.	28.	22.	10.	37.	43.	24.	43.
32	55.	62.	16.	66.	55.	66.	24.	9.
33	23.	40.	48.	23.	19.	60.	24.	31.
34	32.	24.	39.	65.	45.	64.	1.	47.
35	6.	54.	65.	14.	51.	24.	24.	17.
36	65.	19.	6.	6.	65.	65.	24.	52.
37	16.	39.	55.	59.	40.	6.	24.	32.
38	4.	59.	67.	44.	32.	70.	24.	12.
39	36.	37.	35.	5.	29.	7.	24.	34.
40	58.	10.	13.	3.	43.	20.	24.	61.
41	50.	61.	21.	27.	24.	19.	24.	10.
42	56.	35.	15.	25.	70.	59.	1.	36.
43	17.	51.	54.	48.	69.	22.	1.	20.
44	12.	56.	59.	12.	46.	11.	1.	14.
45	33.	53.	38.	9.	28.	17.	24.	18.
46	67.	1.	4.	19.	12.	42.	24.	70.
47	22.	70.	49.	46.	56.	46.	24.	1.
48	57.	52.	14.	62.	8.	37.	1.	19.
49	3.	22.	68.	13.	9.	13.	24.	49.
50	41.	21.	30.	11.	34.	35.	24.	50.
51	27.	65.	44.	26.	5.	3.	24.	6.
52	15.	48.	56.	45.	27.	69.	1.	22.

Appendix B: BRAGFLO Reference Tables

Table B-2 1992 BRAGFLO Ranks of Computed Variable Values for SALADO (Concluded)

<u>Run No.</u>	<u>Porosity</u>	<u>Permeability</u>	<u>Compressibility</u>	<u>BCEXP</u>	<u>BCBRSAT</u>	<u>BCGSSAT</u>	<u>BCFLG</u>	<u>BCPCT</u>
53	46.	58.	25.	58.	50.	32.	24.	13.
54	43.	29.	28.	20.	30.	48.	1.	42.
55	53.	18.	18.	32.	57.	54.	1.	53.
56	38.	2.	33.	51.	17.	10.	1.	69.
57	14.	30.	57.	68.	1.	49.	24.	41.
58	30.	9.	41.	31.	62.	58.	24.	62.
59	62.	8.	9.	67.	15.	55.	24.	63.
60	29.	14.	42.	70.	13.	15.	24.	57.
61	25.	41.	46.	36.	49.	25.	24.	30.
62	39.	16.	32.	7.	63.	44.	24.	55.
63	13.	27.	58.	47.	36.	50.	1.	44.
64	11.	20.	60.	42.	6.	16.	24.	51.
65	26.	46.	45.	4.	47.	62.	24.	25.
66	10.	12.	61.	35.	22.	56.	1.	59.
67	28.	42.	43.	54.	10.	45.	1.	29.
68	37.	23.	34.	50.	53.	53.	1.	48.
69	45.	25.	26.	49.	66.	1.	24.	46.
70	2.	3.	69.	30.	18.	21.	24.	68.

Table B-2 1992 BRAGFLO Computed Variable Values for SHAFT_SEAL

Run No.	Porosity	Permeability	Compressibility	BCEXP	BCBRSAT	BCGSSAT	BCFLG	BCPCT
1	5.6433x10 ⁻²	3.2690x10 ⁻¹⁷	1.8102x10 ⁻⁹	7.0000x10 ⁻¹	2.0000x10 ⁻¹	0.0000	1.0000	2.8327x10 ⁵
2	4.3305x10 ⁻²	1.2730x10 ⁻¹⁷	2.4347x10 ⁻⁹	7.0000x10 ⁻¹	2.0000x10 ⁻¹	0.0000	1.0000	3.9257x10 ⁵
3	4.0073x10 ⁻²	5.5560x10 ⁻¹⁷	2.6512x10 ⁻⁹	7.0000x10 ⁻¹	2.0000x10 ⁻¹	0.0000	1.0000	2.3578x10 ⁵
4	5.8422x10 ⁻²	1.8260x10 ⁻¹⁷	1.7400x10 ⁻⁹	7.0000x10 ⁻¹	2.0000x10 ⁻¹	0.0000	1.0000	3.4650x10 ⁵
5	3.5889x10 ⁻²	4.6190x10 ⁻¹⁹	2.9895x10 ⁻⁹	7.0000x10 ⁻¹	2.0000x10 ⁻¹	0.0000	1.0000	1.2367x10 ⁶
6	4.8739x10 ⁻²	9.4430x10 ⁻¹⁸	2.1354x10 ⁻⁹	7.0000x10 ⁻¹	2.0000x10 ⁻¹	0.0000	1.0000	4.3531x10 ⁵
7	1.8565x10 ⁻²	3.4350x10 ⁻¹⁷	6.0125x10 ⁻⁹	7.0000x10 ⁻¹	2.0000x10 ⁻¹	0.0000	1.0000	2.7846x10 ⁵
8	3.3804x10 ⁻²	1.1320x10 ⁻¹⁸	3.1893x10 ⁻⁹	7.0000x10 ⁻¹	2.0000x10 ⁻¹	0.0000	1.0000	9.0690x10 ⁵
9	8.2847x10 ⁻²	3.6880x10 ⁻¹⁹	1.1533x10 ⁻⁹	7.0000x10 ⁻¹	2.0000x10 ⁻¹	0.0000	1.0000	1.3368x10 ⁶
10	4.8961x10 ⁻²	7.9740x10 ⁻¹⁸	2.1246x10 ⁻⁹	7.0000x10 ⁻¹	2.0000x10 ⁻¹	0.0000	1.0000	4.6154x10 ⁵
11	6.0343x10 ⁻²	3.8050x10 ⁻¹⁸	1.6767x10 ⁻⁹	7.0000x10 ⁻¹	2.0000x10 ⁻¹	0.0000	1.0000	5.9619x10 ⁵
12	5.5800x10 ⁻²	2.0750x10 ⁻¹⁷	1.8336x10 ⁻⁹	7.0000x10 ⁻¹	2.0000x10 ⁻¹	0.0000	1.0000	3.3151x10 ⁵
13	7.2964x10 ⁻²	4.9500x10 ⁻¹⁷	1.3434x10 ⁻⁹	7.0000x10 ⁻¹	2.0000x10 ⁻¹	0.0000	1.0000	2.4539x10 ⁵
14	6.0840x10 ⁻²	4.9160x10 ⁻¹⁸	1.6610x10 ⁻⁹	7.0000x10 ⁻¹	2.0000x10 ⁻¹	0.0000	1.0000	5.4562x10 ⁵
15	5.0585x10 ⁻²	4.2050x10 ⁻¹⁸	2.0484x10 ⁻⁹	7.0000x10 ⁻¹	2.0000x10 ⁻¹	0.0000	1.0000	5.7592x10 ⁵
16	3.5074x10 ⁻²	1.0530x10 ⁻¹⁸	3.0648x10 ⁻⁹	7.0000x10 ⁻¹	2.0000x10 ⁻¹	0.0000	1.0000	9.2988x10 ⁵
17	5.7146x10 ⁻²	6.8710x10 ⁻¹⁹	1.7845x10 ⁻⁹	7.0000x10 ⁻¹	2.0000x10 ⁻¹	0.0000	1.0000	1.0779x10 ⁶
18	8.2074x10 ⁻²	2.9880x10 ⁻¹⁸	1.1666x10 ⁻⁹	7.0000x10 ⁻¹	2.0000x10 ⁻¹	0.0000	1.0000	6.4820x10 ⁵
19	6.3721x10 ⁻²	7.1460x10 ⁻¹⁷	1.5746x10 ⁻⁹	7.0000x10 ⁻¹	2.0000x10 ⁻¹	0.0000	1.0000	2.1611x10 ⁵
20	1.6736x10 ⁻²	4.5930x10 ⁻¹⁸	6.6967x10 ⁻⁹	7.0000x10 ⁻¹	2.0000x10 ⁻¹	0.0000	1.0000	5.5860x10 ⁵
21	4.7082x10 ⁻²	1.9190x10 ⁻¹⁸	2.2194x10 ⁻⁹	7.0000x10 ⁻¹	2.0000x10 ⁻¹	0.0000	1.0000	7.5552x10 ⁵
22	4.6655x10 ⁻²	4.3250x10 ⁻¹⁷	2.2420x10 ⁻⁹	7.0000x10 ⁻¹	2.0000x10 ⁻¹	0.0000	1.0000	2.5712x10 ⁵
23	5.0975x10 ⁻²	1.7220x10 ⁻¹⁸	2.0308x10 ⁻⁹	7.0000x10 ⁻¹	2.0000x10 ⁻¹	0.0000	1.0000	7.8437x10 ⁵
24	6.8520x10 ⁻²	5.2090x10 ⁻¹⁹	1.4468x10 ⁻⁹	7.0000x10 ⁻¹	2.0000x10 ⁻¹	0.0000	1.0000	1.1863x10 ⁶
25	5.1999x10 ⁻²	1.1040x10 ⁻¹⁶	1.9859x10 ⁻⁹	7.0000x10 ⁻¹	2.0000x10 ⁻¹	0.0000	1.0000	1.8592x10 ⁵
26	4.1033x10 ⁻²	1.4510x10 ⁻¹⁹	2.5834x10 ⁻⁹	7.0000x10 ⁻¹	2.0000x10 ⁻¹	0.0000	1.0000	1.8461x10 ⁶
27	6.1762x10 ⁻²	1.1630x10 ⁻¹⁹	1.6324x10 ⁻⁹	7.0000x10 ⁻¹	2.0000x10 ⁻¹	0.0000	1.0000	1.9930x10 ⁶
28	3.7132x10 ⁻²	1.0480x10 ⁻¹⁷	2.8811x10 ⁻⁹	7.0000x10 ⁻¹	2.0000x10 ⁻¹	0.0000	1.0000	4.1990x10 ⁵
29	6.9933x10 ⁻²	4.0080x10 ⁻¹⁸	1.4125x10 ⁻⁹	7.0000x10 ⁻¹	2.0000x10 ⁻¹	0.0000	1.0000	5.8557x10 ⁵
30	4.7777x10 ⁻²	7.9680x10 ⁻¹⁷	2.1834x10 ⁻⁹	7.0000x10 ⁻¹	2.0000x10 ⁻¹	0.0000	1.0000	2.0812x10 ⁵
31	2.2998x10 ⁻²	1.9610x10 ⁻¹⁷	4.8054x10 ⁻⁹	7.0000x10 ⁻¹	2.0000x10 ⁻¹	0.0000	1.0000	3.3806x10 ⁵
32	4.5772x10 ⁻²	5.0000x10 ⁻¹⁶	2.2901x10 ⁻⁹	7.0000x10 ⁻¹	2.0000x10 ⁻¹	0.0000	1.0000	1.1024x10 ⁵
33	5.3975x10 ⁻²	8.1000x10 ⁻¹⁹	1.9040x10 ⁻⁹	7.0000x10 ⁻¹	2.0000x10 ⁻¹	0.0000	1.0000	1.0182x10 ⁶
34	6.6056x10 ⁻²	7.5340x10 ⁻¹⁸	1.5101x10 ⁻⁹	7.0000x10 ⁻¹	2.0000x10 ⁻¹	0.0000	1.0000	4.7069x10 ⁵
35	2.5859x10 ⁻²	1.1420x10 ⁻¹⁷	4.2460x10 ⁻⁹	7.0000x10 ⁻¹	2.0000x10 ⁻¹	0.0000	1.0000	4.0760x10 ⁵
36	2.7519x10 ⁻²	2.6550x10 ⁻¹⁸	3.9748x10 ⁻⁹	7.0000x10 ⁻¹	2.0000x10 ⁻¹	0.0000	1.0000	6.7525x10 ⁵
37	4.9770x10 ⁻²	1.4690x10 ⁻¹⁷	2.0860x10 ⁻⁹	7.0000x10 ⁻¹	2.0000x10 ⁻¹	0.0000	1.0000	3.7359x10 ⁵
38	4.2030x10 ⁻²	1.2620x10 ⁻¹⁸	2.5162x10 ⁻⁹	7.0000x10 ⁻¹	2.0000x10 ⁻¹	0.0000	1.0000	8.7342x10 ⁵
39	3.8123x10 ⁻²	2.4400x10 ⁻¹⁶	2.7997x10 ⁻⁹	7.0000x10 ⁻¹	2.0000x10 ⁻¹	0.0000	1.0000	1.4130x10 ⁵
40	6.2212x10 ⁻²	8.6700x10 ⁻¹⁸	1.6188x10 ⁻⁹	7.0000x10 ⁻¹	2.0000x10 ⁻¹	0.0000	1.0000	4.4837x10 ⁵
41	6.2879x10 ⁻²	6.0530x10 ⁻¹⁹	1.5990x10 ⁻⁹	7.0000x10 ⁻¹	2.0000x10 ⁻¹	0.0000	1.0000	1.1262x10 ⁶
42	5.5614x10 ⁻²	9.7010x10 ⁻¹⁹	1.8405x10 ⁻⁹	7.0000x10 ⁻¹	2.0000x10 ⁻¹	0.0000	1.0000	9.5664x10 ⁵
43	3.3383x10 ⁻²	2.1950x10 ⁻¹⁷	3.2327x10 ⁻⁹	7.0000x10 ⁻¹	2.0000x10 ⁻¹	0.0000	1.0000	3.2513x10 ⁵
44	7.4798x10 ⁻²	1.4780x10 ⁻¹⁸	1.3044x10 ⁻⁹	7.0000x10 ⁻¹	2.0000x10 ⁻¹	0.0000	1.0000	8.2695x10 ⁵
45	6.5132x10 ⁻²	2.7170x10 ⁻¹⁷	1.5350x10 ⁻⁹	7.0000x10 ⁻¹	2.0000x10 ⁻¹	0.0000	1.0000	3.0199x10 ⁵
46	4.5591x10 ⁻²	2.0720x10 ⁻¹⁸	2.3001x10 ⁻⁹	7.0000x10 ⁻¹	2.0000x10 ⁻¹	0.0000	1.0000	7.3573x10 ⁵
47	7.6297x10 ⁻²	3.9130x10 ⁻¹⁷	1.2738x10 ⁻⁹	7.0000x10 ⁻¹	2.0000x10 ⁻¹	0.0000	1.0000	2.6618x10 ⁵
48	9.0000x10 ⁻²	1.6990x10 ⁻¹⁷	1.0418x10 ⁻⁹	7.0000x10 ⁻¹	2.0000x10 ⁻¹	0.0000	1.0000	3.5526x10 ⁵
49	7.8712x10 ⁻²	2.3260x10 ⁻¹⁸	1.2271x10 ⁻⁹	7.0000x10 ⁻¹	2.0000x10 ⁻¹	0.0000	1.0000	7.0687x10 ⁵
50	2.2704x10 ⁻²	2.8780x10 ⁻¹⁷	4.8708x10 ⁻⁹	7.0000x10 ⁻¹	2.0000x10 ⁻¹	0.0000	1.0000	2.9604x10 ⁵
51	2.8140x10 ⁻²	2.3210x10 ⁻¹⁸	3.8816x10 ⁻⁹	7.0000x10 ⁻¹	2.0000x10 ⁻¹	0.0000	1.0000	7.0740x10 ⁵
52	4.2389x10 ⁻²	1.5210x10 ⁻¹⁸	2.4928x10 ⁻⁹	7.0000x10 ⁻¹	2.0000x10 ⁻¹	0.0000	1.0000	8.1879x10 ⁵

Appendix B: BRAGFLO Reference Tables

Table B-2 1992 BRAGFLO Computed Variable Values for SHAFT_SEAL (Concluded)

Run No.	Porosity	Permeability	Compressibility	BCEXP	BCBRSAT	BCGSSAT	BCFLG	BCPCT
53	5.8188x10 ⁻²	6.3790x10 ⁻¹⁸	1.7480x10 ⁻⁹	7.0000x10 ⁻¹	2.0000x10 ⁻¹	0.0000	1.0000	4.9859x10 ⁵
54	6.7354x10 ⁻²	1.5510x10 ⁻¹⁷	1.4762x10 ⁻⁹	7.0000x10 ⁻¹	2.0000x10 ⁻¹	0.0000	1.0000	3.6664x10 ⁵
55	3.9083x10 ⁻²	3.5290x10 ⁻¹⁸	2.7248x10 ⁻⁹	7.0000x10 ⁻¹	2.0000x10 ⁻¹	0.0000	1.0000	6.1193x10 ⁵
56	6.6469x10 ⁻²	8.1660x10 ⁻¹⁸	1.4991x10 ⁻⁹	7.0000x10 ⁻¹	2.0000x10 ⁻¹	0.0000	1.0000	4.5775x10 ⁵
57	5.3429x10 ⁻²	5.3740x10 ⁻¹⁸	1.9260x10 ⁻⁹	7.0000x10 ⁻¹	2.0000x10 ⁻¹	0.0000	1.0000	5.2906x10 ⁵
58	5.4958x10 ⁻²	9.3590x10 ⁻¹⁷	1.8655x10 ⁻⁹	7.0000x10 ⁻¹	2.0000x10 ⁻¹	0.0000	1.0000	1.9685x10 ⁵
59	5.2762x10 ⁻²	5.7450x10 ⁻¹⁸	1.9535x10 ⁻⁹	7.0000x10 ⁻¹	2.0000x10 ⁻¹	0.0000	1.0000	5.1698x10 ⁵
60	2.9620x10 ⁻²	3.1910x10 ⁻¹⁸	3.6751x10 ⁻⁹	7.0000x10 ⁻¹	2.0000x10 ⁻¹	0.0000	1.0000	6.3362x10 ⁵
61	4.0430x10 ⁻²	2.8000x10 ⁻¹⁸	2.6256x10 ⁻⁹	7.0000x10 ⁻¹	2.0000x10 ⁻¹	0.0000	1.0000	6.6294x10 ⁵
62	4.4173x10 ⁻²	6.3220x10 ⁻¹⁷	2.3820x10 ⁻⁹	7.0000x10 ⁻¹	2.0000x10 ⁻¹	0.0000	1.0000	2.2547x10 ⁵
63	5.9404x10 ⁻²	1.2980x10 ⁻¹⁶	1.7071x10 ⁻⁹	7.0000x10 ⁻¹	2.0000x10 ⁻¹	0.0000	1.0000	1.7579x10 ⁵
64	3.2463x10 ⁻²	5.8550x10 ⁻¹⁸	3.3314x10 ⁻⁹	7.0000x10 ⁻¹	2.0000x10 ⁻¹	0.0000	1.0000	5.1360x10 ⁵
65	7.1865x10 ⁻²	2.4680x10 ⁻¹⁷	1.3678x10 ⁻⁹	7.0000x10 ⁻¹	2.0000x10 ⁻¹	0.0000	1.0000	3.1220x10 ⁵
66	4.5003x10 ⁻²	6.8400x10 ⁻¹⁸	2.3335x10 ⁻⁹	7.0000x10 ⁻¹	2.0000x10 ⁻¹	0.0000	1.0000	4.8670x10 ⁵
67	3.1590x10 ⁻²	1.1240x10 ⁻¹⁷	3.4304x10 ⁻⁹	7.0000x10 ⁻¹	2.0000x10 ⁻¹	0.0000	1.0000	4.0985x10 ⁵
68	1.0000x10 ⁻²	2.4420x10 ⁻¹⁹	1.1376x10 ⁻⁸	7.0000x10 ⁻¹	2.0000x10 ⁻¹	0.0000	1.0000	1.5418x10 ⁶
69	5.1572x10 ⁻²	1.3260x10 ⁻¹⁷	2.0044x10 ⁻⁹	7.0000x10 ⁻¹	2.0000x10 ⁻¹	0.0000	1.0000	3.8707x10 ⁵
70	3.7917x10 ⁻²	2.0800x10 ⁻¹⁶	2.8162x10 ⁻⁹	7.0000x10 ⁻¹	2.0000x10 ⁻¹	0.0000	1.0000	1.4933x10 ⁵

Table B-2 1992 BRAGFLO Ranks of Computed Variable Values for SHAFT_SEAL

Run No.	Porosity	Permeability	Compressibility	BCEXP	BCBRSAT	BCGSSAT	BCFLG	BCPCT
1	46.	56.	25.	1.	1.	1.	1.	15.
2	25.	44.	46.	1.	1.	1.	1.	27.
3	20.	61.	51.	1.	1.	1.	1.	10.
4	49.	49.	22.	1.	1.	1.	1.	22.
5	15.	5.	56.	1.	1.	1.	1.	66.
6	33.	40.	38.	1.	1.	1.	1.	31.
7	3.	57.	68.	1.	1.	1.	1.	14.
8	13.	12.	58.	1.	1.	1.	1.	59.
9	69.	4.	2.	1.	1.	1.	1.	67.
10	34.	37.	37.	1.	1.	1.	1.	34.
11	51.	26.	20.	1.	1.	1.	1.	45.
12	45.	51.	26.	1.	1.	1.	1.	20.
13	64.	60.	7.	1.	1.	1.	1.	11.
14	52.	30.	19.	1.	1.	1.	1.	41.
15	36.	28.	35.	1.	1.	1.	1.	43.
16	14.	11.	57.	1.	1.	1.	1.	60.
17	47.	8.	24.	1.	1.	1.	1.	63.
18	68.	23.	3.	1.	1.	1.	1.	48.
19	56.	63.	15.	1.	1.	1.	1.	8.
20	2.	29.	69.	1.	1.	1.	1.	42.
21	31.	17.	40.	1.	1.	1.	1.	54.
22	30.	59.	41.	1.	1.	1.	1.	12.
23	37.	16.	34.	1.	1.	1.	1.	55.
24	61.	6.	10.	1.	1.	1.	1.	65.
25	39.	66.	32.	1.	1.	1.	1.	5.
26	22.	2.	49.	1.	1.	1.	1.	69.
27	53.	1.	18.	1.	1.	1.	1.	70.
28	16.	41.	55.	1.	1.	1.	1.	30.
29	62.	27.	9.	1.	1.	1.	1.	44.
30	32.	64.	39.	1.	1.	1.	1.	7.
31	5.	50.	66.	1.	1.	1.	1.	21.
32	29.	70.	42.	1.	1.	1.	1.	1.
33	42.	9.	29.	1.	1.	1.	1.	62.
34	58.	36.	13.	1.	1.	1.	1.	35.
35	6.	43.	65.	1.	1.	1.	1.	28.
36	7.	21.	64.	1.	1.	1.	1.	50.
37	35.	46.	36.	1.	1.	1.	1.	25.
38	23.	13.	48.	1.	1.	1.	1.	58.
39	18.	69.	53.	1.	1.	1.	1.	2.
40	54.	39.	17.	1.	1.	1.	1.	32.
41	55.	7.	16.	1.	1.	1.	1.	64.
42	44.	10.	27.	1.	1.	1.	1.	61.
43	12.	52.	59.	1.	1.	1.	1.	19.
44	65.	14.	6.	1.	1.	1.	1.	57.
45	57.	54.	14.	1.	1.	1.	1.	17.
46	28.	18.	43.	1.	1.	1.	1.	53.
47	66.	58.	5.	1.	1.	1.	1.	13.
48	70.	48.	1.	1.	1.	1.	1.	23.
49	67.	20.	4.	1.	1.	1.	1.	51.
50	4.	55.	67.	1.	1.	1.	1.	16.
51	8.	19.	63.	1.	1.	1.	1.	52.
52	24.	15.	47.	1.	1.	1.	1.	56.

Appendix B: BRAGFLO Reference Tables

Table B-2 1992 BRAGFLO Ranks of Computed Variable Values for SHAFT_SEAL (Concluded)

<u>Run No.</u>	<u>Porosity</u>	<u>Permeability</u>	<u>Compressibility</u>	<u>BCEXP</u>	<u>BCBRSAT</u>	<u>BCGSSAT</u>	<u>BCFLG</u>	<u>BCPCT</u>
53	48.	34.	23.	1.	1.	1.	1.	37.
54	60.	47.	11.	1.	1.	1.	1.	24.
55	19.	25.	52.	1.	1.	1.	1.	46.
56	59.	38.	12.	1.	1.	1.	1.	33.
57	41.	31.	30.	1.	1.	1.	1.	40.
58	43.	65.	28.	1.	1.	1.	1.	6.
59	40.	32.	31.	1.	1.	1.	1.	39.
60	9.	24.	62.	1.	1.	1.	1.	47.
61	21.	22.	50.	1.	1.	1.	1.	49.
62	26.	62.	45.	1.	1.	1.	1.	9.
63	50.	67.	21.	1.	1.	1.	1.	4.
64	11.	33.	60.	1.	1.	1.	1.	38.
65	63.	53.	8.	1.	1.	1.	1.	18.
66	27.	35.	44.	1.	1.	1.	1.	36.
67	10.	42.	61.	1.	1.	1.	1.	29.
68	1.	3.	70.	1.	1.	1.	1.	68.
69	38.	45.	33.	1.	1.	1.	1.	26.
70	17.	68.	54.	1.	1.	1.	1.	3.

Table B-2 1992 BRAGFLO Computed Variable Values for SHAFT_SEAL_2

Run No.	Porosity	Permeability	Compressibility	BCEXP	BCBRSAT	BCGSSAT	BCFLG	BCPCT
1	5.6433x10 ⁻²	5.5110x10 ⁻²⁰	1.8102x10 ⁻⁹	7.0000x10 ⁻¹	2.0000x10 ⁻¹	0.0000	1.0000	2.5806x10 ⁶
2	4.3305x10 ⁻²	1.7740x10 ⁻²⁰	2.4347x10 ⁻⁹	7.0000x10 ⁻¹	2.0000x10 ⁻¹	0.0000	1.0000	3.8199x10 ⁶
3	4.0073x10 ⁻²	1.3420x10 ⁻²⁰	2.6512x10 ⁻⁹	7.0000x10 ⁻¹	2.0000x10 ⁻¹	0.0000	1.0000	4.2071x10 ⁶
4	5.8422x10 ⁻²	6.5440x10 ⁻²⁰	1.7400x10 ⁻⁹	7.0000x10 ⁻¹	2.0000x10 ⁻¹	0.0000	1.0000	2.4317x10 ⁶
5	3.5889x10 ⁻²	9.3510x10 ⁻²¹	2.9895x10 ⁻⁹	7.0000x10 ⁻¹	2.0000x10 ⁻¹	0.0000	1.0000	4.7673x10 ⁶
6	4.8739x10 ⁻²	2.8360x10 ⁻²⁰	2.1354x10 ⁻⁹	7.0000x10 ⁻¹	2.0000x10 ⁻¹	0.0000	1.0000	3.2475x10 ⁶
7	1.8565x10 ⁻²	2.0950x10 ⁻²¹	6.0125x10 ⁻⁹	7.0000x10 ⁻¹	2.0000x10 ⁻¹	0.0000	1.0000	7.9994x10 ⁶
8	3.3804x10 ⁻²	7.8100x10 ⁻²¹	3.1893x10 ⁻⁹	7.0000x10 ⁻¹	2.0000x10 ⁻¹	0.0000	1.0000	5.0738x10 ⁶
9	8.2847x10 ⁻²	5.3920x10 ⁻¹⁹	1.1533x10 ⁻⁹	7.0000x10 ⁻¹	2.0000x10 ⁻¹	0.0000	1.0000	1.1722x10 ⁶
10	4.8961x10 ⁻²	2.8910x10 ⁻²⁰	2.1246x10 ⁻⁹	7.0000x10 ⁻¹	2.0000x10 ⁻¹	0.0000	1.0000	3.2260x10 ⁶
11	6.0343x10 ⁻²	7.7240x10 ⁻²⁰	1.6767x10 ⁻⁹	7.0000x10 ⁻¹	2.0000x10 ⁻¹	0.0000	1.0000	2.2961x10 ⁶
12	5.5800x10 ⁻²	5.2180x10 ⁻²⁰	1.8336x10 ⁻⁹	7.0000x10 ⁻¹	2.0000x10 ⁻¹	0.0000	1.0000	2.6299x10 ⁶
13	7.2964x10 ⁻²	2.2970x10 ⁻¹⁹	1.3434x10 ⁻⁹	7.0000x10 ⁻¹	2.0000x10 ⁻¹	0.0000	1.0000	1.5748x10 ⁶
14	6.0840x10 ⁻²	8.0630x10 ⁻²⁰	1.6610x10 ⁻⁹	7.0000x10 ⁻¹	2.0000x10 ⁻¹	0.0000	1.0000	2.2623x10 ⁶
15	5.0585x10 ⁻²	3.3260x10 ⁻²⁰	2.0484x10 ⁻⁹	7.0000x10 ⁻¹	2.0000x10 ⁻¹	0.0000	1.0000	3.0733x10 ⁶
16	3.5074x10 ⁻²	8.7150x10 ⁻²¹	3.0648x10 ⁻⁹	7.0000x10 ⁻¹	2.0000x10 ⁻¹	0.0000	1.0000	4.8849x10 ⁶
17	5.7146x10 ⁻²	5.8610x10 ⁻²⁰	1.7845x10 ⁻⁹	7.0000x10 ⁻¹	2.0000x10 ⁻¹	0.0000	1.0000	2.5262x10 ⁶
18	8.2074x10 ⁻²	5.0440x10 ⁻¹⁹	1.1666x10 ⁻⁹	7.0000x10 ⁻¹	2.0000x10 ⁻¹	0.0000	1.0000	1.1996x10 ⁶
19	6.3721x10 ⁻²	1.0340x10 ⁻¹⁹	1.5746x10 ⁻⁹	7.0000x10 ⁻¹	2.0000x10 ⁻¹	0.0000	1.0000	2.0757x10 ⁶
20	1.6736x10 ⁻²	1.7890x10 ⁻²¹	6.6967x10 ⁻⁹	7.0000x10 ⁻¹	2.0000x10 ⁻¹	0.0000	1.0000	8.4486x10 ⁶
21	4.7082x10 ⁻²	2.4580x10 ⁻²⁰	2.2194x10 ⁻⁹	7.0000x10 ⁻¹	2.0000x10 ⁻¹	0.0000	1.0000	3.4123x10 ⁶
22	4.6655x10 ⁻²	2.3690x10 ⁻²⁰	2.2420x10 ⁻⁹	7.0000x10 ⁻¹	2.0000x10 ⁻¹	0.0000	1.0000	3.4561x10 ⁶
23	5.0975x10 ⁻²	3.4400x10 ⁻²⁰	2.0308x10 ⁻⁹	7.0000x10 ⁻¹	2.0000x10 ⁻¹	0.0000	1.0000	3.0377x10 ⁶
24	6.8520x10 ⁻²	1.5650x10 ⁻¹⁹	1.4468x10 ⁻⁹	7.0000x10 ⁻¹	2.0000x10 ⁻¹	0.0000	1.0000	1.7984x10 ⁶
25	5.1999x10 ⁻²	3.7580x10 ⁻²⁰	1.9859x10 ⁻⁹	7.0000x10 ⁻¹	2.0000x10 ⁻¹	0.0000	1.0000	2.9461x10 ⁶
26	4.1033x10 ⁻²	1.4580x10 ⁻²⁰	2.5834x10 ⁻⁹	7.0000x10 ⁻¹	2.0000x10 ⁻¹	0.0000	1.0000	4.0882x10 ⁶
27	6.1762x10 ⁻²	8.7310x10 ⁻²⁰	1.6324x10 ⁻⁹	7.0000x10 ⁻¹	2.0000x10 ⁻¹	0.0000	1.0000	2.2008x10 ⁶
28	3.7132x10 ⁻²	1.0410x10 ⁻²⁰	2.8811x10 ⁻⁹	7.0000x10 ⁻¹	2.0000x10 ⁻¹	0.0000	1.0000	4.5936x10 ⁶
29	6.9933x10 ⁻²	1.7680x10 ⁻¹⁹	1.4125x10 ⁻⁹	7.0000x10 ⁻¹	2.0000x10 ⁻¹	0.0000	1.0000	1.7241x10 ⁶
30	4.7777x10 ⁻²	2.6100x10 ⁻²⁰	2.1834x10 ⁻⁹	7.0000x10 ⁻¹	2.0000x10 ⁻¹	0.0000	1.0000	3.3422x10 ⁶
31	2.2998x10 ⁻²	3.0720x10 ⁻²¹	4.8054x10 ⁻⁹	7.0000x10 ⁻¹	2.0000x10 ⁻¹	0.0000	1.0000	7.0071x10 ⁶
32	4.5772x10 ⁻²	2.1950x10 ⁻²⁰	2.2901x10 ⁻⁹	7.0000x10 ⁻¹	2.0000x10 ⁻¹	0.0000	1.0000	3.5486x10 ⁶
33	5.3975x10 ⁻²	4.4570x10 ⁻²⁰	1.9040x10 ⁻⁹	7.0000x10 ⁻¹	2.0000x10 ⁻¹	0.0000	1.0000	2.7773x10 ⁶
34	6.6056x10 ⁻²	1.2650x10 ⁻¹⁹	1.5101x10 ⁻⁹	7.0000x10 ⁻¹	2.0000x10 ⁻¹	0.0000	1.0000	1.9358x10 ⁶
35	2.5859x10 ⁻²	3.9330x10 ⁻²¹	4.2460x10 ⁻⁹	7.0000x10 ⁻¹	2.0000x10 ⁻¹	0.0000	1.0000	6.4330x10 ⁶
36	2.7519x10 ⁻²	4.5390x10 ⁻²¹	3.9748x10 ⁻⁹	7.0000x10 ⁻¹	2.0000x10 ⁻¹	0.0000	1.0000	6.1218x10 ⁶
37	4.9770x10 ⁻²	3.1000x10 ⁻²⁰	2.0860x10 ⁻⁹	7.0000x10 ⁻¹	2.0000x10 ⁻¹	0.0000	1.0000	3.1490x10 ⁶
38	4.2030x10 ⁻²	1.5890x10 ⁻²⁰	2.5162x10 ⁻⁹	7.0000x10 ⁻¹	2.0000x10 ⁻¹	0.0000	1.0000	3.9683x10 ⁶
39	3.8123x10 ⁻²	1.1340x10 ⁻²⁰	2.7997x10 ⁻⁹	7.0000x10 ⁻¹	2.0000x10 ⁻¹	0.0000	1.0000	4.4596x10 ⁶
40	6.2212x10 ⁻²	9.0770x10 ⁻²⁰	1.6188x10 ⁻⁹	7.0000x10 ⁻¹	2.0000x10 ⁻¹	0.0000	1.0000	2.1714x10 ⁶
41	6.2879x10 ⁻²	9.6150x10 ⁻²⁰	1.5990x10 ⁻⁹	7.0000x10 ⁻¹	2.0000x10 ⁻¹	0.0000	1.0000	2.1286x10 ⁶
42	5.5614x10 ⁻²	5.1350x10 ⁻²⁰	1.8405x10 ⁻⁹	7.0000x10 ⁻¹	2.0000x10 ⁻¹	0.0000	1.0000	2.6445x10 ⁶
43	3.3383x10 ⁻²	7.5310x10 ⁻²¹	3.2327x10 ⁻⁹	7.0000x10 ⁻¹	2.0000x10 ⁻¹	0.0000	1.0000	5.1380x10 ⁶
44	7.4798x10 ⁻²	2.6910x10 ⁻¹⁹	1.3044x10 ⁻⁹	7.0000x10 ⁻¹	2.0000x10 ⁻¹	0.0000	1.0000	1.4909x10 ⁶
45	6.5132x10 ⁻²	1.1680x10 ⁻¹⁹	1.5350x10 ⁻⁹	7.0000x10 ⁻¹	2.0000x10 ⁻¹	0.0000	1.0000	1.9900x10 ⁶
46	4.5591x10 ⁻²	2.1610x10 ⁻²⁰	2.3001x10 ⁻⁹	7.0000x10 ⁻¹	2.0000x10 ⁻¹	0.0000	1.0000	3.5678x10 ⁶
47	7.6297x10 ⁻²	3.0630x10 ⁻¹⁹	1.2738x10 ⁻⁹	7.0000x10 ⁻¹	2.0000x10 ⁻¹	0.0000	1.0000	1.4256x10 ⁶
48	9.0000x10 ⁻²	1.0000x10 ⁻¹⁸	1.0418x10 ⁻⁹	7.0000x10 ⁻¹	2.0000x10 ⁻¹	0.0000	1.0000	9.4665x10 ⁵
49	7.8712x10 ⁻²	3.7730x10 ⁻¹⁹	1.2271x10 ⁻⁹	7.0000x10 ⁻¹	2.0000x10 ⁻¹	0.0000	1.0000	1.3263x10 ⁶
50	2.2704x10 ⁻²	2.9950x10 ⁻²¹	4.8708x10 ⁻⁹	7.0000x10 ⁻¹	2.0000x10 ⁻¹	0.0000	1.0000	7.0689x10 ⁶
51	2.8140x10 ⁻²	4.7890x10 ⁻²¹	3.8816x10 ⁻⁹	7.0000x10 ⁻¹	2.0000x10 ⁻¹	0.0000	1.0000	6.0093x10 ⁶
52	4.2389x10 ⁻²	1.6390x10 ⁻²⁰	2.4928x10 ⁻⁹	7.0000x10 ⁻¹	2.0000x10 ⁻¹	0.0000	1.0000	3.9259x10 ⁶

Appendix B: BRAGFLO Reference Tables

Table B-2 1992 BRAGFLO Computed Variable Values for SHAFT_SEAL_2 (Concluded)

Run No.	Porosity	Permeability	Compressibility	BCEXP	BCBRSAT	BCGSSAT	BCFLG	BPCPT
53	5.8188x10 ⁻²	6.4130x10 ⁻²⁰	1.7480x10 ⁻⁹	7.0000x10 ⁻¹	2.0000x10 ⁻¹	0.0000	1.0000	2.4488x10 ⁶
54	6.7354x10 ⁻²	1.4150x10 ⁻¹⁹	1.4762x10 ⁻⁹	7.0000x10 ⁻¹	2.0000x10 ⁻¹	0.0000	1.0000	1.8622x10 ⁶
55	3.9083x10 ⁻²	1.2320x10 ⁻²⁰	2.7248x10 ⁻⁹	7.0000x10 ⁻¹	2.0000x10 ⁻¹	0.0000	1.0000	4.3335x10 ⁶
56	6.6469x10 ⁻²	1.3110x10 ⁻¹⁹	1.4991x10 ⁻⁹	7.0000x10 ⁻¹	2.0000x10 ⁻¹	0.0000	1.0000	1.9120x10 ⁶
57	5.3429x10 ⁻²	4.2520x10 ⁻²⁰	1.9260x10 ⁻⁹	7.0000x10 ⁻¹	2.0000x10 ⁻¹	0.0000	1.0000	2.8229x10 ⁶
58	5.4958x10 ⁻²	4.8520x10 ⁻²⁰	1.8655x10 ⁻⁹	7.0000x10 ⁻¹	2.0000x10 ⁻¹	0.0000	1.0000	2.6969x10 ⁶
59	5.2762x10 ⁻²	4.0140x10 ⁻²⁰	1.9535x10 ⁻⁹	7.0000x10 ⁻¹	2.0000x10 ⁻¹	0.0000	1.0000	2.8797x10 ⁶
60	2.9620x10 ⁻²	5.4420x10 ⁻²¹	3.6751x10 ⁻⁹	7.0000x10 ⁻¹	2.0000x10 ⁻¹	0.0000	1.0000	5.7493x10 ⁶
61	4.0430x10 ⁻²	1.3840x10 ⁻²⁰	2.6256x10 ⁻⁹	7.0000x10 ⁻¹	2.0000x10 ⁻¹	0.0000	1.0000	4.1625x10 ⁶
62	4.4173x10 ⁻²	1.9120x10 ⁻²⁰	2.3820x10 ⁻⁹	7.0000x10 ⁻¹	2.0000x10 ⁻¹	0.0000	1.0000	3.7221x10 ⁶
63	5.9404x10 ⁻²	7.1230x10 ⁻²⁰	1.7071x10 ⁻⁹	7.0000x10 ⁻¹	2.0000x10 ⁻¹	0.0000	1.0000	2.3614x10 ⁶
64	3.2463x10 ⁻²	6.9560x10 ⁻²¹	3.3314x10 ⁻⁹	7.0000x10 ⁻¹	2.0000x10 ⁻¹	0.0000	1.0000	5.2812x10 ⁶
65	7.1865x10 ⁻²	2.0890x10 ⁻¹⁹	1.3678x10 ⁻⁹	7.0000x10 ⁻¹	2.0000x10 ⁻¹	0.0000	1.0000	1.6274x10 ⁶
66	4.5003x10 ⁻²	2.0540x10 ⁻²⁰	2.3335x10 ⁻⁹	7.0000x10 ⁻¹	2.0000x10 ⁻¹	0.0000	1.0000	3.6310x10 ⁶
67	3.1590x10 ⁻²	6.4510x10 ⁻²¹	3.4304x10 ⁻⁹	7.0000x10 ⁻¹	2.0000x10 ⁻¹	0.0000	1.0000	5.4207x10 ⁶
68	1.0000x10 ⁻²	1.0000x10 ⁻²¹	1.1376x10 ⁻⁸	7.0000x10 ⁻¹	2.0000x10 ⁻¹	0.0000	1.0000	1.0332x10 ⁷
69	5.1572x10 ⁻²	3.6220x10 ⁻²⁰	2.0044x10 ⁻⁹	7.0000x10 ⁻¹	2.0000x10 ⁻¹	0.0000	1.0000	2.9840x10 ⁶
70	3.7917x10 ⁻²	1.1140x10 ⁻²⁰	2.8162x10 ⁻⁹	7.0000x10 ⁻¹	2.0000x10 ⁻¹	0.0000	1.0000	4.4871x10 ⁶

Table B-2 1992 BRAGFLO Ranks of Computed Variable Values for SHAFT_SEAL_2

Run No.	Porosity	Permeability	Compressibility	BCEXP	BCRSAT	BCGSSAT	BCFLG	BCPCT
1	46.	46.	25.	1.	1.	1.	1.	25.
2	25.	25.	46.	1.	1.	1.	1.	46.
3	20.	20.	51.	1.	1.	1.	1.	51.
4	49.	49.	22.	1.	1.	1.	1.	22.
5	15.	15.	56.	1.	1.	1.	1.	56.
6	33.	33.	38.	1.	1.	1.	1.	38.
7	3.	3.	68.	1.	1.	1.	1.	68.
8	13.	13.	58.	1.	1.	1.	1.	58.
9	69.	69.	2.	1.	1.	1.	1.	2.
10	34.	34.	37.	1.	1.	1.	1.	37.
11	51.	51.	20.	1.	1.	1.	1.	20.
12	45.	45.	26.	1.	1.	1.	1.	26.
13	64.	64.	7.	1.	1.	1.	1.	7.
14	52.	52.	19.	1.	1.	1.	1.	19.
15	36.	36.	35.	1.	1.	1.	1.	35.
16	14.	14.	57.	1.	1.	1.	1.	57.
17	47.	47.	24.	1.	1.	1.	1.	24.
18	68.	68.	3.	1.	1.	1.	1.	3.
19	56.	56.	15.	1.	1.	1.	1.	15.
20	2.	2.	69.	1.	1.	1.	1.	69.
21	31.	31.	40.	1.	1.	1.	1.	40.
22	30.	30.	41.	1.	1.	1.	1.	41.
23	37.	37.	34.	1.	1.	1.	1.	34.
24	61.	61.	10.	1.	1.	1.	1.	10.
25	39.	39.	32.	1.	1.	1.	1.	32.
26	22.	22.	49.	1.	1.	1.	1.	49.
27	53.	53.	18.	1.	1.	1.	1.	18.
28	16.	16.	55.	1.	1.	1.	1.	55.
29	62.	62.	9.	1.	1.	1.	1.	9.
30	32.	32.	39.	1.	1.	1.	1.	39.
31	5.	5.	66.	1.	1.	1.	1.	66.
32	29.	29.	42.	1.	1.	1.	1.	42.
33	42.	42.	29.	1.	1.	1.	1.	29.
34	58.	58.	13.	1.	1.	1.	1.	13.
35	6.	6.	65.	1.	1.	1.	1.	65.
36	7.	7.	64.	1.	1.	1.	1.	64.
37	35.	35.	36.	1.	1.	1.	1.	36.
38	23.	23.	48.	1.	1.	1.	1.	48.
39	18.	18.	53.	1.	1.	1.	1.	53.
40	54.	54.	17.	1.	1.	1.	1.	17.
41	55.	55.	16.	1.	1.	1.	1.	16.
42	44.	44.	27.	1.	1.	1.	1.	27.
43	12.	12.	59.	1.	1.	1.	1.	59.
44	65.	65.	6.	1.	1.	1.	1.	6.
45	57.	57.	14.	1.	1.	1.	1.	14.
46	28.	28.	43.	1.	1.	1.	1.	43.
47	66.	66.	5.	1.	1.	1.	1.	5.
48	70.	70.	1.	1.	1.	1.	1.	1.
49	67.	67.	4.	1.	1.	1.	1.	4.
50	4.	4.	67.	1.	1.	1.	1.	67.
51	8.	8.	63.	1.	1.	1.	1.	63.
52	24.	24.	47.	1.	1.	1.	1.	47.

Appendix B: BRAGFLO Reference Tables

Table B-2 1992 BRAGFLO Ranks of Computed Variable Values for SHAFT_SEAL_2 (Concluded)

<u>Run No.</u>	<u>Porosity</u>	<u>Permeability</u>	<u>Compressibility</u>	<u>BCEXP</u>	<u>BCBRSAT</u>	<u>BCGSSAT</u>	<u>BCFLG</u>	<u>BCPCT</u>
53	48.	48.	23.	1.	1.	1.	1.	23.
54	60.	60.	11.	1.	1.	1.	1.	11.
55	19.	19.	52.	1.	1.	1.	1.	52.
56	59.	59.	12.	1.	1.	1.	1.	12.
57	41.	41.	30.	1.	1.	1.	1.	30.
58	43.	43.	28.	1.	1.	1.	1.	28.
59	40.	40.	31.	1.	1.	1.	1.	31.
60	9.	9.	62.	1.	1.	1.	1.	62.
61	21.	21.	50.	1.	1.	1.	1.	50.
62	26.	26.	45.	1.	1.	1.	1.	45.
63	50.	50.	21.	1.	1.	1.	1.	21.
64	11.	11.	60.	1.	1.	1.	1.	60.
65	63.	63.	8.	1.	1.	1.	1.	8.
66	27.	27.	44.	1.	1.	1.	1.	44.
67	10.	10.	61.	1.	1.	1.	1.	61.
68	1.	1.	70.	1.	1.	1.	1.	70.
69	38.	38.	33.	1.	1.	1.	1.	33.
70	17.	17.	54.	1.	1.	1.	1.	54.

Table B-2 1992 BRAGFLO Computed Variable Values for TRANSITION_ZONE

Run No.	Porosity	Permeability	Compressibility	BCEXP	BCBRSAT	BCGSSAT	BCFLG	BCPCT
1	2.8660x10 ⁻²	1.4125x10 ⁻¹⁸	3.8066x10 ⁻⁹	9.6790	8.7890x10 ⁻²	2.3300x10 ⁻¹	0.0000	8.4002x10 ⁵
2	6.9900x10 ⁻³	1.6982x10 ⁻²⁰	1.6383x10 ⁻⁸	4.9660x10 ⁻¹	1.4570x10 ⁻¹	1.2590x10 ⁻¹	1.0000	3.8780x10 ⁶
3	2.8970x10 ⁻²	9.1201x10 ⁻¹⁹	3.7632x10 ⁻⁹	6.7900x10 ⁻¹	1.8490x10 ⁻¹	2.1660x10 ⁻¹	1.0000	9.7730x10 ⁵
4	5.6130x10 ⁻³	5.0119x10 ⁻²⁰	2.0463x10 ⁻⁸	5.1820	1.7260x10 ⁻¹	1.8900x10 ⁻¹	1.0000	2.6668x10 ⁶
5	2.0560x10 ⁻²	1.1482x10 ⁻²⁰	5.4048x10 ⁻⁹	4.0710x10 ⁻¹	1.9880x10 ⁻¹	1.4590x10 ⁻¹	1.0000	4.4405x10 ⁶
6	1.3750x10 ⁻²	1.5136x10 ⁻²⁰	8.2055x10 ⁻⁹	6.1420	3.3170x10 ⁻¹	4.7930x10 ⁻²	0.0000	4.0356x10 ⁶
7	2.5930x10 ⁻²	1.7783x10 ⁻²⁰	4.2337x10 ⁻⁹	1.0990	3.5430x10 ⁻²	1.6220x10 ⁻¹	0.0000	3.8167x10 ⁶
8	3.1850x10 ⁻³	1.8197x10 ⁻¹⁹	3.6253x10 ⁻⁸	6.4480	3.8660x10 ⁻¹	2.8520x10 ⁻²	1.0000	1.7070x10 ⁶
9	2.7270x10 ⁻²	1.2303x10 ⁻²⁰	4.0134x10 ⁻⁹	4.2610x10 ⁻¹	3.4080x10 ⁻¹	1.8690x10 ⁻¹	1.0000	4.3356x10 ⁶
10	9.6770x10 ⁻³	5.2481x10 ⁻¹⁸	1.1764x10 ⁻⁸	1.5170	7.9000x10 ⁻²	3.4810x10 ⁻¹	1.0000	5.3342x10 ⁵
11	2.5730x10 ⁻³	1.3183x10 ⁻²⁰	4.4936x10 ⁻⁸	5.1250x10 ⁻¹	2.7170x10 ⁻¹	2.0030x10 ⁻¹	0.0000	4.2332x10 ⁶
12	9.8270x10 ⁻³	2.2387x10 ⁻¹⁹	1.1581x10 ⁻⁸	7.4960	1.4100x10 ⁻¹	2.8620x10 ⁻¹	1.0000	1.5889x10 ⁶
13	1.6610x10 ⁻²	4.8978x10 ⁻²⁰	6.7496x10 ⁻⁹	2.2490	3.6500x10 ⁻¹	2.9370x10 ⁻¹	1.0000	2.6881x10 ⁶
14	1.9600x10 ⁻²	1.0000x10 ⁻²⁰	5.6818x10 ⁻⁹	3.0620x10 ⁻¹	8.3660x10 ⁻³	1.7360x10 ⁻¹	1.0000	4.6579x10 ⁶
15	1.1590x10 ⁻³	2.0893x10 ⁻²⁰	1.0006x10 ⁻⁷	4.4620x10 ⁻¹	2.3100x10 ⁻¹	3.8350x10 ⁻¹	0.0000	3.6097x10 ⁶
16	5.8700x10 ⁻³	5.1286x10 ⁻¹⁹	1.9556x10 ⁻⁸	5.3590x10 ⁻¹	3.7890x10 ⁻¹	2.1720x10 ⁻¹	1.0000	1.1927x10 ⁶
17	2.3950x10 ⁻²	5.7544x10 ⁻²⁰	4.6044x10 ⁻⁹	5.9190	1.1130x10 ⁻¹	3.8060x10 ⁻¹	0.0000	2.5423x10 ⁶
18	6.1370x10 ⁻³	6.6069x10 ⁻²⁰	1.8695x10 ⁻⁸	5.8730x10 ⁻¹	2.9470x10 ⁻¹	8.6120x10 ⁻³	0.0000	2.4236x10 ⁶
19	6.2550x10 ⁻³	4.5709x10 ⁻²⁰	1.8337x10 ⁻⁸	2.0050	1.1640x10 ⁻¹	1.6670x10 ⁻¹	1.0000	2.7531x10 ⁶
20	1.7070x10 ⁻²	4.4668x10 ⁻²⁰	6.5609x10 ⁻⁹	6.7090x10 ⁻¹	1.2940x10 ⁻¹	3.2110x10 ⁻¹	1.0000	2.7752x10 ⁶
21	2.3500x10 ⁻²	1.1481x10 ⁻¹⁹	4.6974x10 ⁻⁹	2.2590x10 ⁻¹	1.9770x10 ⁻²	2.2330x10 ⁻¹	0.0000	2.0018x10 ⁶
22	2.6030x10 ⁻²	7.4131x10 ⁻²⁰	4.2165x10 ⁻⁹	1.4340	2.1830x10 ⁻¹	1.8710x10 ⁻²	1.0000	2.3290x10 ⁶
23	2.9920x10 ⁻²	3.5481x10 ⁻²⁰	3.6358x10 ⁻⁹	7.0990	2.3880x10 ⁻¹	4.5230x10 ⁻²	1.0000	3.0053x10 ⁶
24	1.4710x10 ⁻²	6.1660x10 ⁻²⁰	7.6537x10 ⁻⁹	4.3270x10 ⁻¹	6.1270x10 ⁻²	2.6430x10 ⁻¹	1.0000	2.4823x10 ⁶
25	2.4720x10 ⁻²	3.2359x10 ⁻²⁰	4.4532x10 ⁻⁹	2.7610	3.0510x10 ⁻¹	9.9900x10 ⁻²	1.0000	3.1026x10 ⁶
26	1.8820x10 ⁻²	2.3988x10 ⁻²⁰	5.9276x10 ⁻⁹	5.2660	2.4700x10 ⁻¹	6.8060x10 ⁻²	1.0000	3.4412x10 ⁶
27	2.2740x10 ⁻³	2.1878x10 ⁻²⁰	5.0877x10 ⁻⁸	8.3330	2.1280x10 ⁻¹	7.5730x10 ⁻²	1.0000	3.5526x10 ⁶
28	2.8830x10 ⁻³	1.9499x10 ⁻²⁰	4.0077x10 ⁻⁸	7.9460	3.4740x10 ⁻¹	1.5270x10 ⁻¹	0.0000	3.6970x10 ⁶
29	1.2680x10 ⁻²	3.0903x10 ⁻²⁰	8.9190x10 ⁻⁹	6.0410x10 ⁻¹	3.3040x10 ⁻¹	3.5780x10 ⁻¹	1.0000	3.1525x10 ⁶
30	8.7910x10 ⁻³	7.4131x10 ⁻²⁰	1.2975x10 ⁻⁸	2.0040x10 ⁻¹	1.4050x10 ⁻²	1.5530x10 ⁻¹	0.0000	2.3290x10 ⁶
31	1.7650x10 ⁻²	3.2359x10 ⁻²¹	6.3371x10 ⁻⁹	3.3160x10 ⁻¹	2.1130x10 ⁻¹	2.4050x10 ⁻¹	1.0000	6.8822x10 ⁶
32	2.0930x10 ⁻²	1.0471x10 ⁻²⁰	5.3048x10 ⁻⁹	8.8800	3.1430x10 ⁻¹	3.7550x10 ⁻¹	1.0000	4.5842x10 ⁶
33	6.6640x10 ⁻³	4.6774x10 ⁻¹⁹	1.7196x10 ⁻⁸	5.2200x10 ⁻¹	1.0530x10 ⁻¹	3.4190x10 ⁻¹	1.0000	1.2313x10 ⁶
34	9.1030x10 ⁻³	1.2303x10 ⁻²⁰	1.2522x10 ⁻⁸	8.6520	2.5150x10 ⁻¹	3.6280x10 ⁻¹	0.0000	4.3356x10 ⁶
35	2.4230x10 ⁻³	2.8184x10 ⁻²⁰	4.7733x10 ⁻⁸	3.9470x10 ⁻¹	2.9070x10 ⁻¹	1.3390x10 ⁻¹	1.0000	3.2545x10 ⁶
36	2.7120x10 ⁻²	1.9953x10 ⁻²⁰	4.0370x10 ⁻⁹	2.7500x10 ⁻¹	3.7090x10 ⁻¹	3.6960x10 ⁻¹	1.0000	3.6677x10 ⁶
37	5.0960x10 ⁻³	2.5704x10 ⁻²⁰	2.2564x10 ⁻⁸	6.9780	2.2650x10 ⁻¹	3.0790x10 ⁻²	1.0000	3.3599x10 ⁶
38	1.8940x10 ⁻³	1.5136x10 ⁻¹⁹	6.1135x10 ⁻⁸	2.9640	1.7810x10 ⁻¹	3.9620x10 ⁻¹	1.0000	1.8193x10 ⁶
39	1.0090x10 ⁻²	5.6234x10 ⁻²⁰	1.1273x10 ⁻⁸	2.6060x10 ⁻¹	1.6330x10 ⁻¹	3.7240x10 ⁻²	1.0000	2.5626x10 ⁶
40	2.2760x10 ⁻²	2.0893x10 ⁻¹⁹	4.8582x10 ⁻⁹	2.4160x10 ⁻¹	2.4340x10 ⁻¹	1.1100x10 ⁻¹	1.0000	1.6273x10 ⁶
41	1.8020x10 ⁻²	3.9811x10 ⁻¹⁹	6.2019x10 ⁻⁹	5.7490x10 ⁻¹	1.3340x10 ⁻¹	1.0650x10 ⁻¹	1.0000	1.3019x10 ⁶
42	2.1990x10 ⁻²	2.3442x10 ⁻²¹	5.0371x10 ⁻⁹	5.4840x10 ⁻¹	3.9640x10 ⁻¹	3.3500x10 ⁻¹	0.0000	7.6943x10 ⁶
43	5.1790x10 ⁻³	2.6915x10 ⁻¹⁹	2.2199x10 ⁻⁸	4.0000	3.9070x10 ⁻¹	1.2040x10 ⁻¹	0.0000	1.4908x10 ⁶
44	3.9010x10 ⁻³	5.3703x10 ⁻²⁰	2.9553x10 ⁻⁸	3.6050x10 ⁻¹	2.5980x10 ⁻¹	5.7350x10 ⁻²	0.0000	2.6038x10 ⁶
45	9.3870x10 ⁻³	9.7724x10 ⁻²⁰	1.2135x10 ⁻⁸	3.2390x10 ⁻¹	1.5830x10 ⁻¹	9.4190x10 ⁻²	1.0000	2.1166x10 ⁶
46	2.8280x10 ⁻²	1.6596x10 ⁻²⁰	3.8611x10 ⁻⁹	4.6060x10 ⁻¹	6.5170x10 ⁻²	2.3880x10 ⁻¹	1.0000	3.9090x10 ⁶
47	6.5700x10 ⁻³	9.1201x10 ⁻²⁰	1.7446x10 ⁻⁸	3.4760	3.1780x10 ⁻¹	2.6060x10 ⁻¹	1.0000	2.1678x10 ⁶
48	2.2390x10 ⁻²	1.4125x10 ⁻²⁰	4.9426x10 ⁻⁹	7.7080	4.5510x10 ⁻²	2.0750x10 ⁻¹	0.0000	4.1332x10 ⁶
49	1.6820x10 ⁻³	6.9183x10 ⁻¹⁹	6.8872x10 ⁻⁸	3.7530x10 ⁻¹	5.0110x10 ⁻²	6.9900x10 ⁻²	1.0000	1.0753x10 ⁶
50	1.2890x10 ⁻²	2.4547x10 ⁻²⁰	8.7696x10 ⁻⁹	3.5390x10 ⁻¹	1.8990x10 ⁻¹	1.9850x10 ⁻¹	1.0000	3.4139x10 ⁶
51	7.8440x10 ⁻³	4.0738x10 ⁻¹⁷	1.4572x10 ⁻⁸	5.6000x10 ⁻¹	2.3180x10 ⁻²	1.1810x10 ⁻²	1.0000	2.6250x10 ⁵
52	4.7130x10 ⁻³	8.7097x10 ⁻²⁰	2.4418x10 ⁻⁸	3.2370	1.5040x10 ⁻¹	3.8860x10 ⁻¹	0.0000	2.2027x10 ⁶

Appendix B: BRAGFLO Reference Tables

Table B-2 1992 BRAGFLO Computed Variable Values for TRANSITION_ZONE (Concluded)

Run No.	Porosity	Permeability	Compressibility	BCEXP	BCBR SAT	BCGSSAT	BCFLG	BCPCT
53	1.5900x10 ⁻²	7.7625x10 ⁻¹⁹	7.0621x10 ⁻⁹	6.7410	2.8470x10 ⁻¹	1.8060x10 ⁻¹	1.0000	1.0334x10 ⁶
54	1.4500x10 ⁻²	1.4454x10 ⁻²⁰	7.7681x10 ⁻⁹	4.7200x10 ⁻¹	1.6590x10 ⁻¹	2.7290x10 ⁻¹	0.0000	4.1004x10 ⁶
55	2.0030x10 ⁻²	1.0233x10 ⁻¹⁷	5.5544x10 ⁻⁹	6.5030x10 ⁻¹	3.2450x10 ⁻¹	3.0330x10 ⁻¹	0.0000	4.2338x10 ⁵
56	1.1650x10 ⁻²	1.0965x10 ⁻²⁰	9.7296x10 ⁻⁹	4.8480	9.2770x10 ⁻²	5.2210x10 ⁻²	0.0000	4.5118x10 ⁶
57	4.5630x10 ⁻³	5.2481x10 ⁻²¹	2.5229x10 ⁻⁸	9.2110	5.1160x10 ⁻³	2.7770x10 ⁻¹	1.0000	5.8219x10 ⁶
58	8.7110x10 ⁻³	3.3884x10 ⁻¹⁹	1.3097x10 ⁻⁸	6.4060x10 ⁻¹	3.4880x10 ⁻¹	3.2980x10 ⁻¹	1.0000	1.3766x10 ⁶
59	2.5160x10 ⁻²	7.9433x10 ⁻²⁰	4.3709x10 ⁻⁹	8.9580	8.5120x10 ⁻²	3.1270x10 ⁻¹	1.0000	2.2740x10 ⁶
60	8.2600x10 ⁻³	9.5499x10 ⁻²⁰	1.3825x10 ⁻⁸	9.8620	7.0380x10 ⁻²	8.1940x10 ⁻²	1.0000	2.1336x10 ⁶
61	7.3840x10 ⁻³	4.1687x10 ⁻²⁰	1.5495x10 ⁻⁸	8.0490x10 ⁻¹	2.7910x10 ⁻¹	1.3890x10 ⁻¹	1.0000	2.8423x10 ⁶
62	1.2250x10 ⁻²	5.4954x10 ⁻¹⁹	9.2408x10 ⁻⁹	2.8630x10 ⁻¹	3.5990x10 ⁻¹	2.5120x10 ⁻¹	1.0000	1.1645x10 ⁶
63	4.1090x10 ⁻³	9.5499x10 ⁻¹⁷	2.8045x10 ⁻⁸	3.7540	2.0010x10 ⁻¹	2.8360x10 ⁻¹	0.0000	1.9548x10 ⁵
64	3.7390x10 ⁻³	2.6915x10 ⁻²⁰	3.0845x10 ⁻⁸	2.4950	2.9320x10 ⁻²	8.7020x10 ⁻²	1.0000	3.3068x10 ⁶
65	7.4700x10 ⁻³	3.7153x10 ⁻²⁰	1.5314x10 ⁻⁸	2.5410x10 ⁻¹	2.6410x10 ⁻¹	3.5100x10 ⁻¹	1.0000	2.9578x10 ⁶
66	3.5330x10 ⁻³	3.9811x10 ⁻²⁰	3.2658x10 ⁻⁸	6.9150x10 ⁻¹	1.2380x10 ⁻¹	3.1630x10 ⁻¹	0.0000	2.8879x10 ⁶
67	8.1910x10 ⁻³	1.3804x10 ⁻¹⁹	1.3944x10 ⁻⁸	5.5890	5.6350x10 ⁻²	2.5370x10 ⁻¹	0.0000	1.8782x10 ⁶
68	1.0760x10 ⁻²	6.7608x10 ⁻²⁰	1.0555x10 ⁻⁸	4.5200	3.0240x10 ⁻¹	2.9970x10 ⁻¹	0.0000	2.4044x10 ⁶
69	1.5190x10 ⁻²	3.3113x10 ⁻²⁰	7.4039x10 ⁻⁹	4.3270	3.7150x10 ⁻¹	4.8390x10 ⁻³	1.0000	3.0780x10 ⁶
70	1.4890x10 ⁻³	1.3490x10 ⁻²¹	7.7831x10 ⁻⁸	6.2770x10 ⁻¹	1.0130x10 ⁻¹	1.1920x10 ⁻¹	1.0000	9.3155x10 ⁶

Table B-2 1992 BRAGFLO Ranks of Computed Variable Values for TRANSITION_ZONE

Run No.	Porosity	Permeability	Compressibility	BCEXP	BCBRSAT	BCGSSAT	BCFLG	BCPCT
1	68.	66.	3.	69.	16.	41.	1.	5.
2	24.	16.	47.	21.	26.	23.	24.	55.
3	69.	65.	2.	34.	33.	38.	24.	6.
4	18.	37.	53.	52.	31.	34.	24.	34.
5	54.	8.	17.	15.	35.	26.	24.	63.
6	42.	14.	29.	56.	59.	9.	1.	57.
7	63.	17.	8.	37.	7.	29.	1.	54.
8	9.	54.	62.	57.	68.	5.	24.	17.
9	66.	9.	5.	16.	60.	33.	24.	61.
10	34.	67.	37.	39.	14.	61.	24.	4.
11	7.	11.	64.	22.	48.	36.	1.	60.
12	35.	56.	36.	61.	25.	51.	24.	15.
13	47.	36.	24.	41.	64.	52.	24.	35.
14	52.	5.	19.	8.	2.	31.	24.	66.
15	1.	20.	70.	18.	41.	68.	1.	51.
16	19.	61.	52.	24.	67.	39.	24.	10.
17	60.	40.	11.	55.	20.	67.	1.	31.
18	20.	42.	51.	28.	52.	2.	1.	29.
19	21.	35.	50.	40.	21.	30.	24.	36.
20	48.	34.	23.	33.	23.	57.	24.	37.
21	59.	51.	12.	2.	4.	40.	1.	20.
22	64.	44.	7.	38.	39.	4.	24.	26.
23	70.	30.	1.	60.	42.	8.	24.	41.
24	44.	41.	27.	17.	11.	47.	24.	30.
25	61.	28.	10.	43.	54.	18.	24.	43.
26	51.	22.	20.	53.	44.	12.	24.	49.
27	5.	21.	66.	64.	38.	14.	24.	50.
28	8.	18.	63.	63.	61.	27.	1.	53.
29	40.	27.	31.	29.	58.	63.	24.	44.
30	31.	44.	40.	1.	3.	28.	1.	26.
31	49.	3.	22.	10.	37.	43.	24.	68.
32	55.	6.	16.	66.	55.	66.	24.	65.
33	23.	60.	48.	23.	19.	60.	24.	11.
34	32.	9.	39.	65.	45.	64.	1.	61.
35	6.	26.	65.	14.	51.	24.	24.	45.
36	65.	19.	6.	6.	65.	65.	24.	52.
37	16.	24.	55.	59.	40.	6.	24.	47.
38	4.	53.	67.	44.	32.	70.	24.	18.
39	36.	39.	35.	5.	29.	7.	24.	32.
40	58.	55.	13.	3.	43.	20.	24.	16.
41	50.	59.	21.	27.	24.	19.	24.	12.
42	56.	2.	15.	25.	70.	59.	1.	69.
43	17.	57.	54.	48.	69.	22.	1.	14.
44	12.	38.	59.	12.	46.	11.	1.	33.
45	33.	50.	38.	9.	28.	17.	24.	21.
46	67.	15.	4.	19.	12.	42.	24.	56.
47	22.	48.	49.	46.	56.	46.	24.	23.
48	57.	12.	14.	62.	8.	37.	1.	59.
49	3.	63.	68.	13.	9.	13.	24.	8.
50	41.	23.	30.	11.	34.	35.	24.	48.
51	27.	69.	44.	26.	5.	3.	24.	2.
52	15.	47.	56.	45.	27.	69.	1.	24.

Appendix B: BRAGFLO Reference Tables

Table B-2 1992 BRAGFLO Ranks of Computed Variable Values for TRANSITION_ZONE (Concluded)

Run No.	Porosity	Permeability	Compressibility	BCEXP	BCBRSAT	BCGSSAT	BCFLG	BCPCT
53	46.	64.	25.	58.	50.	32.	24.	7.
54	43.	13.	28.	20.	30.	48.	1.	58.
55	53.	68.	18.	32.	57.	54.	1.	3.
56	38.	7.	33.	51.	17.	10.	1.	64.
57	14.	4.	57.	68.	1.	49.	24.	67.
58	30.	58.	41.	31.	62.	58.	24.	13.
59	62.	46.	9.	67.	15.	55.	24.	25.
60	29.	49.	42.	70.	13.	15.	24.	22.
61	25.	33.	46.	36.	49.	25.	24.	38.
62	39.	62.	32.	7.	63.	44.	24.	9.
63	13.	70.	58.	47.	36.	50.	1.	1.
64	11.	25.	60.	42.	6.	16.	24.	46.
65	26.	31.	45.	4.	47.	62.	24.	40.
66	10.	32.	61.	35.	22.	56.	1.	39.
67	28.	52.	43.	54.	10.	45.	1.	19.
68	37.	43.	34.	50.	53.	53.	1.	28.
69	45.	29.	26.	49.	66.	1.	24.	42.
70	2.	1.	69.	30.	18.	21.	24.	70.

Table B-2 1992 BRAGFLO Computed Variable Values for UPPER_SHAFT

Run No.	Porosity	Permeability	Compressibility	BCEXP	BCBRSAT	BCGSSAT	BCFLG	BCPCT
1	5.6433x10 ⁻²	2.8110x10 ⁻¹⁹	1.8102x10 ⁻⁹	7.0000x10 ⁻¹	2.0000x10 ⁻¹	0.0000	1.0000	1.4685x10 ⁶
2	4.3305x10 ⁻²	5.6030x10 ⁻¹⁸	2.4347x10 ⁻⁹	7.0000x10 ⁻¹	2.0000x10 ⁻¹	0.0000	1.0000	5.2148x10 ⁵
3	4.0073x10 ⁻²	7.1940x10 ⁻¹⁸	2.6512x10 ⁻⁹	7.0000x10 ⁻¹	2.0000x10 ⁻¹	0.0000	1.0000	4.7827x10 ⁵
4	5.8422x10 ⁻²	5.6960x10 ⁻¹⁹	1.7400x10 ⁻⁹	7.0000x10 ⁻¹	2.0000x10 ⁻¹	0.0000	1.0000	1.1502x10 ⁶
5	3.5889x10 ⁻²	4.5850x10 ⁻¹⁹	2.9895x10 ⁻⁹	7.0000x10 ⁻¹	2.0000x10 ⁻¹	0.0000	1.0000	1.2398x10 ⁶
6	4.8739x10 ⁻²	1.6410x10 ⁻¹⁷	2.1354x10 ⁻⁹	7.0000x10 ⁻¹	2.0000x10 ⁻¹	0.0000	1.0000	3.5955x10 ⁵
7	1.8565x10 ⁻²	4.5900x10 ⁻¹⁷	6.0125x10 ⁻⁹	7.0000x10 ⁻¹	2.0000x10 ⁻¹	0.0000	1.0000	2.5188x10 ⁵
8	3.3804x10 ⁻²	1.4360x10 ⁻¹⁷	3.1893x10 ⁻⁹	7.0000x10 ⁻¹	2.0000x10 ⁻¹	0.0000	1.0000	3.7654x10 ⁵
9	8.2847x10 ⁻²	9.5250x10 ⁻¹⁷	1.1533x10 ⁻⁹	7.0000x10 ⁻¹	2.0000x10 ⁻¹	0.0000	1.0000	1.9566x10 ⁵
10	4.8961x10 ⁻²	1.4640x10 ⁻¹⁶	2.1246x10 ⁻⁹	7.0000x10 ⁻¹	2.0000x10 ⁻¹	0.0000	1.0000	1.6862x10 ⁵
11	6.0343x10 ⁻²	1.9920x10 ⁻¹⁸	1.6767x10 ⁻⁹	7.0000x10 ⁻¹	2.0000x10 ⁻¹	0.0000	1.0000	7.4582x10 ⁵
12	5.5800x10 ⁻²	3.9570x10 ⁻¹⁸	1.8336x10 ⁻⁹	7.0000x10 ⁻¹	2.0000x10 ⁻¹	0.0000	1.0000	5.8817x10 ⁵
13	7.2964x10 ⁻²	2.2680x10 ⁻¹⁹	1.3434x10 ⁻⁹	7.0000x10 ⁻¹	2.0000x10 ⁻¹	0.0000	1.0000	1.5817x10 ⁶
14	6.0840x10 ⁻²	1.4270x10 ⁻¹⁷	1.6610x10 ⁻⁹	7.0000x10 ⁻¹	2.0000x10 ⁻¹	0.0000	1.0000	3.7736x10 ⁵
15	5.0585x10 ⁻²	1.0660x10 ⁻¹⁷	2.0484x10 ⁻⁹	7.0000x10 ⁻¹	2.0000x10 ⁻¹	0.0000	1.0000	4.1743x10 ⁵
16	3.5074x10 ⁻²	1.6750x10 ⁻¹⁸	3.0648x10 ⁻⁹	7.0000x10 ⁻¹	2.0000x10 ⁻¹	0.0000	1.0000	7.9192x10 ⁵
17	5.7146x10 ⁻²	1.7580x10 ⁻¹⁸	1.7845x10 ⁻⁹	7.0000x10 ⁻¹	2.0000x10 ⁻¹	0.0000	1.0000	7.7877x10 ⁵
18	8.2074x10 ⁻²	1.6710x10 ⁻¹⁶	1.1666x10 ⁻⁹	7.0000x10 ⁻¹	2.0000x10 ⁻¹	0.0000	1.0000	1.6108x10 ⁵
19	6.3721x10 ⁻²	1.9530x10 ⁻¹⁷	1.5746x10 ⁻⁹	7.0000x10 ⁻¹	2.0000x10 ⁻¹	0.0000	1.0000	3.3854x10 ⁵
20	1.6736x10 ⁻²	3.4450x10 ⁻¹⁸	6.6967x10 ⁻⁹	7.0000x10 ⁻¹	2.0000x10 ⁻¹	0.0000	1.0000	6.1705x10 ⁵
21	4.7082x10 ⁻²	1.1130x10 ⁻¹⁸	2.2194x10 ⁻⁹	7.0000x10 ⁻¹	2.0000x10 ⁻¹	0.0000	1.0000	9.1222x10 ⁵
22	4.6655x10 ⁻²	1.7830x10 ⁻¹⁷	2.2420x10 ⁻⁹	7.0000x10 ⁻¹	2.0000x10 ⁻¹	0.0000	1.0000	3.4937x10 ⁵
23	5.0975x10 ⁻²	8.0220x10 ⁻¹⁷	2.0308x10 ⁻⁹	7.0000x10 ⁻¹	2.0000x10 ⁻¹	0.0000	1.0000	2.0764x10 ⁵
24	6.8520x10 ⁻²	8.1030x10 ⁻¹⁸	1.4468x10 ⁻⁹	7.0000x10 ⁻¹	2.0000x10 ⁻¹	0.0000	1.0000	4.5898x10 ⁵
25	5.1999x10 ⁻²	6.1670x10 ⁻¹⁸	1.9859x10 ⁻⁹	7.0000x10 ⁻¹	2.0000x10 ⁻¹	0.0000	1.0000	5.0446x10 ⁵
26	4.1033x10 ⁻²	2.2930x10 ⁻¹⁸	2.5834x10 ⁻⁹	7.0000x10 ⁻¹	2.0000x10 ⁻¹	0.0000	1.0000	7.1038x10 ⁵
27	6.1762x10 ⁻²	9.1500x10 ⁻¹⁸	1.6324x10 ⁻⁹	7.0000x10 ⁻¹	2.0000x10 ⁻¹	0.0000	1.0000	4.4009x10 ⁵
28	3.7132x10 ⁻²	1.0160x10 ⁻¹⁸	2.8811x10 ⁻⁹	7.0000x10 ⁻¹	2.0000x10 ⁻¹	0.0000	1.0000	9.4146x10 ⁵
29	6.9933x10 ⁻²	7.3210x10 ⁻¹⁹	1.4125x10 ⁻⁹	7.0000x10 ⁻¹	2.0000x10 ⁻¹	0.0000	1.0000	1.0545x10 ⁶
30	4.7777x10 ⁻²	2.1720x10 ⁻¹⁷	2.1834x10 ⁻⁹	7.0000x10 ⁻¹	2.0000x10 ⁻¹	0.0000	1.0000	3.2631x10 ⁵
31	2.2998x10 ⁻²	1.0000x10 ⁻¹⁵	4.8054x10 ⁻⁹	7.0000x10 ⁻¹	2.0000x10 ⁻¹	0.0000	1.0000	8.6734x10 ⁴
32	4.5772x10 ⁻²	4.2740x10 ⁻¹⁷	2.2901x10 ⁻⁹	7.0000x10 ⁻¹	2.0000x10 ⁻¹	0.0000	1.0000	2.5818x10 ⁵
33	5.3975x10 ⁻²	3.6810x10 ⁻¹⁸	1.9040x10 ⁻⁹	7.0000x10 ⁻¹	2.0000x10 ⁻¹	0.0000	1.0000	6.0306x10 ⁵
34	6.6056x10 ⁻²	1.2150x10 ⁻¹⁷	1.5101x10 ⁻⁹	7.0000x10 ⁻¹	2.0000x10 ⁻¹	0.0000	1.0000	3.9896x10 ⁵
35	2.5859x10 ⁻²	3.0210x10 ⁻¹⁷	4.2460x10 ⁻⁹	7.0000x10 ⁻¹	2.0000x10 ⁻¹	0.0000	1.0000	2.9111x10 ⁵
36	2.7519x10 ⁻²	5.8240x10 ⁻¹⁸	3.9748x10 ⁻⁹	7.0000x10 ⁻¹	2.0000x10 ⁻¹	0.0000	1.0000	5.1454x10 ⁵
37	4.9770x10 ⁻²	8.0100x10 ⁻¹⁹	2.0860x10 ⁻⁹	7.0000x10 ⁻¹	2.0000x10 ⁻¹	0.0000	1.0000	1.0222x10 ⁶
38	4.2030x10 ⁻²	1.1200x10 ⁻¹⁶	2.5162x10 ⁻⁹	7.0000x10 ⁻¹	2.0000x10 ⁻¹	0.0000	1.0000	1.8499x10 ⁵
39	3.8123x10 ⁻²	3.8250x10 ⁻¹⁹	2.7997x10 ⁻⁹	7.0000x10 ⁻¹	2.0000x10 ⁻¹	0.0000	1.0000	1.3201x10 ⁶
40	6.2212x10 ⁻²	4.8060x10 ⁻¹⁷	1.6188x10 ⁻⁹	7.0000x10 ⁻¹	2.0000x10 ⁻¹	0.0000	1.0000	2.4791x10 ⁵
41	6.2879x10 ⁻²	6.2130x10 ⁻¹⁷	1.5990x10 ⁻⁹	7.0000x10 ⁻¹	2.0000x10 ⁻¹	0.0000	1.0000	2.2683x10 ⁵
42	5.5614x10 ⁻²	5.3950x10 ⁻¹⁷	1.8405x10 ⁻⁹	7.0000x10 ⁻¹	2.0000x10 ⁻¹	0.0000	1.0000	2.3819x10 ⁵
43	3.3383x10 ⁻²	4.7020x10 ⁻¹⁸	3.2327x10 ⁻⁹	7.0000x10 ⁻¹	2.0000x10 ⁻¹	0.0000	1.0000	5.5409x10 ⁵
44	7.4798x10 ⁻²	1.7210x10 ⁻¹⁷	1.3044x10 ⁻⁹	7.0000x10 ⁻¹	2.0000x10 ⁻¹	0.0000	1.0000	3.5368x10 ⁵
45	6.5132x10 ⁻²	9.7080x10 ⁻¹⁸	1.5350x10 ⁻⁹	7.0000x10 ⁻¹	2.0000x10 ⁻¹	0.0000	1.0000	4.3116x10 ⁵
46	4.5591x10 ⁻²	2.4720x10 ⁻¹⁷	2.3001x10 ⁻⁹	7.0000x10 ⁻¹	2.0000x10 ⁻¹	0.0000	1.0000	3.1203x10 ⁵
47	7.6297x10 ⁻²	3.0790x10 ⁻¹⁷	1.2738x10 ⁻⁹	7.0000x10 ⁻¹	2.0000x10 ⁻¹	0.0000	1.0000	2.8920x10 ⁵
48	9.0000x10 ⁻²	6.8540x10 ⁻¹⁸	1.0418x10 ⁻⁹	7.0000x10 ⁻¹	2.0000x10 ⁻¹	0.0000	1.0000	4.8635x10 ⁵
49	7.8712x10 ⁻²	1.4730x10 ⁻¹⁸	1.2271x10 ⁻⁹	7.0000x10 ⁻¹	2.0000x10 ⁻¹	0.0000	1.0000	8.2792x10 ⁵
50	2.2704x10 ⁻²	7.9550x10 ⁻¹⁸	4.8708x10 ⁻⁹	7.0000x10 ⁻¹	2.0000x10 ⁻¹	0.0000	1.0000	4.6192x10 ⁵
51	2.8140x10 ⁻²	4.1850x10 ⁻¹⁸	3.8816x10 ⁻⁹	7.0000x10 ⁻¹	2.0000x10 ⁻¹	0.0000	1.0000	5.7687x10 ⁵
52	4.2389x10 ⁻²	5.9300x10 ⁻¹⁶	2.4928x10 ⁻⁹	7.0000x10 ⁻¹	2.0000x10 ⁻¹	0.0000	1.0000	1.0392x10 ⁵

Appendix B: BRAGFLO Reference Tables

Table B-2 1992 BRAGFLO Computed Variable Values for UPPER_SHAFT (Concluded)

Run No.	Porosity	Permeability	Compressibility	BCEXP	BCBRSAT	BCGSSAT	BCFLG	BCPCT
53	5.8188x10 ⁻²	2.6650x10 ⁻¹⁷	1.7480x10 ⁻⁹	7.0000x10 ⁻¹	2.0000x10 ⁻¹	0.0000	1.0000	3.0402x10 ⁵
54	6.7354x10 ⁻²	2.3110x10 ⁻¹⁸	1.4762x10 ⁻⁹	7.0000x10 ⁻¹	2.0000x10 ⁻¹	0.0000	1.0000	7.0846x10 ⁵
55	3.9083x10 ⁻²	1.1210x10 ⁻¹⁷	2.7248x10 ⁻⁹	7.0000x10 ⁻¹	2.0000x10 ⁻¹	0.0000	1.0000	4.1023x10 ⁵
56	6.6469x10 ⁻²	1.3450x10 ⁻¹⁸	1.4991x10 ⁻⁹	7.0000x10 ⁻¹	2.0000x10 ⁻¹	0.0000	1.0000	8.5438x10 ⁵
57	5.3429x10 ⁻²	1.8690x10 ⁻¹⁶	1.9260x10 ⁻⁹	7.0000x10 ⁻¹	2.0000x10 ⁻¹	0.0000	1.0000	1.5496x10 ⁵
58	5.4958x10 ⁻²	3.5380x10 ⁻¹⁷	1.8655x10 ⁻⁹	7.0000x10 ⁻¹	2.0000x10 ⁻¹	0.0000	1.0000	2.7562x10 ⁵
59	5.2762x10 ⁻²	1.2070x10 ⁻¹⁹	1.9535x10 ⁻⁹	7.0000x10 ⁻¹	2.0000x10 ⁻¹	0.0000	1.0000	1.9675x10 ⁶
60	2.9620x10 ⁻²	2.3520x10 ⁻¹⁷	3.6751x10 ⁻⁹	7.0000x10 ⁻¹	2.0000x10 ⁻¹	0.0000	1.0000	3.1745x10 ⁵
61	4.0430x10 ⁻²	9.2530x10 ⁻¹⁷	2.6256x10 ⁻⁹	7.0000x10 ⁻¹	2.0000x10 ⁻¹	0.0000	1.0000	1.9763x10 ⁵
62	4.4173x10 ⁻²	5.1730x10 ⁻¹⁸	2.3820x10 ⁻⁹	7.0000x10 ⁻¹	2.0000x10 ⁻¹	0.0000	1.0000	5.3608x10 ⁵
63	5.9404x10 ⁻²	2.7290x10 ⁻¹⁶	1.7071x10 ⁻⁹	7.0000x10 ⁻¹	2.0000x10 ⁻¹	0.0000	1.0000	1.3594x10 ⁵
64	3.2463x10 ⁻²	3.8080x10 ⁻¹⁷	3.3314x10 ⁻⁹	7.0000x10 ⁻¹	2.0000x10 ⁻¹	0.0000	1.0000	2.6870x10 ⁵
65	7.1865x10 ⁻²	1.3080x10 ⁻¹⁷	1.3678x10 ⁻⁹	7.0000x10 ⁻¹	2.0000x10 ⁻¹	0.0000	1.0000	3.8890x10 ⁵
66	4.5003x10 ⁻²	3.0810x10 ⁻¹⁸	2.3335x10 ⁻⁹	7.0000x10 ⁻¹	2.0000x10 ⁻¹	0.0000	1.0000	6.4136x10 ⁵
67	3.1590x10 ⁻²	4.1580x10 ⁻¹⁶	3.4304x10 ⁻⁹	7.0000x10 ⁻¹	2.0000x10 ⁻¹	0.0000	1.0000	1.1750x10 ⁵
68	1.0000x10 ⁻²	2.8300x10 ⁻¹⁸	1.1376x10 ⁻⁸	7.0000x10 ⁻¹	2.0000x10 ⁻¹	0.0000	1.0000	6.6050x10 ⁵
69	5.1572x10 ⁻²	6.6500x10 ⁻¹⁷	2.0044x10 ⁻⁹	7.0000x10 ⁻¹	2.0000x10 ⁻¹	0.0000	1.0000	2.2156x10 ⁵
70	3.7917x10 ⁻²	2.6470x10 ⁻¹⁸	2.8162x10 ⁻⁹	7.0000x10 ⁻¹	2.0000x10 ⁻¹	0.0000	1.0000	6.7595x10 ⁵

Table B-2 1992 BRAGFLO Ranks of Computed Variable Values for UPPER_SHAFT

Run No.	Porosity	Permeability	Compressibility	BCEXP	BCBRSAT	BCGSSAT	BCFLG	BCPCT
1	46.	3.	25.	1.	1.	1.	1.	68.
2	25.	27.	46.	1.	1.	1.	1.	44.
3	20.	31.	51.	1.	1.	1.	1.	40.
4	49.	6.	22.	1.	1.	1.	1.	65.
5	15.	5.	56.	1.	1.	1.	1.	66.
6	33.	42.	38.	1.	1.	1.	1.	29.
7	3.	55.	68.	1.	1.	1.	1.	16.
8	13.	41.	58.	1.	1.	1.	1.	30.
9	69.	62.	2.	1.	1.	1.	1.	9.
10	34.	64.	37.	1.	1.	1.	1.	7.
11	51.	15.	20.	1.	1.	1.	1.	56.
12	45.	23.	26.	1.	1.	1.	1.	48.
13	64.	2.	7.	1.	1.	1.	1.	69.
14	52.	40.	19.	1.	1.	1.	1.	31.
15	36.	36.	35.	1.	1.	1.	1.	35.
16	14.	13.	57.	1.	1.	1.	1.	58.
17	47.	14.	24.	1.	1.	1.	1.	57.
18	68.	65.	3.	1.	1.	1.	1.	6.
19	56.	45.	15.	1.	1.	1.	1.	26.
20	2.	21.	69.	1.	1.	1.	1.	50.
21	31.	10.	40.	1.	1.	1.	1.	61.
22	30.	44.	41.	1.	1.	1.	1.	27.
23	37.	60.	34.	1.	1.	1.	1.	11.
24	61.	33.	10.	1.	1.	1.	1.	38.
25	39.	29.	32.	1.	1.	1.	1.	42.
26	22.	16.	49.	1.	1.	1.	1.	55.
27	53.	34.	18.	1.	1.	1.	1.	37.
28	16.	9.	55.	1.	1.	1.	1.	62.
29	62.	7.	9.	1.	1.	1.	1.	64.
30	32.	46.	39.	1.	1.	1.	1.	25.
31	5.	70.	66.	1.	1.	1.	1.	1.
32	29.	54.	42.	1.	1.	1.	1.	17.
33	42.	22.	29.	1.	1.	1.	1.	49.
34	58.	38.	13.	1.	1.	1.	1.	33.
35	6.	50.	65.	1.	1.	1.	1.	21.
36	7.	28.	64.	1.	1.	1.	1.	43.
37	35.	8.	36.	1.	1.	1.	1.	63.
38	23.	63.	48.	1.	1.	1.	1.	8.
39	18.	4.	53.	1.	1.	1.	1.	67.
40	54.	56.	17.	1.	1.	1.	1.	15.
41	55.	58.	16.	1.	1.	1.	1.	13.
42	44.	57.	27.	1.	1.	1.	1.	14.
43	12.	25.	59.	1.	1.	1.	1.	46.
44	65.	43.	6.	1.	1.	1.	1.	28.
45	57.	35.	14.	1.	1.	1.	1.	36.
46	28.	48.	43.	1.	1.	1.	1.	23.
47	66.	51.	5.	1.	1.	1.	1.	20.
48	70.	30.	1.	1.	1.	1.	1.	41.
49	67.	12.	4.	1.	1.	1.	1.	59.
50	4.	32.	67.	1.	1.	1.	1.	39.
51	8.	24.	63.	1.	1.	1.	1.	47.
52	24.	69.	47.	1.	1.	1.	1.	2.

Appendix B: BRAGFLO Reference Tables

Table B-2 1992 BRAGFLO Ranks of Computed Variable Values for UPPER_SHAFT (Concluded)

Run No.	Porosity	Permeability	Compressibility	BCEXP	BCBRSAT	BCGSSAT	BCFLG	BCPCT
53	48.	49.	23.	1.	1.	1.	1.	22.
54	60.	17.	11.	1.	1.	1.	1.	54.
55	19.	37.	52.	1.	1.	1.	1.	34.
56	59.	11.	12.	1.	1.	1.	1.	60.
57	41.	66.	30.	1.	1.	1.	1.	5.
58	43.	52.	28.	1.	1.	1.	1.	19.
59	40.	1.	31.	1.	1.	1.	1.	70.
60	9.	47.	62.	1.	1.	1.	1.	24.
61	21.	61.	50.	1.	1.	1.	1.	10.
62	26.	26.	45.	1.	1.	1.	1.	45.
63	50.	67.	21.	1.	1.	1.	1.	4.
64	11.	53.	60.	1.	1.	1.	1.	18.
65	63.	39.	8.	1.	1.	1.	1.	32.
66	27.	20.	44.	1.	1.	1.	1.	51.
67	10.	68.	61.	1.	1.	1.	1.	3.
68	1.	19.	70.	1.	1.	1.	1.	52.
69	38.	59.	33.	1.	1.	1.	1.	12.
70	17.	18.	54.	1.	1.	1.	1.	53.

DISTRIBUTION

(Send Distribution list changes to M.M. Gruebel, Dept. 6342, Sandia
National Laboratories, PO Box 5800, Albuquerque, NM 87185-5800)

Federal Agencies

US Department of Energy (6)
Office of Civilian Radioactive Waste
Management
Attn: Deputy Director, RW-2
Associate Director, RW-10/50
Office of Program and
Resources Management
Office of Contract Business
Management
Director, Analysis and
Verification Division, RW-22
Associate Director, RW-30
Office of Systems and
Compliance
Associate Director, RW-40
Office of Storage and
Transportation
Director, RW-4/5
Office of Strategic Planning
and International Programs
Office of External Relations
Forrestal Building
Washington, DC 20585

US Department of Energy
Albuquerque Operations Office
Attn: National Atomic Museum Library
PO Box 5400
Albuquerque, NM 87185

US Department of Energy (2)
Office of Environmental Restoration
and Waste Management
Attn: EM-1
C. Frank, EM-50
Washington, DC 20585

US Department of Energy (3)
Office of Environmental Restoration
and Waste Management
Attn: M. Frei, EM-34, Trevion II
Director, Waste Management Projects
Washington, DC 20585-0002

US Department of Energy
Office of Environmental Restoration
and Waste Management
Attn: J. Lytle, EM-30, Trevion II
Washington, DC 20585-0002

US Department of Energy
Office of Environmental Restoration
and Waste Management
Attn: S. Schneider, EM-342,
Trevion II
Washington, DC 20585-0002

US Department of Energy (3)
WIPP Task Force
Attn: G.H. Daly
S. Fucigna
B. Bower
12800 Middlebrook Rd., Suite 400
Germantown, MD 20874

US Department of Energy (4)
Office of Environment, Safety and
Health
Attn: R.P. Berube, EH-20
C. Borgstrum, EH-25
R. Pelletier, EH-231
K. Taimi, EH-232
Washington, DC 20585

US Department of Energy (6)
WIPP Project Integration Office
Attn: S. Alcorn
W.J. Arthur III
J. Coffey
L.W. Gage
P.J. Higgins
D.A. Olona
PO Box 5400
Albuquerque, NM 87115-5400

US Department of Energy (2)
WIPP Project Integration Satellite
Office
Attn: R. Batra
R. Becker
PO Box 3090, Mail Stop 525
Carlsbad, NM 88221-3090

US Department of Energy (10)
WIPP Project Site Office (Carlsbad)
Attn: A. Hunt (4)
V. Daub (4)
J. Lippis
K. Hunter
PO Box 3090
Carlsbad, NM 88221-3090

US Department of Energy
Research & Waste Management Division
Attn: Director
PO Box E
Oak Ridge, TN 37831

US Department of Energy (2)
Idaho Operations Office
Fuel Processing and Waste
Management Division
785 DOE Place
Idaho Falls, ID 83402

US Department of Energy
Savannah River Operations Office
Defense Waste Processing
Facility Project Office
Attn: W.D. Pearson
PO Box A
Aiken, SC 29802

US Department of Energy (2)
Richland Operations Office
Nuclear Fuel Cycle & Production
Division
Attn: R.E. Gerton
825 Jadwin Ave.
PO Box 500
Richland, WA 99352

US Department of Energy
Office of Geologic Disposal
Yucca Mountain Project Office
Attn: Associate Director, RW-20
PO Box 98608
Las Vegas, NV 89193-8608

US Department of Energy (3)
Nevada Operations Office
Attn: J.R. Boland
D. Livingston
P.K. Fitzsimmons
2753 S. Highland Drive
Las Vegas, NV 89183-8518

US Department of Energy (2)
Technical Information Center
PO Box 62
Oak Ridge, TN 37831

US Department of Energy
Los Alamos Area Office
528 35th Street
Los Alamos, NM 87544

US Department of Energy (2)
Chicago Operations Office
Attn: J.C. Haugen
9800 South Cass Avenue
Argonne, IL 60439

US Department of Energy (3)
Rocky Flats Area Office
Attn: W.C. Rask
G. Huffman
T. Lukow
PO Box 928
Golden, CO 80402-0928

US Department of Energy
Dayton Area Office
Attn: R. Grandfield
PO Box 66
Miamisburg, OH 45343-0066

US Department of Energy
Attn: E. Young
Room E-178
GAO/RCED/GTN
Washington, DC 20545

US Bureau of Land Management
Carlsbad Office
101 E. Mermod
Carlsbad, NM 88220

US Bureau of Land Management
New Mexico State Office
PO Box 1449
Santa Fe, NM 87507

US Environmental Protection
Agency (2)
Radiation Protection Programs
Attn: M. Oge
ANR-460
Washington, DC 20460

US Environmental Protection
Agency, Region 6
Attn: C. Byrum, 6T-ET
1445 Ross Ave.
Dallas, TX 75202

US Geological Survey (2)
Water Resources Division
Attn: C. Peters
4501 Indian School NE
Suite 200
Albuquerque, NM 87110

US Nuclear Regulatory Commission
Division of Waste Management
Attn: H. Marson
Mail Stop 4-H-3
Washington, DC 20555

US Nuclear Regulatory Commission (4)
Advisory Committee on Nuclear Waste
Attn: D. Moeller
M.J. Steindler
P.W. Pomeroy
W.J. Hinze
7920 Norfolk Ave.
Bethesda, MD 20814

Defense Nuclear Facilities Safety
Board
Attn: D. Winters
625 Indiana Ave. NW
Suite 700
Washington, DC 20004

Nuclear Waste Technical Review Board
Attn: Library (2)
1100 Wilson Blvd.
Suite 910
Arlington, VA 22209-2297

Energy and Science Division
Office of Management and Budget
Attn: K. Yuracko
725 17th Street NW
Washington, DC 20503

State Agencies

New Mexico Bureau of Mines
and Mineral Resources
Socorro, NM 87801

New Mexico Energy, Minerals and
Natural Resources Department
Attn: Librarian
2040 South Pacheco
Santa Fe, NM 87505

New Mexico Energy, Minerals and
Natural Resources Department
New Mexico Radioactive Task Force (2)
(Governor's WIPP Task Force)
Attn: A. Lockwood, Chairman
C. Wentz, Policy Analyst
2040 South Pacheco
Santa Fe, NM 87505

Bob Forrest
Mayor, City of Carlsbad
PO Box 1569
Carlsbad, NM 88221

Carlsbad Department of Development
Executive Director
Attn: C. Bernard
PO Box 1090
Carlsbad, NM 88221

New Mexico Environment Department
Secretary of the Environment (3)
Attn: J. Espinosa
PO Box 968
1190 St. Francis Drive
Santa Fe, NM 87503-0968

New Mexico Environment Department
Attn: P. McCasland
WIPP Project Site Office
PO Box 3090
Carlsbad, NM 88221-3090

New Mexico State Engineer's Office
Attn: M. Chudnoff
PO Box 25102
Santa Fe, NM 87504-5102

Environmental Evaluation Group (5)
Attn: R. Neill
7007 Wyoming Blvd. NE, Suite F-2
Albuquerque, NM 87109

Advisory Committee on Nuclear Facility Safety

John F. Ahearne
Executive Director, Sigma Xi
99 Alexander Drive
Research Triangle Park, NC 27709

James E. Martin
109 Observatory Road
Ann Arbor, MI 48109

WIPP Panel of National Research Council's Board on Radioactive Waste Management

Charles Fairhurst, Chairman
Department of Civil and
Mineral Engineering
University of Minnesota
500 Pillsbury Dr. SE
Minneapolis, MN 55455-0220

John O. Blomeke
3833 Sandy Shore Drive
Lenoir City, TN 37771-9803

John D. Bredehoeft
Western Region Hydrologist
Water Resources Division
US Geological Survey (M/S 439)
345 Middlefield Road
Menlo Park, CA 94025

Rodney C. Ewing
Department of Geology
University of New Mexico
Albuquerque, NM 87131

B. John Garrick
PLG, Inc.
4590 MacArthur Blvd.
Suite 400
Newport Beach, CA 92660-2027

Leonard F. Konikow
US Geological Survey
431 National Center
Reston, VA 22092

Jeremiah O'Driscoll
505 Valley Hill Drive
Atlanta, GA 30350

Chris G. Whipple
ICF Kaiser Engineers
1800 Harrison St.
Oakland, CA 94612-3430

National Research Council (3)
Board on Radioactive
Waste Management
RM HA456
Attn: P.B. Myers (2)
G.J. Grube
2101 Constitution Ave.
Washington, DC 20418

Performance Assessment Peer Review Panel

G. Ross Heath
College of Ocean and Fishery
Sciences, HN-15
583 Henderson Hall
University of Washington
Seattle, WA 98195

Thomas H. Pigford
Department of Nuclear Engineering
4159 Etcheverry Hall
University of California
Berkeley, CA 94720

Thomas A. Cotton
JK Research Associates, Inc.
4429 Butterworth Place NW
Washington, DC 20016

Robert J. Budnitz
President, Future Resources
Associates, Inc.
2000 Center Street, Suite 418
Berkeley, CA 94704

C. John Mann
Department of Geology
245 Natural History Bldg.
1301 West Green Street
University of Illinois
Urbana, IL 61801

Frank W. Schwartz
Department of Geology and Mineralogy
The Ohio State University
Scott Hall
1090 Carmack Rd.
Columbus, OH 43210

National Laboratories

Argonne National Laboratory (2)
Attn: A. Smith
D. Tomasko
9700 South Cass, Bldg. 201
Argonne, IL 60439

Battelle Pacific Northwest
Laboratory (2)
Attn: S. Bates
R.E. Westerman
MSIN P8-44
Battelle Boulevard
Richland, WA 99352

Idaho National Engineering
Laboratory (2)
Attn: H. Loo
R. Klinger
Mail Stop 5108
Idaho Falls, ID 83403-4000

Los Alamos National Laboratory (5)
Attn: B. Erdal, CNC-11
M. Ennis, HS-12
Mail Stop J900
S. Kosiewicz, EM-7
Mail Stop J595
L. Soholt, EM-13
Mail Stop M992
J. Wenzel, HS-12
Mail Stop K482
PO Box 1663
Los Alamos, NM 87545

Oak Ridge National Laboratory
Transuranic Waste Manager
Attn: D.W. Turner
Bldg. 3047
PO Box 2008
Oak Ridge, TN 37831-6060

Pacific Northwest Laboratory
Attn: B. Kennedy
PO Box 999
Richland, WA 99352

Westinghouse-Savannah River
Technology Center (4)
Attn: N. Bibler
J.R. Harbour
M.J. Plodinec
G.G. Wicks
Aiken, SC 29802

Corporations/Members of the Public

Battelle Memorial Institute
Attn: R. Root
J. Kircher
505 Marquette NW
Suite 1
Albuquerque, NM 87102

Benchmark Environmental Corp.
Attn: C. Frederickson
4501 Indian School NE
Suite 105
Albuquerque, NM 87110

Beta Corporation Int.
Attn: E. Bonano
6613 Esther NE
Albuquerque, NM 87109

City of Albuquerque
Public Works Department
Utility Planning Division
Attn: W.K. Summers
PO Box 1293
Albuquerque, NM 87103

Deuel and Associates, Inc.
Attn: R.W. Prindle
7208 Jefferson NE
Albuquerque, NM 87109

Disposal Safety, Inc.
Attn: B. Ross
1660 L Street NW, Suite 314
Washington, DC 20036

Ecodynamics (2)
Attn: P. Roache
R. Blaine
PO Box 9229
Albuquerque, NM 87119-9229

EG & G Idaho (3)
1955 Fremont Street
Attn: C. Atwood
C. Hertzler
T.I. Clements
Idaho Falls, ID 83415

Geomatrix
Attn: K. Coppersmith
100 Pine St., Suite 1000
San Francisco, CA 94111

Golder Associates, Inc.
Attn: R. Kossik
4104 148th Avenue NE
Redmond, WA 98052

INTERA, Inc.
Attn: A.M. LaVenue
1650 University Blvd. NE, Suite 300
Albuquerque, NM 87102

INTERA, Inc.
Attn: J.F. Pickens
6850 Austin Center Blvd., Suite 300
Austin, TX 78731

INTERA, Inc.
Attn: W. Stensrud
PO Box 2123
Carlsbad, NM 88221

INTERA, Inc.
Attn: W. Nelson
101 Convention Center Drive
Suite 540
Las Vegas, NV 89109

IT Corporation (2)
Attn: R.F. McKinney
J. Myers
Regional Office
Suite 700
5301 Central Avenue NE
Albuquerque, NM 87108

John Hart and Associates, P.A.
Attn: J.S. Hart
2815 Candelaria Road NW
Albuquerque, NM 87107

John Hart and Associates, P.A.
Attn: K. Licklitter
1009 North Washington
Tacoma, WA 98406

MAC Technical Services Co.
Attn: D.K. Duncan
8418 Zuni Road SE
Suite 200
Albuquerque, NM 87108

Newman and Holtzinger
Attn: C. Mallon
1615 L Street NW
Suite 1000
Washington, DC 20036

RE/SPEC, Inc. (2)
Attn: W. Coons
4775 Indian School NE
Suite 300
Albuquerque, NM 87110

RE/SPEC, Inc.
Attn: J.L. Ratigan
PO Box 725
Rapid City, SD 57709

Reynolds Electric and Engineering
Company, Inc.
Attn: E.W. Kendall
Building 790
Warehouse Row
PO Box 98521
Las Vegas, NV 89193-8521

Science Applications International
Corporation (SAIC)
Attn: H.R. Pratt
10260 Campus Point Drive
San Diego, CA 92121

Science Applications International
Corporation (2)
Attn: D.C. Royer
C.G. Pflum
101 Convention Center Dr.
Las Vegas, NV 89109

Science Applications International
Corporation (3)
Attn: M. Davis
R. Guzowski
J. Tollison
2109 Air Park Road SE
Albuquerque, NM 87106

Science Applications International
Corporation (2)
Attn: J. Young
D. Lester
18706 North Creek Parkway, Suite 110
Bothell, WA 98011

Southwest Research Institute
Center for Nuclear Waste Regulatory
Analysis (2)
Attn: P.K. Nair
6220 Culebra Road
San Antonio, TX 78228-0510

Systems, Science, and Software (2)
Attn: E. Peterson
P. Lagus
Box 1620
La Jolla, CA 92038

TASC
Attn: S.G. Oston
55 Walkers Brook Drive
Reading, MA 01867

Tech Reps, Inc. (7)
Attn: J. Chapman
C. Crawford
D. Marchand
T. Peterson
J. Stikar
D. Scott
F. Puffer
5000 Marble NE, Suite 222
Albuquerque, NM 87110

Tolan, Beeson & Associates
Attn: T.L. Tolan
2320 W. 15th Avenue
Kennewick, WA 99337

TRW Environmental Safety Systems (2)
Attn: I. Sacks, Suite 800
L. Wildman, Suite 1300
2650 Park Tower Drive
Vienna, VA 22180-7306

Sanford Cohen and Associates
Attn: J. Channell
7101 Carriage Rd NE
Albuquerque, NM 87109

Westinghouse Electric Corporation (5)
Attn: Library
C. Cox
L. Fitch
B.A. Howard
R.F. Kehrman
PO Box 2078
Carlsbad, NM 88221

Westinghouse Hanford Company
Attn: D.E. Wood, MSIN HO-32
PO Box 1970
Richland, WA 99352

Western Water Consultants
Attn: P.A. Rechard
PO Box 4128
Laramie, WY 82071

Western Water Consultants
Attn: D. Fritz
1949 Sugarland Drive #134
Sheridan, WY 82801-5720

P. Drez
8816 Cherry Hills Road NE
Albuquerque, NM 87111

David Lechel
9600 Allende Rd. NE
Albuquerque, NM 87109

C.A. Marchese
PO Box 21790
Albuquerque, NM 87154

Arend Meijer
3821 Anderson SE
Albuquerque, NM 87108

D.W. Powers
Star Route Box 87
Anthony, TX 79821

Shirley Thieda
PO Box 2109, RR1
Bernalillo, NM 87004

Jack Urich
c/o CARD
144 Harvard SE
Albuquerque, NM 87106

Universities

University of California
Mechanical, Aerospace, and
Nuclear Engineering Department (2)
Attn: W. Kastenberg
D. Browne
5532 Boelter Hall
Los Angeles, CA 90024

University of California
Engineering and Applied Science Attn:
D. Okrent
48-121A Engineering IV
Los Angeles, CA 90024-1597

University of California
Mine Engineering Department
Rock Mechanics Engineering
Attn: N. Cook
Berkeley, CA 94720

University of Hawaii at Hilo
Business Administration
Attn: S. Hora
Hilo, HI 96720-4091

University of New Mexico
Geology Department
Attn: Library
Albuquerque, NM 87131

University of New Mexico
Research Administration
Attn: H. Schreyer
102 Scholes Hall
Albuquerque, NM 87131

University of Wyoming
Department of Civil Engineering
Attn: V.R. Hasfurther
Laramie, WY 82071

University of Wyoming
Department of Geology
Attn: J.I. Drever
Laramie, WY 82071

University of Wyoming
Department of Mathematics
Attn: R.E. Ewing
Laramie, WY 82071

Libraries

Thomas Brannigan Library
Attn: D. Dresp
106 W. Hadley St.
Las Cruces, NM 88001

New Mexico State Library
Attn: N. McCallan
325 Don Gaspar
Santa Fe, NM 87503

New Mexico Tech
Martin Speere Memorial Library
Campus Street
Socorro, NM 87810

New Mexico Junior College
Pannell Library
Attn: R. Hill
Lovington Highway
Hobbs, NM 88240

Carlsbad Municipal Library
WIPP Public Reading Room
Attn: L. Hubbard
101 S. Halagueno St.
Carlsbad, NM 88220

University of New Mexico
Zimmerman Library
Government Publications Department
Albuquerque, NM 87131

NEA/Performance Assessment Advisory Group (PAAG)

P. Duerden
ANSTO
Lucas Heights Research Laboratories
Private Mail Bag No. 1
Menai, NSW 2234
AUSTRALIA

Gordon S. Linsley
Division of Nuclear Fuel Cycle and
Waste Management
International Atomic Energy Agency
PO Box 100
A-1400 Vienna, AUSTRIA

Nicolo Cadelli
Commission of the European
Communities
200, Rue de la Loi
B-1049 Brussels, BELGIUM

R. Heremans
Organisme Nationale des Déchets
Radioactifs et des Matières Fissiles
(ONDRAF)
Place Madou 1, Boitec 24/25
B-1030 Brussels, BELGIUM

J. Marivoet
Centre d'Etudes de l'Energie
Nucléaire (CEN/SCK)
Boeretang 200
B-2400 Mol, BELGIUM

P. Conlon
Waste Management Division
Atomic Energy Control Board (AECB)
PO Box 1046
Ottawa, Ontario KIP 559, CANADA

A.G. Wikjord
Manager, Environmental and Safety
Assessment Branch
Atomic Energy of Canada Limited
Whiteshell Research Establishment
Pinewa, Manitoba ROE 1LO
CANADA

Teollisuuden Voima Oy (TVO) (2)
Attn: Timo Äikäs
Jukka-Pekka Salo
Annankatu 42 C
SF-00100 Helsinki Suomi
FINLAND

Timo Vieno
Technical Research Centre of Finland
(VTT)
Nuclear Energy Laboratory
PO Box 208
SF-02151 Espoo, FINLAND

Division de la Sécurité et de la
Protection de l'Environnement (DSPE)
Commissariat à l'Energie Atomique
Agence Nationale pour la Gestion des
Déchets Radioactifs (ANDRA) (2)

Attn: Gérald Ouzounian

M. Claude Ringear
Route du Panorama Robert Schuman
B. P. No. 38
F-92266 Fontenay-aux-Roses Cedex
FRANCE

Claudio Pescatore
Division of Radiation Protection and
Waste Management
OECD Nuclear Energy Agency
38, Boulevard Suchet
F-75016 Paris, FRANCE

M. Dominique Greneche
Commissariat à l'Energie Atomique
IPSN/DAS/SASICC/SAED
B.P. No. 6
F-92265 Fontenay-aux-Roses Cedex
FRANCE

Robert Fabriol
Bureau de Recherches Géologiques et
Minières (BRGM)
B.P. 6009
45060 Orléans Cedex 2, FRANCE

P. Bogorinski
Gesellschaft für Reaktorsicherheit
(GRS) MBH
Schwertnergasse 1
D-5000 Köln 1, GERMANY

R. Storck
GSF - Institut für Tieflagerung
Theodor-Heuss-Strabe 4
D-3300 Braunschweig, GERMANY

Ferruccio Gera
ISMES S.p.A
Via del Crociferi 44
I-00187 Rome, ITALY

Hiroyuki Umeki
Isolation System Research Program
Radioactive Waste Management Project
Power Reactor and Nuclear Fuel
Development Corporation (PNC)
1-9-13, Akasaka, Minato-ku
Tokyo 107, JAPAN

P. Carboneras Martinez
ENRESA
Calle Emilio Vargas, 7
R-28043 Madrid
SPAIN

Tönis Papp
Swedish Nuclear Fuel and Waste
Management Co.
Box 5864
S 102 48 Stockholm
SWEDEN

Conny Hägg
Swedish Radiation Protection
Institute (SSI)
Box 60204
S-104 01 Stockholm
SWEDEN

J. Hadermann
Paul Scherrer Institute
Waste Management Programme
CH-5232 Villigen PSI
SWITZERLAND

J. Vigfusson
HSK-Swiss Nuclear Safety Inspectorate
Federal Office of Energy
CH-5232 Villigen-HSK
SWITZERLAND

D.E. Billington
Departmental Manager-Assessment
Studies
Radwaste Disposal R&D Division
AEA Decommissioning & Radwaste
Harwell Laboratory, B60
Didcot Oxfordshire OX11 0RA
UNITED KINGDOM

P. Grimwood
Waste Management Unit
BNFL
Sellafield
Seascale, Cumbria CA20 1PG
UNITED KINGDOM

Alan J. Hooper
UK Nirex Ltd
Curie Avenue
Harwell, Didcot
Oxfordshire, OX11 0RH
UNITED KINGDOM

Jerry M. Boak
Yucca Mountain Project Office
US Department of Energy
PO Box 98608
Las Vegas, NV 89193

Seth M. Coplan (Chairman)
US Nuclear Regulatory Commission
Division of High-Level Waste
Management
Mail Stop 4-H-3
Washington, DC 20555

A.E. Van Luik
INTERA/M&O
The Valley Bank Center
101 Convention Center Dr.
Las Vegas, NV 89109

**NEA/Probabilistic System Assessment
Group (PSAG)**

Shaheed Hossain
Division of Nuclear Fuel Cycle and
Waste Management
International Atomic Energy Agency
Wagramerstrasse 5
PO Box 100
A-1400 Vienna, AUSTRIA

Alexander Nies (PSAC Chairman)
Gesellschaft für Strahlen- und
Institut für Tieflagerung
Abteilung für Endlagersicherheit
Theodor-Heuss-Strasse 4
D-3300 Braunschweig, GERMANY

Eduard Hofer
Gesellschaft für Reaktorsicherheit
(GRS) MBH
Forschungsgelände
D-8046 Garching, GERMANY

Andrea Saltelli
Commission of the European
Communities
Joint Resarch Centre of Ispra
I-21020 Ispra (Varese)
ITALY

Alejandro Alonso
Cátedra de Tecnología Nuclear
E.T.S. de Ingenieros Industriales
José Gutiérrez Abascal, 2
E-28006 Madrid, SPAIN

ENRESA (2)
Attn: M. A. Cuñado
F. J. Elorza
Calle Emilio Vargas, 7
E-28043 Madrid, SPAIN

Pedro Prado
CIEMAT
Instituto de Tecnología Nuclear
Avenida Complutense, 22
E-28040 Madrid, SPAIN

Nils A. Kjellbert
Swedish Nuclear Fuel and Waste
Management Company (SKB)
Box 5864
S-102 48 Stockholm, SWEDEN

Björn Cronhjort
Royal Institute of Technology
Automatic Control
S-100 44 Stockholm, SWEDEN

Richard A. Klos
Paul-Scherrer Institute (PSI)
CH-5232 Villigen PSI, SWITZERLAND

Nationale Genossenschaft für die
Lagerung Radioaktiver Abfälle (2)
Attn: C. McCombie
F. Van Dorp
Hardstrasse 73
CH-5430 Wettingen, SWITZERLAND

N. A. Chapman
Intera Information Technologies
Park View House
14B Burton Street
Melton Mowbray
Leicestershire LE13 1AE
UNITED KINGDOM

Daniel A. Galson
Galson Sciences Ltd.
35, Market Place
Oakham
Leicestershire LE15 6DT
UNITED KINGDOM

David P. Hodgkinson
Intera Information Technologies
45 Station Road, Chiltern House
Henley-on-Thames
Oxfordshire RG9 1AT
UNITED KINGDOM

Brian G.J. Thompson
Department of the Environment: Her
Majesty's Inspectorate of Pollution
Room A5.33, Romney House
43 Marsham Street
London SW1P 2PY
UNITED KINGDOM

Intera Information Technologies
Attn: M.J.Apted
3609 South Wadsworth Blvd.
Denver, CO 80235

US Nuclear Regulatory Commission (2)
Attn: R. Codell
N. Eisenberg
Mail Stop 4-H-3
Washington, DC 20555

Battelle Pacific Northwest
Laboratories
Attn: P.W. Eslinger
MS K2-32
PO Box 999
Richland, WA 99352

Center for Nuclear Waste Regulatory
Analysis (CNWRA)
Southwest Research Institute
Attn: B. Sagar
PO Drawer 28510
6220 Culebra Road
San Antonio, TX 78284

Geostatistics Expert Working Group (GXG)

Rafael L. Bras
R.L. Bras Consulting Engineers
44 Percy Road
Lexington, MA 02173

Jesus Carrera
Universidad Politécnic de Cataluña
E.T.S.I. Caminos
Jordi, Girona 31
E-08034 Barcelona
SPAIN

Gedeon Dagan
Department of Fluid Mechanics and
Heat Transfer
Tel Aviv University
PO Box 39040
Ramat Aviv, Tel Aviv 69978
ISRAEL

Ghislain de Marsily (GXG Chairman)
University Pierre et Marie Curie
Laboratoire de Geologie Applique
4, Place Jussieu
T.26 - 5^e etage
75252 Paris Cedex 05, FRANCE

Alain Galli
Centre de Geostatistique
Ecole des Mines de Paris
35 Rue St. Honore
77035 Fontainebleau, FRANCE

Christian Ravenne
Geology and Geochemistry Division
Institut Francais du Pétrole
1 & 4, Av. de Bois-Préau B.P. 311
92506 Rueil Malmaison Cedex
FRANCE

Peter Grindrod
INTERA Information Technologies Ltd.
Chiltern House
45 Station Road
Henley-on-Thames
Oxfordshire, RG9 1AT, UNITED KINGDOM

Alan Gutjahr
Department of Mathematics
New Mexico Institute of Mining and
Technology
Socorro, NM 87801

C. Peter Jackson
Harwell Laboratory
Theoretical Studies Department
Radwaste Disposal Division
Bldg. 424.4
Oxfordshire Didcot Oxon OX11 0RA
UNITED KINGDOM

Rae Mackay
Department of Civil Engineering
University of Newcastle Upon Tyne
Newcastle Upon Tyne NE1 7RU
UNITED KINGDOM

Steve Gorelick
Department of Applied Earth Sciences
Stanford University
Stanford, CA 94305-2225

Peter Kitanidis
60 Peter Coutts Circle
Stanford, CA 94305

Dennis McLaughlin
Parsons Laboratory
Room 48-209
Department of Civil Engineering
Massachusetts Institute of Technology
Cambridge, MA 02139

Shlomo P. Neuman
College of Engineering and Mines
Department of Hydrology and Water
Resources
University of Arizona
Tucson, AZ 85721

Yoram Rubin
Department of Civil Engineering
University of California
Berkeley, CA 94720

Foreign Addresses

Studiecentrum Voor Kernenergie
Centre D'Energie Nucleaire
Attn: A. Bonne
SCK/CEN
Boeretang 200
B-2400 Mol
BELGIUM

Atomic Energy of Canada, Ltd. (3)
Whiteshell Research Establishment
Attn: M.E. Stevens
B.W. Goodwin
D. Wushke
Pinewa, Manitoba ROE 1L0, CANADA

Juhani Vira
Teollisuuden Voima Oy (TVO)
Annankatu 42 C
SF-00100 Helsinki Suomi
FINLAND

Jean-Pierre Olivier
OECD Nuclear Energy Agency (2)
38, Boulevard Suchet
F-75016 Paris
FRANCE

D. Alexandre, Deputy Director
ANDRA
31 Rue de la Federation
75015 Paris
FRANCE

Claude Sombret
Centre D'Etudes Nucleaires
De La Vallee Rhone
CEN/VALRHO
S.D.H.A. B.P. 171
30205 Bagnols-Sur-Ceze, FRANCE

Bundesministerium fur Forschung und
Technologie
Postfach 200 706
5300 Bonn 2, GERMANY

Bundesanstalt fur Geowissenschaften
und Rohstoffe
Attn: M. Langer
Postfach 510 153
3000 Hanover 51, GERMANY

Gesellschaft fur Reaktorsicherheit
(GRS) (2)
Attn: B. Baltes
W. Muller
Schwertnergasse 1
D-5000 Cologne, GERMANY

Institut fur Tieflagerung (2)
Attn: K. Kuhn
Theodor-Heuss-Strasse 4
D-3300 Braunschweig, GERMANY

Physikalisch-Technische
Bundesanstalt
Attn: P. Brenneke
Postfach 33 45
D-3300 Braunschweig, GERMANY

Shingo Tashiro
Japan Atomic Energy Research
Institute
Tokai-Mura, Ibaraki-Ken
319-11, JAPAN

Netherlands Energy Research
Foundation (ECN)
Attn: L.H. Vons
3 Westerduinweg
PO Box 1
1755 ZG Petten, THE NETHERLANDS

Johan Andersson
Swedish Nuclear Power Inspectorate
Statens Kärnkraftinspektion (SKI)
Box 27106
S-102 52 Stockholm, SWEDEN

Fred Karlsson
Svensk Karnbransleforsorjning
AB SKB
Box 5864
S-102 48 Stockholm, SWEDEN

Nationale Genossenschaft für die
Lagerung Radioaktiver Abfälle (2)
Attn: S. Vomvoris
P. Zuidema
Hardstrasse 73
CH-5430 Wettingen, SWITZERLAND

AEA Technology
Attn: J.H. Rees
D5W/29 Culham Laboratory
Abington
Oxfordshire OX14 3DB, UNITED KINGDOM

AEA Technology
Attn: W.R. Rodwell
O44/A31 Winfrith Technical Centre
Dorchester
Dorset DT2 8DH, UNITED KINGDOM

AEA Technology
Attn: J.E. Tinson
B4244 Harwell Laboratory
Didcot, Oxfordshire OX11 0RA
UNITED KINGDOM

D.R. Knowles
British Nuclear Fuels, plc
Risley, Warrington
Cheshire WA3 6AS, 1002607
UNITED KINGDOM

Internal

1 A. Narath
20 O.E. Jones
1502 J.C. Cummings
1511 D.K. Gartling
6000 D.L. Hartley
6115 P.B. Davies
6115 R.L. Beauheim
6119 E.D. Gorham
6119 Staff (14)
6121 J.R. Tillerson
6121 Staff (7)
6233 J.C. Eichelberger
6300 D.E. Ellis
6302 L.E. Shephard
6303 S.Y. Pickering

6303 W.D. Weart
6305 S.A. Goldstein
6305 A.R. Lappin
6306 A.L. Stevens
6312 F.W. Bingham
6313 L.S. Costin
6331 P.A. Davis
6341 Sandia WIPP Central Files (100)
6342 D.R. Anderson
6342 Staff (30)
6343 V. Harper-Slaboszewicz
6343 Staff (3)
6345 R.C. Lincoln
6345 Staff (9)
6347 D.R. Schafer
6348 J.T. Holmes
6348 Staff (4)
6351 R.E. Thompson
6352 D.P. Garber
6352 S.E. Sharpton
6400 N.R. Ortiz
6613 R.M. Cranwell
6613 R.L. Iman
6613 C. Leigh
6622 M.S.Y. Chu
6641 R.E. Luna, Acting
7141 Technical Library (5)
7151 Technical Publications
7613-2 Document Processing for
DOE/OSTI (10)
8523-2 Central Technical Files

THIS PAGE INTENTIONALLY LEFT BLANK